Microgel Particles Stabilised High Internal Phase Emulsions for Applications in Tissue Engineering

A thesis submitted in partial fulfilment of the requirements for the degree of
Doctor of Philosophy

Wei Yuan

Department of Chemistry

Imperial College London

Declaration

The work described in this thesis is the work of the author, unless otherwise stated.

The copyright of this thesis rests with the author and is made available under a Creative Commons Attribution Non-Commercial No Derivatives licence. Researchers are free to copy, distribute or transmit the thesis on the condition that they attribute it, that they do not use it for commercial purposes and that they do not alter, transform or build upon it. For any reuse or redistribution, researchers must make clear to others the licence terms of this work.

Acknowledgements

Above all, I am so grateful for a China-UK Scholarships for Excellence award from the China Scholarship Council, which financed my PhD study. It was a great honour to have the opportunity.

Many thanks go to my supervisors, Dr. Joachim H. G. Steinke and Prof. Alexander Bismarck, for their continuous input into this project with expertise, insight, encouragement and enlightenment. It has been great experience to study under their supervisions, which can only make me strong and confident. Sadly, Joachim passed away in January 2013, which is such a great loss. He will be sorely missed by us all while his instructions will guide me forward in the pursuit of truth.

Then, I want to thank members of the Steinke Group and the PaCE Group for the help and for the fun, especially Dr. Fanshun Meng, Dr. Natasha Shirshova, Jonathan Martinelli, Christopher Drake, James Serginson, Sally Ewen, Edyta Sidorowicz, Shengzhong Zhou and David Rees; Dr. Angelica Menner, Urosh Vukicevic, Steven Lamoriniere, Kingsley Ho and Ranting Wu. What I also have to mention is the help from neighbouring labs. I am grateful to Katherine Orchard and Robert Menzel in the NanoHAC Group, to Dr. Savaas Georgiades in the Villa Group and to Xinzhu Liu in the Mimi Group.

Meanwhile, this work cannot be done without all the technical support in the college. Special thanks go to Ms. Patricia Carry for trainings in the analytical lab (Department of Chemical Engineering) and Dr. Ambrose Taylor for help with SEM (Department of Mechanical Engineering).

Finally, I cannot thank my family enough for their support throughout my studies. I am so grateful for the positive energy transmitted over each of their phone calls. This thesis is dedicated to them.

Abstract

Tissue engineering using polymeric scaffolds to support cell growth and tissue regeneration is currently under development as a promising solution to tissue loss or organ failure. This thesis focuses on fabricating multifunctional scaffolds for tissue engineering using emulsion templating.

Poly(*N*-isopropylacrylamide-*co*-acrylic acid) [poly(NIPAAm-*co*-AA)] microgel particles were found capable of stabilising both w/o and o/w high internal phase emulsions (HIPEs), depending on the temperature, pH and salt concentration. PolyHIPEs were prepared by photo-polymerisation of both HIPEs containing monomers in the continuous phase and exhibited pore structures with sizes of a few hundred micrometers. For oil-soluble monomers, e.g., divinylbenzene (DVB), microgel particles stabilised w/o HIPEs were obtained at 40 °C using a microgel suspension (0.4 wt %) in 1 mM KCl solution at pH 4. For water-soluble monomers, e.g., potassium acrylate (KAA), the crosslinker content was found crucial to the formation of an open porous structure in poly(KAA) HIPEs. It was shown by cryo-scanning electron microscopy that the interconnections were not generated upon polymerisation but during solvent extraction. Highly interconnected poly(KAA) HIPEs prepared using 80 vol % internal phase possessed a low density of ca. 0.03 g/cm^3 and a porosity up to 97~98%.

By using active ingredient (A.I.) loaded microgel particles as emulsifiers, polyHIPEs with delivery functionality were developed. The emulsifying ability of A.I. loaded microgels was found to be dependent on A.I.-microgel interactions. Paracetamol drug loaded microgel particles resulted in stable o/w HIPEs at either low (400 rpm) or high stirring speed (1000 rpm) and hence polyHIPEs with tunable morphologies after polymerisation.

Microgel particles stabilised o/w HIPEs were also used to fabricate macroporous dextran and dextran-*co*-polyNIPAAm. The pH of the aqueous phase was found crucial to HIPE stability and pH 6.8 resulted in stable HIPEs without coalescence and macropores with narrow pore size distribution after freeze-drying. By thermostating HIPEs prior to freezing or by varying dextran concentration, the morphology of macroporous dextran was tunable. Macroporous dextran-*co*-polyNIPAAm could potentially be used as a multiply responsive scaffold. Besides the stimuli-responsiveness of microgel particles, polyNIPAAm segments of the copolymers enabled scaffold integrity in water at physiological temperature.

Microgel particles stabilised HIPEs were established as a truly versatile template to fabricate macroporous polymers for potential applications as tissue engineering scaffolds.

Contents

Declaration ***2***

Acknowledgements ***3***

Abstract ***4***

Contents ***5***

List of Figures ***9***

List of Tables ***17***

List of Abbreviations ***19***

Project Aims and Objectives ***22***

Chapter 1 Introduction ***24***

1.1 Bone tissue and Bone tissue engineering 25

1.1.1 Bones and bone cells 26

1.1.1.1 Composition and mechanical properties of bones 26

1.1.1.2 Introduction to native bone cells 27

1.1.1.3 Adult stem cells for tissue engineering application 28

1.1.2 Formation and healing process of bone 29

1.1.2.1 Formation of bone 29

1.1.2.2 Bone fracture healing 30

1.1.2.3 Current treatment of bone defects 31

1.1.3 Bone tissue engineering 31

1.1.3.1 Current research in bone tissue engineering 31

1.1.3.2 Biomaterials for bone tissue engineering 32

1.1.3.3 Scaffold fabrication 33

1.1.3.4 Bioreactor for in-vitro tissue cultivation 36

1.2 HIPEs and polyHIPEs 37

1.2.1 Versatility of HIPEs and polyHIPEs 38

1.2.1.1 Tunability of pore architectures and mechanical properties of polyHIPEs 39

1.2.1.2 Poly(Pickering HIPEs) as novel polyHIPEs 40

1.2.2 Applications of polyHIPEs as tissue engineering scaffolds 44

Chapter 2 Microgel particles stabilised DVB based emulsions ***46***

2.1 Overview 46

2.2 Synthesis, purification and characterisation of poly(NIPAAm-*co*-AA) microgel particles 47

2.2.1 Assessment of the environmental sensitivity of microgel particles 48

2.2.1.1 Particle size of microgels as a function of temperature at various pH 49

2.2.1.2 Particle size of microgels as a function of temperature at various ionic strengths 52

2.2.1.3 Particle size of microgels at various concentrations as a function of temperature 55

2.2.2 Assessment of the effect of surfactant and purification procedures on microgel size 57

2.2.2.1 Effect of dialysis type used in purification on the particle size of microgels 58

2.2.2.2 Effect of six different purification procedures on the particle size of microgels 61
2.2.2.3 Batch-to-batch variation in the particle size of synthesized microgels.....63
2.3 Preparation and characterisation of styrene/DVB based polyHIPEs.....65
2.4 Preliminary investigations of microgel particle stabilised emulsions.....66
2.4.1 Effect of phase volume ratio on the stability of microgel stabilised emulsions 67
2.4.2 Effect of particle concentration on stability of microgel-stabilised emulsions.....70
2.4.3 Effect of preparation temperature on the stability emulsions 73
2.5 Investigation of the thermal sensitivity of microgel stabilised emulsions.....75
2.5.1 Effect of the preparation temperature on emulsion stability investigated at pH 3..75
2.5.2 Creaming of microgel stabilised emulsions investigated at pH 2.5, pH 3 and pH 4 77
2.5.3 Thermal sensitivity of microgel-stabilised emulsions investigated above the VPTT at pH 4.....80
2.5.3.1 Thermal sensitivity of microgel-stabilised emulsions prepared at pH 4 using different temperatures 81
2.5.3.2 Effect of microgel concentration on stability of the emulsions prepared at pH 4 86
2.6 Preparation of polyHIPEs from microgel-stabilised w/o emulsions.....88
2.6.1 Effect of preparation conditions on the morphology of DVB based polyHIPEs....89
2.6.2 Formation of stable microgel layers at the interface essential for stable w/o HIPEs 93
2.7 Summary.....95

***Chapter 3 PolyHIPEs from microgels stabilised o/w HIPEs*.....97**
3.1 Overview.....97
3.2 Preparation of microgels stabilised o/w HIPEs containing KAA.....98
3.2.1 Preliminary tests on KAA-microgel aqueous mixtures prior to emulsification 98
3.2.1.1 Effect of KAA concentration on microgel dispersion in the aqueous mixtures 98
3.2.1.2 Effect of temperature on microgel dispersion in the aqueous mixtures.....100
3.2.2 Emulsification of microgel suspensions in KAA solutions with the oil phase.....101
3.2.2.1 Effect of KAA concentration on the stability of microgel-stabilised o/w HIPEs 101
3.2.2.2 Effect of stirring protocol on the stability of microgel-stabilised o/w HIPEs103
3.2.2.3 Effect of microgel concentration on stability of the resultant o/w HIPEs 107
3.2.2.4 Effect of temperature on the stability of microgel-stabilised o/w HIPEs 109
3.3 Selecting initiator and crosslinker for the polymerisation of o/w HIPEs 111
3.3.1 Polymerisation of microgel-stabilised o/w HIPEs using redox initiation.....111
3.3.2 Photo-polymerisation of microgel-stabilised o/w HIPEs 114
3.3.2.1 Photo-initiation methods for the polymerisation of microgel-stabilised o/w HIPEs 114
3.3.2.2 Effect of initiator amount on polymerisation of microgel-stabilised o/w HIPEs 117
3.4 Controlling the pore structure of poly(KAA) Pickering-HIPEs 119
3.4.1 Varying the extraction and drying conditions to produce open porous polyHIPEs ... .119
3.4.1.1 Effect of extraction time and extraction-drying protocol on the pore structures 119

3.4.1.2 Other attempts to produce pore throats in the extraction and drying process 123
3.4.2 Tuning the HIPE composition for open porous poly(KAA) Pickering-HIPEs 125
3.4.2.1 Effect of the internal phase volume ratio on pore structures 125
3.4.2.2 Effect of the cross-linker content on pore structures of polyHIPEs 127
3.4.2.3 Interplay of KAA concentration, BIS content and $\phi_{int.}$ for pore-throat formation 133
3.4.3 Effect of stirring speed on the pore structures of poly(KAA) Pickering-HIPEs .. 136
3.4.3.1 Effect of crosslinker content on the pore structure at increased stirring speed 137
3.4.3.2 Effect of microgel concentration on the pore structure at increased stirring speed 142
3.4.4 Investigation of pore-throat formation by cryo-SEM 144
3.4.4.1 Closed-pore structures after polymerisation evidenced by cryo-SEM 144
3.4.4.2 Open porous structures generated during Soxhlet extraction with MeOH 147
3.5 Surface area and porosity of poly(KAA) Pickering-HIPEs 150
3.5.1 BET surface area 151
3.5.2 Porosity of poly(KAA) Pickering-HIPEs 156
3.5.2.1 Porosity from liquid displacement measurements 157
3.5.2.2 Porosities by mercury intrusion porosimetry and a designed indirect method 159
3.6 Preparation and characterisation of KAA based polyHIPE composites 163
3.6.1 Hydrophilic silica filled poly(KAA) Pickering-HIPE composites 163
3.6.2 45S5 Bioglass® filled poly(KAA) Pickering-HIPE composites 167
3.7 Preparation of poly(potassium methacrylate) Pickering-HIPEs 174
3.8 Summary 176

Chapter 4 High internal phase emulsions stabilised with dye- and drug-loaded microgel particles 178
4.1 Overview 178
4.2 Mixing dye molecules with microgel particles for HIPE preparation 179
4.2.1 Effect of centrifugation of the aqueous mixtures on emulsion stability 179
4.2.1.1 Mixing of R6G into aqueous suspensions prior to emulsification 179
4.2.1.2 Efficiency of dye-loaded microgel particles as emulsifiers 181
4.2.1.3 Microgel-dye interactions revealed by particle size measurements 182
4.2.2. Effect of dye concentration in the aqueous suspension on HIPE stability 184
4.2.3 Effect of using buffer in the aqueous phase on HIPE stability 185
4.2.4 Effect of using dye-loaded microgels as emulsifiers on the polyHIPE morphology 186
4.3 HIPEs stabilised with drug-loaded microgel particles 188
4.3.1 Investigation into the microgel-drug interactions 189
4.3.2 Drug-loaded microgels with 1 mol % crosslinking degree as HIPE stabilisers ... 190
4.3.3 Drug-loaded microgels with 2 mol % crosslinking degree as HIPE stabilisers ... 193
4.4 Summary 195

Chapter 5 Microgel-stabilised o/w HIPEs for the preparation of macroporous materials containing dextran and its derivative 197
5.1 Overview 197
5.2 Dextran macroporous structures from microgels stabilised o/w HIPEs 197

5.2.1 Effect of pH on stability of the template and the resultant porous structures.....198
5.2.2. Effects of temperature on the morphology of dextran macroporous structures...202
5.2.3 Effect of dextran concentration and molecular weight on the pore structures 206
5.3 Dextran-*co*-polyNIPAAm macroporous structures from microgels stabilised o/w HIPEs 210
5.3.1 Morphologies and thermal properties of dextran-*co*-polyNIPAAm macroporous structures 210
5.3.2 Morphologies of dextran-*co*-polyNIPAAm macroprous structures after durability tests in water 214
5.4 Summary 216

Chapter 6 Conclusions and perspectives for future work 217
6.1 Conclusions.....217
6.2 Perspectives for future work 219

Chapter 7 Experimental.....221
7.1 Materials 221
7.2 Synthesis and purification of poly(NIPAAm-*co*-AA) microgel particles 222
7.3 Analytical techniques and characterisation methods 223
7.4 Preparation and characterisation of emulsions, HIPEs and polyHIPEs.....228
7.4.1 Preparation of poly(styrene/DVB) HIPEs using surfactants as the emulsifier.....228
7.4.2 Microgel particles stabilised emulsions using DVB as the oil phase 229
7.4.2.1 Emulsions prepared using microgel suspensions at pH 5 229
7.4.2.2 Emulsions prepared using microgel suspensions at pH 2.5, 3 and 4 230
7.4.2.3 Polymerisation of microgel particles stabilised water-in-DVB HIPEs.....231
7.4.3 Poly(KAA) Pickering-HIPEs prepared from microgels stabilised o/w HIPEs.....233
7.4.3.1 Selecting aqueous suspensions and organic solvents for HIPE preparation..233
7.4.3.2 Selecting crosslinker and initiator for polymerisation of HIPEs containing KAA 234
7.4.3.3 Tuning the morphologies of poly(KAA) Pickering-HIPEs 237
7.4.3.4 Surface area measurements of poly(KAA) Pickering-HIPEs 241
7.4.3.5 Porosity measurements of poly(KAA) Pickering-HIPEs 241
7.4.4 Preparation and characterisation of poly(KAA) Pickering-HIPE composites.....246
7.4.5 Microgel particles stabilised o/w HIPEs containing potassium methacrylate 248
7.4.6 Poly(KAA) HIPEs prepared using dye/drug loaded-microgels as the emulsifiers..... 248
7.4.6.1 Poly(KAA) HIPEs prepared using dye-loaded microgels as the emulsifiers 248
7.4.6.2 Poly(KAA) HIPEs prepared using drug-loaded microgels as the emulsifiers 250
7.4.7 Microgel particles stabilised o/w HIPEs containing dextran and its derivatives..252
7.4.7.1 Synthesis and characterisation of dextran-*co*-polyNIPAAm 252
7.4.7.2 Preparation of microgel particles stabilised o/w HIPEs containing dextran and dextran-*co*-polyNIPAAm.....252
7.4.7.3 Characterisation of macroprous dextran and dextran-*co*-polyNIPAAm 254

References 258

List of Figures

Fig. 1.1 In one major approach to tissue engineering, 3-D highly porous scaffolds composed of synthetic polymers serve as cell transplant devices.[4,5] (Reproduced from ref.[5]) **25**
Fig. 1.2 Origins and locations of bone cells (Reproduced from ref.[12]) **27**
Fig. 1.3 The mesengenic process diagram originated in the late 1980s as a hypothesis based on what was known about mesenchymal progenitors in embryos (Reproduced from ref.[18]) **28**
Fig. 1.4 The four phases of skeletal development. Migration of preskeletal cells to sites of future skeletogenesis is followed by these cells interacting with an epithelium and an epithelial basement membrane. This in turn leads to mesenchymal condensation and subsequent differentiation to chondroblasts or osteoblasts. (Reproduced from ref.[25]) **29**
Fig. 1.5 A scheme of main activities in bone tissue engineering research **32**
Fig. 1.6 A schematic diagram showing macrophagic response to biomaterials. Marcophages respond to small particles (<10 μm) by phagocytosis (I). For large particles, macrophages fuse to form foreign body giant cells (FBGC) to either engulf the particles (II) or remain on the surface of bulk materials (III). (Reproduced from ref.[39]) **33**

Fig. 2.1 Average particle size of **GP1-1** as a function of temperature at pH 2 (0.048 wt %), pH 2.5 (0.10 wt %), pH 3.0 (0.031 wt %) and pH 3.5 (0.035 wt %) in 1 mM KCl solutions. Numbers in the brackets were particle concentrations of the suspensions characterised. **49**
Fig. 2.2 Average particle size of **GP1-1** as a function of temperature at pH 4.0 (0.037 wt %), pH 5.0 (0.073 wt %), pH 6.0 (0.046 wt %) and pH 7.0 (0.047 wt %) in 1 mM KCl solutions. Numbers in the brackets indicate particle concentrations of the suspensions studied. **51**
Fig. 2.3 Average particle size of microgels (**GP1-1**) as a function of temperature measured using microgel suspensions of different KCl concentrations at pH 5. The KCl concentrations were 0.001 M, 0.02 M and 0.2 M, respectively. Minor differences existed in microgel concentration of the three suspensions studied, which were 0.073 wt %, 0.066 wt % and 0.062 wt %, respectively **53**
Fig. 2.4 Average particle size of microgels (**GP1-1**) as a function of temperature and particle concentration, which was varied from 0.020 wt % to 0.10 wt %, 0.20 wt % and 0.40 wt % in microgel suspensions at pH 5 containing 1 mM KCl. **56**
Fig. 2.5 Average particle sizes of **GP1-2** microgels as a function of temperature measured in microgel suspensions (0.2 wt %) of pH 5 in 1mM KCl solution. The microgels were purified using three procedures: **DT60-OH** (alkaline dialysis at 60 °C), **DT60-H** (acidic dialysis at 60 °C) and **DT60-OH-EX** (alkaline dialysis at 60 °C followed by ion exchange). **59**
Fig. 2.6 Average particle sizes of **GP1-3** microgels as a function of temperature measured in microgel suspensions (0.2 wt %) of pH 5 in 1mM KCl solution. The microgels were purified using three procedures: **DT60-OH** (alkaline dialysis at 60 °C), **DT60-H** (acidic dialysis at 60 °C) and **DT60-OH-EX** (alkaline dialysis at 60 °C followed by ion exchange). **60**
Fig. 2.7 Average particle size of **GP1-4** as a function of temperature measured in an microgel suspensions (0.2 wt %) of pH 5 in 1mM KCl solution. **GP1-4** was purified using six different procedures: **D20-OH-EX** (alkaline dialysis at 20 °C using untreated tubing), **DT20-OH-EX** (alkaline dialysis at 20 °C using treated tubing), **DT60-OH** (alkaline dialysis at 60 °C), **DT60-OH-EX** (alkaline dialysis at 60 °C followed by ion exchange), **DT60-H** (acidic dialysis at 60 °C) and **DT60-H-EX** (acidic dialysis at 60 °C followed by ion exchange). **62**
Fig. 2.8 SEM images of St/DVB based polyHIPEs. For preparation, an oil phase consisting of 4 ml styrene, 4 ml DVB, 1 mol % AIBN and 2 ml Hypermer 2296 and an aqueous phase containing 40 ml 0.068 M KCl solution were used. **65**
Fig. 2.9 Photographs of 10 ml microgel aqueous suspension-DVB mixtures of various ratios after emulsified by hand shaking (a) and by homogenizing (b). The volume ratios of DVB (from left to right) are 80%, 60%, 50%, 40% and 20%, respectively in both groups. Arrows indicate the boundaries after phase volumes became stable. **68**
Fig. 2.10 Optical microscope images of the droplets taken from emulsions prepared by homogenizing microgel suspension-DVB mixtures at various DVB ratios after emulsion volumes became stable (Scale bar 100 μm) **69**

Fig. 2.11 Photographs of 10 ml emulsions prepared using 40 vol % DVB and various microgel concentrations in the aqueous suspension: (from left to right) 0.02 wt %, 0.1 wt %, 0.2 wt % and 0.4 wt%. The dash lines indicate the boundaries after creaming. **71**
Fig. 2.12 Optical microscope images of droplets from emulsions prepared using the same DVB ratio of 40 vol % but various microgel concentrations ranging from 0.02 wt % to 0.4 wt % (Scale bar 100 μm). **71**
Fig. 2.13 SEM images of the polymerised products of DVB-in-water emulsions prepared using various DVB ratios and microgel concentrations at pH 5 **73**
Fig. 2.14 Photographs of emulsions prepared at 40 °C (left) and 50 °C (right). The arrows indicate the position of interface immediately after emulsions were transferred into cylinders. **74**
Fig. 2.15 Average particle size of poly(NIPAAm-*co*-AA) microgels as a function of temperature. The measurements were carried out using microgel suspensions (0.4 wt %) in 1 mM KCl solutions of pH 2.5, 3 and 4, respectively. **76**
Fig. 2.16 SEM images of the polymerised product of DVB-in-water emulsions prepared at pH 3 **77**
Fig. 2.17 The creaming volume ratios of microgel-stabilised emulsions as a function of time after aged at 25 °C and 32 °C. (Error of volume: ± 0.1 ml.) Emulsions were prepared using 40 vol % DVB and microgel suspensions (0.4 wt %) in 1 mM KCl solution of pH 2.5, 3 and 4, respectively. **78**
Fig. 2.18 Optical microscope images of emulsions taken at the beginning of aging and after emulsion volumes became stable (scale bar 100 μm). Emulsions were prepared using 40 vol % DVB and microgel suspension (0.4 wt %) in 1 mM KCl of pH 3. The temperatures of emulsions after homogenisation were 22.5 °C for (a)(b) and 21 °C for (c)(d), respectively. **79**
Fig. 2.19 Average particle size of poly(NIPAAm-*co*-AA) microgels as a function of temperature measured using microgel suspensions with 0.4 wt % and 0.8 wt % microgels, respectively. The suspensions were prepared using 1 mM KCl solution as the background and were adjusted to pH 4 prior to measurement. **81**
Fig. 2.20 Optical micrographs of microgel-stabilised emulsions taken after emulsification at 15 °C and during aging at 50 °C. Emulsification was carried out using a microgel (0.4 wt %) suspension in 1 mM KCl solution of pH 4 and 40 vol % DVB. **82**
Fig. 2.21 Optical micrographs of microgel-stabilised emulsions taken after preparation at 37 °C and during aging at 50 °C (scale bar 50 μm). Emulsification was carried out using a microgel (0.4 wt %) suspension in 1 mM KCl solution of pH 4 and 40 vol % DVB **83**

Fig. 3.1 Chemical structures of the monomers, crosslinker and photoinitiator used in the preparation of macroporous hydrogels from microgel-stabilised o/w HIPEs. The monomers are potassium acrylate (KAA) and potassium methacrylate (KMAA); the crosslinker is *N*, *N'*-methylenebisacrylamide (BIS); the photoinitiator is 2-hydroxy-1-[4-(2-hydroxyethoxy) phenyl]-2-methyl-1-propanone (Irgacure2959 or I2959). **98**
Fig. 3.2 Images of aqueous mixtures made up with 1 ml microgel suspension (0.8 wt % in 1 mM KCl solution) and 4 ml KAA solution of various concentrations at 25 °C. The concentration of KAA is gradually decreased from "1-1" (2.05 M) to "1-16" (0.51 M). Microgel particles aggregated and precipitated in mixtures "1-1" to "1-8" (1.33 M) while suspensions from "1-9" (1.23 M) to "1-16" remained stable and transparent. **99**
Fig. 3.3 Images of a series of 5 ml microgel suspensions in KAA solutions at 32 °C. KAA concentration gradually decreased from "1-1" (2.05 M) to "1-16" (0.51 M). From "1-1" to "1-8" (1.33 M), large-sized microgel clusters precipitated out; from "1-9" (1.23 M) to "1-12" (0.92 M), mixtures were turbid; from "1-13" (0.82 M) to "1-16", suspensions were transparent. **101**
Fig. 3.4 Images showing the stability of o/w HIPE prepared using 20 ml toluene and 5 ml microgel suspension in KAA solutions with various KAA concentration: (a) [KAA] = 1.33 M, t = 0; (b) [KAA] = 1.33 M, t = 0.5 h; (c) [KAA] = 1.33 M, t = 2.5 h; (d) [KAA] = 1.12 M, t = 0; (e) [KAA] = 1.12 M, t = 71 h; (f) [KAA] = 1.02 M, t = 69 h; (g) [KAA] = 0.92 M, t = 29 h; (h) [KAA] = 0.82 M, t = 25 h. The microgel content in each HIPE was 8 mg. **102**
Fig. 3.5 Images of microgel-stabilised o/w HIPEs prepared using a two-speed protocol. An aqueous phase containing 0.82 M KAA and 8 mg microgels was used together with 80 vol % oil phase for all. The oil and the 2nd stirring speed in the stirring protocol (400 rpm as the 1st stirring speed during addition) were varied. (a) HIPEs just after preparation, toluene and 1000 rpm; (b) phase separation, toluene and 2000 rpm; (c) HIPEs after creaming (~2.1 ml aqueous phase on the bottom of the tube), hexane and 1000 rpm; (d) HIPEs after creaming, hexane and 2000 rpm; (e) phase separation, hexane, 2000 rpm and microgels with 2 mol % crosslinking degree used in contrast to those with 1 mol % crosslinking degree for the others. **104**
Fig. 3.6 Optical microscope images of emulsion drops taken from microgel-stabilised hexane-in-water HIPEs after creaming occurred. Scale bar 200 μm. 1000 rpm (left) and 2000 rpm (right) were used as the 2nd stirring speed in a two-speed stirring protocol for emulsification, respectively. **105**

Fig. 3.7 Average particle size of poly(NIPAAm-*co*-AA) microgels suspended in KAA solutions (0.82 M) at microgel concentrations of 1.6 mg/ml and 3.2 mg/ml, respectively. **108**
Fig. 3.8 Images of microgel-stabilised o/w HIPEs containing KAA after creaming occurred at RT. The oil phase (80 vol %) was toluene for (a) and (b) in contrast to hexane for (c) and (d). Microgel concentrations in the aqueous suspensions were 1.6 mg/ml, 3.2 mg/ml, 1.6 mg/ml and 4.0 mg/ml, respectively. Air bubbles were present in (d). **108**
Fig. 3.9 Images of microgel-stabilised o/w HIPEs that experienced creaming at different temperatures. (a) and (b) were toluene-in-water HIPEs prepared at RT (~22 ºC) but subjected to creaming tests at RT and 30 ºC, respectively; (c) and (d) were hexane-in-water HIPEs that were prepared and tested at RT and at 31~32 ºC, respectively. **110**
Fig. 3.10 Photographs of samples prepared using 5 ml microgel suspension (1.6 mg/ml) in KAA solutions (0.82 M) and 20 ml toluene but using various stirring protocols for the addition of TMEDA. APS and BIS (10 mol %) were mixed into the aqueous suspension prior to emulsification. (a) Polymerised o/w HIPEs after 60 h at 31 °C, 3.7 ml toluene expelled, TMEDA added at the end of a one-speed stirring protocol (400 rpm); (b) 13.3 ml toluene expelled, TMEDA added during stirring at 1000 rpm in a two-speed stirring protocol (400→1000 rpm); (c) polymerised o/w HIPEs after 52 h at RT and 2 d at 31 °C, 4.3 ml toluene expelled, TMEDA added during stirring at the 3rd speed in a three-speed stirring protocol (400→1000→240 rpm). **113**
Fig. 3.11 Photographs of samples prepared using 5 ml microgel suspension (1.6 mg/ml) in KAA solutions (0.82 M) and 20 ml toluene. APS and DEGDVE (20 mol %) were mixed into the aqueous suspension prior to emulsification. (a) TMEDA added during stirring at 1000 rpm in a two-speed stirring protocol (400→1000 rpm) and ~12 ml toluene expelled after stirring (in the tube on the left); (b) TMEDA added prior to stirring at 1000 rpm in a two-speed stirring protocol (400→1000 rpm) and ~1.3 ml toluene expelled after stirring (in the tube on the left); (c) the sample shown in (b) were not solidified after 3 d at 30 °C. **113**
Fig. 3.12 SEM images of poly(KAA) Pickering-HIPEs prepared by photo-polymerisation of microgel-stabilised o/w HIPEs with a manual rotation protocol during UV exposure. The aqueous phase of the HIPEs contained 0.82 M KAA, 10 mol % BIS, 2 mol % photo-initiator I2959 and 1.6 mg/ml microgels while the oil phase was toluene (80 vol %). After polymerisation, the sample was purified using a two-step Soxhlet extraction with HCl in MeOH solution (0.8 M) and acetone in sequence. **115**
Fig. 3.13 SEM images of poly(KAA) Pickering-HIPEs prepared by UV-initiated free radical polymerisation using a continuous rotation protocol during UV exposure. The o/w HIEPs were emulsified using microgel suspension in KAA solution (1.6 mg/ml microgels, 0.82 M KAA, 10 mol % BIS, 2 mol % I2959), toluene (80 vol %) and a one-speed stirring protocol (400 rpm). A pore and a "potential pore throat" (not open) were marked in the pore structure. **116**
Fig. 3.14 Average particle size of poly(NIPAAm-*co*-AA) microgels in KAA solutions (0.82 M) with and without BIS (10 mol % relative to KAA) and an initiator (I2959 or APS, 2 mol % relative to the total double bonds). **117**
Fig. 3.15 Photographs of photo-polymerised microgel-stabilised HIPEs by using various amounts of I2959. From left to right: the initiator amount was 2.0 mol %, 1.5 mol %, 1.0 mol % and 0.5 mol % (relative to the total double bonds), respectively. The HIPEs were emulsified using 5 ml microgel suspension in KAA solution (1.6 mg/ml microgels, 0.82 M KAA, 10 mol % BIS) and 20 ml toluene. Black lines marked the positions below which gels were formed after photo-polymerisation. **118**
Fig. 3.16 Photographs of the preparation process of poly(KAA) Pickering-HIPEs (a) A sample of microgel-stabilised o/w HIPEs in a glass tube of 25 mm in diameter; (b) HIPEs cured after UV exposure; (c) the gel-like sample was taken out of the tube by cracking the glass with a diamond knife; (d) the sample was taken out of an extraction thimble after experiencing a designed Soxhlet-extraction procedure; (e) dried sample, a polyHIPE. **118**
Fig. 3.17 SEM images of poly(KAA) Pickering-HIPEs prepared using various purification and drying protocols. (a) One-step extraction with HCl in MeOH for 40 h, vacuum drying (one-step); (b) One-step extraction, two-step drying (drying in a convection oven before vacuum drying); (c) Extraction with HCl in MeOH for 40 h followed by extraction with acetone for 24 h (two-step extraction), one-step drying; (d) two-step extraction, two-step drying. The drying temperature is 50 °C for all. **121**
Fig. 3.18 SEM images of poly(KAA) Pickering-HIPEs prepared using various purification and drying protocols. (a) One-step extraction with HCl in MeOH for 40 h, vacuum drying (one-step); (b) One-step extraction, two-step drying (drying in a convection oven before vacuum drying); (c) Extraction with HCl in MeOH for 40 h followed by extraction with acetone for 24 h (two-step extraction), one-step drying; (d) two-step extraction, two-step drying. The drying temperature is 70 °C for all. **122**

Fig. 3.19 SEM images of poly(KAA) Pickering-HIPEs purified using extraction with HCl in MeOH for 72 h plus extraction with acetone for 24 h but dried using either a one-step (a) or a two-step (b) protocol at 70 °C. **123**
Fig. 3.20 SEM images of poly(KAA) Pickering-HIPEs (a) freeze-dried polyHIPE hydrogel, (distilled water/dry polyHIPEs= 200, w/w) (b) polyHIPEs extracted first with a 1:1 (v/v) mixture of HCl in MeOH and distilled water ([HCl]= 0.15 M) for 26 h and then with acetone for 24 h, followed by vacuum drying at 60-70 °C. **124**
Fig. 3.21 SEM images of poly(KAA) Pickering-HIPEs at two magnifications (×50 and ×250). The HIPEs were prepared using a microgel suspension in KAA solution (1.6 mg/ml microgels, 0.82 M KAA, 10 mol % BIS and 2 mol % I2959), 85.0 vol % or 90.0 vol % toluene as the internal phase and a one-speed stirring protocol (400 rpm). **126**
Fig. 3.22 SEM images of poly(KAA) Pickering-HIPEs prepared by polymerisation of HIPEs containing constant $\phi_{int.}$ (80%) and KAA amount (0.82 M) but various BIS contents. During emulsification, a one-speed stirring protocol (400 rpm) was used. **130**
Fig. 3.23 Photographs of poly(KAA) Pickering-HIPEs prepared by polymerisation of HIPEs containing 2.5 mol % BIS. (a) A sample taken out of the glass tube after polymerisation and left in a dry Petri dish; (b) another sample taken out of the glass tube after polymerisation and left in an toluene-wetted Petri dish; (c) the sample shown in (b) after solvent extraction (a piece of filter paper used to wrap the sample prior to extraction) and vacuum drying. **131**
Fig. 3.24 SEM images of poly(KAA) Pickering-HIPEs prepared by polymerisation of HIPEs containing 2.5 mol % BIS. (a) and (b) were from sample that was purified using Soxhlet extraction and dried under vacuum; filter paper was used to wrap the sample during extraction. (c) and (d) were from sample that was freeze-dried after polymerisation; *p*-xylene was used instead of toluene as the internal phase. **132**
Fig. 3.25 SEM images of poly(KAA) Pickering-HIPEs prepared by polymerisation of microgel-stabilised HIPEs containing various KAA concentrations, BIS contents and internal phase volume rations. The magnifications of the images are ×100 (left) and ×250 (right) for each polyHIPEs. **134**
Fig. 3.26 Photographs of polymerised Pickering o/w HIPEs prepared by polymerisation of HIPEs containing 10 mol % BIS. From left to right: stirring speed of 400, 600, 700, 800 and 1000 rpm were used during emulsification, respectively. The transparent part on the bottom, as marked (4 mm in height), was polymerised aqueous solution (containing KAA and BIS) that separated from the bulk emulsions due to creaming. **137**
Fig. 3.27 Photographs of polymerised Pickering o/w HIPEs prepared by polymerisation of HIPEs containing various BIS contents (BIS/KAA, mol/mol). From left to right: a BIS content of 10.0%, 5.0%, 4.0%, 3.2% and 2.5% was employed, respectively. The HIPEs were emulsified using a two-speed stirring protocol (400→1000 rpm). Glass tubes have a diameter of 25 mm. **138**
Fig. 3.28 SEM images of poly(KAA) Pickering-HIPEs prepared by polymerisation of HIPEs that were emulsified using a two speed stirring protocol (400→1000 rpm). The BIS contents in the HIPEs were 10 mol %, 5 mol %, 4 mol %, 3.2 mol % and 2.5 mol %, respectively. **139**
Fig. 3.29 SEM images of poly(KAA) Pickering-HIPEs prepared by polymerisation of HIPEs containing the same crosslinking level (BIS/KAA = 2.5 mol %). During emulsification, a two-speed stirring protocol (400→1000 rpm) was used for (a) in contrast to a one-speed stirring protocol (400 rpm) for (b)(c)(d); Soxhlet extraction and vacuum drying used for (a)(b)(c) in contrast to freeze-drying for (d) after photo-polymerisation; during extraction, filter paper was used for sample wrapping in the case of (a) and (c). **140**
Fig. 3.30 Photographs of poly(KAA) Pickering-HIPEs after solvent extraction and vacuum drying. From left to right: the crosslinking levels (BIS/KAA, mol/mol) used were 10.0%, 4.0% and 2.5%, respectively. **141**
Fig. 3.31 SEM/EDX analysis of poly(KAA) Pickering-HIPEs showing obvious potassium peaks in different parts (left: SEM images; right: the element analysis on the specified parts). For lower-magnification images of the sample, see **Fig. 3.28** (b). **142**
Fig. 3.32 SEM images of poly(KAA) Pickering-HIPEs prepared by polymerisation of HIPEs containing 1.5 wt % microgels and 2.5 mol % BIS. A two-speed stirring protocol (400→1000 rpm) was used during emulsification. **143**
Fig. 3.33 Cryo-SEM micrographs of unextracted polymerised HIPEs under three sublimation conditions (temperature, time): (a) -120 °C, 3 min; (b) -100 °C, 3 min 10 s; (c) -100 °C, 45 min. The HIPEs were prepared using 0.15 wt % microgels, 0.82 M KAA, 2.5 mol % BIS, 2 mol % I2959, 80 vol % toluene and a two-speed stirring protocol (400→1000 rpm). **145**
Fig. 3.34 Cryo-SEM micrographs of poly(KAA) Pickering-HIPEs after a one-step extraction with MeOH (sublimation conditions: -110 ºC, 3 min). The HIPEs were prepared using 0.15 wt % microgels, 0.82 M KAA, 2.5 mol % BIS, 2 mol % I2959, 80 vol % toluene and a two-speed stirring protocol (400→1000 rpm). **147**

Fig. 3.35 SEM images of poly(KAA) Pickering-HIPEs vacuum-dried at 70 ºC after one-step extraction with MeOH. The HIPEs were prepared using 0.15 wt % microgels, 0.82 M KAA, 2.5 mol % BIS, 2 mol % I2959, 80 vol % toluene and the two-speed stirring protocol (400→1000 rpm). **148**
Fig. 3.36 2-D schematics illustrating the proposed formation of pore throats in poly(KAA) Pickering-HIPEs. T, G, M and P stand for toluene, poly(KAA) gel, MeOH and polymer, respectively. **149**
Fig. 3.37 Cryo-SEM micrographs of poly(KAA) Pickering-HIPEs after extraction with acetone (sublimation conditions: -84 ºC, 3 min). The HIPEs were prepared using 0.15 wt % microgels, 0.82 M KAA, 2.5 mol % BIS, 2 mol % I2959, 80 vol % toluene and a two-speed stirring protocol (400→1000 rpm). The polymerised HIPEs were purified using Soxhlet extraction with MeOH and acetone in sequence. **149**
Fig. 3.38 TGA of poly(KAA) Pickering-HIPEs under N_2 atmosphere (heating rate: 10 °C/ min). The tested polyHIPEs were prepared by polymerisation of HIPEs that were emulsified using 0.82 M KAA, 10 mol % BIS, 0.15 wt % microgels and 85 vol % toluene and using a one-speed stirring protocol. **151**
Fig. 3.39 N_2 adsorption-desorption isotherms of poly(KAA) Pickering HIPEs measured after various degassing durations from 4 h to 12 h and 24 h. The polyHIPEs were prepared using 10 mol % BIS and 80 vol % internal phase. **153**
Fig. 3.40 Representative adsorption-desorption isotherms of poly(KAA) Pickering HIPEs that underwent three degas-test cycles. The isotherms of polyHIPEs No.1 (closed porous) and No.5 (open porous) were both showed to move upwards in subsequent tests in comparison to the previous tests. The compositions of these polyHIPEs are listed in **Table 3.6**. **155**
Fig. 3.41 Three cycles of BET surface area tests on poly(KAA) Pickering-HIPEs. The compositions of these polyHIPEs are listed in **Table 3.6**. **156**
Fig. 3.42 Scheme of porosity measurement by a designed indirect method. A polymer block was prepared using identical composition to the continuous phase of HIPEs, whose density was measured by Accupyc1330 and taken as the skeleton density of the polyHIPEs. Foam density of polyHIPEs was determined by measuring the weights and dimensions of cuboids that were cut out of the polyHIPEs. Porosity was then calculated using Equation (7.1). **160**
Fig. 3.43 Photographs showing the production of a polymer block. (a) A piece of gel obtained by photo-polymerising the aqueous solution having identical composition to the continuous phase of HIPEs; (b) after Soxhlet extraction; (c) after drying. **161**
Fig. 3.44 SEM images of poly(KAA) Pickering-HIPEs and its silica composites prepared using the one-speed stirring protocol (400 rpm). The silica amounts used were 0, 1, 5, 10 and 15 wt %, respectively, relative to the total weight of KAA and BIS. **165**
Fig. 3.45 SEM images of poly(KAA)/silica Pickering-HIPE composites prepared using the two-speed stirring protocol (400→1000 rpm). Silica loadings were 1, 5, 10 and 15 wt %, respectively, relative to the total weight of KAA and BIS. **166**
Fig. 3.46 Photographs of poly(KAA)/silica Pickering-HIPE composite during a swelling test using simulated body fluid as the medium. A slice was cut out of the dry sample for the test. **167**
Fig. 3.47 SEM images of poly(KAA)/Bioglass® Pickering-HIPE composites prepared using the two-speed stirring protocol for emulsification. The HIPEs containing 0.15 wt % microgels, 0.85 M KAA, 3.2 mol % BIS, 2 mol % I2959 and 80 vol % toluene for all but containing 2, 5, 10, 15 and 20 wt % Bioglass®, respectively. **170**
Fig. 3.48 TGA of poly(KAA)/Bioglass® Pickering-HIPE composites in N_2 and air (heating rate: 10 °C/ min). **171**
Fig. 3.49 TGA of poly(KAA)/Bioglass® Pickering-HIPE composite ranging from 900 °C to 1000 °C. The composite was prepared using a nominal loading of 10 wt % Bioglass®, relative to the weight sum of KAA and BIS. **172**
Fig. 3.50 TGA of Bioglass® in air using a heating rate of 10 °C/ min **172**
Fig. 3.51 Residual weights of poly(KAA)/Bioglass® Pickering-HIPE composites after TGA tests in air. A procedure consisting of a ramp from RT to 900 °C at 10 °C/min and an isothermal duration of 40 min at 900 °C was used. The weight percentages showing on the horizontal axis were the mixing ratios of Bioglass® to the weight sum of KAA and BIS. The theoretical ratio of Bioglass® was a calculated ratio of Bioglass® in the polyHIPE composite, i.e., the weight of Bioglass® divided by the total weight of Bioglass®, KAA and BIS. **173**
Fig. 3.52 Average particle size of poly(NIPAAm-*co*-AA) microgels in KMAA solution as a function of temperature. Identical to the microgel suspension in KAA solution, the concentrations of microgels and KMAA were 1.6 mg/ml and 0.85 M, respectively. **174**
Fig. 3.53 SEM images of poly(KMAA) Pickering-HIPEs prepared by polymerisation of microgel-stabilised o/w HIPEs containing 15, 5.0 and 3.2 mol % BIS, respectively. **176**

Fig. 4.1 Chemical structures of model active ingredients to be loaded into microgel particles **178**

Fig. 4.2 Photographs of aqueous solutions/suspensions of **S(2)-S(5)** before and after centrifugation at 5000 rpm for 1 h (Sample volumes used for centrifugation were 3ml, 3 ml, 7 ml and 7 ml, respectively.) Briefly, **S(2)** and **S(3)** were dye solutions without and with microgels, respectively; **S(4)** was **S(3)** with KAA; **S(5)** was **S(4)** with BIS and I2959. ..... **180**

Fig. 4.3 Fluorescence spectra of R6G dye solutions without and with microgels. The dye solution tested was prepared by mixing 2.32 ml dye solution (196 μg dye) with 1 ml KCl solution (1 mM), i.e., **S(2)**; the dye solution with microgels was prepared by mixing 1.5 ml **S(2)** with 0.5 ml microgel suspension (8 mg/ml in 1 mM KCl solution). The excited wavelength was 528 nm. **180**

Fig. 4.4 Photographs of emulsions prepared using either un-centrifuged **S(5)** or supernatant of centrifuged **S(5)**: (a) sample prepared using supernatant of centrifuged **S(5)** as the aqueous phase and the two-speed stirring protocol (400→1000 rpm); (b) unpolymerised HIPEs, prepared using un-centrifuged **S(5)** and the one-speed stirring protocol (400 rpm); (c)-1 & (c)-2 photo-polymerised HIPEs (b); (d)-1 & (d)-2, prepared using supernatant of centrifuged **S(5)** and the one-speed stirring protocol. Photograph (d)-2 was taken 4 min after (d)-1. Emulsification was all carried out using 2.5 ml aqueous suspension and 10 ml *p*-xylene. **181**

Fig. 4.5 Photograph of photo-polymerised HIPEs, stabilised with dye-loaded microgel particles. The microgel particles and R6G dye were mixed at a ratio of 8 mg/ 0.39 mg (per 5 ml aqueous phase) in the loading process but the loading percentage was not yet quantified. Subsequently, the polymerised sample was frozen in LN_2 and freeze-dried, leading to poly(KAA) Pickering-HIPEs. **184**

Fig. 4.6 Photograph of *p*-xylene-in-water HIPEs stabilised by dye-loaded microgel particles. The aqueous phase was prepared by mixing a phosphate-buffered solution (10 mM, pH 6.5) of microgel particles and R6G dye (8 mg/0.39 mg per 3.32 ml) with the KAA stock solution (2.54 M, 1.68 ml). The volume ratio of *p*-xylene was 80%. **185**

Fig. 4.7 SEM images of poly(KAA) Pickering-HIPEs prepared by polymerising o/w HIPEs that were stabilised with dye-loaded microgels. The mixing ratio of microgels to R6G dye was 8 mg to 0.19 mg in 5 ml aqueous phase. After polymerisation, solvents were removed via freezing in LN_2 and freeze-drying. **187**

Fig. 4.8 SEM images of poly(KAA) Pickering-HIPEs prepared by polymerising o/w HIPEs that were stabilised with dye-loaded microgels. The mixing ratio of microgels to R6G dye was 8 mg to 0.39 mg in 5 ml aqueous phase. After polymerisation, solvents were removed via freezing in LN_2 and freeze-drying. **188**

Fig. 4.9 Average particle size of unmixed microgels and paracetamol-loaded microgels as a function of temperature measured in solutions containing 0.85 M KAA **190**

Fig. 4.10 Photographs of HIPEs stabilised by paracetamol-loaded microgel particles and their polymerisated products. The microgel particles used had a crosslinking degree of 1 mol %. KAA, BIS and I2959 were mixed into the aqueous suspension prior to emulsification. (a), HIPEs prepared with the one-speed stirring protocol (400 rpm); (b), HIPEs prepared with the two-speed stirring protocol (400→1000 rpm); 1, before polymerisation; 2 and 2', after polymerisation (2' vial on its head showing HIPEs were polymerised); 3, after freeze-dried. **191**

Fig. 4.11 Morphologies of poly(KAA) Pickering HIPEs prepared using paracetamol-loaded microgels with 1 mol % crosslinking degree as emulsifiers and using the one-speed stirring protocol (400 rpm) during emulsification. **192**

Fig. 4.12 Morphologies of poly(KAA) Pickering-HIPEs prepared using paracetamol-loaded microgels with 1 mol % crosslinking degree as emulsifiers and using the two-speed stirring protocol (400 rpm→1000 rpm) during emulsification. **192**

Fig. 4.13 Photographs of HIPEs stabilised by paracetamol-loaded microgel particles and their polymerisated products. The microgel particles used had a crosslinking degree of 2 mol %. KAA, BIS and I2959 were mixed into the aqueous suspension prior to emulsification. (a) HIPEs prepared with the one-speed stirring protocol; (b), HIPEs prepared with the two-speed stirring protocol; 1, before polymerisation; 2 and 2', after polymerisation (2' vial on its head showing HIPEs were polymerised); 3, after freeze-dried. **193**

Fig. 4.14 Morphologies of poly(KAA) Pickering-HIPEs prepared using paracetamol-loaded microgels with 2 mol % crosslinking degree as emulsifiers and using the one-speed stirring protocol (400 rpm) during emulsification. **194**

Fig. 4.15 Morphologies of poly(KAA) Pickering-HIPEs prepared using paracetamol-loaded microgels with 2 mol % crosslinking degree as emulsifiers and using the two-speed stirring protocol (400 rpm→1000 rpm) during emulsification **195**

Fig. 5.1 Particle size dependence of microgels on pH in the aqueous suspension (0.4 wt % in 1 mM KCl) at 22 °C (from left to right: 3.7, 4.7, 5.5, and 6.8; inset: image of dextran-containing HIPEs prepared using microgel suspension with a pH of 6.8.) **199**

Fig. 5.2 Morphologies of solid HIPEs of dextran prepared using microgel suspension of pH 4.7 showing both the macropores (a), (b) and the microstructures on the pore wall (c), (d). **200**
Fig. 5.3 Morphologies of solid HIPEs of dextran prepared using microgel suspension of pH 5.5 showing both the macropores (a), (b) and the microstructures on the pore wall (c), (d). **201**
Fig. 5.4 Morphologies of solid HIPEs of dextran prepared using microgel suspension of pH 6.8 showing both the macropores (a) and the microstructures on the pore wall (b)-(d). **202**
Fig. 5.5 Pore size distributions of solid emulsions/HIPEs of dextran prepared using microgel suspensions with a pH of 4.7, 5.5 and 6.8, respectively. The emulsions/HIPEs containing dextran were frozen by liquid N_2 and then freeze-dried, resulting in solid emulsions/HIPEs. **202**
Fig. 5.6 Average particle size of poly(NIPAAm-*co*-AA) microgels as a function of temperature measured using a microgel suspension (0.4 wt % in 1 mM KCl) of pH 6.8 ..... **203**
Fig. 5.7 Morphologies of solid HIPEs of dextran prepared by using a thermostating step at 45 ºC for 1 h after emulsification but prior to freeze-drying. Circles mark the fusion of pores. **204**
Fig. 5.8 Morphologies of solid HIPEs of dextran prepared by using a thermostating step at 50 ºC for 1 h after emulsification but prior to freeze-drying. Circles mark the fusion of pores. **204**
Fig. 5.9 Morphologies of solid HIPEs of dextran prepared by using a thermostating step at 55 ºC for 1 h after emulsification but prior to freeze-drying. Circles mark the fusion of pores. **204**
Fig. 5.10 Morphologies of solid HIPEs of dextran prepared by using a thermostating step at 60 ºC for 1 h after emulsification but prior to freeze-drying. Circles mark the fusion of pores. **205**
Fig. 5.11 Pore size distribution for solid HIPEs of dextran prepared either by freezing the HIPEs directly after emulsification or by using a thermostating step at 50 ºC for 1 h after emulsification but prior to freezing. **206**
Fig. 5.12 Morphologies of solid HIPEs of dextran prepared using a molecular weight (Mr) of 40, 000 and a polymer concentration (C_p) of 8 w/v %. Arrows mark polymer beads. **207**
Fig. 5.13 Morphologies of solid HIPEs of dextran prepared using a molecular weight (Mr) of 6, 000 and a polymer concentration (C_p) of 20 w/v %. The circle marks pore fusion. **207**
Fig. 5.14 Morphologies of solid HIPEs of dextran prepared using a molecular weight (Mr) of 6, 000 and a polymer concentration (C_p) 8 w/v %. Arrows mark polymer beads. **208**
Fig. 5.15 Pore size distributions for solid HIPEs of dextran prepared using dextran with a molecular weight (Mr) of 40 k and 6 k, respectively, and a polymer concentration (C_p) of 20 w/v % and 8 w/v %, respectively. **209**
Fig. 5.16 Morphologies of dextran-*co*-polyNIPAAm macroporous structures prepared by directly freezing the HIPEs in LN_2 after emulsification and then freeze-drying. **211**
Fig. 5.17 Morphologies of dextran-*co*-polyNIPAAm macroporous structures prepared by thermostating the HIPEs at 38 °C for 30 min prior to the freezing and freeze-drying process. **211**
Fig. 5.18 Pore size distribution for dextran-*co*-polyNIPAAm macroporous structures prepared either by using a thermostating step (38 °C for 30 min) after emulsification but prior to the freezing and freeze-drying step or by freezing the HIPEs in LN_2 directly after emulsification and then freeze-drying. **212**
Fig. 5.19 Partial DSC curves for dextran-*co*-polyNIPAAm macroporous structures prepared either using or without using a thermostating step. The curves were obtained from the 2nd heating cycle at a heating rate of 20 °C/min and the rest of curves ranging from -50 °C to 100 °C were linear lines. **213**
Fig. 5.20 Morphologies of dextran-*co*-polyNIPAAm macroporous structures frozen in LN_2 and freeze-dried after a 14 d durability test in water. The original emulsion-templated macroporous structures transformed into various new structures after freeze-drying. **215**
Fig. 5.21 Morphologies of dextran-*co*-polyNIPAAm macroporous structures frozen in LN_2 and freeze-dried after a 14 d durability test in water. A thermostating step was used when preparing the original emulsion-templated macroporous structures prior to the test. **215**

Fig. 7.1 Synthesis of poly(NIPAAm-*co*-AA) microgel particles **222**
Fig. 7.2 Set-up for cyro-SEM: (A) Preparation chamber (1-Vacuum transfer device (VTD), 2-Pump assembly box, 3-Optical microscope, 4-Liquid N_2 filling port, 5-Sputter coater, 6-Fracture knife, 7-Ball valve assembly); (B) Keypad; (C) Slushing station; (D) Liquid N_2 bucket; (E) SEM chamber. **225**
Fig. 7.3 Schematic process of a cryo-SEM experiment **226**
Fig. 7.4 Apparatus used in emulsion preparation: (a) assembled mechanical stirrer; (b) flask shaker; (c) ultrasonic nozzle; (d) rotor-stator homogenizer. **228**
Fig. 7.5 A modified column in condenser for the addition of microgel suspensions. The apparatus was connected to the neck of the vessel lid. Microgel suspension in the column was warmed up by circulated water in the condenser and added through the needle into the vessel containing DVB. **232**

Fig. 7.6 Set-up for UV-polymerisation of o/w HIPEs. The glass tube containing HIPEs was rotated at a stirring speed of 50~70 rpm during UV exposure. A water bath was used to maintain the sample temperature around room temperature. **236**
Fig. 7.7 Four purification-drying routes for poly(KAA) Pickering-HIPEs (a) One-step extraction and one-step drying; (b) one-step extraction and two-step drying; (c) two-step extraction and one-step drying; (d) two-step extraction and two-step drying. **237**
Fig. 7.8 An established procedure for purification and drying of poly(KAA) Pickering-HIPEs **238**
Fig. 7.9 Assembled device for density measurement using liquid displacement. The device was made up with a plastic syringe (50 ml), a two-way Young's tap, a graduated glass tube (20 ml, ± 0.1 ml), a wire-wrapped metal block, rubber tubings and connectors. **243**
Fig. 7.10 Absorbance of paracetamol in phosphate buffer (peak wavelength at 243 nm) **251**
Fig. 7.11 TGA of macroporous dextran and dextran-*co*-polyNIPAAm and control samples **255**

List of Tables

Table 1.1 Mean values for the mechanical properties of human bone materials **26**
Table 1.2 Origins and functions of bone cells **27**
Table 1.3 Coordination of cellular activities over the human life cycle[11] **30**
Table 1.4 Phases in the normal fracture healing sequence[27] **30**

Table 2.1 List of parameters that were varied in the preparation of gel particles (**GP1**) **48**
Table 2.2 Original pH of the aqueous suspensions of **GP1-4** purified via different procedures **61**
Table 2.3 Size comparisons among different microgel particles in aqueous suspensions **64**
Table 2.4 Physical properties of styrene/DVB based polyHIPEs **66**
Table 2.5 Summary of the emulsions prepared using various DVB ratios **68**
Table 2.6 Summary of the emulsions prepared using various microgel concentrations **72**
Table 2.7 Stability of microgel-stabilised emulsions prepared at various temperatures **74**
Table 2.8 10 ml microgel suspension-DVB mixture emulsified at different temperatures **76**
Table 2.9 Conditions for the emulsification and polymerisation of microgel-stabilised HIPEs **89**

Table 3.1 Compositions of KAA solutions prior to mixing with 1 ml microgel suspensions **99**
Table 3.2 The protocols used in the purification and drying of poly(KAA) Pickering-HIPEs **120**
Table 3.3 Numbers* of "potential pore throats" and pore throats in poly(KAA HIPEs) **135**
Table 3.4 Surface areas of poly(KAA) HIPEs measured after degassing for 4 h at 60 °C **152**
Table 3.5 Surface areas of poly(KAA) HIPEs measured after degassing for 12 h at 60 °C **154**
Table 3.6 Surface areas results of poly(KAA) Pickering-HIPEs obtained in the third tests **154**
Table 3.7 Densities and porosities of polyKAA foams measured from liquid displacement **157**
Table 3.8 Densities and porosities of poly(styrene) HIPEs measured with various methods **158**
Table 3.9 Porosities of poly(KAA) HIPEs measured by MIP and a designed indirect method **160**
Table 3.10 The volume ratios of removed liquids from poly(KAA) Pickering-HIPEs **162**
Table 3.11 Swelling of poly(KAA)/silica Pickering-HIPE composite in SBF at 36 °C **167**

Table 4.1 Particle size measurements on aqueous solutions/suspensions of **S(1)-S(5)** at 22 °C **182**

Table 5.1 A summary of glass transition temperatures (T_g) determined by DSC **214**

Table 7.1 Preparation of emulsions using DVB and microgel aqueous suspension of pH 5 ..... **229**
Table 7.2 Emulsification of DVB and microgel suspension of pH 3 at different temperatures **230**
Table 7.3 Stability study on microgel particles stabilised emulsions containing DVB **231**
Table 7.4 Emulsification of microgel suspension in KAA solutions with various oils **234**
Table 7.5 Polymerisation of microgel-stabilised o/w HIPEs using redox initiation **235**
Table 7.6 Preparation of poly(KAA) Pickering-HIPEs using various t_{UV} and t_{stand} **236**
Table 7.7 Various extraction and drying conditions for poly(KAA) Pickeirng-HIPEs **237**
Table 7.8 Poly(KAA) HIPEs prepared using various compositions and stirring protocols **239**
Table 7.9 Preparation of o/w HIPEs for a nominal internal phase volume ratio of 92.5% **240**
Table 7.10 Conditions for cryo-SEM study on poly(KAA) Pickering-HIPEs **240**
Table 7.11 Surface areas of poly(KAA) HIPEs measured using various degassing durations **241**
Table 7.12 Porosity measurements using hexane as the displacement liquid **242**
Table 7.13 Porosity measurements using *p*-xylene as the displacement liquid **243**
Table 7.14 Porosity measurements of poly(KAA) Pickering-HIPEs using MIP **244**
Table 7.15 Weights and dimensions of cuboid pieces of poly(KAA) Pickering-HIPEs **245**
Table 7.16 Dimensional measurements of polymer blocks in both wet and dry states **246**
Table 7.17 Dimensions of poly(KAA) Pickering-HIPEs in the wet and dry states **246**
Table 7.18 TGA of Bioglass® and poly(KAA)/Bioglass® Pickering-HIPE composites **247**
Table 7.19 Emulsification using dye-loaded microgel particles as the emulsifiers **249**
Table 7.20 Compositions of the aqueous solutions/suspensions used in dye loading study **250**

Table 7.21 Absorbance of drug paracetamol and drug-loaded microgel particles at 243 nm **251**
Table 7.22 Variables in preparation of macroporous dextran and dextran-*co*-polyNIPAAm **253**
Table 7.23 Pore structure analysis of macroporous dextran and dextran-*co*-polyNIPAAm **254**
Table 7.24 Different test procedures used in DSC analysis of macroporous dextran **255**
Table 7.25 Summaries of steps and endothermic peaks observed in DSC **255**

List of Abbreviations

2-D	two-dimensional
3-D	three-dimensional
AA	acrylic acid
AAm	acrylamide
A.I.	active ingredient
AIBN	*α, α'*-azoisobutyronitrile
APS	ammonium persulfate
a.u.	arbitrary unit
BET	Brunauer-Emmett-Teller
BIS	*N, N'*-methylenebisacrylamide
BMP-2	bone morphogenetic protein-2
cm	centimetre
CMC	critical micelle concentration
CNTs	carbon nanotubes
C_p	polymer concentration
cryo-SEM	cryo-scanning electron microscopy
c/w	CO_2-in-water
d	day
DEGDVE	di(ethyleneglycol) divinyl ether
dextran-*co*-polyNIPAAm	copolymers of dextran and poly(*N*-isopropylacrylamide)
D_h	hydrodynamic diameter
DLS	dynamic light scattering
DSC	differential scanning calorimetry
DVB	divinylbenzene
ECM	extracellular matrix
EDX	energy-dispersive X-ray spectroscopy
GP	(micro/nano)gel particles
GPC	gel permeation chromatogrphy
h	hour
HEMA	2-hydroxyethyl methacrylate

HIPEs	high internal phase emulsions
HLB	hydrophilic-lipophilic balance
I2959	Irgacure 2959
iPSC	induced pluripotent stem cells
KAA	potassium acrylate
KCl	potassium chloride
KMAA	potassium methacrylic acid or potassium methacrylate
LCST	lower critical solution temperature
LN_2	liquid nitrogen
logK_{ow}	octanol/water partition coefficient
M	molar or moles per litre
MeOH	methanol
mg	milligram
min	minute
MIP	mercury intrusion porosimetry
mm	millimetre
mol %	molar percentage
mp	melting point
MWCO	molecular weight cut-off
MSCs	mesenchymal stem cells
NaDBS	sodium dodecylbenzene sulfonate
NIPAAm	*N*-isopropylacrylamide
nm	nanometre
NMR	nuclear magnetic resonance
o/o	oil-in-oil
o/w	oil-in-water
PAA	poly(acrylic acid)
poly(DVB)	polydivinylbenzene
pK_a	acid dissociation constant
polyHIPE	polymerised (high internal phase emulsions)
poly(KAA)	poly(potassium acrylate)
poly(KMAA)	poly(potassium methacrylic acid)
polyNIPAAm	poly(*N*-isopropylacrylamide)

poly(NIPAAm-*co*-AA)	poly(*N*-isopropylacrylamide-*co*-acrylic acid)
PPF	poly(propylene fumarate)
PPH	polymerised (Pickering high internal phase emulsions)
ppm	parts per million
PS	polystyrene
R6G	rhodamine 6G
rpm	revolutions per minute
RT	room temperature
s	second
SEM	scanning electron microscopy
St	styrene
T_g	glass transition temperature
TGA	thermal gravimetric analysis
TIPS	thermally induced phase separation
TMEDA	*N, N, N', N'*-tetramethylethylenediamine
UV	ultra violet
UV-vis	ultra violet-visible
VEGF	vascular endothelial growth factor
vol %	percent by volume
VPT	volume phase transition
VPTT	volume phase transition temperature
w/o	water-in-oil
wt %	percent by weight
$\phi_{con.}$	continuous phase volume ratio
$\phi_{int.}$	internal phase volume ratio
γ	interfacial tension
λ_D	the Debye screening length
μm	micrometre
θ	contact angle

Project Aims and Objectives

In my PhD, I aim to prepare three-dimensional (3-D), macroporous, polymeric scaffolds with potential applications in tissue engineering. Our approach employs emulsion templating for scaffold fabrication, in which stimuli-responsive microgel particles are exploited as emulsifiers of high internal phase emulsions (HIPEs). Apart from providing pore structures for ingrowth of cells, the polymeric matrices are also expected to be biocompatible, biodegradable and multifunctional. This general aim is divided into the following parts or steps, each of which has its own objectives and major challenges.

(i) Microgel particles as emulsifiers of HIPEs

Since microgel particles are sensitive to environmental stimuli, such as pH, temperature and salt concentration, it is necessary to determine how the type and stability of microgel-stabilised emulsions is affected by these stimuli. Both water-in-oil (w/o) and oil-in-water (o/w) HIPEs shall be prepared.

(ii) Selection of monomers / macromers / polymers as the building materials of scaffolds

The monomers / macromers / polymers to be selected are expected to be compatible with the emulsion template, resulting in stable HIPEs of either w/o or o/w type. After solidification, they are expected to provide suitable surfaces for cell attachment and a biocompatible environment for cell growth.

(iii) Formation of macroporous scaffolds

The aim is to prepare polymer networks within the continuous phase of HIPEs, using either a chemical or a physical crosslinking method. The chemical approach is to polymerise HIPEs containing monomers and an initiator, leading to polyHIPEs after removal of the internal phase. The polymerisation conditions depend on the nature of the selected monomers and initiator. The physical approach is expected to result in macroporous scaffolds via phase separation of a polymer solution, such as thermally induced phase separation (TIPS). Overall, the primary objective is to produce macroporous scaffolds that can maintain structural stability and integrity during tissue engineering.

(iv) Control over the morphology of macroporous scaffolds

A control over the porous structures is essential in order to meet the requirements for ingrowth of cells into any scaffolds. For example, pore sizes of 100-300 μm[1,2] and high degree of interconnectivity[3] are expected for potential application as bone tissue engineering scaffolds.

(v) Multifunctional scaffolds

Ideally a scaffold should be injectable to minimize invasive surgery but could also benefit from drug delivery functions to enable the scaffolds to supply growth factors or other essential biomolecules for cell growth in a controlled manner.

To address these aims and objectives, the seven chapters of the thesis are organized as follows. **Chapter 1** gives an introduction to bone tissue engineering as well as HIPEs and polyHIPEs. **Chapter 2** firstly discusses the stimuli-responsiveness of microgels and the effects of surfactant source and purification procedures on the particle size of microgels. Following this, there is a discussion of the use of microgel particles as emulsifiers in water-divinylbenzene (DVB) systems aiming to produce w/o HIPE templates from which polyHIPEs can be synthesised. **Chapter 3** focuses on the application of microgel particles in o/w HIPEs containing water-soluble monomers, e.g., potassium acrylate (KAA). It discusses the stability of o/w HIPEs, polymerisation of HIPE templates, control over pore size and pore interconnectivity of the resultant polyHIPEs, densities and porosities, swelling properties and polyHIPE composites. **Chapter 4** presents the idea of polyHIPE scaffolds with drug delivery functionality by using dye/drug-loaded microgels as emulsifiers. **Chapter 5** demonstrates the formation of macroporous scaffolds using a physical crosslinking method for solidification of HIPEs. **Chapter 6** lists the conclusions of the thesis and gives the prospective for future work. **Chapter 7** details the experimental procedures used in the experiments discussed in the thesis.

Chapter 1 Introduction

Tissue loss or organ failure caused by disease or accident is one of the most tragic and costly problems in human health care. The major solutions currently available are either reconstructive or transplantation surgery or the use of mechanical devices to replace or augment the function of the existing organs. However, surgical reconstruction can result in long-term problems while transplantation is currently limited by increasing donor shortages or problems associated with immuosuppression drugs. Finally, a mechanical device cannot perform all the functions of a single organ and thus cannot prevent progressive patient deterioration. Tissue engineering[4,5] is a recently proposed concept that promises novel solutions to tissue damage or loss (**Fig. 1.1**). By combining the developing expertise in engineering, biology, chemistry, materials and medicine,[6] tissue engineering aims to create new tissues by utilising a patient's own cells. Seeding of cells can be done on surfaces but the three-dimensionality of tissue requires a scaffold matrix with three-dimensional (3-D) interconnected porous structures, not only able to mechanically support the growth of cells, but also able to facilitate nutrient supply to and waste removal from cells during their proliferation and differentiation. Therefore, both the biomaterials used as scaffolds and the fabricating methods to create interconnected porous structures are crucial to the final performance of scaffolds and the range of tissues that can be grown and ultimately given to the patient.

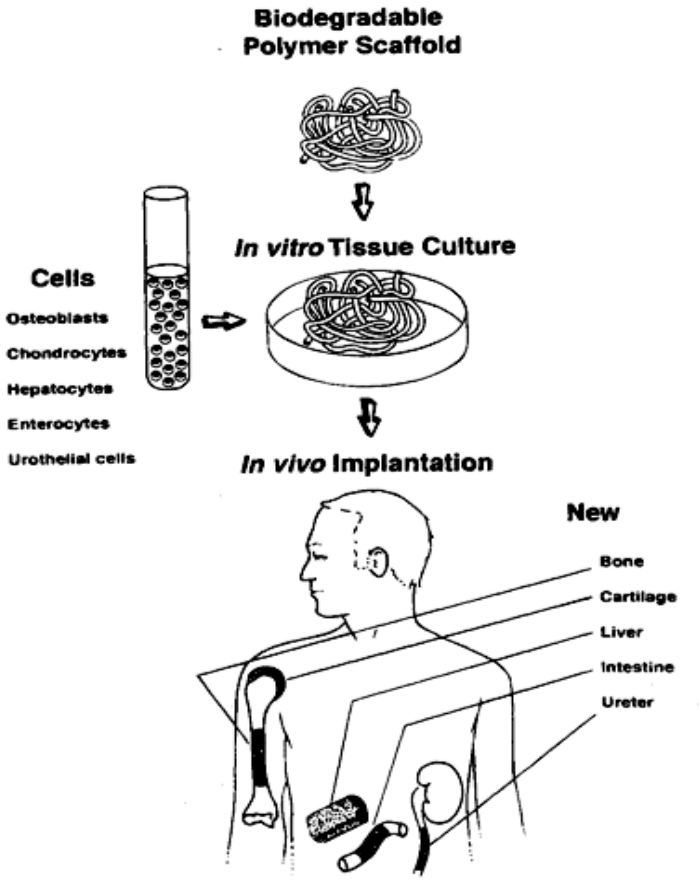


Fig. 1.1 In one major approach to tissue engineering, 3-D highly porous scaffolds composed of synthetic polymers serve as cell transplant devices.[4,5] (Reproduced from ref.[5])

1.1 Bone tissue and Bone tissue engineering

When we consider tissue engineering, several facts should always be kept in mind. Tissue engineering is based on the following observations:[4] (i) every tissue undergoes remodeling; (ii) isolated cells tend to reform the appropriate tissue structure under appropriate experimental conditions; (iii) although isolated cells have the capacity to form the appropriate tissue structure, they do so only to a limited degree when placed as a suspension into a tissue; these cells begin without any intrinsic organization and have no template to guide restructuring; (iv) cells will not survive if they are located more than a few hundred micrometres from the nearest capillary. The challenges[6-8] that lie ahead include finding suitable cells and cell sources, determining the most appropriate biomaterial and developing reliable ways of expanding the cells and growing them in a 3-D environment. The following section will briefly introduce bone-related cells, bone composition and morphology, bone

formation and the healing of fractured bones. Other subjects of importance, including biomaterials, scaffold fabrication methods and bioreactors will also be covered.

1.1.1 Bones and bone cells

1.1.1.1 Composition and mechanical properties of bones

Bone is composed of approximately 70% minerals, 22% protein (organic matrix), and 8% water.[9] 95% of the organic matrix is type I collagen and the remaining 5% are composed of 200 or more non-collagenous proteins,[10] such as proteoglycans. Crystalline salts are mainly calcium and phosphate in the form of hydroxyapatite.[11] In terms of morphology, there are two forms of bone: cortical (compact) bone and cancellous (spongy) bone. Collagen fibrils are densely packed in cortical bone and form concentric lamellae, while cancellous bone has a loosely organized, porous matrix. Cortical bone provides mechanical and protective functions and cancellous bone provides metabolic functions.[11] Different mechanical properties of bone in different loading directions, i.e., anisotropy, are summerised in **Table 1.1**.[9]

Table 1.1 Mean values for the mechanical properties of human bone materials

Type of bone	Direction and type of load	Apparent density (g/cm^3)	Ultimate strength (MPa)	Modulus of elasticity (MPa)
Cortical (midfemur)	Longitudinal tension	1.85	133	17,000
	Longitudinal compression	1.85	193	17,000
	Longitudinal shear	1.85	68	3,000
	Transverse tension	1.85	51	11,500
	Transverse compression	1.85	33	11,500
Trabecular (vertebral body)	Compression	0.31	6	76

As bone tissue engineering requires scaffolds of similar mechanical properties to native bone, the strengths and moduli listed in **Table 1.1** can serve as targets for the scaffolds used for different bone defects of the body.

1.1.1.2 Introduction to native bone cells

There are four types of bone cells in human bone tissue as shown in **Fig. 1.2**:[12] osteoblasts, osteoclasts, and bone lining cells are on the surface while osteocytes exist in the mineralized interior.

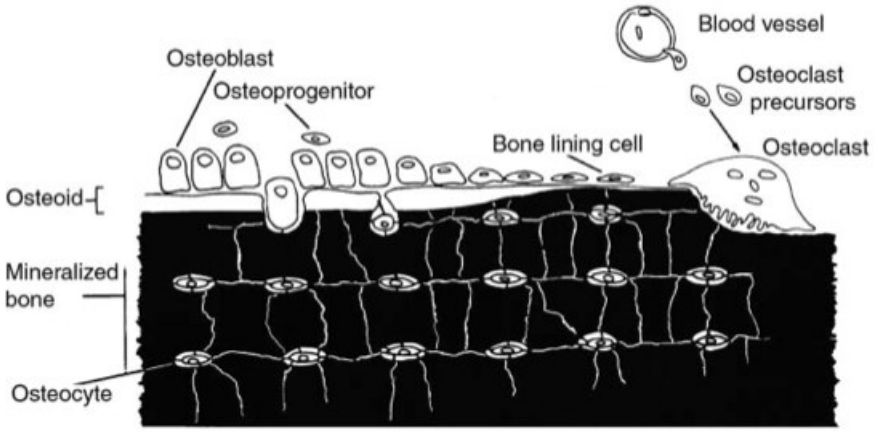


Fig. 1.2 Origins and locations of bone cells (Reproduced from ref.[12])

These four types of cells serve different functions in the human body, and work together to maintain a healthy bone tissue. The origins, and functions of bone cells are shown in **Table 1.2**.[11]

Table 1.2 Origins and functions of bone cells

Cell types	Osteoblasts	Osteocytes	Bone lining cells	Osteoclasts
Originate from	Local osteoprogenitor cells			Fusion of mononuclear precursors
Description	Fully differentiated cells	Mature osteoblasts	Flat, elongated, inactive cells	Large, multinucleated cells
Function	Make bone matrix	Maintain bone, i.e. produce and resorb bone matrix	Receive and deliver signals[13]	Resorb bone

It can be seen from **Table 1.2** that osteoblasts are the major cell type to make up the bone matrix. Currently in bone tissue engineering, osteoblasts are therefore used as the cell type for bone regeneration. However, it is unlikely that only osteoblasts will be sufficient to form a fully developed bone tissue without the addition of other types of bone cells.

1.1.1.3 Adult stem cells for tissue engineering application

Adult mesenchymal stem cells (MSCs) were discovered in bone marrow but have been found to be derivable from many other sources,[14,15] such as umbilical cord blood, adipose tissue, etc. MSCs are investigated for use in tissue repair and regeneration due to two attractive features. First, MSCs can give rise to a series of cell types that will generate specific mesenchymal tissues,[16-18] such as bone, cartilage, muscle, marrow stroma, tendon, fat and other connective tissues (**Fig. 1.3)**. Second, MSCs can secrete bioactive macromolecules that are immunoregulatory and crucial to tissue regeneration.[18,19]

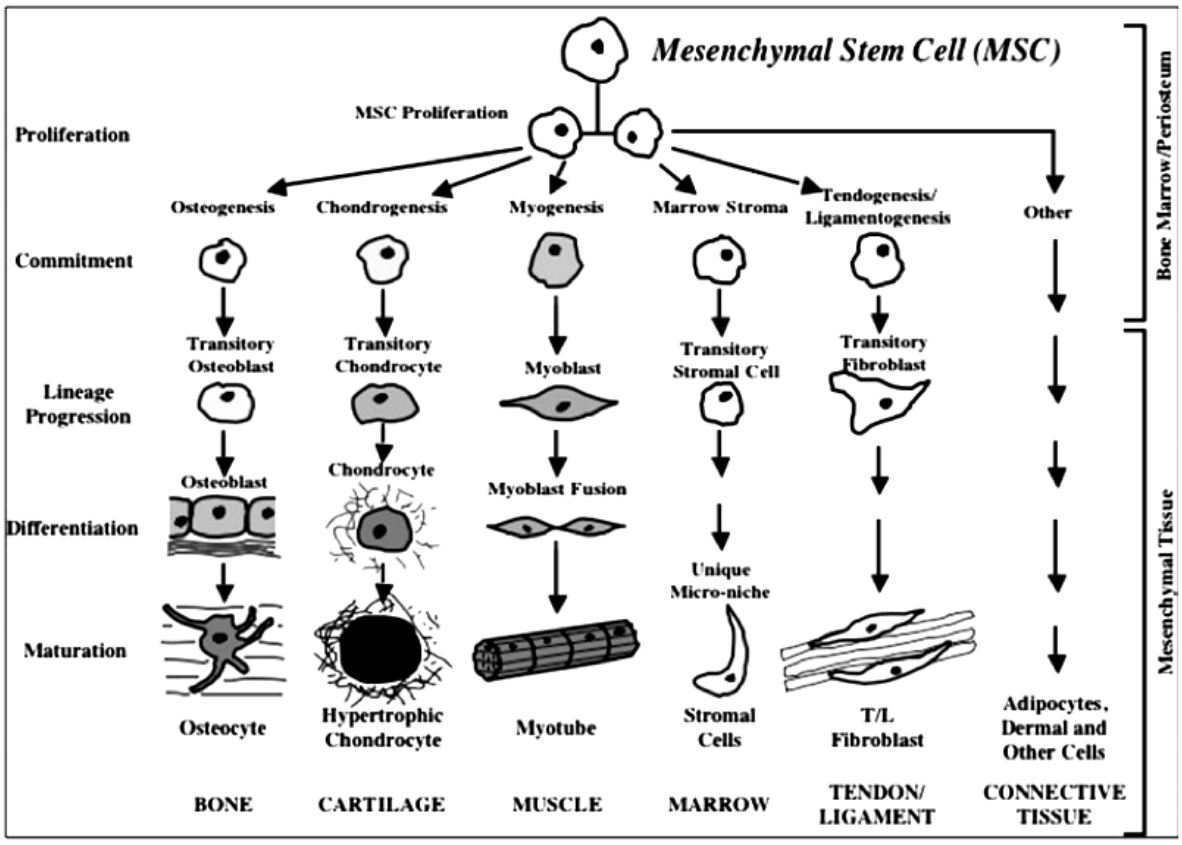


Fig. 1.3 The mesengenic process diagram originated in the late 1980s as a hypothesis based on what was known about mesenchymal progenitors in embryos (Reproduced from ref.[18])

Induced pluripotent stem (iPS) cells are reprogrammed cells that can potentially differentiate into various types of cells. The first reported iPS cells were reprogrammed from mouse fibroblasts[20] and were soon followed by those from human fibroblasts.[21,22] As a newly developed cell species, the application of iPS cells in tissue engineering is under way.[23]

1.1.2 Formation and healing process of bone

1.1.2.1 Formation of bone

Bone formation is realized either through intramembranous ossification (direct) or endochondral ossification (indirect).[11] Both require a solid base and a well-developed vascular supply for the elaboration and mineralization of the extracellular matrix (ECM).[11] Intramembranous ossification occurs during embryonic development by the direct transformation of mesenchymal cells into osteoblasts, which includes four phases[24] as shown in **Fig. 1.4**.[25] The type of ossification for entire bones is restricted to those of the cranial vault, some facial bones and part of the mandible and clavicle.[11] On the other hand, bones that participate in joints and bear weight come into being via endochondral ossification. In this process, the unique properties of cartilage and bone are developed, which provide a mechanism for the formation and growth of the skeleton during the growth of the individual. In these bones, the condensed embryonic mesenchyme transforms into cartilage, and forms the eventual bone at the site.[11]

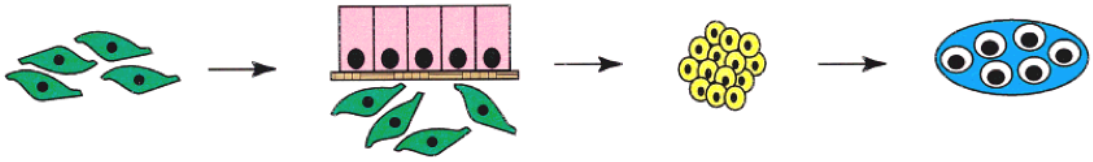


Fig. 1.4 The four phases of skeletal development. Migration of preskeletal cells to sites of future skeletogenesis is followed by these cells interacting with an epithelium and an epithelial basement membrane. This in turn leads to mesenchymal condensation and subsequent differentiation to chondroblasts or osteoblasts. (Reproduced from ref.[25])

Under normal conditions, bone formation (BF) and bone resorption (BR) are coupled to each other,[26] and the long-term maintenance of skeleton is achieved through the intricate action of systemic hormones and local mediators. The coordination of cellular activities over the human life cycle is shown in **Table 1.3**.[11] In general, the principal physiological processes of skeletal formation and maintenance include pattern formation, transition from cartilage to bone, bone matrix synthesis and secretion, and bone resorption and remodeling.[11]

Table 1.3 Coordination of cellular activities over the human life cycle[11]

	Development	**Maintenance**	**Osteoporosis**
Age	0-20	20-50	50+
Sequence	BF→ BR Modeling	BR→ BF Remolding	BR→ BF
Activity	BF>BR	BF=BR	BF<BR

1.1.2.2 Bone fracture healing

The study of fracture healing provides important insight into the mechanisms and courses of bone recovery. A normal fracture healing sequence subdivides into five major stages as shown in **Table 1.4**: induction, inflammation, formation of soft callus, formation of hard callus and remodeling.[27]

Table 1.4 Phases in the normal fracture healing sequence[27]

Phase	**Time**	**Activities**
Induction	0 to 2 days	Hematoma formation; release soluble inductive, growth, and inflammatory factors
Inflammation	2 to 14 days	Polymorphonuclear neutrophils; macrophages
Soft callus	2 to 8 weeks	Highly cellular and collagenous material in fracture gap; chondrogenesis and angiogenesis
Hard callus	2 to 12 months	Woven bone forms; considered healed at this stage
Remodeling	1 or more years	Lamellar bone forms

Table 1.4 provides a timetable of bone healing, which is helpful in planning the procedures of implantation surgery, such as the implantation time and the biopsy-taken time. Also, for bone tissue engineering, when biodegradable polymers are used as the scaffolds, the recovery cycle of bone could be useful in scaffold design. For example, the degradation rate and life cycle of the scaffolds are directly related to the healing process.

1.1.2.3 Current treatment of bone defects

Currently, bone grafting and bone-graft substitutes are widely applied in the treatment of bone defects.[28] Bone graft can be divided into autograft, allograft and xenograft according to the source of bone donor.[27,29]

Autografting involves harvesting a bone from a healthy part of a patient and implanting it to the defect site of his own body. The method provides a distinct possibility of healing the defect site but at the same time it can cause donor site pain, morbidity, potential infection and extra blood loss. Importantly, when the defect site volume is large enough, or if the patients are geriatric or pediatric, autografting is not an advisable method. As an alternative, allografting uses human cadaver bone instead. Compared to autografting, allografting has a more frequent failure besides possible immune rejection from the host body and potential disease transmission. In some rather special cases where both autografting and allografting are not feasible, xenografting may be used. This involves the use of animal bones and carries a high risk of immunogenicity and disease transmission.

On the other hand, there are a number of materials under review as bone-graft substitutes, such as metals, ceramics, composites, bone derivatives and polymers.[28,29] Although titanium is used for bone reconstruction due to its biocompatibility, resistance to corrosion and high strength,[30] metals generally cannot provide all the functions of a bone tissue and have poor overall integration with the tissues at the implantation site.[28] Ceramics are widely used as bone-graft substitutes,[31] although the brittleness may limit their application in load-bearing locations. Meanwhile, ceramics are also being investigated as scaffold candidates in the field of bone tissue engineering. Since 3-D porous ceramics are preferred in both bone grafts and bone tissue engineering, the boundary of the two is not so clearly distinguished.

1.1.3 Bone tissue engineering

1.1.3.1 Current research in bone tissue engineering

Nowadays, a great number of investigations are being conducted worldwide to improve the treatment of bone defects. Fundamentally, there are studies on solving the problems in current implantation with metals or ceramics as mentioned above. However, methods that start with cells – including bone tissue engineering,[28,32] gene therapy strategies[33-35] and the combination of tissue engineering and gene therapy[36] – represent novel and promising routes

in the treatment of bone defects. The following section will give a general introduction to the current research in bone tissue engineering. A summary of the main research directions is shown in **Fig. 1.5**.

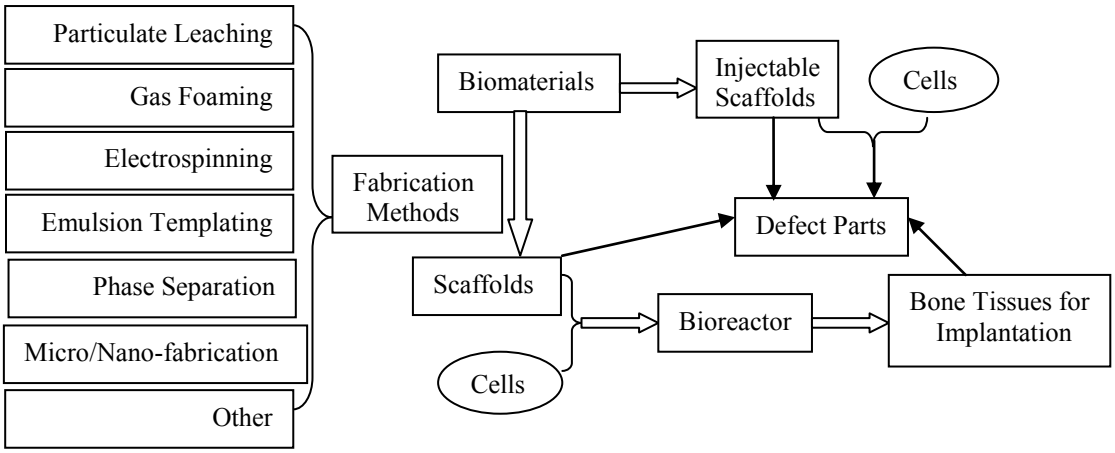


Fig. 1.5 A scheme of main activities in bone tissue engineering research

1.1.3.2 Biomaterials for bone tissue engineering

Biomaterials have been experiencing rapid development in the past few decades.[37,38] One of the most important driving forces is the investigation of cell-biomaterial interactions, which has led to extensive research of biomaterials for tissue engineering and regenerative medicine. When used as tissue engineering scaffolds, biomaterials need to be biocompatible. This means that they should be engineered in such a way that will elicit minimal immune responses. Macrophages, as members of the host immune system, play an important role in clearing the effete host cells and molecules as well as in defending against foreign invasion.[39] They can actively respond to biomaterial implants in a size-dependent manner (**Fig. 1.6**).[39] It is important to note that the meaning of biocompatibility for a tissue engineering scaffold may differ from that for an implantable medical device,[40] because tissue engineering scaffolds are expected to support cellular activity rather than simply avoid undesired host responses.

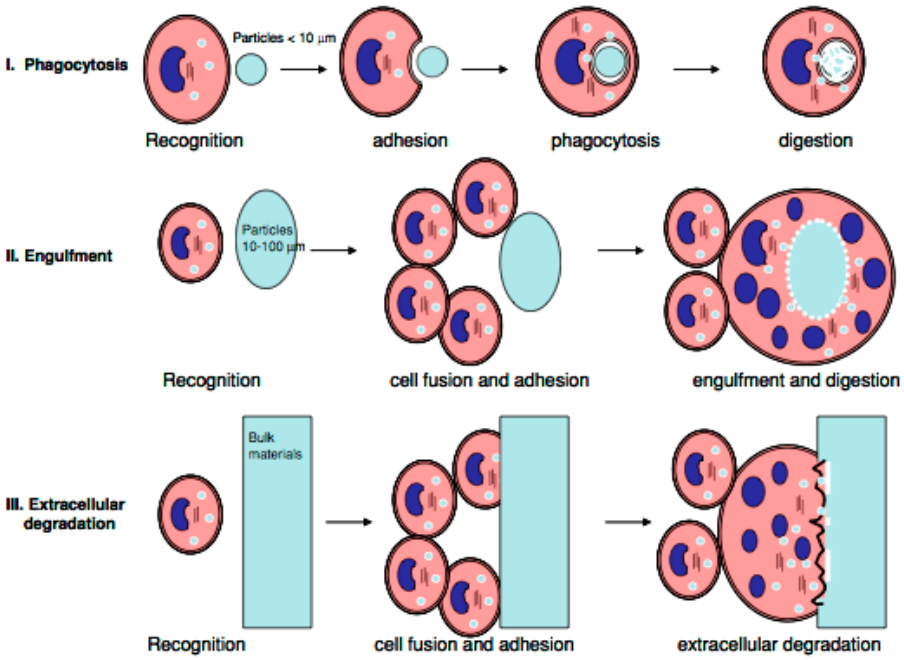


Fig. 1.6 A schematic diagram showing macrophagic response to biomaterials. Marcophages respond to small particles (<10 μm) by phagocytosis (I). For large particles, macrophages fuse to form foreign body giant cells (FBGC) to either engulf the particles (II) or remain on the surface of bulk materials (III). (Reproduced from ref.[39])

The biomaterials investigated for bone tissue engineering include inorganic materials, polymers and composites.[31,41] Inorganic materials of a similar composition to the mineral phase of bone (calcium phosphates, hydroxyapatite (HA), bioactive glasses, glass-ceramics, etc) are widely investigated for bone tissue engineering.[42] Natural and synthetic polymers are also candidates for bone tissue applications,[31] such as type I collagen, hyaluronic acid, chitosan, polyanhydrides, poly(propylene fumarate) (PPF), poly(ε-caprolactone) (PCL), polyphosphazenes, poly(lactic acid) (PLA), poly(glycolic acid) (PGA), and poly(lactide-*co*-glycolide) (PLGA). Since biodegradability is expected from polymer scaffolds, the use of non-biodegradable polymers is restricted to those modifiable to ensure their elimination from the body.[43] Composites are also frequently used in bone tissue engineering to mimic the composite structure of bone and to obtain optimal properties. A variety of polymer-ceramic composites,[42,44] either polymer-based or ceramic-based have been investigated. In addition to ceramics, trials have also been made using other inorganic components in the composites, such as carbon nanotubes (CNTs).[45,46]

1.1.3.3 Scaffold fabrication

Scaffold fabrication is the process of turning biomaterials into environments appropriate for cell growth. Alongside the physical properties of biomaterials (**Section 1.1.3.2**), it has also been experimentally found that the nature of a 3-D scaffold also plays a significant role in cell survival and growth. The relevant variables include porosity,[47] average pore size,[47,48] pore interconnectivity,[48] surface characteristics,[49,50] and mechanical properties.[51,52] However, there is hardly a quick answer to the question of optimal values for these properties for bone tissue engineering due to the complexity of bone formation, especially when starting from cells and an artificial scaffold. Studies have been extensively carried out to minimize the gap in our understanding of the formation process. A number of biological indices are used to evaluate the scaffold parameters, such as cellular attachment, intracellular signaling, cellular penetration, osteoblast proliferation, the extent of mineralization, bone ingrowth, vascularization, etc. Generally, scaffolds need to be porous[53] for bone regeneration but can be high or low in porosity.[47] A pore size of more than 100 μm was found essential for mineralized bone ingrowth into ceramic scaffolds.[1] Meanwhile, the required pore size is not expected to be the same as the largest size possible. Ishaug *et al.* reported that cell proliferation was not affected by increasing the pore size of PLGA scaffolds above 150-300 μm.[54] This is echoed by a recent study which revealed that PCL scaffolds of pore sizes between 350 μm and 800 μm had limited effect on bone regeneration.[55] Moreover, a balance between pore size and mechanical properties needs to be considered since an increase in pore size and porosity does lead to an reduction in the mechanical strength of scaffolds.[47] Pore interconnectivity within scaffolds is clearly necessary in order for cell penetration and vascularization to be able to take place.[48]

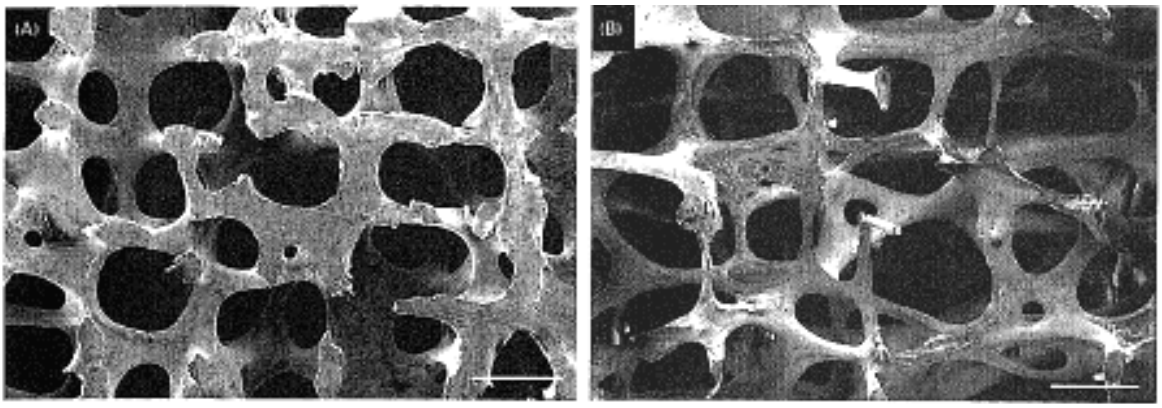


Fig. 1.7 Scanning electron micrographs of vertical sections through the bodies of the third lumber vertebrae (after removal of bone cells and soft tissues) of a normal 30-year old woman (A) and a 71-year-old woman (B), respectively. For the older woman severe osteoporotic changes are evident; the trabeculae are eroded to thin mechanically-insufficient rods. Scale bars 500 μm. (Reproduced from ref.[56])

Since artificial scaffold fabrication aims to create an environment for cell growth, it is sensible to learn from nature. **Fig. 1.7** shows examples of decellularized bone matrices (third lumber vertebrae) from a normal 30 year-old woman and a 71 year-old woman with severe osteoporosis.[56] The healthy matrix has interconnected pores of a few hundred microns in diameter, indicating the validity of experimental results on pore architectures. Currently, a variety of scaffold fabrication methods are under investigation and development (**Fig. 1.5**), such as particulate leaching,[57-60] gas foaming,[61] electro-spinning,[62-65] phase separation,[66] solid freeform fabrication (SFF)[67], emulsion templating[68] and micro/nano-fabrication.[69-73] Of these methods, emulsion templating is a relatively new approach for scaffold fabrication. It is mainly based on high internal phase emulsions (HIPEs) and is detailed in **Section 1.2**. The relative advantages and disadvantages of these methods have been summarized in a few reviews.[74-76] Another lesson learned from nature is that scaffolds with drug delivery capability[77] are crucial for cell survival and growth prior to the production of a fully functional ECM by seeded cells. For example, delivery of bone morphogenetic protein-2 (BMP-2) and vascular endothelial growth factor (VEGF) is frequently investigated in bone tissue engineering.[78-81] **Fig. 1.8** shows the effect of BMP-2 and VEGF delivered from gelatin particles within porous PPF scaffolds on bone regeneration in a rat cranial critical size defect. It was found that bone formation at 4 weeks was significantly higher for the dual release group than all other groups.[78]

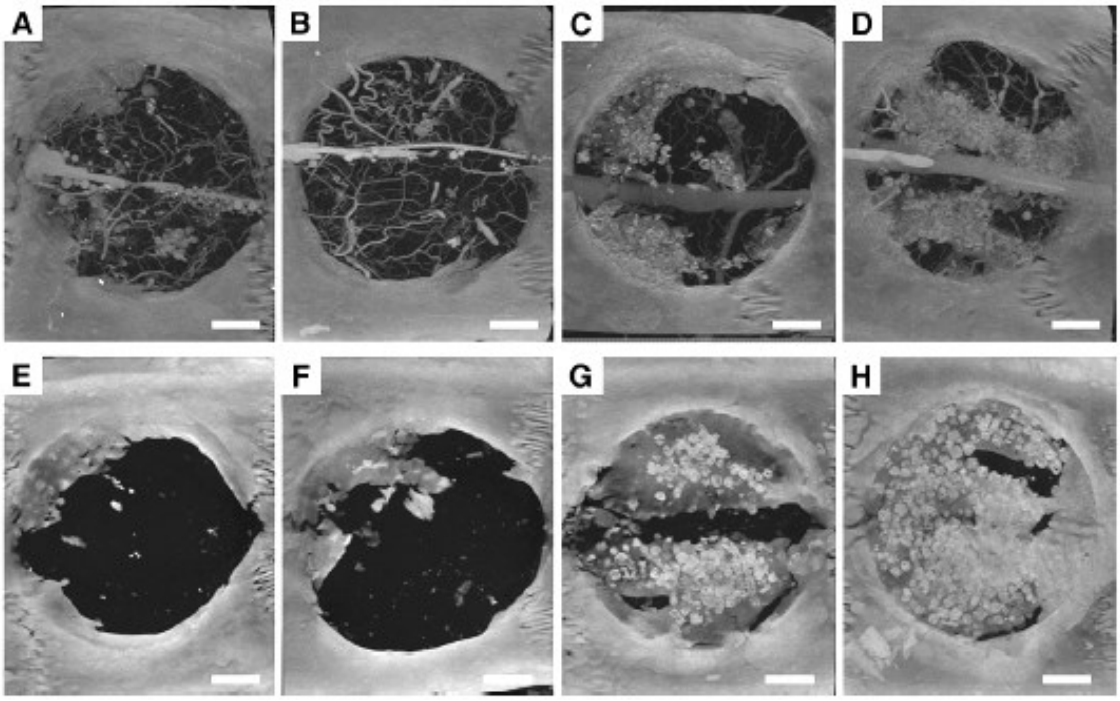


Fig. 1.8 MicroCT images (maximum intensity projections) of cranial defects at 4 and 12 weeks. Panels A-D represent BLANK, VEGF, BMP-2, and DUAL groups at 4 weeks prior to decalcification; both blood vessels and bone were visible. Panels E-H represent BLANK, VEGF, BMP-2, and DUAL groups at 12 weeks; no blood vessels were visible because Microfil perfusion was not done at this time period. Bar represents 200 μm for all panels. (Reproduced from ref.[78])

1.1.3.4 Bioreactor for in-vitro tissue cultivation

Tissue engineering scaffolds can be either injected[82,83] or implanted into defect sites (**Fig. 1.5**). However, implantation after in-vitro tissue cultivation may become the only option for large defects or whole organ replacement. The concept of a bioreactor is to provide an environment that can mimic the physiological conditions for in-vitro tissue cultivation.[84] Thus, bioreactor design is supposed to be tissue-specific.[85] Ideally, all the parameters for tissue growth, such as temperature, pH, biochemical gradients and mechanical stresses, should be continuously controlled during the period of cultivation. For bone tissue engineering, a variety of bioreactors have been investigated or commercialized in order to prepare functional bone grafts.[86,87] Bioreactor types include spinner flask bioreactors, rotating bioreactor systems and perfusion bioreactors. An example of a perfusion bioreactor is shown in **Fig. 1.9**, which was used to study the effect of hydrodynamic perfusion and mechanical stimulation on cell proliferation and differentiation.[88] Despite the advance in bioreactors, more efforts still need to be made prior to the clinical application of engineered bone grafts.[87]

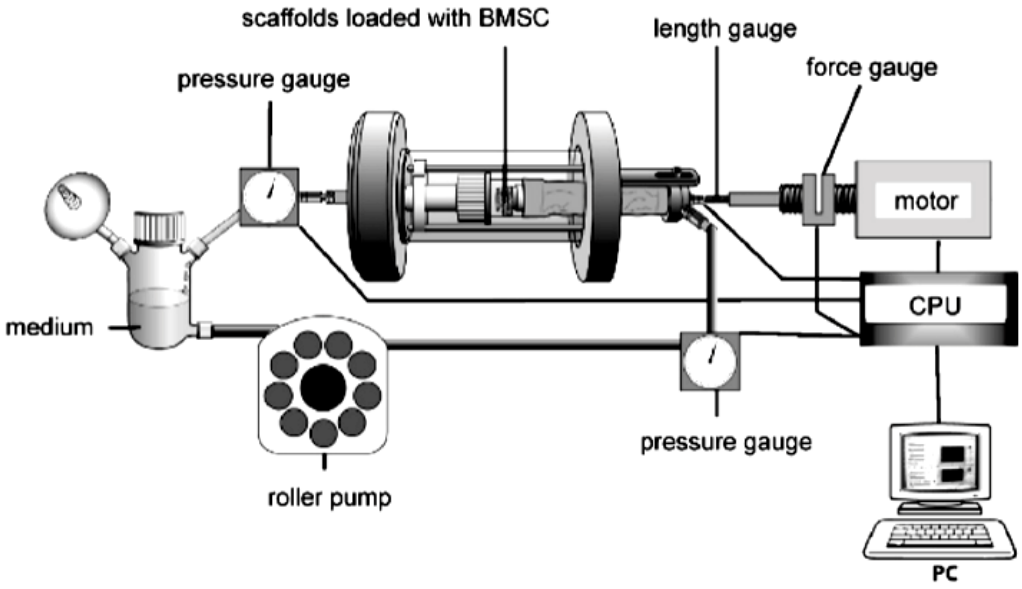


Fig. 1.9 Perfusion-mechano-bioreactor used for the stimulation of 3-D scaffolds seeded with BMSCs (Reproduced from ref.[88], BMSCs stand for bone marrow stromal cells.)

1.2 HIPEs and polyHIPEs

It was already mentioned in **Section 1.1.3.3** that emulsion templating can be used to prepare scaffolds for tissue engineering. A detailed introduction to the method is given in this section. Emulsions are produced from two liquid phases that are either insoluble or only slightly miscible. When emulsions are used as templates for preparation of porous materials, two steps are usually involved: solidification of the continuous phase and removal of the dispersed (droplet) phase. Emulsion templating is widely applied to both inorganic and organic materials,[89] although different gelation and drying methods will be used. For example, sol-gel chemistry is employed for the gelation of inorganic materials,[90] whereas polymerisation of monomers[91] or emulsion freeze-drying[92] is used for organic materials (polymers). The emulsion freeze-drying technique as reported typically uses a w/o emulsion prepared from water and an organic solution of polymer and solidifies the template by quenching in liquid nitrogen (LN_2) and freeze-drying. However, the technique is apparently extendable to those applying an emulsifier[93] and to o/w emulsions containing a hydrophilic polymer.

Polymerising monomers in order to solidify the continuous phase is an increasingly popular method of preparing porous polymers, especially when the internal (droplet) phase volume ratio (ϕ) is above 74%. This volume ratio represents the close packing limit of

uniform, non-deformable spheres, thus emulsions with $\phi \geq 74\%$ must have either droplets of a polydisperse size or droplets that are non-spherical. These emulsions are referred to as high internal phase emulsions (HIPEs) while the highly porous polymers that result from polymerisation of the continuous phase are called as polyHIPEs.

1.2.1 Versatility of HIPEs and polyHIPEs

Initially, polyHIPEs were prepared mainly from w/o HIPEs via free-radical polymerisation of hydrophobic monomers, typically styrene/divinylbenzene (St/DVB). However, in the last two decades, polyHIPEs underwent tremendous development and are now regarded as an extremely versatile means of preparing porous polymers. Firstly, HIPEs are no longer limited to a w/o system; it is now possible to prepare HIPEs from o/w (see **Section 3.2**), CO_2-in-water (c/w),[94] oil-in-oil (o/o),[95,96] oil-in-alcohol[97] and ionic liquid-in-oil,[98,99] and ionic liquid-in-water[100] systems. Secondly, the emulsifiers of HIPEs are not exclusively low molecular weight surfactants, but can also be polymeric surfactants,[95,101,102] a variety of particles (see **Section 1.2.1.2**) and a combination of surfactant and particle.[103-106] Thirdly, the polymer chemistry employed for polyHIPE synthesis has been significantly diversified. Besides radical chain-growth polymerisation as frequently used, step-growth polymerization has also been realized within HIPE template, e.g., hydrosilylation,[107] isocyanate-hydroxyl,[108] thiol-ene[109-111] and thiol-yne[109] reactions. Moreover, for chain growth polymerisation, ring-opening metathesis polymerization (ROMP)[112-116] and controlled/living radical polymerisations including atom transfer radical polymerisation (ATRP)[117-121] and reversible addition-fragmentation chain transfer (RAFT) polymerization[122] have also been reported for systhesis or functionalization of polyHIPEs. Due to these advances, polyHIPEs can now be prepared from an enormous family of monomers[91,123,124] and are being exploited for various applications[91,125,126] as recently reviewed. The aim here is not to give a comprehensive introduction to polyHIPEs. Instead, the focus is on work concerning the tuning of pore architectures and mechanical properties of polyHIPEs particularly in conventional polyHIPEs. This will be followed by a brief summary of novel polyHIPEs prepared using particles as emulsifiers.

1.2.1.1 Tunability of pore architectures and mechanical properties of polyHIPEs

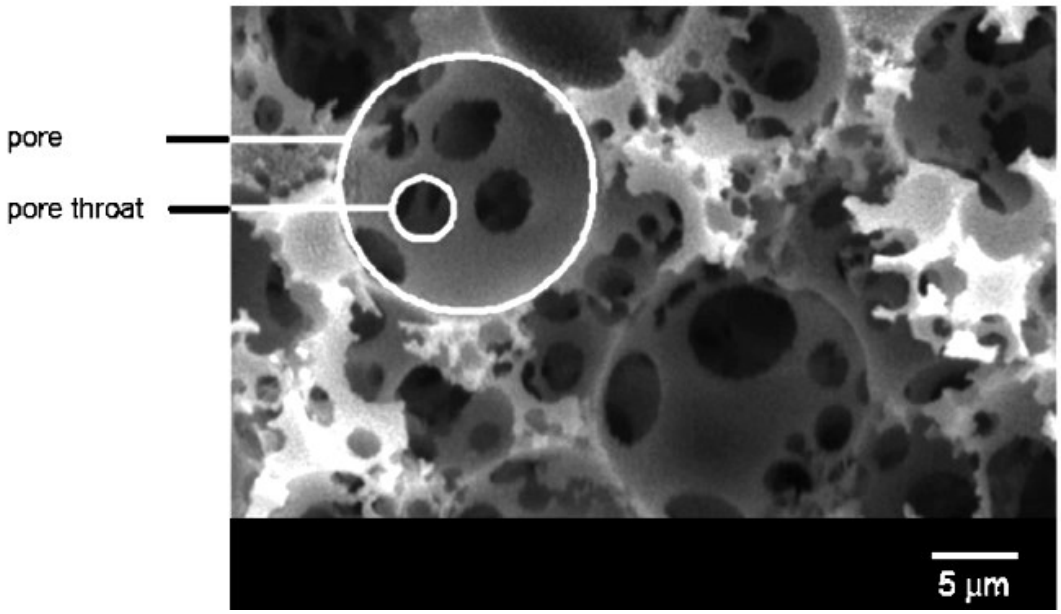


Fig. 1.10 Definition of pores and pore throats of polyHIPEs (Reproduced from ref.[127])

Fig. 1.10 shows the morphology of a typical crosslinked polystyrene (PS) polyHIPE, which consist of pores of 9-19 µm and pore throats of 2-7 µm.[127] In the literature, pores are also referred to as cells or voids while pore throats can be referred to as windows or interconnects. Since the pores of polyHIPEs originate from the emulsion droplets, their size variation is closely related to the HIPE stability. Measures that can enhance the HIPE stability, such as increasing the surfactant concentration or adding an electrolyte,[128] will reduce the average pore sizes of polyHIPEs. Those that can decrease the HIPE stability, such as increasing temperature[129-131] or adding organic additives,[130-133] will increase the pore sizes. The destabilization mechanisms involve promotion of coalescence, increase of Ostwald ripening[134,135] or removal of surfactant molecules from the interface. On the other hand, the formation of pore throats is closely related to the thin layers between two droplets. For example, PS polyHIPEs that were prepared using 5 wt % surfactant, relatively to the monomer phase, remained closed-pore even at an internal phase volume ratio of 97%. However, an increase in the surfactant concentration led to open porous structures.[136] Since the preparation of polyHIPEs involves emulsification, polymerisation, purification and drying, the actual mechanism for the formation of pore throats is not straightforward. The proposed mechanisms include shrinkage during polymerisation,[137] surfactant removal during polymerisation,[138] and mechanical actions during drying.[127]

The mechanical properties of polyHIPEs are mostly rather poor. For example, PS polyHIPEs prepared from HIPEs of 20 vol % continuous phase exhibited a Young's modulus of 5 ± 1 MPa and a crush strength of 0.3 ± 0.1 MPa.[139] A few approaches have been adopted to improve their mechanical properties. Firstly, a reduction of the internal phase volume ratio can effectively enhance the mechanical properties,[139,140] although the porosity of polyHIPEs is also decreased. Secondly, the crosslinker is of importance for the mechanical properties of polyHIPEs. The use of a long-chained crosslinker, such as polyethylene glycol dimethacrylate (PEGDMA) instead of DVB resulted in foams of reduced brittleness and chalkiness.[139] Another example is the use of vinyl silsesquioxane (VSQ) as the crosslinker and reinforcing agent for poly(2-ethylhexyl acrylate) (polyEHA) polyHIPE materials. It was found that room temperature modulus and stress at 40% strain increased in a linear fashion with increasing VSQ content.[141] Thirdly, the mechanical properties of polyHIPEs can also be improved by preparing polyHIPE composites. For example, when 1 wt % silica particles were used, the Young's modulus of PS polyHIPEs was improved by 280% without varying the pore structures.[142] Other fillers have also been investigated for polyHIPE reinforcement, such as carbon black,[143] clay,[144] titania (TiO_2) nanoparticles,[145] TiO_2 nanorods[145] and carbon nanotubes.[145]

1.2.1.2 Poly(Pickering HIPEs) as novel polyHIPEs

Besides surfactants, particles are important emulsifiers. Particle stabilised emulsions are also known as Pickering (or Ramsden) emulsions due to the pioneering work by Pickering and Ramsden at the beginning of the last century.[146,147] The similarities and differences between surfactant stabilised emulsions and Pickering emulsions have been intensely studied.[148,149] To characterise the emulsifying ability, the wettability of particles is used – this can be regarded as the counterpart of the hydrophilic-lipophilic balance (HLB) number used to describe non-ionic surfactants. The phase that wets particles better tends to form the continuous phase. The contact angle (**Fig. 1.11**) is usually employed to describe the position of particles at the interface and the energy of attachment for a spherical particle at the oil-water interface can be expressed by Equation (1.1):[148,150]

$$E = \pi R^2 \gamma_{ow} (1 \pm \cos\theta)^2 \qquad (1.1)$$

where R is the particle radius, γ_{ow} is the oil-water interfacial tension and θ is the contact angle formed between the oil-water interface and the surface of the solid particle. The sign within the bracket is positive for removal of the particle into the oil and negative for removal into the water phase. It is clearly shown that particles of intermediate hydrophobicity (contact angles close to 90° from either side) have a very high energy of attachment at the interface. This can explain why Pickering emulsions normally display higher stability to coalescence than those stabilised by surfactants. Nevertheless, it is obvious that particle detachment can become significant for very small particles (< 1 nm radius) and unstable emulsions will be produced in these cases. The wettability of particles can be tuned via coating or by using *in situ* measures such as pH variation and salt or surfactant addition.[149] Along with wettability, other factors can also play a role in determining the type and stability of Pickering emulsions. The factors include phase volume ratio, particle location, oil type, particle size, particle shape and particle concentration.[149,151] The proposed stabilisation mechanisms of Pickering emulsions include particle bilayer stabilisation, stabilisation by a "bridging" particle monolayer, the formation of a two-dimenional (2-D) network of aggregated particles on the droplet surface or the formation of a 3-D network of particles between droplets.[151] The particles used for emulsion stabilisation can be either inorganic[152] or organic. Due to their tunablity in size, structure, hydrophobicity and even degradability, organic particles have received growing interest as Pickering emulsifiers. Typical examples are PS latexes with various particle sizes and surface functionalities[153-159] while microgel particles and particles of natural origin are attracting increasing attention. In contrast to latex particles, microgel particles are swollen particles and have the potential to encapsulate and release active ingredients (see **Section 2.2**). Interestingly, some synthetic particles can undergo a latex-microgel transition upon pH change but the microgel state of these particles was usually used for demulsification.[160,161] Particles of natural origin with or without modification as stabilisers of emulsions and HIPEs include ferritin,[162-164] bovine serum albumin (BSA),[165] geltatin,[166] soy protein,[167,168] fat crystals,[169,170] cellulose,[171-176] chitosan,[177,178] lignin,[179-181] starch[182-184] and chitin.[185,186] These natural polymer particles together with PLGA particles[187,188] can offer biocompatibility and biodegradability for food or biomedical applications. In general, Pickering emulsions can find applications in the industries of cosmetics, food and petroleum as well in the fields ranging from drug delivery, polymer blends to preparation of porous materials.[189]

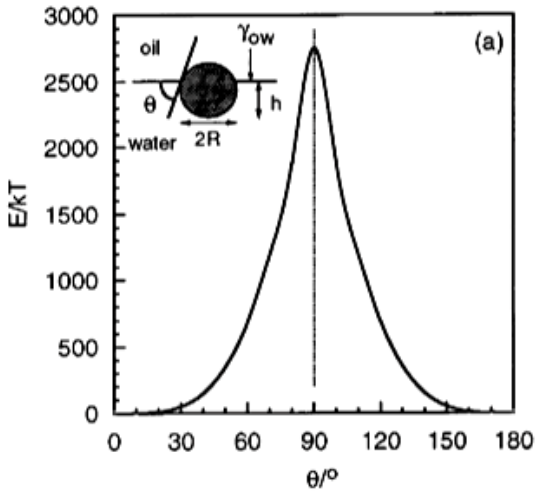


Fig. 1.11 Variation of the energy of attachment, E (relative to kT), of a spherical particle (R = 1×10^{-8} m) at a planner oil-water interface (γ_{ow} = 0.036 N.m^{-1}) as a function of contact angle θ (measured through the water phase) at 298 K. (Reproduced from ref.[150].)

The preparation of polyHIPEs from a Pickering HIPE template, i.e. poly(Pickering HIPEs) (PPH) was first reported in 2007.[190,191] Colver *et al.* obtained PPHs from a Pickering template stabilised by DVB-crosslinked poly(methyl methacrylate) (PMMA) particles.[190] In the same year, Menner *et al.* reported porous polymer foams from Pickering emulsions using multiwalled carbon nanotubes (CNTs) as the stabiliser and an internal phase of 60 vol % (i.e. not a HIPE)[192] as well as functionalized titania nanoparticles as the stabiliser and an internal phase volume ratio up to 80%.[191] In the following years, many other particles were investigated as the stabilisers of Pickering HIPEs for the preparation of PPHs, e.g., modified oxides of silica[193,194] and magnetite,[195,196] polymeric particles of poly(St-AA-MMA)[197,198] and poly(urethane urea),[199,200] and single walled CNTs.[201] The particle species investigated in this thesis are particles of stimuli-responsive poly(NIPAAm-*co*-AA) microgels. Besides the advantages of Pickering emulsions over conventional emulsions in emulsion stabilisation, the preparation of PPHs can also represent a novel approach to polyHIPE composites or nanocomposites. Within this relatively new field of research, three aspects were of particular interest: PPH morphology, particle locus and PPH properties.

Firstly, pores of a few hundred microns were commonly exhibited in PPHs[190,191,193] and these were obviously larger than those of typical polyHIPEs (< 100 μm). This feature potentially extends the application of polyHIPEs to a wider range. However, closed-pore structures have been frequently obtained in PPHs[190,191,193,194,196,199,202] except few examples.[103,200] Since open porous foams are required for most applications, it is essential to

find out why closed pores are present and how to generate pore throats in PPHs. This is discussed in detail in **Section 3.4**.

The particle locus in PPHs plays an important role in the applications of PPHs. For example, the reinforcement of polyHIPEs requires uniform particle distribution whereas polyHIPEs for catalysis purpose need particles at the interface. As Pickering emulsions have various stabilisation mechanisms, the particle locus in PPHs is not always at the pore surface as may be expected. In a study by Gurevitch *et al.*, it was found that when the initiator was in the dispersed phase, particles that were pre-mixed in the continuous phase would be located within the polyHIPE walls, far from the polyHIPE surface.[120,194] Conversely, when the initiator was in the continuous phase, particles that were pre-dispersed in the internal phase would normally be visible at the pore surface of the resultant PPH.[190] Furthermore, Zhang *et al.* found that the presence of visible particles on the pore surface depended on the salt concentration and particle concentration in the aqueous phase as well as the nature of the particles.[197,198] When the locus of initiation was in the continuous phase, particles that were also pre-dispersed in the continuous phase would be visible at the surface of the pore wall and within the polymer matrix.[120,192,195] Gurevitch *et al.* attributed the appearance of particles within the pore wall to the changes in droplet shape and size upon HIPE destabilization during polymerisation.[120] Vilchez *et al.* found that the hydrophobicity of particles could play a role in determining their location in PPH and particles of a low affinity to the polymer matrix could only stay at the interface.[196] In the case of particles used as both the stabiliser and as an atom transfer radical polymerisation (ATRP) initiator, they would also be located only at the interface after polymerisation.[120]

The properties of PPHs were preliminarily investigated aiming for potential applications. Since PPHs normally exhibited closed pores of much larger sizes than their conventional counterparts, particles hardly showed an obvious effect of reinforcement[192] or even caused a reduction in mechanical properties due to particle aggregation.[202] Nevertheless, Li *et al.* recently obtained PPHs of similar sizes to conventional polyHIPEs using surface-modified magnetite nanoparticles and γ-rays for initiation and found a reinforcement effect of particles below 20 wt % loading.[195] The compression strength and Young's modulus of the PPH at 20 wt % particles were 5.29 and 69.7 MPa, obviously higher than those of a conventional polyHIPE prepared using 3 wt % Span 80 (2.36 and 41.9 MPa).[195] In addition, PPHs prepared using CNTs or magnetite particles exhibited conductivity[192,201] or superparamagnetic

behavior.[195,196] All these properties show that preparation of PPHs can be a promising approach to macroporous polymer composites or nanocomposites.

1.2.2 Applications of polyHIPEs as tissue engineering scaffolds

Due to their versatility in structures and properties, polyHIPEs have been exploited for a variety of potential applications,[91,125,126,203] such as catalyst supports,[204,205] ionic exchange modules,[206] media for protein separation or purification[207,208] and tissue engineering scaffolds. Although the study of polyHIPE scaffolds for tissue engineering only started at the beginning of this century, recent advances have led to an increased understanding of the cell-scaffold interactions.

Firstly, cell growth in polyHIPE matrices has been shown to be superior to that in 2-D conditions. Hayman *et al.* reported the use of polystyrene (PS) based polyHIPEs for cell culture tests and found that human neural precursors could differentiate and form neutral networks on 2-D surfaces but their ability to continue to differentiate was significantly enhanced on inert solid 3-D PS matrices.[132] Bokhari *et al.* cultured hepG2 liver cells on PS polyHIPEs of 120 μm in thickness and found that 3-D culture was more conductive to enhanced cell function and less susceptible to cytotoxin than 2-D culture.[209,210] In comparison to 2-D culture, Barbetta *et al.* also found better-preserved hepatocyte viability after 48 h and a much higher level of albumin production in gelatin based polyHIPE matrices.[211,212]

Secondly, polyHIPE scaffolds have been preliminarily investigated for bone tissue engineering. Akay *et al.* investigated three PS based polyHIPEs of different pore sizes (40 μm, 60 μm and 100 μm) and pore throat sizes (15 μm, 20 μm and 30 μm) for the culture of primary rat osteoblasts.[129] It was found that pore size influenced the rate of cell penetration but did not influence cell viability, cell differentiation or the maximal depth of cell penetration (~1.4 mm at 35 days).[129] Moreover, compared to pure PS polyHIPEs, polyHIPEs modified with hydroxyapatite showed more cells within the matrix, earlier collagen I expression and significantly more bone nodule formation at 28 and 35 days;[129] polyHIPEs coated with a peptide hydrogel could significantly increase the ability of the scaffold to support osteoblast activity and bone formation.[213]

In addition to this, both synthetic and natural biopolymers have been fabricated via polyHIPEs aiming for biocompatible and biodegradable scaffolds. Typically, macromers of the biopolymers were prepared and used alone or together with a co-monomer in the

continuous phase of HIPEs. The macromers of synthetic biopolymers are normally oil-soluble, such as PCL-diacrylate,[214-217] PLA-diacrylate,[215] PPF and propylene fumarate diacrylate (PFDA)[68] and propylene fumarate dimethacrylate (PFDMA).[218] In contrast, the macromers of the natural biopolymers investigated are water-soluble, such as methacrylated dextran,[219] pullulan[219] or gelatin,[211,212,219,220] and degraded alginate.[221] Moreover, biopolymers that can lead to scaffolds with good mechanical properties have been exploited for bone tissue engineering. Moglia *et al.*[218] reported that PPF polyHIPEs could reach an average compressive modulus and strength of 33 MPa and 5 MPa, respectively. These values are as high as those of the cancellous bone and suggest a great potential for PPF polyHIPEs in the field.

Finally, it was shown that drug delivery from polyHIPE scaffolds is possible. Hayman *et al.* coated PS polyHIPEs with bioactive molecules by immersing the polyHIPE scaffold into an aqueous solution of poly-D-lysine and laminin and found the differentiation of human neuron cells was enhanced.[133] In another case, Akay *et al.* modified PS polyHIPEs by dissolving hydroxyapatite into the aqueous phase prior to emulsification and found that the ability of osteoblasts to penetrate and migrate into the scaffolds was improved.[129]

So far, there are no reported poly(Pickering HIPEs) (PPHs) used as tissue engineering scaffolds. By using a particle stabiliser instead of conventional surfactants, PPHs are expected to offer improved features, such as larger pore sizes and higher biocompatibility. Moreover, using a particle stabiliser that is capable of carrying and releasing drugs or bioactive molecules – such as the microgels as investigated in this work – would represent a novel step forward for the use of polyHIPEs in tissue engineering applications.

Chapter 2 Microgel particles stabilised DVB based emulsions

2.1 Overview

Poly(*N*-isopropylacrylamide-*co*-acrylic acid) [poly(NIPAAm-*co*-AA)] microgel particles have been studied as stimuli-responsive emulsifiers for high internal phase emulsions (HIPE) to fabricate novel multifunctional polymeric scaffolds. Before microgel particles of poly(NIPAAm-*co*-AA) were investigated as emulsifiers, their responsiveness to temperature, pH and KCl concentration together with the effect of microgel concentration were investigated via particle size measurements. Meanwhile, the factors involved in microgel preparation – including surfactant source and purification procedures – were evaluated in terms of their effect on particle size. It was found that only the surfactant source had a significant effect on the particle size. In addition, a purification procedure without using acid or base was sufficient for our use as emulsifiers, i.e., dialysis with distilled water at 60 °C followed by an ion exchange process.

Investigations of microgel particles as emulsifiers in divinylbenzene (DVB) based emulsions were then carried out. The aim of these experiments was to find out whether w/o Pickering HIPEs and poly(Pickering HIPEs) could be obtained. At pH 5, it was found that swollen microgel particles were so hydrophilic that only o/w Pickering emulsions could be produced regardless of phase volume ratio (varied from 20% to 80%) or particle concentration (varied from 0.02 wt % to 0.4 wt %). Attempts using shrunken microgel particles at pH 5 to prepare HIPEs above the volume phase transition temperature (VPTT), either at 50 °C or at 65 °C, resulted in phase separation during homogenisation due to microgel aggregation. At pH 2.5 or pH 3, it was found that only o/w emulsions were obtained below 32 °C and that phase separation occurred above 32 °C due to particle aggregation. At pH 4, however, the shrunken microgel particles did stabilise w/o emulsions (60 vol % internal phase) and HIPEs at temperatures above the VPTT, from which poly(DVB) Pickering-HIPEs were obtained. Further investigation into the stabilisation mechanism indicated that the charges of collapsed microgel particles were crucial for the formation of stable particle layers at the interface so that w/o HIPEs were stabilised.

2.2 Synthesis, purification and characterisation of poly(NIPAAm-*co*-AA) microgel particles

Microgel particles are cross-linked polymeric particles that are swollen in a good solvent[222-224] and are normally of colloidal dimensions. Those presenting stimuli responsiveness[225-227] in an aqueous environment have been extensively investigated for applications in biomedicine and industry.[223,228-232] Since first reported as novel particulate emulsifiers in 2005,[233,234] microgel and composite microgel particles have not only shown the ability to stabilise surfactant-free emulsions,[148,149] but also enabled tunable emulsion stability and demulsification on demand via variation in temperature,[233,235] pH,[233-237] salt concentration[235,236] or magnetic field.[238] In this thesis, we aim to create tissue-engineering scaffolds by exploiting microgel particles as novel emulsifiers of high internal phase emulsions (HIPEs). Classically, surfactants have been the dominant type of emulsifiers for HIPEs as detailed in **Chapter 1**. As an alternative to conventional surfactants for our purposes, microgel particles have the additional benefit that they can serve as carriers[239-245] of bioactive molecules[246] that are essential for cell growth and tissue development. Attractively, their stimuli-responsiveness could be potentially used as triggers[245,247] for drug release under physiological conditions.

Within the growing family of stimuli-responsive microgel particles, poly(*N*-isopropylacrylamide) (polyNIPAAm) and its derivatives have attracted considerable attention since first reported by Pelton and Chibante in 1986.[248] PolyNIPAAm microgel particles,[225,249-251] similar to the analogous linear polymers[252-254] and macro-gels,[255] undergo a typical thermo-reversible phase separation when the temperature of the aqueous solution is raised above ca. 32 °C. In contrast to the coil-to-globule transition[253,256-261] observed in linear polyNIPAAm, microgels or macro-gels exhibit a sharp volume phase transition (VPT)[255,262-265] (shrinkage). This phenomenon is attributed to a balance between hydration and hydrophobic aggregation of the isopropyl groups.[266] The transition temperature is commonly referred to as lower critical solution temperature (LCST) for linear polymers and as the volume phase transition temperature[225] (VPTT) for both gel species. In this thesis, copolymer microgel particles of poly(*N*-isopropylacrylamide-*co*-acrylic acid) [poly(NIPAAm-*co*-AA)][267-269] are employed since copolymerisation with acrylic acid (AA) enables an increase of the VPTT close to physiologically relevant temperatures (37 °C) as well as a larger

swelling capacity[267,269,270] at temperatures below the VPTT and additional sensitivity to pH[268,271] and ionic strength, which are equally useful for biomedical applications.

The poly(NIPAAm-*co*-AA) microgel particles in our work were prepared using surfactant-assisted emulsion polymerisation.[270,272] **Table 2.1** lists the parameters that were investigated in the synthesis and purification of poly(NIPAAm-*co*-AA) microgel particles. Microgel responsiveness to environmental stimuli including temperature, pH and ionic strength was characterised by dynamic light scattering (DLS), i.e., particle size measurements in aqueous suspensions.

Table 2.1 List of parameters that were varied in the preparation of gel particles (**GP1**)

GP species	Molar feed ratio (NIPAAm:BIS:AA)	NaDBS source	GP batch No.	Purification procedures*
GP1	94:1:5	BDH	**GP1-1**	D20-OH-EX
		Aldrich	**GP1-2**	DT60-OH
				DT60-H
				DT60-OH-EX
		Aldrich	**GP1-3**	DT60-OH
				DT60-H
				DT60-OH-EX
		BDH	**GP1-4**	D20-OH-EX
				DT20-OH-EX
				DT60-OH
				DT60-OH-EX
				DT60-H
				DT60-H-EX

* Purification procedures (a combination of the following four factors):
(1) Treatment of dialysis tubing: washing with distilled water (D), followed by treatment with sodium sulphide and sulphuric acid (DT);
(2) Dialysis temperature: room temperature (20) or 60 °C (60);
(3) Dialysis type: alkaline dialysis (OH) or acidic dialysis (H);
(4) Exchange resin: whether applied (EX) or not.

2.2.1 Assessment of the environmental sensitivity of microgel particles

GP1 of poly(NIPAAm-*co*-AA) microgel particles were prepared at a molar feed ratio (NIPAAm:BIS:AA) of 94:1:5, in contrast to 93:2:5 for **GP2** (used in **Chapter 3** and **4**). 5

mol % AA was employed for both microgel species aiming to induce a sharp swelling-deswelling transition caused by pH change at 37 °C.[271,273] A small amount of *N*, *N'*-methylenebisacrylamide (BIS, 1-2 mol %) was used as crosslinker to create a significant variation in microgel volume at the transition.[274-279] Prior to being studied as emulsifiers, microgel suspensions of **GP1-1** (batch 1 of **GP1**) with predetermined KCl concentration, pH and microgel concentration were characterised by particle size measurement in a temperature range of 20-70 °C to establish the environmental sensitivity of the particles.

2.2.1.1 Particle size of microgels as a function of temperature at various pH

Understanding the response of poly(NIPAAm-*co*-AA) microgel particles to temperature and pH is essential for emulsification using the particles as stabilisers as well as for drug uptake and release (**Chapter 4**). **Fig. 2.1** and **Fig. 2.2** show the size variation of **GP1-1** as a function of temperature in the pH range from 2.0 to 7.0 in 1 mM KCl solution, which was chosen to provide a weak screening environment. The behaviour of microgel particles that are suspended in KCl solutions of higher concentrations will be discussed in **Section 2.2.1.2**.

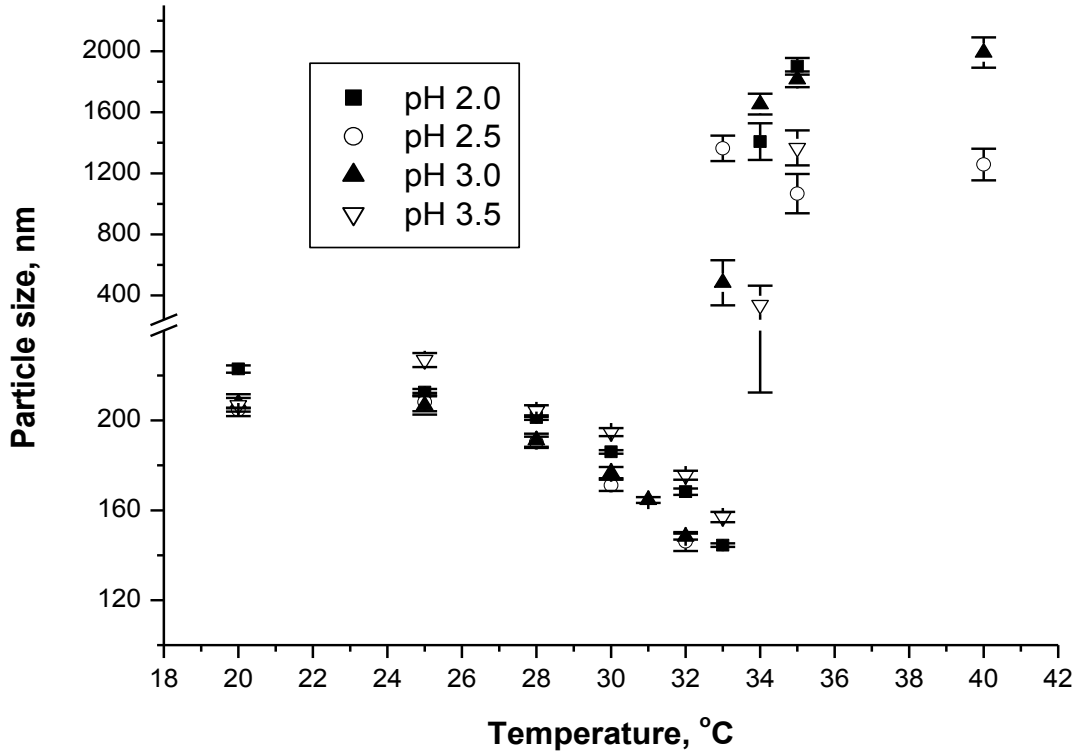


Fig. 2.1 Average particle size of **GP1-1** as a function of temperature at pH 2 (0.048 wt %), pH 2.5 (0.10 wt %), pH 3.0 (0.031 wt %) and pH 3.5 (0.035 wt %) in 1 mM KCl solutions. Numbers in the brackets were particle concentrations of the suspensions characterised.

For all pH values (2.0-3.5), at temperatures below 32 °C, the particle sizes of **GP1-1** decreased with temperature from 200-230 nm to 140-160 nm (**Fig. 2.1**), indicating a process of temperature induced gradual collapse of individual microgel particles. However, above 32 °C for pH 2.5 and pH 3.0 and above 33 °C for pH 2.0 and pH 3.5, an abrupt increase of particle size from about 150 nm to over 1000 nm was seen, suggesting loss of colloidal stability[249,274,280] in the aqueous medium. Although microgel concentrations in these suspensions were varied within a range from 0.03 wt % to 0.10 wt %, the influence of this variable on the tendency of microgel particles upon temperature increase is believed to be negligible; our subsequent investigations (**Fig. 2.15**) having shown identical results in more highly concentrated suspensions containing 0.4 wt % of microgels. For comparison, reported polyNIPAAm microgel particles[249] employing the same background electrolyte (1 mM KCl), presented a typical volume phase transition process (shrinkage) without coagulation over a temperature range from 10 to 50 °C. Thus, it is naturally deduced that PAA moieties in our poly(NIPAAm-*co*-AA) microgel particles played a role in the coagulation of microgel particles within the current pH range. So far, ambiguities and controversies[281] still exist in comprehensively understanding the forces exposing to microgel particles in the aqueous medium. However, in terms of the colloidal stability in microgel suspensions, analysis can be carried out based on a qualitative understanding that hydrophobic hydration[282-286] and electrostatic repulsion provide counter-interactions to those attractive ones including hydrophobic interaction[287-290] between isopropyl groups, van der Waals attraction,[223,288,291] and inter-particle hydrogen bonding.[292] The electrostatic repulsion among poly(NIPAAm-*co*-AA) microgel particles is believed to originate from two sources:[293] the ionized fragments of initiators[249,294,295] (sulphate group, $-OSO_3^-$) and ionisable co-monomer AA, and to manifest through the resultant electrical double layers.[286,296] The pH range (**Fig. 2.1**) is above the pK_a of sulphate group (2.0[293]) but well below that of acrylic acid (4.25[297]). Indeed, the pK_a of carboxyl groups shifts to 4.7[298,299] in PAA or even increases with temperature above 32 °C in poly(NIPAAm-*co*-AA) copolymers of low AA contents.[300] Titrations[270,301-303] showed that the carboxylic acid groups in poly(NIPAAm-*co*-AA) microgels hardly ionized at or below pH 3.5, indicating PAA only contributed to attractive rather than repulsive interactions under these conditions. Thus, upon increase of the temperature above 32 °C, dissociation of the hydrophobic interaction between NIPAAm segments and water (or hydrophobic hydration)[283,304] facilitated the hydrophobic interactions between isopropyl groups, leading to

microgel collapse. The driving forces for particle coagulation were attributed to increased inter-particle attractive interactions,[292,305] mainly hydrogen bonding[269,292] arising from protonated carboxylic acid groups and amide groups.

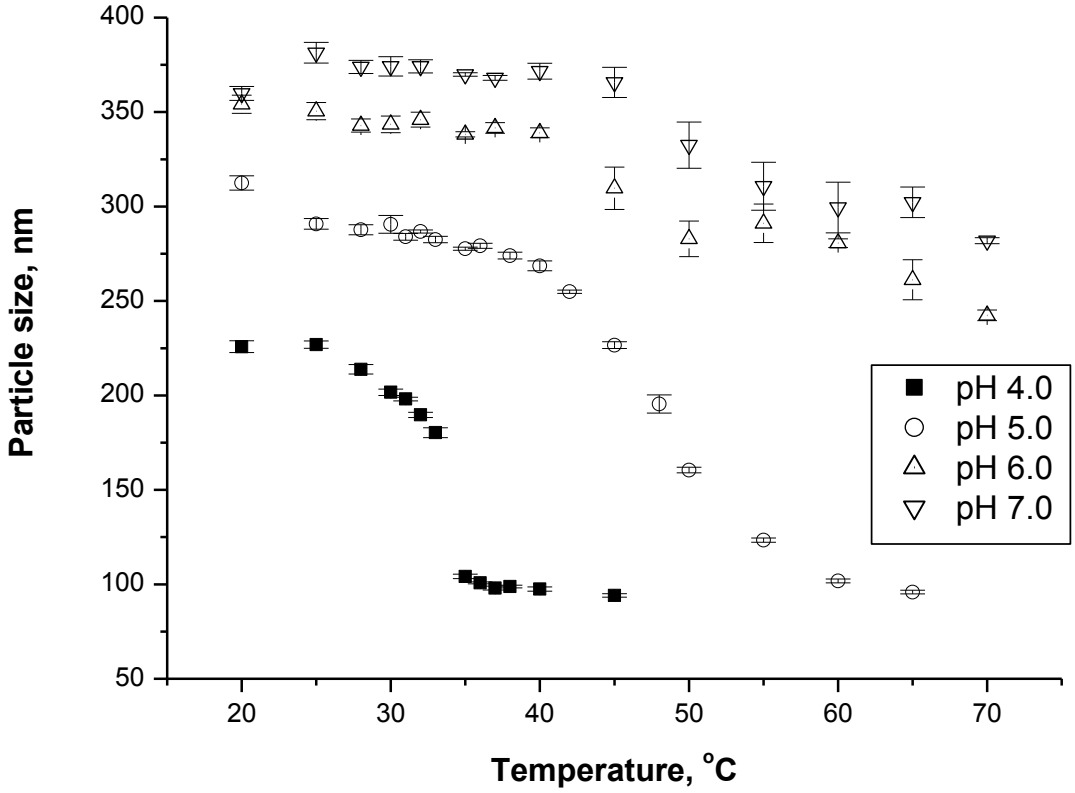


Fig. 2.2 Average particle size of **GP1-1** as a function of temperature at pH 4.0 (0.037 wt %), pH 5.0 (0.073 wt %), pH 6.0 (0.046 wt %) and pH 7.0 (0.047 wt %) in 1 mM KCl solutions. Numbers in the brackets indicate particle concentrations of the suspensions studied.

At pH 4.0 (**Fig. 2.2**), when the temperature was increased from 32 °C to 35 °C, particles displayed a volume phase transition (VPT) with a sharp decrease of size from 190 nm to 100 nm. The disappearance of microgel aggregation above 32 °C at pH 4.0 in contrast to pH 2.0-3.5 was thus attributed to a slight ionization[301,303] of the carboxylic acid groups, which enhanced the electrostatic repulsion among microgels and maintained the colloidal stability during VPT. It can be seen from **Fig. 2.2** that an increase in pH from 4.0 to 7.0 had significant effects on particle size and the VPT process. In the swollen state, particle size of the ionic microgels became larger with an increase of pH, which is due to increase of the Donnan potential[306-308] within the particles accompanied by an increase in the osmotic pressure[307,309] under the same bulk salt concentration (1 mM KCl). Meanwhile, it is interesting to note that the VPT appeared to be sharper at pH 4 than that at and above pH 5. This is similar to the behaviour of macroscopic gels of poly(NIPAAm-*co*-AA),[300,310] whose

VPT changed from a discontinuous transition to a continuous one when pH was increased above 7.5. The occurrence of this sharper transition at pH 4 rather than at pH 5 was attributed to a lower osmotic pressure and the presence of stronger intra-particle interactions at pH 4, including hydrogen bonds and hydrophobic interactions. The formation of intra-particle hydrogen bonds[311-313] was expected since ionization of the AA moieties was still at a very low level at pH 4.[302,303] At and above pH 5, with a significant increase in degree of ionization of the carboxylic acid groups and thus the electrostatic repulsion arising from $–COO^-$, it became more difficult to form intra-particle hydrogen bonds as well as to deswell the particles.[314] As a result, the VPT process became more continuous and covered a broader temperature range from 40 °C to 60 °C. Moreover, comparisons can be drawn among the collapsed states of the particles at various pHs. The same size of 100 nm was reached at pH 4 and at pH 5 whereas – due to further ionization of the –COOH groups – microgel particles in suspensions of pH 6.0 and 7.0 hardly shrank to below 240 nm even at 70 °C. Thus, an order of the magnitude of temperature-induced volume changes [$V_{swollen}/V_{shrunken} = (d_{swollen}/d_{shrunken})^3$] at different pHs can be obtained: 34.6 (pH 5) > 13.3 (pH 4) > 2.5 (pH 6) > 2.0 (pH 7), using particle sizes at 65 °C as the sizes of collapsed particles for pH 5-7. Clearly, the temperature-induced volume change of **GP1-1** reached a maximum at pH 5 and attenuated sharply with increasing pH. On the other hand, it can also be seen that a pH change from 4.0 to 7.0 at 37 °C brought about a significant size change of poly(NIPAAm-*co*-AA) microgel particles from 100 nm to 370 nm, equivalent to a 50.7 fold change in volume. This striking variation can be a promising feature for drug delivery systems, i.e., uptake of hydrophobic drugs at pH 4 followed by release at pH 7.[250]

To conclude, the swelling behaviour of poly(NIPAAm-*co*-AA) microgels (**GP1-1**) has shown a strong pH-dependence in the studied pH range from 2 to 7 with 1 mM KCl as electrolyte background. Charges arising from ionization of the –COOH groups determine the stability of microgel particles against aggregation upon temperature increase, the VPTT, breadth of the VPT and the magnitude of temperature-induced deswelling. Significant volume changes can be induced either through temperature variation at pH 4 and pH 5, or through pH variation between 4 and 7 at 37 °C.

2.2.1.2 Particle size of microgels as a function of temperature at various ionic strengths

Since microgel particles are to be used in an environment containing salts during emulsification, it is essential to investigate the behaviour of microgel particles in suspensions of various ionic strengths. Although the charges of our poly(NIPPAm-*co*-AA) microgel particles stem from the initiator (APS) and AA as discussed in **Section 2.2.1.1**, it is of significance to study the effects of ionic strength on the swelling behaviour of microgel particles only when –COOH from AA are sufficiently ionized.[307] Meanwhile, the salt species remains KCl in accordance with the previous section since it is not our aim here to cover the entire Hofmeister series.[315-317] Therefore, based on **Fig. 2.2**, microgel suspensions with KCl as background electrolyte and pH 5 as the predetermined pH were selected for investigation in this section. Furthermore, three ionic strengths, 0.001 M, 0.02 M and 0.2 M, were chosen since the critical salt concentration for microgel aggregation was expected to lie between 0.02 M and 0.2 M.[269,318]

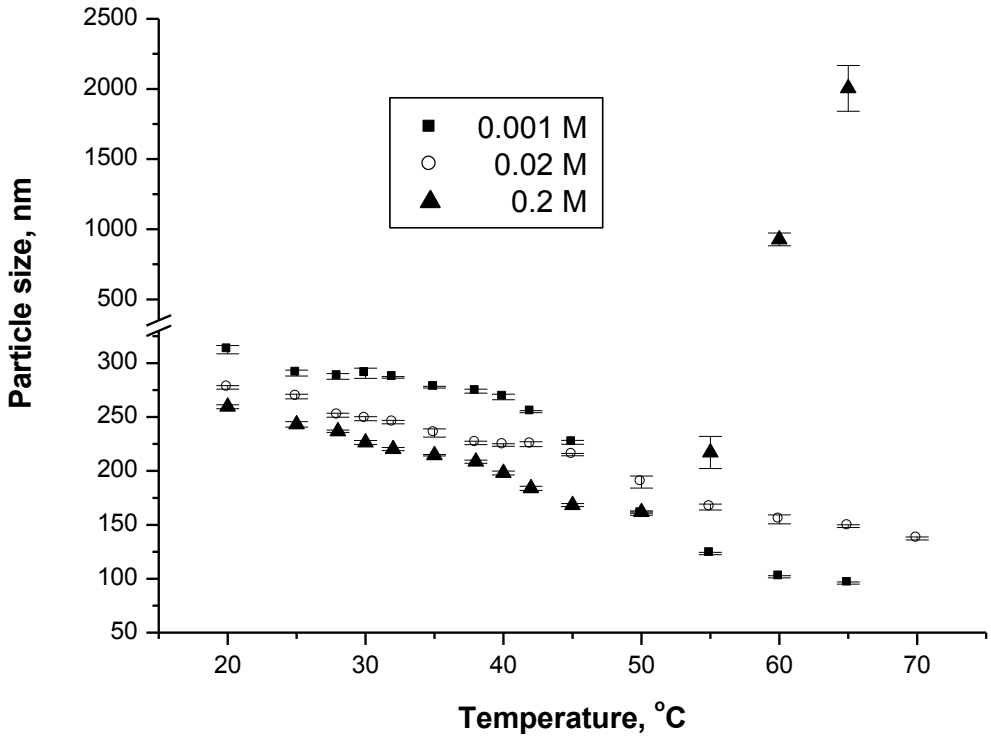


Fig. 2.3 Average particle size of microgels (**GP1-1**) as a function of temperature measured using microgel suspensions of different KCl concentrations at pH 5. The KCl concentrations were 0.001 M, 0.02 M and 0.2 M, respectively. Minor differences existed in microgel concentration of the three suspensions studied, which were 0.073 wt %, 0.066 wt % and 0.062 wt %, respectively.

Fig. 2.3 shows the effects of salt concentration and temperature on the average particle size of **GP1-1** at pH 5.0 in 0.001 M, 0.02 M and 0.2 M KCl background electrolyte solutions,

respectively. Microgel aggregation appeared in the KCl solution of 0.2 M rather than 0.02 M as expected. The critical temperature for aggregation was about 50 °C, in close agreement with the VPTT,[319] suggesting aggregation occurred during VPT since the overall inter-particle interaction became attractive. This can be explained by calculating the Debye screening length λ_D at 25 °C according to Equation (2.1):[320]

$$\lambda_D = \frac{3.04 \times 10^{-10}}{z_i \sqrt{c_i}} \quad \text{.....(2.1)}$$

where z_i and c_i are valency of ion i and electrolyte concentration, respectively. Increase of KCl concentration from 0.001 M to 0.02 M and 0.2 M led to a reduction of the Debye screening length from 9.6 nm to 2.1 nm and 0.7 nm, respectively, at 25 °C. Thus, once the hydration was largely dissociated upon VPT, a very short Debye screening length at high KCl concentration allows particles to come sufficiently close so that inter-particle attractive forces, including hydrogen bonding as well as hydrophobic interaction and van der Waals forces, can manifest significantly, leading to aggregation. The occurrence of microgel aggregation[269,318,319] during and/or after the VPT rather than in the swollen state indicated the existence of strong hydration of particles in the swollen state, including hydrogen bonds between water molecules and carbonyl groups and amide groups together with hydrophobic hydration of the isopropyl groups. Meanwhile, it is noticed that in the swollen state, increasing the ionic strength clearly caused a reduction in particle size. Taking 25 °C as an example, upon increasing the KCl concentration from 1 mM to 20 mM and 200 mM, the particle size decreased from 290 nm to 270 and 240 nm, respectively (**Fig. 2.3**). This was attributed to a decreasing ionic osmotic pressure with increasing salt concentration.[307] On the contrary, in the aggregation-free shrunken state, microgel particles were larger in suspensions of higher KCl concentration. For example, at 60 °C, increasing the KCl concentration from 0.001 M to 0.02 M resulted in a size increase from 100 nm to 160 nm, which was due to the fact that a higher concentration of ions was trapped inside the microgel upon VPT in the case of 0.02 M and subsequently caused resistance against the contraction of microgel network. Kratz *et al.*[269] reported similar effects of salt concentration on the sizes of swollen and collapsed poly(NIPAAm-*co*-AA) microgels with higher AA content (12.5 mol %) and crosslinking degree (6~7 mol %) than our microgels (5 mol % AA, 1 mol % BIS), i.e, microgels were smaller in the swollen state but larger in the collapsed state upon adding more

salts. This indicated that the amount of microgel charges had little effect on this trend, although it was found to have a linear relationship with the critical salt concentration for microgel aggregation.[269] It is also worth mentioning that the effect of minor differences in microgel concentration is believed to be negligible. This is evidenced by our subsequent study (**Fig. 2.4**) that a variation in microgel concentration from 0.02 wt % to 0.10 wt % had little effect on sizes of either swollen or shrunken microgels in 1 mM KCl. Thus, it can be deduced from **Fig. 2.2** and **Fig. 2.3** that based on microgel suspensions of pH 5 in 1 mM KCl solutions, either increasing pH or increasing KCl concentration can lead to a reduction in the magnitude of temperature-induced volume change of microgel particles, but through different mechanisms.

To conclude, the effect of KCl concentration on the swelling of poly(NIPAAm-*co*-AA) microgels prior to VPT can be well accounted for as a process driven by osmotic pressure difference between the interior of microgels and their surroundings for the studied KCl concentrations. Meanwhile, microgel aggregation tends to occur during VPT once the KCl concentration was increased to or above the critical point, where the attractive interactions prevailed over the electrostatic repulsion due to reduction of the Debye screening length.

2.2.1.3 Particle size of microgels at various concentrations as a function of temperature

Particle concentration is an important factor in particle-stabilised emulsions since it is related to the degree of droplet surface coverage[321] and plays a role in determining the emulsion stability[321,322] and the droplet size.[235,323] Meanwhile, for emulsions stabilised by microgel particles, the characteristic swelling behaviour of microgels has a major effect on the resultant emulsions.[233,234] Therefore, besides the effects of pH and ionic strength on microgel swelling previously discussed, it is also of interest to evaluate the effect of microgel concentration on the swelling behaviour prior to emulsification, which can support the understanding of microgel interactions in suspensions as well as at the water-oil interface.

Since higher concentration of particles simply means shorter inter-particle distance in the suspension, inter-particle interactions are very likely to be affected by particle concentration. Studies were carried out (**Fig. 2.4**) to determine the effects of microgel concentration – including 0.020 wt %, 0.10 wt %, 0.20 wt % and 0.40 wt % – on particle size in the temperature range from 20 to 70 °C in a 0.001 M KCl solution of pH 5.0. This KCl solution was chosen as a baseline composition of high sensitivity for this study since the temperature-

induced volume change of microgel particles reached a maximum degree as concluded from **Section 2.2.1.1** and **Section 2.2.1.2**. On the other hand, a particle concentration range from 0.020 wt % to 0.40 wt % was also sufficient for this current purpose.

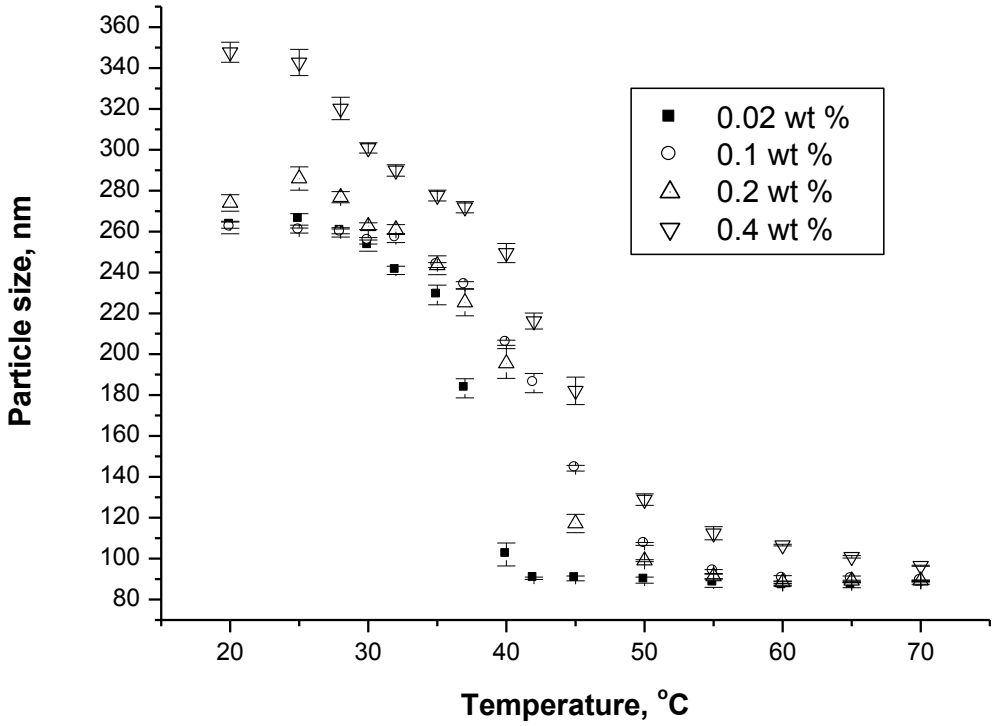


Fig. 2.4 Average particle size of microgels (**GP1-1**) as a function of temperature and particle concentration, which was varied from 0.020 wt % to 0.10 wt %, 0.20 wt % and 0.40 wt % in microgel suspensions at pH 5 containing 1 mM KCl.

A 20-fold increase of the microgel concentration from 0.020 wt % to 0.40 wt % in the suspension led to an increase in particle size in the swollen state. At 25 °C, the particle sizes were 260-270 nm for microgel suspensions of 0.020 wt % and 0.10 wt %, 280-290 nm for suspension of 0.20 wt % and 340-350 nm for suspension of 0.40 wt % whereas at 65 °C, the sizes were 90 nm for suspensions of 0.020 ~0.20 wt % and 100 nm for suspension of 0.40 wt %. The particle collapse process was also affected, especially the breadth of VPT process. For suspension of 0.02 wt %, the collapse of microgels occurred in a narrow range from 35 °C to 40 °C. However, the transition range became broader with increasing microgel concentrations. To reach a similar shrunken state of microgels (~90 nm), the suspensions needed to be heated up to 55-60 °C for suspensions of 0.1 wt % and 0.2 wt % and to 70 °C for suspension of 0.40 wt %.

To explain the effect of microgel concentration, the concentration-dependent inter-particle interactions[305] are first taken into account. The lightly-crosslinked poly(NIPAAm-*co*-AA) microgel particles (1 mol % BIS in feed) were not homogeneous spheres, but rather shells of dangling chains connected to a cross-linked core[279,293,324-326] due to a faster reaction kinetics of BIS than NIPAAm during the synthesis of particles.[280] Since these extended chains also contribute to the hydrodynamic diameters,[293,325-327] it is not surprising that the swelling behaviour of microgel particles observed is influenced by the interactions between the dangling chains.[292,328] Thermodynamically, if the entropy penalty of stretching can be overcome by enthalpy gain,[292] the dangling chains at the microgel surfaces can remain extended. This enthalpy gain is more likely to be available in suspensions of swollen microgel particles with higher concentration, e.g., W_4, which can arise from inter-chain hydrogen bonding. In addition, the technique used for size measurement, i.e. DLS, can also result in a slightly smaller particle size at lower particle concentration due to an increase in the diffusion coefficient.[329,330]

The above phenomenon brought about by microgel concentration is not just for suspensions at pH 5. Our subsequent study at pH 4 (**Fig. 2.19**) showed that an increase in microgel concentration from 0.40 wt % to 0.80 wt % also led to a considerable increase of the hydrodynamic diameters for the swollen particles but had no obvious effect on the shrunken microgels. For example, at 25 °C, a size variation from 220 nm to 260 nm was observed. The independence of particle size on microgel concentration observed above VPT at pH 4 was attributed to stronger intra-particle hydrogen bonding than that at pH 5 (**Section 2.2.1.1**).

To conclude, the particle concentration has an obvious effect on the hydrodynamic diameters of swollen microgels as well as the VPT of lightly crosslinked microgels, especially when the particle concentration reached 0.4 wt % as investigated in 1 mM KCl solution. The reasons mainly lie in the fact that the structural features of microgel particles become more and more important with increasing microgel concentration and the dangling chains in the shell layer of microgels start to interact with those of neighbouring microgels.

2.2.2 Assessment of the effect of surfactant and purification procedures on microgel size

When microgel particles are used as emulsifiers, their wettability[149,150,331] at the interfaces are closely related to the swelling degree. This is because variations of the swelling degree are accompanied by changes in the water content inside the microgel network[264,279,332-335] and

the number of water molecules hydrogen-bonded to each repeat unit inside the gel,[313,336-341] and thus will influence the overall hydrophilicity or hydrophobicity of microgels,[233,235] – an important factor in determining particle wettability. Meanwhile, particle size (i.e., hydrodynamic diameter) can indicate the variation in swelling degree with the environmental stimuli (**Section 2.2.1**). Therefore, measuring particle sizes of microgels can be a very useful tool for studying microgel-stabilised emulsions.

In this section, we aim to assess the effects of the surfactant source and purification procedures on the particle size of **GP1**. This will help minimize the batch-to-batch variation before these particles are used as emulsifiers. The surfactant NaDBS used was either from BDH (yellow and sticky solid, 80% active constituent with sodium sulphate as the remainder) or from Aldrich (white or light yellow powder, technical grade, unspecified purity). The purification of microgels involves multi-step procedures (**Section 7.2**), of which the choice of options may influence the final states of microgels. For example, alkaline dialysis (0.1 M NaOH used as the medium between two steps of dialysis with distilled water) and acidic dialysis (0.1 HCl used as the medium between two steps of dialysis with distilled water) can determine the nature of microgel charges.[270] Therefore, a step-by-step procedure for our purpose is needed practically. In total, four factors were considered to obtain an understanding of how each factor affected the particle size: (i) treatment of dialysis tubing, either simply washed with water (D) or to follow a three-step procedure[342] involving treatment with sodium sulphide and sulphuric acid (DT); (ii) dialysis temperature, room temperature (20) or 60 °C as recommended by the manufacturer[343] (60); (iii) dialysis type,[270] either alkaline dialysis (OH) or acidic dialysis (H); (iv) ion exchange resin,[272,344] whether applied (EX) or not. For example, purification of **GP1-1** followed procedure **D20-OH-EX**, i.e., a combination of the choices made upon the four factors.

2.2.2.1 Effect of dialysis type used in purification on the particle size of microgels

GP1-2 (batch 2 of **GP1**) was prepared using the NaDBS from Aldrich and purified by three different procedures, including **DT60-OH** (alkaline dialysis at 60 °C), **DT60-H** (acidic dialysis at 60 °C) and **DT60-OH-EX** (alkaline dialysis at 60 °C followed by ion exchange). The effect of these purification procedures on the particle size was assessed in microgel suspensions (0.2 wt %) of pH 5 in 1 mM KCl solution (**Fig. 2.5**). The sizes of swollen microgels (25 °C) were 150-160 nm, 215-230 nm and 180-190 nm, respectively, whereas no

obvious difference was shown in the VPT or in the shrunken state (~50 nm at 70 °C) of the three. On the other hand, an identical batch to **GP1-2**, **GP1-3** (batch 3 of **GP1**) was also prepared and evaluated in the same way (**Fig. 2.6**). The sizes of swollen **GP1-3** (25 °C) were 150-160 nm, 180-190 nm and 170-180 nm under the three conditions while the collapsed microgels exhibited a size of 60-70 nm, respectively.

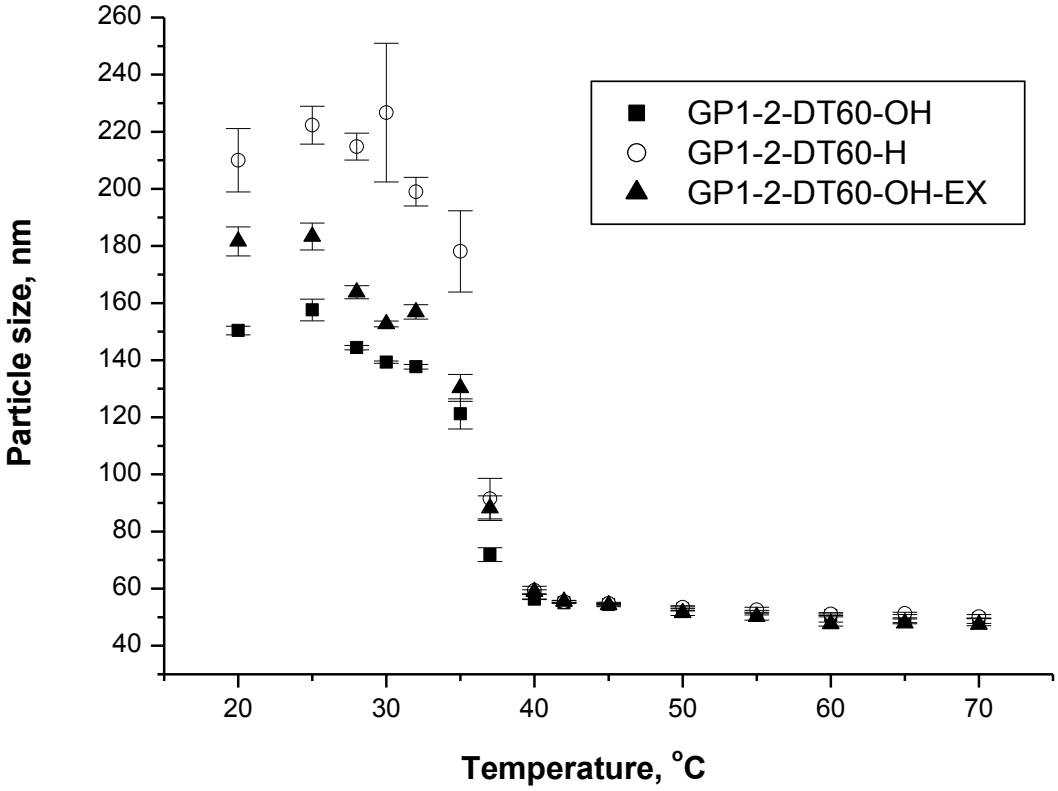


Fig. 2.5 Average particle sizes of **GP1-2** microgels as a function of temperature measured in microgel suspensions (0.2 wt %) of pH 5 in 1mM KCl solution. The microgels were purified using three procedures: **DT60-OH** (alkaline dialysis at 60 °C), **DT60-H** (acidic dialysis at 60 °C) and **DT60-OH-EX** (alkaline dialysis at 60 °C followed by ion exchange).

When comparing the three purification procedures applied to **GP1-2** and **GP1-3**, differences in particle size were mainly observed in the swollen state of microgels. This variation was attributed to two major aspects. Firstly, a difference in ionic strength of microgel suspension was probably introduced when pH was adjusted to 5.0 for all three microgel suspensions by using either HCl or KOH solutions before particle size measurements. The pH values of the microgel suspensions prior to pH adjustment were either 6.9 or 4.6 (**Table 2.2**). According to reported titration results,[270,301,302] the amount of HCl needed to change pH from 6.9 (**DT60-OH**) to 5.0 was more than that of KOH needed to

adjust pH from 4.6 (**DT60-H** or **DT60-OH-EX**) to 5.0. Thus, it is reasonable to expect that the ionic strength of the suspension containing microgels of **DT60-OH** was relatively higher than that of the suspensions containing microgels of **DT60-H** and **DT60-OH-EX**. According to our understanding of the effect of ionic strength (**Section 2.2.1.2**), it is not surprising that smaller particle sizes were exhibited in suspensions of **GP1-2-DT60-OH** and **GP1-3-DT60-OH** prior to the VPT. Secondly, there was a higher possibility of surfactant binding to microgels for acidic dialysis at 60 °C (**DT60-H**), which would typically result in larger particle sizes.[345-347] This is because collapsed and protonated microgel particles were more hydrophobic (**Section 2.1.1.1**) and would facilitate the binding of microgels with the hydrocarbon tails of the surfactant.[348] Thus, the removal of surfactant molecules may become more difficult and time-consuming. This may also explain the size deviation of swollen **GP1-3-DT60-H** from **GP1-2-DT60-H** (15~20%, 25 °C), since the surfactant molecules binding to microgels can have a considerable batch-to-batch variation. In contrast, the batch-to-batch variation was negligible for microgels purified under alkaline conditions due to the existence of $-COO^-$.

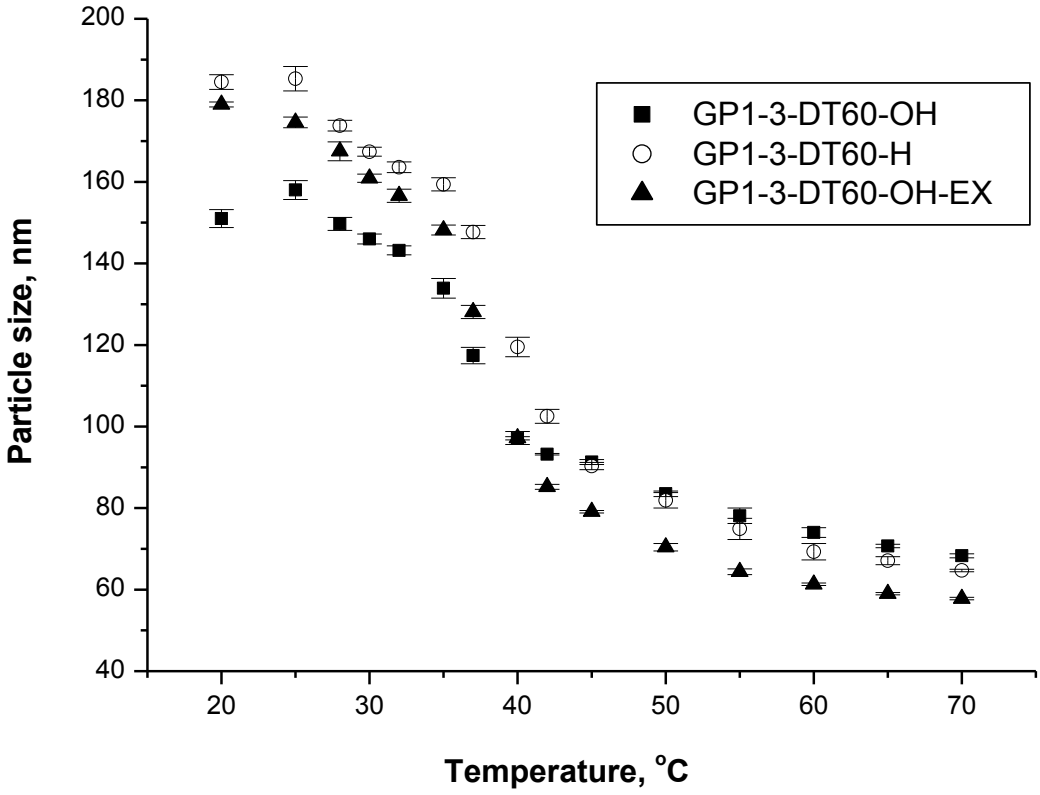


Fig. 2.6 Average particle sizes of **GP1-3** microgels as a function of temperature measured in microgel suspensions (0.2 wt %) of pH 5 in 1mM KCl solution. The microgels were purified using three procedures: **DT60-OH** (alkaline dialysis at 60 °C), **DT60-H** (acidic dialysis at 60 °C) and **DT60-OH-EX** (alkaline dialysis at 60 °C followed by ion exchange).

To conclude, the purification procedures can influence the original pH of the microgel suspensions (i.e., prior to pH adjustment using either HCl or KOH), and the variation in particle size will be observed if differences in ionic strength of the suspensions are brought about by the subsequent adjustment of pH. Meanwhile, surfactant binding to microgels is more likely for dialysis under acidic conditions.

2.2.2.2 Effect of six different purification procedures on the particle size of microgels

The particle sizes of **GP1-2** and **GP1-3** (**Section 2.2.2.1**) were about 30% smaller than that of **GP1-1** in both the swollen and collapsed states. In order to fully assess the effect of NaDBS sources and purification procedures on particle size, **GP1-4** (batch 4 of **GP1**) was prepared using NaDBS from BDH, the same source as used for **GP1-1**, and purified using six different procedures, which were different from each other with respect to the treatment of dialysis tubing, dialysis temperature, dialysis type and ion exchange process. Before a batch-to-batch comparison is carried out (**Section 2.2.2.3**), this section assesses the effect of purification procedures on the particle size using **GP1-4**. Prior to adjustment to pH 5 for particle size measurement, the original pHs of six microgel suspensions (0.2 wt % microgels in 1 mM KCl solution) are listed in **Table 2.2**.

Table 2.2 Original pH of the aqueous suspensions of **GP1-4** purified via different procedures

	D20-OH-EX	**DT20-OH-EX**	**DT60-OH**	**DT60-OH-EX**	**DT60-H**	**DT60-H-EX**
pH	4.60	4.60	6.91	4.62	4.67	4.60

The measured pH of the suspensions containing differently purified **GP1-4** can show the efficiencies of purification procedures in changing counter ions (NH_4^+, Na^+) for H^+. For alkaline dialysis, adding an ion exchange step was obviously more effective, compared to a sole dialysis procedure (**GP1-4-DT60-OH**). The acidic dialysis (**GP1-4-DT60-H**) clearly helped remove counter ions to a level equivalent to that attained by using ion exchange, which was similar to acid washing[349] as applied in the purification of polystyrene latexes. The particle sizes of these six products of **GP1-4** were also compared in microgel suspensions (0.2 wt %) of pH 5 in 1mM KCl solution over a temperature range of 20-70 °C (**Fig. 2.7**).

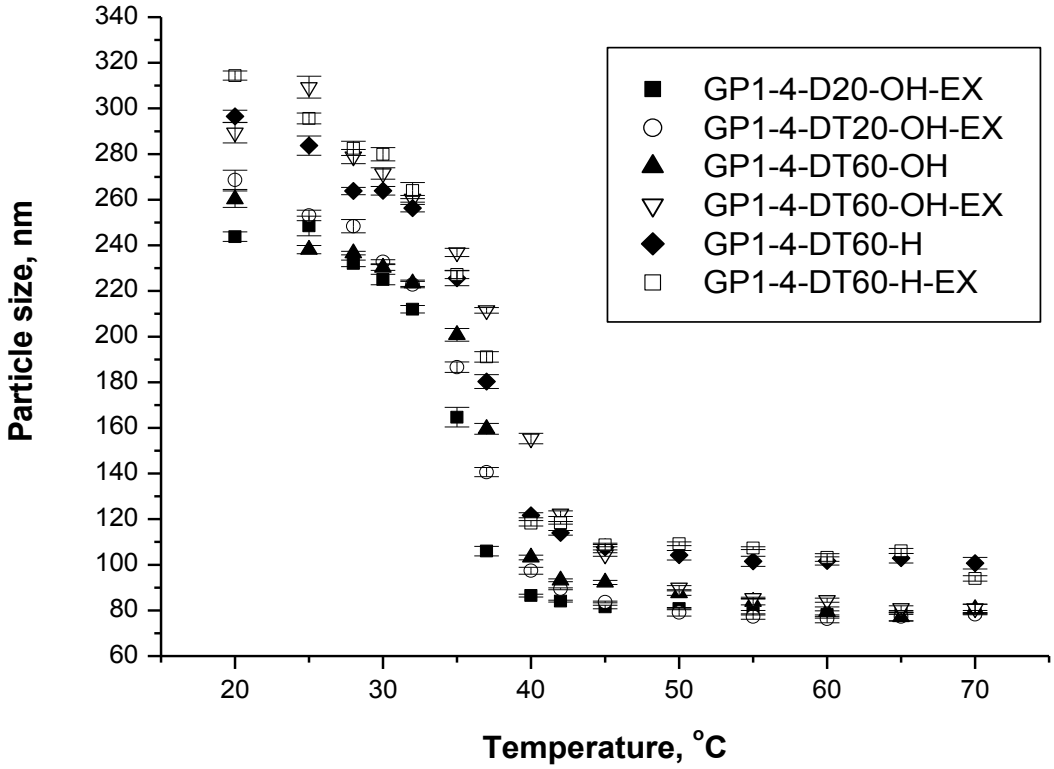


Fig. 2.7 Average particle size of **GP1-4** as a function of temperature measured in an microgel suspensions (0.2 wt %) of pH 5 in 1mM KCl solution. **GP1-4** was purified using six different procedures: **D20-OH-EX** (alkaline dialysis at 20 °C using untreated tubing), **DT20-OH-EX** (alkaline dialysis at 20 °C using treated tubing), **DT60-OH** (alkaline dialysis at 60 °C), **DT60-OH-EX** (alkaline dialysis at 60 °C followed by ion exchange), **DT60-H** (acidic dialysis at 60 °C) and **DT60-H-EX** (acidic dialysis at 60 °C followed by ion exchange).

It can be deduced by comparing **D20-OH-EX** (248.5 ± 4.3 nm, 25 °C; 79.5 ± 0.5 nm, 70 °C) and **DT20-OH-EX** (253.1 ± 2.3 nm, 25 °C; 78.3 ± 0.2 nm, 70 °C) that treatment of the dialysis tubing had no obvious effect on the average particle size over the tested temperature range. This largely eliminated the concern of possible contamination caused by weak acid residues[342,350,351] in the tubing, which required a time-consuming and chemical-involved washing procedure[342] for complete removal. Thus, cleaning the tubing solely by washing with distilled water for removal of glycerol (used as humectant)[351] was satisfactory. Regarding the dialysis temperature, although 60 °C is recommended by the manufacturer in terms of the tubing performance,[343] the state of microgel particles also needs to be taken into account. The size difference of **DT60-OH-EX** (309.3 ± 4.8 nm, 25 °C; 80.9 ± 1.9 nm, 70 °C) from **DT20-OH-EX** may indicate that 60 °C as the dialysis temperature was not so efficient for surfactant removal as RT (20 °C). This is probably because microgels were swollen at RT and less hydrophobic than they were at 60 °C. For the purification with dialysis under acidic

conditions (**DT60-H** and **DT60-H-EX**), larger particle sizes were observed in both the swollen and the shrunken states of microgels. This was in agreement with **GP1-2** and **GP1-3** and was attributed to a higher possibility of surfactant binding to microgels (**Section 2.2.2.1**). As stated before, acidic dialysis aimed to help remove counter ions, which however can be effectively achieved by ion exchange. Therefore, acidic dialysis at 60 °C is not an ideal procedure for microgel purification here and its function can also be replaced. As for alkaline dialysis or dialysis solely against distilled water, the possibility of surfactant binding was lower due to the presence of $–COO^-$. In addition, the particle sizes of **GP1-4-DT60-OH** (230-240 nm, 25 °C) were obviously smaller than that of **GP1-4-DT60-OH-EX**, (300-310 nm, 25 °C) in the swollen state. This behaviour was similar to what was observed in **GP1-2** and **GP1-3** (**Section 2.2.2.1**) and was attributed to the difference in ionic strength brought about by pH adjustment to pH 5 using either HCl or KOH.

To conclude, cleaning of dialysis tubing by solely washing with distilled water without applying the chemical-involved procedures had no significant effect on microgel purification. Acidic dialysis at 60 °C for microgel purification had a higher possibility of surfactant binding, compared to alkaline dialysis or dialysis against distilled water, and the removal of counter ions was possible with ion exchange.

2.2.2.3 Batch-to-batch variation in the particle size of synthesized microgels

The above two sections have assessed the effect of purification procedures on the particle size of **GP1** in detail. This section aims to summarize the results and reveal whether the surfactant source had a significant effect on particle sizes. The average particle sizes of microgels from four batches, i.e., **GP1-1**, **2**, **3** and **4**, were compared in microgel suspensions (0.2 wt %) of pH 5 in 1mM KCl solution (**Table 2.3**).

Table 2.3 Size comparisons among different microgel particles in aqueous suspensions

Particles	Size at 25 °C / nm	Size at 37 °C / nm	Size at 70 °C / nm	Sharpest size drop		NaDBS source	Purification procedures**
				|Δd/ΔT|*	Temp /°C		
GP1-1	275.1 ± 1.3	180.5 ± 1.7	88.3 ± 0.6	25.8	37-40	BDH	**D20-OH-EX**
GP1-2	157.6 ± 3.8	71.9 ± 2.4	49.6 ± 0.1	24.7	35-37	Aldrich	**DT60-OH**
	222.3 ± 6.6	91.5 ± 7.1	50.2 ± 0.7	43.3	35-37		**DT60-H**
	183.3 ± 4.7	88.2 ± 4.3	47.4 ± 0.4	21.1	35-37		**DT60-OH-EX**
GP1-3	158.0 ± 2.3	117.4 ± 2.0	68.3 ± 0.5	8.3	35-37	Aldrich	**DT60-OH**
	185.3 ± 3.0	147.7 ± 1.6	64.7 ± 0.3	9.4	37-40		**DT60-H**
	174.6 ± 1.3	128.1 ± 1.6	57.8 ± 0.3	10.3	37-40		**DT60-OH-EX**
GP1-4	248.5 ± 4.3	106.0 ± 2.1	79.5 ± 0.5	29.4	35-37	BDH	**D20-OH-EX**
	253.1 ± 2.3	140.6 ± 2.0	78.3 ± 0.2	23.0	35-37		**DT20-OH-EX**
	238.1 ± 1.8	159.6 ± 2.4	80.6 ± 2.1	20.1	35-37		**DT60-OH**
	309.3 ± 4.8	211.5 ± 1.2	80.9 ± 1.9	18.7	37-40		**DT60-OH-EX**
	283.7 ± 4.2	180.3 ± 3.0	100.7 ± 2.5	22.7	35-37		**DT60-H**
	295.6 ± 2.4	191.1 ± 2.3	94.0± 1.2	24.3	37-40		**DT60-H-EX**

* $|\Delta d/\Delta T|=|(d_2-d_1)/(T_2-T_1)|$, where d stands for particle size and T for temperature.
** Purification procedures (a combination of the following 4 factors):
(1) Treatment of dialysis tubing: washing with distilled water (D), followed by treatment with sodium sulphide and sulphuric acid (DT);
(2) Dialysis temperature: room temperature (20) or 60 °C (60);
(3) Dialysis type: alkaline dialysis (OH) or acidic dialysis (H);
(4) Exchange resin: whether applied (EX) or not.

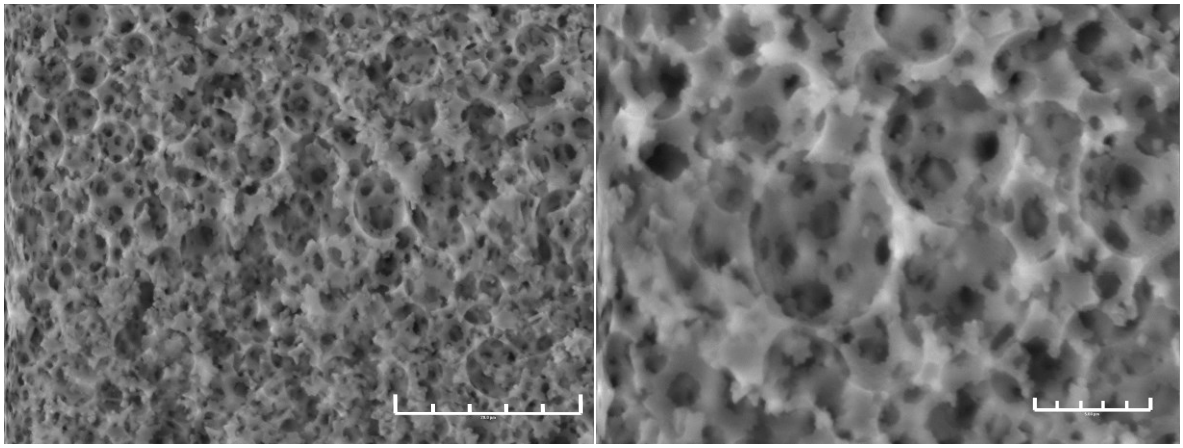
When using the same purification procedure **D20-OH-EX**, particle sizes of **GP1-4-D20-OH-EX** (270-280 nm at 25 °C and 90 nm at 70 °C) showed resemblance to **GP1-1** (240-250 nm at 25 °C and 80 nm at 70 °C), indicating the repeatability of particle preparation when using NaDBS from the same source. Comparisons between particles from **GP1-4** and **GP1-2** or **GP1-3** using the same purification procedures suggest NaDBS from a different source does have a significant effect on the particle size. Specifically, particles made using NaDBS from Aldrich are ~100 nm smaller at 25 °C and 20~30 nm smaller at 70 °C than particles made with NaDBS from BDH. This variation arising from surfactant source was explained in two aspects. Firstly, the active content of each surfactant was taken into consideration. The BDH surfactant has 80% active content with sodium sulphate as the remainder, and the Aldrich one is categorised as technical grade (purity unspecified). If it is assumed that the Aldrich one has a higher active content, it can be deduced that when the same amount (nominal concentration, 0.01 M) of surfactant is used, smaller particles[274,280,339] will be

obtained using the Aldrich surfactant. This is in agreement with our measured results. Thus, an active content of more than 80% in the Aldrich surfactant is a reasonable speculation. Secondly, since the nominal concentration of NaDBS for synthesis was not much above or close to the critical micelle concentration (CMC) of NaDBS (0.005 M[352]), an increased ionic strength in the synthesis medium by the presence of sodium sulphate in the BDH surfactant can possibly play a role in the formation of larger particles.[350]

Therefore, particle size variations can originate from the surfactant source as well as the purification process. To reduce the possibility of surfactant binding to microgels, alkaline dialysis or dialysis at room temperature is more efficient. The size variation due to microgel charges can be eliminated by using ion exchange as the final step of purification or using buffer solutions[353] as background of the microgel suspensions.

2.3 Preparation and characterisation of styrene/DVB based polyHIPEs

Prior to the investigation into microgel stabilised high internal phase emulsions (HIPEs), those stabilised by surfactant, i.e., conventional HIPEs, were prepared as a reference. Here we start with preparation of water-in-(styrene/DVB) HIPEs using non-ionic surfactant Hypermer 2296 as the emulsifier and production of a conventional polyHIPE since styrene (St) and DVB have been widely investigated as the oil phase in conventional HIPEs and polyHIPEs,[128,136,143,213,354-359] and Hypermer 2296 (HLB 4.9) has proved to be an efficient surfactant for w/o HIPE.[145,191] Morphologies of the resultant polyHIPEs are shown in **Fig. 2.8**.



(a) scale bar 20 μm (b) scale bar 5 μm

Fig. 2.8 SEM images of St/DVB based polyHIPEs. For preparation, an oil phase consisting of 4 ml styrene, 4 ml DVB, 1 mol % AIBN and 2 ml Hypermer 2296 and an aqueous phase containing 40 ml 0.068 M KCl solution were used.

The pores in the polyHIPEs were well interconnected (**Fig. 2.8**). Pore sizes were 3~8 μm in diameter while sizes of the pore throats were in the range of 0.5~2.5 μm. These sizes were in close agreement with those of a reported polyHIPE,[145] prepared using identical procedures and compositions except $CaCl_2$ (0.03 M) as the electrolyte. Both of these polyHIPEs exhibited small pore sizes due to the use of a relatively high salt concentration.[128] Besides morphology, other physical properties of the polyHIPEs (**Table 2.4**), including skeleton density, envelope density, porosity and BET surface area, were also comparable to the reported values.[145]

Table 2.4 Physical properties of styrene/DVB based polyHIPEs

Skeleton density /g.cm^{-3}	Envelope density /g.cm^{-3}	Porosity /%	BET surface area (at p/p° =0.200) /m² g^{-1}
1.13	0.16	85.7	4.90

2.4 Preliminary investigations of microgel particle stabilised emulsions

To prepare polyHIPEs based on microgel stabilised emulsions, efforts should be made to address three questions: (1) whether emulsions or HIPEs can be stabilised by our synthesised poly(NIPAAm-*co*-AA) microgels; (2) what types of emulsions can be obtained; (3) how stable the emulsions are. The emulsion type is important because the polymerisable components need to be incorporated into the continuous (external) phase of the emulsions for preparation of a polyHIPE.[89,360] Meanwhile, the emulsion stability needs to be maintained throughout the polymerisation process in order to obtain polyHIPEs.

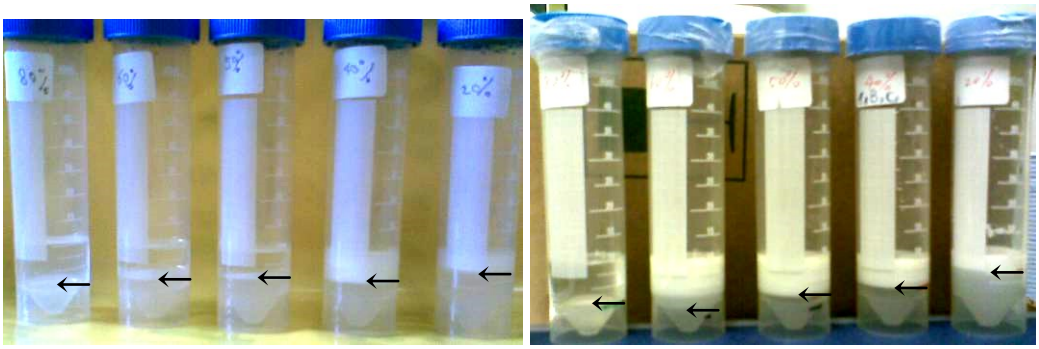
In this study, a water-oil system made up with an aqueous suspension of poly(NIPAAm-*co*-AA) microgels (**GP1**) and DVB was used. The aqueous suspensions for emulsification were prepared in the same way as those used for particle size measurements, i.e., suspensions in KCl solutions with known KCl concentration, pH and particle concentration, which could facilitate the correlation[235] of microgel behaviours in the suspensions and their efficiency for emulsification. Initially, microgel suspensions prepared using 1 mM KCl, pH 5 and variable microgel concentration were selected, since the microgel behaviour in these suspensions was well studied (**Section 2.2.1**). For the oil phase, DVB was used as the sole polymerisable

component (without styrene),[128,361-363] and AIBN was added in the cases where polymerisation was desired. The effects of phase volume ratio, microgel concentration and preparation temperature on the type and stability of microgel-stabilised emulsions were all of concern. Since temperature played a key role in determining the behaviour of **GP1**, a step of pre-mixing the two phases in a tube prior to emulsification was adopted, which allowed for temperature control by placing the tube into a thermostatted bath during emulsification. The available methods included hand shaking[321] and homogenisation with a rotor-stator homogeniser as discussed below. Binks *et al.*[152] found that the speed of a homogeniser ranging from 8,000 rpm to 24,000 rpm had little effect on the drop diameters of water in toluene emulsions (ϕ_w= 0.1) that were stabilised by 2 wt % of H30 hydrophobic silica. Thus, the homogenisation speed was not considered to be an important variable in our study and a speed of 15,000 rpm was selected for all emulsifications.

2.4.1 Effect of phase volume ratio on the stability of microgel stabilised emulsions

When DVB is used as the oil phase, w/o HIPEs are targeted in order to prepare polyHIPEs.[89,360] However, it is not a simple process due to two challenging aspects. On one hand, a tendency to o/w rather than w/o emulsions was reported for systems using polyNIPAAm-based microgel particles as emulsifiers.[233,235,364,365] On the other hand, increasing the internal phase volume of particle-stabilised emulsions (also known as Pickering emulsions[146,147]) above ca. 70% may lead to phase inversion,[152,321,366] indicating volume phase ratio is an important factor in determining emulsion type and stability. Therefore, we initially studied whether w/o emulsions and HIPEs were obtainable by varying the phase volume ratio.

At a fixed aqueous composition (1 mM KCl, pH 5 and 0.2 wt % microgels), 10 ml water-oil mixtures of various DVB ratios (ϕ_{DVB}) were emulsified via hand shaking or homogenizing with a rotor-stator homogeniser. The maximum ϕ_{DVB} that could be emulsified was 40% [**Fig. 2.9** (a)] by shaking but was over 60% [**Fig. 2.9** (b)] by homogenising. This indicated that homogenising could provide sufficient energy to produce relatively concentrated emulsions.

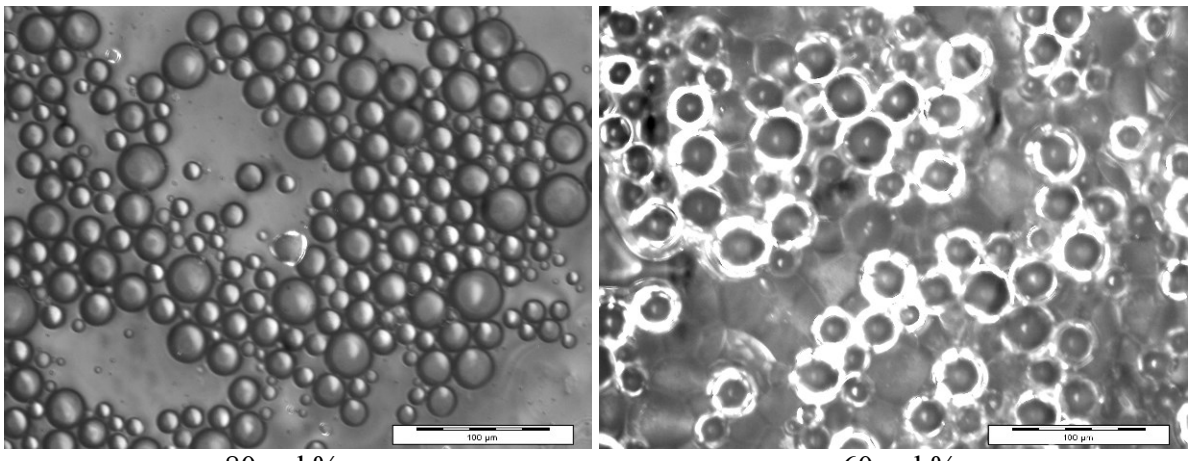


(a) Emulsification by hand shaking (b) Emulsification by homogenizing

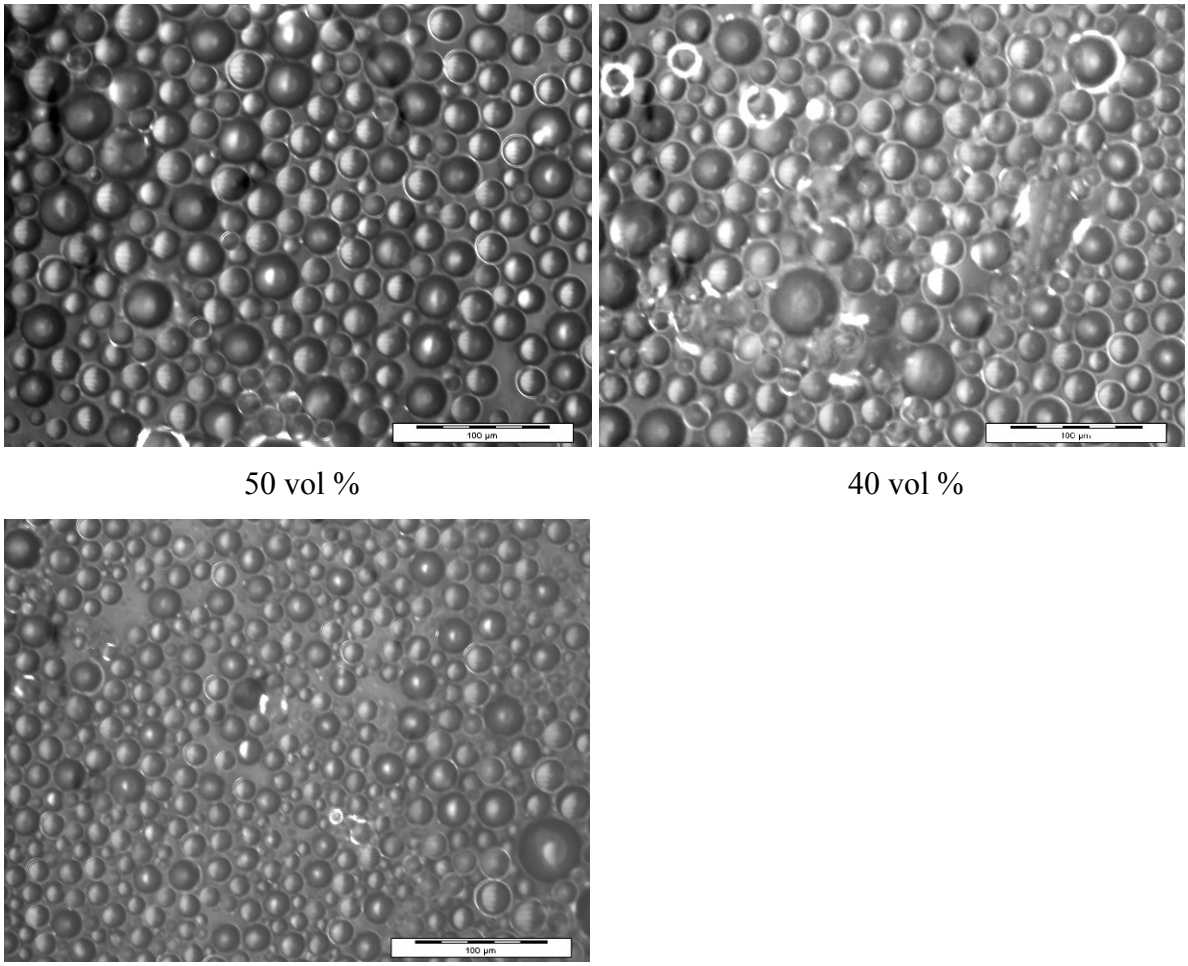
Fig. 2.9 Photographs of 10 ml microgel aqueous suspension-DVB mixtures of various ratios after emulsified by hand shaking (a) and by homogenizing (b). The volume ratios of DVB (from left to right) are 80%, 60%, 50%, 40% and 20%, respectively in both groups. Arrows indicate the boundaries after phase volumes became stable.

Table 2.5 Summary of the emulsions prepared using various DVB ratios

DVB ratio, vol %	80	60	50	40	20
Aqueous suspension	1 mM KCl, pH 5 and 0.2 wt % microgel particles				
Emulsion type	o/w	o/w	o/w	o/w	o/w
$V_{emulsion,\ 20\ min}$, ml	<2.5	>8.0	>8.0	9.75	10
$V_{emulsion,\ 20\ h\ or\ more}$, ml	<2.5	>8.0	7.5	5.5-6.0	3.0
Max $_{droplet\ size}$, μm	40-45	40	35-40	~35	35-40
Min $_{droplet\ size}$, μm	5-10	10-15	~15	10-15	5-10



80 vol % 60 vol %



50 vol %

40 vol %

20 vol %

Fig. 2.10 Optical microscope images of the droplets taken from emulsions prepared by homogenizing microgel suspension-DVB mixtures at various DVB ratios after emulsion volumes became stable (Scale bar 100 μm)

Droplet morphology (**Fig. 2.10**) and the variation in emulsion volume (**Table. 2.5**) were also characterised. The emulsion type of those prepared using a DVB ratio (ϕ_{DVB}) from 20 vol % to 60 vol % can be easily determined to be o/w because creaming occurred after homogenising and the emulsion droplets were on the top. This was not surprising, since microgel particles were in their swollen state under the preparation conditions (**Fig. 2.2**) and were hydrophilic enough to stabilise o/w emulsions.[233,235] For the sample prepared using a ϕ_{DVB} of 80%, the possibility of the droplets being w/o emulsions due to a catastrophic inversion[150,152,235,366] was ruled out, since more than 90% of the DVB liquid was on the top (**Table 2.5**). This was similar to a reported case by Yan *et al.*,[367] where an aqueous suspension containing hydrophilic silica particles (contact angle 60°) was mixed with 80% toluene. Ngai *et al.*[235] reported the occurrence of a catastrophic inversion from o/w to w/o with increasing oil volume ratio at or above 0.6 at 25 °C in an octanol-water system stabilised

by poly(*N*-isopropylacrylamide)-*co*-(methacrylic acid) [poly(NIPAAm-*co*-MAA)] microgels at pH 9.4. This indicates that the phase with relatively higher volume ratio does form the continuous phase. However, our DVB-in-water emulsions were attainable at ϕ_{oil} of 0.6, which raised the question of what exactly determined the phase volume ratio for catastrophic phase inversion. On one hand, the nature of the oil phase[368] may play a role since the interfacial tension of octanol-water (8.5 $mN.m^{-1}$, 20 °C) was much lower than that of DVB-water (35-38 $mN.m^{-1}$, 20 °C) in the absence of any surface-active agents.[369] The low interfacial tension would contribute to the instability[360,370] against phase inversion. On the other hand, the hydrophobicity[149,150,371] of microgel particles had a significant effect on the phase inversion. Stiller *et al.*[371] showed that 80 vol % oil was dispersed phase when using relatively hydrophilic TiO_2 particles as the emulsifiers whereas 40 vol % oil was able to form the continuous phase when TiO_2 particles of relatively high hydrophobicity were used. However, further reduction of the oil volume ratio to 30% resulted in catastrophic inversion while further increase of the particle hydrophobicity led to phase separation.[371] Their results provided valuable insight into the effect of particle hydrophobicity on the volume ratio limit for catastrophic inversion. From this point of view, it was suggested that poly(NIPAAm-*co*-AA) microgel particles were currently still too hydrophilic and w/o HIPEs might only be obtainable when microgel particles became more hydrophobic.

Therefore, when emulsification was carried out at RT using microgel suspensions of pH 5, only o/w emulsions were obtained regardless of the phase volume ratio due to the hydrophilic nature of swollen microgel particles.

2.4.2 Effect of particle concentration on stability of microgel-stabilised emulsions

The particle concentration also has a profound influence on the resultant emulsions[235,321-323,372,373] and in some cases even on the emulsion type.[322,373] Therefore, trials were made to confirm whether w/o emulsions were obtainable by varying particle concentration while keeping other conditions constant (RT, 1 mM KCl, pH 5 and 40 vol % DVB). In this study, the microgel concentration in the aqueous phase was increased from 0.020 wt % to 0.40 wt %. The photos of homogenised samples after creaming (**Fig. 2.11**) hardly shows any obvious difference. However, the effect of particle concentration manifest when comparing the droplet morphologies (**Fig. 2.12**) and the emulsion stability (**Table 2.6**).



Fig. 2.11 Photographs of 10 ml emulsions prepared using 40 vol % DVB and various microgel concentrations in the aqueous suspension: (from left to right) 0.02 wt %, 0.1 wt %, 0.2 wt % and 0.4 wt%. The dash lines indicate the boundaries after creaming.

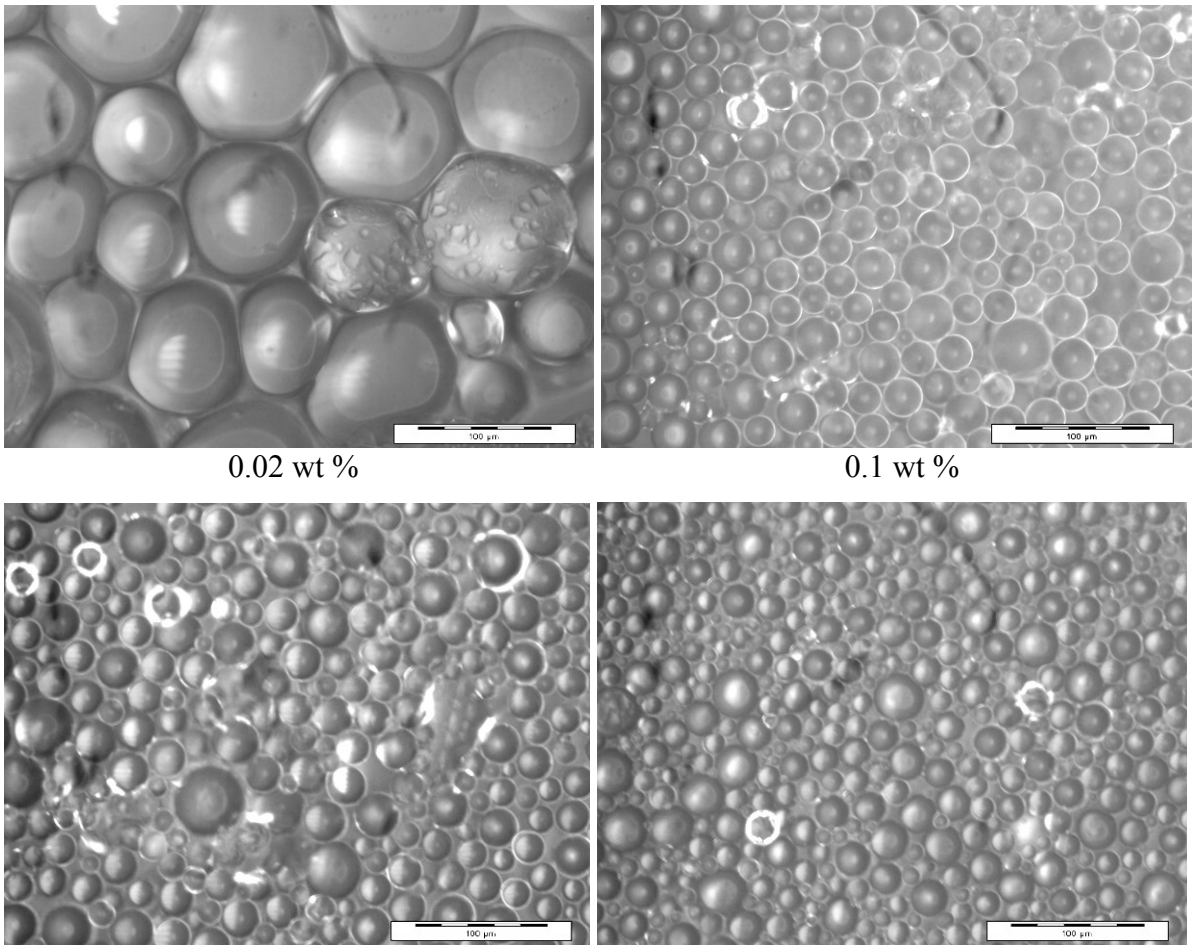
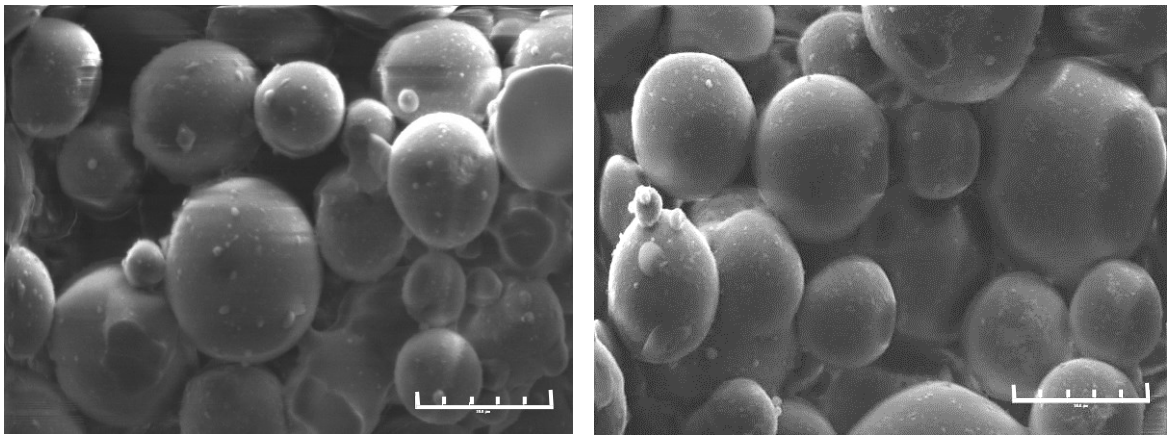


Fig. 2.12 Optical microscope images of droplets from emulsions prepared using the same DVB ratio of 40 vol % but various microgel concentrations ranging from 0.02 wt % to 0.4 wt % (Scale bar 100 μm).

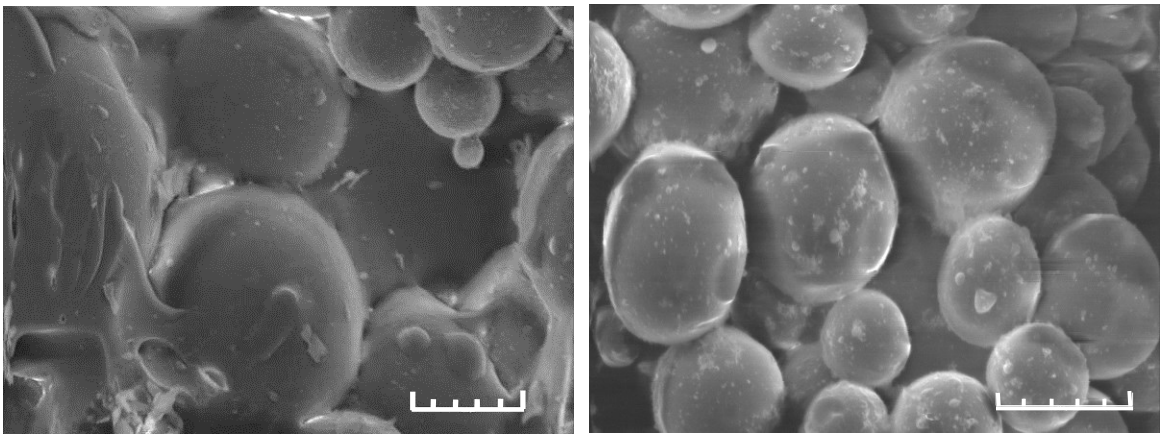
Table 2.6 Summary of the emulsions prepared using various microgel concentrations

Composition	DVB ratio, vol %	40			
	microgel concentration, wt %	0.02	0.1	0.2	0.4
	pH	5			
	KCl concentration, M	0.001			
Emulsion type		o/w	o/w	o/w	o/w
$V_{emulsion,\ 20\ min}$, ml		5.8	7.5	9.75	10
$V_{emulsion,\ 20\ h\ or\ more}$, ml		5.5	5.5	5.5-6.0	5.5
$Max_{\ droplet\ size}$, μm		>100	30-35	~35	35-40
$Min_{\ droplet\ size}$, μm		~50	10-15	10-15	5-10

When different amounts of particles were used for emulsion preparation, the emulsion volumes after aging for 20 h were similar for all four samples (**Fig. 2.11**), although the initial emulsion volumes ($V_{emulsion,\ 20\ min}$) increased with increasing particle concentration (**Table 2.6**). Moreover, the emulsion type remained o/w regardless of the particle concentration. The reported phenomenon of phase inversion from o/w to w/o induced by increasing the concentration of silica particles[322,373] was not observed. However, with increasing particle concentration, the droplet size reduced. At low particle concentration, limited coalescence[321,374-376] occurred, i.e., coalescence of smaller droplets whose interfaces were not sufficiently covered by the particles to form larger drops, which were sufficiently stabilised against further coalescence. In addition, the o/w emulsions containing AIBN (half-life at 70 °C about 4.1 h[377]) were polymerised at 70 °C and led to brittle products after purification and drying consisting of fused polymer beads (**Fig. 2.13**). Therefore, in order to make poly(DVB) Pickering-HIPEs rather than fused spheres, the oil phase should be the continuous phase for polymerisation.[89,360]



ϕ_{DVB}= 60%, 0.2 wt % microgels (scale bar 30 μm) ϕ_{DVB}= 50%, 0.2 wt % microgels (scale bar 30 μm)



ϕ_{DVB}= 40%, 0.02 wt % microgels (scale bar 50 μm) ϕ_{DVB}= 40%, 0.1 wt % microgels (scale bar 30 μm)

Fig. 2.13 SEM images of the polymerised products of DVB-in-water emulsions prepared using various DVB ratios and microgel concentrations at pH 5

2.4.3 Effect of preparation temperature on the stability emulsions

In the above two sections, the emulsions that were prepared at RT using pre-mixed microgel suspensions of pH 5 and DVB turned out to be o/w emulsions, and it was clear that phase volume and microgel concentration had no direct influence on the emulsion types. Since microgel particles were in their swollen state at RT and held a considerably high level of water in their networks,[264,279,332-335] they exhibited a relatively high hydrophilicity so that only o/w emulsions can be stabilised. To make microgel particles less hydrophilic and to obtain microgel stabilised w/o HIPEs, measures that can be taken according to **Section 2.2.1** include increasing temperature and/or decreasing pH. In this section, trials were made by emulsifying 2 ml DVB and 8 ml microgel suspension at increased temperatures: 40 °C, 50 °C and 65 °C, while pH of the microgel suspension (0.2 wt % microgels in 1 mM KCl) was

maintained at pH 5. These three temperatures were selected to see how poly(NIPAAm-*co*-AA) microgel particles behaved as emulsifiers in three states (**Fig. 2.4**): (1) particles were still swollen at 40 °C but about to undergo the VPT; (2) at 50 °C, microgel particles shrank and just passed the VPT; (3) at 65 °C, microgel particles were in their collapsed state.

Stability of the resultant emulsions was recorded at RT (**Table 2.7** and **Fig. 2.14**). For emulsions prepared at 40 °C, the microgel suspension and DVB were almost fully emulsified, similar to those prepared using the same compositions but at RT. For 50 °C as the preparation temperature, solid clusters were observed in the emulsion part, which were attributed to aggregated microgels. Meanwhile, most of the aqueous solutions appeared as a separate phase in the cases of 50 °C and 65 °C, suggesting microgel particles were not efficient emulsifiers at these temperatures. It was interesting to note that aggregation did not appear in the microgel suspensions alone above the VPTT. The aggregation occurred possibly at the oil-water interface[364,378] during the emulsification process. Therefore, it is important to keep particles from aggregating at the water-oil interface when reducing the hydrophilicity of microgel particles by increasing the temperature.

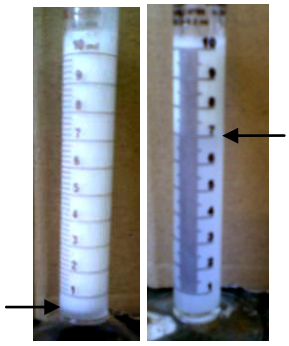


Fig. 2.14 Photographs of emulsions prepared at 40 °C (left) and 50 °C (right). The arrows indicate the position of interface immediately after emulsions were transferred into cylinders.

Table 2.7 Stability of microgel-stabilised emulsions prepared at various temperatures

Preparation temperature, °C	40	50	65
Volume of emulsions at t = 0, ml	9.6	3*	2.6**
Volume of emulsions at t = 1 h, ml	9.6	3	-
Volume of emulsions at t =18 ~19 h, ml	3.8	3	2.6

* Some solid clusters were observed inside the emulsions. ** About 0.2 ml clear DVB was on the top.

To summarise **Section 2.4,** it was found that swollen-state microgel particles at pH 5 were hydrophilic so that only o/w Pickering emulsions were produced regardless of variation of

phase volume ratio from 20% to 80%, or variation of particle concentration from 0.02 wt % to 0.4 wt %. Meanwhile, attempts to prepare HIPEs using shrunken microgel particles at pH 5 above the VPTT, either at 50 °C or at 65 °C, resulted in phase separation during homogenisation due to microgel aggregation. To prepare the desired w/o emulsions, it is essential to further reduce the hydrophilicity of microgel particles without causing microgel aggregation at the interface.

2.5 Investigation of the thermal sensitivity of microgel stabilised emulsions

According to **Fig. 2.2**, increasing the pH above 5 renders microgel particles more hydrophilic; therefore it becomes less likely to produce w/o emulsions. In order to prepare microgel stabilised w/o HIPEs and the corresponding polyHIPEs, microgel suspensions of pH lower than 5 were investigated, including pH 2.5, pH 3 and pH 4. The oil phase (DVB) was used at a phase ratio of 40 vol % to verify the availability of w/o emulsions (this section) and was used at 20 vol % to prepare the polyHIPEs (**Section 2.6**). The thermal sensitivity of the emulsions produced at these three pH was investigated, i.e. the effect of temperature – including the preparation temperature and the aging temperature – on the stability and the type of emulsions. A list of the preparation temperatures and the aging temperatures for stability assessment is referred to **Table 7.3** (**Section 7.4.2.2**).

2.5.1 Effect of the preparation temperature on emulsion stability investigated at pH 3

An investigation into the effect of preparation temperature on the emulsion stability of was carried out using three temperatures (**Table 2.8**) for the emulsification of 6 ml microgel suspension (pH 3, 0.4 wt % microgels and 1 mM KCl) and 4 ml DVB. Since emulsification using a rotor-stator homogeniser (15,000 rpm for 2.5 min, 2 min's pause applied every 30 s) caused temperature increase, 10 ml emulsions were obtained only when a water bath of 18.5 °C was used. Partial or complete phase separation occurred for emulsification at RT without temperature control or at 34 °C. This indicated that the preparation temperatures from start to end should affect the emulsion stability. Microgels in the aqueous suspension (0.4 wt %) reached their minimum sizes at 32 °C and started to aggregate upon further increasing the temperature (**Fig. 2.15**). Therefore, the phase separation observed at preparation temperatures

above 32 °C was attributed to microgel aggregation. However, subsequent polymerisation of the obtained emulsions (AIBN as the initiator) at 70 °C led to phase separation as indicated by **Fig. 2.16**. This was likely due to microgel aggregation during polymerisation. In addition, it is noticed that the swelling-deswelling behaviour of microgels presented in **Fig. 2.15** was similar to those presented in **Fig. 2.1** and **Fig. 2.2**, although the microgel concentration here (0.4 wt %) was four-, thirteen- and eleven-times of those at pH 2.5, 3 and 4, respectively.

Table 2.8 10 ml microgel suspension-DVB mixture emulsified at different temperatures

No.	**1**	**2**	**3**
Temp $_{Start}$, °C	18.5 (water bath used)	22 (RT, no bath used)	34 (water bath used)
Temp $_{End}$, °C	22	33~34	34
Outcome	Emulsions	Phase separation	Phase separation

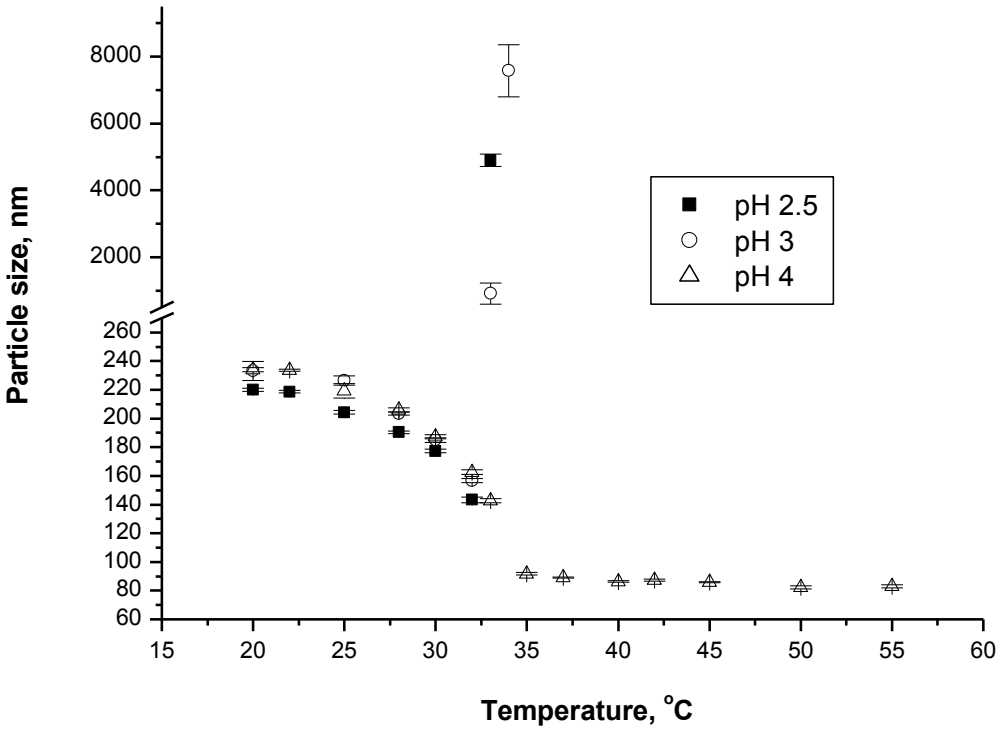


Fig. 2.15 Average particle size of poly(NIPAAm-*co*-AA) microgels as a function of temperature. The measurements were carried out using microgel suspensions (0.4 wt %) in 1 mM KCl solutions of pH 2.5, 3 and 4, respectively.

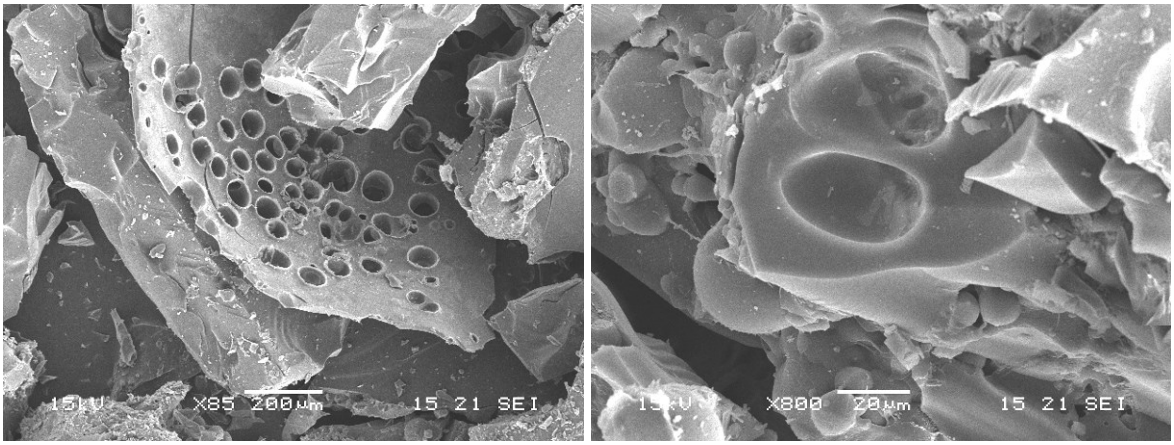


Fig. 2.16 SEM images of the polymerised product of DVB-in-water emulsions prepared at pH 3

It is deduced from the above investigation at pH 3 that the thermal sensitivity of microgel stabilised emulsions needs to be considered during emulsification and polymerisation in order to avoid phase separation. It is essential to prepare a stable emulsion and to study its stability against temperature prior to investigation into whether polyHIPEs could be obtained.

2.5.2 Creaming of microgel stabilised emulsions investigated at pH 2.5, pH 3 and pH 4

Since emulsification using a 18.5 °C water bath led to stable emulsions (22 °C) (**Table 2.8**), we standardise the emulsification conditions by using a water bath of 15~16 °C and study the stability of the resultant emulsions at various aging temperatures. This section discusses the emulsion stability at aging temperatures of 25 °C and 32 °C. These two temperatures were chosen based on **Fig. 2.15**. Phase separation with aggregated microgels forming a network on the tube wall was observed when emulsions prepared at pH 3 were aged at 37 °C (above the VPTT). Creaming was observed over time and was characterised using the variation of creaming volume ratio with time, i.e. $V_{creaming}$ / V = f (t) (**Fig. 2.17**). $V_{creaming}$ denotes volume of the aqueous solution below the emulsions and V stands for total volume of the sample. Thus, the values of $V_{creaming}$ / V can indicate the creaming extent while the slope of the plot (after lined) indicates the creaming rate. Meanwhile, the occurrence of creaming to these microgel-stabilised emulsions indicated that they were o/w emulsions below the VPTT of microgel particles. This method for assessing the stability to creaming is similar to the one reported by Bink *et al.* that the increase with time of the position of the clear water-emulsion interface was monitored.[150]

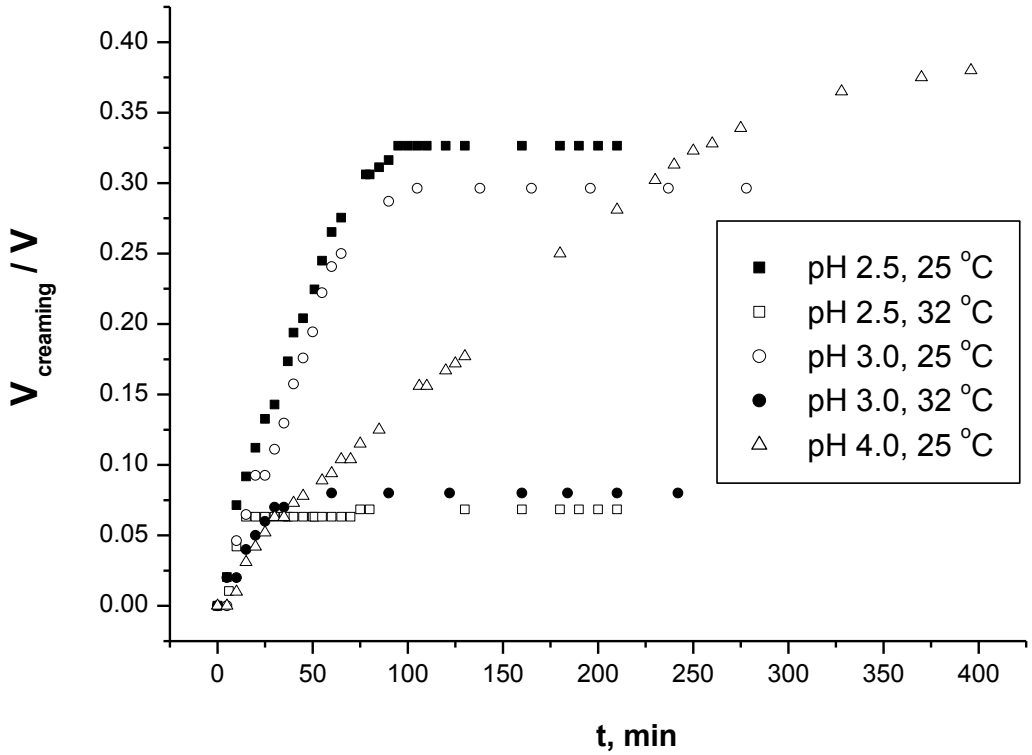
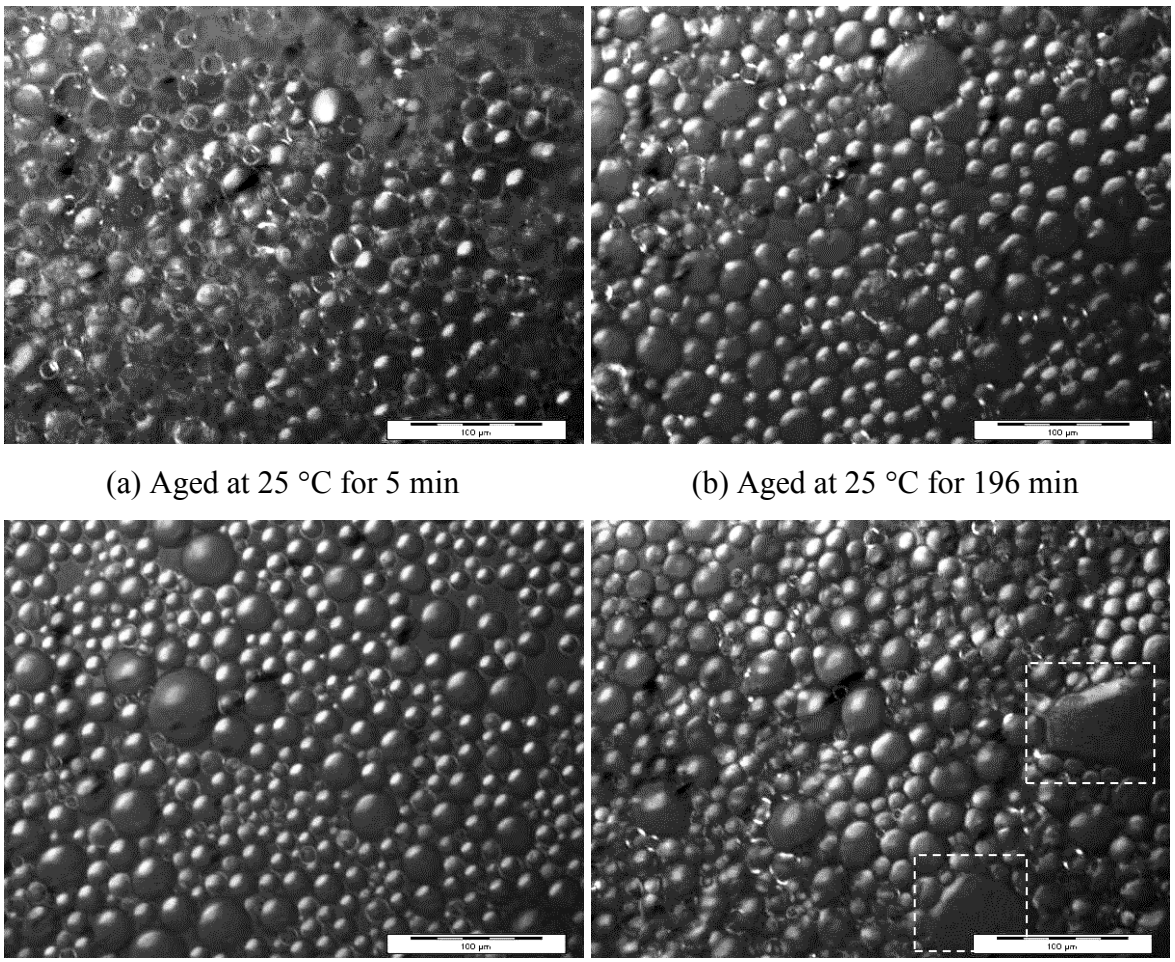


Fig. 2.17 The creaming volume ratios of microgel-stabilised emulsions as a function of time after aged at 25 °C and 32 °C. (Error of volume: ± 0.1 ml.) Emulsions were prepared using 40 vol % DVB and microgel suspensions (0.4 wt %) in 1 mM KCl solution of pH 2.5, 3 and 4, respectively.

It was clearly shown (**Fig. 2.17**) that the creaming volume ratio ($V_{creaming}$ / V) was significantly reduced at 32 °C, compared to 25 °C for both pH 2.5 and pH 3. This was explained from the point of view of the 3-D microgel network[152,379,380] around emulsion droplets. Destribats *et al.* reported that core-shell structured polyNIPAAm microgel particles at the interface of o/w emulsions connected with each other through their deformed shells forming an entangled filament network.[381] We believe that formation of such a microgel network around the emulsion droplets also fits our poly(NIPAAm-*co*-AA) particles due to the structural similarity to polyNIPAAm microgels and a complete protonation[303] of the PAA moieties at pH 2.5 or pH 3. A stronger particle network was expected to withstand the buoyancy of o/w emulsion droplets so that further motion of droplets upwards was restricted. With a temperature increase from 25 °C to 32 °C, particle size decreased from 204 nm to 143 nm at pH 2.5 and from 227 nm to 157 nm at pH 3 (**Fig. 2.15**). This indicated that particles became less hydrophilic due to deswelling, which resulted in increased attractive inter-particle interactions,[266,288,292,305] and thus enhanced the stability of the particle network. Meanwhile, the aging process was traced using optical micrographs of the emulsion droplets.

Taking emulsions prepared at pH 3 as an example (**Fig. 2.18**), no obvious differences in drop size were shown during aging at either 25 °C or 32 °C except that some bigger droplets visible [**Fig. 2.18** (d)]. This was a sign of coalescence in local areas because 32 °C was so closed to the aggregation temperature of microgels at pH 3.



(a) Aged at 25 °C for 5 min (b) Aged at 25 °C for 196 min

(c) Prior to aging at 32 °C (d) Aged at 32 °C for 210 min

Fig. 2.18 Optical microscope images of emulsions taken at the beginning of aging and after emulsion volumes became stable (scale bar 100 μm). Emulsions were prepared using 40 vol % DVB and microgel suspension (0.4 wt %) in 1 mM KCl of pH 3. The temperatures of emulsions after homogenisation were 22.5 °C for (a)(b) and 21 °C for (c)(d), respectively.

As for the creaming rate, a comparison was made at aging temperature of 25 °C among emulsions prepared using 40 vol % DVB and microgel suspensions of pH 2.5, 3 and 4, respectively. The creaming rate at pH 4 was about one third of that at pH 3 or pH 2.5 (**Fig. 2.17**). This was attributed to the increased electrostatic repulsion among the oil droplets arising from the ionisation of carboxyl groups of microgels at pH 4.[301-303] It was also interesting to observe that increasing pH from 2.5 or 3 to 4 only reduced the creaming rate

rather than the creaming extent at 25 °C whereas increasing temperature from 25 °C to 32 °C significantly reduced the creaming extent at pH 2.5 or 3. This indicated that a stronger particle network formed due to the increase of inter-particle attraction was more efficient to reduce creaming, while the pH-induced increase of the electrostatic repulsion among emulsion droplets did not reduce creaming but significantly slow down the process.

In addition, Ngai *et al.* reported that the octanol-in-water emulsions stabilised by poly(NIPAAm-*co*-MAA) microgels became unstable below pH 6 and underwent phase separation below pH 3.[233,235] This was in contrast to the fact that our microgel particles of **GP1** were capable of stabilising o/w emulsions at pH 2.5. This was attributed to the nature of oil used rather than the difference between PAA and PMAA since carboxyl groups in both particles were fully protonated at or below pH 3.[303] Due to a much lower interfacial tension of octanol (8.5 $mN.m^{-1}$) than that of DVB (35-38 $mN.m^{-1}$)[369], the desorption energy of particles from the octanol-water interface was significantly lower according to Equation (1.1), which facilitated phase separation of the emulsions. Brugger *et al.* also investigated the stimuli-sensitivity of poly(NIPAAm-*co*-MAA) microgel-stabilised emulsions and found that phase separation occurred to the octanol-in-water emulsions rather than to the toluene-in-water emulsions when adding acid.[364] This further confirms our analysis since toluene has a similar interfacial tension (36.1 $mN.m^{-1}$)[369] to DVB.

To summarise, o/w emulsions were resulted at pH 2.5 and pH 3 due to the hydrophilic nature of microgel particles. These emulsions were stable to phase separation at temperatures below 32 °C and exhibited improved stability against creaming upon temperature increase from 25 °C to 32 °C. Since microgels aggregated above 32 °C at pH 2.0-3.5 (**Fig. 2.1**) rather than at pH 4.0 (**Fig. 2.15**), microgels at pH 4 were expected to be less hydrophilic after further deswelling above the VPTT and thus to possibly stabilise the desired w/o emulsions.

2.5.3 Thermal sensitivity of microgel-stabilised emulsions investigated above the VPTT at pH 4

Since microgel particles of poly(NIPAAm-*co*-AA) did not aggregate above the VPTT at pH 4 (**Fig. 2.2** or **Fig. 2.19**), the preparation temperature for microgel-stabilised emulsions was varied in the investigation of their thermal sensitivity. On the other hand, the effect of particle concentration on the emulsion stability was studied at pH 4 using suspensions containing 0.40 wt % and 0.80 wt % microgels for emulsification with DVB, respectively.

The size variation of particles in the two suspensions was measured as a function temperature (**Fig. 2.19**). It is noticed that the VPT process of mirogels remained identical to the one presented in **Fig. 2.2**, despite ten-fold (0.4 wt %) or 20-fold (0.8 wt %) more microgels used here. However, particle concentration did affect the measured size in the swollen state, which was similar to that at pH 5 as discussed in **Section 2.2.1.3**.

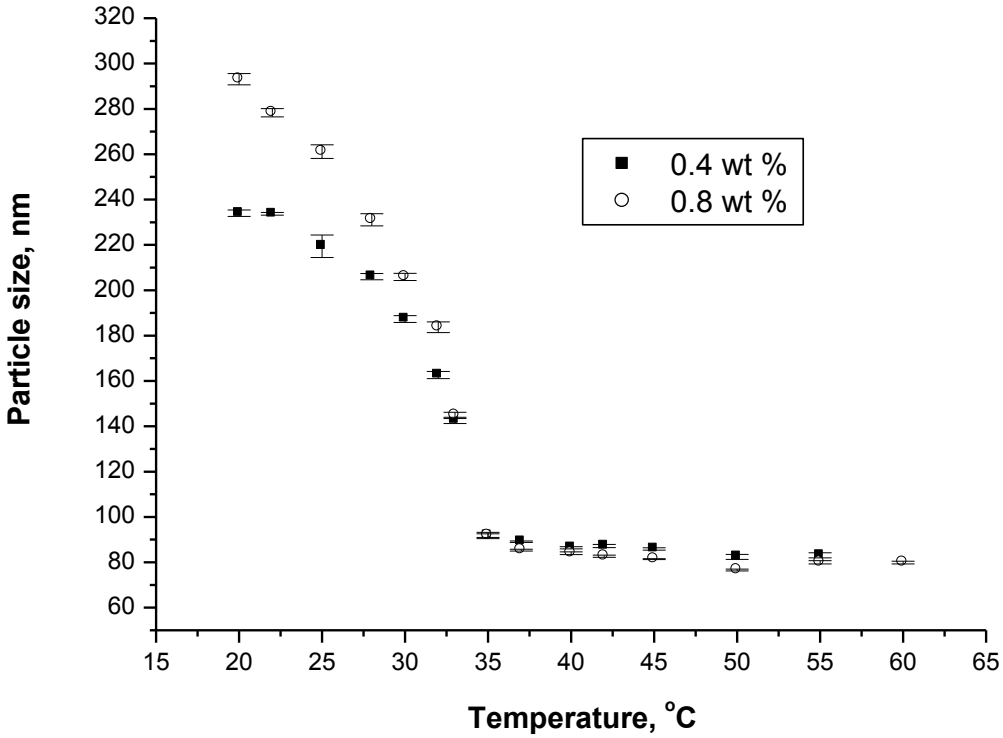
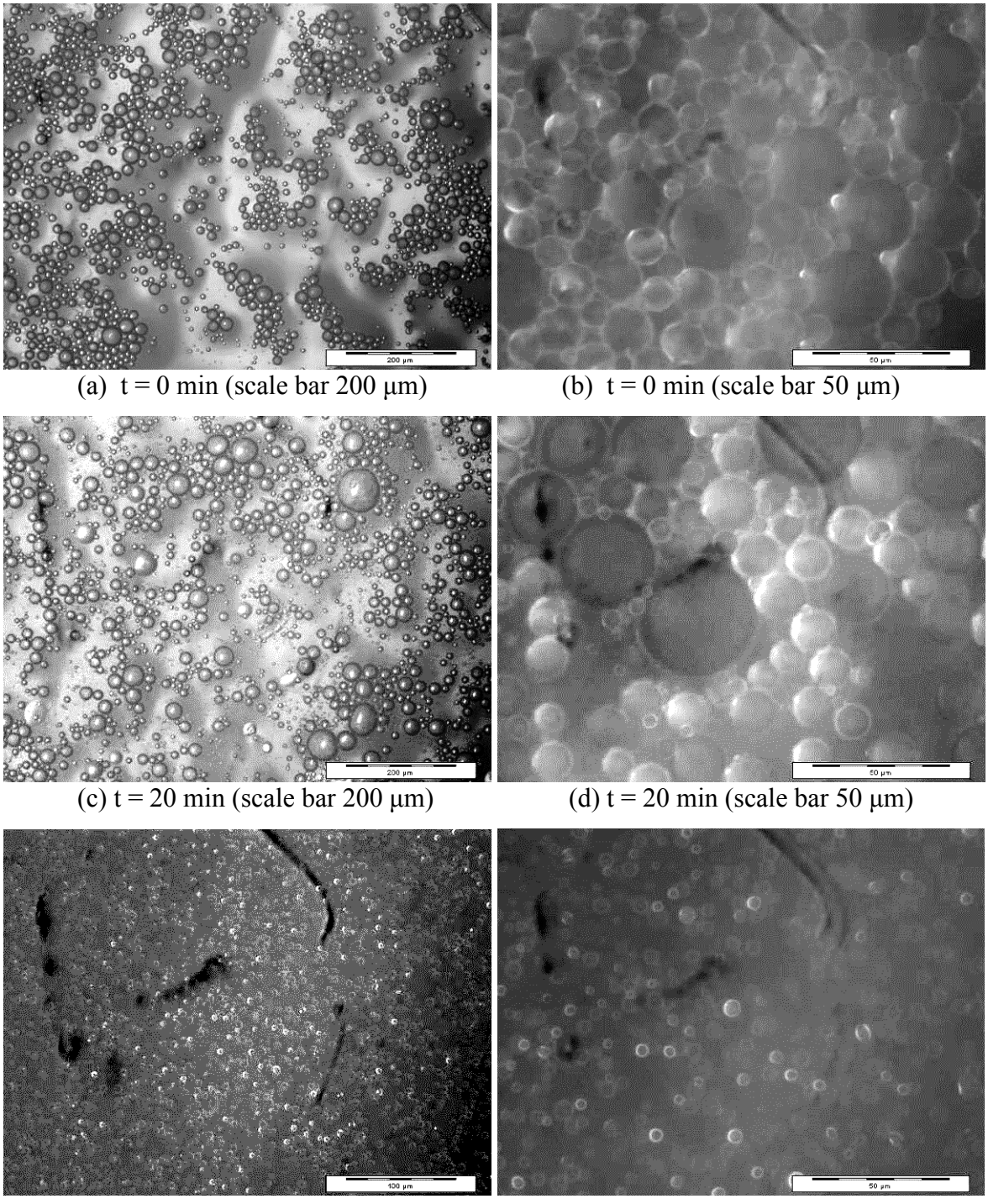


Fig. 2.19 Average particle size of poly(NIPAAm-*co*-AA) microgels as a function of temperature measured using microgel suspensions with 0.4 wt % and 0.8 wt % microgels, respectively. The suspensions were prepared using 1 mM KCl solution as the background and were adjusted to pH 4 prior to measurement.

2.5.3.1 Thermal sensitivity of microgel-stabilised emulsions prepared at pH 4 using different temperatures

In this study, 15 °C, 37-38 °C and 50 °C were used as the temperatures for emulsification of microgel suspension-DVB mixtures (0.4 wt % microgels in 1 mM KCl of pH 4, 40 vol % DVB) while 50 °C was chosen as the aging temperature of the resultant emulsions. The use of 15 °C as the emulsification temperature aimed to obtain emulsions around RT (< VPTT); emulsification at 37-38 °C – slightly above the VPTT (**Fig. 2.19**) and around the body temperature – was of significance when considering scaffold fabrication via injection of

emulsions into the body; a temperature well above the VPTT of microgel particles (50 °C) could demonstrate the efficiency of shrunken microgels as the emulsifier.



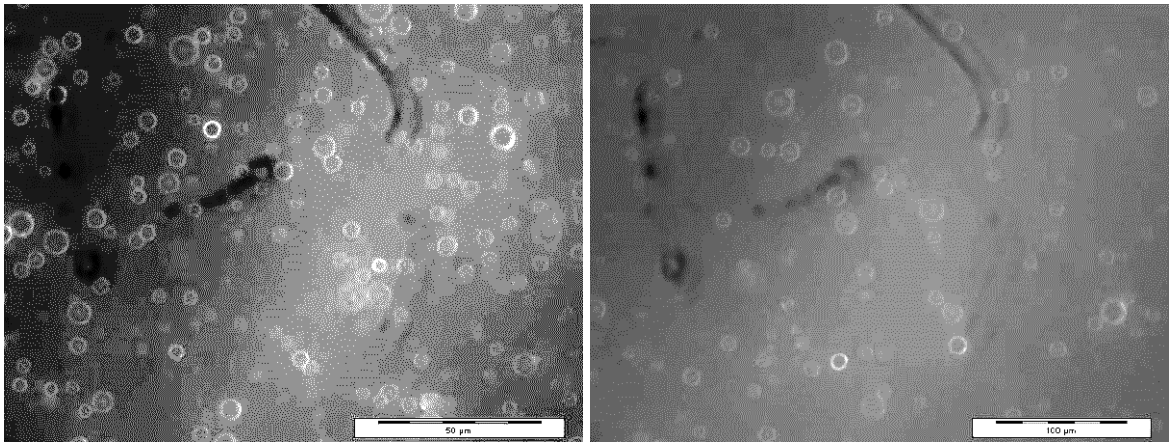
(a) t = 0 min (scale bar 200 μm) (b) t = 0 min (scale bar 50 μm)

(c) t = 20 min (scale bar 200 μm) (d) t = 20 min (scale bar 50 μm)

(e) t = 2.5 h (scale bar 100 μm) (f) t = 2.5 h (scale bar 50 μm)

Fig. 2.20 Optical micrographs of microgel-stabilised emulsions taken after emulsification at 15 °C and during aging at 50 °C. Emulsification was carried out using a microgel (0.4 wt %) suspension in 1 mM KCl solution of pH 4 and 40 vol % DVB.

Optical microscope images of emulsions taken just after preparation at 15 °C and during aging at 50 °C (**Fig. 2.20**) suggested the occurrence of a transition from o/w to w/o emulsions. This was also identified by "drop tests", i.e. inferring the emulsion type via observing the miscibility of a few emulsion drops with either of the pure liquid.[152,155] At t = 0 min, the size of emulsion droplets was less than 30 μm in diameter. At t = 20 min, oil droplets of size over 50 μm were visible, indicating that coalescence of oil droplets occurred. After the emulsions were aged at 50 °C for an extended period, such as 2.5 h [**Fig. 2.20** (e) and (f)], monodisperse water droplets of size ~5 μm were resulted. This phase inversion fit into the category of transitional phase inversion,[152,373,382,383] i.e. an inversion caused by the change of particle hydrophobicity. The variation in particle hydrophobicity here was attributed to a temperature-induced shrinkage of microgels from 230 nm (20 °C) to 80 nm (50 °C) in diameter. It was also implied that the hydrophilicity of microgels was sufficiently reduced under the conditions of pH 4 and 50 °C so that the desired w/o emulsions were obtained. It is worth noting that this transitional phase inversion has not been reported in other microgel-stabilised emulsions, although a catastrophic phase inversion from o/w to w/o was shown by Ngai *et al.*[235] via increasing the oil volume ratio above 0.6 at 25 °C in an octanol-water system stabilised by poly(NIPAAm-*co*-MAA) microgels at pH 9.4.



(a) t = 10 min (b) t = 1.5 h

Fig. 2.21 Optical micrographs of microgel-stabilised emulsions taken after preparation at 37 °C and during aging at 50 °C (scale bar 50 μm). Emulsification was carried out using a microgel (0.4 wt %) suspension in 1 mM KCl solution of pH 4 and 40 vol % DVB.

For emulsions prepared at 37 °C, sedimentation was observed after emulsification and the emulsion type was w/o as confirmed by drop tests. The subsequent increase of temperature from 37 °C to 50 °C during aging had little effect on the emulsion droplets (**Fig. 2.21**),

identical to the emulsion droplets obtained via phase inversion [**Fig. 2.20** (e)(f)]. For 50 °C as the emulsification temperature, identical emulsions [**Fig. 2.22** (c)] to those prepared at 37 °C [**Fig. 2.22** (b)] were resulted. This indicated that w/o emulsions were obtainable using shrunken microgels at pH 4 irrespective of whether the temperature was increased above the VPTT before or after emulsification. This was in contrast to a reported PS latex stabilised n-hexadecane-water emulsion system.[384] In their experiments, a temperature-induced phase inversion from o/w to w/o was only observed when a series of emulsions were prepared at different temperatures; coalescence rather than phase inversion was resulted if an obtained o/w emulsion was heated. This contrast indicated that the transitional phase inversion occurring to microgel-stabilised emulsion (**Fig. 2.20**) was not just due to a variation of the particle wettability at the interface. The concomitant shrinkage of microgels might also play an important role in microgels crossing the interface, leading to w/o emulsions. In addition, the size reduction in emulsion droplets upon inversion from o/w to w/o was also observed in reported surfactant-stabilised emulsions[385] and other Pickering emulsions.[382,384,386]

On the other hand, the emulsion volume ratio of the sample during aging at 50 °C, i.e. emulsion volume relative to the total sample volume ($V_{emulsion}/V$), was recorded as a function of time (**Fig. 2.23**). An agglomeration was removed from the emulsions prepared at 15 °C at the beginning of the aging process to facilitate volume recording, which was attributed to microgel aggregates formed during phase inversion. Otherwise, the emulsion volume ratio hardly showed any obvious variation, indicating the w/o emulsions were stable to aging at 50 °C. Meanwhile, it was estimated that the oil (transparent) on top of the emulsions (milky) constituted about 30-35% of the total volume (**Fig. 2.22**). Thus, the oil phase ratio in the emulsions was actually less than 20 vol %, suggesting the possibility of preparing w/o HIPEs by using less oil.



(a) (b) (c) (d) (e) (f)

Fig. 2.22 Photos of microgel-stabilised emulsions taken after the volumes became stable during aging. All emulsions were prepared using 40 vol % DVB and a micrigel suspension in 1 mM KCl solution of pH 4. The microgel concentrations used in (a)-(d) and (e)-(f) were 0.4 wt % and 0.8 wt %, respectively. (a) Emulsified at 15 °C and aged at 50 °C; (b) emulsified at 37 °C and aged at 50 °C; (c) emulsified at 50 °C and aged at 50 °C; (d) emulsified at 15 °C and aged at 25 °C; (e) emulsified at 15 °C and aged at 25 °C; (f) emulsified at 15 °C and aged at 50 °C. Agglomeration was removed from (a) and (f) during aging.

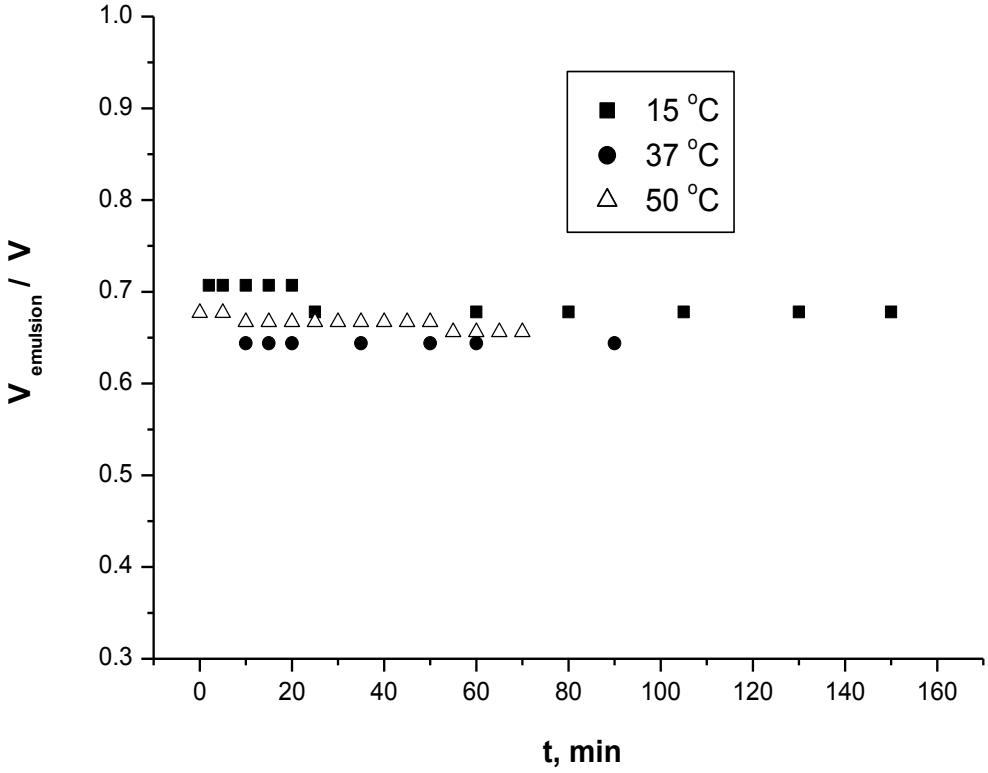
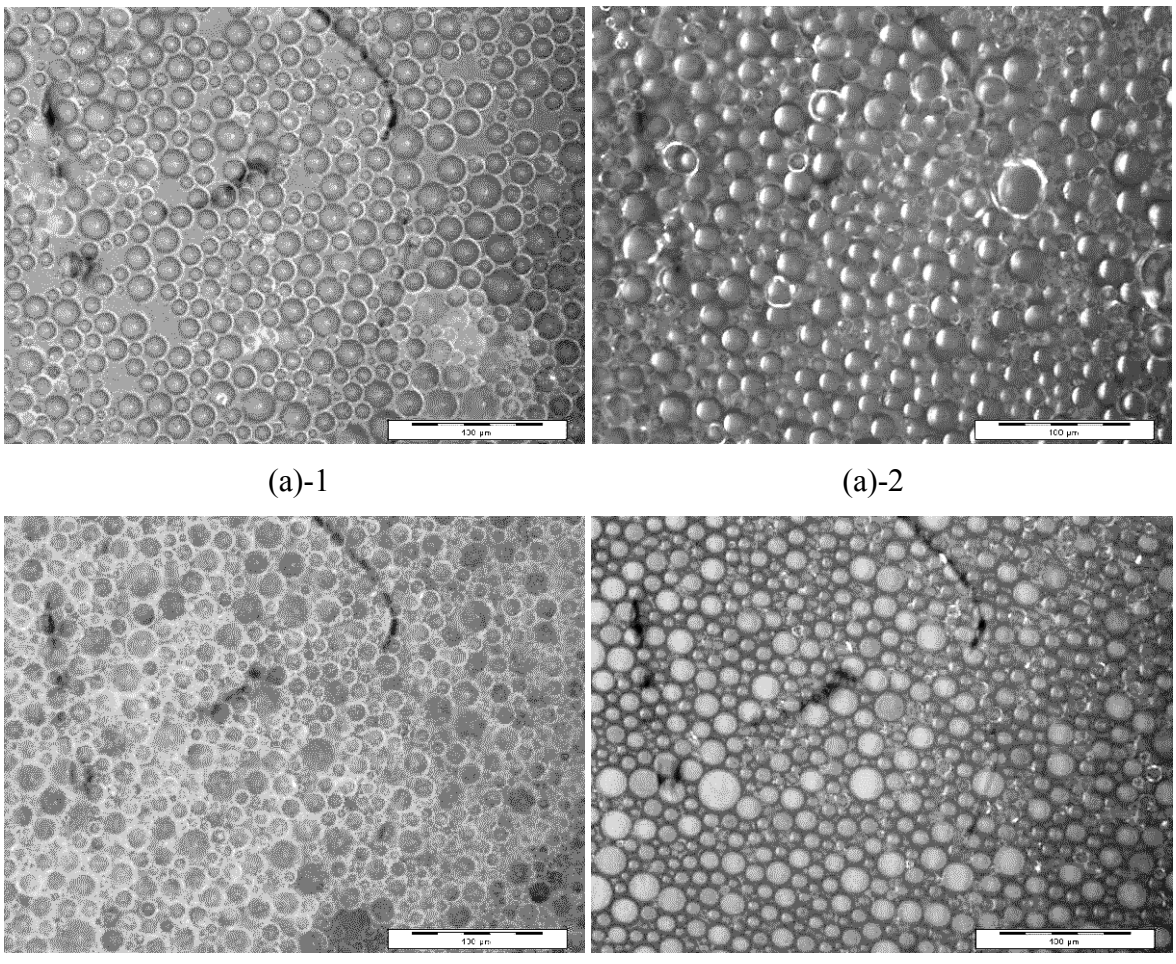


Fig. 2.23 Emulsion volume ratio of microgel-stabilised emulsions as a function of time recorded during aging at 50 °C (error of volume: ± 0.1 ml). The three emulsions were prepared using the same composition at 15 °C, 37 °C and 50 °C, respectively. The decrease of $V_{emulsion}/V$ observed in sample prepared at 15 °C at 20 min was due to removal of an agglomeration.

To sum up, the desired microgel-stabilised w/o emulsions were obtained at pH 4 and 40 vol % DVB either through a temperature-induced phase inversion or through emulsification directly at temperatures above the VPTT of microgels, such as 37 °C and 50 °C. Microgel-stabilised water-in-DVB HIPEs were expected to be produced under these conditions.

2.5.3.2 Effect of microgel concentration on stability of the emulsions prepared at pH 4

It is showed that microgel particles at pH 4 were capable of stabilising either o/w emulsions below the VPTT or w/o emulsions above the VPTT. It is noticed that microgel concentration and DVB volume ratio were set at 0.4 wt % and 40%. Prior to preparing w/o HIPEs using 20% DVB (**Section 2.6**), this section discusses whether increasing the microgel concentration from 0.4 wt % to 0.8 wt % could affect the stability of emulsions.



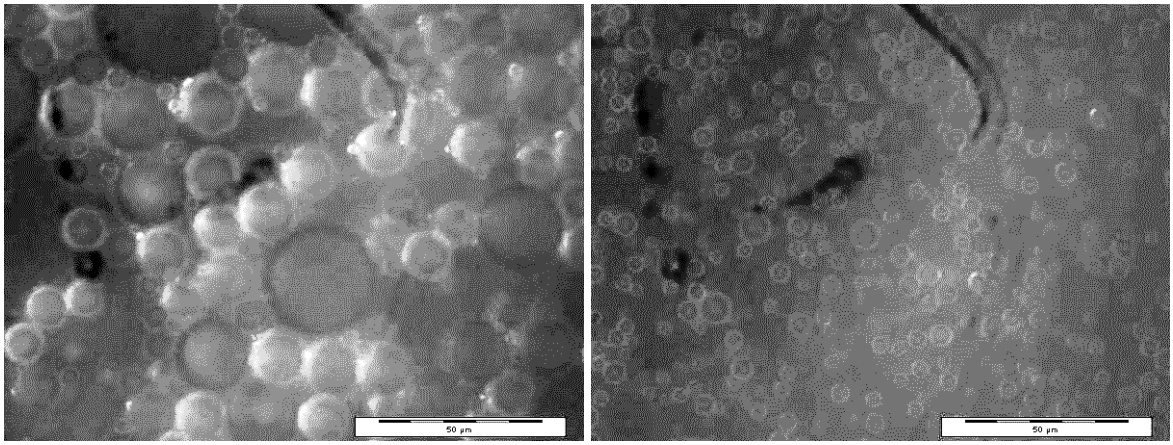
(a)-1 (a)-2

(b)-1 (b)-2

Fig. 2.24 Optical micrographs of microgel-stabilised emulsions taken after emulsification at 15~16 °C (left) and after creaming during aging at 25 °C (right) (scale bar 100 μm). Samples (a) and (b) were prepared using 0.4 wt % and 0.8 wt % microgels, respectively.

The o/w emulsions obtained by emulsifying 40 vol % DVB and microgel suspensions (pH 4) containing 0.4 wt % and 0.8 wt % microgels at 15~16 °C were tested using optical microscope (**Fig. 2.24**). It was shown that the size of emulsion droplets was hardly affected by the aging process at 25 °C or the microgel concentration. Meanwhile, the increase in particle concentration had little effect on the creaming extent of emulsions [**Fig. 2.22** (d)(e)], although whether the creaming rate was affected was unknown due to an ambiguous boundary between emulsions and the aqueous phase in the case of 0.8 wt % microgels used [**Fig. 2.22** (e)]. This was in contrast to the study reported by Ngai *et al.*,[235] which showed that increasing the concentration of poly(NIPAAm-*co*-MAA) microgel particles from 0.28 wt % to 1.0 wt % and 2.0 wt % clearly reduced the creaming extent of octanol-in-water emulsions at pH 9.4. This was attributed to a significant reduction of drop sizes in their system.

On the other hand, the effect of aging at 50 °C on the stability of sample prepared by emulsifying microgel suspension (0.8 wt %) and 40 vol % DVB at 15 °C was investigated. The net-like clusters observed on the tube wall at the beginning of the aging process were attributed to microgel aggregates, similar to those observed in sample prepared using 0.4 wt % microgels. Optical micrographs taken at t = 0 and t = 81 min in the aging test (**Fig. 2.25**), together with drop tests of the emulsions, showed that a transitional phase inversion from o/w to w/o occurred during aging at 50 °C or in the process of temperature increase from 24 °C (after emulsification) to 50 °C. This phase inversion was also identical to that observed in sample prepared using 0.4 wt % microgels during aging at 50 °C (**Fig. 2.20**) and led to small water droplets of about 5 μm in diameter. The resultant w/o emulsions maintained stable to coalescence at 50 °C for at least 285 min [**Fig. 2.22** (f)], after which solidification of DVB on the top became significant. Although it was expected to improve the stability to sedimentation by increasing microgel concentration,[155] the actual concentrations were varied due to the removal of microgel agglomeration during aging. Indeed, there was no obvious difference in the volume of clear oil between the two samples [**Fig. 2.22** (a) and (f)]. For the preparation of microgel-stabilised w/o HIPEs, it is sensible to use preparation temperatures above the VPTT rather than adopt the route of phase inversion so that microgel loss due to agglomeration can be avoided.



(a) t = 0 min (b) t = 81 min

Fig. 2.25 Optical micrographs of microgel-stabilised emulsions taken at t = 0 and t = 81 min during an aging test at 50 °C (scale bar 50 μm). The emulsions were prepared by homogenising 40 vol % DVB and a microgel suspension (0.8 wt %) in 1 mM KCl solution at 15 °C.

To sum up, increasing microgel concentration from 0.4 wt % to 0.8 wt % had no obvious effect on the stability of o/w emulsions prepared below VPTT or that of the w/o emulsions prepared using a temperature-induced phase inversion approach.

2.6 Preparation of polyHIPEs from microgel-stabilised w/o emulsions

It was demonstrated above (**Section 2.5.3.1**) that the desired w/o emulsions were obtained by emulsifying 40 vol % DVB and microgel suspension of pH 4 above the VPTT of microgels. However, the average drop size of the emulsions (< 10 μm) was not sufficiently large to prepare polyHIPE scaffolds for bone tissue engineering (> 100 μm). This was attributed to the relatively high speed (15, 000 rpm) used during emulsification with a rotor-stator homogeniser. Although w/o HIPEs were indeed obtained at 20 vol % DVB and microgel suspension of pH 4 at 37 °C (not shown), it was necessary to replace the rotor-stator homogeniser with a mechanical stirrer in order to prepare polyHIPEs with larger pore sizes. The following will discuss microgel-stabilised HIPEs prepared using a mechanical stirrer under mild stirring intensities, e.g., 400-1000 rpm.

2.6.1 Effect of preparation conditions on the morphology of DVB based polyHIPEs

To prepare poly(DVB) Pickering-HIPEs using a mechanical stirrer instead of a rotor-stator homogeniser, a new set of preparation conditions need to be optimized. The factors under investigation included temperature control during emulsification, polymerisation temperature and the stirring protocol (**Table 2.9**).

Table 2.9 Conditions for the emulsification and polymerisation of microgel-stabilised HIPEs

No.	Emulsification		Polymerisation		Observation
	Stirring protocol	**Temperature ***	**Initiation #**	**Temperature**	
1	400 rpm	45 ºC (V), RT (F)	Thermal	70 ºC	Partially expelled water
2	400 rpm	45 ºC (V), RT (F)	Thermal	50 ºC	Partially expelled water
3	400 → 600 rpm	40 ºC (V), 40 ºC (F)	Photo-	40 ºC	Partially expelled water
4	400 → 800 rpm	40 ºC (V), 40 ºC (F)	Photo-	40 ºC	-
5	400 → 1000 rpm	40 ºC (V), 40 ºC (F)	Photo-	40 ºC	No expelled water

***** The oil phase was warmed up in a reaction vessel (V) prior to emulsification, while the microgel aqueous suspension was placed in a dropping funnel (F) attached to the vessel. # AIBN was used as the initiator.

Firstly, a comparison was made between two polymerisation temperatures, 70 °C and 50 °C. During emulsification, the same stirring protocol and temperature control measures were applied to both. Although 70 °C can lead to faster decomposition of initiator AIBN,[377] the product from polymerisation at 50 °C exhibited pores with more intact profiles (**Fig. 2.26**). This indicated that emulsions were more stable when polymerised at 50 ºC. On the other hand, expelled water and polymer beads were observed in both samples. Since water-in-DVB emulsions remained stable at 50 °C (**Fig. 2.23**), the coalescence was likely due to the heat released during polymerisation. This negative effect of heat on emulsion stability was in agreement with reported literatures.[130,235,360,387,388] Meanwhile, the presence of both pores and beads (**Fig. 2.26**) probably indicated a coexistence of w/o and o/w emulsions or possibly the formation of o/w/o multiple emulsions[373] prior to polymerisation. Since the aqueous phase underwent a temperature increase from RT (funnel) to 45 ºC (vessel) when added, production of microgels with various hydrophobicity and therefore different emulsion types was possible, especially at high water volume ratios.

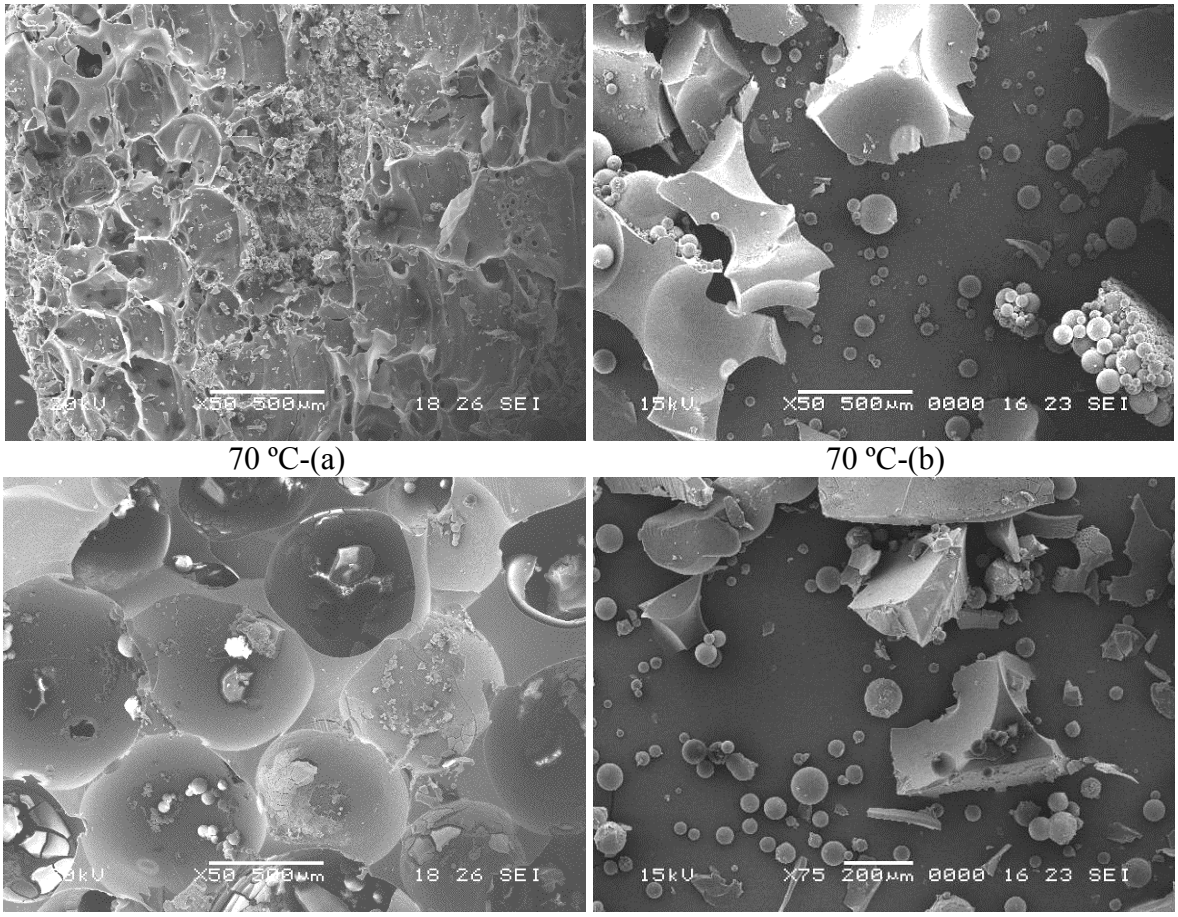


Fig. 2.26 SEM images of polyDVB samples prepared by polymerising microgel-stabilised HIPEs at 70 ºC and 50 ºC, respectively. Images (a) and (b) were taken from specimen of a big piece and broken pieces, respectively.

Secondly, the effect of stirring protocol on the preparation of DVB based polyHIPEs was investigated. From above, it was found necessary to reduce polymerisation temperature as well as to warm up the aqueous phase above the VPTT. Therefore, photo-initiation instead of thermal initiation was adopted so that the polymerisation temperature was set at 40 ºC. Meanwhile, the microgel suspension was thermostatted at ~40 ºC via a designed apparatus enabling warm water circulation (**Fig. 7.5**). Li *et al.*[389] recently found that the adsorption of polyNIPAAm microgels to the heptane-water interface was slowed down with increasing temperature above the VPTT, despite a constant microgel size. This may support why 40 ºC was beneficial in our case. The stirring protocol investigated was a two-speed stirring protocol, i.e., 400 rpm during addition of the aqueous dispersion followed by 600, 800 or 1000 rpm for 10 min (**Table 2.9**). By increasing the second stirring speed from 600 rpm to 1000 rpm, the expelled water was almost eliminated (**Fig. 2.27**). This indicated that the HIPE stability was improved at 1000 rpm.



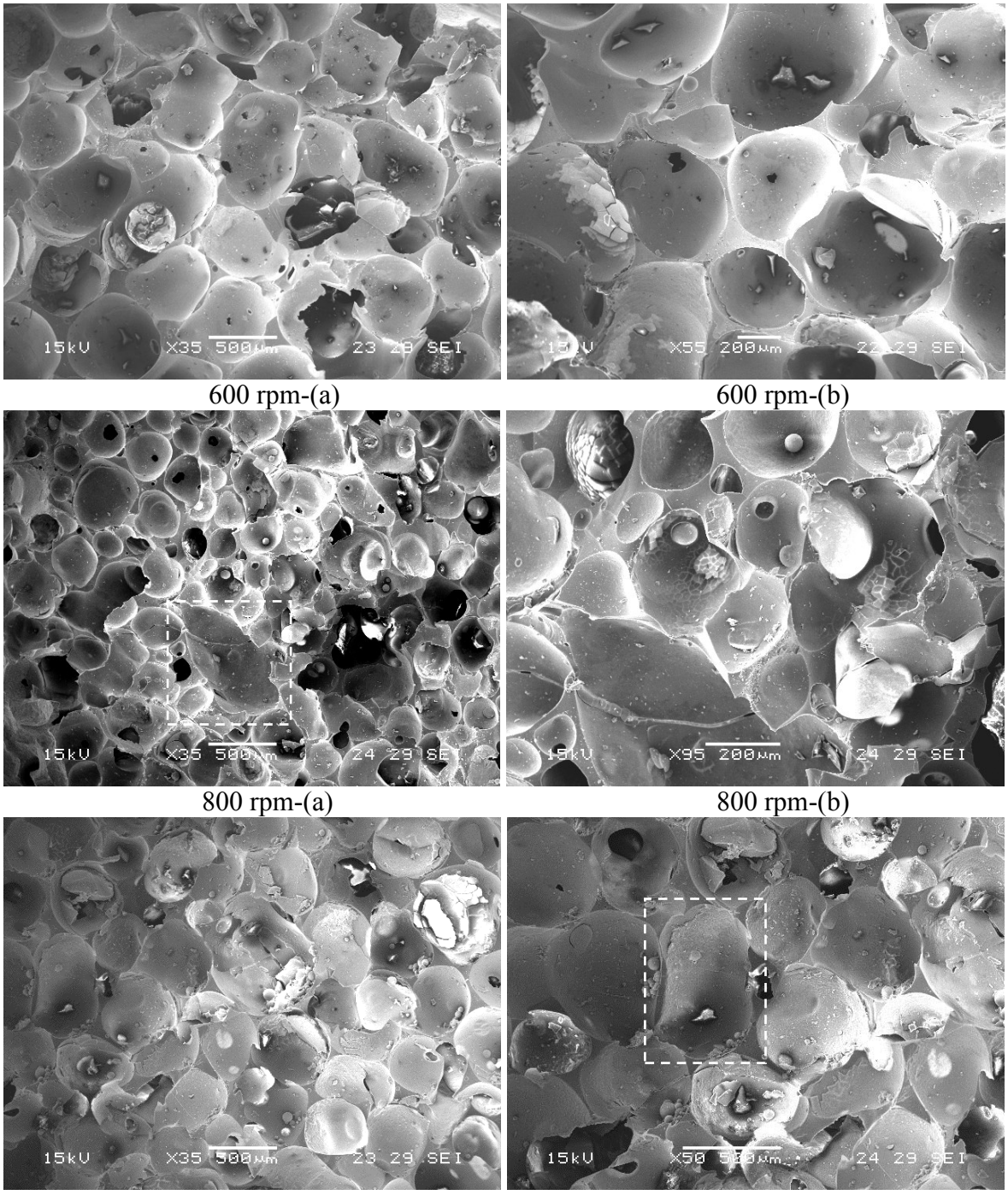
(a) (b) (c)

Fig. 2.27 Photos of microgel-stabilised HIPEs prepared using a two speed stirring protocol and the resultant polyHIPEs. (a) HIPEs emulsified using the two-speed stirring protocol of (400→600 rpm) at 40 °C prior to photo-polymerisation. The arrow points at the interface between HIPEs (top) and a small amount of expelled water (bottom); (b) HIPEs emulsified using the two-speed stirring protocol of (400→1000 rpm) at 40 °C; (c) poly(DVB) Pickering-HIPEs prepared by photo-polymerising the HIPEs shown in (b). The external diameter of the glass tubes is 25 mm.

Meanwhile, the variation in stirring speed had some effects on the morphology of polyHIPEs. PolyHIPEs prepared using 600 rpm as the second stirring speed (porosity 73 ± 3%) exhibited morphology of closed pores with diameter up to 500 μm while polyHIPEs prepared using 800 rpm (porosity 79 ± 1%) and 1000 rpm (porosity 76 ± 2%) showed similar morphology but smaller pore sizes (**Fig. 2.28**). This effect of stirring speed on pore size may be partially explained by its effect on the size of emulsion droplets as estimated (within an order of magnitude) with the "Hinze-Clay relation"[390]:

$$x_{\max} = C\upsilon^{-6/5} X^{-4/5} \rho_C^{-3/5} \gamma^{3/5} \quad \text{.....(2.2)}$$

where C is a constant, ν the revolution rate, X stirrer diameter, ρ_c the density of the continuous phase and γ the interfacial tension. Thus, the maximum drop size obtained at 600 rpm can be 1.5 times of that at 1000 rpm. Practically, partial or arrested coalescence[391] observed in polyHIPEs prepared using 800 rpm and 1000 rpm (**Fig. 2.28**, boxed) increased the drop size contrarily.



600 rpm-(a) 600 rpm-(b)

800 rpm-(a) 800 rpm-(b)

1000 rpm-(a) 1000 rpm-(b)

Fig. 2.28 SEM images of poly(DVB) Pickering-HIPEs prepared by photo-polymerising microgel-stabilised w/o HIPEs. During emulsification, 600, 800 and 1000 rpm were used as the second stirring speed, respectively, following 400 rpm in the two-speed stirring protocol.

Therefore, poly(DVB) Pickering-HIPEs with suitable pore sizes for bone tissue engineering were successfully obtained from microgel-stabilised w/o HIPEs. Besides using microgel dispersion of pH 4 above the VPTT, it was found beneficial to use mild polymerisation conditions, such as photo-polymerisation at 40 °C.

2.6.2 Formation of stable microgel layers at the interface essential for stable w/o HIPEs

For microgel particles consisting of polyNIPAAm or its copolymers as the emulsifier, o/w emulsions were normally obtained except two recent examples. Schmidt *et al.*[392] found that water-in-octanol emulsions or HIPEs could be stabilised by microgels of poly(NIPAAm-*co*-MAA) either in the neutral state (pH 3) or in the charged state (pH 9) with charges located in the core. Destribats *et al.*[393] obtained polyNIPAAm microgel-stabilised w/o emulsions using several fatty alcohols as the oil phase. Although the oil phase being alcohols was considered crucial in stabilising w/o emulsions in both studies, DVB used here did result in w/o emulsions and HIPEs. Therefore, an analysis into our case is necessary and helpful to further understand the interfacial behaviour of microgels and their capability as emulsifiers.

In order to stabilise w/o emulsions, poly(NIPAAm-*co*-AA) microgels were required to move from the bulk to the interface after the microgel suspension was added dropwise into DVB. Brugger *et al.*[364] measured the dynamic interfacial tensions of heptane/water with poly(NIPAAm-*co*-MAA) microgels at pH 3 and 9 at RT and found that the equilibrium values were about 13.5 and 16.5 mN/m, respectively. These were much lower than that of heptane/water (50.2 mN/m)[369] without microgels, indicating microgels considerably reduced the interfacial tension. Monteux *et al.*[394] found that the interfacial tension of dodecane/water (without microgels, 52.8 mN/m[369]) with 1 wt % polyNIPAAm microgels at pH 2 was below 20 mN/m in the range of 20-45 °C and passed a minimum value of 14.6 mN/m at the VPTT (33 °C). Li *et al.*[389] very recently showed that the heptane-water interfacial tension was reduced by polyNIPAAm microgels in a concentration- and time-dependent manner. At 40 °C, the interfacial tension in the presence of 5×10^{-3} g/ml microgels was reduced to 20 mN/m in ~5 min. These studies suggested that microgels were very likely to move from the bulk to the interface spontaneously during emulsification. Meanwhile, the nature of microgels being less hydrophilic above the VPTT may also contribute to this tendency.

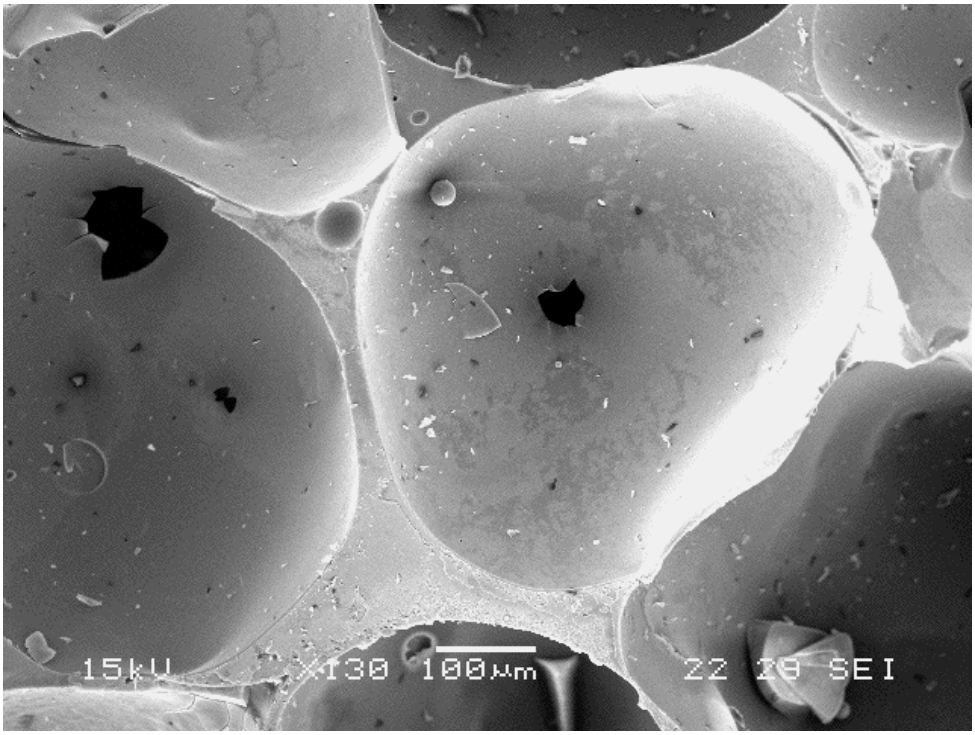


Fig. 2.29 SEM image of poly(DVB) Pickering-HIPEs showing microgel layers inside the pores. In the preparation of this polyHIPE sample, the two speed stirring protocol of (400→600 rpm) was used during emulsification.

However, microgels being able to move to the interface is far from sufficient for the production of w/o emulsions or HIPEs. The formation of stable close-packed particle layers at the interface[159,395] was essential for the stability of w/o emulsions. The existence of such interfacial layers at the water-in-DVB emulsions was partially verified by the layers of dried microgels observed inside the pores of poly(DVB) Pickering-HIPEs (**Fig. 2.29**). A crude estimation of the particle coverage (*Cov*) was expressed by the ratio of particle monolayer surface area ($S_{monolayer}$,) and the total interfacial area ($S_{interface}$) in Equation (2.3):

$$Cov = \frac{S_{monolayer}}{S_{interface}} = \frac{\sqrt{3} m_p D_d}{2\pi \rho_p d_p V_{water}} \quad \text{.....(2.3)}$$

where d_p, m_p and ρ_p are the hydrodynamic diameter, mass and density of microgels; D_d is the diameter of a single water droplet; V_{water} is the volume of water phase. To calculate the monolayer surface area,[396] it is assumed that microgels are hexagonally arranged at the interface. Using the dry weight of microgels as m_p, d_p= 60 nm (hydrodynamic diameter of microgels at 40 ºC) and ρ_p= 0.3 g/cm^3 (the density of collapsed polyNIPAAm microgels measured by Wu *et al.*[264]), D_d= 400 µm as the pore diameter [**Fig. 2.28**, 600 rpm] and V_{water}=

20 ml, the calculated particle coverage (*Cov*) is 24.5. Thus, microgels were expected to form multiple layers at the water-DVB interface. Indeed, the formation of close-packed microgel layers at the interface of w/o emulsions was observed *via* cryo-SEM in both recent cases[392,393] as mentioned earlier in this section.

Schmidt *et al.*[392] attributed the formation of water-in-octanol emulsions at pH 3 to the fact that octanol could swell poly(NIPAAm-*co*-MAA) microgels; they also found water-in-octanol emulsions were available at pH 9 when the MAA moieties of microgels located in the core rather than in the shell. Destribats *et al.*[393] found that polyNIPAAm microgels lost the characteristic thermo-responsiveness and were nondeformed at the interface of w/o emulsions due to octanol uptake. Clearly, the strong affinity of microgels to the oil phase (octanol or other fatty alcohols[393]) in these two cases played a significant role in the formation of stable microgel interfacial layers and hence stable w/o emulsions. Nevertheless, this cannot explain why water-in-DVB emulsions were stabilised since the polarity of DVB is much lower assuming it is similar to that of toluene or xylene. Instead, we believe the reduced hydrophilicity of microgels above the VPTT together with a modest charge density resulted in the stability of microgel layers at the interface. The importance of microgels above the VPTT was obvious since o/w emulsions were obtained otherwise. The amount of charges proved crucial since microgel agglomerate at the interface and hence phase separation of emulsions was observed in the cases of pH 3 and pH 5 above the VPTT. The partially ionised carboxyl groups of microgels at pH 4 probably contributed to a balance of particle interactions at the interface.[378,397,398]

To sum up, the formation of stable microgel layers at the water-DVB interface was essential for the stability of w/o HIPEs and hence the preparation of polyHIPEs. This was achieved using microgels in the collapsed state at pH 4, under which the charges played a crucial role in preventing microgel from agglomerating at the interface.

2.7 Summary

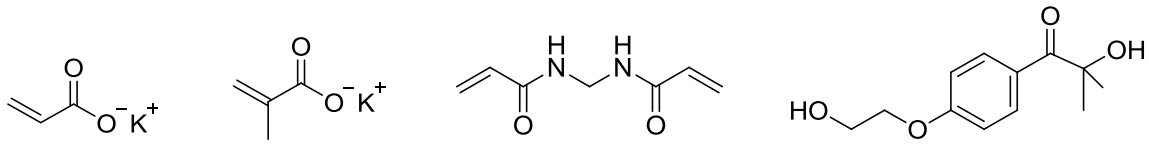
Poly(NIPAAm-*co*-AA) microgel particles stabilised w/o HIPEs were obtained by emulsification of microgel suspension of pH 4 with DVB at 40 ºC. Under these conditions (pH, temperature), the shrunken microgel particles were capable of forming efficient layers at the interface and stabilising the w/o HIPEs. Other conditions were also investigated only resulting in o/w emulsions or phase separation. Poly(DVB) Pickering-HIPEs were obtained

by photo-polymerisation of the w/o HIPEs at 40 ºC. Pores with sizes of a few hundred micrometers were exhibited, within the required pore size range for bone tissue engineering. It would be valuable to make interconnected pore structures and to investigate oils other than DVB that can lead to biocompatible and biodegradable polyHIPEs.

Chapter 3 PolyHIPEs from microgels stabilised o/w HIPEs

3.1 Overview

Besides poly(divinylbenzene) HIPEs prepared using poly(NIPAAm-*co*-AA) microgel-stabilised w/o HIPEs (**Chapter 2**), polyHIPEs based on microgel-stabilised o/w HIPEs were also prepared (this chapter) in order to obtain polymer scaffolds with more hydrophilic surfaces, i.e., macroporous hydrogels. Investigations were carried out into three aspects: (i) stability of the o/w HIPE template, (ii) polymerisation of the template and (iii) properties of the resultant polyHIPEs. Initially, it was found that there existed a temperature-dependent critical concentration of potassium acrylate (KAA, **Fig. 3.1**), the selected monomer, below which microgels were stable against aggregation in the microgel-KAA aqueous suspensions. The stability study on HIPEs made using microgels in KAA solution as the continuous phase revealed that the stirring protocol had a greater influence than the microgel concentration or the aging temperature on HIPE stability against creaming. For polymerisation of the o/w HIPEs, UV initiation was found to be more convenient and efficient than initiation using a chosen redox pair while *N*, *N'*-methylenebisacrylamide (BIS, **Fig. 3.1**) was selected as crosslinker because of its relatively high solubility and reactivity. Of the properties of poly(KAA) Pickering-HIPEs, attention was particularly paid to the morphology, although their BET surface area, density and porosity were also assessed. It was found that the BIS content (BIS/KAA, mol/mol) significantly affected the formation of pore throats in polyHIPEs. The effect of other factors on pore throat formation, such as internal phase volume ratio ($\phi_{int.}$), KAA concentration and stirring speed, were negligible at 10.0 mol % BIS but increasingly noticeable with decreasing BIS content. It was further evidenced by cryo-SEM that the pore throats in open porous poly(KAA) Pickering-HIPEs formed after polymerisation during solvent extraction. In addition, towards applying this template of macroporous hydrogels in the physiological environment, efforts were made to prepare polyHIPE composites of poly(KAA)/silica and poly(KAA)/Bioglass® and to use alternative monomers, such as potassium methacrylate (KMAA, **Fig. 3.1**).



KAA KMAA BIS Irgacure 2959

Fig. 3.1 Chemical structures of the monomers, crosslinker and photoinitiator used in the preparation of macroporous hydrogels from microgel-stabilised o/w HIPEs. The monomers are potassium acrylate (KAA) and potassium methacrylate (KMAA); the crosslinker is *N*, *N'*-methylenebisacrylamide (BIS); the photoinitiator is 2-hydroxy-1-[4-(2-hydroxyethoxy) phenyl]-2-methyl-1-propanone (Irgacure2959 or I2959).

3.2 Preparation of microgels stabilised o/w HIPEs containing KAA

Besides polyHIPEs prepared from w/o HIPEs, those from o/w HIPEs have been explored for applications as tissue engineering scaffolds due to the availability of hydrophilic and biocompatible surfaces for cell attachment and growth.[399,400] In this o/w HIPE template, surfactants were conventionally used as emulsifiers, while a variety of water-soluble monomers or crosslinkable polymers were investigated, such as acrylic acid[401] (AA), acrylamide[402] (AAm), 2-hydroxyethyl methacrylate[403,404] (HEMA), *N*-isopropylacrylamide[405,406] (NIPAAm), and crosslinkable derivatives of dextran,[219] pullulan,[219] gelatin,[212,219,220] and alginate.[221] To make use of the advantages[149] of particulate emulsifiers over conventional surfactants and the potential of microgel particles as drug-carriers,[239-242,244,245] we aimed to fabricate multifunctional scaffolds by preparing polyHIPEs from microgel stabilised o/w HIPEs. Although o/w emulsions[233,235,364,365,381,394] and even HIPEs[407-409] stabilised by polyNIPAAm-based microgels were recently reported, fabrication of 3-D tissue engineering scaffolds via polymerising microgel-stabilised o/w HIPEs is rarely reported. For this purpose, a neutralised potassium salt of acrylic acid (KAA) was selected here as monomer because of its high solubility and reactivity in water as well as the biocompatibility[410] of the resultant hydrogel matrix.

3.2.1 Preliminary tests on KAA-microgel aqueous mixtures prior to emulsification

3.2.1.1 Effect of KAA concentration on microgel dispersion in the aqueous mixtures

As discussed in **Section 2.2.1**, the swelling-deswelling behaviours of poly(NIPAAm-*co*-AA) microgel particles were strongly dependent on temperature, pH, salt concentration and

microgel concentration in water. Therefore, it is necessary to assess the influence of KAA on microgel particles in the aqueous phase prior to emulsification. For this purpose, a series of aqueous mixtures were prepared using 1 ml microgel suspension (0.8 wt % in 1 mM KCl solution) and 4 ml KAA solutions of gradually decreased concentrations (**Table 3.1**). These aqueous mixtures were labelled as "1-1", "1-2", … and "1-16", respectively. The effect of KAA concentration on the state of microgels at 25 °C is clearly shown in **Fig. 3.2**.

Table 3.1 Compositions of KAA solutions prior to mixing with 1 ml microgel suspensions

No.	**1**	**2**	**3**	**4**	**5**	**6**	**7**	**8**
KAA stock solution, ml	4.0	3.8	3.6	3.4	3.2	3.0	2.8	2.6
Distilled H_2O, ml	0	0.2	0.4	0.6	0.8	1.0	1.2	1.4
pH	7.09	7.09	7.07	6.98	6.89	6.88	6.87	6.82
No.	**9**	**10**	**11**	**12**	**13**	**14**	**15**	**16**
KAA stock solution /ml	2.4	2.2	2.0	1.8	1.6	1.4	1.2	1.0
Distilled H_2O /ml	1.6	1.8	2.0	2.2	2.4	2.6	2.8	3.0
pH	6.83	6.77	6.75	6.78	6.72	6.63	6.60	6.59

* KAA stock solution has a concentration of 2.56 ± 0.07 M.

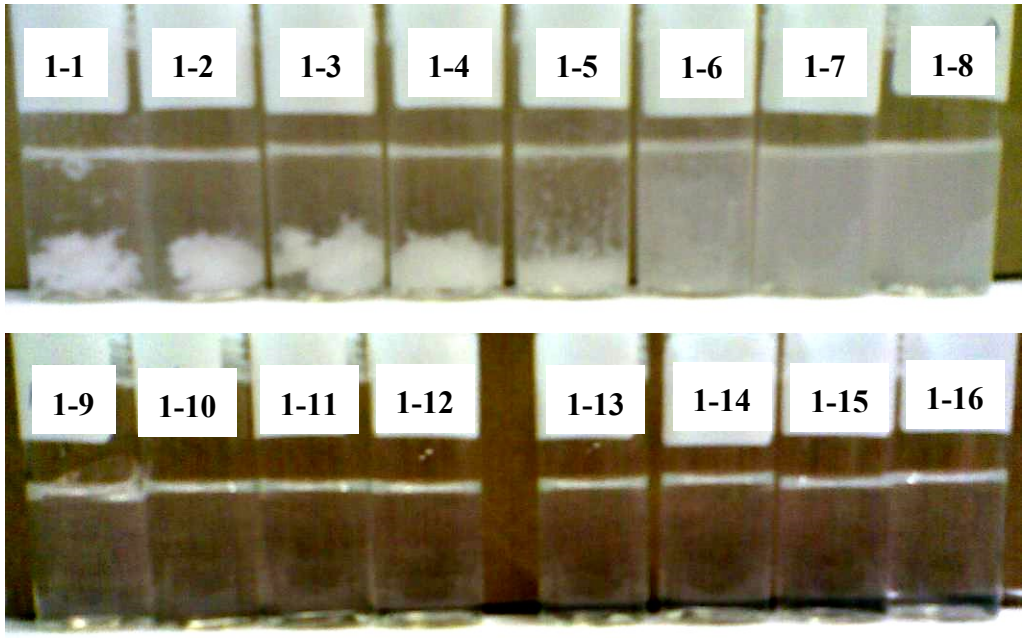


Fig. 3.2 Images of aqueous mixtures made up with 1 ml microgel suspension (0.8 wt % in 1 mM KCl solution) and 4 ml KAA solution of various concentrations at 25 °C. The concentration of KAA is gradually decreased from "1-1" (2.05 M) to "1-16" (0.51 M). Microgel particles aggregated and precipitated in mixtures "1-1" to "1-8" (1.33 M) while suspensions from "1-9" (1.23 M) to "1-16" remained stable and transparent.

Aggregation of microgel particles was observed in the aqueous mixtures from "1-1" ([KAA]= 2.05 M) to "1-8" (1.33 M). Large microgel clusters were visible in mixtures of higher KAA concentrations, from "1-1" to "1-5" (1.64 M). This loss of colloidal stability at relatively high concentrations of KAA was attributed to a significant reduction of the Debye screening length according to Equation (2.1)[320] and an ensuing increase in the interparticle attractive interactions, including hydrogen bonding, the van der Waals forces, and hydrophobic interactions (**Section 2.2.1.2**). At low KAA concentrations, from "1-9" (1.23 M) to "1-16" (0.51 M), particles remained stable against aggregation in the suspensions.

3.2.1.2 Effect of temperature on microgel dispersion in the aqueous mixtures

The 16 microgel-KAA aqueous suspensions were also thermo-sensitive. In contrast to the states of microgel particles at 25 °C (**Fig. 3.2**), "1-8" became transparent at 14 °C (not shown) but exhibited large-sized microgel clusters at 32 °C (**Fig. 3.3**). Meanwhile, suspensions from "1-9" to "1-12" were transparent at 25 °C (**Fig. 3.2**) but appeared turbid at 32 °C (**Fig. 3.3**). These changes illustrated that microgel particles separated from the aqueous medium upon temperature increase, which was due to a temperature-induced disruption of the hydrogen bonding between water and amide groups of the microgels together with a dissociation of the hydrophobic interaction between polyNIPAAm and water (or hydrophobic hydration) (**Section 2.2.1.2**). The extent of phase separation was reflected here by the state of the suspensions, which turned from transparent to turbid, and eventually to large clusters.

As described in **Section 2.5.1**, aggregated microgel particles were unable to stabilise emulsions. Therefore, these preliminary tests of the effect of KAA concentration and temperature on the states of microgel particles provided some initial indication for selecting KAA concentration and temperature for HIPE preparation and polymerisation. Although higher KAA concentrations are generally preferred in order to prepare robust polyHIPEs, HIPE stability has to be guaranteed. Meanwhile, the resultant HIPEs should remain stable under the polymerisation conditions: polymerisation needs to be carried out at temperatures at which the chosen KAA concentration does not cause microgel aggregation.

In addition, the pH of the 16 KAA solutions prior to mixing with microgel suspension exhibited a slight decrease from 7.09 to 6.59 (**Table 3.1**) upon gradual dilution with distilled water (pH ~5.3). The addition of microgel suspension did not significantly affect the pH.

Since the pH of these mixtures were well above the pK_a of the PAA moieties (4.7[298,299]) of poly(NIPAAm-*co*-AA) microgel particles, the pH differences among them, from "1-8" to "1-15", were unlikely to have a significant effect on the microgel behaviour according to **Section 2.2.1.1**, in contrast to the effects of KAA concentration and temperature.

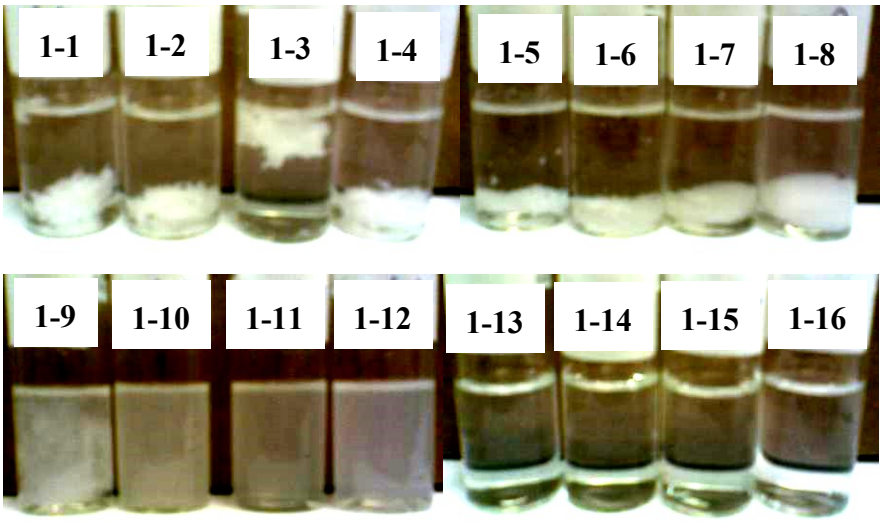


Fig. 3.3 Images of a series of 5 ml microgel suspensions in KAA solutions at 32 °C. KAA concentration gradually decreased from "1-1" (2.05 M) to "1-16" (0.51 M). From "1-1" to "1-8" (1.33 M), large-sized microgel clusters precipitated out; from "1-9" (1.23 M) to "1-12" (0.92 M), mixtures were turbid; from "1-13" (0.82 M) to "1-16", suspensions were transparent.

To sum up **Section 3.2.1**, effects of KAA concentration (from 2.05 M to 0.51 M) and temperature (25 °C and 32 °C) on the state of microgel suspensions in aqueous KAA solutions were assessed. The critical KAA concentration, $[KAA]_C$, above which obvious microgel aggregation started to occur, was between 1.33 M ("1-8") and 1.23 M ("1-9") at 25 °C while between 0.92 M ("1-12") and 0.82 M ("1-13") at 32 °C. Microgel suspensions in KAA solutions with KAA concentrations below $[KAA]_C$ were expected to result in stable emulsions upon emulsification with the oil phase.

3.2.2 Emulsification of microgel suspensions in KAA solutions with the oil phase

3.2.2.1 Effect of KAA concentration on the stability of microgel-stabilised o/w HIPEs

Trials of HIPE preparation were carried out using 5 ml aqueous suspensions of various KAA concentrations (**Fig. 3.2**) and 20 ml toluene ($\phi_{internal}$ = 80%) and using a one-speed

stirring protocol[401] (only 400 rpm) together with a slow addition rate for toluene at room temperature (RT). As a result, HIPEs were obtained immediately after stirring (t = 0) for all the samples but differed in stability over time (**Fig. 3.4**).



(a) (b) (c) (d) (e) (f) (g) (h)

Fig. 3.4 Images showing the stability of o/w HIPE prepared using 20 ml toluene and 5 ml microgel suspension in KAA solutions with various KAA concentration: (a) [KAA] = 1.33 M, t = 0; (b) [KAA] = 1.33 M, t = 0.5 h; (c) [KAA] = 1.33 M, t = 2.5 h; (d) [KAA] = 1.12 M, t = 0; (e) [KAA] = 1.12 M, t = 71 h; (f) [KAA] = 1.02 M, t = 69 h; (g) [KAA] = 0.92 M, t = 29 h; (h) [KAA] = 0.82 M, t = 25 h. The microgel content in each HIPE was 8 mg.

The HIPEs prepared using 1.33 M KAA underwent a fast phase separation over time [**Fig. 3.4** (a)-(c)]. About 50% toluene was expelled within 0.5 h and a complete phase separation was observed in 2.5 h. In contrast, HIPEs prepared using lower KAA concentrations exhibited improved stability. Typically, toluene was partially expelled and creaming occurred over time. The volume of separated toluene was about 70% in HIPEs prepared using 1.12 M KAA after 71 h [**Fig. 3.4** (d) and (e)] but maintained below 20% in HIPEs prepared using 1.02 M KAA after 69 h [**Fig. 3.4** (f)]. This dependence of HIPE stability on KAA concentration was attributed to the state of microgel particles at the water-oil interface.[235] As discussed in **Section 3.2.1**, when [KAA] ≥ $[KAA]_C$, microgel particles tended to form macroscopic aggregates in the aqueous suspension due to a reduction of the repulsive forces between particles. Since this reduction of repulsive inter-particle forces was maintained even after particles attached to the oil-water interface,[411] the mobility[398] of particles at the interface caused the formation of microgel aggregates. Thus, it was unlikely for particles of this state to form efficient barriers and prevent oil droplets from coalescing.[235,387,412] This was also in agreement with the observation in particle-stabilised emulsions that efficient stabilisation of emulsions could be achieved by particles in a state of weak flocculation whereas no emulsions were stabilised by completely flocculated particles with strong bonds.[372,395,413,414]

Apparently, the microgel aggregates observed at high KAA concentrations were irreversible at that temperature due to the formation of hydrogen bonding[269,292] as well as an enhancement of other inter-particle attractive interactions at smaller particle separation, such as the van der Waals forces and hydrophobic interactions. Secondly, an increase of the KAA concentration did reduce the double layer repulsions[372,415] between the oil droplets, contributing to the instability of HIPEs to coalescence. Thirdly, Ruckenstein *et al.* found that the interfacial tension between styrene and aqueous acrylic acid solutions at 25 °C decreased upon increasing acrylic acid concentration from 0 to 1.5 M.[416,417] This can fit into my case due to the similarity between toluene and styrene as the oil phase and indicated a negative effect of higher KAA concentration on HIPE stability. Thus, it was not surprising that further decreasing the KAA concentration from 1.0 M to 0.92 M and 0.82 M led to stable HIPEs [**Fig. 3.4** (g) and **Fig. 3.4** (h)].

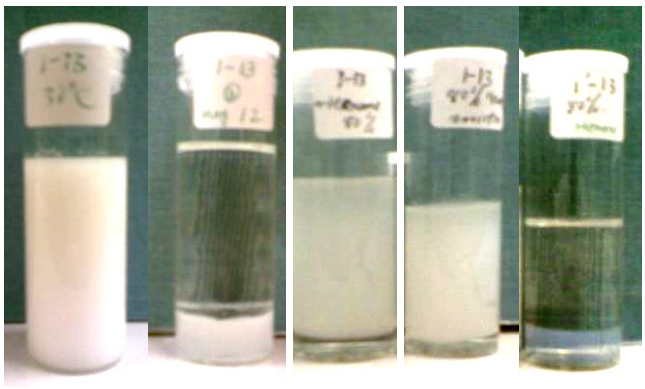
Therefore, our aqueous microgel suspensions with KAA concentrations below 1.0 M were found capable to stabilize HIPEs when a one-speed stirring protocol was applied at RT.

3.2.2.2 Effect of stirring protocol on the stability of microgel-stabilised o/w HIPEs

To further improve HIPE stability prior to polymerisation, attention was paid to the stirring protocol. In contrast to the one speed stirring protocol as discussed in **Section 3.2.2.1**, a two-speed stirring protocol was used for emulsification, i.e., 400 rpm during addition of the internal phase followed by stirring at a higher speed for 5-10 min. This effect of stirring speed on HIPE stability was tested because the maximum drop size would be reduced when the stirring speed was increased according to Equation (2.2).

Firstly, we considered the factors that might cause drop coalescence when using a higher stirring speed (1000 or 2000 rpm). With an identical composition (0.82 M KAA, 8 mg microgels and 80 vol % toluene), w/o HIPEs were prepared using either 1000 rpm or 2000 rpm as the second stirring speed. As a result, HIPEs with little expelled oil were obtained in the case of 1000 rpm [**Fig. 3.5** (a)] but phase separation occurred in the case of 2000 rpm [**Fig. 3.5** (b)] suggesting that there might exist a limit in stirring speed for HIPE preparation at this composition. However, when hexane was used as the oil phase instead of toluene, stable HIPE were obtained for both 1000 rpm [**Fig. 3.5** (c)] and 2000 rpm [**Fig. 3.5** (d)] as the second stirring speed. Compared with toluene-in-water HIPEs, these hexane-in-water HIPEs were more viscous and more transparent, which was attributed to a better-matched refractive

indices[418-420] of the two phases [n_D^{20}: 1.333 (pure water), 1.375 (hexane), 1.497 (toluene)]. It is worth noting that the aqueous phase indeed had a closer refractive index than pure water to that of hexane due to the presence of salts. Importantly, this match in refractive indices of the two phases would lead to a reduction of the inter-drop attractive forces according to Kizling *et al.* and thus an improved HIPE stability to coalescence.[360,420] This might contribute to the availability of stable HIPE using hexane rather than toluene as the internal phase at 2000 rpm. Another example to show the sensitivity of emulsion stability upon stirring at 2000 rpm was that HIPEs prepared using more (2 mol %) instead of less (1 mol %) crosslinked microgels phase-separated after they were stirred at 2000 rpm [**Fig. 3.4** (e)]. The better HIPE stability shown by less crosslinked microgels was in agreement with the study of Destribats *et al.* and was attributed to the higher overlapping ability of these microgels at the interface in comparison with more crosslinked microgels.[381]



(a) (b) (c) (d) (e)

Fig. 3.5 Images of microgel-stabilised o/w HIPEs prepared using a two-speed protocol. An aqueous phase containing 0.82 M KAA and 8 mg microgels was used together with 80 vol % oil phase for all. The oil and the 2nd stirring speed in the stirring protocol (400 rpm as the 1st stirring speed during addition) were varied. (a) HIPEs just after preparation, toluene and 1000 rpm; (b) phase separation, toluene and 2000 rpm; (c) HIPEs after creaming (~2.1 ml aqueous phase on the bottom of the tube), hexane and 1000 rpm; (d) HIPEs after creaming, hexane and 2000 rpm; (e) phase separation, hexane, 2000 rpm and microgels with 2 mol % crosslinking degree used in contrast to those with 1 mol % crosslinking degree for the others.

Secondly, the stability to creaming of the o/w HIPEs obtained using a two speed stirring protocol was emphasised. The average droplet size of HIPEs prepared using 1000 rpm was bigger than that of HIPEs prepared using 2000 rpm (**Fig. 3.6**), in agreement with Equation (2.2), that a higher stirring speed resulted in smaller droplet sizes. This was of importance when using stirring speed to tune the pore sizes of polyHIPEs since a relatively fast polymerisation of the emulsion template normally led to pores of identical sizes to those of

the emulsion droplets. Meanwhile, the stability to creaming was another aspect crucial to the properties of the resultant polyHIPEs because the aqueous phase expelled from o/w HIPEs during creaming also contained monomer and crosslinker and represented a loss to the polyHIPEs.

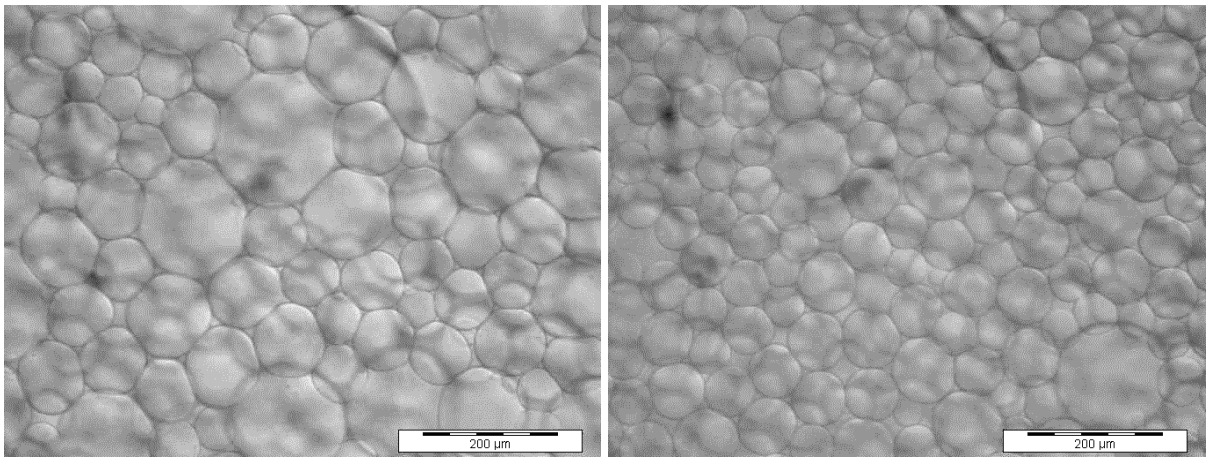


Fig. 3.6 Optical microscope images of emulsion drops taken from microgel-stabilised hexane-in-water HIPEs after creaming occurred. Scale bar 200 µm. 1000 rpm (left) and 2000 rpm (right) were used as the 2nd stirring speed in a two-speed stirring protocol for emulsification, respectively.

The creaming process of HIPEs prepared using different stirring speeds was analyzed with Equation (3.1), expressing a Boltzmann-type equilibrium distribution[134] of the droplets.

$$C_d(h) = C_d(0)\exp(-\frac{mgh}{kT}) \quad \text{(3.1)}$$

where $C_d(0)$ and $C_d(h)$ are the droplet concentration C_d at baseline (i.e., the bottom of the tube) and at a height of h above the baseline; m is the effective mass of a droplet, expressed by Equation (3.2):[134]

$$m = \frac{4}{3}\pi a^3 \Delta\rho \quad \text{(3.2)}$$

where a is the hydrodynamic radius of the droplets and $\Delta\rho$ is the density difference between the two liquid phases.

From Equation (3.1), it can be deduced that in an extreme case where $kT >> \frac{4}{3}\pi a^3 \Delta\rho g h$, $C_d(h)$ is approximately equal to $C_d(0)$ and thus no creaming will occur. Importantly, it is expected that creaming will be reduced when stirring speed is increased from 400 rpm to 1000 rpm or further up to 2000 rpm due to a reduction of the droplet size. This was in agreement with our observation that the creaming volume in **Fig. 3.5** (d) (2000 rpm) was smaller than that in **Fig. 3.5** (c) (1000 rpm). Meanwhile, reduction of $\Delta\rho$ is also expected to increase the stability of HIPE against creaming, i.e., an oil with density closer to water will lead to emulsions of higher stability against creaming.

On the other hand, the benefit of reducing drop sizes of HIPE by using a higher stirring speed also lies in a reduction of creaming rate. According to Stokes' law as expressed by Equation (3.3), the creaming rate υ is expressed by Equation (3.4).[390]

$$\frac{4}{3}\pi a^3 \Delta\rho g = 6\pi\eta_0 a\upsilon \quad \text{(3.3)}$$

$$\upsilon = \frac{2\Delta\rho g a^2}{9\eta_0} \quad \text{(3.4)}$$

where η_0 is the viscosity of the continuous phase. It can be deduced that the creaming rate will decrease when the droplet size is reduced. The importance of the creaming rate can be demonstrated using **Fig. 3.5** (c) as an example. The creaming volume of the hexane-in-water HIPEs was 2.1 ml, about 40% of the total aqueous phase (5 ml), which would not be incorporated into the resultant porous architectures if the emulsion template was cured at a sufficiently slow rate. On the contrary, a slow creaming process together with a fast polymerisation would help increase the polymer content in polyHIPEs as clearly shown in **Section 3.4.6**.

From Equation (3.1) and Equation (3.4), it can be deduced that HIPEs prepared using toluene (0.87 g/cm^3) as the oil phase were supposed to have better stability against creaming than those prepared using hexane (0.66 g/cm^3) due to a lower $\Delta\rho$ between the two phases. Princen[421] pointed out that a higher interfacial tension also contributed to a smaller tendency towards creaming, besides smaller drop size and lower $\Delta\rho$. From this point of view, hexane gained some advantages due to a higher interfacial tension of hexane-water (51.1 mN/m), compared with that of toluene-water (36.1 mN/m).[369,422] Indeed, no obvious difference was

shown between the creaming volume of toluene-in-water HIPEs and that of hexane-in-water HIPEs prepared using 1000 rpm as the 2nd stirring speed [**Fig. 3.8** (a) and (c)].

To conclude, a two-speed stirring protocol in which a higher stirring speed is applied as the 2nd stirring speed in emulsification can reduce drop sizes of HIPEs and enable an obvious improvement in the HIPE stability to creaming.

3.2.2.3 Effect of microgel concentration on stability of the resultant o/w HIPEs

In **Section 2.4.2**, the creaming process of DVB-in-water emulsions (40 vol % DVB) was investigated using microgel concentrations ranging from 0.02 wt % to 0.4 wt %. Since HIPEs have distinct structures and properties from emulsions of lower internal phase volumes[360] and KAA (0.82 M) was also present in the continuous phase, the effect of microgel concentration on the stability of o/w HIPEs was investigated here. Meanwhile, the emulsification using a two-speed stirring protocol resulted in HIPEs with improved stability against creaming (**Section 3.2.2.2**), therefore attention was paid to the question whether the HIPE stability could be further improved by increasing the microgel concentration.

Particle size measurements (**Fig. 3.7**) on microgel suspensions of two concentrations (1.6 mg/ml and 3.2 mg/ml) in the presence of KAA (0.82 M) showed that particles reached their minimum sizes of about 140 nm at 32 ºC and started to aggregate upon a further temperature increase, which was in good agreement with the behaviour of poly(NIPAAm-*co*-AA) microgels at low pH (2-3.5) in the absence of KAA (**Fig. 2.1**). Although pH of the suspension here was 6.6, the presence of KAA clearly not only provided a screening effect as a salt but also deprotonated the microgels by affecting the ionisation equilibrium of PAA moieties. This became more obvious when comparing with the case (**Fig. 2.3**) where microgel aggregation took place above 50 ºC rather than above 32 ºC in the presence of 0.2 M KCl salt due to microgel protonation at pH 5. Minor differences were also observed between microgel sizes in the two suspensions, such as a 20 nm advance for microgels in the suspension with higher microgel concentration (3.2 mg/ml) at temperatures below 25 ºC, which was consistent with the effects of particle concentration on the dimensions of swollen microgels at pH 5 (**Section 2.2.1.3**) and at pH 4 (**Section 2.5.3**) in the absence of KAA.

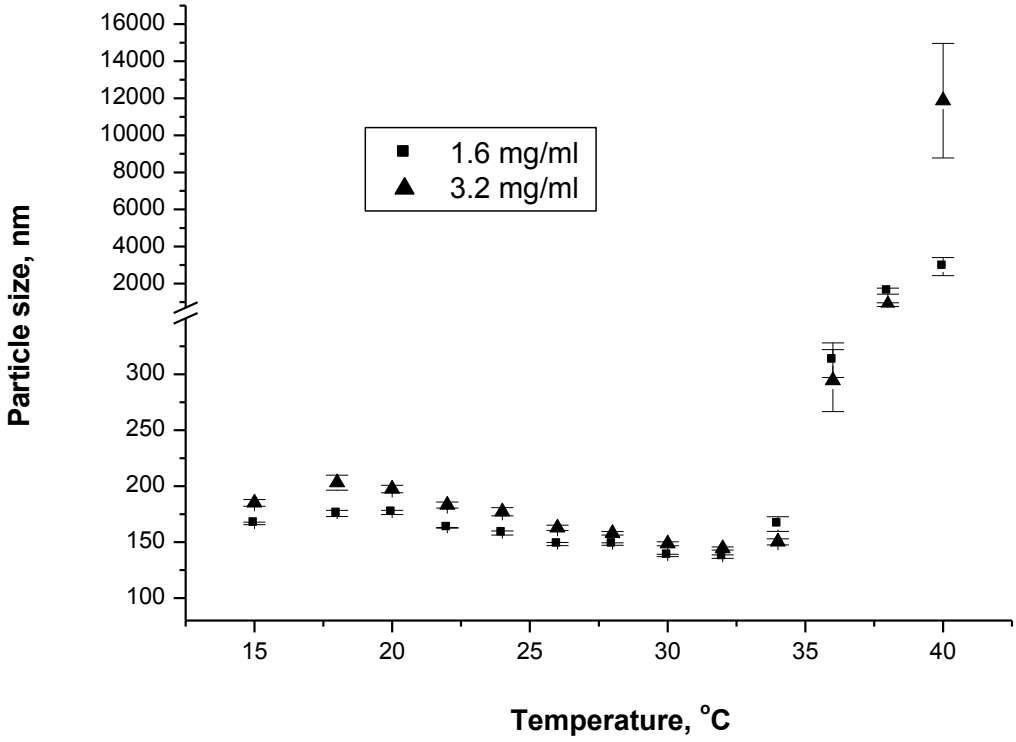
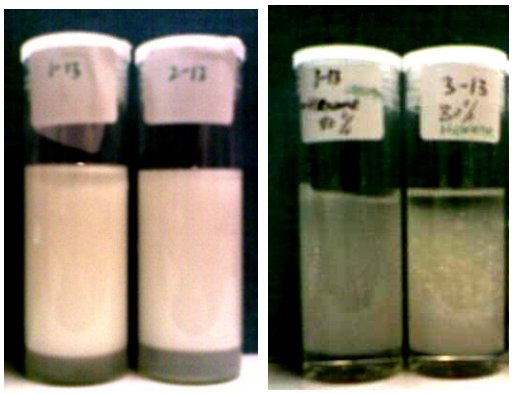


Fig. 3.7 Average particle size of poly(NIPAAm-*co*-AA) microgels suspended in KAA solutions (0.82 M) at microgel concentrations of 1.6 mg/ml and 3.2 mg/ml, respectively.



(a) (b) (c) (d)

Fig. 3.8 Images of microgel-stabilised o/w HIPEs containing KAA after creaming occurred at RT. The oil phase (80 vol %) was toluene for (a) and (b) in contrast to hexane for (c) and (d). Microgel concentrations in the aqueous suspensions were 1.6 mg/ml, 3.2 mg/ml, 1.6 mg/ml and 4.0 mg/ml, respectively. Air bubbles were present in (d).

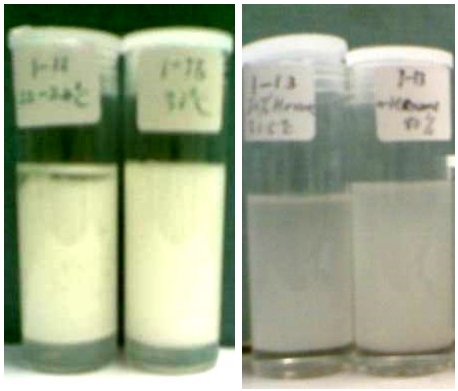
The effect of microgel concentration on HIPE stability was compared for HIPEs with toluene and hexane internal phase (**Fig. 3.8**). For toluene-in-water HIPEs, increasing microgel concentration from 1.6 mg/ml [or 0.15 wt %, **Fig. 3.8** (a),] to 3.2 mg/ml [or 0.31 wt %, **Fig. 3.8** (b)] hardly caused any obvious reduction in the creaming extent of HIPEs at RT. For hexane-in-water HIPEs, entrapment of air bubbles together with a small amount of

un-emulsified oil was observed after increasing microgel concentration from 1.6 mg/ml [**Fig. 3.8** (c)] to 4.0 mg/ml [or 0.38 wt %, **Fig. 3.8** (d)] whereas the creaming extent of HIPEs remained more or less the same. The creaming extent was unaffected in both systems likely due to an insensitivity of droplet size to the variation of microgel concentration according to Equation (3.1). Li *et al.*[407] reported that no obvious changes in average emulsion droplet size were visible upon variation of poly(NIPAAm-*co*-MAA) microgel concentration from 0.05 wt % to 2.0 wt % in hexane-in-water HIPEs. Indeed, although increasing particle concentration generally resulted in a reduced droplet size in a reversely proportional manner,[321,366,413,423] the appearance of a plateau of droplet sizes was also reported upon further increasing the particle concentration.[235,323] Thus, increasing microgel concentration was not always beneficial in terms of emulsion stability. Air entrapment and un-emulsified oil observed in the highly viscous hexane-in-water HIPEs [**Fig. 3.8** (d)] instead indicated negative effects of a high microgel concentration (0.38 wt %). Since hexane-in-water HIPEs were more viscous than the toluene-in-water HIPEs (**Section 3.2.2.2**), a further increase of the microgel concentration in the continuous phase resulted in more viscous HIPEs, which made it difficult to disperse more oil droplets into the continuous phase.[360,417,424]

Therefore, increasing the microgel concentration from 0.15 wt % up to 0.38 wt % had no obvious effect on the creaming extent of the o/w HIPEs. A high microgel concentration (e.g., 0.38 wt %) in a highly viscous HIPE could cause difficulty in emulsification.

3.2.2.4 Effect of temperature on the stability of microgel-stabilised o/w HIPEs

Since microgel particles started to aggregate upon heating above 32 ºC (**Fig. 3.7**) and became less efficient emulsifiers, the temperature during HIPE polymerisation should be controlled below 32 ºC in order to maintain HIPE stability against coalescence.[417] In this section, comparisons were drawn on microgel-stabilised o/w HIPEs in terms of their stability when aged at RT (~22 ºC) and at temperatures below but close to 32 ºC (**Fig. 3.9**) to support the selection of an optimal polymerisation temperature for the HIPE template.



(a) (b) (c) (d)

Fig. 3.9 Images of microgel-stabilised o/w HIPEs that experienced creaming at different temperatures. (a) and (b) were toluene-in-water HIPEs prepared at RT (~22 ºC) but subjected to creaming tests at RT and 30 ºC, respectively; (c) and (d) were hexane-in-water HIPEs that were prepared and tested at RT and at 31~32 ºC, respectively.

For toluene-in-water HIPEs, variation of the aging temperature from RT [**Fig. 3.9** (a)] to 30 ºC [**Fig. 3.9** (b)] did not show any obvious influence on the stability to creaming, indicating an insensitivity to temperature after microgel adsorption onto the interface. This appears to contradict the observations in microgel-stabilised DVB-in-water emulsions at pH 2.5 or pH 3 (**Section 2.5.2**), which showed a significant reduction in creaming extent upon increasing temperature from 25 ºC to 32 ºC. However, this contradiction can be resolved by drawing a comparison among the temperature-induced size changes in the microgel suspensions. The particle size of the microgels used in DVB-in-water emulsions dropped by about 70 nm upon temperature increase from 25 ºC to 32 ºC (microgel aggregation observed at 33 ºC), forming microgel networks to resist creaming due to an increase of hydrophobic interaction. In contrast, the microgel particles used to stabilise toluene-in-water HIPEs exhibited a minor change in particle size by 25 nm when the temperature was increased from 22 ºC (RT) to 30 ºC (**Fig. 3.7**), indicating that interactions between the microgels were more or less unaffected. Hence, an insensitivity of the creaming extent to temperature change was exhibited [**Fig. 3.9** (a) and (b)]. For hexane-in-water HIPEs, uniformity in the preparation temperature and the aging temperature for each sample allowed us to check whether microgel adsorption was affected by a temperature change from RT [**Fig. 3.9** (c)] to 31-32 ºC [**Fig. 3.9** (d)]. However, this was hardly evident from the observation of creaming extents. It was only obvious that these o/w HIPEs containing KAA in the continuous phase were stable to coalescence at RT and temperatures close to 32 ºC.

To sum up **Section 3.2.2**, microgel-stabilised o/w HIPEs whose aqueous phase contained KAA were stable to coalescence when the KAA concentration was below 1.0 M. Further

investigations at a KAA concentration of 0.82 M showed that a two-speed stirring protocol in comparison with a one-speed stirring protocol was capable of reducing the droplet sizes and improving HIPE stability against creaming whereas an increase of the microgel concentration from 0.16 wt % up to 0.4 wt % or an increase of the aging temperature from RT to those close to 32 ºC had no obvious effect on the creaming extent of HIPEs.

3.3 Selecting initiator and crosslinker for the polymerisation of o/w HIPEs

Since the stability of microgel-stabilised o/w HIPEs in the presence of KAA is limited when microgel particles start to aggregate (**Section 3.2.2.1**), it is essential to control the temperature below the aggregation temperature of microgels (**Fig. 3.7**) when polymerising these HIPEs. Thus, an initiating system capable of producing radicals at low temperatures is required. Also, polymerisation at relatively low temperatures is of critical importance when bioactive molecules[425] and living cells[426-428] are involved. For this purpose, we have investigated two possibilities other than the conventional approach of thermal-initiation, including a redox initiating pair of ammonium persulphate (APS)/*N,N,N',N'*-tetramethylethylenediamine (TMEDA) and a photo-initiating system using 2-hydroxy-1-[4-(2-hydroxyethoxy) phenyl]-2-methyl-1-propanone (Irgacure 2959 or I2959, see **Fig. 3.1** for its chemical structure). APS/TMEDA was studied here since it is commonly used for polymerising hydrophilic monomers in o/w emulsions[401-403,405,429,430] or in CO_2-in-water emulsions.[431] On the other hand, a photo-initiating system proved to be highly efficient in polymerising w/o HIPEs.[101,109,118,119,205,432-434] To photo-polymerise o/w HIPEs in our case, Irgacure 2959 was chosen due to its water-solubility and promising performances in injectable scaffolds with living cells encapsulated.[435-444]

3.3.1 Polymerisation of microgel-stabilised o/w HIPEs using redox initiation

To polymerise o/w HIPEs using redox initiation (APS/TMEDA), how TMEDA was added was the key issue since APS could be simply mixed into the aqueous suspensions prior to emulsification. Although TMEDA may be mixed with APS prior to emulsification under well-controlled conditions[429,445,446] together with a very short emulsifying period, it is generally added after an emulsion has been formed.[447] In our case, emulsification of microgel suspensions in KAA solutions with toluene or hexane can be achieved using either a one-

speed stirring protocol (400 rpm) or a two-speed stirring protocol (400→1000 rpm) (**Section 3.2.2**). Thus, the adding moment of TMEDA (0.02~0.05 ml) via an instant injection was investigated for both stirring protocols in order not to compromise the stability of o/w HIPEs.

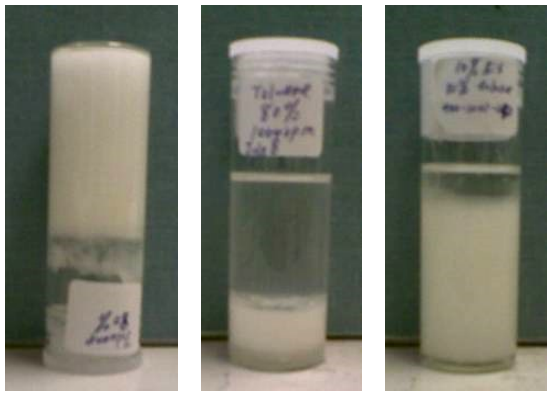
Firstly, TMEDA was added 3 min before the end of stirring in a one-speed stirring protocol, in accordance with the procedure used by Krajnc *et al*. in the polymerisation of a surfactant-stabilised o/w HIPEs.[401] As a result, stable HIPEs were obtained after stirring. For example, microgel-stabilised HIPEs containing 10 mol % BIS relative to KAA in the continuous phase were polymerised after maintained at 31 °C for about 60 h [**Fig. 3.10** (a)].

Secondly, when TMEDA was added during stirring at 1000 rpm in a two-speed stirring protocol (400→1000 rpm), phase separation was observed after stirring, e.g., HIPEs containing 10 mol % BIS [**Fig. 3.10** (b)] and HIPEs containing 20 mol % di(ethylene glycol) divinyl ether (DEGDVE) [**Fig. 3.11** (a)]. However, stable HIPEs were found available when TMEDA was added prior to stirring at 1000 rpm in a two-speed stirring protocol [e.g., HIPEs containing 20 mol % DEGDVE, **Fig. 3.11** (b)] or during stirring at the 3rd speed in a three-speed stirring protocol [400→1000→240 (or 400) rpm] [e.g., HIPEs containing 10 mol % BIS, **Fig. 3.10** (c)].

It was indicated that mixing TMEDA at a higher stirring speed (1000 rpm) was harmful to the HIPE stability to coalescence. Indeed, HIPE stability upon addition of TMEDA was not directly related to whether a higher speed was used for emulsification as long as TMEDA was added at a lower stirring speed. As reported by Kovacic *et al.*,[403] it was even satisfactory to reduce the stirring speed to 20 rpm during TMEDA addition for their o/w HIPEs containing HEMA. Zhang *et al.* used homogenization (much higher stirring speed) after TMEDA was added into o/w HIPEs containing NIPAAm.[405] The reason for phase separation of microgel-stabilised HIPEs upon TMEDA addition at 1000 rpm was similar to the demulsification of clay particles stabilised o/w emulsions by the addition of fresh oil.[448,449] Yan *et al.* found that an increase in stirring speed from 200 rpm to 800 rpm resulted in much faster demusilifcation and attributed this to more fresh oil droplets produced, higher collision frequency and more effective collision between fresh oil droplets and emulsion droplets.[449] We believe their explanation can also fit into our case and the collision of TMEDA droplets and emulsion droplets became much more effective at 1000 rpm, leading to phase separation.

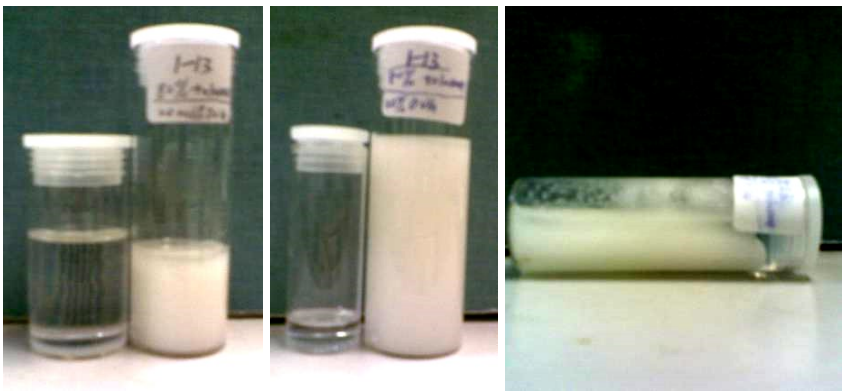
Meanwhile, the nature of the crosslinker, especially its solubility and reactivity,[450,451] was crucial to the polymerisation of o/w HIPEs. BIS, soluble in the neutralised AA solution[401,452] and sufficiently reactive,[401,453,454] was found suitable [**Fig. 3.10** (a) and (c)]. Other

crosslinkers such as di(ethylene glycol) divinyl ether (DEGDVE) and 1,5-hexadiene-3,4-diol (DVG) did not produce solid polyHIPEs [**Fig. 3.11** (c)] either due to a low water solubility[455] or a low reactivity.[450,456,457]. Indeed, BIS has been widely used as the crosslinker in the preparation of polyHIPEs with hydrophilic monomers.[94,140,200,401-406,430,431]



(a) (b) (c)

Fig. 3.10 Photographs of samples prepared using 5 ml microgel suspension (1.6 mg/ml) in KAA solutions (0.82 M) and 20 ml toluene but using various stirring protocols for the addition of TMEDA. APS and BIS (10 mol %) were mixed into the aqueous suspension prior to emulsification. (a) Polymerised o/w HIPEs after 60 h at 31 °C, 3.7 ml toluene expelled, TMEDA added at the end of a one-speed stirring protocol (400 rpm); (b) 13.3 ml toluene expelled, TMEDA added during stirring at 1000 rpm in a two-speed stirring protocol (400→1000 rpm); (c) polymerised o/w HIPEs after 52 h at RT and 2 d at 31 °C, 4.3 ml toluene expelled, TMEDA added during stirring at the 3rd speed in a three-speed stirring protocol (400→1000→240 rpm).



(a) (b) (c)

Fig. 3.11 Photographs of samples prepared using 5 ml microgel suspension (1.6 mg/ml) in KAA solutions (0.82 M) and 20 ml toluene. APS and DEGDVE (20 mol %) were mixed into the aqueous suspension prior to emulsification. (a) TMEDA added during stirring at 1000 rpm in a two-speed stirring protocol (400→1000 rpm) and ~12 ml toluene expelled after stirring (in the tube on the left); (b) TMEDA added prior to stirring at 1000 rpm in a two-speed stirring protocol (400→1000 rpm) and ~1.3 ml toluene expelled after stirring (in the tube on the left); (c) the sample shown in (b) were not solidified after 3 d at 30 °C.

To sum up, microgel-stabilised o/w HIPEs were stable as long as addition of TMEDA was carried out during stirring at a relatively low speed, irrespective of whether or when a higher speed of 1000 rpm was used. A crosslinker of good solubility and high reactivity was required and BIS was found to be a suitable crosslinker for polymerisation of the o/w HIPEs.

3.3.2 Photo-polymerisation of microgel-stabilised o/w HIPEs

3.3.2.1 Photo-initiation methods for the polymerisation of microgel-stabilised o/w HIPEs

To make use of photo-initiation for the polymerisation of microgel-stabilised o/w HIPEs, two protocols have been developed: a manual rotation protocol and a continuous rotation protocol during UV exposure.

First, as used for the polymerisation of water-in-DVB HIPEs (**Section 2.6.1**), a protocol involving manual rotation of the glass tube of HIPEs by 120° twice was used for the polymerisation of microgel-stabilised o/w HIPEs (80 vol % toluene, 0.82 M KAA and 10 mol % BIS). It was necessary to rotate the sample tube (25 mm in diameter) because of the limited penetration depth of UV[433,434,458] through the emulsions which manifested itself by the fact that half of the HIPEs in the back of the vial remained liquid while the HIPEs exposed to UV gelled. Manually rotating the glass tube by 120° twice guaranteed a full exposure of the sample surface to UV light. Moreover, a water bath of 25 °C was used to maintain the sample temperature to avoid HIPE destabilisation by temperature-induced microgel aggregation. As a result, the o/w HIPEs completely gelled after a total exposure time of 30~35 min, which suggested a much more efficient initiation and gelation in comparison with that using an identical amount of APS (2 mol% relative to the total double bonds) together with TMEDA [**Fig. 3.10** (c)]. Meanwhile, in contrast to the two-step addition of APS/TMEDA, photo-initiator I2959 was dissolved into the aqueous phase prior to emulsification. This was believed to contribute to the efficient gelation as well because the generation of free radicals occurred at RT upon exposure to UV light for I2959 but required contact of APS and TMEDA within the HIPE template. 1.45 ml toluene (7%) was expelled from the HIPEs during the polymerisation, suggesting better-maintained emulsion stability than systems using the redox initiation. The pore structure of purified polyHIPEs (**Fig. 3.12**)

showed pores of up to a few hundred micrometers in diameter, which proved the feasibility of photo-polymerisation for the preparation of poly(KAA) Pickering-HIPEs.

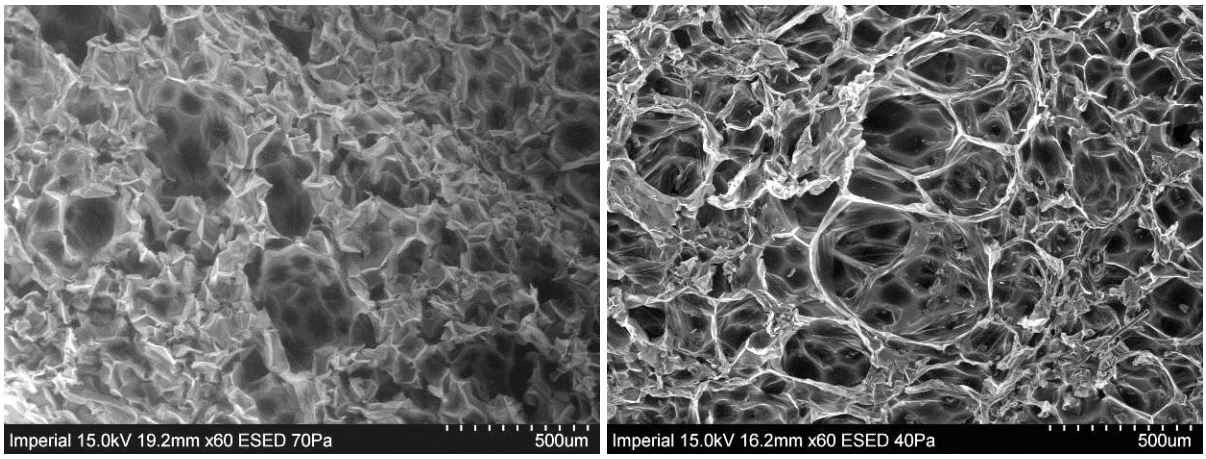


Fig. 3.12 SEM images of poly(KAA) Pickering-HIPEs prepared by photo-polymerisation of microgel-stabilised o/w HIPEs with a manual rotation protocol during UV exposure. The aqueous phase of the HIPEs contained 0.82 M KAA, 10 mol % BIS, 2 mol % photo-initiator I2959 and 1.6 mg/ml microgels while the oil phase was toluene (80 vol %). After polymerisation, the sample was purified using a two-step Soxhlet extraction with HCl in MeOH solution (0.8 M) and acetone in sequence.

Second, a protocol using an overhead stirrer to continuously rotate a HIPE sample at 50-70 rpm during UV exposure was developed (**Fig. 7.6**). Thus, the sample was continuously exposed to the UV light, supposedly leading to a more homogeneous polymerisation of the sample from all directions. This protocol was used to polymerise all the rest o/w HIPEs and proved to be efficient. An example of the poly(KAA) Pickering-HIPEs prepared using this protocol (**Fig. 3.13**) showed un-collapsed pores of up to a few hundred microns were obtained, within the size range for bone tissue engineering scaffolds.[1,2,459] "Potential pore throats" (small circle) were visible in the pores (big circle) but still not open as evidenced by the fact that underlying pore structures were completely covered. Therefore, how to break the "potential pore throats" open and make interconnected structures[3,460] is of significance for application of this template as tissue engineering scaffolds (**Section 3.4**).

Moreover, temperature control during photo-initiation was further optimized. Adding BIS (10 mol % relative to KAA) and I2959 clearly affected the swelling behaviour of poly(NIPAAm-*co*-AA) microgel particles (**Fig. 3.14**). Microgels reached the minimum size of ca. 100 nm at 28 °C and 24 °C before and after addition of BIS & I2959, respectively, and then aggregated with further increasing the temperature. Moreover, prior to the onset of aggregation, microgel particles were 30-50 nm smaller in the presence of BIS and I2959 at

the same temperatures. This suggested that addition of these small organic molecules, especially BIS, enhanced the tendency of microgel deswelling, which was attributed to a partial replacement of hydrogen bonds between microgels and water by those between microgels and BIS. A minor difference was also observed between the two initiators regarding their effects on microgel behaviour. I2959 shifted the onset of microgel aggregation to a slightly lower temperature (25-26 °C) than APS (ca. 28 °C), indicating its higher affinity to microgel particles. Therefore, the temperature should be ideally controlled below 25 °C to maintain the HIPE stability during UV polymerisation. In practice, due to a considerable amount of heat generated by the UV lamp (100 W) in an enclosed box, the water-bath temperature was adjusted to ca. 20-22 °C prior to UV exposure.

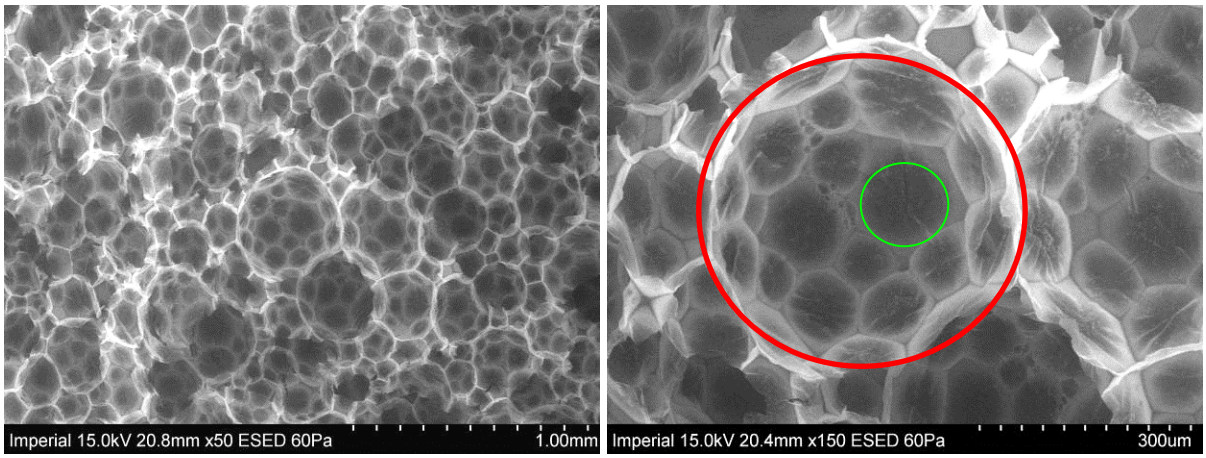


Fig. 3.13 SEM images of poly(KAA) Pickering-HIPEs prepared by UV-initiated free radical polymerisation using a continuous rotation protocol during UV exposure. The o/w HIEPs were emulsified using microgel suspension in KAA solution (1.6 mg/ml microgels, 0.82 M KAA, 10 mol % BIS, 2 mol % I2959), toluene (80 vol %) and a one-speed stirring protocol (400 rpm). A pore and a "potential pore throat" (not open) were marked in the pore structure.

In addition, although the emulsion template can be photo-polymerised rapidly within less than one hour or even within a second,[433] it was observed in our case that the HIPE sample remained partially fluidic after UV exposure and became an integral gel in the glass tube (external diameter: 25 mm) through a standing period (after UV exposure but prior to purification via Soxhlet extraction). Apart from the penetration depth of UV light through emulsions, this delay of complete gelation may arise from the inhibiting effect of O_2.[461,462] Indeed, when replacing the air layer on top of HIPEs with argon before UV exposure, complete gelation was resulted in the glass tube immediately after UV exposure. This indicated that a removal of the O_2 in the air layer could effectively eliminate the inhibiting effect.

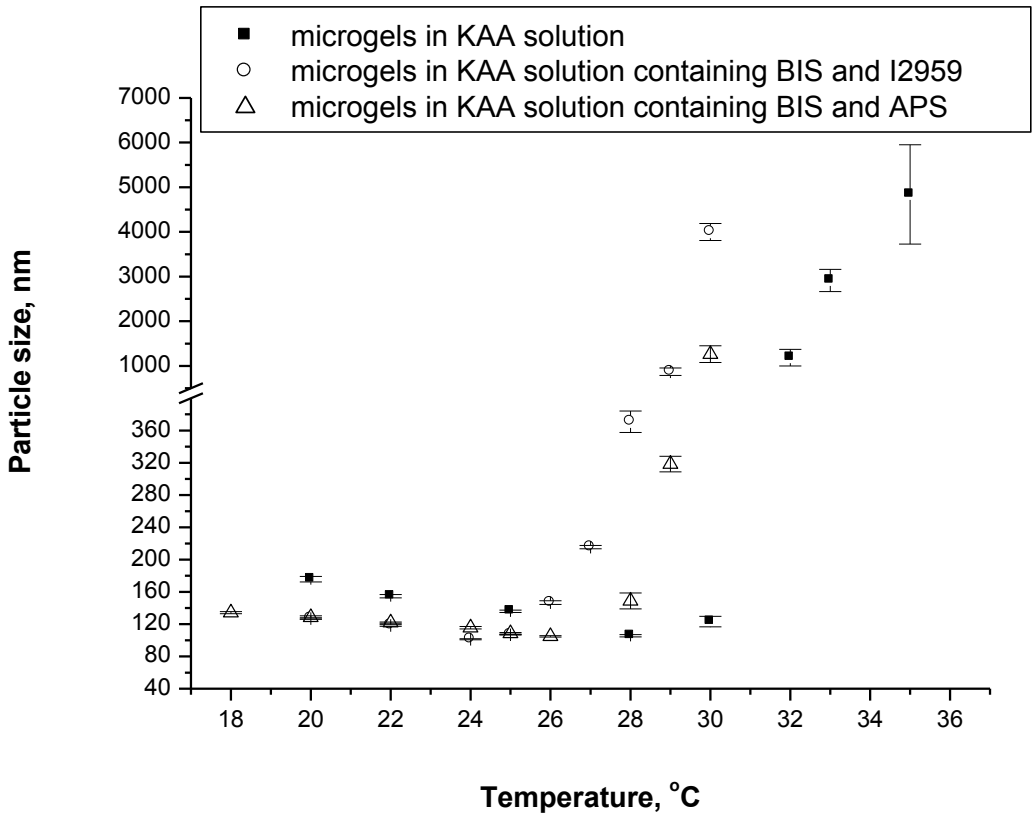


Fig. 3.14 Average particle size of poly(NIPAAm-*co*-AA) microgels in KAA solutions (0.82 M) with and without BIS (10 mol % relative to KAA) and an initiator (I2959 or APS, 2 mol % relative to the total double bonds).

3.3.2.2 Effect of initiator amount on polymerisation of microgel-stabilised o/w HIPEs

Since the initiator amount does influence the penetration depth of UV light in the emulsions,[433,434] i.e., a lower initiator amount allows a deeper UV penetration, effects of varying the initiator amount on gelation of o/w HIPEs were preliminarily investigated. Based on the HIPE template (1.6 mg/ml microgels, 0.82 M KAA, 10 mol % BIS and 80 vol % toluene), the amount of photo-initiator I2959 was varied from 2.0 mol % to 1.5 mol %, 1.0 mol % and 0.5 mol % respectively. A large portion of HIPEs could still flow in the case of 0.5 mol % initiator (argon used on the top) after photo-polymerisation (**Fig. 3.15**), indicating 0.5 mol % I2959 was insufficient to initiate the polymerisation. On the contrary, other HIPEs using more initiators were all completely cured after polymerisation. Meanwhile, a slight increase of the creaming volume, i.e., the volume of aqueous phase resolved at the bottom of the glass tube, was observed with decreasing initiator content, suggesting that the most rapid curing here was attained at the highest content of initiator (2 mol %).



Fig. 3.15 Photographs of photo-polymerised microgel-stabilised HIPEs by using various amounts of I2959. From left to right: the initiator amount was 2.0 mol %, 1.5 mol %, 1.0 mol % and 0.5 mol % (relative to the total double bonds), respectively. The HIPEs were emulsified using 5 ml microgel suspension in KAA solution (1.6 mg/ml microgels, 0.82 M KAA, 10 mol % BIS) and 20 ml toluene. Black lines marked the positions below which gels were formed after photo-polymerisation.

To sum up **Section 3.3.2**, a UV-polymerisation protocol has been developed (**Fig. 3.16**) for the preparation of polyHIPEs from microgel-stabilised o/w HIPEs.

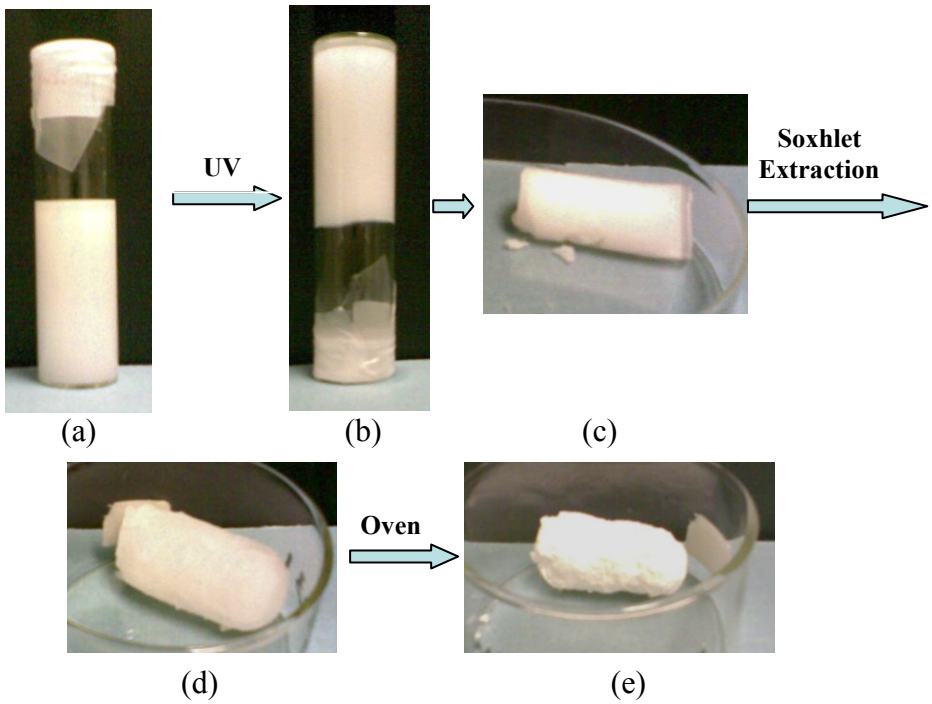


Fig. 3.16 Photographs of the preparation process of poly(KAA) Pickering-HIPEs (a) A sample of microgel-stabilised o/w HIPEs in a glass tube of 25 mm in diameter; (b) HIPEs cured after UV exposure; (c) the gel-like sample was taken out of the tube by cracking the glass with a diamond knife; (d) the sample was taken out of an extraction thimble after experiencing a designed Soxhlet-extraction procedure; (e) dried sample, a polyHIPE.

3.4 Controlling the pore structure of poly(KAA) Pickering-HIPEs

As briefly mentioned in **Section 3.3.2.1**, the poly(KAA) Pickering-HIPEs obtained are mainly closed celled (**Fig. 3.13**) but open pores with high degree of interconnectivity are required for bone tissue engineering applications. Similarly, other polyHIPEs based on Pickering emulsions, i.e., poly(Pickering HIPEs), were also reported with morphologies of large (up to a few hundred microns) but closed pores.[190,191,193,197] Nevertheless, polyHIPEs based on surfactant-stabilised emulsions (conventional polyHIPEs) can also have closed-pore morphologies,[360,463-465] within which pore-throat production was investigated.[136,137,356] Since the preparation of polyHIPEs involves multiple steps and a number of factors, the mechanisms for pore-throat formation are still under debate.[103,358] The principle question concerns the exact time in the process and how pore throats are generated. Proposed causes for the formation of pore throats include the separation of surfactant molecules from the oil phase during polymerisation,[138] thinning of the oil layer surrounding the water droplets due to an increase of the surfactant/monomer ratio,[136] volume contraction on conversion of monomer to polymer,[137,203] and mechanical forces during Soxhlet extraction and drying.[127,191] We carried out a systematic investigation aiming to find out whether pore throats can be produced in poly(KAA) Pickering-HIPEs and the nature of any underlying mechanisms. In the following discussion, contributions from other researchers on this matter will also be covered.

3.4.1 Varying the extraction and drying conditions to produce open porous polyHIPEs

3.4.1.1 Effect of extraction time and extraction-drying protocol on the pore structures

Since the removal of internal phase from polyHIPEs involves solvent extraction and drying (**Fig. 3.16**), it is natural to consider the two processes together when evaluating their effect on the degree of interconnectivity of polyHIPEs. Although the formation of pore throats in polyHIPEs has been conventionally attributed to the polymerisation step,[136-138] the effects of solvent extraction and drying on pore interconnectivity have recently been stressed.[127,191,466,467] In the case of poly(Pickering HIPEs), it's been further proposed that mechanical actions arising from Soxhlet extraction and drying were responsible for the

occasional appearance of pore throats.[127,191,197] This initiated our attempt to produce pore throats for poly(KAA) Pickering-HIPEs by varying the conditions of Soxhlet extraction and drying. Based on an established microgel-stabilised o/w HIPE template (0.82 M KAA, 10 mol % BIS, 2 mol % I2959 and 80 vol % toluene), various extraction and drying conditions were investigated first (**Table 3.2**).

Table 3.2 The protocols used in the purification and drying of poly(KAA) Pickering-HIPEs

	Fig. 3.13	**Fig. 3.17**	**Fig. 3.18**	**Fig. 3.19**
Extraction with HCl in MeOH	0.8 M, 24 h	0.15 M, 40 h	0.15 M, 40 h	0.15 M, 72 h
Drying temperature, °C	50	50	70	70
One-step extraction and one-step drying	-	√	√	-
One-step extraction and two-step drying	-	√	√	-
Two-step extraction and one-step drying	√	√	√	√
Two-step extraction and two-step drying	-	√	√	√

* Soxhlet extraction with HCl in MeOH (one-step extraction) was followed by extraction with acetone for 24 h in a two-step extraction protocol; one-step drying refers to vacuum drying while two-step drying means polyHIPE was dried in a convection oven before being moved into a vacuum oven.

On the one hand, a comparison on the morphology of polyHIPEs was made among those experiencing the protocol of two-step extraction and one-step drying, i.e., Soxhlet extraction in sequence with HCl in MeOH and acetone followed by vacuum drying. Assuming pore throat formation occurs by mechanical actions, extending the extraction duration or increasing the drying temperature should increase this effect on polyHIPEs. Thus, from left to right in **Table 3.2**, the impact of purification and drying on polyHIPEs is supposed to increase and pore throats are expected to appear. However, all polyHIPEs exhibited intact closed-pore structures [**Fig. 3.13**, **Fig. 3.17** (c), **Fig. 3.18** (c) and **Fig. 3.19** (a)]. In addition, although 0.8 M and 0.15 M HCl in MeOH were used, the effect of HCl concentration on purification is believed to be negligible since both concentrations were excessive as indicated by the acidic nature of the post-extraction liquids. The closed-pore structures under various conditions may suggest two possibilities: either that the mechanical actions exposed so far are not strong enough to rupture the thinned pore wall or that pore throats are indeed not generated during the process of extraction and drying at all. In practice, we did not further increase the drying temperature to avoid deformation of the polymers (the glass transition

temperature ~105 °C[468]). Meanwhile, an extraction process with an even greater duration than 4 d would also be inefficient. Instead, it is sensible to look into other factors involved in the preparation of polyHIPEs, such as internal phase volume ratio, crosslinker content, monomer content and stirring speed as discussed in the following sections. Therefore, it is not yet obvious here what impact the process of extraction and drying may have on the interconnectivity of polyHIPEs if there is any.

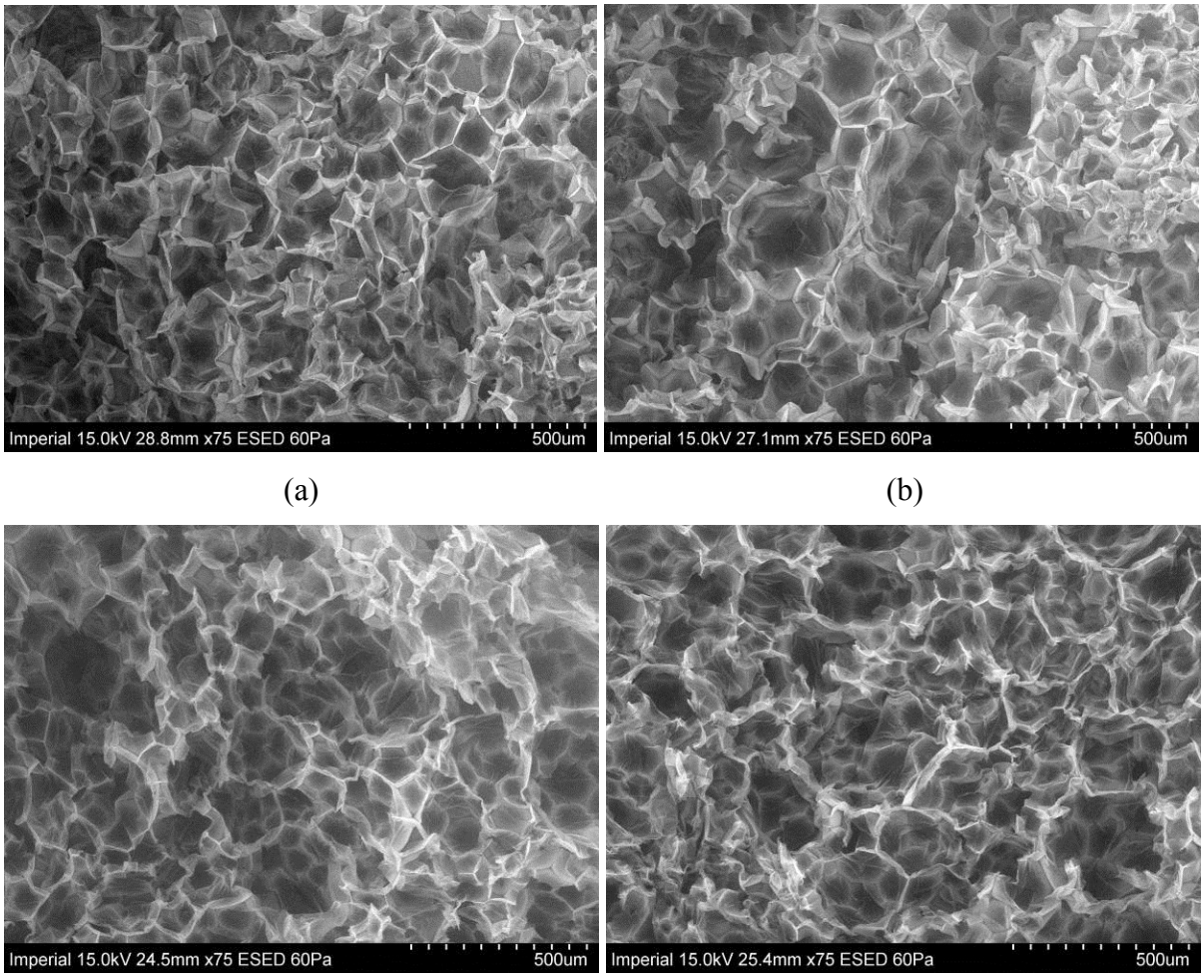


Fig. 3.17 SEM images of poly(KAA) Pickering-HIPEs prepared using various purification and drying protocols. (a) One-step extraction with HCl in MeOH for 40 h, vacuum drying (one-step); (b) One-step extraction, two-step drying (drying in a convection oven before vacuum drying); (c) Extraction with HCl in MeOH for 40 h followed by extraction with acetone for 24 h (two-step extraction), one-step drying; (d) two-step extraction, two-step drying. The drying temperature is 50 °C for all.

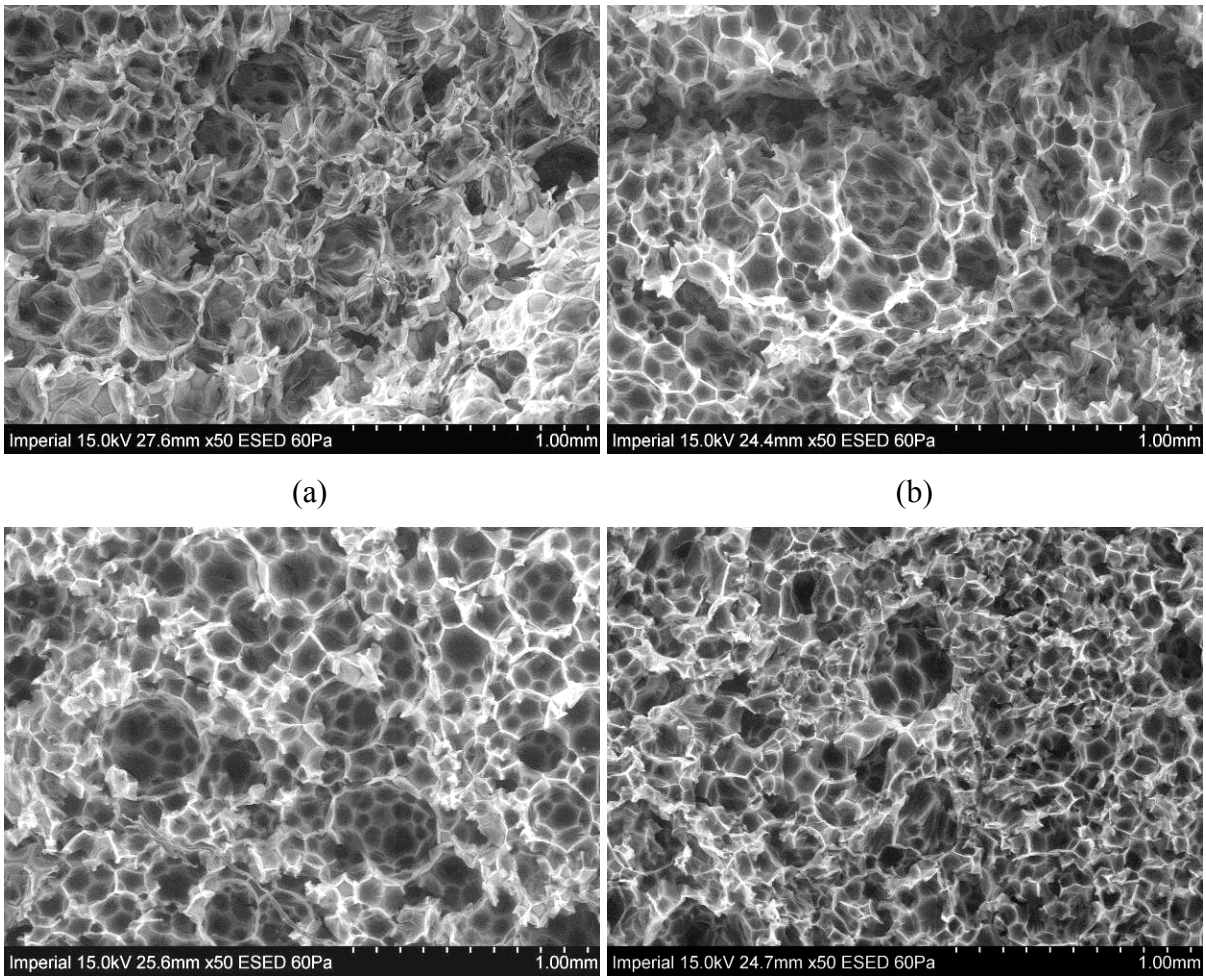
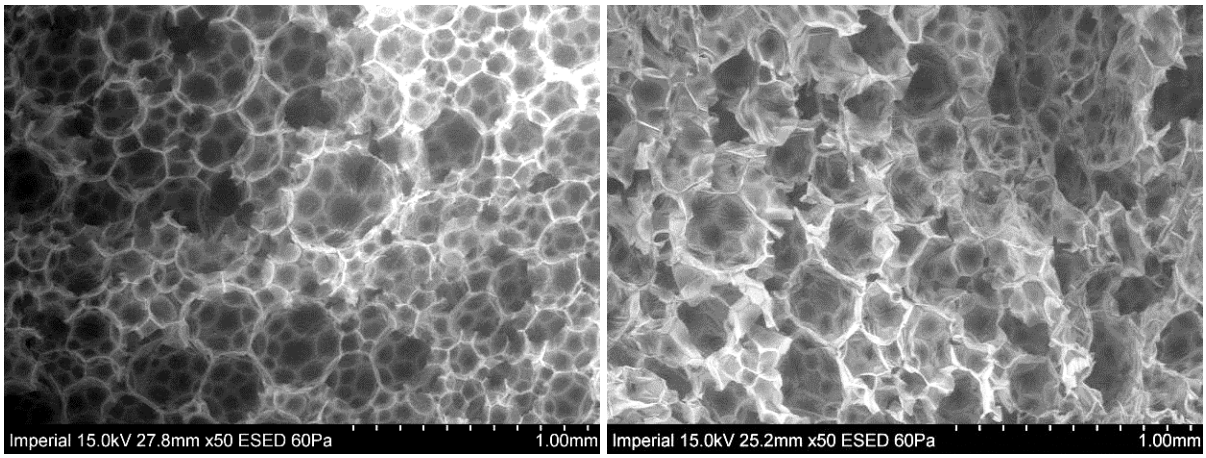


Fig. 3.18 SEM images of poly(KAA) Pickering-HIPEs prepared using various purification and drying protocols. (a) One-step extraction with HCl in MeOH for 40 h, vacuum drying (one-step); (b) One-step extraction, two-step drying (drying in a convection oven before vacuum drying); (c) Extraction with HCl in MeOH for 40 h followed by extraction with acetone for 24 h (two-step extraction), one-step drying; (d) two-step extraction, two-step drying. The drying temperature is 70 °C for all.

On the other hand, the effect of different protocols of purification and drying on the pore structure were evaluated. Firstly, protocols using either one-step or two-step extraction differ in the solvent to which the polymers are exposed and from which they were dried. Since MeOH and acetone are a good solvent and a non-solvent for PAA, respectively,[469,470] it is interesting to know whether one-step and two-step extraction may have any different impacts on the micro-structures of PAA and even on the formation of pore throats. Secondly, one-step (vacuum drying only) and two-step drying (drying in a convection oven followed by vacuum drying) at the same temperature differ in the drying rate. Since solvent is supposed to be removed at a slower rate in a convection oven, it will be possible to see what effect this variation may have on the morphology of polyHIPEs. In contrast to the protocol of two-step

extraction and one-step drying [**Fig. 3.18** (c)], one-step extraction and one-step drying [**Fig. 3.18** (a)] resulted in a corrugated pore walls.[471] This is likely because polymers were quickly dried at 70 °C from a rubbery state after extraction with MeOH whereas a second extraction with acetone made the polymer chains more rigid and glassy before drying.[472-477] This corrugating effect became less obvious when reducing the drying rate by either using the protocol of one-step extraction and two-step drying [**Fig. 3.18** (b)] or drying at a lower temperature [50 °C, **Fig. 3.17** (a)], which allowed the solvated polymer chains to gradually adjust their configuration upon removal of MeOH. In addition, a faster removal of acetone from the pore surface using vacuum drying [**Fig. 3.17** (c), **Fig. 3.18** (c) and **Fig. 3.19** (a)] yielded rigid pores without distortion in comparison to the two-step drying protocols [**Fig. 3.17** (d), **Fig. 3.18** (d) and **Fig. 3.19** (b)]. Therefore, varying the purification and drying protocol did not change the predominance of closed-pore morphology and the shape of pores was best maintained in the case of two-step extraction followed by vacuum drying at 70 °C.



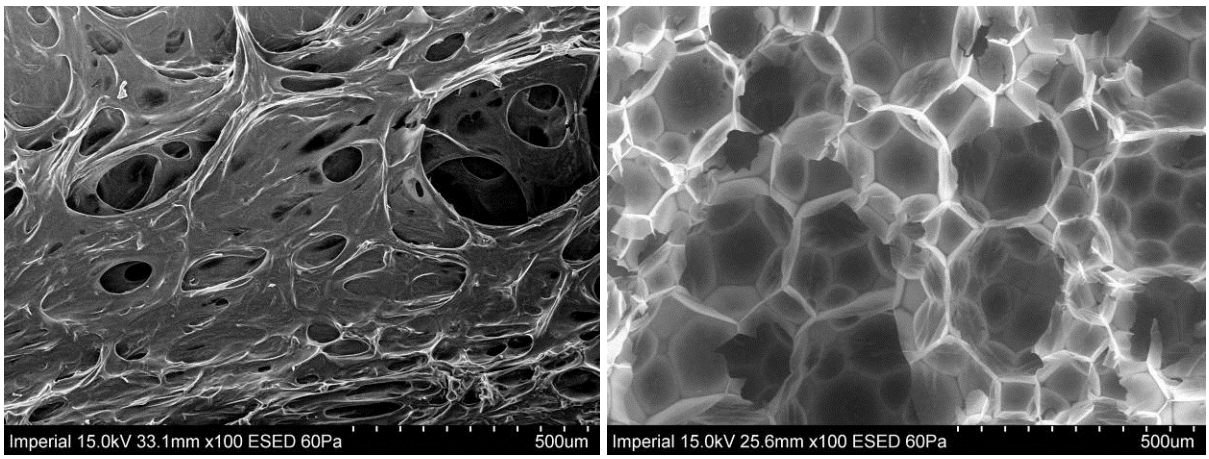
(a) (b)

Fig. 3.19 SEM images of poly(KAA) Pickering-HIPEs purified using extraction with HCl in MeOH for 72 h plus extraction with acetone for 24 h but dried using either a one-step (a) or a two-step (b) protocol at 70 °C.

3.4.1.2 Other attempts to produce pore throats in the extraction and drying process

Using the same composition to prepare poly(KAA) Pickering-HIPEs (0.82 M KAA, 10 mol % BIS, 2 mol % I2959 and 80 vol % toluene), another two approaches were carried out to produce open porous structures. The concept of both involves making plyHIPEs swell to a larger extent and expects to produce pore throats via the subsequent drying. The first approach is to prepare a hydrogel using a sample of obtained the poly(KAA) Pickering-

HIPEs by allowing it to absorb water (1:200, w/w) and subsequently to freeze-dry the hydrogel sample. Pore throats were obtained [**Fig. 3.20** (a)] through a thermally induced phase separation (TIPS) process,[470,478] however, the overall structures of polyHIPEs were completely lost due to collapse and overlap of the pore layers during freeze-drying.[479] The second approach is to employ an extracting solvent of greater solvating power[469] for the polymers – a mixture of HCl in MeOH and distilled water (1:1, v/v) – instead of HCl in MeOH (**Fig. 3.13**). Similarly, closed pores were still dominant in the morphology [**Fig. 3.20** (b)]. Due to the volume confinement of polyHIPEs by the extraction thimble during extraction, a larger swelling degree may not be practically achieved, and clearly the subsequent replacement of MeOH/water by acetone showed little effect on pore-throat formation.



(a) (b)

Fig. 3.20 SEM images of poly(KAA) Pickering-HIPEs (a) freeze-dried polyHIPE hydrogel, (distilled water/dry polyHIPEs= 200, w/w) (b) polyHIPEs extracted first with a 1:1 (v/v) mixture of HCl in MeOH and distilled water ([HCl]= 0.15 M) for 26 h and then with acetone for 24 h, followed by vacuum drying at 60-70 °C.

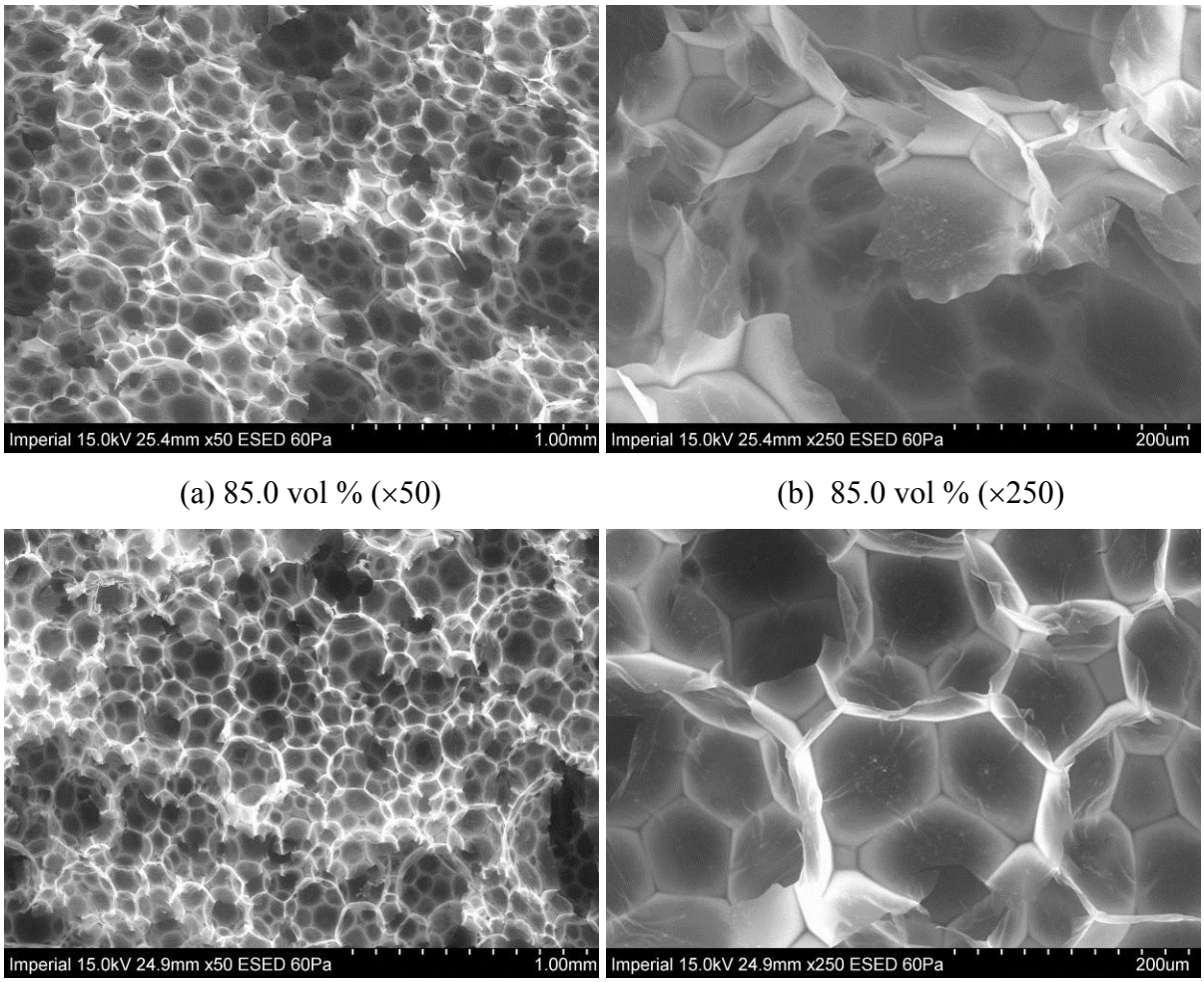
To sum up, despite a proposed mechanism that pore throats are possibly produced during the extraction and drying processes, closed-pore morphologies have been predominantly exhibited in polyHIPEs prepared using a fixed composition (0.82 M KAA, 10 mol % BIS, 2 mol % I2959 and 80 vol % toluene) under various conditions of extraction and drying. Whether the extraction and drying processes may have any effect on pore throat formation at other HIPE compositions is worth further investigating into.

3.4.2 Tuning the HIPE composition for open porous poly(KAA) Pickering-HIPEs

When evaluating the impact of HIPE composition on the morphology of polyHIPEs, it is useful to take the polymerisation process into account to interpret the formation of the pore walls. Since the polymerisation in the continuous phase of a HIPE is generally a free-radical crosslinking polymerisation, the formation of pore walls may be well understood by referring to the analogous situation in macroporous copolymer resin beads[356] or a hydrogel matrix, especially in the presence of a diluent during polymerisation. As comprehensively studied in the preparation of macroporous resin beads[480-483] or hydrogels,[484-489] their porous structures can be influenced by the nature of the diluent, the monomer/diluent ratio and the crosslinker content as well as the processes of solvent extraction and drying. Indeed, based on the analogy, the variation of many properties of the polyHIPEs can be better interpreted,[361-363,404,490-493] such as porosity, wall roughness and surface area. However, it is worth noting that the pores in resin beads or hydrogel matrices are normally on the nanometre scale, i.e. smaller than the size of pore throats in polyHIPEs. It is still unknown whether the formation of pore throats in polyHIPEs is related to these polymerisation-induced nanometre-sized pores. In this section, since H_2O is the diluent, the HIPE composition, including internal phase volume ratio, concentrations of crosslinker (BIS) and monomer (KAA) were varied. For purification and drying of the produced polyHIPEs, the same protocol (two-step extraction followed by vacuum drying at 70 °C) was used.

3.4.2.1 Effect of the internal phase volume ratio on pore structures

Although the internal phase of a Pickering emulsion template is believed to have little effect on the polymerisation occurring in the continuous phase, the internal phase volume ratio ($\phi_{int.}$) of a HIPE template may affect the resultant morphologies due to its influence on the total water-oil interfacial area. The nominal $\phi_{int.}$ was increased from 80.0% as previously used to 85.0% and 90.0% during emulsification, respectively, while the aqueous composition was maintained constant (1.6 mg/ml microgels, 0.82 M KAA, 10 mol % BIS and 2 mol % I2959). As a result of coalescence of a small percentage of toluene droplets during emulsification (volume measured by a 1.0 ml syringe), the actual $\phi_{int.}$ were 84.5% and 89.0%, respectively.



(a) 85.0 vol % (×50) (b) 85.0 vol % (×250)

(c) 90.0 vol % (×50) (d) 90.0 vol % (×250)

Fig. 3.21 SEM images of poly(KAA) Pickering-HIPEs at two magnifications (×50 and ×250). The HIPEs were prepared using a microgel suspension in KAA solution (1.6 mg/ml microgels, 0.82 M KAA, 10 mol % BIS and 2 mol % I2959), 85.0 vol % or 90.0 vol % toluene as the internal phase and a one-speed stirring protocol (400 rpm).

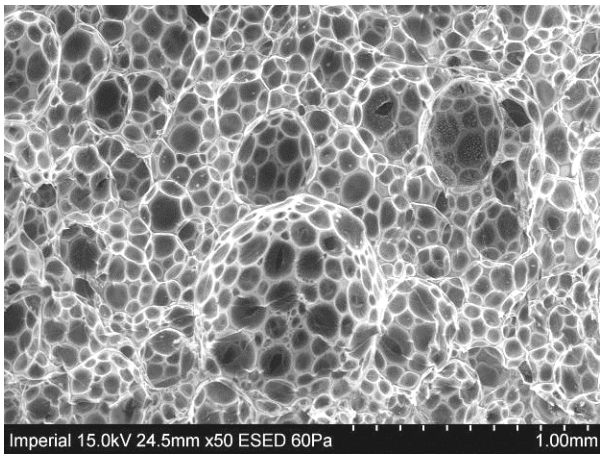
Similar to poly(KAA) Pickering-HIPEs prepared using 80 vol % toluene (**Fig. 3.13**), polyHIPEs prepared using 85 vol % and 90 vol % toluene (**Fig. 3.21**) exhibited closed pore morphologies and "potential pore throats" (not real pore throats). This insensitivity of pore-throat formation to the increase of $\phi_{int.}$ was in agreement with what Williams *et al.*[136] found in conventional polyHIPEs, where closed-pore structures were produced at low surfactant content for $\phi_{int.}$ even up to 97%. This may lead to speculation that closed-pore morphologies in poly(Pickering HIPEs) were due to a low concentration of the emulsifiers, i.e., particles. Indeed, the content of microgel particles employed in the aqueous phase was rather low (ca. 0.15 wt %). Interestingly, Hermant *et al.*[201] reported a dependence of pore-throat formation in Pickering HIPEs on the content of the Pickering emulsifier, modified single-walled carbon nanotubes (SWCNTs) by an amphiphilic block copolymer (1:12, w/w). They found that with

increasing SWCNT content from 0.01 wt % up to 0.1 wt % in HIPEs of 75 vol % internal phase, the resultant polyHIPEs exhibited a morphological change from large pores (500 μm) with little connectivity into smaller pores (50 μm) and more pore throats. Ikem *et al.* reported of closed pore morphologies in poly(Pickering HIPEs) prepared using 2-4 wt % silica particles at $\phi_{int.}$ of 90%[193] or 10 wt % titania particles at $\phi_{int.}$ of 80%.[202] Zhu *et al.*[200] reported open pores in hydrophilic polyHIPEs prepared using 8-16 wt % poly(urethane urea) nanoparticles at $\phi_{int.}$ of 80-92%. Therefore, it is worth confirming the speculation that closed-pore morphologies are preferred at relatively low content of particulate emulsifiers.

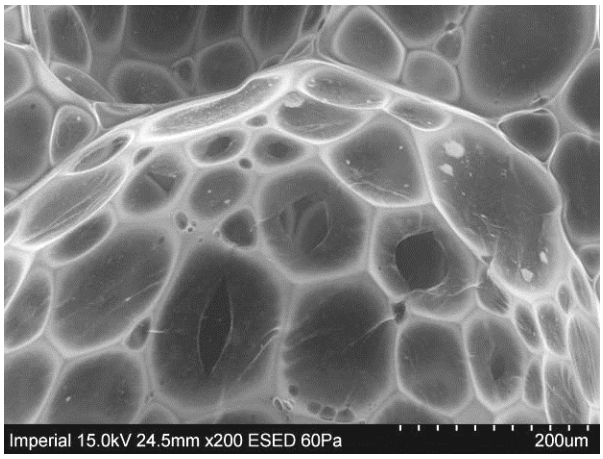
No aqueous phase was visible on the bottom of these two resultant polyHIPEs in comparison to the polyHIPEs prepared using 80 vol % toluene, indicating an elimination of creaming by compacting toluene droplets due to an increase of $\phi_{int.}$. This was in agreement with what Princen[421] observed in surfactant-stabilised o/w HIPEs. In addition, a further increase of $\phi_{int.}$ for the current system proved to be difficult; the maximum $\phi_{int.}$ available was 90.6% (**Table 7.9**), slightly lower than the upper limit reported in other Pickering HIPEs,[191,193,197,200] which is possibly dependent on particle type, particle concentration and the overall viscosity of the continuous phase.

3.4.2.2 Effect of the cross-linker content on pore structures of polyHIPEs

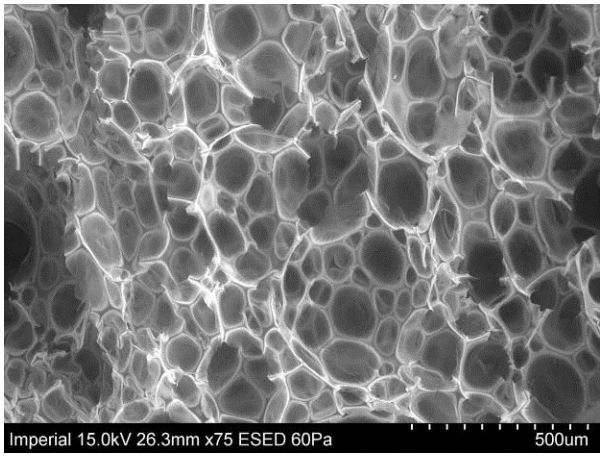
The internal phase is generally regarded as an inert template during polymerisation, attention is paid to the factors closely involved in the polymerisation in the following two sections: the crosslinker content and monomer concentration. In this section, with a constant KAA amount (0.82 M) and a constant $\phi_{int.}$ of 80%, the cross-linker content (BIS/KAA, mol/mol) in the aqueous composition was reduced from 10.0% (**Fig. 3.13**) gradually down to 2.5%. As a result, a few remarkable morphological changes were exhibited in this series of poly(KAA) Pickering-HIPEs (**Fig. 3.22**).



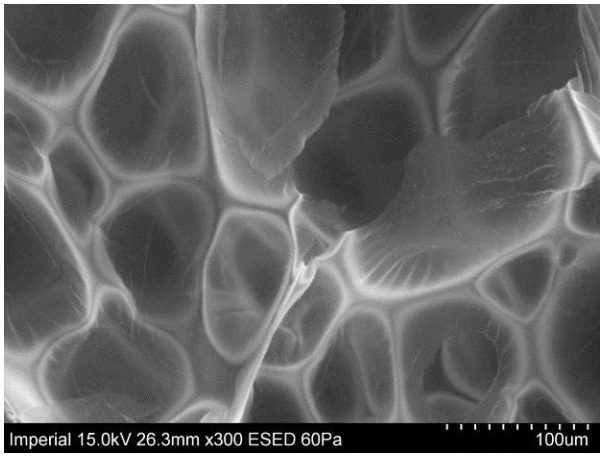
(a) 7.5 mol % BIS



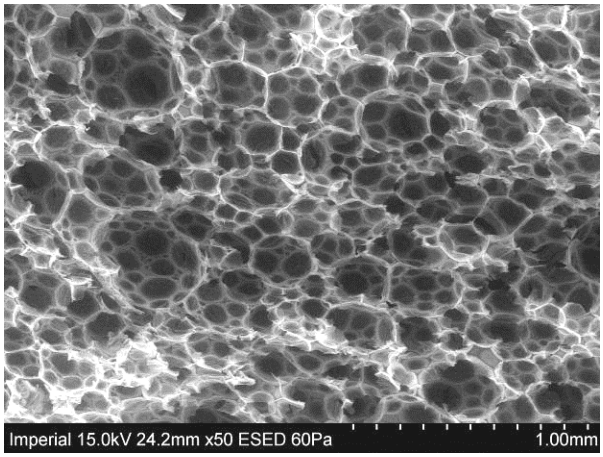
(b) 7.5 mol % BIS



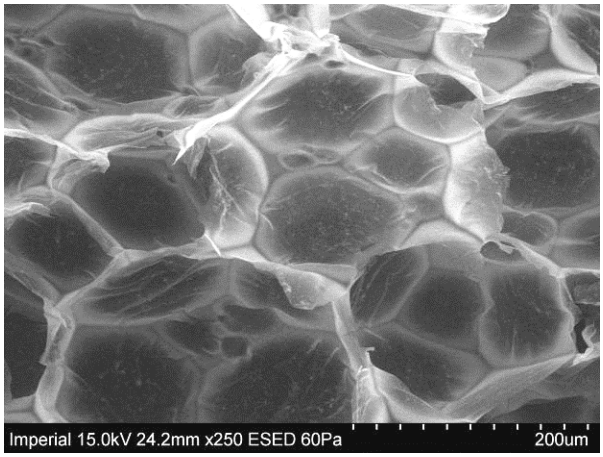
(c) 5.0 mol % BIS



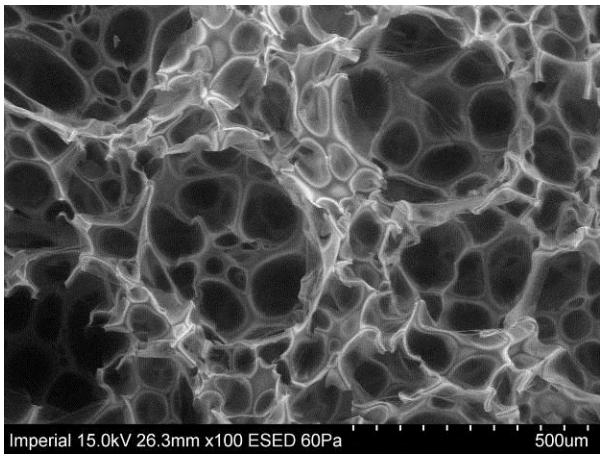
(d) 5.0 mol % BIS



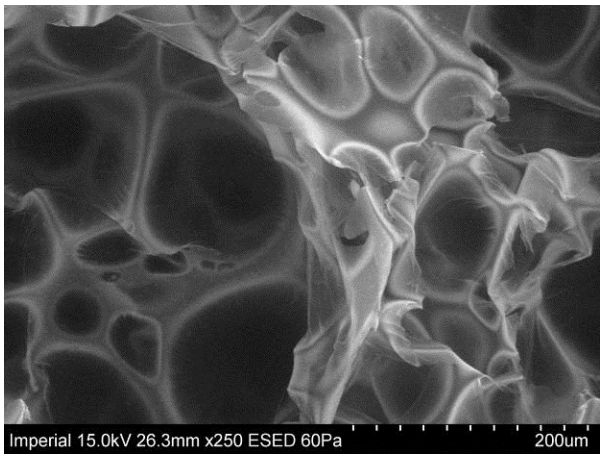
(e) 4.0 mol % BIS



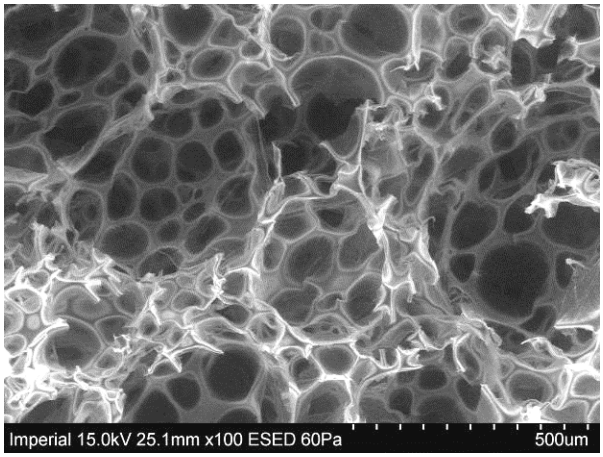
(f) 4.0 mol % BIS



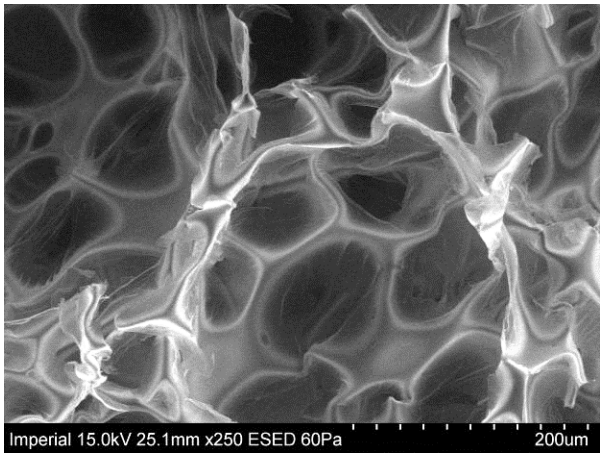
(g) 3.8 mol % BIS



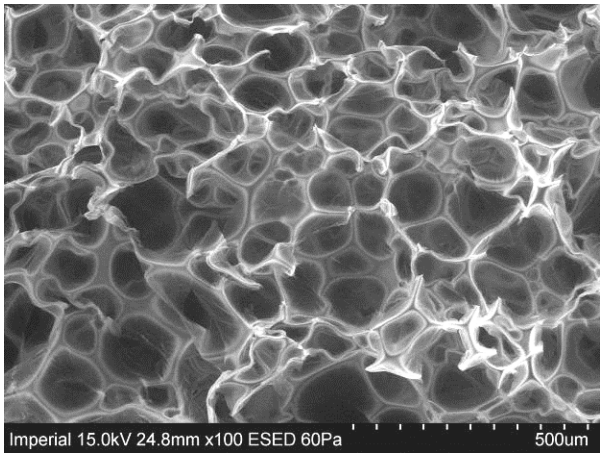
(h) 3.8 mol % BIS



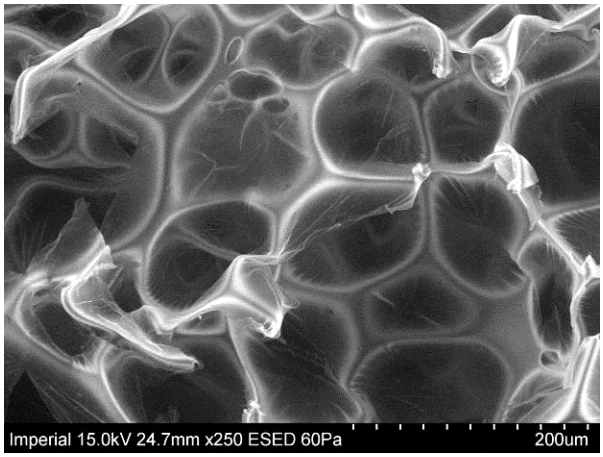
(i) 3.6 mol % BIS



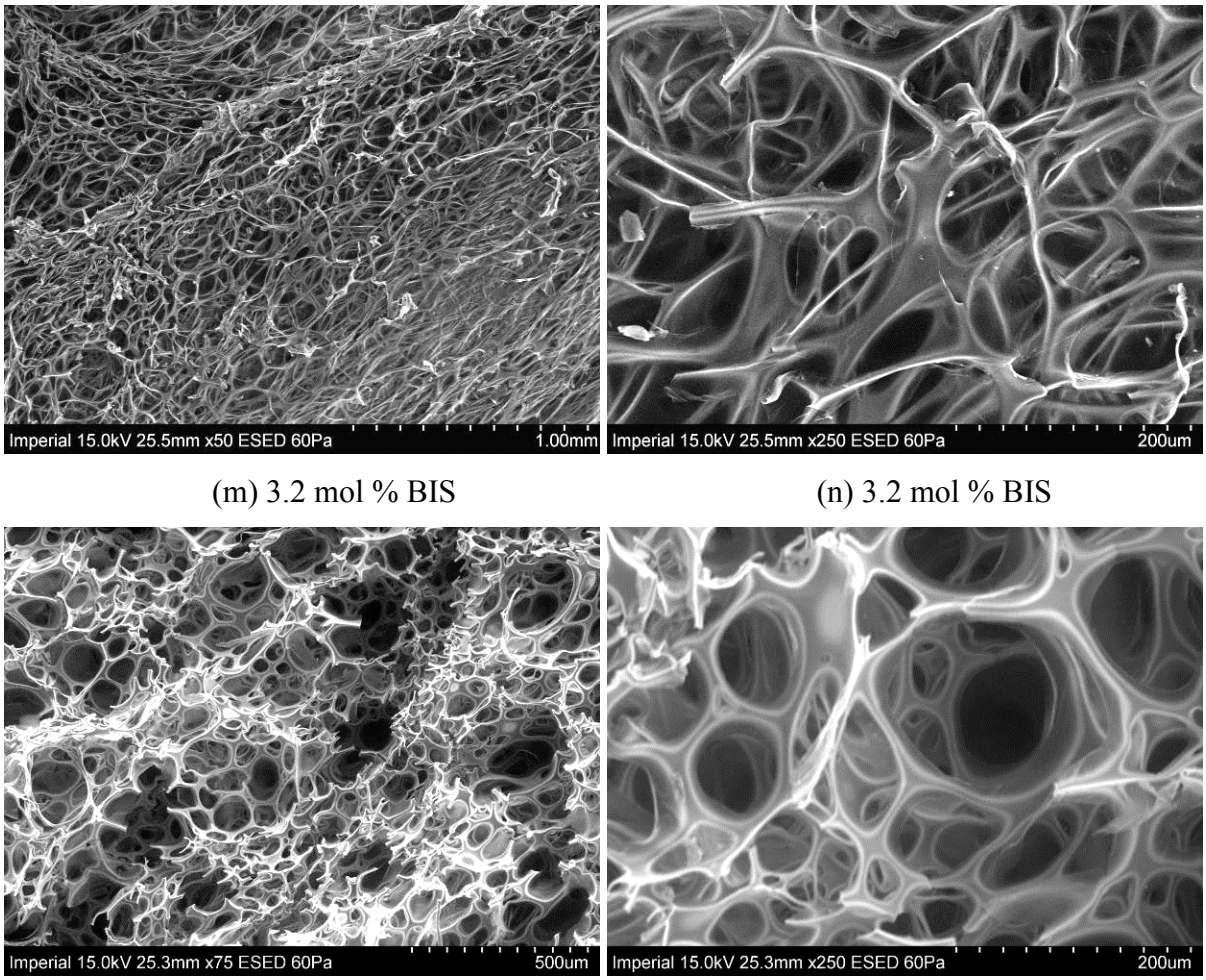
(j) 3.6 mol % BIS



(k) 3.4 mol % BIS



(l) 3.4 mol % BIS



(m) 3.2 mol % BIS (n) 3.2 mol % BIS

(o) 2.5 mol % BIS (p) 2.5 mol % BIS

Fig. 3.22 SEM images of poly(KAA) Pickering-HIPEs prepared by polymerisation of HIPEs containing constant $\phi_{int.}$ (80%) and KAA amount (0.82 M) but various BIS contents. During emulsification, a one-speed stirring protocol (400 rpm) was used.

Above all, it is obvious that open porous structures are obtainable not just in conventional polyHIPEs but also in poly(Pickering-HIPEs). "Potential pore throats" gradually became pore throats with decreasing crosslinker content. The critical point for a predominance of open pores in the morphology occurred at BIS content of 3.2 mol %. Prior to this composition, the polymer films separating two pores were thinned with decreasing BIS content and even became transparent [e.g., **Fig. 3.22** (d)] to allow the pores below to be visible. It is also indicated that pore-throat formation in this series is unlikely to have resulted from phase separation of polymers from the continuous phase during polymerisation,[494,495] since this type of phase separation has a tendency to occur upon an increase rather than decrease of the crosslinker content in the presence of a solvating diluent.[475,477,486,496,497] The weight ratio of water in the monomer solution was slightly increased from 88.5% to 89.4% when reducing the BIS content from 10 mol % to 2.5 mol %, further suggesting that phase separation during

polymerisation was less likely to occur at lower BIS content. Okay *et al.*[498] reported a maximum monomer (sodium acrylate) concentration of 11 w/v % for linear chains remaining soluble in the solution during polymerisation. Since the KAA concentration used (0.82 M) was ca. 9.4 w/v % as calculated, the resultant poly(KAA) chains alone were expected to remain soluble. Yasuda *et al.*[499] found that homogeneous hydrogels could be synthesised at very high water ratios if the resultant polymer had sufficient hydrophilicity. Indeed, poly(KAA) is very hydrophilic[500] and the copolymerisation of KAA and BIS in the aqueous phase resulted in homogeneous hydrogels as evidenced by the hydrogels [**Fig. 3.41** (a)] prepared by solely polymerising an aqueous solution of the monomers. Thus, the production of pore throats is supposed to occur during solvent extraction and drying.

Secondly, the intact pore shape of poly(Pickering HIPEs) prepared using 10 mol % BIS (**Fig. 3.13**) became blurred with decreasing BIS content, i.e., the pore boundaries in the case of open porous poly(Pickering HIPEs) were difficult to identify. This is in agreement with what Williams *et al.*[128] found in conventional polyHIPEs. Meanwhile, pore throats exhibited circular or oval profiles rather than cracks in the thin films, which may shed some light on how pore throats are formed in poly(KAA) Pickering-HIPEs at low BIS content and will be further discussed in **Section 3.4.4**.



(a) (b) (c)

Fig. 3.23 Photographs of poly(KAA) Pickering-HIPEs prepared by polymerisation of HIPEs containing 2.5 mol % BIS. (a) A sample taken out of the glass tube after polymerisation and left in a dry Petri dish; (b) another sample taken out of the glass tube after polymerisation and left in an toluene-wetted Petri dish; (c) the sample shown in (b) after solvent extraction (a piece of filter paper used to wrap the sample prior to extraction) and vacuum drying.

However, loss of sample integrity became an issue in the cases where low crosslinker contents, especially 2.5%, were used for the preparation of polyHIPEs. **Fig. 3.23** (a) clearly shows that the networks of polymerised HIPEs were not strong enough to overcome the adhesive forces between the gel and the glass. To obtain an open-porous morphology as well as integrity of the polyHIPEs, two approaches were carried out. One approach was to wet the

dish with toluene so that the adhesive forces were reduced on contact [**Fig. 3.23** (b)]. To handle with more ease, a trimmed piece of filter paper was also wetted with toluene, with which the sample was wrapped and put into a thimble for solvent extraction. As a result, an integral piece of dried polyHIPEs [**Fig. 3.23** (c)] with open porous structures [**Fig. 3.24** (a) and (b)] was obtained. The other approach was freeze-drying[92,205,405,406] for solvent removal after polymerisation, i.e., the sample was actually not taken out of glass tube. In the process, *p*-xylene (mp, 12-13 °C) was used instead of toluene (mp, -93 °C) as the internal phase for a better freezing. Without causing any noticeable differences in stability during emulsification and polymerisation, the approach also led to open porous structures after freeze-drying [**Fig. 3.24** (c) and (d)]. Nevertheless, the freeze-drying approach did not result in an integral sample piece as **Fig. 3.23** (c) and a complete removal of *p*-xylene was difficult.

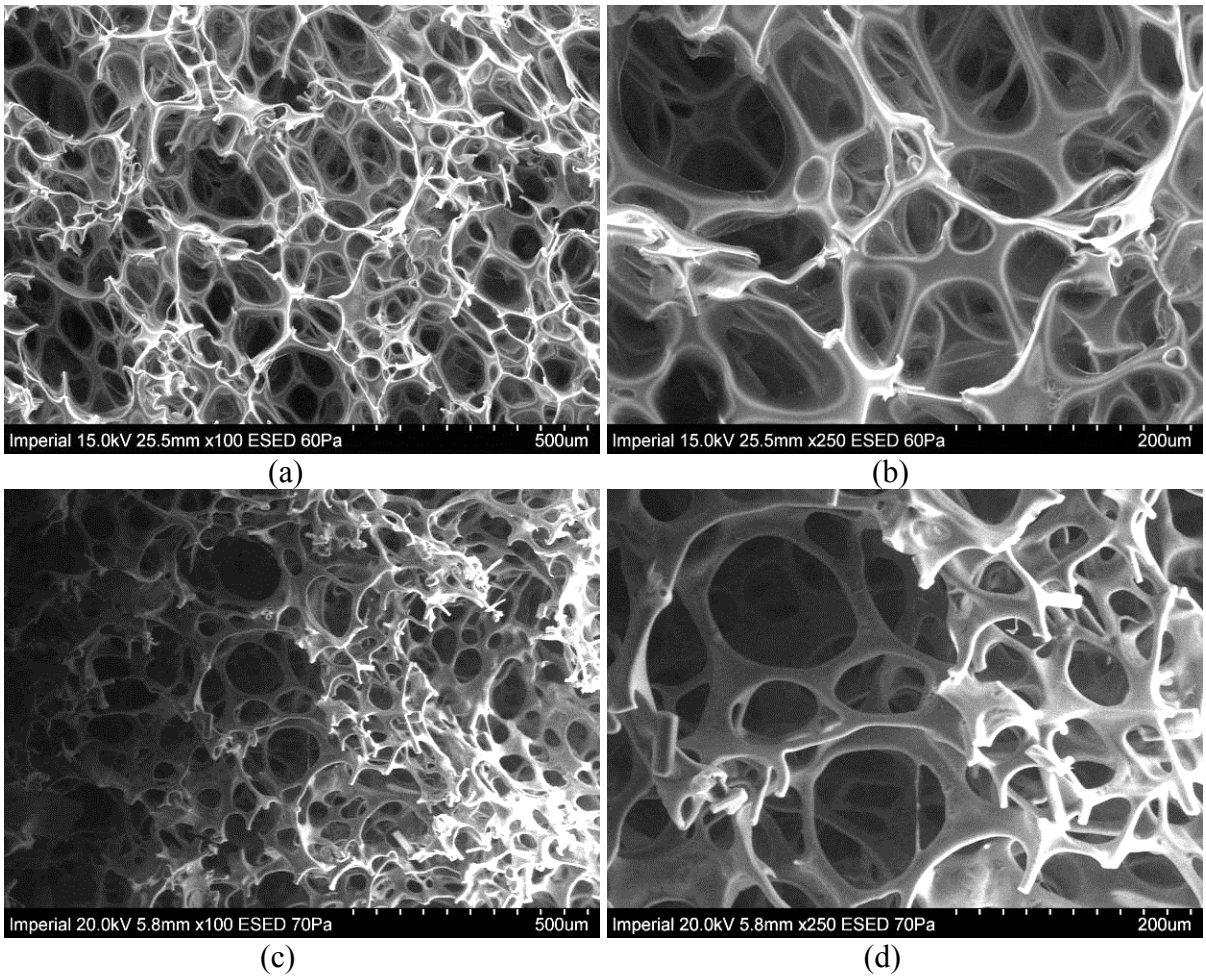
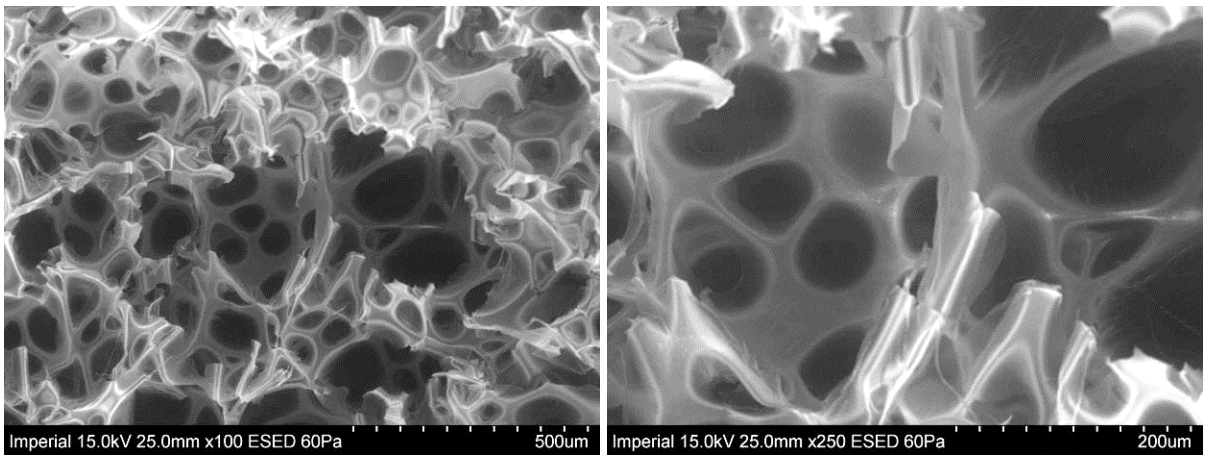


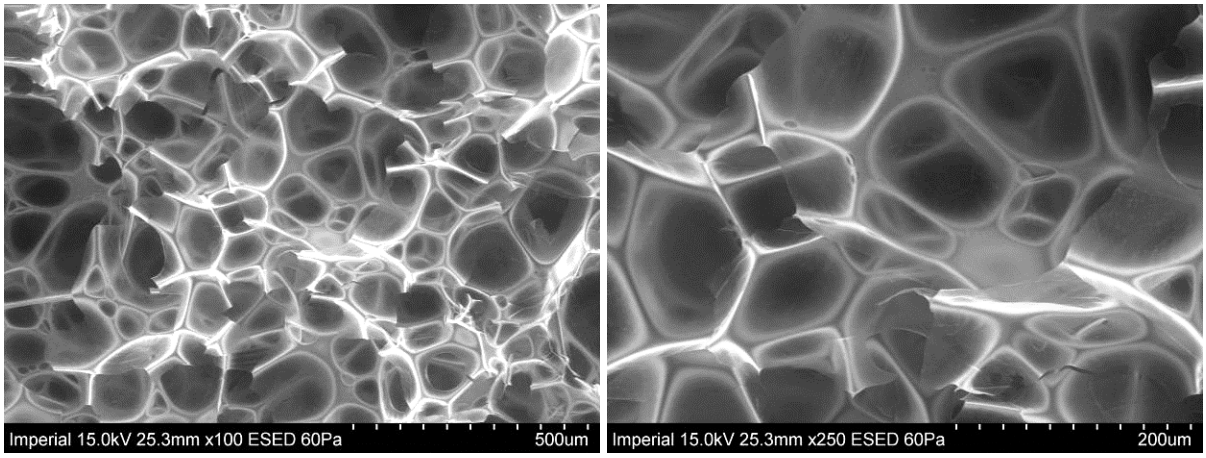
Fig. 3.24 SEM images of poly(KAA) Pickering-HIPEs prepared by polymerisation of HIPEs containing 2.5 mol % BIS. (a) and (b) were from sample that was purified using Soxhlet extraction and dried under vacuum; filter paper was used to wrap the sample during extraction. (c) and (d) were from sample that was freeze-dried after polymerisation; *p*-xylene was used instead of toluene as the internal phase.

3.4.2.3 Interplay of KAA concentration, BIS content and $\phi_{int.}$ for pore-throat formation

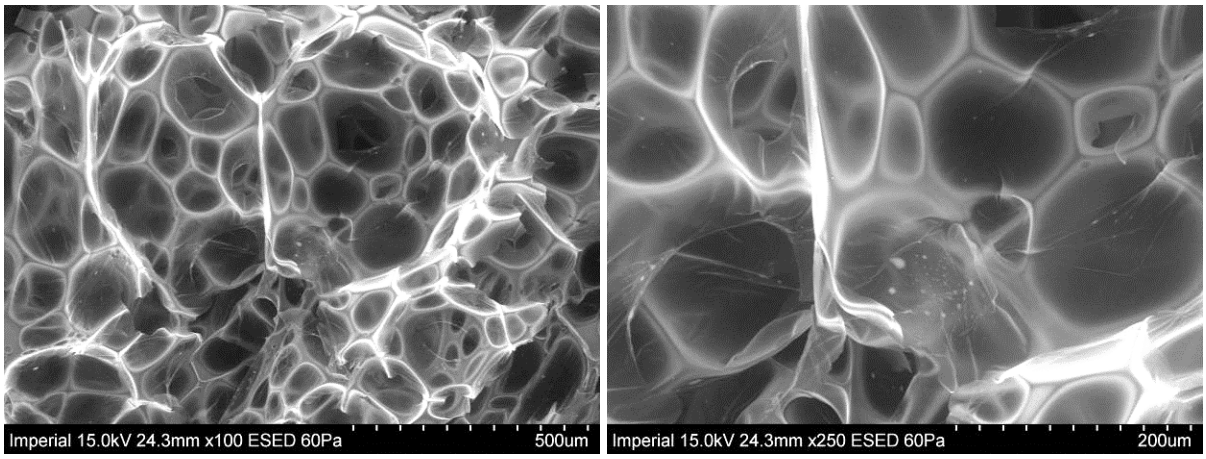
In the above section, it was shown that open porous poly(KAA) Pickering-HIPEs are available at BIS content (BIS/KAA, mol/mol) lower than 3.2%. It is interesting to know whether open porous polyHIPEs could be made at higher BIS content by varying other factors, such as $\phi_{int.}$ and the KAA amount, in order for better mechanical properties or for tuning of porosity. In comparison to the polyHPEs prepared at 5.0 mol % and 2.5 mol % BIS (0.82 M KAA and 80 vol % toluene, **Fig. 3.22**), polyHIPEs (**Table 7.8**) were prepared using various KAA concentrations (from 0.74 M to 1.07 M), internal phase volume ratios (80% or 85%) and BIS contents (2.5 mol % or 5.0 mol %). Characterisation of the resultant morphologies was performed using SEM (**Fig. 3.25**) and a statistical analysis on the numbers of "potential pore throats" and pore throats (**Table 3.3**).



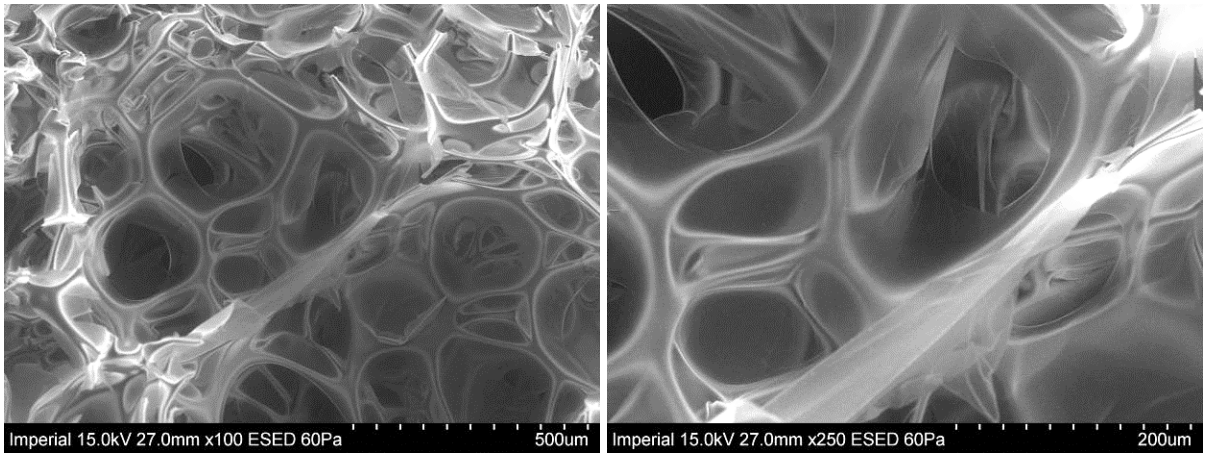
(a) 0.96 M KAA, 2.5 mol % BIS, 80 vol % toluene



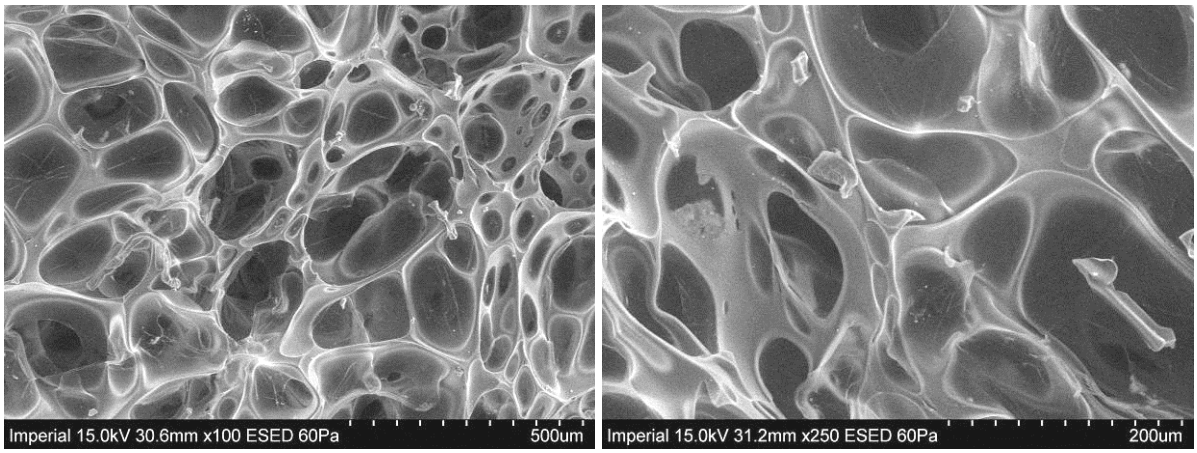
(b) 0.74 M KAA, 5.0 mol % BIS, 80 vol % toluene



(c) 0.85 M KAA, 5.0 mol % BIS, 85 vol % toluene



(d) 0.96 M KAA, 2.5 mol % BIS, 85 vol % toluene



(e) 0.96 M KAA, 16.5 mg BIS (2.2 mol %), 80 vol % toluene

Fig. 3.25 SEM images of poly(KAA) Pickering-HIPEs prepared by polymerisation of microgel-stabilised HIPEs containing various KAA concentrations, BIS contents and internal phase volume rations. The magnifications of the images are ×100 (left) and ×250 (right) for each polyHIPEs.

Table 3.3 Numbers* of "potential pore throats" and pore throats in poly(KAA HIPEs)

	KAA amount**	**Cross-linker (BIS) amount**	**$\phi_{int.}$,** vol %	**"Potential" pore throats**	**Pore throats**	**Pore throat ratio*****
Fig. 3.22 (c)(d)	4.27 mmol	32.9 mg (5.0 mol %)	80	260	10	3.8%
Fig. 3.22 (o)(p)	4.27 mmol	16.5 mg (2.5 mol %)	80	57	211	78.7%
Fig. 3.25 (a)	4.81 mmol	18.5 mg (2.5 mol %)	80	211	35	14.2%
Fig. 3.25 (b)	3.74 mmol	28.8 mg (5.0 mol %)	80	210	20	8.7%
Fig. 3.25 (c)	4.27 mmol	32.9 mg (5.0 mol %)	85	233	30	11.4%
Fig. 3.25 (d)	4.81 mmol	18.5 mg (2.5 mol %)	85	22	90	80.4%
Fig. 3.25 (e)	4.81 mmol	16.5 mg	80	156	26	14.3%

* Counted in SEM images of ×50 magnification; **The microgel suspensions in KAA solution (5 ml) containing 3.74 mmol, 4.27 mmol and 4.81 mmol KAA were identical to "1-14", "1-13" and "1-12" as listed in **Table 3.1**, respectively; *** pore throat ratio was calculated using (the number of pore throats)/(the total number of pore throats and "potential" pore throats).

Firstly, the effect of KAA concentration on the pore interconnectivity of poly(KAA) Pickering-HIPEs were investigated at constant $\phi_{int.}$ of 80 vol %. On the one hand, aqueous solutions of increasing KAA concentration from 0.85 M to 0.96 M and 1.07 M were used for polyHIPE preparation at constant BIS content (16.5 mg). Unfortunately, phase separation occurred in the case of 1.07 M KAA in contrast to the lasting stability shown by its counterpart without BIS and I2959 [**Fig. 3.4** (f)]. This attenuation of the emulsifying ability of microgels was likely due to a synergic effect of adding KAA and organic molecules. The comparison between polyHIPEs prepared using 0.85 M KAA [**Fig. 3.22** (o) and (p)] and 0.96 M KAA [**Fig. 3.25** (e)] clearly revealed that increasing KAA concentration at a constant low amount of BIS (16.5 mg) led to a dramatic decrease in the pore interconnectivity (**Table 3.3**). Indeed, an open porous morphology turned into a closed-pore one. On the other hand, at BIS content of 5 mol %, decreasing the KAA concentration from 0.85 M [**Fig. 3.22** (c) and (d)] to 0.74 M [**Fig. 3.25** (b)] did not change the closed-pore morphology and only resulted in a slight increase in pore interconnectivity. Although both comparisons suggested an inverse relationship between pore interconnectivity and KAA concentration, such dependence was more sensitive at lower cross-linker level. The crucial role the crosslinker content played in the formation of open porous structures was further manifested when comparing Entry 2 and Entry 4 in **Table 3.3**. In the aqueous phase, the monomer content and BIS content were 8.4 wt %, 0.55 wt % for Entry 4 and 9.2 wt %, 0.31 wt % for Entry 2, respectively. Obviously, a lower BIS content despite higher total monomer content did result in polyHIPEs with higher interconnectivity.

Secondly, the effect of internal phase volume ratio ($\phi_{int.}$) on the pore structure was investigated at specified concentrations of KAA and BIS. Although increasing $\phi_{int.}$ from 80% up to 89% did obviously not affect the pore interconnectivity of polyHIPEs made by polymerisation of HIPEs containing 10 mol % BIS content (**Section 3.4.2.1**), it is worth re-examining its effect at lower BIS contents. A comparison is drawn between two polyHIPEs both prepared with 0.85 M KAA and 5.0 mol % BIS. An increase of $\phi_{int.}$ from 80% [**Fig. 3.22** (c) and (d)] to 85% [**Fig. 3.25** (c)] led to an increase of the pore-throat ratio from 3.8% to 11.4% (**Table 3.3**). Meanwhile, when 0.96 M KAA and 2.5 mol % BIS were used for polyHIPE preparation, increasing $\phi_{int.}$ from 80% to 85% resulted in a change from closed-pore structures [**Fig. 3.25** (a)] to open porous ones [**Fig. 3.25** (d)]. Clearly, it is shown that pore interconnectivity in poly(KAA) Pickering-HIPEs became sensitive to the increase of $\phi_{int.}$ at low BIS contents. This sensitivity had a reverse relationship with BIS content. In addition, Entry 2 and Entry 6 in **Table 3.3** exhibited an equivalent level of pore interconnectivity, suggesting that at BIS content of 2.5 mol %, increasing $\phi_{int.}$ from 80% to 85% was similar to reducing KAA concentration from 0.96 M to 0.85 M in terms of their effect on pore interconnectivity.

To sum up **Section 3.4.2.3**, both decreasing KAA concentration and increasing $\phi_{int.}$ can contribute to pore-throat formation in poly(KAA) Pickering-HIPEs. However, their effects depend on the BIS content and only become significant at low BIS content, e.g. 2.5 mol %.

3.4.3 Effect of stirring speed on the pore structures of poly(KAA) Pickering-HIPEs

As previously discussed in **Section 2.6.1** and **Section 3.2.2.2**, stirring speed is one of the dominant factors affecting emulsion drop size and thereby affects HIPE stability and polyHIPE morphology. Indeed, the effect of stirring speed on HIPE stability also manifests in poly(KAA) Pickering-HIPEs (**Fig. 3.26**). Upon photo-polymerisation, the HIPEs prepared using a one-speed stirring protocol (400 rpm) turned into a polymerised HIPE together with a transparent gel of 4 mm in height. Obviously, the gel was the polymerised product of the aqueous phase (containing KAA and BIS) that separated out due to creaming. Its height was gradually reduced to zero when 600 rpm, 700 rpm, 800 rpm and 1000 rpm were used, respectively, as a second stirring speed during emulsification, indicating a better HIPE stability to creaming at a higher stirring speed. However, it is unclear whether stirring speed

plays a role in pore-throat formation in poly(KAA) Pickering-HIPEs. To clarify this point, we discuss in this section those polyHIPEs prepared with a selected two-speed stirring protocol (400→1000 rpm), in comparison with those prepared with a one-speed stirring protocol (400 rpm, **Section 3.4.2**).

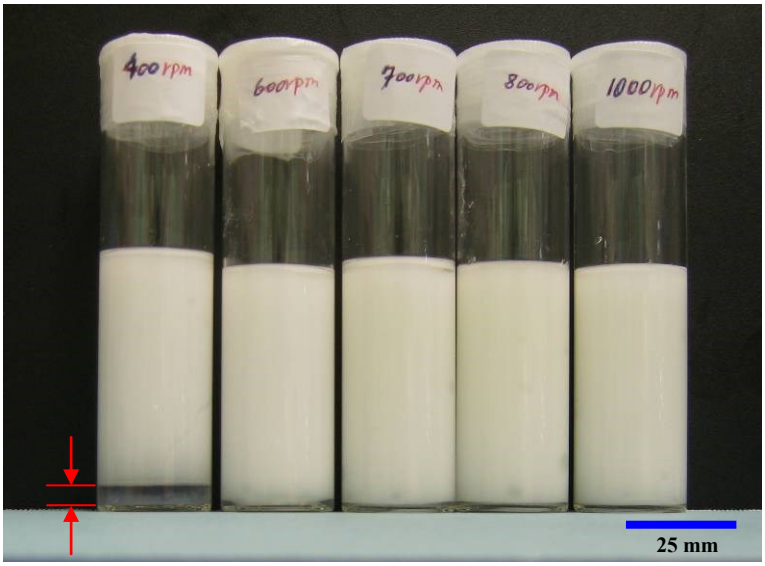


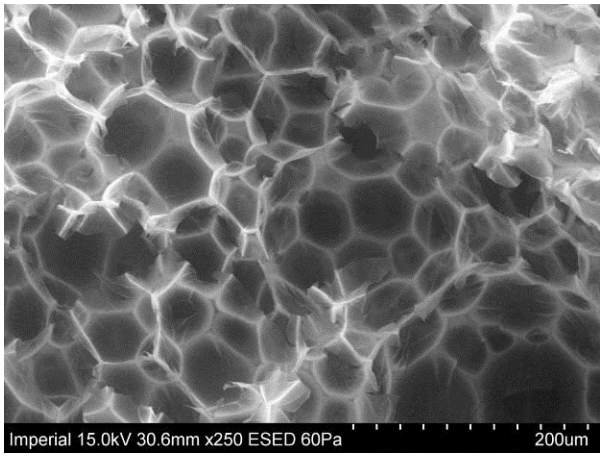
Fig. 3.26 Photographs of polymerised Pickering o/w HIPEs prepared by polymerisation of HIPEs containing 10 mol % BIS. From left to right: stirring speed of 400, 600, 700, 800 and 1000 rpm were used during emulsification, respectively. The transparent part on the bottom, as marked (4 mm in height), was polymerised aqueous solution (containing KAA and BIS) that separated from the bulk emulsions due to creaming.

3.4.3.1 Effect of crosslinker content on the pore structure at increased stirring speed

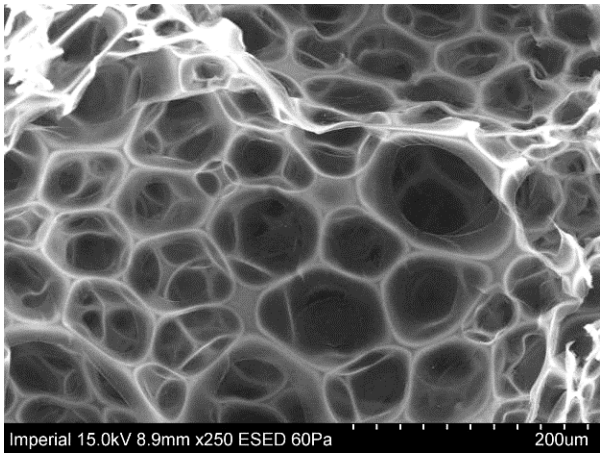
It was revealed that pore-throat formation largely depends on the crosslinker content and that a critical BIS content existed allowing for open porous poly(KAA) Pickering-HIPEs to form (**Section 3.3.2**). How this dependence is affected by increasing stirring speed (1000 rpm) was investigated using polyHIPEs (**Fig. 3.27**) prepared with a BIS content of 10 mol %, 5 mol %, 4 mol %, 3.2 mol % and 2.5 mol %, respectively, and characterised by SEM (**Fig. 3.28**).



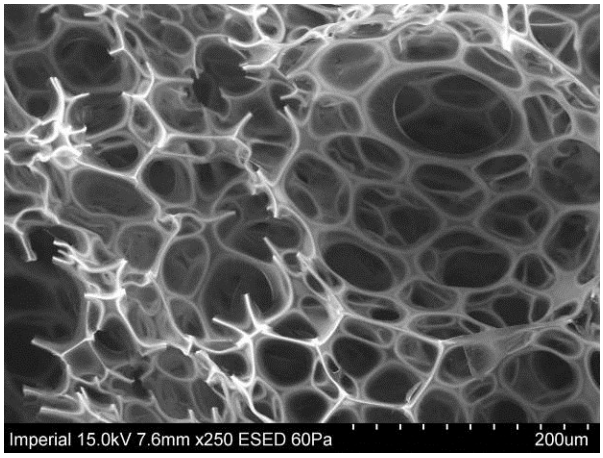
Fig. 3.27 Photographs of polymerised Pickering o/w HIPEs prepared by polymerisation of HIPEs containing various BIS contents (BIS/KAA, mol/mol). From left to right: a BIS content of 10.0%, 5.0%, 4.0%, 3.2% and 2.5% was employed, respectively. The HIPEs were emulsified using a two-speed stirring protocol (400→1000 rpm). Glass tubes have a diameter of 25 mm.



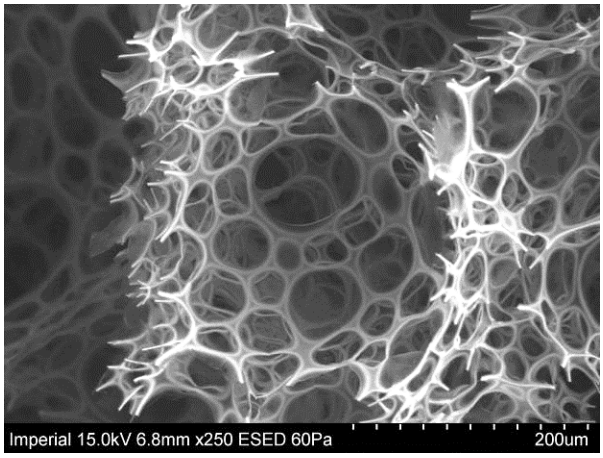
(a) 10 mol % BIS



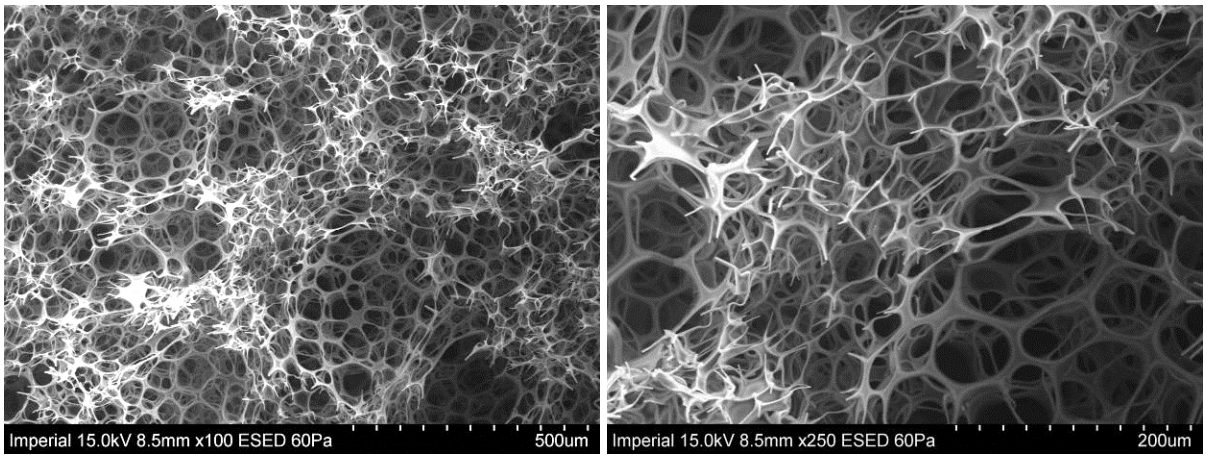
(b) 5.0 mol % BIS



(c) 4.0 mol % BIS



(d) 3.2 mol % BIS

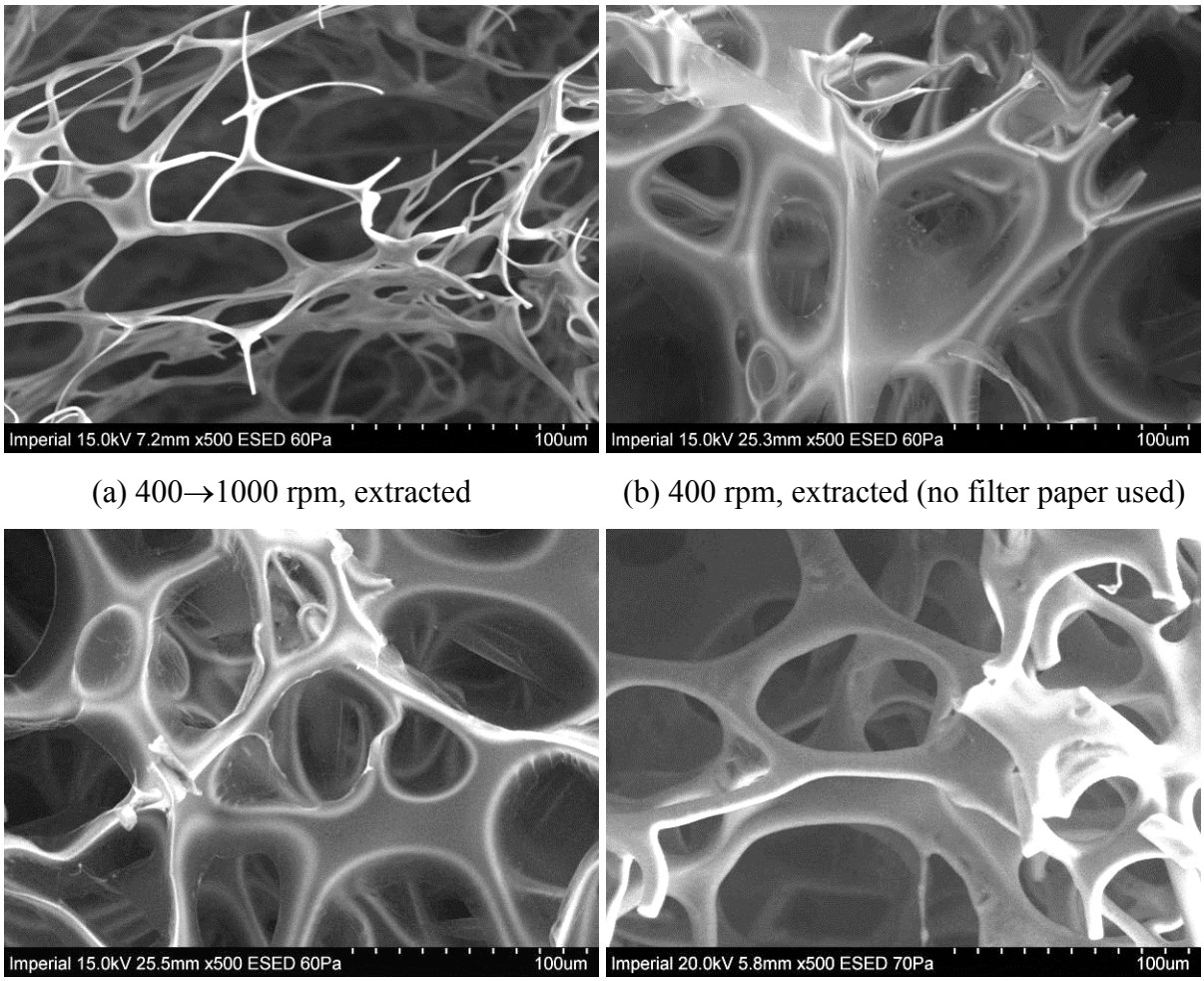


(e) 2.5 mol % BIS (f) 2.5 mol % BIS

Fig. 3.28 SEM images of poly(KAA) Pickering-HIPEs prepared by polymerisation of HIPEs that were emulsified using a two speed stirring protocol (400→1000 rpm). The BIS contents in the HIPEs were 10 mol %, 5 mol %, 4 mol %, 3.2 mol % and 2.5 mol %, respectively.

As expected all five samples exhibited good stability to creaming during polymerisation (**Fig. 3.27**) and displayed two remarkable morphological features induced by using 1000 rpm during emulsification (**Fig. 3.28**). Firstly, despite the closed-pore morphology at BIS content of 10.0 mol %, decreasing it to 5.0 mol % led to an open porous structure. This is in contrast to the closed-pore polyHIPEs prepared using an identical BIS content but 400 rpm as the stirring speed [**Fig. 3.22** (c) and (d)] and suggests that increasing the stirring speed during emulsification played a constructive role in pore-throat formation and increased the critical BIS content for open porous polyHIPEs. Gurevitch *et al.*[194] also found that increasing the mixing intensity reduced the wall thickness and enabled pore throats to form more easily. Secondly, upon decreasing BIS content from 5.0 mol % to 2.5 mol %, pore-throat margins moved outwards, resulting in an increase of the pore-throat size and a reduction of the strut width. This change induced by BIS content is more noticeable for polyHIPEs prepared using a higher speed of 1000 rpm. It is indicated that pore-throat formation is probably induced by shrinkage of the polymer films, the extent of which is dependent on the cross-linking level. At BIS content of 2.5 mol %, a comparison drawn between polyHIPEs prepared using a two-speed stirring protocol (400→1000 rpm) [**Fig. 3.28** (e) and (f)] and those prepared solely with 400 rpm [**Fig. 3.22** (o) and (p), **Fig. 3.24**] clearly shows that 1000 rpm reduced the wall thickness of the polymer films and resulted in decrease of the strut width from more than 10 μm to as thin as 1 μm (**Fig. 3.29**). From this point of view, the higher stirring speed of 1000 rpm contributed to increase of pore throat size. On the other hand, increase of the stirring speed can reduce the pore size,[138,194,501] which in general will decrease the pore-throat size.

Thus, the effect of increasing stirring speed on pore-throat size becomes less straightforward. Indeed, the pore-throat radii of polyHIPEs prepared using 1000 rpm [**Fig. 3.28** (e) and (f)] and 400 rpm [**Fig. 3.22** (o) and (p)] are 24.6 ± 5.8 μm (63 pore throats counted), and 31.8 ± 12.9 μm (67 pore throats counted), respectively, suggesting increase of the stirring speed clearly reduced the distribution of pore-throat size rather than the size.



(a) 400→1000 rpm, extracted (b) 400 rpm, extracted (no filter paper used)

(c) 400 rpm, extracted (d) 400 rpm, freeze-dried

Fig. 3.29 SEM images of poly(KAA) Pickering-HIPEs prepared by polymerisation of HIPEs containing the same crosslinking level (BIS/KAA = 2.5 mol %). During emulsification, a two-speed stirring protocol (400→1000 rpm) was used for (a) in contrast to a one-speed stirring protocol (400 rpm) for (b)(c)(d); Soxhlet extraction and vacuum drying used for (a)(b)(c) in contrast to freeze-drying for (d) after photo-polymerisation; during extraction, filter paper was used for sample wrapping in the case of (a) and (c).

Therefore, the stirring speed appears to be an efficient tool that can substantially vary how polymers are spatially distributed and organized in polyHIPEs by affecting the emulsion drop size. In this process, sample integrity is not compromised (**Fig. 3.30**) even in the case of a low BIS content (2.5 mol %). This tool is of further significance when degradation of these

emulsion-templated scaffolds (e.g., BIS was replaced by a degradable crosslinker) is taken into consideration, since both the width and the thickness of the scaffold struts are tunable by stirring speed and other factors, such as cross-linker content.

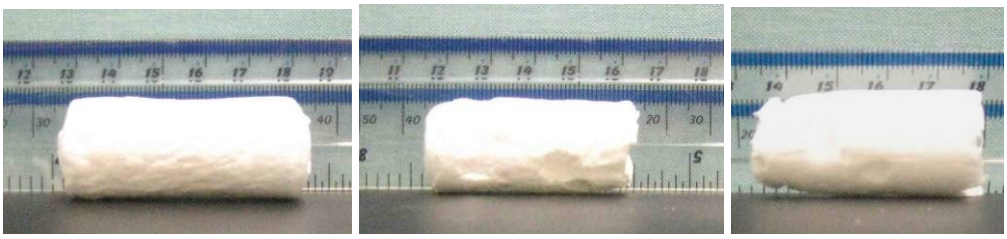
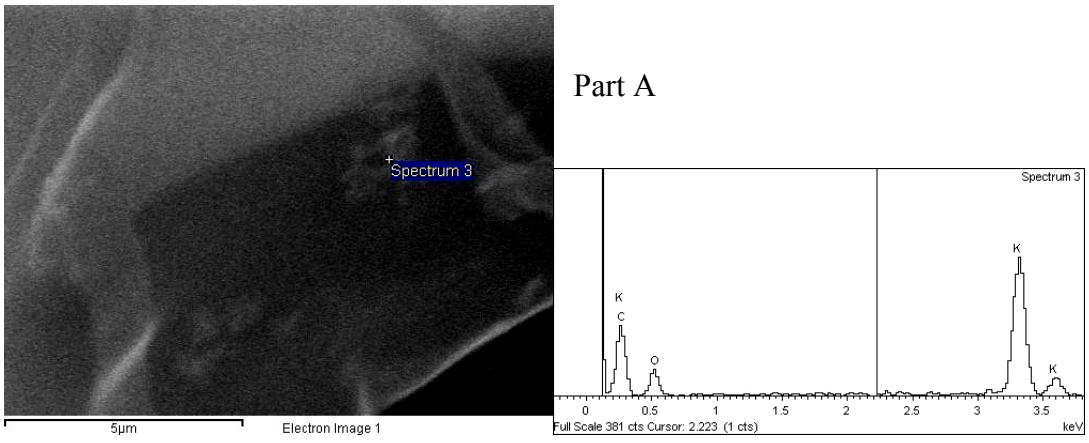
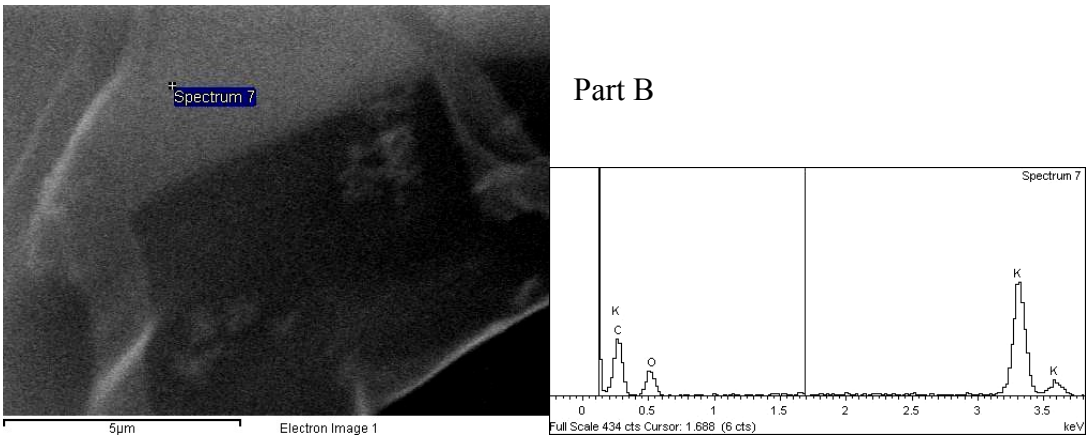


Fig. 3.30 Photographs of poly(KAA) Pickering-HIPEs after solvent extraction and vacuum drying. From left to right: the crosslinking levels (BIS/KAA, mol/mol) used were 10.0%, 4.0% and 2.5%, respectively.

In addition, it is worth mentioning that although extraction with HCl in MeOH was used to protonate the carboxyl groups in poly(KAA), investigations using Energy-dispersive X-ray spectroscopy (EDX) (**Fig. 3.31**) indicate that potassium ions still exist in multitude. Therefore, these polyHIPEs are still defined as poly(KAA) Pickering-HIPEs.





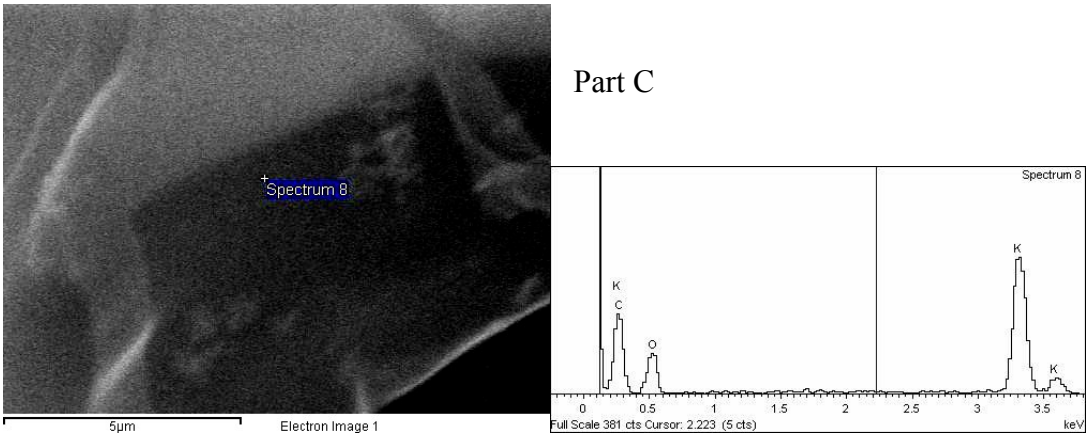


Fig. 3.31 SEM/EDX analysis of poly(KAA) Pickering-HIPEs showing obvious potassium peaks in different parts (left: SEM images; right: the element analysis on the specified parts). For lower-magnification images of the sample, see **Fig. 3.28** (b).

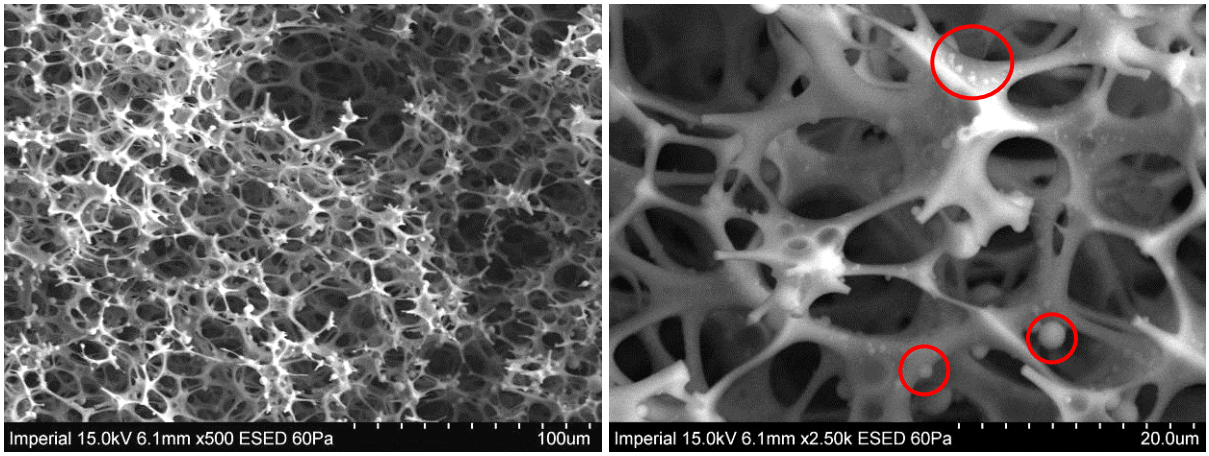
3.4.3.2 Effect of microgel concentration on the pore structure at increased stirring speed

As revealed in **Section 3.2.2.3**, an increase in microgel content from 0.15 wt % to 0.31 wt % in the aqueous phase had no obvious effect on the creaming extent of the water-in-toluene HIPEs. According to Equation (3.1) and (3.2), it appears that the emulsion drop size was the same in the two HIPEs. However, this is not necessarily true for the drop size in polymerised HIPEs, especially by photo-polymerisation, since creaming kinetics was not considered. Indeed, creaming even became negligible during the polymerisation (**Fig. 3.27**, BIS and I2959 was added) due to the fast polymerisation rate. Thus, the drop size evolution with time due to limited coalescence[321,374-376] is negligible and the original state of HIPE after emulsification was maintained. Consequently, it becomes very likely that the microgel content will have an effect on the pore structure of polyHIPEs. To verify this speculation, poly(KAA) Pickering-HIPEs were prepared by polymerisation of HIPEs containing 1.5 wt % microgels and 2.5 mol % BIS, in comparison with 0.15 wt % microgels as discussed before.

The resultant morphology (**Fig. 3.32**) showed two distinct features from that of polyHIPEs using 0.15 wt % microgels [**Fig. 3.28** (e)(f) and **Fig. 3.29** (a)]. Firstly, spheres of various sizes [**Fig. 3.32** (b)] were observed attached to the polymer surfaces in contrast to smooth surfaces observed in polyHIPEs prepared using 0.15 wt % microgels. The large spheres of size up to several micrometers were unlikely to be microgel particles but rather polymer particles.[194] Secondly, pore-throat sizes are significantly reduced as obviously shown in the ×500 images [**Fig. 3.29** (a) and **Fig. 3.32** (a)] of the interconnected structures. It has been reported that particle content is determinant of the pore size in poly(Pickering

HIPEs)[190,198,200-202] due to its influence on the drop size prior to polymerisation. Zhu *et al.*[200] also reported a pore-throat size decrease in accompany with a pore-size decrease upon increasing particle content from 8 wt % to 16 wt %. Li *et al.*[195] reported that poly(St/DVB) Pickering-HIPEs prepared using 20 wt % 12-acryloxy-9-octadecenoic acid (AOA)-modified magnetite nanoparticles as stabilisers exhibited average pore size of 14.9 μm, at equivalent level to those prepared using 3 wt % Span 80 (both relative to the total weight of monomers). Thus, it is clear now that large pores up to a few hundred microns present in poly(KAA) Pickering-HIPEs (**Fig. 3.13**) or in poly(Pickering-HIPEs) reported in the pioneering work[191,193] are not only due to the nature of emulsifiers but also due to relatively low content.

Therefore, it is revealed that microgel content has an obvious effect on the morphology of poly(KAA) Pickering-HIPEs. Increase of microgel content can reduce the pore size as well as the pore-throat size.



(a) (b)

Fig. 3.32 SEM images of poly(KAA) Pickering-HIPEs prepared by polymerisation of HIPEs containing 1.5 wt % microgels and 2.5 mol % BIS. A two-speed stirring protocol (400→1000 rpm) was used during emulsification.

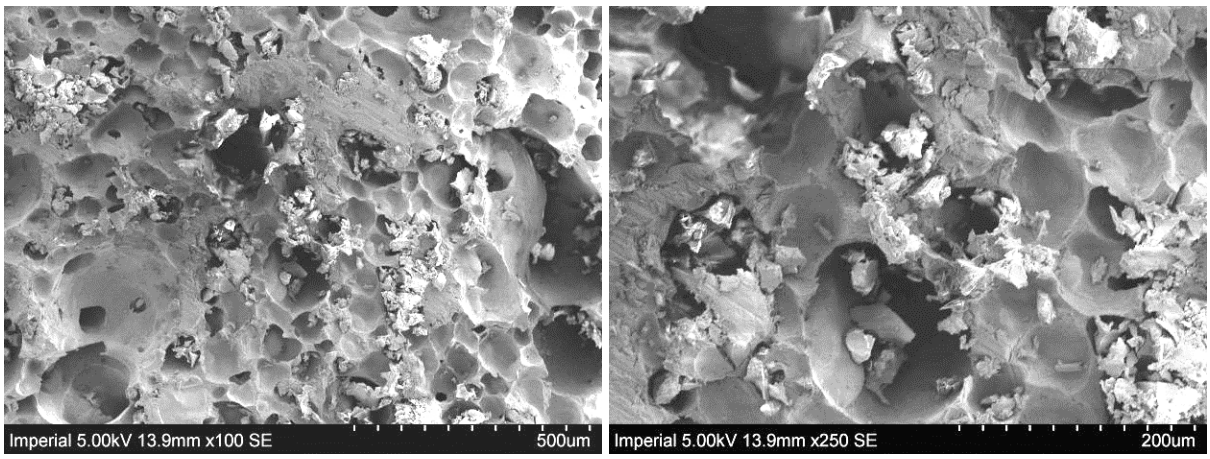
To sum up **Section 3.4.1~3.4.3**, poly(KAA) Pickering-HIPEs with open porous morphology are attainable. It has been found that BIS content (BIS/KAA, mol/mol) determines the formation of pore throats whereas the effects of other factors – including $\phi_{int.}$, KAA concentration and stirring speed – are negligible at 10.0 mol% BIS but increasingly noticeable with decreasing BIS content. Although it is yet to be revealed how exactly pore throats are generated (**Section 3.4.4**), it has been indicated that pore throats in poly(KAA) Pickering-HIPEs are not generated during polymerisation but during solvent extraction and drying.

3.4.4 Investigation of pore-throat formation by cryo-SEM

This section aims to find out the driving force for pore-throat formation in poly(KAA) Pickering-HIPEs and to obtain a better understanding of the process not only in poly(KAA) Pickering-HIPEs but also in other poly(Pickering-HIPEs) and conventional polyHIPEs. For this purpose, cryo-SEM technique is employed to study the morphology change since the technique was efficient in revealing the original state of wet samples, such as hydrogel networks.[487,502,503] In a pioneering work, Cameron *et al.*[137] used cryo-SEM during the copolymerisation of St/DVB in a w/o HIPE template to investigate how pore throats formed. For poly(KAA) Pickering-HIPEs here, since pore throats were unlikely to form due to phase separation during polymerisation (**Section 3.4.2.2**), cryo-SEM was used to study polymerised HIPEs (2.5 mol % BIS and a two-speed stirring protocol used during preparation) at different stages of purification (**Fig. 7.8**): (1) after polymerisation but before solvent extraction; (2) after extraction with MeOH (or HCl in MeOH) and (3) after extraction with acetone. For the corresponding SEM images of purified and dried polyHIPEs, see **Fig. 3.28** (e) and (f).

3.4.4.1 Closed-pore structures after polymerisation evidenced by cryo-SEM

For the first stage (polymerised HIPEs prior to solvent extraction), in order to make the polymer films and pore structures visible, it is ideal to sublimate toluene (m.p. -93 ºC) rather than water. Cryo-SEM was carried out on unextracted polymerised HIPEs using three sublimation conditions (**Fig. 3.33**).



(a)-1 (a)-2

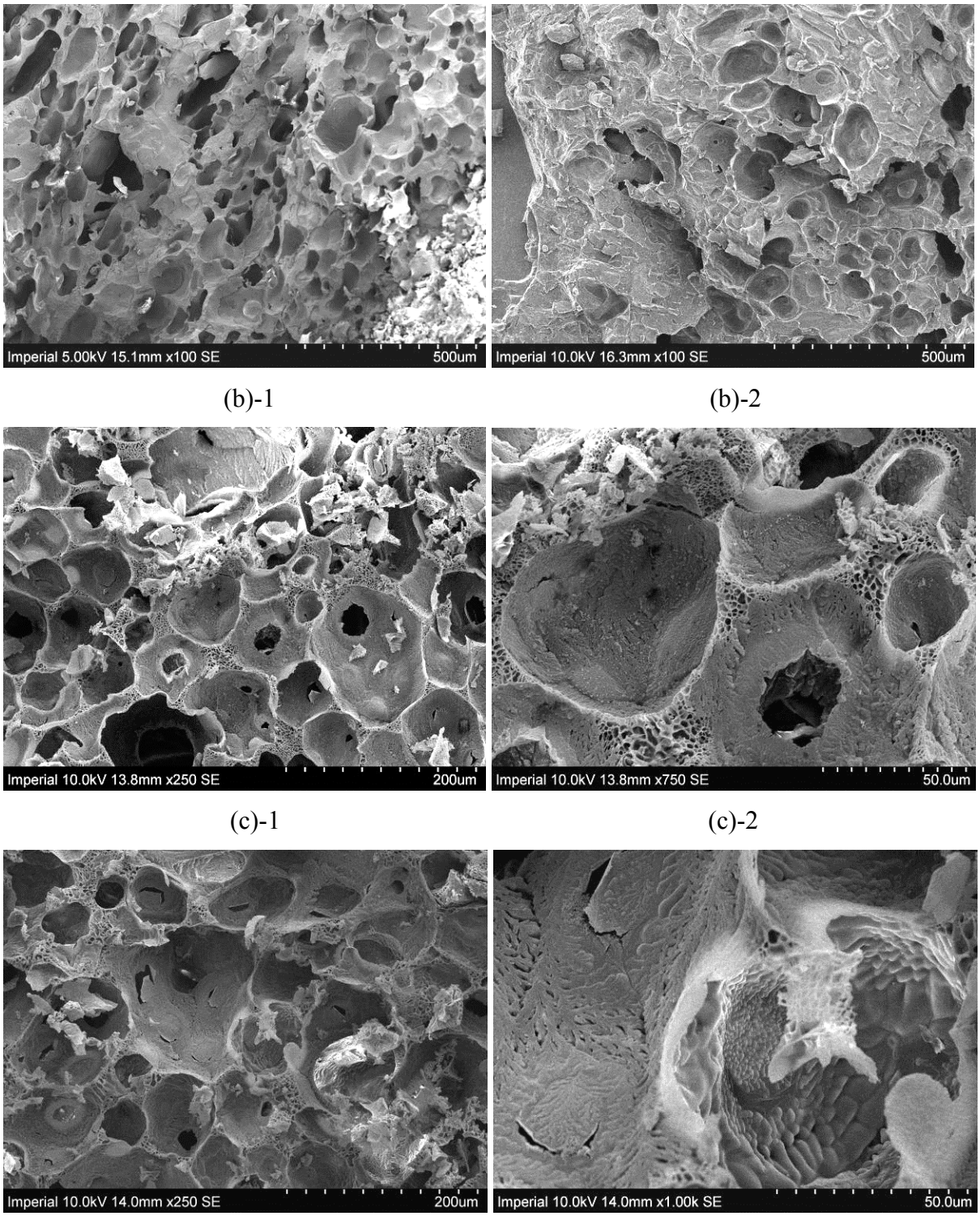


Fig. 3.33 Cryo-SEM micrographs of unextracted polymerised HIPEs under three sublimation conditions (temperature, time): (a) -120 °C, 3 min; (b) -100 °C, 3 min 10 s; (c) -100 °C, 45 min. The HIPEs were prepared using 0.15 wt % microgels, 0.82 M KAA, 2.5 mol % BIS, 2 mol % I2959, 80 vol % toluene and a two-speed stirring protocol (400→1000 rpm).

After sublimation at -120 °C for 3 min [**Fig. 3.33** (a)] or at -100 °C for about 3 min [**Fig. 3.33** (b)], the sample exhibited shallow pores due to the removal of toluene in the top layer. The intact pore profiles indicated that closed pores were dominant. Increasing the sublimation temperature from -120 °C to -100 °C had no obvious effect on the pore structures in 3 min. To better understand the cyro-SEM micrographs, sublimation was carried out at -100 °C for 45 min. Two remarkable features were observed [**Fig. 3.33** (c)]. Firstly, clusters of small holes (1-5 μm) were clearly visible surrounding the pores [**Fig. 3.33** (c)-2] in contrast to **Fig. 3.33** (b). The appearance of these holes was attributed to sublimation of ice crystals that evolved from amorphous ice during standing at -100 °C.[504] Secondly, cracks of different scales and a few pore throats were visible inside the pores. It was strongly indicated [**Fig. 3.33** (c)-3 and (c)-4] that these throats were produced at the thinner parts of the glassy polymer films by attack of toluene vapours from underneath layers, i.e., toluene vapours induced the development of cracks on the films. Meanwhile, the rough profiles of the throats were clear signs of a mechanical rupture, distinct from smooth ones as observed in purified and dried polyHIPEs [**Fig. 3.28** (e) and (f)]. Thus, it becomes clear that the polymerised HIPEs had closed-pore morphology [**Fig. 3.33** (a) and (b)] before solvent extraction, confirming that pore-throat formation in poly(KAA) Pickering HIPEs is not due to phase separation during polymerisation (**Section 3.4.2.2** and **Section 3.4.3.1**). Although the formation of pore throat in a conventional St/DVB based polyHIPEs was attributed to a volume contraction upon conversion of monomers to polymers,[137] Kimmins and Cameron speculated that the lack of contraction at gel points for poly(Pickering HIPEs) (and thereby closed pores) was due to the stability of Pickering emulsions.[91] However, in the case of poly(KAA) Pickering-HIPEs, a missing shrinkage during polymerisation was clearly due to the presence of a solvating diluent (**Section 3.4.2.2**) rather than the stability of Pickering emulsions. In addition, it is worth noting that cryo-SEM technique is more effective when investigating an o/w HIPE template as shown above in comparison with a w/o HIPE template, because the oil phase, such as toluene or styrene/DVB in the process of polymerisation,[137] has a lower melting point than the aqueous phase in the presence/absence of salts. Thus, when water needs to be removed from a w/o HIPE template for observation of the pore structures, the continuous phase would be inevitably disrupted during sublimation, which was also noticed by Cameron *et al.*[137] Therefore, it is evidenced by cryo-SEM that the pore throats in open porous poly(KAA) Pickering-HIPEs are yet formed after polymerisation. In fact,

pore-throat formation in polyHIPEs is not necessarily related to phase separation during polymerisation.

3.4.4.2 Open porous structures generated during Soxhlet extraction with MeOH

Since it has been revealed that pore-throat formation in poly(KAA) Pickering-HIPEs (2.5 mol % BIS, two-speed stirring protocol) occurs during solvent extraction and drying, we now try to specify the actual driving force for pore-throat formation. At the first stage of solvent extraction (**Fig. 7.8**), HCl in MeOH solution (or MeOH) was applied to the polymerised o/w HIPE samples. During the process, MeOH was expected to disassemble the emulsion template due to its miscibility with both toluene and water. Morphological investigations were carried out using cryo-SEM on MeOH-extracted wet samples (**Fig. 3.34**) and normal SEM on the vacuum-dried sample after extraction with MeOH (**Fig. 3.35**).

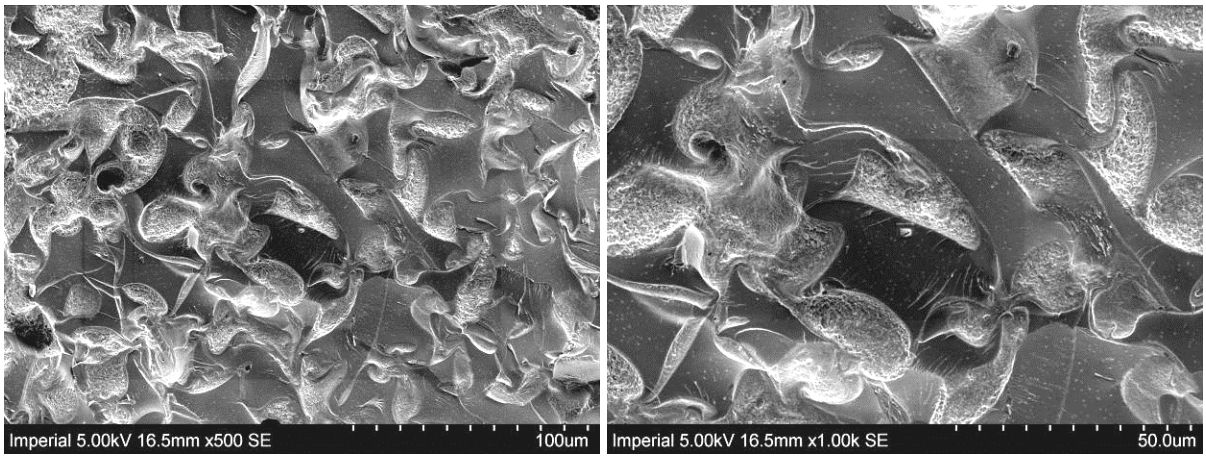


Fig. 3.34 Cryo-SEM micrographs of poly(KAA) Pickering-HIPEs after a one-step extraction with MeOH (sublimation conditions: -110 ºC, 3 min). The HIPEs were prepared using 0.15 wt % microgels, 0.82 M KAA, 2.5 mol % BIS, 2 mol % I2959, 80 vol % toluene and a two-speed stirring protocol (400→1000 rpm).

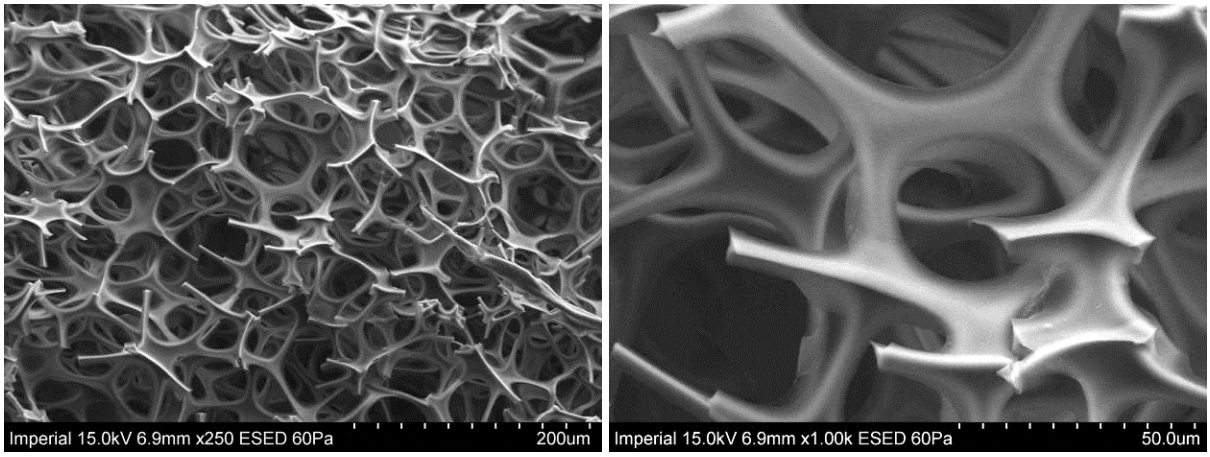
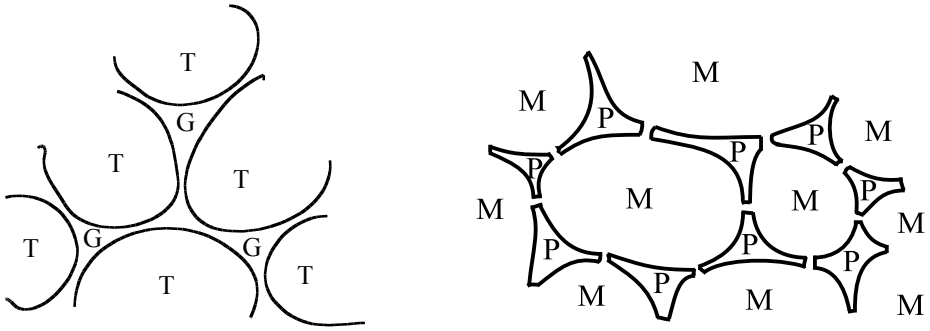


Fig. 3.35 SEM images of poly(KAA) Pickering-HIPEs vacuum-dried at 70 ºC after one-step extraction with MeOH. The HIPEs were prepared using 0.15 wt % microgels, 0.82 M KAA, 2.5 mol % BIS, 2 mol % I2959, 80 vol % toluene and the two-speed stirring protocol (400→1000 rpm).

Since there was only one solvent (MeOH, m.p. -97 ºC) present in the polymer networks, the cryo-SEM micrographs (**Fig. 3.34**) showed how polymer network (dark and smooth) looked in MeOH (grey and rough). It is strongly indicated by the change from loosely packed polymer films [**Fig. 3.33** (c)] prior to extraction into smooth polymer struts that pore throats were formed during extraction. This shrinkage caused by MeOH can be attributed to its role as a non-solvent for the polyelectrolyte chains.[469,498,505,506] It is worth noting that using MeOH instead of HCl in MeOH as the extracting solvent prior to cryo-SEM (to avoid any equipment corrosion by HCl) was not expected to make significant differences since poly(KAA) remained the major constituent despite extraction with HCl in MeOH as revealed by EDX (**Fig. 3.31**). On the other hand, the interconnected structures of dried polyHIPEs after extraction with MeOH (**Fig. 3.35**) were in agreement with the polymer struts observed by cryo-SEM (**Fig. 3.34**, comparing the images at 1 k magnification), indicating that pore-throat formation mainly occurs during extraction with MeOH. Thus, it is clarified that the driving force for pore-throat formation in poly(KAA) Pickering-HIPEs is non-solvent induced phase separation[478,507] of polymers from water as illustrated by a 2-D schematic (**Fig. 3.36**). Apparently, the resistance of the gel layer to shrinkage depends on its "tightness" and thickness. The "tightness" of the gel layer is determined by the degree of crosslinking while the thickness of the gel layer is more likely affected by the stirring speed or the internal phase volume ratio during emulsification. Meanwhile, due to a higher chance of network inhomogeneity for poly(KAA) gels with lower cross-linking density,[508-510] the gel layers with

2.5 mol % crosslinking degree were more vulnerable to shrinkage upon contact with MeOH in comparison with those with 10 mol %.



(a) Before solvent extraction (b) After extraction with MeOH

Fig. 3.36 2-D schematics illustrating the proposed formation of pore throats in poly(KAA) Pickering-HIPEs. T, G, M and P stand for toluene, poly(KAA) gel, MeOH and polymer, respectively.

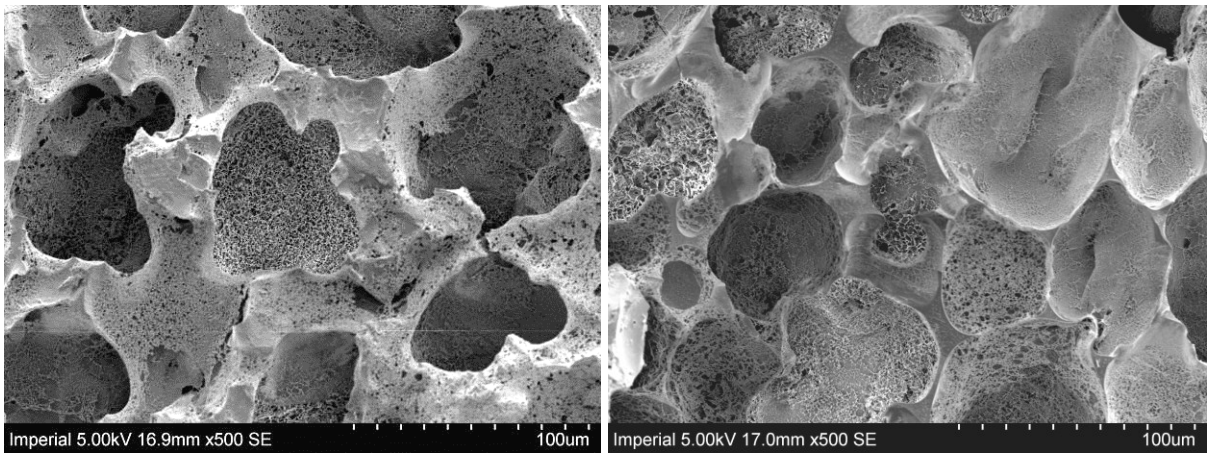


Fig. 3.37 Cryo-SEM micrographs of poly(KAA) Pickering-HIPEs after extraction with acetone (sublimation conditions: -84 ºC, 3 min). The HIPEs were prepared using 0.15 wt % microgels, 0.82 M KAA, 2.5 mol % BIS, 2 mol % I2959, 80 vol % toluene and a two-speed stirring protocol (400→1000 rpm). The polymerised HIPEs were purified using Soxhlet extraction with MeOH and acetone in sequence.

Cryo-SEM on acetone-extracted samples using sublimation temperature below the melting point of acetone (-94.9 ºC) was expected to exhibit similar morphologies to those of MeOH-extracted ones (**Fig. 3.34**), because the examined wet sample simply consisted of polymer networks and a non-solvent. Instead, a temperature (-84 ºC) above the melting point of acetone was applied during sublimation (3 min), aiming to remove acetone deeper from within the bulk polymer (**Fig. 3.37**). Clearly, the polymer struts were displayed on the top while acetone on the same layer was removed, leaving a number of very small holes. In

addition, it was revealed in **Section 3.4.1.1** that two-step extraction (HCl in MeOH and acetone) led to more rigid pore structures (10 mol % BIS used) in comparison with one-step extraction (HCl in MeOH only). This probably indicated that polymer networks of 2.5 mol % crosslinking degree as discussed here would further shrink when MeOH was replaced by acetone although pore throats already formed.

To sum up, this cryo-SEM investigation clearly showed the role solvent extraction played in pore-throat formation, i.e., the interaction between extracting solvents and the polymer gel layers – containing polymers, emulsifiers and diluents (water here) – is the driving force for throat generation in poly(KAA) Pickering-HIPEs. Of course, to obtain open porous structures, it is essential for this interaction to overcome the resistance from polymer networks. From this point of view, morphologies of a number of reported poly(Pickering HIPEs) can be well interpreted. For Pickering emulsion templates without diluent in the continuous phase, closed-pore morphology was exhibited when no solvent extraction step was applied[173,190,191,193,196,202] or when an extracting solvent had little interaction with the polymer layers.[120,192,199] For Pickering emulsion templates with diluent present in the continuous phase, a closed-pore morphology was preferred when the extracting solvent had little interaction with the polymer layers[194] whereas open porous structures can be obtained when the extracting solvent interacted with the polymer gels.[200] This case of open porous poly(Pickering HIPEs) is in agreement with our poly(KAA) Pickering-HIPEs, where the extracting solvent is miscible with the diluent but is a non-solvent for the polymer, although causes for the throat formation was not further identified.

3.5 Surface area and porosity of poly(KAA) Pickering-HIPEs

Besides the morphological requirement, surface features[511,512] and porosity[47,513] are other important parameters to consider during the fabrication of polymeric scaffolds for bone tissue. For KAA-based poly(Pickering HIPEs), a series of measures have been taken in order to control its morphology (**Section 3.4**). Thus, it is interesting to know what effects these measures may have on the surface features and porosity of the resultant monoliths. For an initial assessment here, specific surface area has been solely considered of all the surface properties, which may influence the adsorption of protein[514] as well as the degradation of polymer matrices.[515]

3.5.1 BET surface area

When measuring the surface area, a degassing process is essential in order to remove moisture from polyHIPEs prior to N_2 adsorption. A thermal gravimetric analysis (TGA) was carried out on poly(KAA) Pickering-HIPEs (**Fig. 3.38**) to trace the moisture removal process. It was showed that the polyHIPE sample reached a constant weight after about 4 hours' heating at 60 °C in N_2 and lost another 1~2% weight upon further increasing temperature to 150 °C. To avoid any possible decomposition of poly(KAA) at higher temperatures,[468,516] we chose 60 °C as the degassing temperature (helium as the backfill gas) for poly(KAA) Pickering-HIPEs. Indeed, 60 °C as the degassing temperature was also reported in measuring the surface area of AAm and AA based polyHIPEs.[94,402] It is worth noting that the tested polyHIPEs might vary in their physical appearances (**Table 7.11**). For example, the shape of polyHIPEs was well maintained in some cases whereas partial shrinkage occurred upon drying in other cases. However, comparisons have been drawn among their surface areas without considering the effect of physical appearance since identical preparation protocol (**Fig. 3.16**) and degassing conditions were applied to all polyHIPEs.

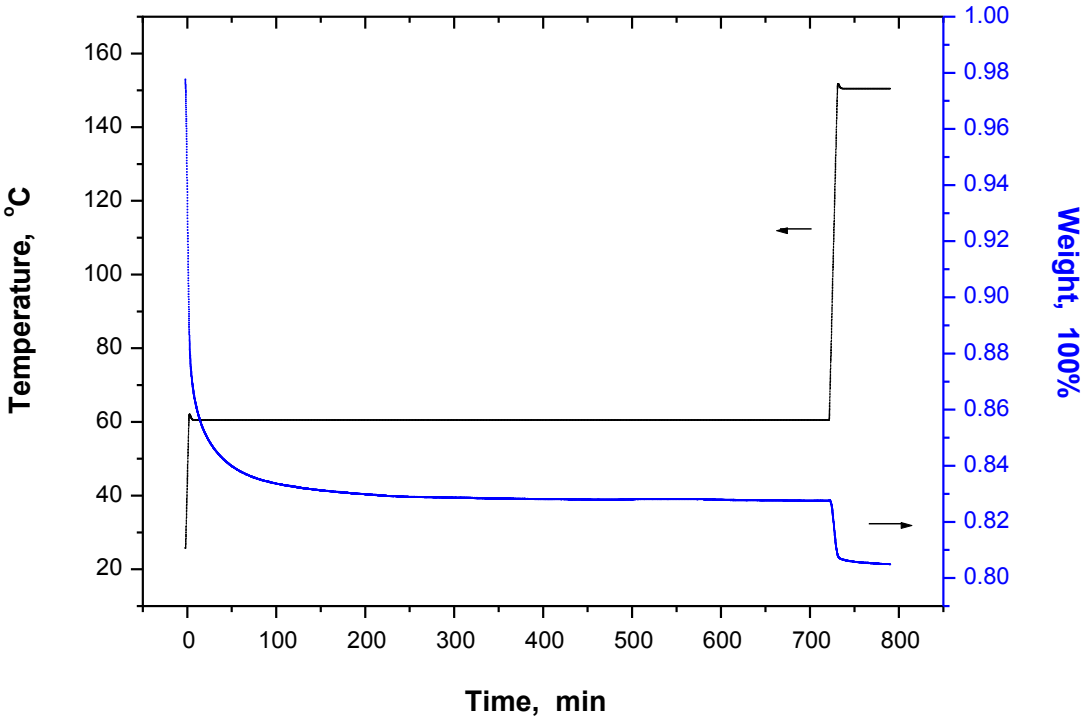


Fig. 3.38 TGA of poly(KAA) Pickering-HIPEs under N_2 atmosphere (heating rate: 10 °C/ min). The tested polyHIPEs were prepared by polymerisation of HIPEs that were emulsified using 0.82 M KAA, 10 mol % BIS, 0.15 wt % microgels and 85 vol % toluene and using a one-speed stirring protocol.

It can be seen that poly(KAA) Pickering-HIPEs with higher BIS content and KAA concentration have higher surface areas (**Table 3.4**), which was likely due to formation of smaller polymer nuclei[477] during polymerisation. This effect of crosslinker content on surface area was also observed in other reported polyHIPEs.[356,404,492,517] However, all surface areas were below 1 m^2/g, much smaller than those of styrene/DVB based polyHIPEs prepared in the presence of a solvating diluent.[356,361-363] Similarly, Zhang *et al.*[402] reported a low value of surface area (0.7 m^2/g) in AA based polyHIPE beads. This was probably related to the homogeneous nature of polymerising AA/BIS in water (**Section 3.4.2**). Meanwhile, influence of the degassing process on surface area[518,519] may require further attention.

Table 3.4 Surface areas of poly(KAA) HIPEs measured after degassing for 4 h at 60 °C

Morphology	Composition			BET surface area, m^2/g
	KAA, mmol	BIS, mol %	$\phi_{int.}$, vol %	
Fig. 3.13	4.27	10.0	80	0.60
Fig. 3.22 (e)(f)	4.27	4.0	80	0.28
Fig. 3.22 (m)(n)	4.27	3.2	80	0.27
Fig. 3.22 (o)(p)	4.27	2.5	80	0.10
Fig. 3.25 (a)	4.81	2.5	80	0.37

Firstly, the degassing duration of polyHIPE specimen was elongated to 12 h prior to N_2 absorption. As a result, a significant increase in surface area from 0.60 m^2/g (4 h, **Table 3.4**) to 1.68 m^2/g (12 h, **Table 3.5**) occurred to polyHIPEs with 10 mol % crosslinking degree whereas little change for those with lower crsslinking degrees. It is indicated that moisture removal in polyHIPEs with 10 mol % crosslinking degree was slower, probably due to its closed-pore morphology (**Fig. 3.13**). Compared to that of polyHIPE specimen degassed for 4 h, the adsorption-desorption isotherm of polyHIPEs degassed for 12 h clearly moved upwards (**Fig. 3.39**), although both showed a type II adsorption isotherm together with a H3 hysteresis loop in the IUPAC classification.[519] This type of adsorption indicated the macroporous nature of the polyHIPE materials and a lack of mesopores. The drop in adsorption quantity observed in the middle section of the isotherms was probably due to release of moisture from polyHIPEs in the process of pressure increase. With 12 h as the degassing time (**Table 3.5**), the surface area of polyHIPEs increased with crosslinking degree, in agreement with the

trend obtained under 4 h degassing. Moreover, the surface area decreased when $\phi_{int.}$ increased from 80% (1.68 m^2/g) to 89% (1.32 m^2/g). Similarly, Barbetta *et al.*[362] reported a decrease in surface area with increasing $\phi_{int.}$ in DVB based polyHIPEs prepared in the presence of a polar diluent. In contrast, Youssef *et al.*[140] reported the opposite for 1-vinyl-5-aminotetrazole/BIS based polyHIPEs when $\phi_{int.}$ was increased from 76% to 88%. Apparently, this is a complicated matter since some diluents can contribute to the surface area whereas others do not. For the latter case, the surface area does increase if more water-oil interfaces are formed in the emulsions upon increasing $\phi_{int.}$. In addition, with an extra degassing cycle of up to 24 h, the BET surface areas of poly(KAA) Pickering-HIPEs prepared using $\phi_{int.}$ of 80% and 89% were 1.81 m^2/g and 1.17 m^2/g, respectively. These values were more or less at the same level as the previous results, indicating maximum surface areas were likely reached. This was also verified by the fact that the adsorption-desorption isotherm of polyHIPEs was almost unchanged when elongating the degassing duration from 12 h to 24 h (**Fig. 3.39**).

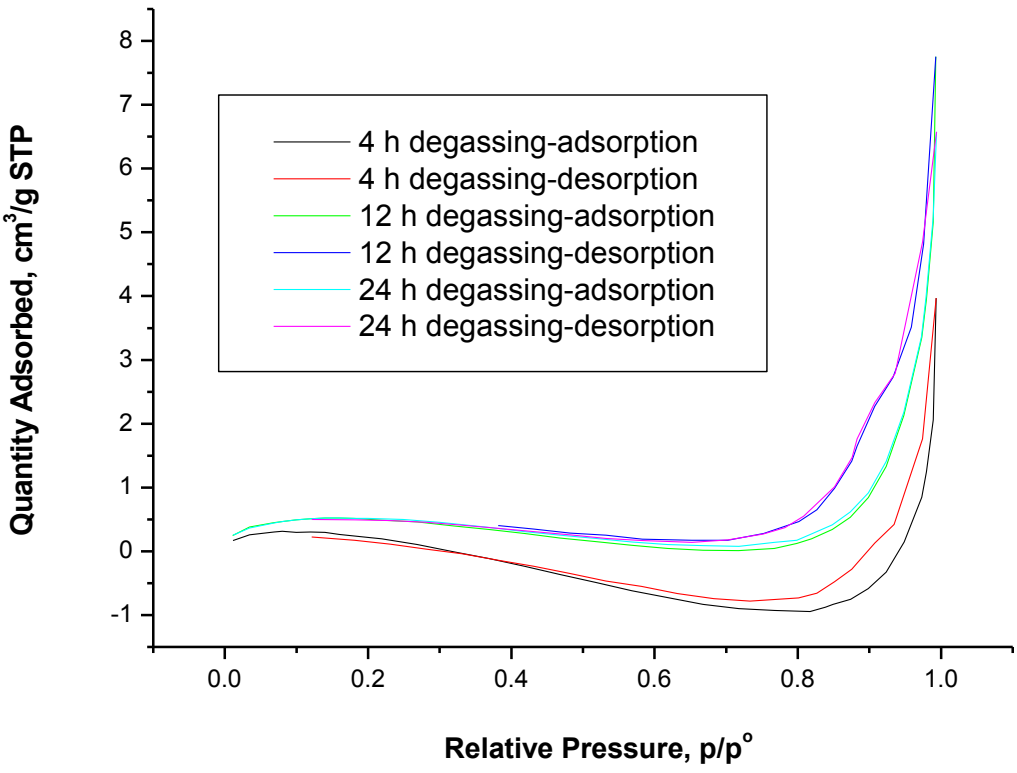


Fig. 3.39 N_2 adsorption-desorption isotherms of poly(KAA) Pickering HIPEs measured after various degassing durations from 4 h to 12 h and 24 h. The polyHIPEs were prepared using 10 mol % BIS and 80 vol % internal phase.

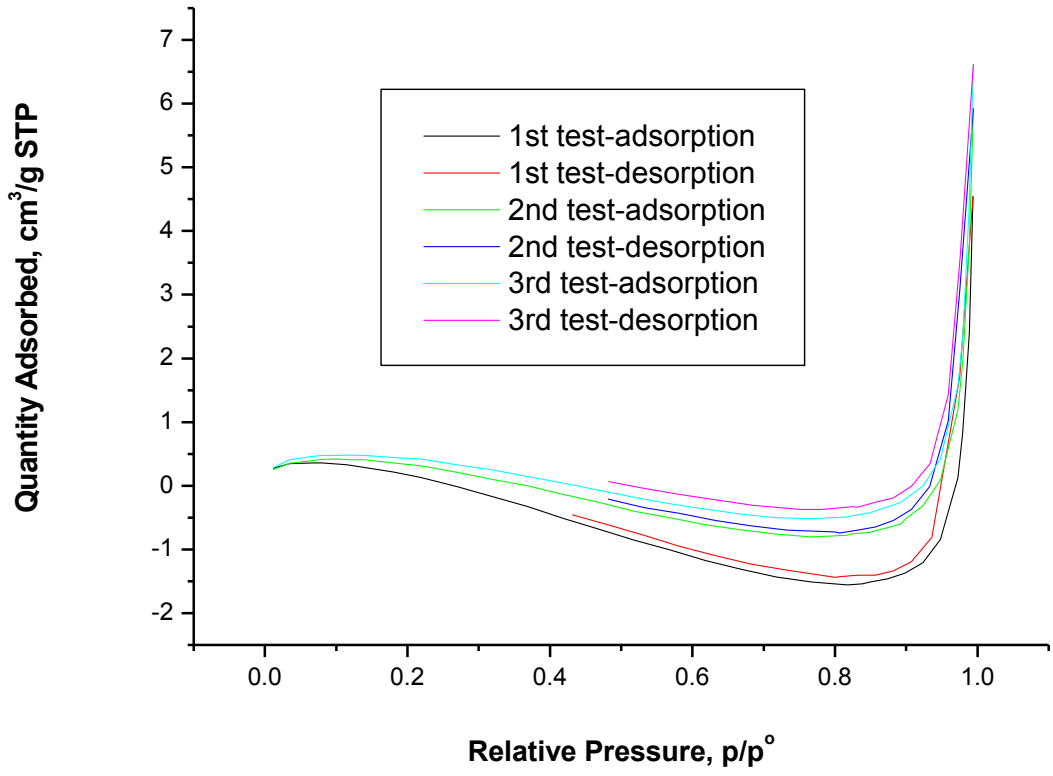
Table 3.5 Surface areas of poly(KAA) HIPEs measured after degassing for 12 h at 60 °C

Morphology	Composition			BET surface area, m^2/g
	KAA, mmol	BIS, mol %	$\phi_{int.}$, vol %	
Fig. 3.13	4.27	10	80	1.68
Fig. 3.21 (c)(d)	4.27	10	89	1.32
Fig. 3.22 (e)(f)	4.27	4.0	80	0.25
Fig. 3.25 (a)	4.81	2.5	80	0.45

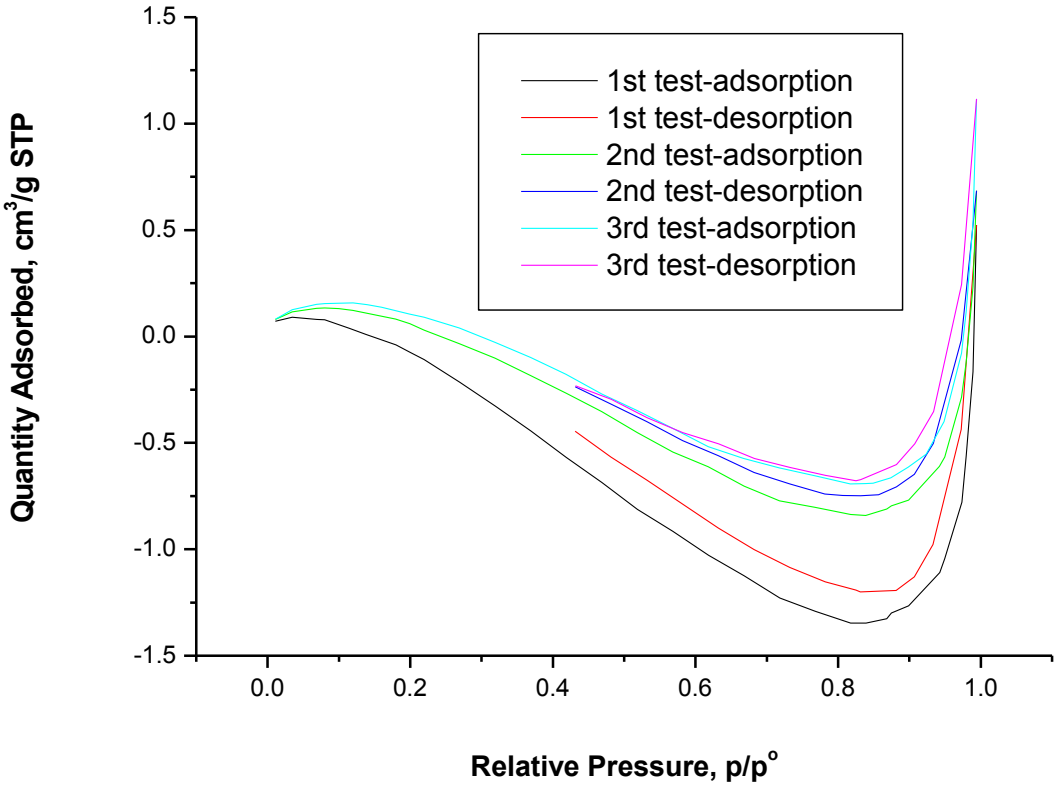
Secondly, surface area measurements were carried out using three degas-test cycles, i.e., the same samples were degassed again at 60 °C and tested after a previous degas-test cycle. The reason for doing so is to check whether more surface area can be created, since poly(KAA) is hydroscopic.[520] As a result, the adsorption-desorpiton isotherms were observed move upwards in later cycles (**Fig. 3.40**) and surface areas of all tested samples presented a significant increase in subsequentcycles in comparison to the results obtained in the first cycle (**Fig. 3.41**). This indicated that a complete moisture removal from poly(KAA) Pickering-HIPEs was difficult. For the third test (**Table 3.6**), polyHIPEs **No.1** showed a relatively higher surface area (1.37 m^2/g) than others, likely due to its higher BIS content. It is worth noting that polyHIPEs **No.6** samples were shrunken pieces prior to the degassing process, which was probably responsible for the extremely low surface areas.

Table 3.6 Surface areas results of poly(KAA) Pickering-HIPEs obtained in the third tests

No.	Morphology	Composition			BET surface area, m^2/g
		KAA, mmol	BIS, mol %	$\phi_{int.}$, vol %	
3	**Fig. 3.25**(b)	3.74	5 (28.8 mg)	80	0.57
4	**Fig. 3.25**(c)	4.27	5 (32.9 mg)	85	0.64
5	**Fig. 3.25**(d)	4.81	2.5 (18.5 mg)	85	0.28
1	**Fig. 3.21**(a)(b)	4.27	10	85	1.32
2	**Fig. 3.22**(a)	4.27	7.5	80	0.31
6	**Fig. 3.25**(e)	4.81	16.5 mg	80	0.08



(a) **No.1**



(b) **No.5**

Fig. 3.40 Representative adsorption-desorption isotherms of poly(KAA) Pickering HIPEs that underwent three degas-test cycles. The isotherms of polyHIPEs **No.1** (closed porous) and **No.5** (open porous) were both showed to move upwards in subsequent tests in comparison to the previous tests. The compositions of these polyHIPEs are listed in **Table 3.6**.

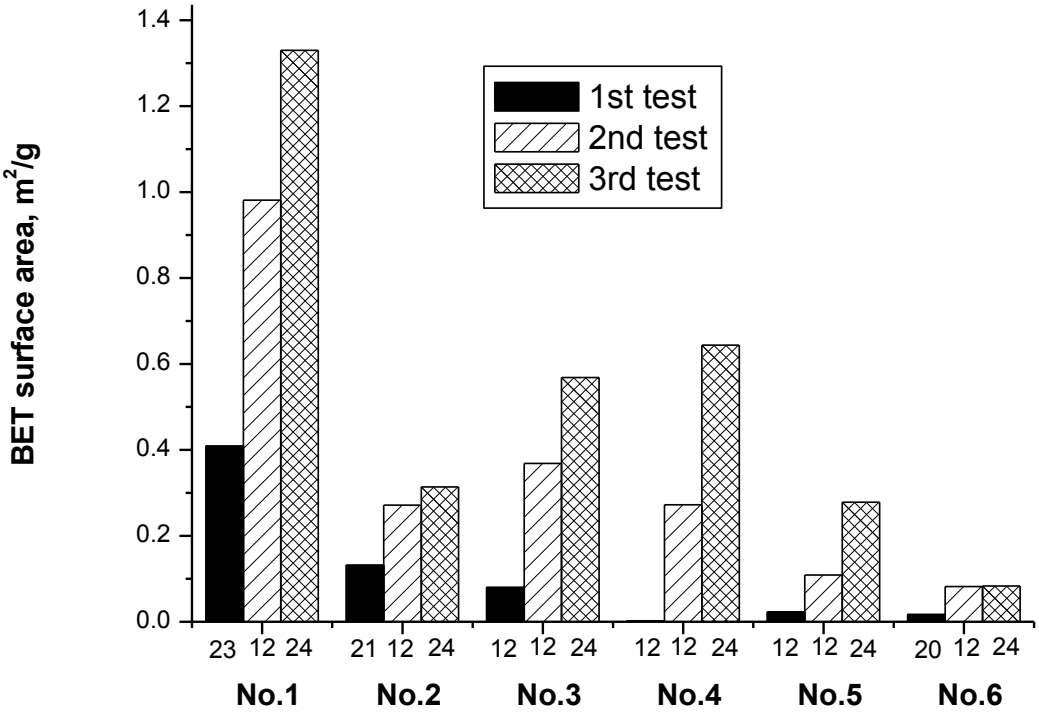


Fig. 3.41 Three cycles of BET surface area tests on poly(KAA) Pickering-HIPEs. The compositions of these polyHIPEs are listed in **Table 3.6**.

To sum up, poly(KAA) Pickering-HIPEs exhibit surface areas below 2 m^2/g, indicating that removal of water did not produce mesopores in polyHIPEs. On the other hand, it has been found that the degassing process and the sample state prior to test does influence the results. Measures such as elongating the degassing duration or applying multiple freeze/thaw cycles can lead to an increase in surface area due to further removal of moisture. It has also been shown that higher crosslinking degree tends to produce higher surface areas.

3.5.2 Porosity of poly(KAA) Pickering-HIPEs

To measure the porosities of poly(KAA) foams, the method used for styrene-based polyHIPEs (**Section 2.3**), i.e. Geopyc1360 plus Accupyc1330, is practically not suitable due to the soft and hydroscopic nature of the foams. Attempts have been made using other methods, including liquid displacement, mercury intrusion porosimetry and a designed indirect method.

3.5.2.1 Porosity from liquid displacement measurements

Liquid displacement (**Section 7.3** and **Section 7.4.3.5.1**) is a method to measure porosity and density of polymer foams,[220,521-524] in which a nonsolvent of the polymer is chosen as the displacement liquid. To carry out the evacuation-repressurization cycles, a self-designed device (**Fig. 7.9**) was used for the measurements. Initially, the effectiveness of the device has been shown by two facts: a large number of air bubbles come out of the specimen during evacuation; the created vacuum is kept above the standard vapour pressure of *p*-xylene (the displacement liquid) at RT. With this method, porosities of two series of poly(KAA) Pickering-HIPEs (**Table 3.7**, for details see **Table 7.13**) were measured: (1) $\phi_{int.}$ as the variable at BIS content of 10 mol %; (2) BIS content as the variable at $\phi_{int.}$ of 80%.

Table 3.7 Densities and porosities of polyKAA foams measured from liquid displacement

Morphology	Composition			ρ_{Foam} /g.cm^{-3}	$\rho_{Skeleton}$ /g.cm^{-3}	Porosity /%
	KAA /mmol	BIS /mol %	$\phi_{int.}$ /vol %			
Fig. 3.13	4.27	10.0	80	0.024±0.002	0.108±0.042	76.1±6.7
Fig. 3.21 (a)	4.27	10.0	85	0.033±0.002	0.313±0.234	85.8±10.2
Fig. 3.21 (b)	4.27	10.0	89	0.050±0.040	0.116±0.087	57.2±8.6
Fig. 3.22 (e)(f)	4.27	4.0	80	0.031±0.008	0.157±0.049	79.7±1.8
Fig. 3.22 (o)(p)	4.27	2.5	80	0.100	0.502	80.0

* The numbers of tested specimens were 3, 2, 3, 3 and 1, respectively.

For the series taking $\phi_{int.}$ as the variable, the reported inverse relationship[220] between foam density of polyHIPEs and $\phi_{int.}$ was not present. Instead, a slight increase from 0.024 g.cm^{-3} to 0.031 g.cm^{-3} was observed when $\phi_{int.}$ was increased from 80% to 85%. One important reason was that KAA/BIS in the aqueous solution did not fully turn into the matrix of polyHIPEs due to creaming during photo-polymerisation (**Section 3.4.2.1**). This loss of materials occurring to polyHIPEs prepared using 80 vol % internal phase rather than those prepared using 85 vol % internal phase, decreased its foam density. In addition, the densities of polyHIPEs prepared using 85 vol % or 89 vol % internal phase exhibited larger deviations than those of polyHIPEs prepared using 80 vol % internal phase, indicating that the pore structures of the foam might become less uniform upon increasing $\phi_{int.}$. For the series of

various BIS contents, foam densities and skeleton densities of polyHIPEs with 10 mol % and 4 mol % crosslinking degrees were similar but smaller than those of polyHIPEs with 2.5 mol % crosslinking degree. This was probably determined by whether the BIS content of polyHIPEs was above or below the critical BIS content (3.2 mol%, **Section 3.4.2.2**) for open porous morphology. The open porous morphology of polyHIPEs with 2.5 mol % crosslinking degree could help attain an easier penetration of *p*-xylene into the specimen interior and a more complete removal of air. Thus, the density results measured with liquid displacement were morphology dependent. The porosities of this series (**Table 3.7**) were all around 80%, their nominal $\phi_{int.}$.

Meanwhile, it is worth noting that the measured skeleton densities (**Table 3.7**) were all below 0.6 g.cm^{-3}, much lower than the reported densities of dehydrated PAA or PAA salts (1.4~1.7 g.cm^{-3}).[525-527] This issue was not mentioned in the reported cases where liquid displacement was applied. To stress this issue, control tests were carried out on a more rigid polymer foam, a styrene-based polyHIPE (**Section 2.3**), using *p*-xylene or water as the displacement liquid (**Table 3.8**). It can be seen that porosities from liquid displacement were in good agreement with those from Geopyc1360 plus Accupyc1330 whereas densities were approximately 20% lower. This indicated according to Equation (7.3) that occupation of the pores by liquids was incomplete despite an open porous morphology (**Fig. 2.8**) and that the matrix volume assessed by applying helium to sample powders, i.e., via Accupyc1330, was more accurate. Thus, it can be deduced that not only open porous morphologies but also sufficiently large pores and interconnections (or pore throats) of the foams are necessary in order for more precise density measurements. On the other hand, the identical porosity results (**Table 3.8**) suggested that porosity measured with liquid displacement could still be reliable to some extent.

Table 3.8 Densities and porosities of poly(styrene) HIPEs measured with various methods

Testing methods		ρ_{Foam} / g.cm^{-3}	$\rho_{Skeleton}$ / g.cm^{-3}	Porosity / %
Geopyc1360 & Accupyc1330		0.162	1.13	85.7
Liquid displacement*	*p*-Xylene	0.134	0.873	84.6
	Water	0.119	0.835	85.7

* One specimen was tested for either displacement liquid.

Therefore, liquid displacement is suitable for density and porosity measurement of soft and hydroscopic polymer foams only when they possess open porous morphologies and sufficiently large pore throats to facilitate liquid penetration. The shortcomings of the method include low efficiency and manual evacuation.

3.5.2.2 Porosities by mercury intrusion porosimetry and a designed indirect method

Mercury intrusion porosimetry (MIP) is also a method for porosity measurement of polyHIPEs.[140,201,528,529] In the cases where a solvent coexisted with the monomers in the continuous phase of HIPEs, it was reported that porosities of the resultant polyHIPEs were close to the volume ratios of the internal phase ($\phi_{int.}$), i.e., the solvent in the continuous phase did not generate a secondary porosity.[140,528] However, the porosities of poly(KAA) Pickering-HIPEs (**Table 3.9**) were about 6~15% higher than their nominal $\phi_{int.}$, 80%. This significant difference suggested that the removal of water did contribute to the porosities of the foams in our case. This was consistent with the fact that poly(KAA) Pickering-HIPEs exhibited little shrinkage as a whole during water removal (**Fig. 3.30**). On the other hand, most skeleton densities measured by MIP were still below 1.0 g.cm^{-3} except two specimens of polyHIPEs with 3.2 mol % crosslinking degree (1.1 and 1.3 g.cm^{-3}). The lowest skeleton densities were only 0.3~0.4 g.cm^{-3}, obtained from polyHIPEs with 10 mol % crosslinking degree, which could be attributed to the presence of closed pores or a less dense polymer network.[201] Nonetheless, the relatively low skeleton densities of the open porous polyHIPEs with 2.5 mol % crosslinking degree remind us that measurements by MIP may become erroneous for flexible materials with porosity higher than 90% because the high pressure (228 MPa) can rupture the pore structures.[530]

Since liquid displacement and MIP were both prone to give skeleton densities of poly(KAA) Pickering-HIPEs that were lower than 1.0 g.cm^{-3}, their accuracy in porosity measurements should be compromised to some extent. In order to assess the skeleton densities and porosities more precisely, an indirect method was designed (**Fig. 3.42**) using the density of a polymer block (PB) as the skeleton density of the polyHIPEs. The polymer blocks were prepared by solely polymerising the aqueous solutions that had identical compositions to the aqueous phases of HIPEs. The photographs of a polymer block (**Fig. 3.43**) showed that the poly(KAA) gel shrank dramatically into polymer block (data see **Table 7.16**). Since poly(KAA) Pickering-HIPEs itself exhibited little or minor shrinkage (**Fig. 3.30**), this

dramatic shrinkage of the polymer network again suggested that the removal of water together with the internal phase contributed to the porosity of poly(KAA) Pickering-HIPEs, in agreement with the conclusion drawn from MIP.

Table 3.9 Porosities of poly(KAA) HIPEs measured by MIP and a designed indirect method

BIS content /mol %	Porosity by MIP			Porosity by an indirect method		
	ρ_{Bulk} /g.cm^{-3}	$\rho_{Skeleton}$ /g.cm^{-3}	Porosity /%	ρ_{Foam} /g.cm^{-3}	$\rho_{Skeleton}$ /g.cm^{-3}	Porosity /%
10.0	0.034±0.006	0.351±0.081	89.9±4.2	0.020±0.002	1.346	98.5±0.2
5.0	0.086	0.629	86.3	0.039±0.008	1.294	97.0±0.6
4.0	0.063±0.002	0.790±0.118	92.0±1.0	0.027±0.002	1.193	97.7±0.2
3.2	0.080±0.005	0.980±0.382	90.9±3.6	0.034±0.009	1.325	97.5±0.6
2.5	0.053±0.011	0.659±0.167	91.8±0.3	0.026±0.002	1.248	97.9±0.2

* The above poly(KAA) Pickering-HIPEs were prepared by polymerisation of HIPEs containing 0.82 M KAA, various BIS content and 80 vol % toluene. During emulsification a two-speed stirring protocol was used. For morphologies, see **Fig. 3.28**.

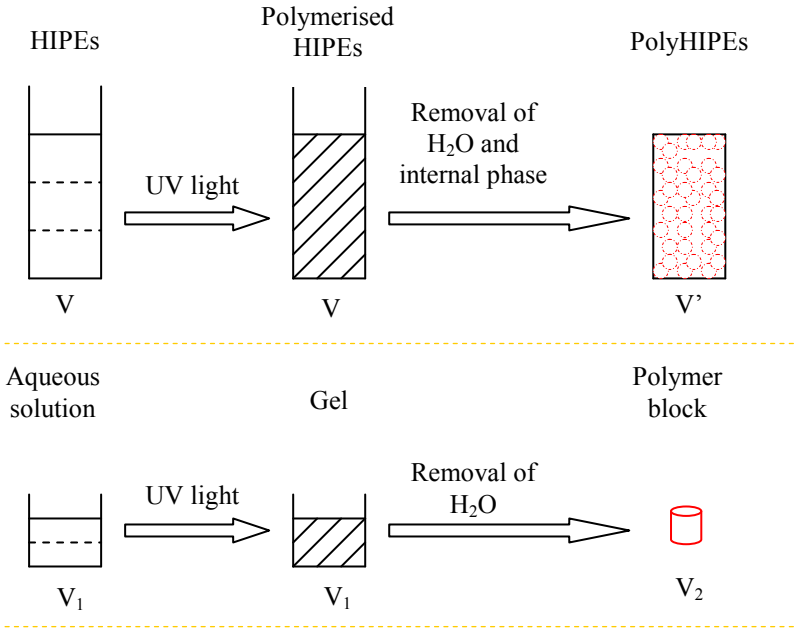
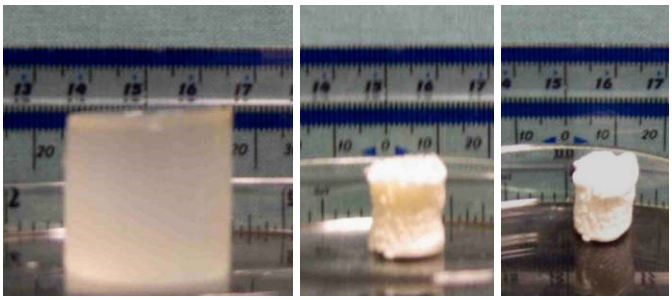


Fig. 3.42 Scheme of porosity measurement by a designed indirect method. A polymer block was prepared using identical composition to the continuous phase of HIPEs, whose density was measured by Accupyc1330 and taken as the skeleton density of the polyHIPEs. Foam density of polyHIPEs was determined by measuring the weights and dimensions of cuboids that were cut out of the polyHIPEs. Porosity was then calculated using Equation (7.1).



(a) (b) (c)

Fig. 3.43 Photographs showing the production of a polymer block. (a) A piece of gel obtained by photo-polymerising the aqueous solution having identical composition to the continuous phase of HIPEs; (b) after Soxhlet extraction; (c) after drying.

Obviously, measurement with the designed indirect method avoided going inside the porous structures of polyHIPEs and generating errors that were caused by destruction of the pore structures, such as the high pressure used in MIP. The skeleton densities measured with Accupyc1330 (**Table 3.9**) were 1.19~1.35 g.cm^{-3}, close to the reported densities of dehydrated PAA and its salts (1.4~1.7 g.cm^{-3}).[525-527] These results were reasonably reliable since the presence of water as well as protonation during washing would bring about a density reduction.[525,526] Foam densities of poly(KAA) Pickering-HIPEs measured using weights and dimensions of the polyHIPE cuboids (**Table 7.15**) were in the range of 0.02~0.04 g.cm^{-3}, lower than the bulk densities obtained from MIP (**Table 3.9**). As a result, the calculated porosities according to Equation (7.1) were higher than those obtained from MIP and reached 97~98% irrespective of BIS content. This strongly indicated that porosity of poly(KAA) Pickering-HIPEs was contributed by both oil and water. Meanwhile, it is worth noting that these high porosity results reflected the porosity of the interior of polyHIPEs, where the tested cuboids were sourced. As to the outer layer, the porosity was likely to be lower (not measured) since this layer of UV-polymerised samples was normally denser. Thus, the poly(KAA) Pickering-HIPEs (**Fig. 3.30**) were made of an interior of extremely high porosity and a surface layer of lower porosity, which helped resist shrinkage of the whole polyHIPEs.

In addition, the volume ratios of removed liquids ($\phi_{Removal}$) from poly(KAA) Pickering-HIPEs were estimated using Equation (3.5) and compared with their porosity results.

$$\phi_{Removal} = \phi_{int.} + \phi_{con.}(1 - \frac{V_{Dry}}{V_{Wet}}) \quad \text{.....(3.5)}$$

where V_{Dry} is the volume of dry polymer block measured using Accupyc1330, V_{wet} is the volume of poly(KAA) gel obtained by measuring its diameter and height prior to Soxhlet extraction and V_{Dry} / V_{Wet} stands for the shrinkage ratio of poly(KAA) gel to dry solid.

Table 3.10 The volume ratios of removed liquids from poly(KAA) Pickering-HIPEs

BIS content mol %	$\phi_{int.}$ (theo.) /%	$\phi_{int.}$ (actual) /%	Volumes of polymer blocks			$\phi_{Removal}$ /%
			V_{Dry} /cm^3	V_{Wet} /cm^3	V_{Dry}/ V_{Wet}	
10.0	80	79.7	0.438±0.001	7.238	0.0605	98.8
5.0	80	79.3	0.448±0.001	2.799	0.1601	96.7
4.0	80	79.3	0.952±0.001	9.764	0.0975	98.0
3.2	80	79.5	0.778±0.001	10.179	0.0764	98.4
2.5	80	79.2	0.835±0.001	9.141	0.0913	98.1

***** The above poly(KAA) Pickering-HIPEs were prepared by polymerisation of HIPEs containing 0.82 M KAA, various BIS content and 80 vol % toluene. During emulsification a two-speed stirring protocol was used. For morphologies, see **Fig. 3.28**.

The actual $\phi_{int.}$ was slightly smaller than the theoretical $\phi_{int.}$, because a small amount of toluene was expelled out of the HIPE template during polymerisation. Meanwhile, the shrinkage ratio of polymer blocks (V_{Dry}/V_{Wet}) was assumedly taken as that of the poly(KAA) gel in the fabrication of polyHIPEs. Thus, Equation (3.5) would not be suited to those parts of the polyHIPEs that exhibited little or minor shrinkage. Since the calculated $\phi_{Removal}$ (**Table 3.10**) was in good agreement with the interior porosity of poly(KAA) Pickering-HIPEs assessed by the designed indirect method, it was deduced that polymer networks in the interiors of polyHIPEs dramatically shrank as the polymer blocks. In other words, the internal porosity of polyHIPEs was equivalent to the volume ratio sum of oil and water. Nevertheless, when overall shrinkage of polyHIPEs was not negligible, especially at very low BIS content (**Table 7.17**), the use of $\phi_{Removal}$ for internal porosity assessment could become vulnerable, since it was unknown whether $\phi_{int.}$ fully contributed to porosity.

To sum up **Section 3.5.2.2**, removal of water in the continuous phase also contributed to the porosity of poly(KAA) Pickering-HIPEs. Skeleton densities measured by MIP were mostly below 1.0 $g.cm^{-3}$ and were even lower for polyHIPEs with closed-pore morphology. However, measurements by a designed indirect method effectively resulted in skeleton

densities of 1.19~1.35 g.cm^{-3}, close to that of the reported PAA or poly(KAA). Meanwhile, the method revealed that the porosity of the interior of polyHIPEs was as high as 97~98%, in agreement with the calculated volume ratio sum of removed oil and water.

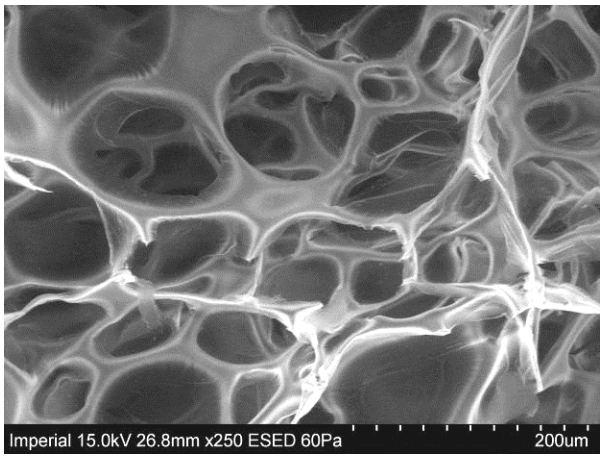
3.6 Preparation and characterisation of KAA based polyHIPE composites

To improve the properties of polymer materials for certain applications, the composite approach is usually taken.[531-535] For the fabrication of 3-D porous scaffolds for tissue engineering, it is also common to use polymer composites instead of neat polymers in order to enhance cell attachment,[536] protein adsorption,[537,538] mechanical properties,[539] bioactivity[42,540], etc. As a unique method to produce highly porous polymers, polyHIPE has recently been absorbing the concept of polymer composites for the purpose of improved properties and practical applications, leading to polyHIPE composites.[142-145,541] More interestingly, polyHIPEs itself can become composite when a Pickering HIPE template is used, i.e., poly(Pickering HIPEs). However, microgel particles as employed here in poly(KAA) Pickering-HIPEs were expected to introduce controlled drug-delivery functions to the composite (**Chapter 4**). Considering mechanical properties or bioactivity of polyHIPEs, it is essential to use other particle species than microgels. Thus, it is our aim to prepare poly(Pickering HIPE) composites for potential applications as multifunctional scaffolds, which has not been reported to our best knowledge.

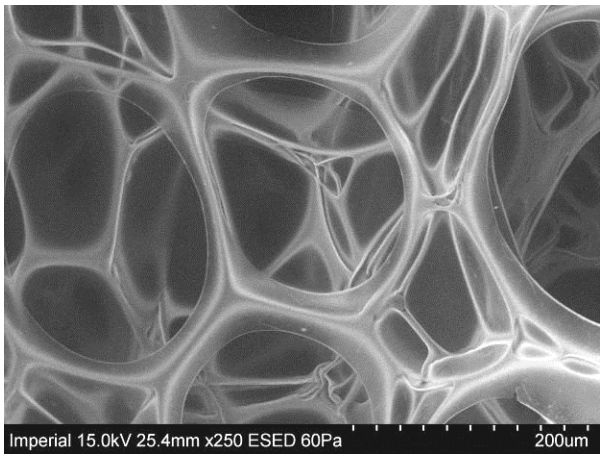
3.6.1 Hydrophilic silica filled poly(KAA) Pickering-HIPE composites

Silica is a widely used particulate reinforcement in polymer composites,[542] and has recently been used after modification as filler in conventional polyHIPE composites[102,142] and as Pickering HIPE stabiliser in poly(Pickering HIPEs).[193,194] The modification rendered silica particles less hydrophilic and improved their interaction with the hydrophobic matrices. However, since silica here is designed to disperse within the aqueous phase containing KAA in an o/w HIPE template, the hydrophilic particles were used without modification and expected to have good affinity to the resultant hydrophilic polymer matrix. The dispersion of silica, the morphology and swelling properties of polyHIPE composites are of concern in this preliminary investigation.

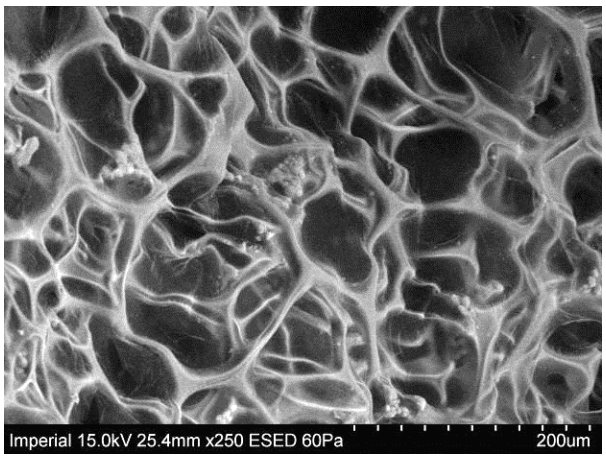
A control experiment replacing microgel particles with an identical amount of silica in KAA-toluene system phase separated during emulsification. This indicated that silica particles were too hydrophilic to serve as a Pickering emulsifier, in agreement with others' findings.[193,194] On the other hand, incorporation of silica into microgel-stabilised HIPEs – containing 0.15 wt % microgels, 0.82 M KAA, 3.2 mol % BIS, 2 mol % I2959 and 80 vol % toluene – was carried out using either the one-speed (400 rpm) or the two speed (400→1000 rpm) stirring protocol. As a result, stable HIPEs were obtained in either case. The choice of this composition was because it had a critical BIS content for open porous poly(Pickering HIPEs) (**Section 3.4.2.2**). The dispersion of various amounts of silica into the polyHIPE composites was investigated using these two stirring protocols.



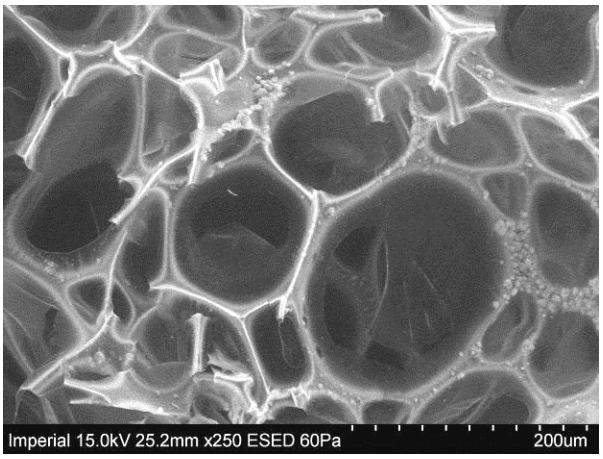
(a) No silica



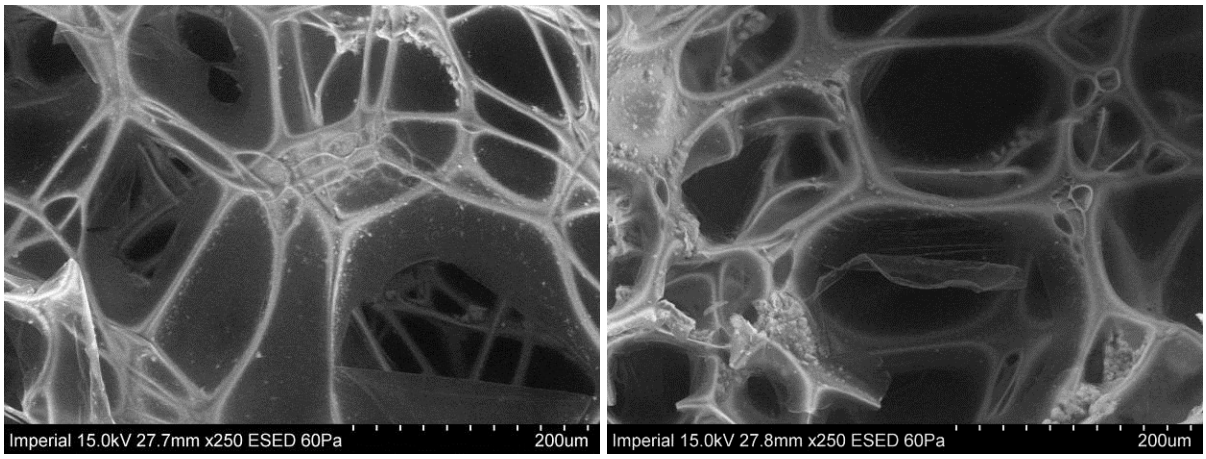
(b) 1 wt % silica



(c) 5 wt % silica



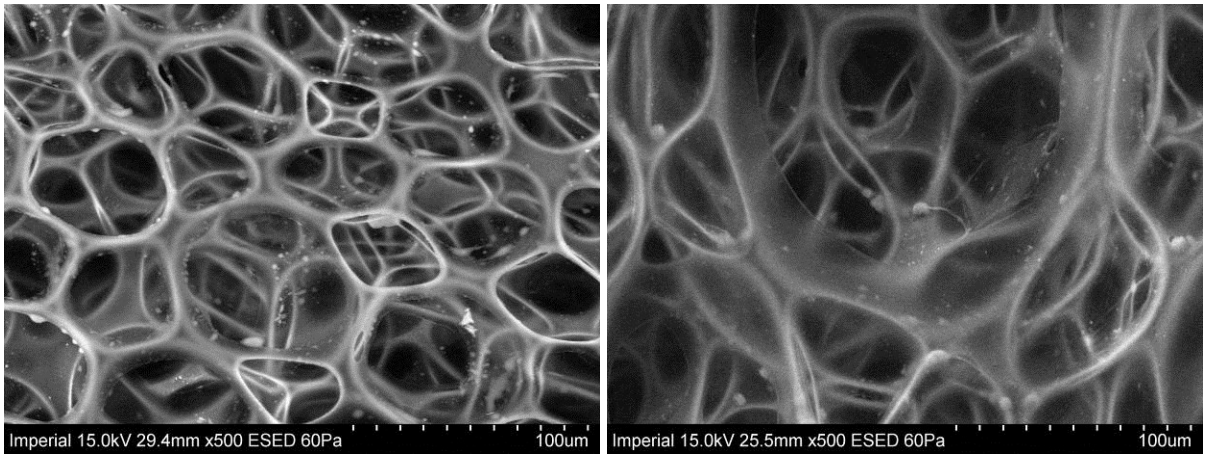
(d) 10 wt % silica



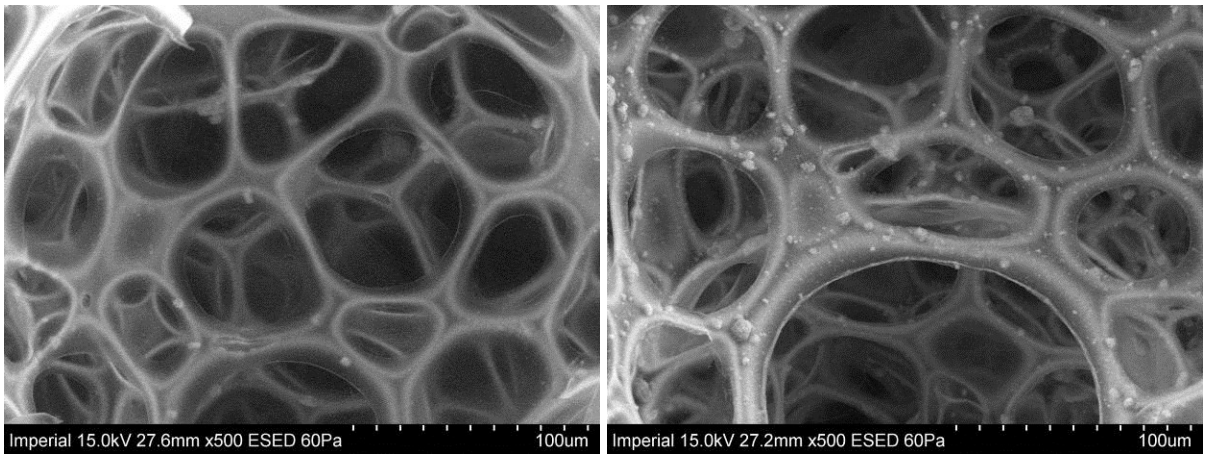
(e) 15 wt % silica (f) 15 wt % silica

Fig. 3.44 SEM images of poly(KAA) Pickering-HIPEs and its silica composites prepared using the one-speed stirring protocol (400 rpm). The silica amounts used were 0, 1, 5, 10 and 15 wt %, respectively, relative to the total weight of KAA and BIS.

Using the one-speed stirring protocol (400 rpm), silica particles were visible in polyHIPE composites in contrast to the neat polyHIPEs [**Fig. 3.44** (a)]. At the loading of 5 wt % or above, the clusters of larger than 30 μm seen in the composites indicated that the dispersion and the distribution of silica was poor. However, using 1000 rpm in the two-speed stirring protocol (400→1000 rpm) resulted in more homogeneous open-porous structures [**Fig. 3.28** (d)] and obviously better dispersion and distribution of silica (**Fig. 3.45**). Particle clusters larger than 10 μm in diameter were hardly visible in the composites even at the highest loading of 15 wt %. Thus, increasing stirring speed prior to polymerisation proved effective in reducing silica aggregation.



(a) 1 wt % silica (b) 5 wt % silica



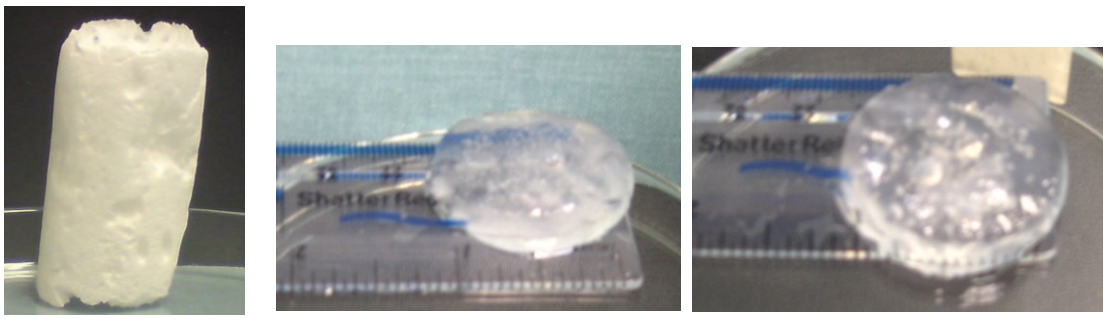
(c) 10 wt % silica (d) 15 wt % silica

Fig. 3.45 SEM images of poly(KAA)/silica Pickering-HIPE composites prepared using the two-speed stirring protocol (400→1000 rpm). Silica loadings were 1, 5, 10 and 15 wt %, respectively, relative to the total weight of KAA and BIS.

Since poly(Pickering HIPE) composites should be used as tissue engineering scaffolds, their wet-state properties are of practical importance. Firstly, taking poly(KAA)/silica Pickering-HIPE composites prepared using a two-speed stirring protocol and 10 wt % loading [**Fig. 3.45** (c)] as an example, a preliminary swelling test of the composite was carried out in simulated body fluid (SBF). Photographs of the specimen at different stages (**Fig. 3.46**) together with tracing measurements of its size and weight (**Table 3.11**) showed a swelling ratio of more than 6000 wt % and a volume expansion of 3~5 times. Besides a very high hydrophilicity and a low crosslinking degree (3.2 mol %) of the polyHIPE composite, the aqueous medium for swelling test also significantly affected the swelling ratio. Of all the ions present in the medium, the concentration of Ca^{2+} played a significant role.[543] For example, simple tests showed that a sample piece of the polyHIPE composite lost its mechanical stability in distilled water but hardly swell in a saturated $CaCl_2$ solution. Secondly, assessment of the mechanical properties of these polyHIPE composite hydrogels was desirable. Unfortunately, the composite hydrogel in SBF (**Fig. 3.46**) was so pliable that no forces were detected during compression conducted with a micro-deformation apparatus.[544] Apparently, a reduction of the swelling ratio would make the hydrogel mechanically stronger. There are options that only involve composition tuning but hardly affect the open porous morphology, such as increasing the crosslinking degree to 5 mol % or more (**Section 3.4.3**). Other options that involve introducing new components will be discussed in the following sections of the chapter.

Table 3.11 Swelling of poly(KAA)/silica Pickering-HIPE composite in SBF at 36 °C

Time	Size (D × h) /mm	Volume /cm^3	Weight /g	Swelling ratio /wt %
t_0 (dry state)	17.0 ± 0.1 × 7.0 ± 1.0	1.59 ± 0.23	0.0884	-
t_1 =25 h 20 min	32.0 ± 0.1 × 8.3 ± 2.5	6.67 ± 2.01	5.442	6056
t_2 =117 h 45 min	30.5 ± 0.5 × 8.0 ± 2.0	5.84 ± 1.47	5.956	6638



(a) t_0 (b) t_1 (c) t_2

Fig. 3.46 Photographs of poly(KAA)/silica Pickering-HIPE composite during a swelling test using simulated body fluid as the medium. A slice was cut out of the dry sample for the test.

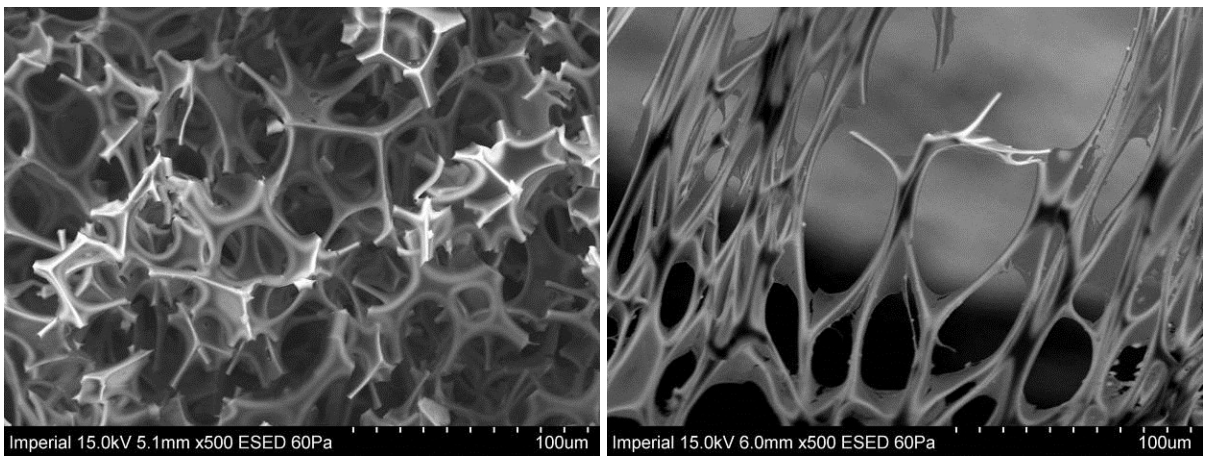
To sum up this preliminary study, it was revealed that the dispersion of unmodified silica in poly(KAA)/silica Pickering-HIPE composites was dependent on the stirring speed. PolyHIPE composite with 15 wt % silica were obtained without particle clusters larger than 10 μm using a higher stirring speed (1000 rpm). A porous composite with 10 wt % nominal loading exhibited a swelling ratio in SBF up to over 6000 wt %. Further investigations into the composition-morphology-property relationship of the composites are necessary in order to exploit this approach for cell growth or bone repair.

3.6.2 45S5 Bioglass® filled poly(KAA) Pickering-HIPE composites

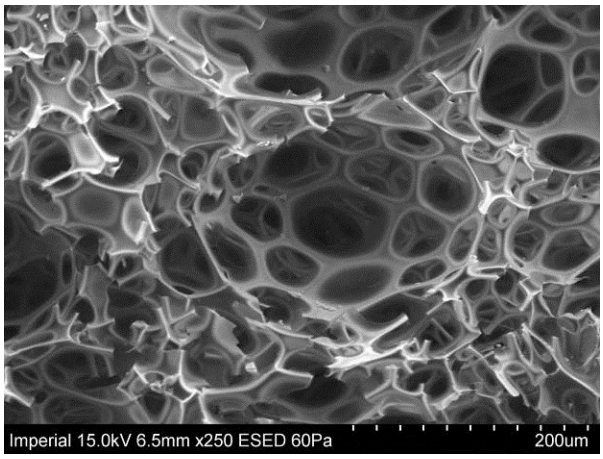
Bioactive glasses have attracted much attention in biomedical applications due to their high bioactivity, i.e., the capability of reacting with physiological fluids and forming chemical bonds to bone (or soft) tissues.[545] In this family, 45S5 Bioglass® (or Bioglass®), possessing a composition of 45% SiO_2, 24.5% Na_2O, 24.5% CaO, and 6% P_2O_5 (wt %), was the first reported[546] and most frequently investigated bioactive glass species.[547] For tissue engineering applications, Bioglass® has been recently incorporated into porous polymer scaffolds aiming for bioactive composite scaffolds.[548-554] In principle, apart from improving

the interfacial bonding of composites to surrounding bone tissue, Bioglass® is also expected to manifest in the scaffolds its stimulating effect on gene expression,[555] angiogenesis,[556,557] mineralization,[558] etc. On the other hand, there are two extra motivations to prepare Bioglass® filled poly(KAA) Pickering-HIPE composites. Firstly, it is attractive to fabricate bioactive scaffolds using polyHIPEs, especially poly(Pickering HIPEs), as a template. Secondly, it is also interesting to use poly(KAA) instead of the commonly reported hydrophobic polymers[559] as the matrix, since the resultant poly(KAA) hydrogel not only enables larger water absorption but also has the possibility to undergo calcification[560] as well as to interact with Bioglass® and the surrounding tissue. In this preliminary study, poly(KAA)/Bioglass® Pickering-HIPE composites with various loadings were prepared using the two-speed stirring protocol (400→1000 rpm) for HIPE preparation and characterized with SEM and TGA.

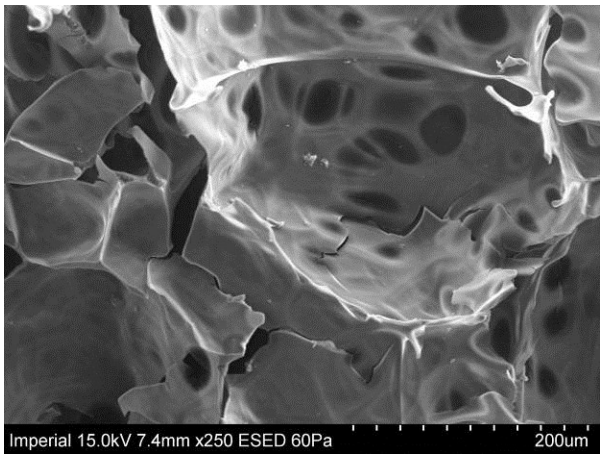
Particulate Bioglass® was only sporadically visible in poly(KAA) Pickering-HIPE composites even at 20 wt % loading (**Fig. 3.47**), in contrast to silica in poly(KAA) Picking-HIPE composites (**Section 3.6.1**) or Bioglass® in other polymer composite foams.[552,553] One probable cause could be the high reactivity of Bioglass® in the aqueous medium, evidenced by some "paste" covered pore throats [**Fig. 3.47** (d), (f) and (i)]. The "paste" on the polymer surface was not observed in neat poly(KAA) Pickering-HIPEs [**Fig. 3.28** (d)] and was likely formed due to the dissolution[561] of Bioglass® in the aqueous phase. It was also possible that the original particles turned into smaller ones during dissolution. Nevertheless, Roether *et al.*[548] reported the use of a Bioglass® aqueous slurry for poly($_{D,L}$-lactide) foam coating and found the composite scaffolds still to be bioactive. Apart from those "paste" covered throats, interconnected pore structures were exhibited, similar to the neat poly(KAA) Pickering-HIPEs [**Fig. 3.28** (d)].



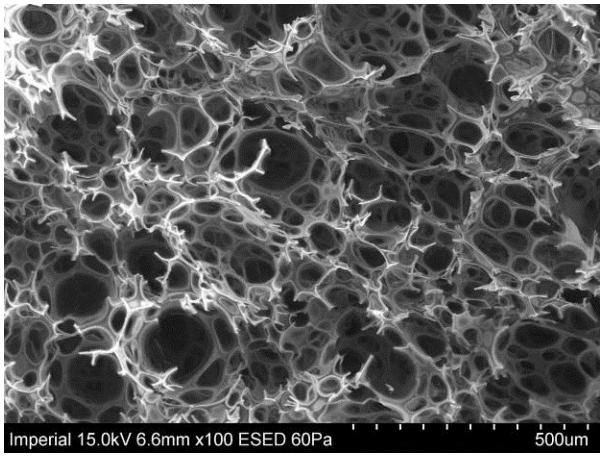
(a) 2 wt %　　(b) 2 wt %



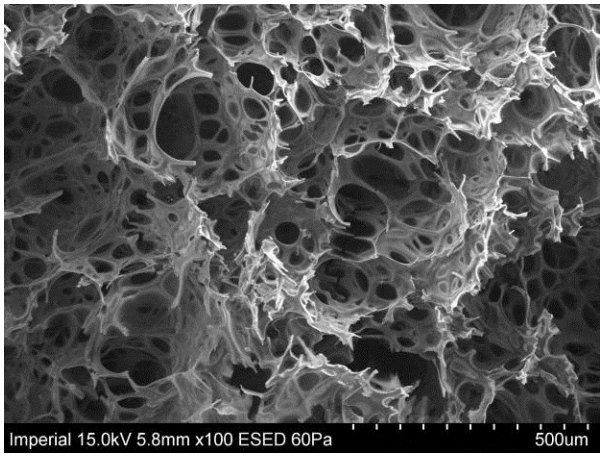
(c) 5 wt %



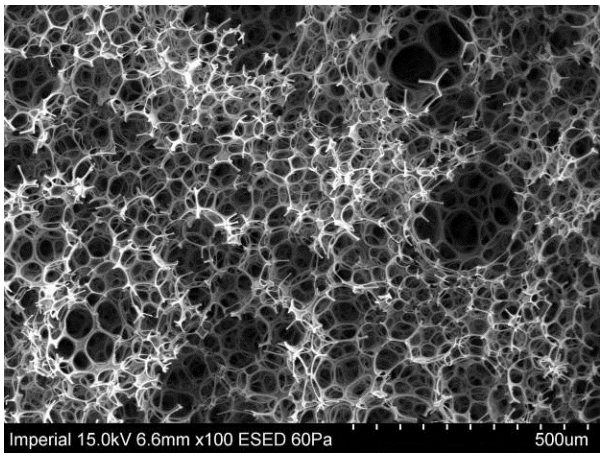
(d) 5 wt %



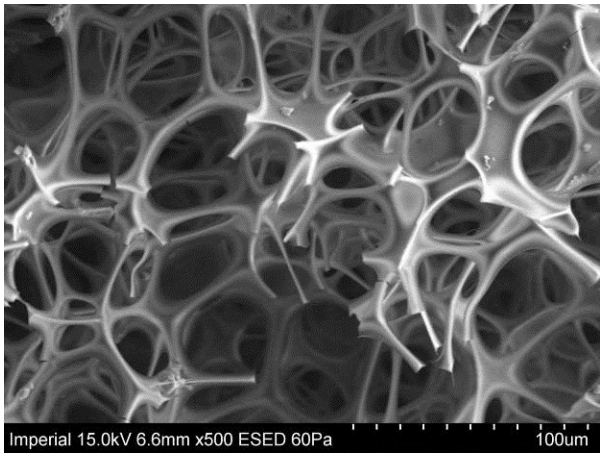
(e) 10 wt %



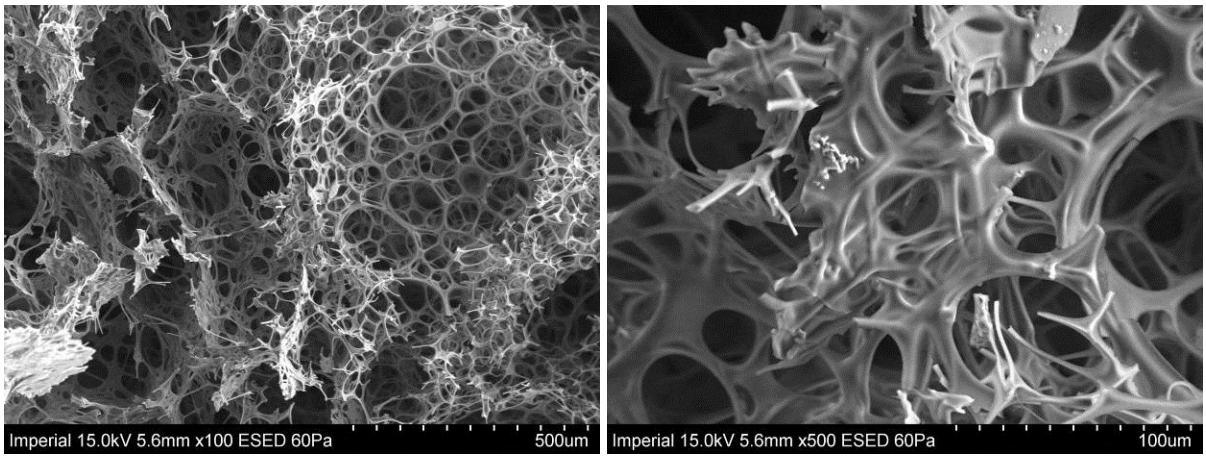
(f) 10 wt %



(g) 15 wt %



(h) 15 wt %



(i) 20 wt % (j) 20 wt %

Fig. 3.47 SEM images of poly(KAA)/Bioglass® Pickering-HIPE composites prepared using the two-speed stirring protocol for emulsification. The HIPEs containing 0.15 wt % microgels, 0.85 M KAA, 3.2 mol % BIS, 2 mol % I2959 and 80 vol % toluene for all but containing 2, 5, 10, 15 and 20 wt % Bioglass®, respectively.

The content and distribution of Bioglass® in the composites was investigated with TGA. More than 50% weight remained when specimens were heated up to 600 °C in either N_2 or air (**Fig. 3.48**). This high percentage of residual weight is similar to reported TGA data of poly(KAA)[562] rather than PAA,[563] which resulted in 20 wt % residue when heated in TGA up to 500 °C in N_2.[563] Thus, it is again confirmed that poly(KAA) is the major component of the polyHIPE matrix despite extraction with HCl in MeOH used during purification. On the other hand, the weight loss between 250 °C and 500 °C was attributed to two processes: an initial dehydration followed by decomposition, which was responsible for the sharp weight loss. The decomposition of the polyHIPE composites in N_2 occurred in the range of 450~500 °C whereas a sharper weight loss in air occurred at ~400 °C. As a result, the residue in the plateau between 500~600 °C was mainly a mixture of potassium carbonate[562] and Bioglass®. Therefore, a TGA up to 600 °C is not sufficient to probe Bioglass® contents in polyHIPE composites.

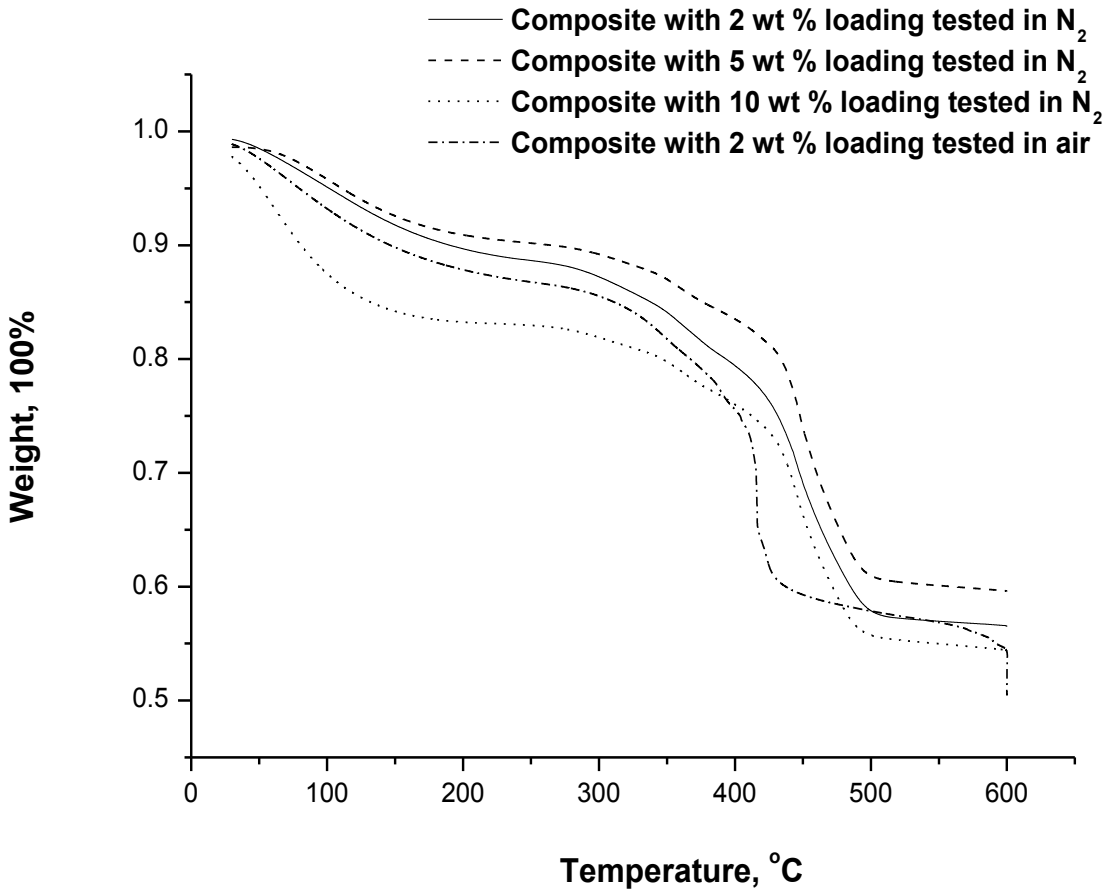


Fig. 3.48 TGA of poly(KAA)/Bioglass® Pickering-HIPE composites in N_2 and air (heating rate: 10 °C/ min).

A further increase of temperature up to 900 °C resulted in a dramatic weight loss. About 21.4% weight was detected for polyHIPE composite with 2 wt % nominal loading, which was isothermally heated at 900 °C for 10 min after a ramp from RT to 900 °C at 10 °C/min. Moreover, it was observed from polyHIPE composite with 10 wt % nominal loading (**Fig. 3.49**) that the isothermal duration at 900 °C also had an effect on the residual weight. A consistent loss of weight was shown when the polyHIPE composite was isothermally heated at 900 °C, especially during the first 30 min (22% loss). This was attributed to the decomposition of potassium carbonate[564] starting from 900 °C since Bioglass® alone did not show any weight loss during this process[565] (**Fig. 3.50**).

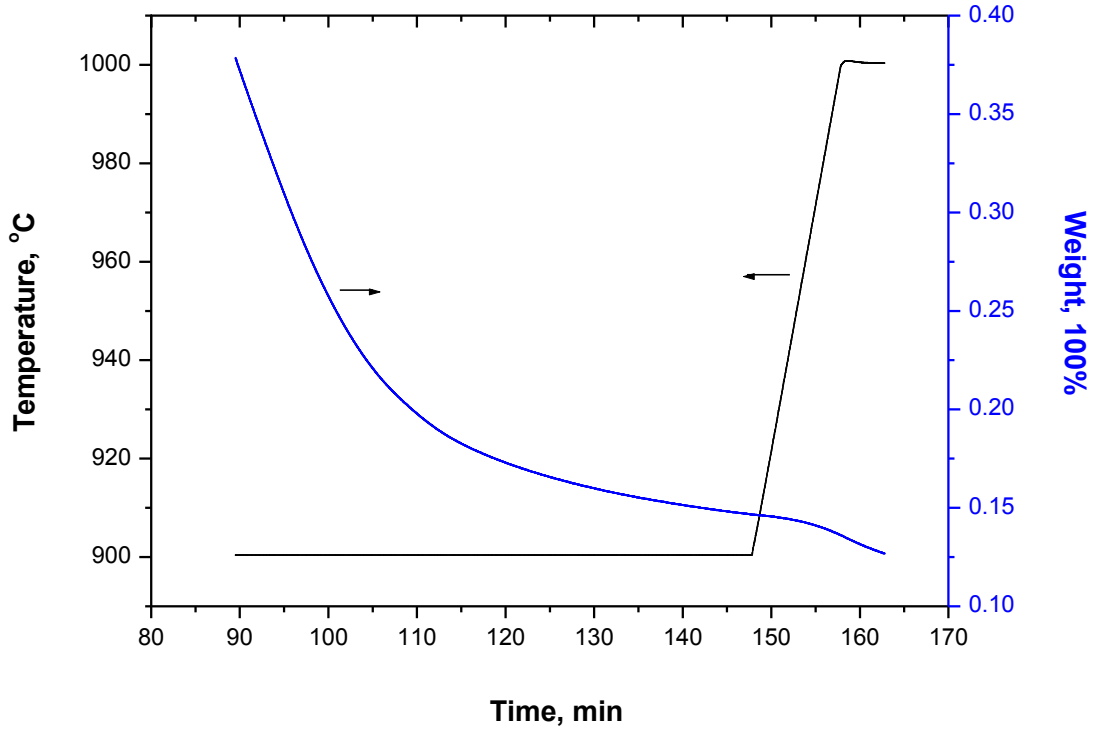


Fig. 3.49 TGA of poly(KAA)/Bioglass® Pickering-HIPE composite ranging from 900 °C to 1000 °C. The composite was prepared using a nominal loading of 10 wt % Bioglass®, relative to the weight sum of KAA and BIS.

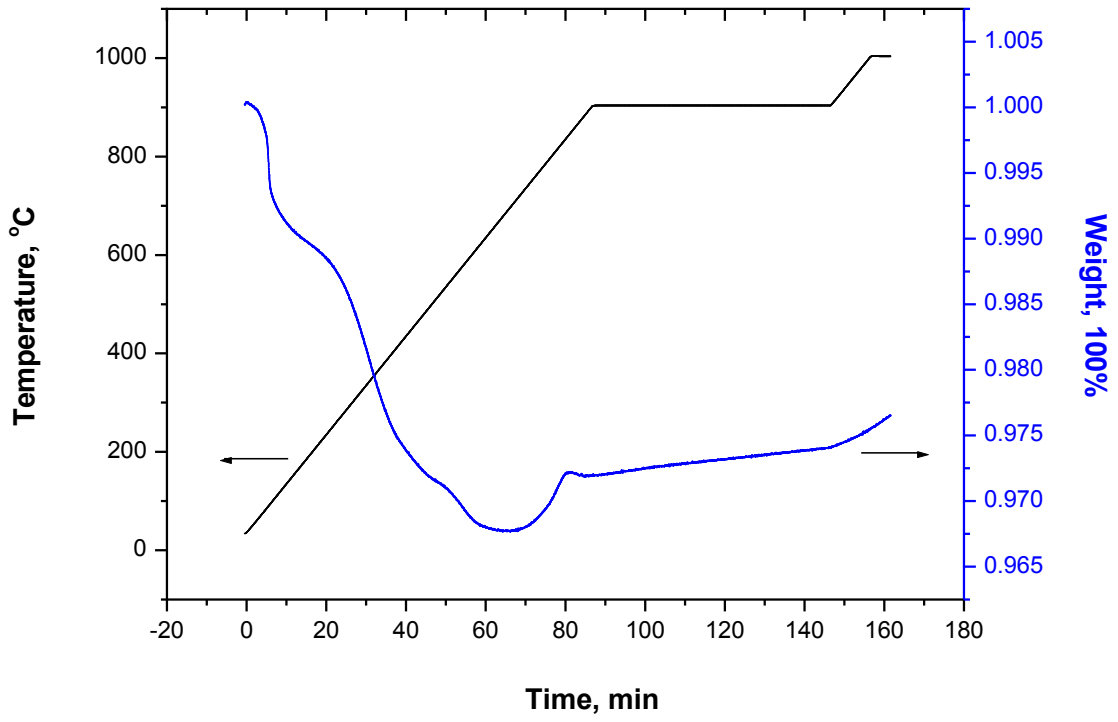


Fig. 3.50 TGA of Bioglass® in air using a heating rate of 10 °C/ min

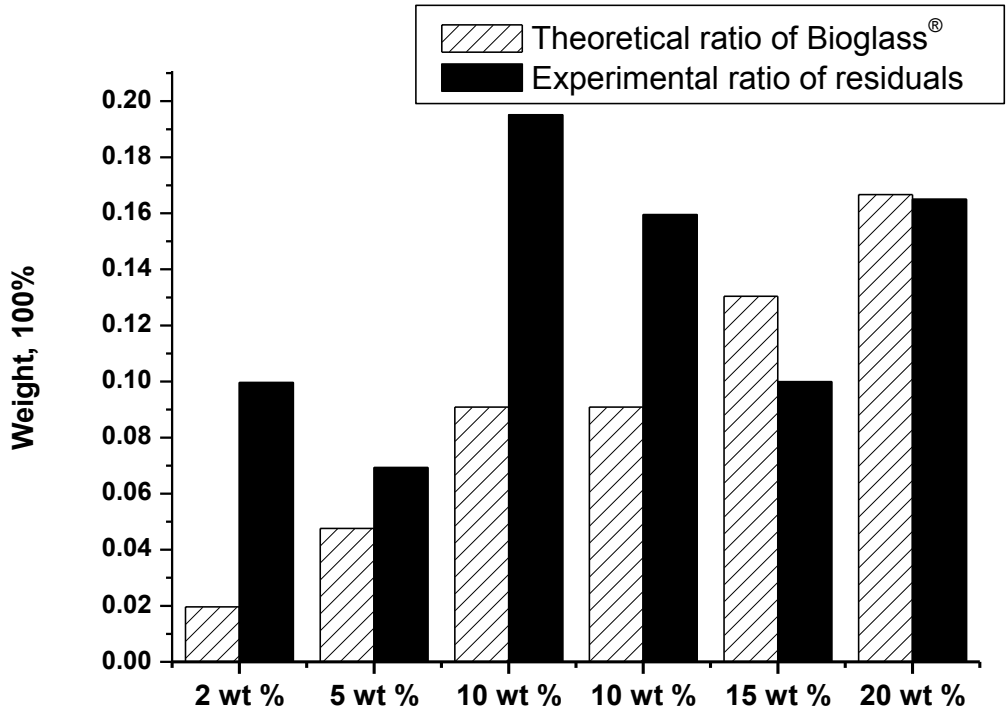


Fig. 3.51 Residual weights of poly(KAA)/Bioglass® Pickering-HIPE composites after TGA tests in air. A procedure consisting of a ramp from RT to 900 °C at 10 °C/min and an isothermal duration of 40 min at 900 °C was used. The weight percentages showing on the horizontal axis were the mixing ratios of Bioglass® to the weight sum of KAA and BIS. The theoretical ratio of Bioglass® was a calculated ratio of Bioglass® in the polyHIPE composite, i.e., the weight of Bioglass® divided by the total weight of Bioglass®, KAA and BIS.

The residual weights of poly(KAA)/Bioglass® Pickering-HIPE composites were hence measured using an isothermal duration of 40 min at 900 °C and compared with the theoretical ratios of Bioglass® in the composites (**Fig. 3.51**). As a result, the experimental ratios of residuals were higher than the theoretical ratios of Bioglass® in tested composites with 2~10 wt % nominal loadings. This was reasonably attributed to the presence of K_2O in the residues, the decomposition product of K_2CO_3 but the distribution of Bioglass® might not be uniform. Therefore, determination of Bioglass® contents in poly(KAA) Pickering-HIPE composites via TGA was influenced by the formation and decomposition of K_2CO_3.

To sum up, Bioglass® can be incorporated into microgels stabilised HIPEs without compromising emulsion stability. However, Bioglass® resulted in "paste"-covered pores in the resultant polyHIPE composites likely due to its reactivity in the aqueous phase. TGA became ineffective in determining Bioglass® content and distribution in the composites due to formation and decomposition of K_2CO_3. Whether the resultant polyHIPE composites are

bioactive and whether Bioglass® also brings about reinforcing effect to the composites are of interest for investigation in the future.

3.7 Preparation of poly(potassium methacrylate) Pickering-HIPEs

As deduced in **Section 3.6.1**, the poor mechanical properties exhibited by poly(KAA) Pickering-HIPE hydrogels were largely related to the superabsorbent nature of poly(KAA). In order to obtain poly(Pickering HIPE) hydrogels with better mechanical properties to support cell growth, it is worth trying to reduce the swelling degree of the polymer matrices. A simple approach based on microgels stabilised HIPE template is to introduce hydrophobic groups into poly(KAA) networks, e.g., to use potassium methacrylate (KMAA) instead of KAA as monomer. The influence of changing KAA for KMAA on HIPE stability as well as the polyHIPE morphology is the topic of this short section.

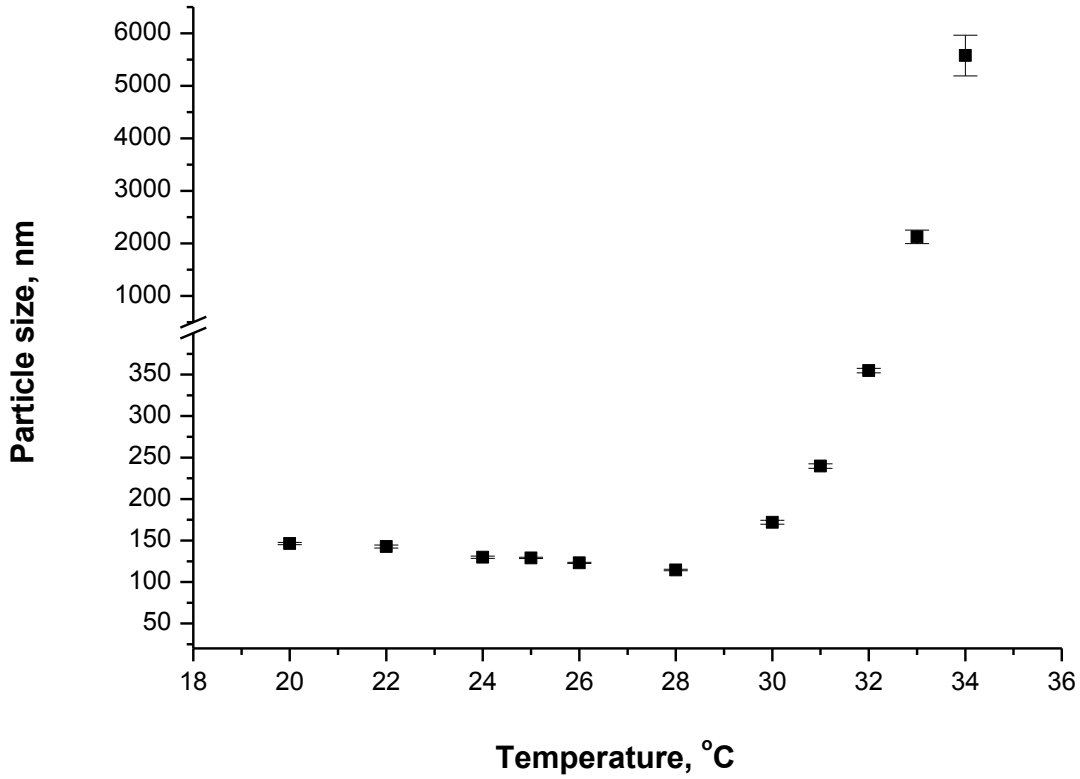
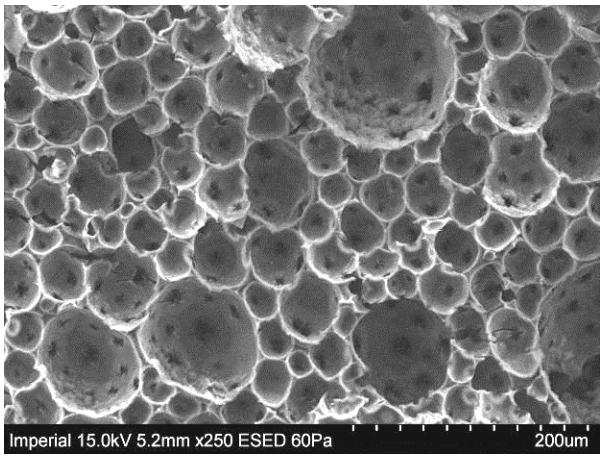
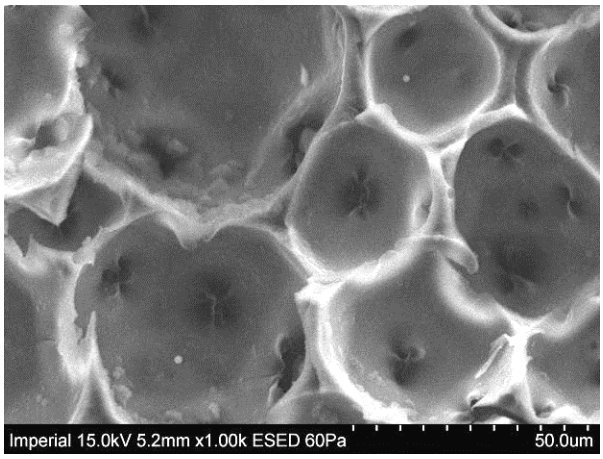


Fig. 3.52 Average particle size of poly(NIPAAm-*co*-AA) microgels in KMAA solution as a function of temperature. Identical to the microgel suspension in KAA solution, the concentrations of microgels and KMAA were 1.6 mg/ml and 0.85 M, respectively.

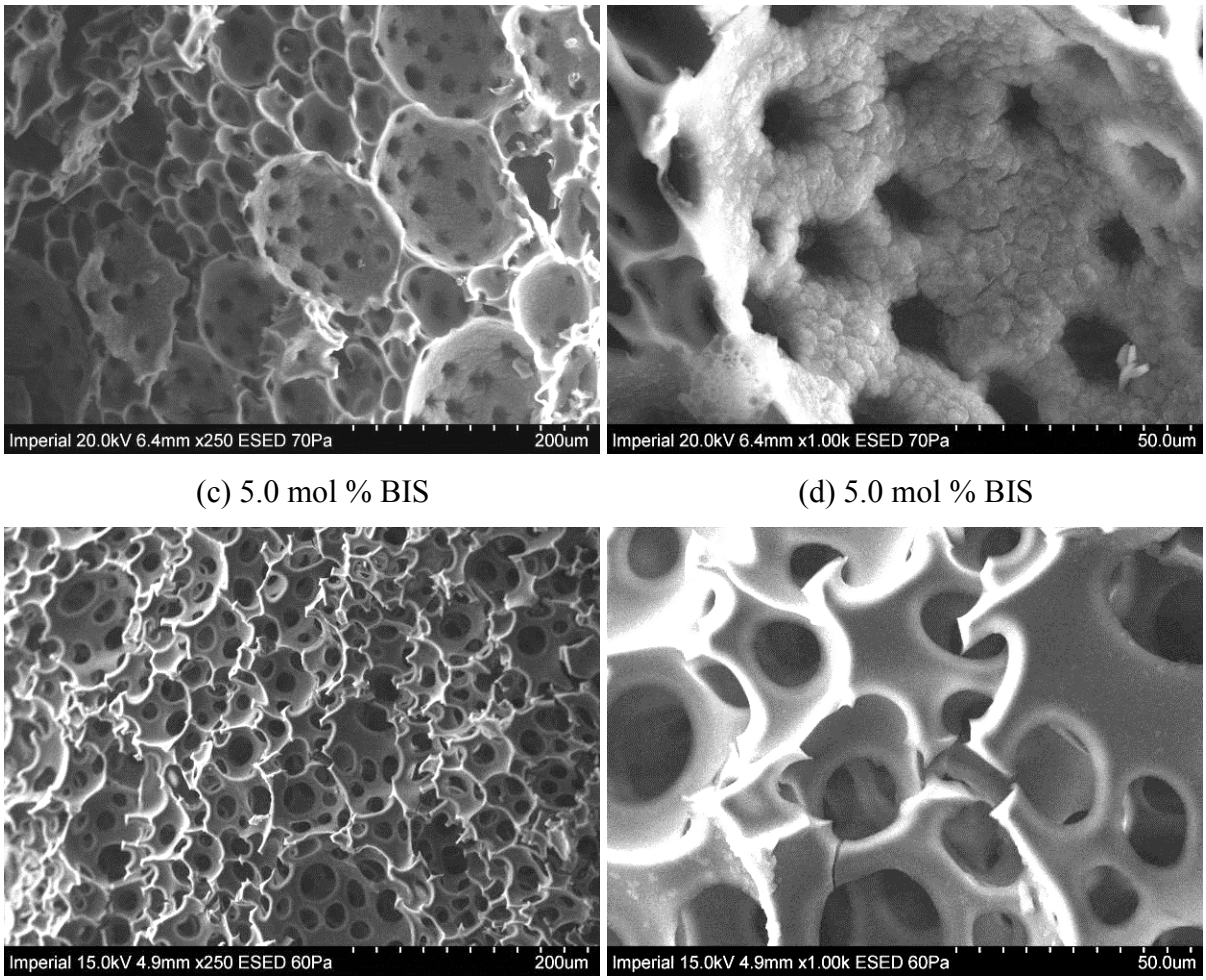
The size-temperature relationship of poly(NIPAAm-*co*-AA) microgel particles in KMAA (**Fig. 3.52**) was similar to that in KAA solution (**Fig. 3.14**). Particles reached the minimum size of ca. 110 nm at 28 °C and began to aggregate upon further increasing the temperature. Thus, RT was chosen for HIPE preparation. With identical concentrations of monomer (0.85 M) and microgels (1.6 mg/ml) to those in the KAA system, stable o/w HIPEs containing KMAA and various BIS contents were obtained. This indicated that changing KAA for KMAA had no obvious effect on HIPE stability. The effect of BIS content on morphology of the resultant poly(KMAA) Pickering-HIPEs was also investigated (**Fig. 3.53**). A reduction of BIS content from 15 mol % [**Fig. 3.53** (a) and (b)] to 3.2 mol % [**Fig. 3.53** (e) and (f)] led to a clear transition of the polyHIPE morphology from closed to open pores. This morphological effect of BIS content on poly(KMAA) Pickering-HIPEs was consistent with that on poly(KAA) Pickering-HIPEs (**Section 3.4.3.1**); only that 5.0 mol % BIS resulted in less open porous structures in poly(KMAA) Pickering-HIPEs [**Fig. 3.53** (c) and (d)] than in poly(KAA) Pickering-HIPEs [**Fig. 3.28** (b)]. In addition, the gradual transition of "potential pore throats" into pore throats indicated that shrinkage of polymer films starts from thinner centres and propagates outwards. Due to a lower swelling degree of poly(MAA) in aqueous media[566,567], poly(KMAA) Pickering-HIPE hydrogels are expected to have better mechanical properties than poly(KAA) Pickering-HIPE hydrogels.



(a) 15 mol % BIS



(b) 15 mol % BIS



(c) 5.0 mol % BIS (d) 5.0 mol % BIS

(e) 3.2 mol % BIS (f) 3.2 mol % BIS

Fig. 3.53 SEM images of poly(KMAA) Pickering-HIPEs prepared by polymerisation of microgel-stabilised o/w HIPEs containing 15, 5.0 and 3.2 mol % BIS, respectively.

3.8 Summary

PolyHIPEs with hydrophilic surfaces and pore sizes of a few hundred micrometers were obtained by photo-polymerisation of poly(NIPAAm-*co*-AA) microgel particles stabilised o/w HIPEs. Stability of the HIPEs containing KAA, the selected water-soluble monomer, was investigated prior to the polymerisation. It was found that emulsifying ability of microgel particles and HIPE stability to coalescence were dependent on KAA concentration and temperature while HIPE stability to creaming was obviously affected by the stirring speed used to produce the HIPEs. Polymerisation using BIS as the crosslinker and using an optimized UV-initiation protocol proved efficient and convenient.

Pore structures of poly(KAA) Pickering-HIPEs were investigated by varying the duration of solvent extraction, drying rate, internal phase volume ratio ($\phi_{int.}$), BIS content (BIS/AA, mol %), KAA concentration, stirring speed and microgel concentration. It was found that BIS content played a crucial role in the formation of pore throats (or interconnections). As revealed by cryo-SEM, non-solvent induced phase separation during solvent extraction was the driving force for pore throat formation. This explained why BIS content mattered to the formation of the pore throats, since the phase separation process occurred more easily at lower BIS content.

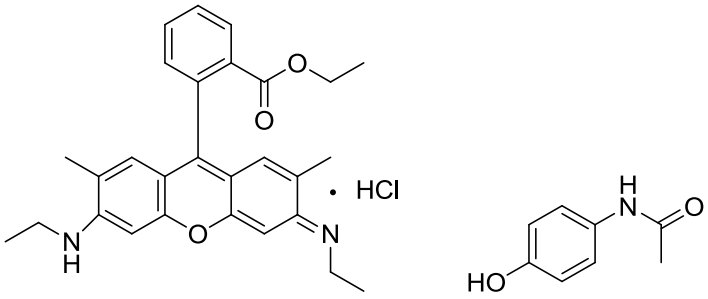
The measured BET surface areas of poly(KAA) Pickering-HIPEs were below 2 m^2/g, although increased by deep removal of moisture. Densities and porosities of the polyHIPEs were measured using liquid displacement, mercury intrusion porosimetry and a designed indirect method. Skeleton densities obtained from the indirect method were 1.19~1.35 $g.cm^{-3}$, close to that of PAA or poly(KAA), while porosities of the interior of polyHIPEs were as high as 97~98%.

Poly(KAA)/silica and poly(KAA)/Bioglass® Pickering-HIPE composites as well as poly(KMAA) Pickering-HIPEs were prepared. It was found that the dispersion of silica in the composites was obviously improved when using an increased stirring speed (1000 rpm) during emulsification. A preliminary test was carried out on polyHIPEs in the wet state, i.e., macroporous hydrogels. Poly(KAA)/silica polyHIPE composites showed a swelling ratio up to over 6000 wt % in SBF. It would be very important to test and tune the mechanical properties of macroporous hydrogels for cell growth purpose.

Chapter 4 High internal phase emulsions stabilised with dye- and drug-loaded microgel particles

4.1 Overview

This chapter describes the preparation of poly(NIPAAm-*co*-AA) microgel particles loaded with dye and drug molecules and their application as the emulsifiers for HIPEs aiming to produce poly(Pickering HIPEs). This could combine the emulsifier function of microgel particles in HIPEs with controlled release[228,568-571] of active ingredients (A.I.) and provide an attractive and novel means of introducing cell signaling molecules within tissue engineering scaffolds.[572,573] Moreover, although drug molecules can be released from polymer scaffolds, delivery through microgels may be more efficient when drugs have weak interactions with the scaffolds, e.g., hydrophobic drugs can be encapsulated into microgels in the case of hydrophilic matrices.[574,575]



(a) Rhodamine 6G (R6G) (b) Paracetamol

Fig. 4.1 Chemical structures of model active ingredients to be loaded into microgel particles

On the basis of their reported uptake into poly(NIPAAm-*co*-AA) microgels,[576,577] water-soluble dye Rhodamine 6G (R6G) and drug paracetamol (also known as acetaminophen) (**Fig. 4.1**) were used as active ingredients (i.e., A.I.) to investigate the potential of A.I. loaded microgel particles as emulsifiers. The established o/w HIPE template (**Chapter 3**) containing KAA was used with modification. 3.2 mol % crosslinker (BIS/KAA) was used because it represented the critical amount for open-porous polyHIPEs produced using the one-speed stirring protocol (**Section 3.4.2.2**). After photo-polymerisation, the internal phase was removed via freeze-drying rather than via Soxhlet extraction to avoid removing A.I. during

solvent extraction. *p*-Xylene (mp, 12-13 °C) was used instead of toluene (mp, -93 °C) as the internal phase (80 vol %) of HIPEs because its higher melting point means that it is more easily freeze-dried. Thus, we aimed to prepare open-porous poly(KAA) Pickering-HIPEs with the potential of controlled drug release.

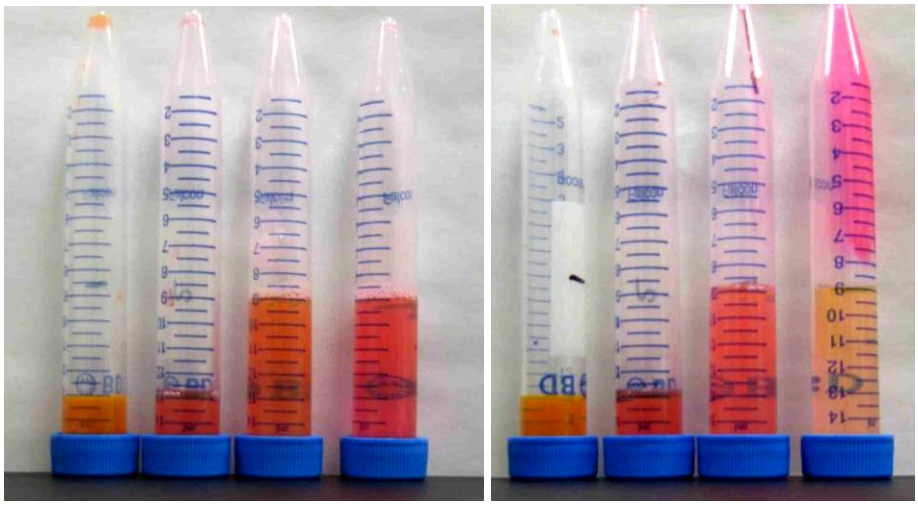
4.2 Mixing dye molecules with microgel particles for HIPE preparation

The model dye molecules (R6G, **Fig. 4.1**) were mixed with poly(NIPAAm-*co*-AA) microgel suspension prior to mixing with other components (KAA, BIS and I2959) to allow dye molecules to diffuse into microgel particles. A series of aqueous solutions or suspensions ranging from **S(1)** to **S(10)** (see **Table 7.20** for details) were used for this study. Prior to mixing with KAA stock solution (2.54 M), the background electrolytes of these solutions or suspensions were 1 mM KCl for **S(1)-S(5)** and 10 mM phosphate buffer (pH 6.5) for **S(6)-S(10)**, respectively. Centrifugation was used to quantify the loading of dye into the microgels. Effects of centrifugation, dye amount and the background electrolyte on emulsion stability were investigated. Attention was also paid to morphologies of the obtained polyHIPEs.

4.2.1 Effect of centrifugation of the aqueous mixtures on emulsion stability

4.2.1.1 Mixing of R6G into aqueous suspensions prior to emulsification

The mixing process prior to emulsification was carried out in three steps: (a) mixing 2.32 ml R6G solution (192 μg solute) with 1.00 ml microgel suspension (8 mg/ml in 1 mM KCl solution) to obtain **S(3)**; (b) adding 1.68 ml KAA stock solution into **S(3)** to obtain 5 ml **S(4)** and (c) adding crosslinker BIS and photo-initiator I2959 into **S(4)** to obtain **S(5)**. **S(5)** represented an aqueous mixture of R6G dye with the aqueous phase of the selected HIPE template. The reason for this procedure was to introduce R6G without varying the established aqueous composition for HIPE preparation and to evaluate the effect of adding R6G. The microgel-dye interaction was indicated by a colour change from orange in **S(2)** (R6G solution without micogels) to pink in **S(3)** before centrifugation [**Fig. 4.2** (a)] as well as a 9 nm red shift of the peak wavelength in fluorescence spectra of dye solutions without and with microgel particles (**Fig. 4.3**). The also observed decrease of fluorescence intensity at peak wavelength was attributed to dilution of the dye solution by adding microgel suspension.



(a) Before centrifugation (b) After centrifugation

Fig. 4.2 Photographs of aqueous solutions/suspensions of **S(2)-S(5)** before and after centrifugation at 5000 rpm for 1 h (Sample volumes used for centrifugation were 3ml, 3 ml, 7 ml and 7 ml, respectively.) Briefly, **S(2)** and **S(3)** were dye solutions without and with microgels, respectively; **S(4)** was **S(3)** with KAA; **S(5)** was **S(4)** with BIS and I2959.

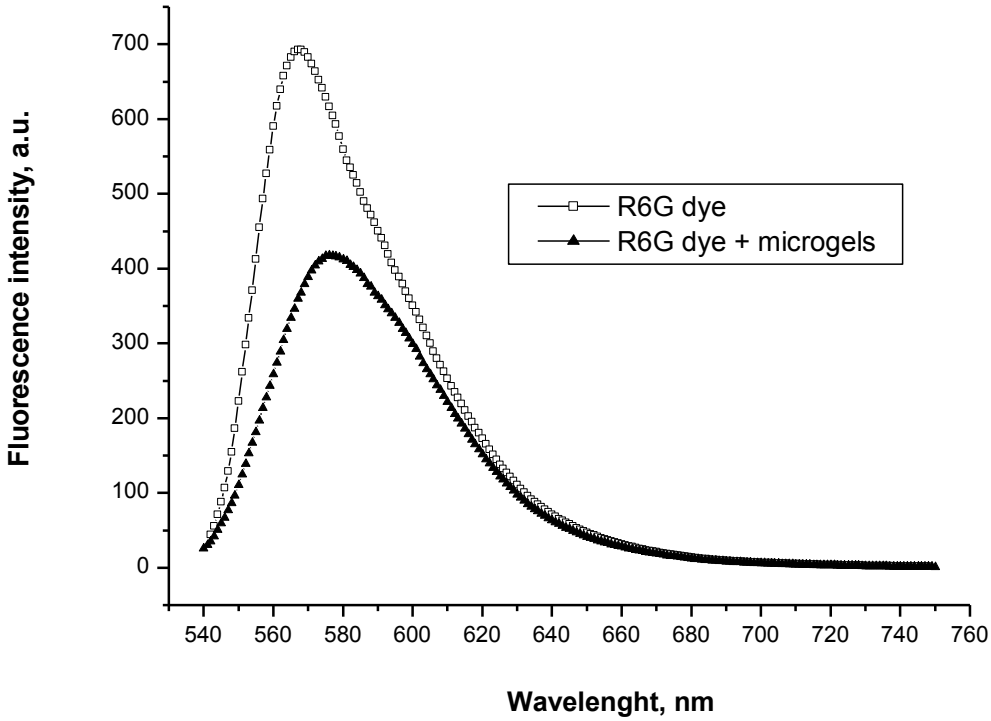


Fig. 4.3 Fluorescence spectra of R6G dye solutions without and with microgels. The dye solution tested was prepared by mixing 2.32 ml dye solution (196 µg dye) with 1 ml KCl solution (1 mM), i.e., **S(2)**; the dye solution with microgels was prepared by mixing 1.5 ml **S(2)** with 0.5 ml microgel suspension (8 mg/ml in 1 mM KCl solution). The excited wavelength was 528 nm.

Centrifugation was used to remove excess dye molecules from the aqueous mixture according to the reported uptake procedure.[576] In our case, this was also carried out prior to HIPE preparation. As a result, the centrifugation (5000 rpm, 1 h) applied to **S(2)-S(5)** resulted in obvious precipitates in **S(4)** and **S(5)** rather than in **S(3)** [**Fig. 4.2** (b)]. Although the volume of **S(3)** used was smaller than those of **S(4)** and **S(5)**, these results suggested that the degree of precipitation of dye-loaded particles was not sufficient in **S(3)** under current conditions but was enhanced by addition of KAA and BIS. Meanwhile, the colour differences among the original **S(4)** & **S(5)** [**Fig. 4.2** (a)] and their supernatants after centrifugation [**Fig. 4.2** (b)] indicated that addition of BIS and I2959 might affect the dye-microgel interactions.

4.2.1.2 Efficiency of dye-loaded microgel particles as emulsifiers

The ability of blank microgel suspension **S(1)** to result in poly(Pickering HIPEs) has already been shown (**Chapter 3**) after KAA, BIS and I2959 were all added. Here the preparation of poly(Pickering HIPEs) using dye-loaded microgel particles was attempted. Initially, emulsification was carried out using either un-centrifuged **S(5)** or supernatant of **S(5)** as the aqueous phase. Photos of the resultant emulsions are shown in **Fig. 4.4** (a)-(d).



(a) (b) (c)-1 (c)-2 (d)-1 (d)-2

Fig. 4.4 Photographs of emulsions prepared using either un-centrifuged **S(5)** or supernatant of centrifuged **S(5)**: (a) sample prepared using supernatant of centrifuged **S(5)** as the aqueous phase and the two-speed stirring protocol (400→1000 rpm); (b) unpolymerised HIPEs, prepared using un-centrifuged **S(5)** and the one-speed stirring protocol (400 rpm); (c)-1 & (c)-2 photo-polymerised HIPEs (b); (d)-1 & (d)-2, prepared using supernatant of centrifuged **S(5)** and the one-speed stirring protocol. Photograph (d)-2 was taken 4 min after (d)-1. Emulsification was all carried out using 2.5 ml aqueous suspension and 10 ml *p*-xylene.

Fig. 4.4 (a) and (d) show that supernatant of centrifuged **S(5)** did not result in a stable HIPEs no matter whether the one-speed (400 rpm) or two-speed stirring protocol (400→1000

rpm) was used for its preparation. In contrast, when un-centrifuged **S(5)** was emulsified with *p*-xylene under the one-speed stirring protocol, a pink HIPE sample was obtained with visible large droplets. The HIPEs creamed with time [**Fig. 4.4** (b)]. Moreover, the photo-polymerisation procedure did efficiently solidify the HIPE sample [**Fig. 4.4** (c)-1 and (c)-2]. Together with the images of **S(5)** (**Fig. 4.2**), it can be deduced that there were insufficient particles left in the supernatant of centrifuged **S(5)** and dye-loaded microgel particles were in the pink precipitates [**Fig. 4.2** (b)].

4.2.1.3 Microgel-dye interactions revealed by particle size measurements

The preliminary study described in **Section 4.2.1.1** and **4.2.1.2** demonstrated the capability of A.I. loaded microgel particles to act as emulsifiers. Although the mechanism is not fully understood, the interaction between microgels and R6G dye might play a role in the formation of large droplets [**Fig. 4.4** (b)]. Since the stability of Pickering emulsions is determined by the performance of particles at the water-oil interface,[148,150] particle size measurement was carried out (**Table 4.1**) to characterise the microgel-dye interaction and to reveal the effects of mixing process and centrifugation on particle emulsifying ability.

Table 4.1 Particle size measurements on aqueous solutions/suspensions of **S(1)-S(5)** at 22 °C

Entry	Sample	Mean /nm	Std. error /nm	Average count rate /kilo counts per second (kcps)
1	**S(1)**	286.0	7.6	443.4
2	Uncentrifuged **S(2)**	3615.8	155.9	51.2
3	Supernatant of **S(2)**	2094.4	162.6	19.5
4	Uncentrifuged **S(3)**	360.0	13.9	189.4
5	Supernatant of **S(3)**	456.5	25.2	235.2
6	Uncentrifuged **S(4)**	784.5	77.9	446.4
7	Supernatant of **S(5)**	43663.8	6170.8	10.7

Entry 1 (**Table 4.1**) shows the size of microgel particles prior to mixing with R6G and serves as a control. Size values in Entry 2, 3 and 7 appeared too high while the count rates were too low, an indication of too diluted suspensions. Since **S(2)** was a microgel-free solution of R6G, the erroneous results (Entry 2 and Entry 3) were not surprising. Likewise, it

was probable that **S(5)** supernatant (Entry 7) was microgel-free. This was also supported by the orange colour of the supernatant [**Fig. 4.2** (b)], since a trace of carboxyl groups would result in pink colour.[578] Thus, it was likely that polymerisation occurred to the monomers (KAA and BIS) in **S(5)** during centrifugation at RT and the resultant polymers together with microgels went to the precipitates. On the other hand, it is interesting to notice that particle size increased slightly from ~300 nm (Entry 1) to ~350 nm (Entry 4) upon adding R6G but jumped to 700-800 nm (doubled) after further adding KAA solution (Entry 6). This suggested that the attractive interactions among dye-loaded microgels were increased upon addition of KAA, resulting in the formation of dimers. Sivakumaran *et al.*[579] reported a similar phenomenon of limited aggregation of poly(NIPAAm-*co*-AA) microgels in the presence of a high concentration of bupivacaine (pK_a= 8.2[580,581]), a cationic drug. The cause of aggregation in their case was attributed to neutralization of -COO^- by the cationic drug.[579] In our case, the cationic nature of R6G dye (pK_a= 7.5[582]) contributed to its interaction with -COO^- of microgels but were not sufficient to result in the formation of dimmers, since the particle size doubled (entry 6) only when KAA (0.85 M) was added. Meanwhile, microgels without dye were capable of maintaining their colloidal stability in the presence of KAA below 28 °C (**Fig. 3.14**, **Section 3.3.2.1**). Therefore, the screening effect of KAA on the -COO^- of microgels reduced the repulsive interactions among dye-loaded microgels and contributed to the limited aggregation together with dye-microgel interaction. Due to this larger size of dye-loaded particles, it was not surprising to observe large droplets in the resultant HIPEs [**Fig. 4.4** (b)]. In addition, it was deduced from Entry 5 that dye-loaded microgel particles did not precipitate out of **S(3)** (suspension without KAA) after centrifugation, although expected in order to quantify dye loading into microgels. This was also in agreement with the observation that **S(3)** supernatant remained pink [**Fig. 4.2** (b)] – an indication of the existence of carboxyl groups (from microgels) in the suspension.[578]

In summary, it was revealed that the dye-microgel interaction together with the screening effect of KAA caused a limited aggregation (dimmer formation) of dye-loaded microgel particles. These large particles could stabilise KAA-containing HIPEs of large drop sizes, from which poly(KAA) Pickering-HIPEs were obtained upon photo-polymerisation.

4.2.2. Effect of dye concentration in the aqueous suspension on HIPE stability

For HIPE preparation using A.I. loaded microgel particles as emulsifiers [**Fig. 4.4** (b)], a recipe of 0.19 mg R6G dye and 8 mg microgels (per 5 ml aqueous phase) was used, of which the microgel amount was the same as for microgel-stabilised HIPEs [**Fig. 3.22** (m)(n)] while the R6G/microgel ratio followed a reported one[576]. However, the poly(NIPAAm-*co*-AA) microgels in the reported case[576] were synthesised using different NIPAAm/AA molar ratio (9:1) and crosslinking degree (4 mol %) from our microgels (NIPAAm/AA/BIS= 94:5:1, mol). Although the dye loading was not yet quantified under current centrifugation conditions (5000 rpm for 1 h at RT), we focused on whether HIPEs could be stabilised in the presence of more dye molecules. Thus, another R6G/microgel ratio of 8 mg/ 0.39 mg (per 5 ml aqueous phase) was investigated for HIPE preparation. As a result, the effect of doubling the dye concentration on HIPE stability was negligible, since stable HIPEs were obtained using an un-centrifuged aqueous suspension and using the one-speed stirring protocol (400 rpm). Also, the subsequent photo-polymerisation successfully solidified the HIPE template (**Fig. 4.5**). Nevertheless, HIPEs phase-separated upon increasing the stirring speed from 400 rpm to 1000 rpm. Thus, the two-speed stirring protocol (400→1000 rpm) was not successful for dye-loaded microgel particles stabilised HIPEs, although it proved efficient in microgel-stablised HIPEs (**Section 3.4.3**). It was indicated that aggregated R6G-loaded microgel particles (e.g., 700-800 nm, **Table 4.1**) were not efficient stabilisers for smaller emulsion droplets.



Fig. 4.5 Photograph of photo-polymerised HIPEs, stabilised with dye-loaded microgel particles. The microgel particles and R6G dye were mixed at a ratio of 8 mg/ 0.39 mg (per 5 ml aqueous phase) in the loading process but the loading percentage was not yet quantified. Subsequently, the polymerised sample was frozen in LN_2 and freeze-dried, leading to poly(KAA) Pickering-HIPEs.

4.2.3 Effect of using buffer in the aqueous phase on HIPE stability

Although the use of a buffered aqueous solution is not necessary for HIPE preparation, it is very common in A.I. uptake/release investigations.[577] In order to facilitate the tests of A.I. uptake before emulsification and its release from the resultant polyHIPEs, this section investigated HIPE preparation using a phosphate buffer (10 mM, pH 6.5)[577] as the dispersion medium for microgel particles and R6G dye instead of the established KCl solution (1 mM). As a result, stable HIPEs were obtained either using an R6G-containing aqueous suspension (**Fig. 4.6**) or using an R6G-free aqueous suspension (not shown), suggesting that replacement of KCl by this phosphate buffer had no obvious effect on HIPE stability. This was reasonable because the major component in the aqueous phase was KAA (0.85 M).



Fig. 4.6 Photograph of *p*-xylene-in-water HIPEs stabilised by dye-loaded microgel particles. The aqueous phase was prepared by mixing a phosphate-buffered solution (10 mM, pH 6.5) of microgel particles and R6G dye (8 mg/0.39 mg per 3.32 ml) with the KAA stock solution (2.54 M, 1.68 ml). The volume ratio of *p*-xylene was 80%.

To quantify the dye loading into microgel particles, further effort was made using higher-speed centrifugation on phosphate buffered R6G-microgel mixture solutions (see **Table 7.20**) prior to emulsification. It was encouraging that pink precipitates were observed after **S(7)** was centrifuged at 12 k rpm for 0.5 h and at 15 k rpm for 1 h in sequence (at 4 °C). However, emulsification using a dispersion of these precipitates together with KAA, BIS and I2959 [**S(9)**] failed to result in stable HIPEs. This was likely due to a lack of sufficient particles in **S(9)**. This similarity of inefficient precipitation to **S(3)** (KCl as the background electrolyte, **Fig. 4.2**) might suggest that it was difficult to precipitate R6G-loaded microgel particles in the absence of KAA. Further investigation using more powerful centrifugation is essential in order to precipitate R6G-loaded microgel particles and to quantify the R6G loading. However, it is still of practical importance to use un-centrifuged aqueous mixture for polyHIPE

preparation, since any excessive A.I. molecules will probably attach to the porous matrices after freeze-drying.[66,583,584] Due to a distinct profile of drug release from microgel,[569,579] it will be possible to evaluate the release from microgels and that from the surrounding matrices.

4.2.4 Effect of using dye-loaded microgels as emulsifiers on the polyHIPE morphology

The above section showed the capability of R6G-loaded microgel particles to stabilise HIPEs. Subsequently, it is important to evaluate their effect on the polyHIPE morphology, since we aim to obtain macroporous materials with controlled-release properties as tissue engineering scaffolds. Thus, the morphologies of poly(KAA) Pickering-HIPEs prepared using dye-loaded microgel particles as emulsifiers at microgel/R6G mixing ratios of 8 mg/0.19 mg (**Fig. 4.7**) and 8 mg/0.39 mg (**Fig. 4.8**) were compared with those of the polyHIPEs prepared using unmixed microgels as emulsifiers (**Section 3.4.2.2**).

An obvious difference was that polyHIPEs prepared using dye-loaded microgels as emulsifiers (3.2 mol % BIS used) exhibited thin films rather than struts as observed in those prepared using unmixed microgels as emulsifiers [**Fig. 3.22** (m)(n), 3.2 mol % BIS]. It should be noticed that freezing in LN_2 and freeze-drying were used for solvent removal after polymerisation here in comparison with the Soxhlet extraction and vacuum drying procedures for polyHIPEs prepared using unmixed microgels as emulsifiers. However, the freezing and freeze-drying procedures did result in struts as shown either in another case of poly(KAA) Pickering-HIPEs [**Fig. 3.24** (c)(d), 2.5 mol % BIS] or in a reported case.[205] The formation of an open porous morphology [**Fig. 3.24** (c)(d)] was related to the liquid-liquid phase separation[478] occurring in the poly(KAA) gel layers during freeze-drying. It was probable that pore walls and pore throats were developed from the polymer-rich and polymer-poor domains, respectively. In contrast to the predominance of pore throats of more than 50 μm [**Fig. 3.24** (c)(d)], the polymer films observed here in **Fig. 4.7** and **Fig. 4.8** might suggest an insufficient phase separation. Further evidence for this came from the small holes of less than 2 μm within the films [**Fig. 4.8** (d)]. Since R6G incorporation into microgels caused an increase in particle size (**Section 4.2.1.3**), larger emulsion droplets should result,[151,155] as confirmed by the large pores of 200-700 μm [**Fig. 4.8** (a) and (b)]. Thus, the resultant poly(KAA) gel layers would be thicker and hence have higher resistance to phase separation during freeze-dying.

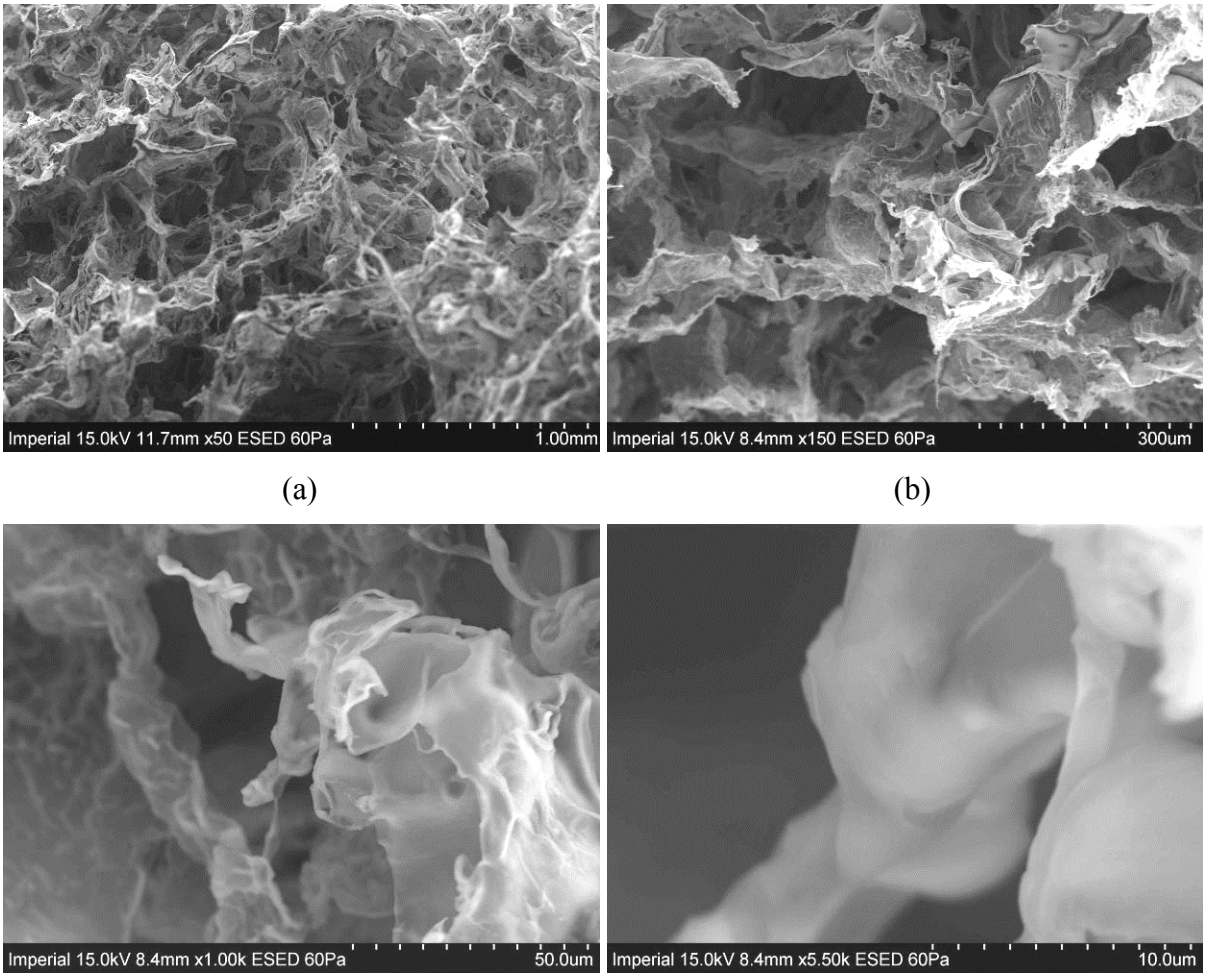
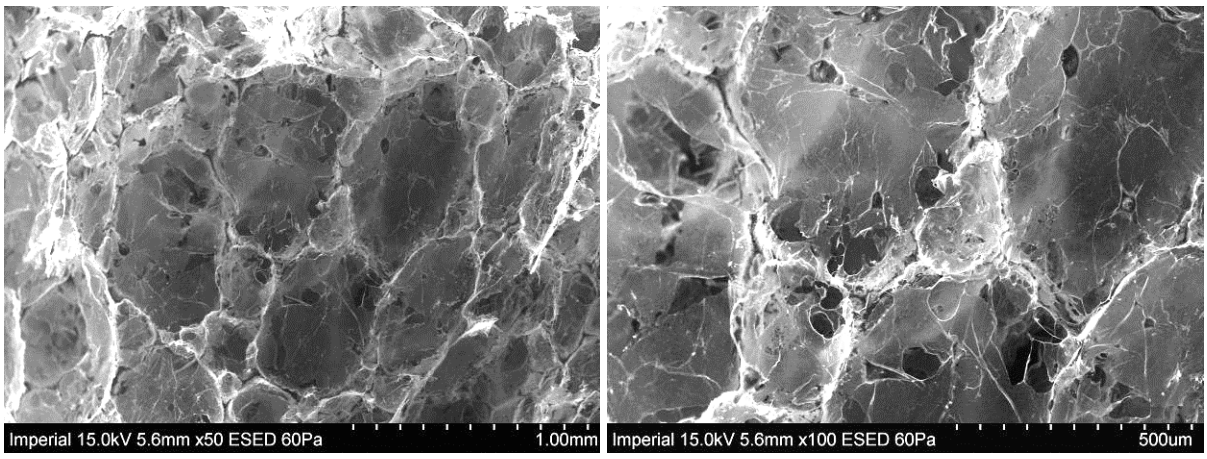
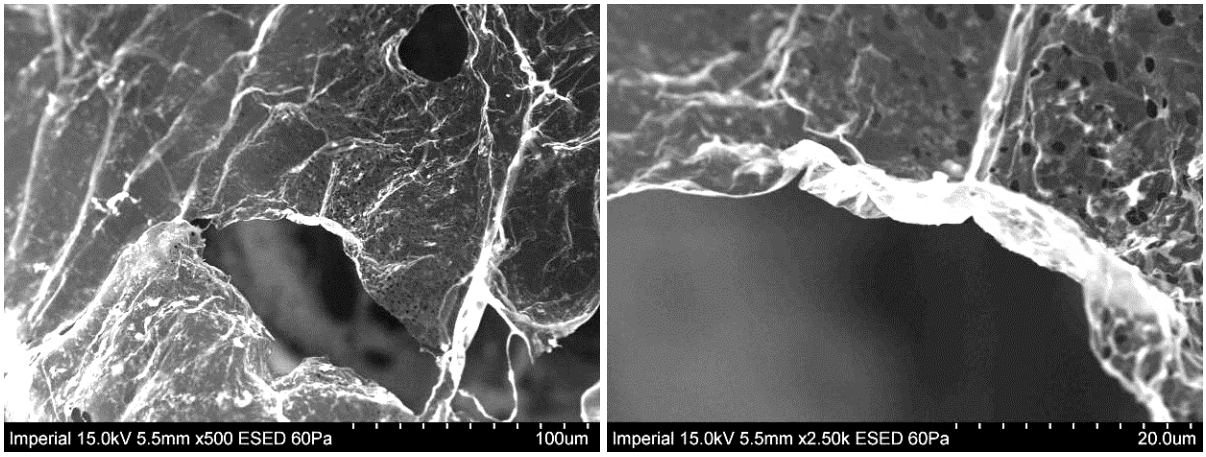


Fig. 4.7 SEM images of poly(KAA) Pickering-HIPEs prepared by polymerising o/w HIPEs that were stabilised with dye-loaded microgels. The mixing ratio of microgels to R6G dye was 8 mg to 0.19 mg in 5 ml aqueous phase. After polymerisation, solvents were removed via freezing in LN_2 and freeze-drying.





(c) (d)

Fig. 4.8 SEM images of poly(KAA) Pickering-HIPEs prepared by polymerising o/w HIPEs that were stabilised with dye-loaded microgels. The mixing ratio of microgels to R6G dye was 8 mg to 0.39 mg in 5 ml aqueous phase. After polymerisation, solvents were removed via freezing in LN_2 and freeze-drying.

To sum up, the dye-microgel interaction caused dye-loaded microgel particles to aggregate to a limited extent (e.g., dimer) in KAA containing suspensions. As a result, although HIPEs could be prepared using these particles, HIPE stability and the resultant polyHIPE morphology were obviously affected.

4.3 HIPEs stabilised with drug-loaded microgel particles

It was preliminarily shown when using dye-loaded microgel particles as emulsifiers that the microgel-dye interaction played a significant role in emulsion stability and polyHIPE morphology. To prepare polyHIPEs using other A.I. loaded microgel particles as emulsifiers, such as drugs, the microgel-drug interaction should be emphasized. Since the interactions of drugs with polyNIPAAm-based hydrogels[585] or microgels[577] are closely related to the physicochemical properties of drugs, such as pK_a, octanol/water partition coefficient (logK_{ow}), etc., we also aimed to further evaluate the effect of these properties on the emulsifying ability of A.I. loaded micogel particles. Moreover, since the crosslinking degree of microgels may affect drug uptake,[277,586] effort was made to investigate the emulsifying ability of drug-loaded microgel particles with 1 mol % and 2 mol % crosslinking degrees, respectively.

4.3.1 Investigation into the microgel-drug interactions

Based on a reported study on the interactions of drugs and polyNIPAAm-based micrigels,[577] we selected paracetamol (also known as acetaminophen) as another A.I. to mix with our poly(NIPAAm-*co*-AA) microgel particles and used a ratio of 90 μmol drug : 3.32 ml buffer : 8 mg microgels : 1.68 ml KAA. Before and after mixing KAA (2.54 M, pH 7.0) into the microgel/paracetamol aqueous suspension (10 mM phosphate buffer, pH 6.5), the suspension was shaken on a shaker at 70 osc./min overnight to allow drug molecules to reach an equilibrium of diffusion into microgel particles. Nevertheless, the loading percentage was not yet characterised because precipitate was hardly obtained under the current centrifugation conditions (15,000 rpm). This was probably due to an insufficient centrifugation speed in use, in comparison with the reported ultracentrifugation (45,000 rpm),[577] since the density of swollen microgels was unlikely to differ much from that of water ($\rho_{polyNIPAAm}$ = 1.07 g/cm^3)[587].

The effect of paracetamol incorporation on the particle size of microgels with 1 mol % crosslinking degree (**Fig. 4.9**) was investigated in aqueous solutions containg KAA (0.85 M). Over the temperature range of 10~28 °C, the drug-loaded microgel particles reached a maximum size at 18 °C as the unmixed microgels did. Unlike the unmixed microgels however, the drug-loaded micrgels exhibited a greater temperature sensitivity before the maximum. In addition to this, the drug-loaded microgels reached their minimum size of 110 nm at 28 °C and started to aggregate upon further increasing the temperature. In contrast, the unmixed microgels reached 110 nm at 30 °C. This aggregation of drug-loaded microgel particles at a slightly lower temperature was similar to the effect of adding BIS into microgels (**Fig. 3.14**). It is worth noting that aggregation of R6G-loaded microgel particles into dimers was observed even at 22 °C (**Table 4.1**). This was attributed to the properties of these small molecules. The cationic dye R6G, possessing a pK_a of 7.5[582] and a logK_{ow} of 2.37, should be expected to interact with –COO$^-$ of microgels upon mixing and reduce the surface charge density of microgels. In contrast, paracetamol, possessing a pK_a of 9.4 and a logK_{ow} of 0.46, was neutral at pH 6.5.[577] Thus, R6G not only had a stronger interaction with the hydrophobic segments of microgels due to a higher logK_{ow} but also rendered micrgels prone to aggregation via electrostatic interaction. Huo *et al.*[586] calculated the contact angles of poly(NIPAAm-*co*-AA) microgels on a glass plate (dried from solutions of pH 5 under ambient temperature) and found an increase from 22.9° to 45.4° after binding with bovine serum albumin (BSA).

Clearly, the interaction between microgels and A.I. could change the wettablity of microgels and hence affect their emulsifying efficiency or even the resultant emulsion type.

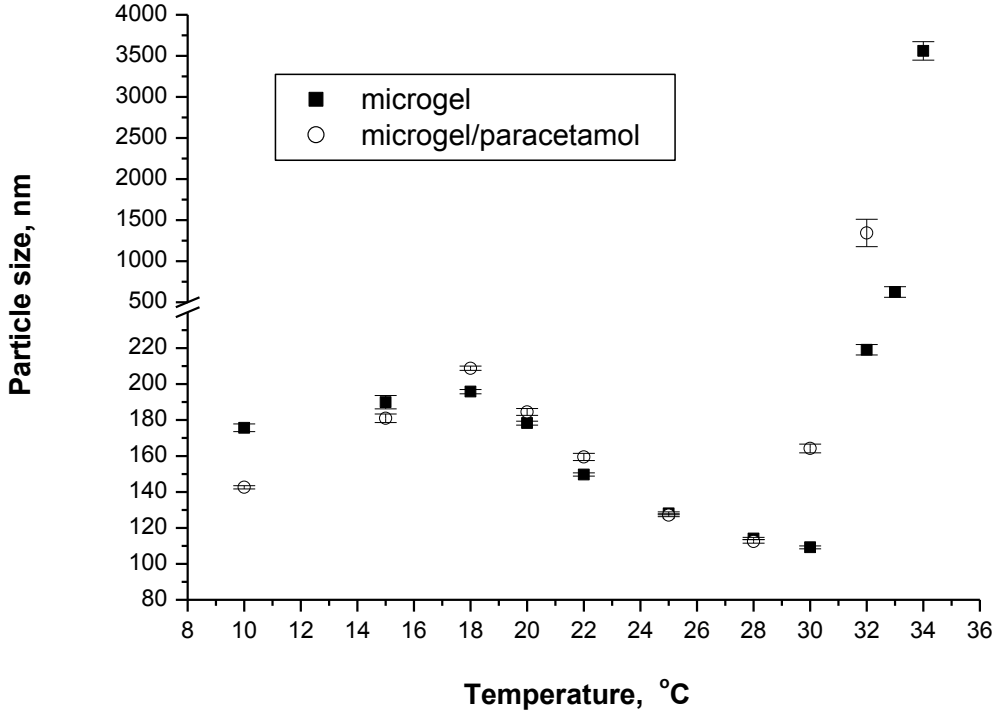
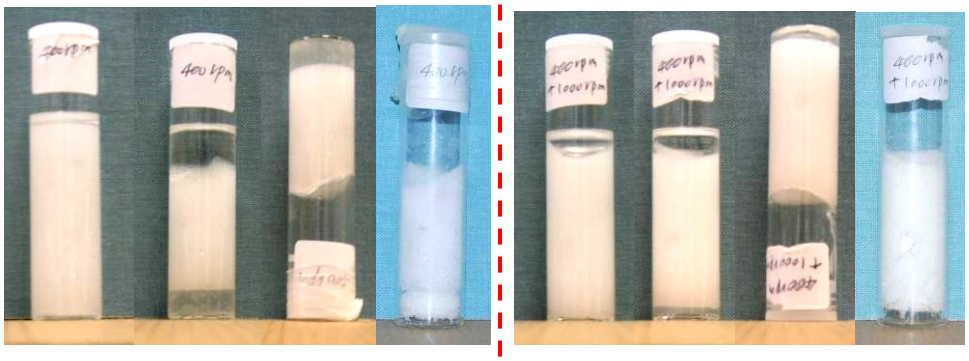


Fig. 4.9 Average particle size of unmixed microgels and paracetamol-loaded microgels as a function of temperature measured in solutions containing 0.85 M KAA

4.3.2 Drug-loaded microgels with 1 mol % crosslinking degree as HIPE stabilisers

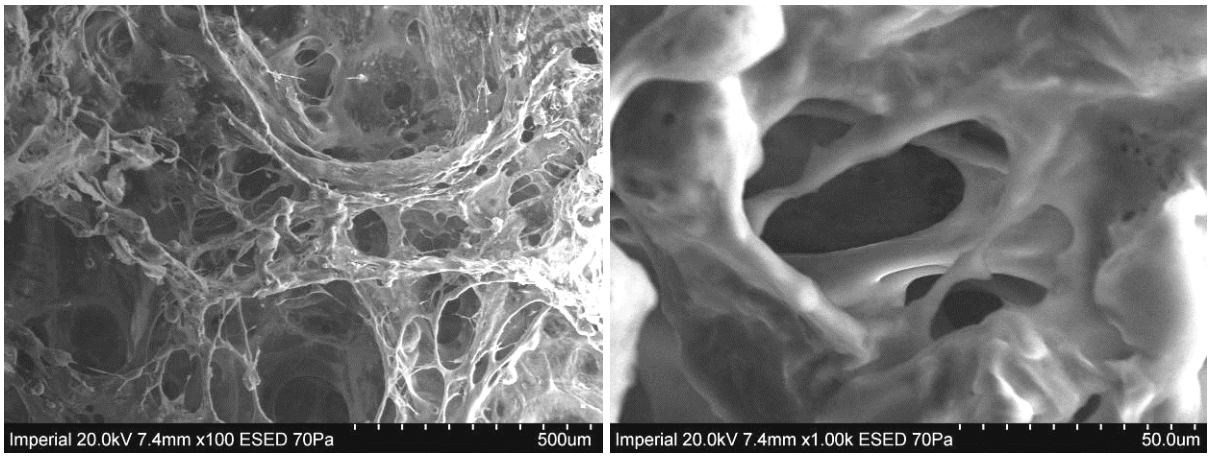
The solution containing drug-loaded microgels and KAA (and possibly with free drugs) was used for HIPE preparation at 22 °C after BIS (3.2 mol %) and I2959 (2 mol %) were added. Despite the effect of paracetamol on microgel particle size (**Fig. 4.9**), we expected that its effect on the emulsifying ability would be only significant at 30 °C or above but negligible at 22 °C. Consistent with our expectation, stable HIPEs were obtained using the one-speed [**Fig. 4.10** (a)-1] and two-speed stirring protocol [**Fig. 4.10** (b)-1], similar to those prepared using unmixed microgels. This confirmed that the emulsifying ability of microgels was not obviously affected by incorporation of paracetamol at 22 °C in contrast to the incorporation of R6G. Meanwhile, it was clearly seen that creaming was less significant in the polymerised HIPEs that were prepared using the two-speed stirring protocol, due to smaller emulsion drops obtained at 1000 rpm (**Section 3.4.3**).

The effect of stirring protocol on the morphology of resultant poly(KAA) Pickering-HIPEs was evaluated (**Fig. 4.11** and **Fig. 4.12**). The polyHIPEs prepared using the one-speed protocol during emulsification exhibited a multi-layer structure and pores ranging from tens microns to a few hundred microns [**Fig. 4.11** (a) and (b)]. In contrast, the polyHIPEs prepared using the two-speed stirring protocol during emulsification showed layers that were closer or even overlapped [**Fig. 4.12** (a) and (b)], indicating lower pore volume. This was likely because the bigger emulsion drops obtained at lower stirring speed (400 rpm) left more space after removal.

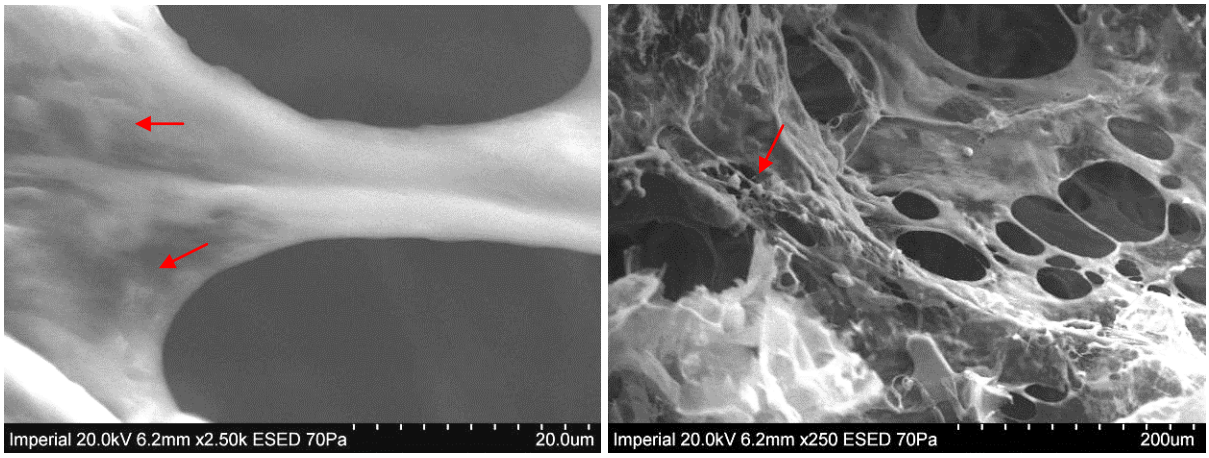


(a)-1 (a)-2 (a)-2’ (a)-3 (b)-1 (b)-2 (b)-2’ (b)-3

Fig. 4.10 Photographs of HIPEs stabilised by paracetamol-loaded microgel particles and their polymerisated products. The microgel particles used had a crosslinking degree of 1 mol %. KAA, BIS and I2959 were mixed into the aqueous suspension prior to emulsification. (a), HIPEs prepared with the one-speed stirring protocol (400 rpm); (b), HIPEs prepared with the two-speed stirring protocol (400→1000 rpm); 1, before polymerisation; 2 and 2’, after polymerisation (2’ vial on its head showing HIPEs were polymerised); 3, after freeze-dried.

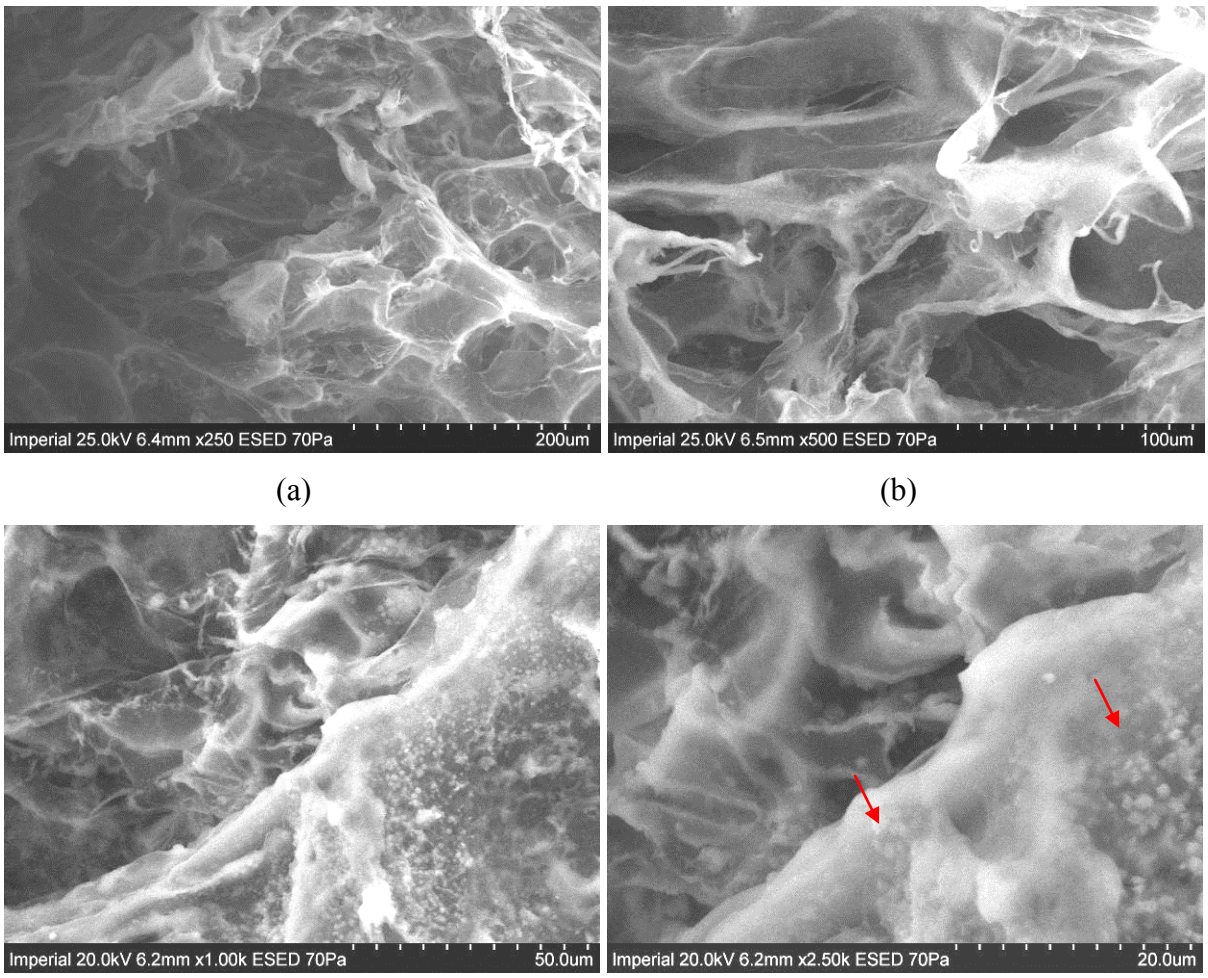


(a) (b)



(c) (d)

Fig. 4.11 Morphologies of poly(KAA) Pickering HIPEs prepared using paracetamol-loaded microgels with 1 mol % crosslinking degree as emulsifiers and using the one-speed stirring protocol (400 rpm) during emulsification.



(a) (b)

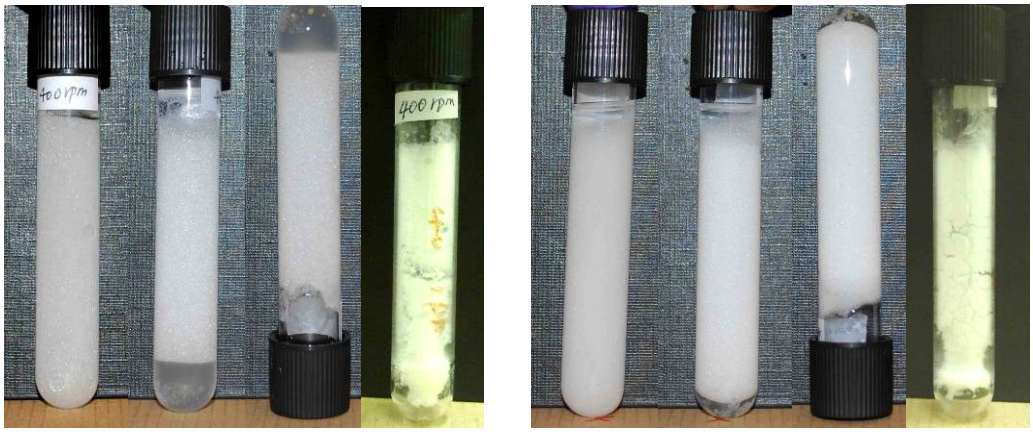
(c) (d)

Fig. 4.12 Morphologies of poly(KAA) Pickering-HIPEs prepared using paracetamol-loaded microgels with 1 mol % crosslinking degree as emulsifiers and using the two-speed stirring protocol (400 rpm→1000 rpm) during emulsification.

Particles were clearly visible on the surfaces of poly(KAA) films [**Fig. 4.11** (c) and **Fig. 4.12** (d)], although it was not yet determined whether they were microgels, drug crystals or a mixture of both. It can be safely said that those with a diameter between a few hundred nanometers to 1-1.5 μm [**Fig. 4.12** (d)] were likely to be drug crystals,[588] since the excessive drugs were not separated from the aqueous phase prior to emulsification. In addition, it is worth noting that the bead-like structures [**Fig. 4.11** (d)] were assumed to be poly(KAA), which probably formed alongside the interconnected porous structures during freeze-drying through a nucleation and growth mechanism and a spinodal decomposition mechanism, respectively.[478,589,590]

4.3.3 Drug-loaded microgels with 2 mol % crosslinking degree as HIPE stabilisers

In the same manner as microgels with 1 mol % crosslinking degree, microgels with 2 mol % crosslinking degree were mixed with paracetamol, KAA and BIS & I2959 in sequence prior to emulsification. Stable HIPEs were obtained using the one-speed [**Fig. 4.13** (a)-1] and two-speed stirring protocol [**Fig. 4.13** (b)-1]. Also, the creaming extent was obviously reduced [**Fig. 4.13** (b)-2] in the case where the two speed stirring protocol (400→1000 rpm) was used during emulsification.



(a)-1 (a)-2 (a)-2’ (a)-3 (b)-1 (b)-2 (b)-2’ (b)-3

Fig. 4.13 Photographs of HIPEs stabilised by paracetamol-loaded microgel particles and their polymerisated products. The microgel particles used had a crosslinking degree of 2 mol %. KAA, BIS and I2959 were mixed into the aqueous suspension prior to emulsification. (a) HIPEs prepared with the one-speed stirring protocol; (b), HIPEs prepared with the two-speed stirring protocol; 1, before polymerisation; 2 and 2’, after polymerisation (2’ vial on its head showing HIPEs were polymerised); 3, after freeze-dried.

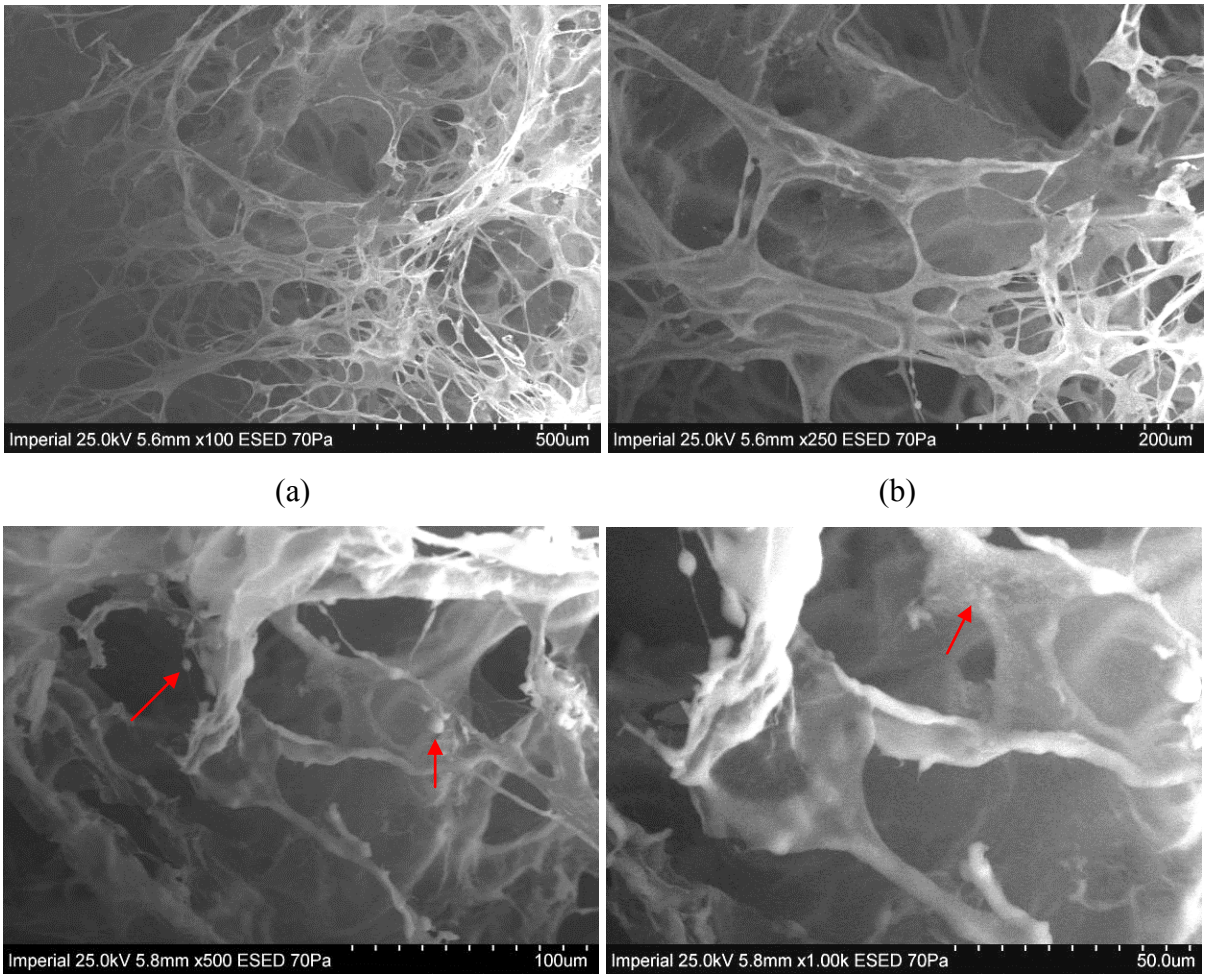
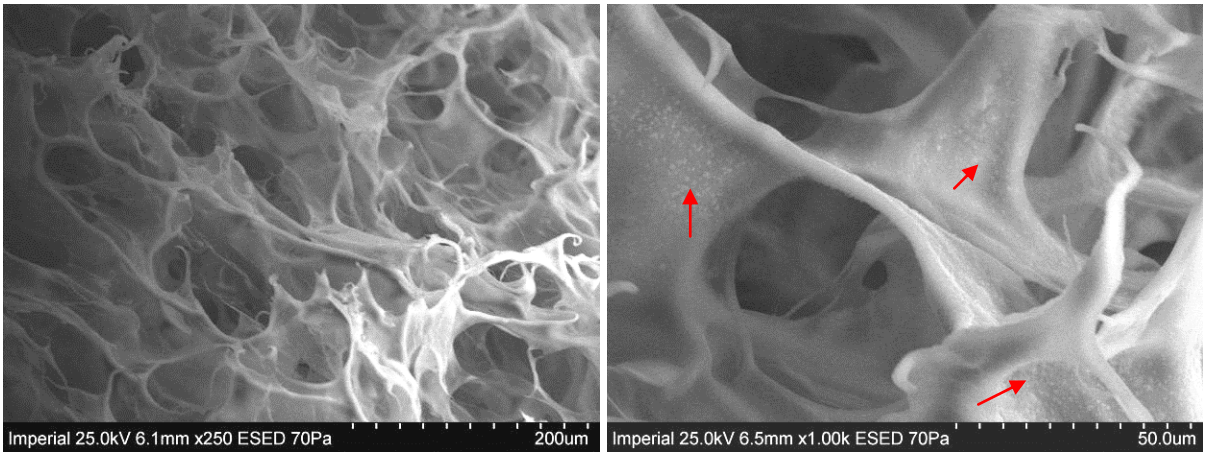
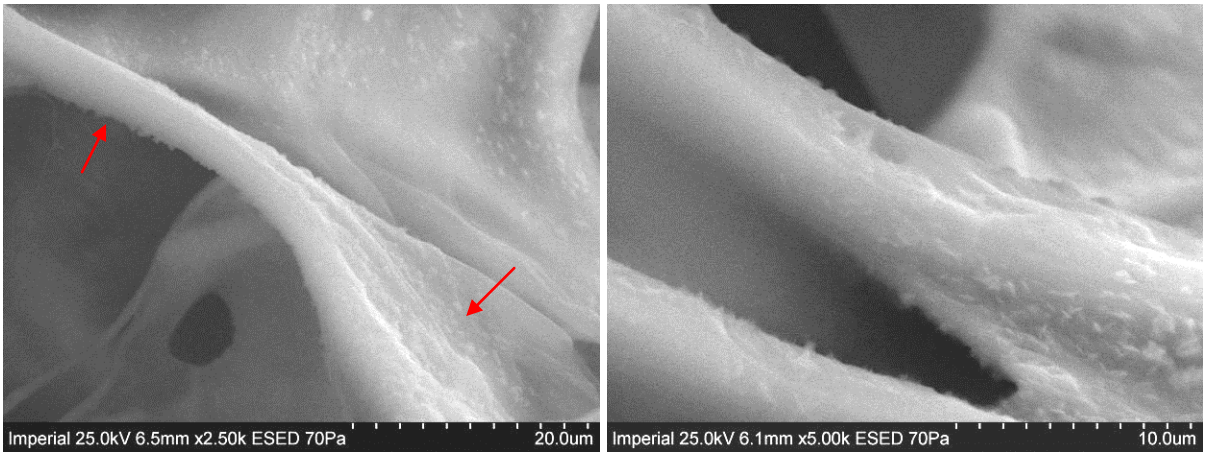


Fig. 4.14 Morphologies of poly(KAA) Pickering-HIPEs prepared using paracetamol-loaded microgels with 2 mol % crosslinking degree as emulsifiers and using the one-speed stirring protocol (400 rpm) during emulsification.





(c) (d)

Fig. 4.15 Morphologies of poly(KAA) Pickering-HIPEs prepared using paracetamol-loaded microgels with 2 mol % crosslinking degree as emulsifiers and using the two-speed stirring protocol (400 rpm→1000 rpm) during emulsification

The morphologies of poly(KAA) Pickering-HIPEs prepared using microgels with 2 mol % crosslinking degree as emulsifiers (**Fig. 4.14** and **Fig. 4.15**) showed a series of similar features to those of polyHIPEs prepared using microgels with 1 mol % crosslinking degree as emulsifiers (**Fig. 4.11** and **Fig. 4.12**). The pore structures with either larger pore size or smaller pore size were tunable by the stirring speed [**Fig. 4.14** (b) and **Fig. 4.15** (a)]. Also in this case, bead-like structures [**Fig. 4.14** (c)] were visible together with interconnected structures. Furthermore, microgels or crystals of unseparated drugs were clearly seen [**Fig. 4.14** (d) and **Fig. 4.15** (b)]. Interestingly, they were on both sides of the polymer films [**Fig. 4.15** (c)] and were either spherical [**Fig. 4.15** (b) and (c)] or needle-shaped [**Fig. 4.15** (d)]. In summary, no obvious differences were visible in the HIPEs stabilised by paracetamol-loaded microgels with 1 mol % or 2 mol % crosslinking degree or in the morphologies of the resultant polyHIPEs.

4.4 Summary

The emulsifying ability of A.I. loaded poly(NIPAAm-*co*-AA) microgel particles was obviously affected by R6G dye rather than by paracetamol drug due to the electrostatic interaction between swollen microgels and R6G dye. Similar to unmixed microgel particles, paracetamol loaded microgel particles resulted in stable HIPEs at either low or high stirring speed and hence poly(KAA) Pickering-HIPEs of tunable morphologies. Further efforts are

required to separate the excessive A.I. molecules from the aqueous suspension prior to emulsification so that the loading percentage of A.I. into microgels can be quantified. The release of A.I. from microgel particles and from the resultant polyHIPEs should also be followed.

Chapter 5 Microgel-stabilised o/w HIPEs for the preparation of macroporous materials containing dextran and its derivative

5.1 Overview

Dextran is a natural biopolymer consisting of an α-(1→6) linked D-glucose main chain and other branched linkages. This structural feature not only gives it water-solubility and biodegradability[591] but also renders it readily modifiable for various new functional polymers.[592] Consequently, dextrans and modified dextrans have been investigated widely for controlled drug delivery[593] and recently for tissue engineering scaffolds.[219,524,594-600] The fabrication of macroporous dextran-based scaffolds by emulsion templating was reported in a few cases[219,524,600,601] and showed interconnected structures of high porosity. Nevertheless, surfactants were used as the emulsifiers in all these cases. Considering the biocompatibility of scaffolds, we stress the need of using particulate emulsifiers as an attractive alternative to surfactants. For example, Zhou *et al.*[602] investigated hydroxyapatite nanoparticles as the emulsifiers of o/w HIPEs to fabricate scaffolds containing dextran modified by glycidyl methacrylate (GMA). In this chapter, microgels as the particulate emulsifiers of o/w HIPEs for the preparation of macroporous materials containing dextran and modified dextran will be discussed. In contrast to the chemical crosslinking method used in the formation of poly(KAA) Pickering-HIPEs (**Chapter 3** and **Chapter 4**) and in the study by Zhou *et al.*,[602] this work aims to prepare macroporous structures using physical crosslinking method, i.e., polymer molecules of the building materials are expected to form networks via non-covalent interactions, such as hydrogen bonding and hydrophobic interactions. For this aim, dextran and polyNIPAAm-modified dextran (synthesised and characterised by Zhou[600]) were selected as the building materials.

5.2 Dextran macroporous structures from microgels stabilised o/w HIPEs

Due to the water solubility of dextran,[591] we aim to put dextran in the continuous phase of a microgel-stabilised o/w HIPE template. In order to understand whether macroporous

structures can be formed with this template, we use a freeze-drying method after emulsification. Besides removing the internal phase (the oil phase, *p*-xylene), freeze-drying is also expected to fabricate dextrans via thermal induced phase separation[478,603] (TIPS) in the aqueous phase. The factors that may influence the HIPE stability and the resultant porous structures have been investigated, including pH, temperature, molecular weight of dextran and polymer concentration.

5.2.1 Effect of pH on stability of the template and the resultant porous structures

Since environmental stimuli (pH, temperature and ionic strength) do affect the particle sizes of poly(NIPAAm-*co*-AA) microgels (**Section 2.2.1**), they can affect the swelling/ deswelling behaviour of microgels and their emulsifying ability. Thus, the effect of pH on the stability of dextran containing HIPEs was investigated using microgel suspensions (0.4 wt % in 1 mM KCl) with a pH 3.7, 4.7, 5.5 and 6.8, respectively. Other conditions were kept constant for this study, including dextran moleculear weight (Mr, 40, 000), dextran concentration (20 w/v %), volume ratio of the oil phase (*p*-xylene, 80%) and the emulsification temperature (room temperature, 22 °C).

Firstly, the effect of pH on HIPE stability was observed during preparation. More than half of the oil phase was expelled from the emulsion template using the aqueous phase with a pH of 3.7. At pH 4.7, more oil was emulsified but coalescence was visible after stirring stopped. More stable HIPEs were produced at pH 5.5 with more than 90% oil emulsified. At pH 6.8, stable and viscous HIPEs were obtained with no free oil visible (**Fig. 5.1**, inset). Clearly, HIPE stability was improved by increasing the pH of microgel suspension from 3.7 to 6.8, which was attributed to pH-induced variation in the emulsifying ability of microgels. As characterised by particle size measurements (**Fig. 5.1**), a gradual diameter increase from 100 nm to 350 nm – an over 40-fold expansion in volume – was observed by increasing pH from 3.7 to 6.8, due to an increased dissociation of carboxylic acid groups.[303] Thus, it can be deduced that microgels reached an optimal emulsifying ability at pH 6.8 for dextran containing o/w HIPEs.

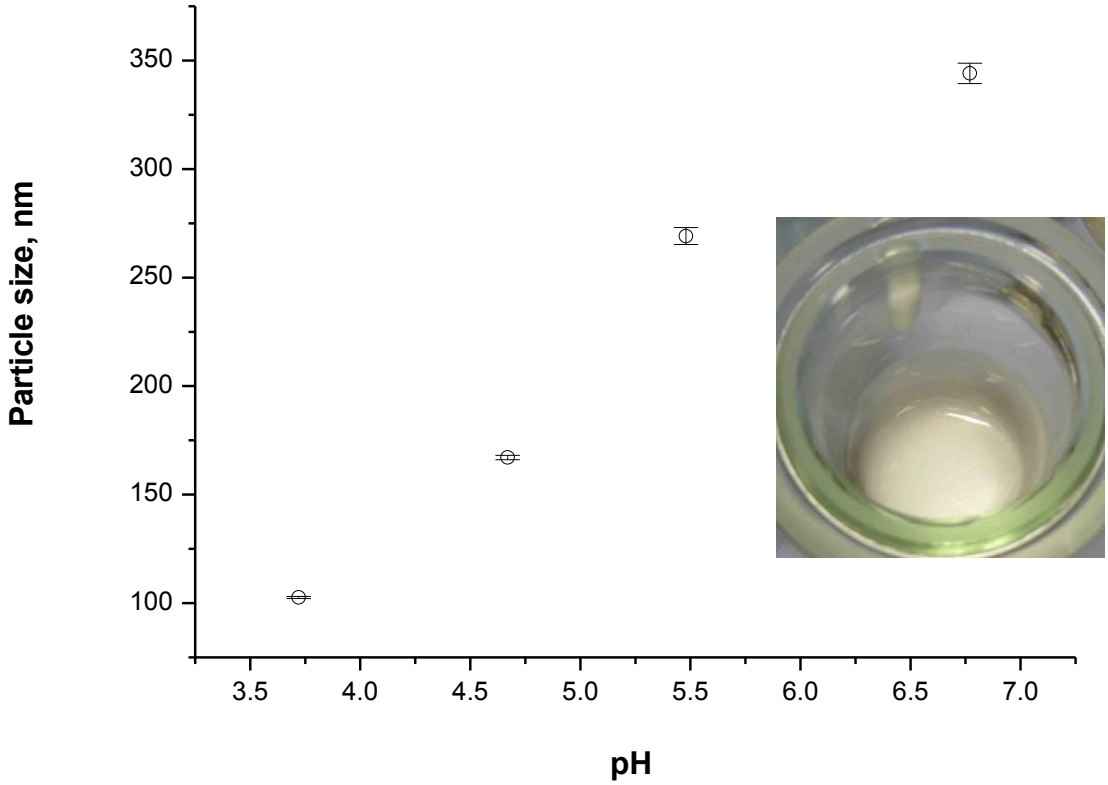


Fig. 5.1 Particle size dependence of microgels on pH in the aqueous suspension (0.4 wt % in 1 mM KCl) at 22 °C (from left to right: 3.7, 4.7, 5.5, and 6.8; inset: image of dextran-containing HIPEs prepared using microgel suspension with a pH of 6.8.)

Secondly, the effect of pH on the morphologies of freeze-dried emulsions/HIPEs was studied (**Fig. 5.2**~**Fig. 5.4**). Typically, the morphology consisted of both macropores and microstructures, which originated from the removal of oil droplets and the water in the dextran solution, respectively. Since the same stirring protocol and composition were used during emulsification, pore size of the macropores reflected the effect of pH on HIPE stability prior to freeze-drying. A statistical comparison on the pore sizes (**Fig. 5.5**) clearly showed that nearly 90% pores of the solid HIPEs prepared using pH 6.8 were within the range of 20-60 μm; this was a much narrower pore size distribution than those prepared using either pH 4.7 or pH 5.5. The large pores of up to 200 μm in diameter observed in solid HIPEs prepared using lower pH (4.7 or 5.5) indicated the occurrence of coalescence prior to freeze-drying; this was in agreement with what was observed during emulsification as discussed above. Therefore, microgel suspensions of pH 6.8 led to stable HIPE as well as macropores with narrower pore size distribution after freeze-drying. Furthermore, the microstructures on the pore walls need to be considered in order to understand the formation of solid HIPEs. They were likely formed through a process of solid-liquid phase separation[604] consisting of liquid-liquid demixing[478] upon quenching in LN_2 and freeze-drying. Liquid-liquid demixing

resulted in dextran-rich and dextran-lean domains. The formation and removal of ice crystals during freeze-drying further compacted the dextran-rich domains and generated grooves in the pore walls. Since no chemical crosslinking was used, physical crosslinking of dextran chains via hydrogen bonding was believed to be responsible for the structural integrity of solid HIPEs after freeze-drying. Meanwhile, dextran-lean domains turned into thin films [marked with arrows in **Fig. 5.2** (d)] or submicrometer-sized holes [**Fig. 5.2** (d) and **Fig.5.3** (d)] after ice removal, indicating that the extent of phase separation affected the formation of pore throats. Thus, the freeze-drying process (duration, control over temperature and pressure) and the polymer concentration (studied in **Section 5.2.3**) may also play a role in determining the microstructures of solid HIPEs. In addition, the orientations of the grooves were either aligned or unalined [**Fig. 5.2** (c) and **Fig. 5.4** (b) (c)], which was likely determined by the pathway of water vapors during sublimation, i.e., the freeze-drying direction.

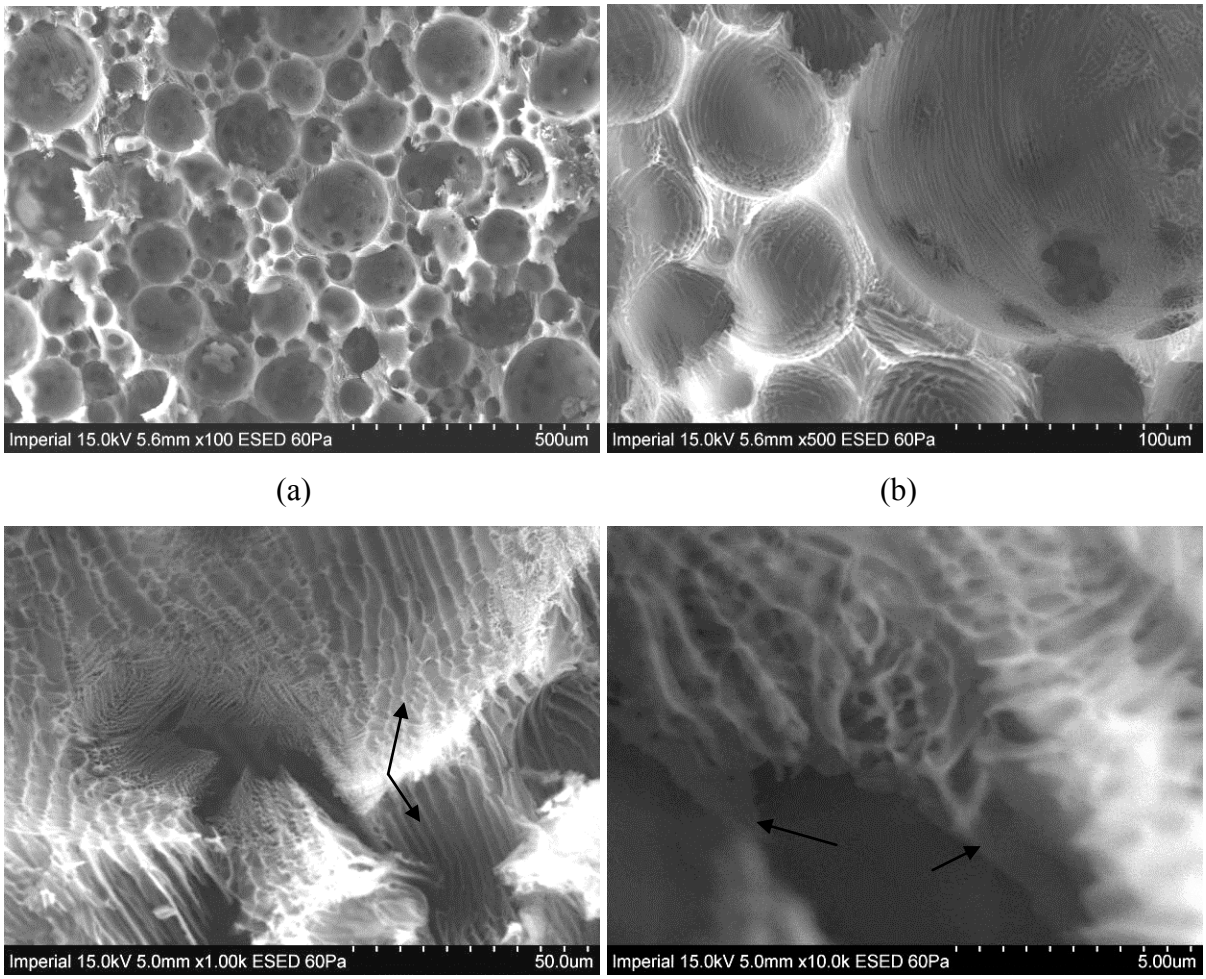


Fig. 5.2 Morphologies of solid HIPEs of dextran prepared using microgel suspension of pH 4.7 showing both the macropores (a), (b) and the microstructures on the pore wall (c), (d).

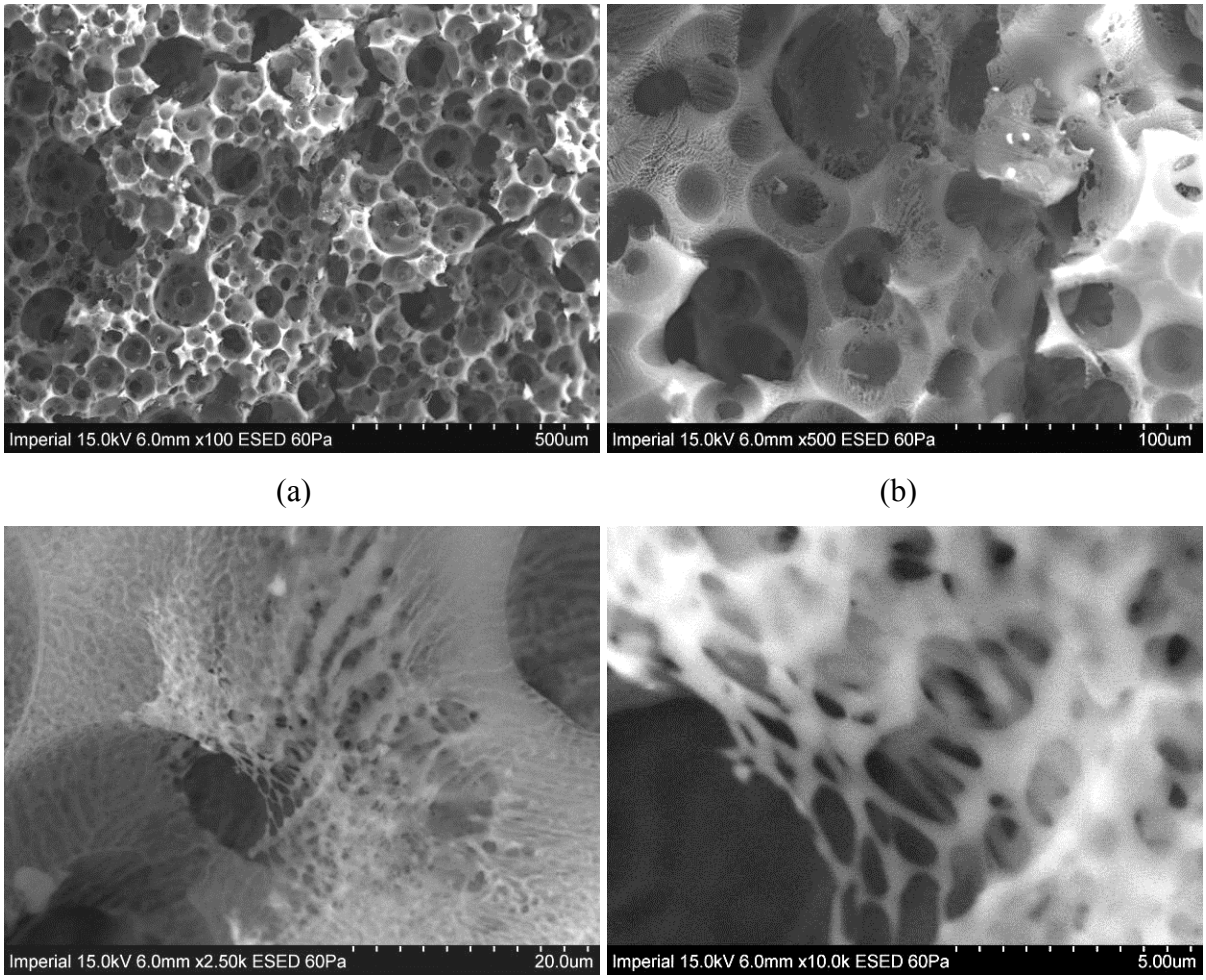
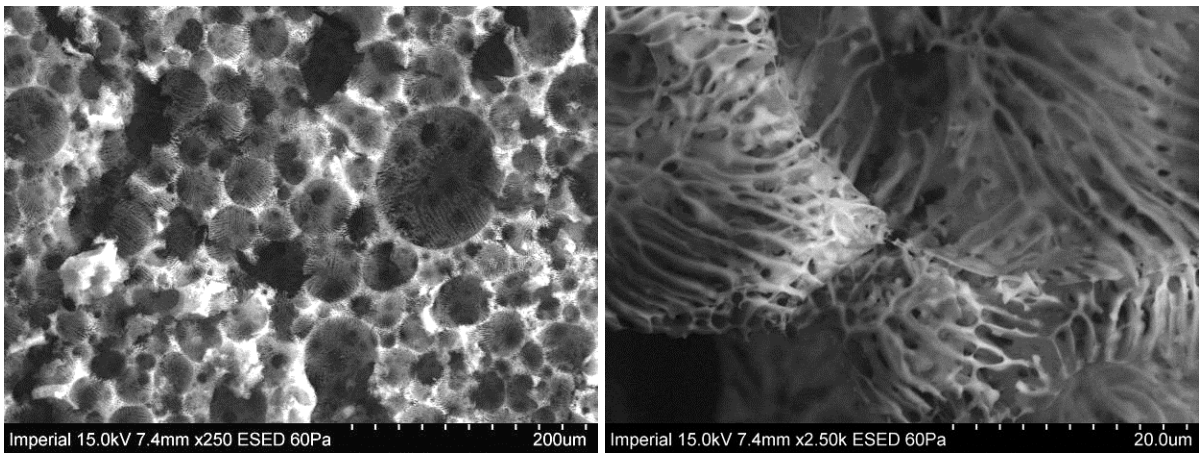
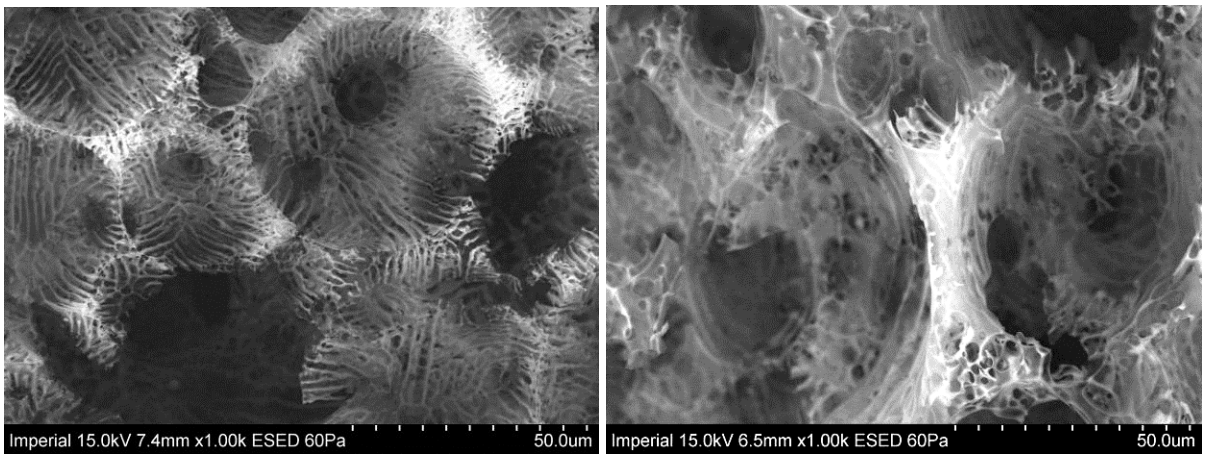


Fig. 5.3 Morphologies of solid HIPEs of dextran prepared using microgel suspension of pH 5.5 showing both the macropores (a), (b) and the microstructures on the pore wall (c), (d).





(c) (d)

Fig. 5.4 Morphologies of solid HIPEs of dextran prepared using microgel suspension of pH 6.8 showing both the macropores (a) and the microstructures on the pore wall (b)-(d).

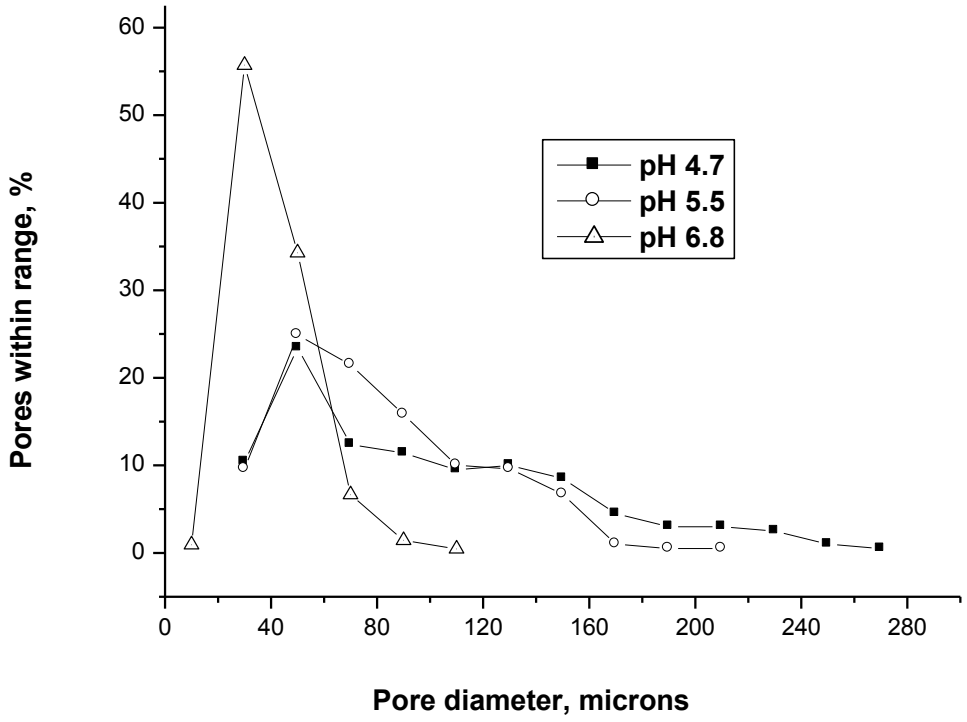


Fig. 5.5 Pore size distributions of solid emulsions/HIPEs of dextran prepared using microgel suspensions with a pH of 4.7, 5.5 and 6.8, respectively. The emulsions/HIPEs containing dextran were frozen by liquid N_2 and then freeze-dried, resulting in solid emulsions/HIPEs.

5.2.2. Effects of temperature on the morphology of dextran macroporous structures

Since poly(NIPAAm-*co*-AA) microgels are also thermo-sensitive (**Section 2.2.1**), it is natural to assume that temperature may have an effect on the morphology of dextran

macroporous structures. Particle size measurements on one particular microgel suspension (0.4 wt % in 1 mM KCl, pH 6.8) showed a minor size change from 340 nm at 22 ºC to 300 nm at 45 ºC and a sharp decreasing trend upon further heating to 70 ºC (**Fig. 5.6**). Thus, it is expected that this temperature-induced shrinkage of microgels may affect HIPE stability and thereby the pore morphology. To study this, a thermostating step was added after emulsification at RT but before quenching with liquid N_2. HIPEs containing dextran were prepared using identical composition (pH 6.8) and were then heated at 45 °C, 50 °C, 55 °C, and 60 °C, respectively for 1 h prior to freeze-drying.

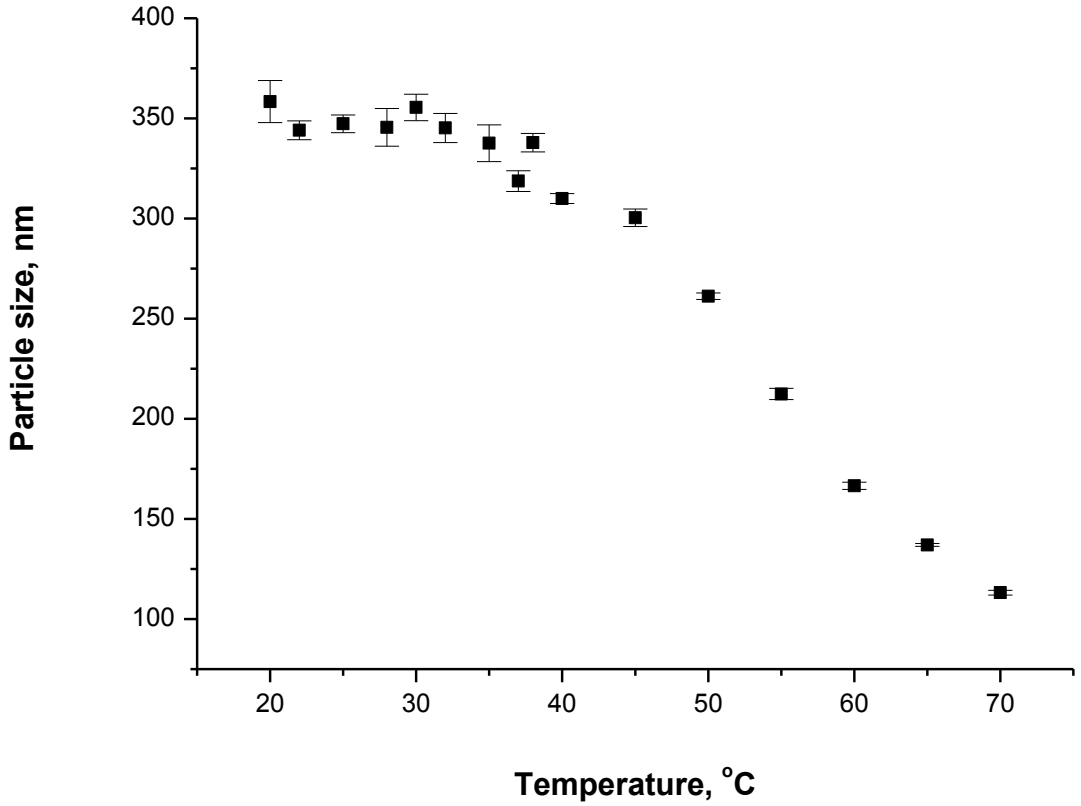


Fig. 5.6 Average particle size of poly(NIPAAm-*co*-AA) microgels as a function of temperature measured using a microgel suspension (0.4 wt % in 1 mM KCl) of pH 6.8

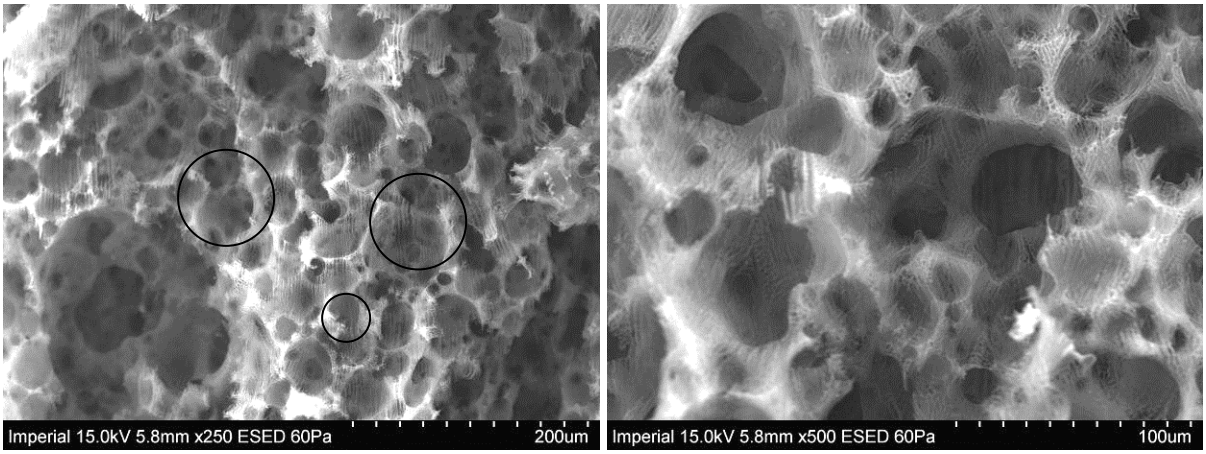


Fig. 5.7 Morphologies of solid HIPEs of dextran prepared by using a thermostating step at 45 ºC for 1 h after emulsification but prior to freeze-drying. Circles mark the fusion of pores.

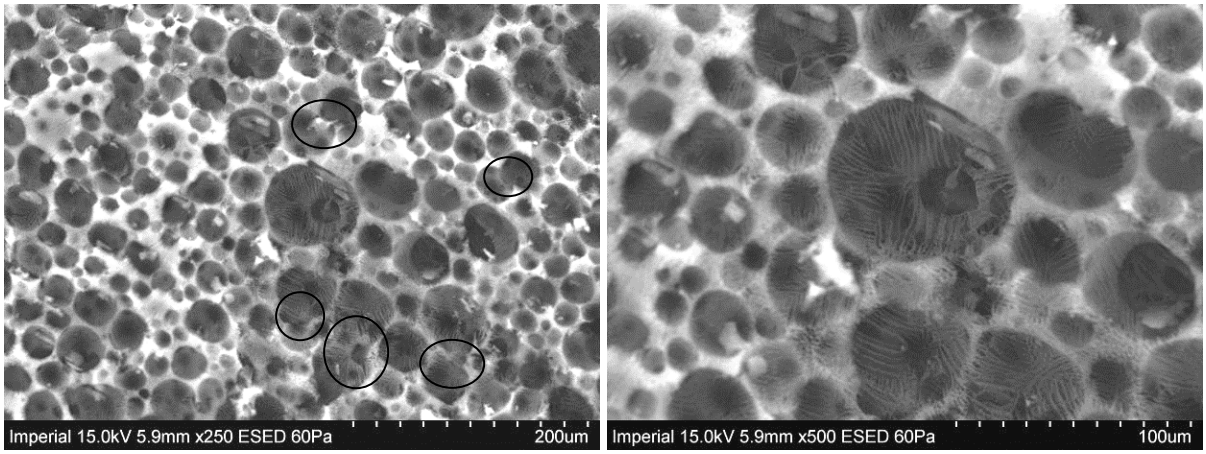


Fig. 5.8 Morphologies of solid HIPEs of dextran prepared by using a thermostating step at 50 ºC for 1 h after emulsification but prior to freeze-drying. Circles mark the fusion of pores.

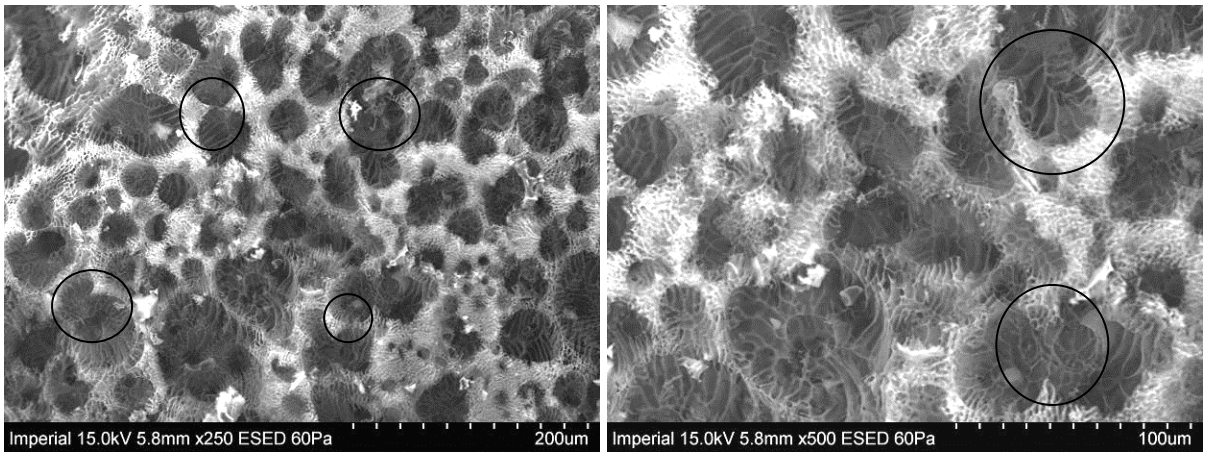


Fig. 5.9 Morphologies of solid HIPEs of dextran prepared by using a thermostating step at 55 ºC for 1 h after emulsification but prior to freeze-drying. Circles mark the fusion of pores.

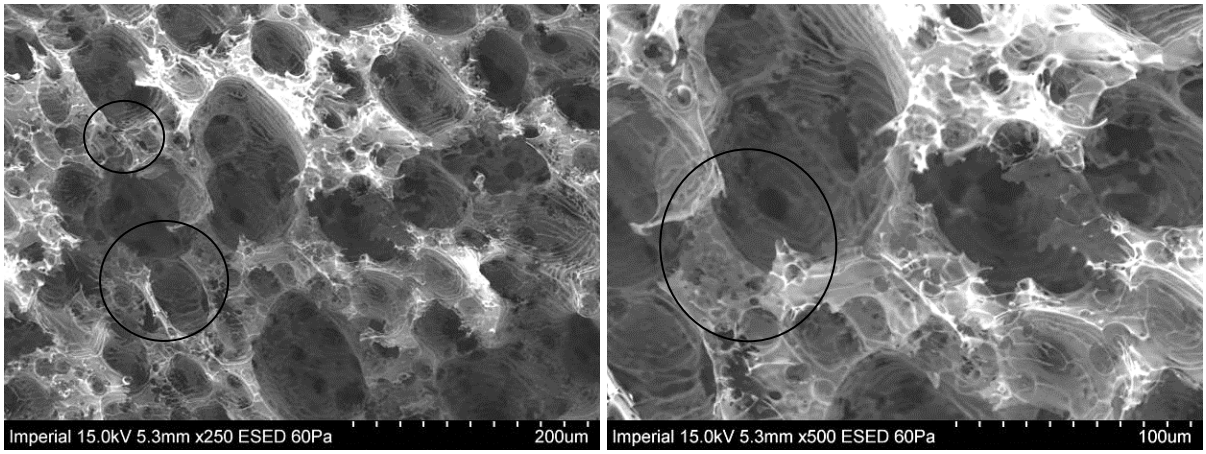


Fig. 5.10 Morphologies of solid HIPEs of dextran prepared by using a thermostating step at 60 ºC for 1 h after emulsification but prior to freeze-drying. Circles mark the fusion of pores.

The resultant morphologies of freeze-dried HIPEs (**Fig. 5.7**~**Fig. 5.10**) showed that the pore walls between neighboring pores partially disappeared as marked by circles, indicating ongoing coalescence of oil droplets upon temperature increase.[130,384] Analysis (**Fig. 5.11**) of the pore sizes of one of the solid HIPEs, which was prepared using 50 ºC in the heating step after emulsification (**Fig. 5.8**), showed that pores with clear boundaries still had a similar size distribution to those of the solid HIPEs prepared without using a heating step (**Fig. 5.4**). This suggested that the extent of coalescence remained low at 50 ºC. This continued stability against coalescence was attributed to the viscous nature of the aqueous phase[68] arising from a high dextran concentration (20 w/v %). In contrast to thermostating the HIPEs at 50 ºC (**Fig. 5.8**), thermostating at 60 ºC resulted in a thin layer of oil on the top prior to freeze-drying as well as intensive pore fusion and distorted pore shapes after freeze-drying (**Fig. 5.10**). This indicated that the extent of droplet coalescence was significantly increased at 60 ºC over 50 ºC. However, this effect of temperature increase on HIPE stability and pore structures could not solely be an effect of microgel shrinkage. More importantly, heating the emulsions could increase the contact frequency of droplets[130] as well as reduce the viscosity of the dextran solution[605], which in turn facilitated the rupture of interfacial films and droplet coalescence. Meanwhile, coarsening[606-608] of the textures or microstructures of the pore walls were observed in comparison with solid HIPEs prepared without using a heating step (**Fig. 5.4**), especially in solid HIPEs prepared using higher thermostating temperatures (55 ºC and 60 ºC). This was because the thermostating temperatures used were above the theta temperature of dextran[605] (43 ºC) and could possibly cause phase separation of dextran in the aqueous phase prior to freezing with LN_2.

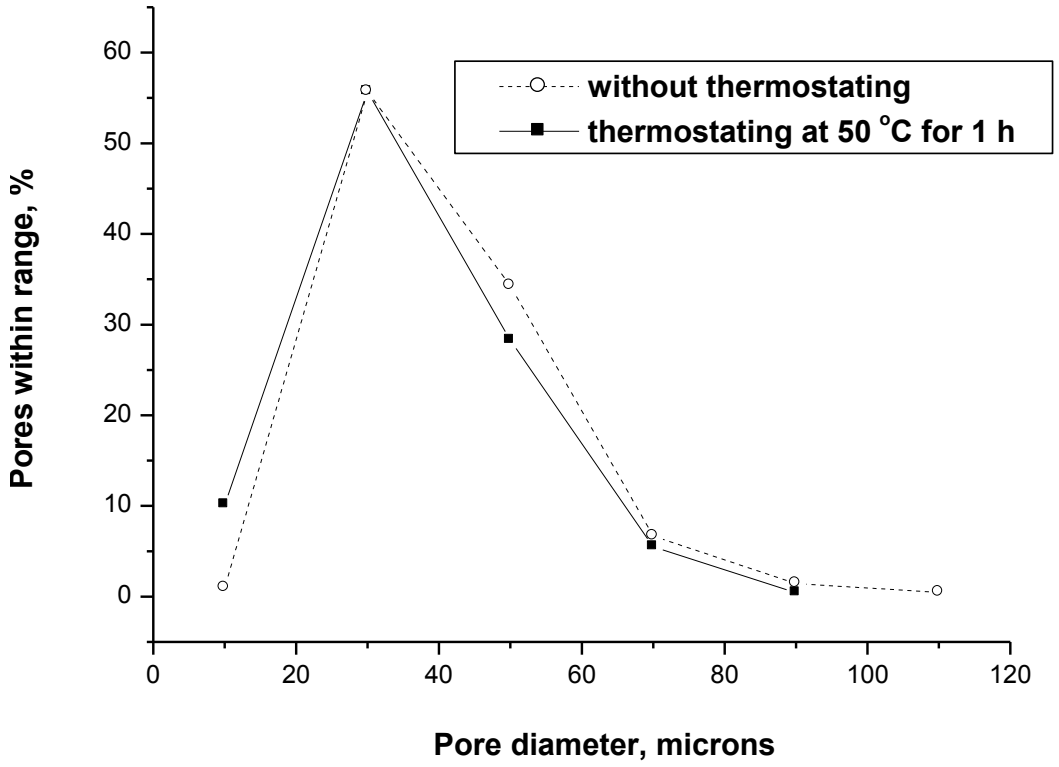


Fig. 5.11 Pore size distribution for solid HIPEs of dextran prepared either by freezing the HIPEs directly after emulsification or by using a thermostating step at 50 ºC for 1 h after emulsification but prior to freezing.

Therefore, thermostating the dextran-containing HIPEs above the theta temperature of dextran affected both the pore morphology and the microstructures of the pore walls. These were attributed to thermostating temperature-induced coalescence of emulsion droplets and phase separation of dextran solution, respectively. Thus, temperature can be used to tune the pore interconnectivity and the microstructures of the pore walls in solid HIPEs of dextran.

5.2.3 Effect of dextran concentration and molecular weight on the pore structures

Since polymer concentration (C_p) and polymer molecular weight will influence the viscosity of the continuous phase[68,220,221] and therefore the HIPE stability, it is possible that the morphology of solid HIPEs of dextran may be tuned by varying polymer concentration and polymer molecular weight. Investigations were carried out using an identical stirring protocol (400 rpm), volume ratio of *p*-xylene (80%) and microgel suspension (0.4 wt % in 1 mM KCl, pH 6.8). Since the o/w HIPEs containing dextran (Mr, 40,000; 20 w/v %) as discussed above (**Fig. 5.4**) was already very viscous, lower molecular weight dextran (Mr,

6,000) and lower dextran concentration (8 w/v %) were selected for the study (**Fig. 5.12~Fig. 5.14**).

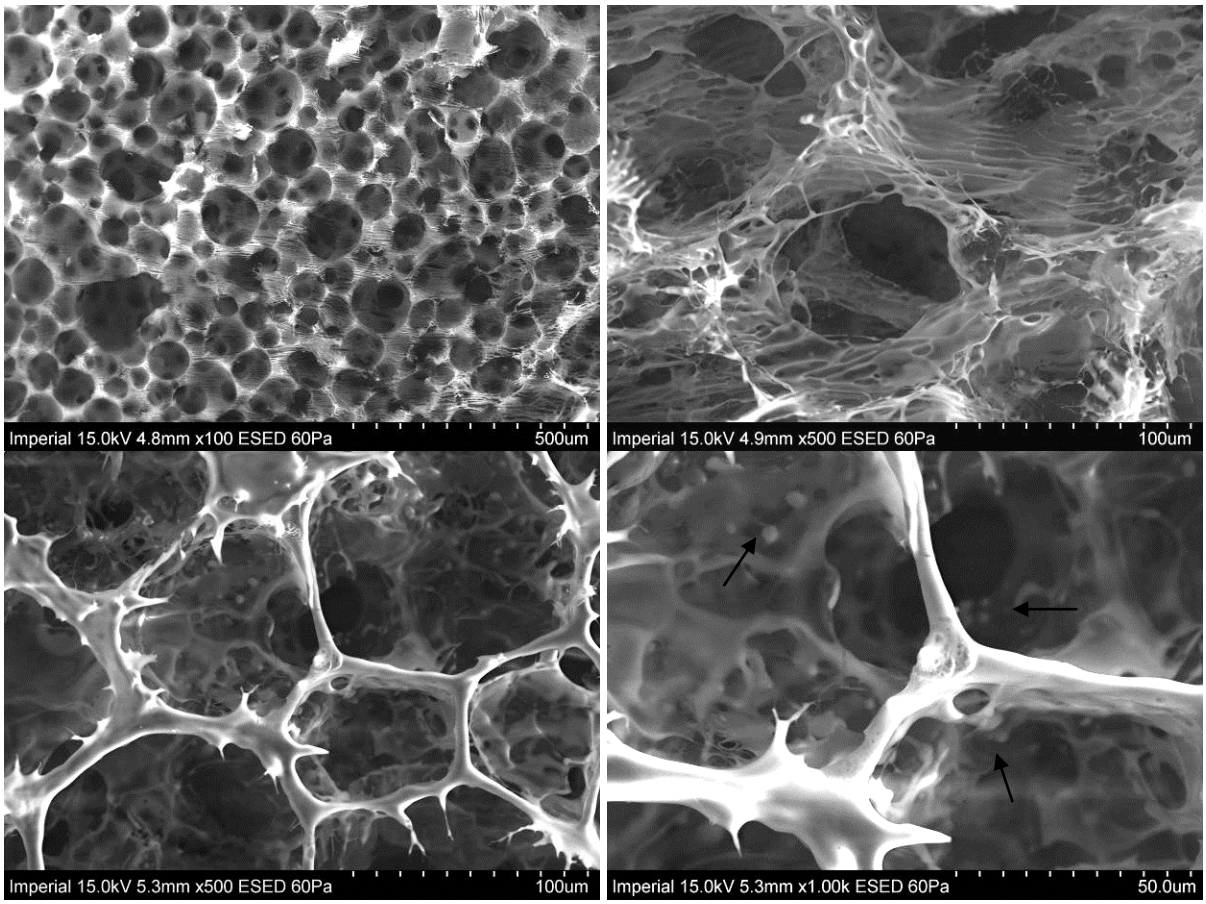


Fig. 5.12 Morphologies of solid HIPEs of dextran prepared using a molecular weight (Mr) of 40, 000 and a polymer concentration (C_p) of 8 w/v %. Arrows mark polymer beads.

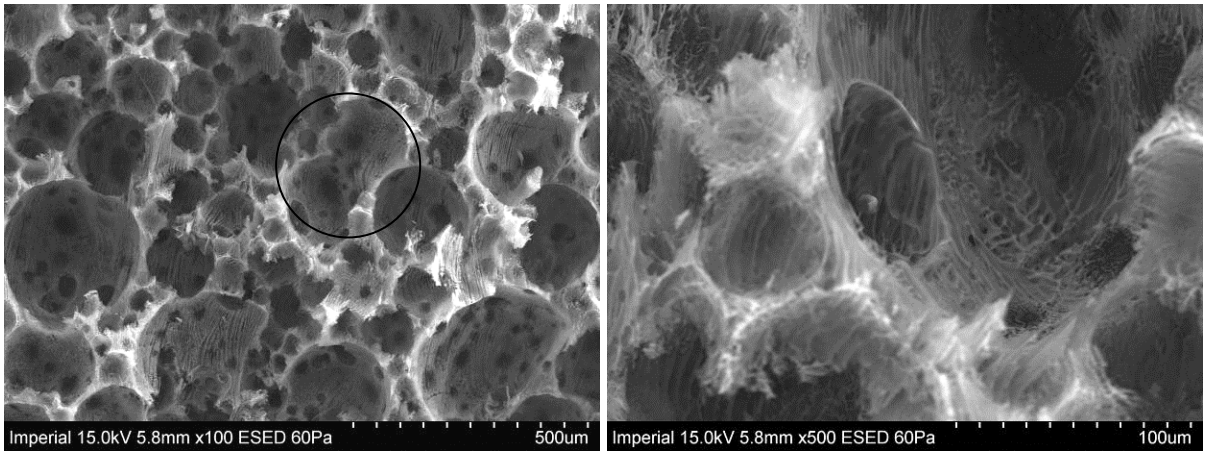


Fig. 5.13 Morphologies of solid HIPEs of dextran prepared using a molecular weight (Mr) of 6, 000 and a polymer concentration (C_p) of 20 w/v %. The circle marks pore fusion.

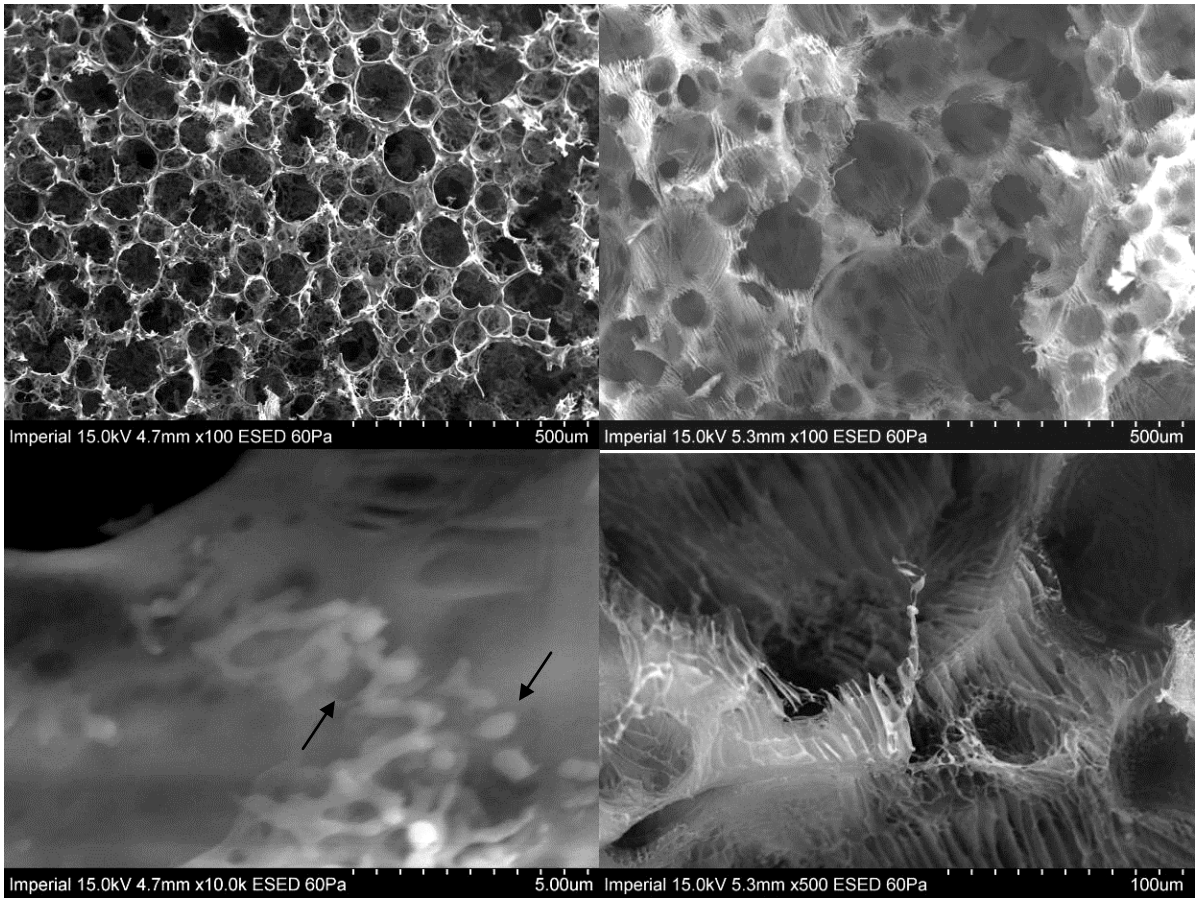


Fig. 5.14 Morphologies of solid HIPEs of dextran prepared using a molecular weight (Mr) of 6, 000 and a polymer concentration (C_p) 8 w/v %. Arrows mark polymer beads.

The effects of dextran concentration on the pore structure of solid HIPEs are clearly seen in the cases where a molecular weight of 40, 000 was used [**Fig. 5.4** and **Fig. 5.12**]. Firstly, a more interconnected pore structure resulted when using a lower dextran concentration (8 w/v %, **Fig. 5.12**) indicating a larger extent of phase separation. Secondly, solid HIPEs prepared using a C_p of 8 w/v % (85.3 ± 32.1 μm) exhibited a clear shift towards larger pore sizes (**Fig. 5.15**), in comparison with those prepared using a C_p of 20 w/v % (41.5 ± 14.5 μm). This was likely because a higher viscosity of the aqueous phase at 20 w/v % dextran led to a higher energy input into emulsions during emulsification and therefore smaller emulsion droplets. Thirdly, polymer beads were sporadically visible within solid HIPEs prepared at lower C_p (**Fig. 5.12**, marked with arrows), likely due to a nucleation and growth mechanism[478,589,590] during phase separation of dextran solution. These bead-like structures were also observed in solid HIPEs prepared using 8 w/v % of low Mr (6,000) Dextran (**Fig. 5.14**, marked with arrows). Nam *et al.*[590] reported the appearance of bead-like, ladder-like and tube-like structures at C_p of 4, 6 and 9 w/v %, respectively, when PLGA/dioxane was quenched into LN_2. Thus, bead-like structures were more likely produced at low C_p and it

was not surprising that they were visible in solid HIPEs prepared using 8 w/v % (**Fig. 5.12** and **Fig. 5.14**) rather than in those prepared using 20 w/v % dextran of either molecule weight (**Fig. 5.4** and **Fig. 5.13**).

The effect of dextran molecular weight on the pore structure was not straightforward. For solid HIPEs prepared using a C_P of 8 w/v % (**Fig. 5.12** and **Fig. 5.14**), a nearly identical pore size distribution was resulted (**Fig. 5.15**), irrespective of the molecular weight, indicating that molecular weight had no obvious effect on HIPE stability at this polymer concentration. In contrast, solid HIPEs prepared using 20 w/v % lower molecular weight dextran (Mr, 6,000) exhibited a much broader pore size range than all the other three solid HIPEs (**Fig. 5.15**). Stenekes *et al.*[609] reported that the dissolution of dextran with a molecular weight of 6, 000 in concentrated aqueous solution was surprisingly more difficult than dextran with a molecular weight of 40, 000. We believe that this lower solubility of dextran with a molecular weight of 6,000 was responsible for a reduced HIPE stability and therefore a broader pore size range observed in solid HIPEs here. It was evidenced by the fusion of pores (**Fig. 5.13**, marked by circle) that coalescence of emulsion droplets did occur.

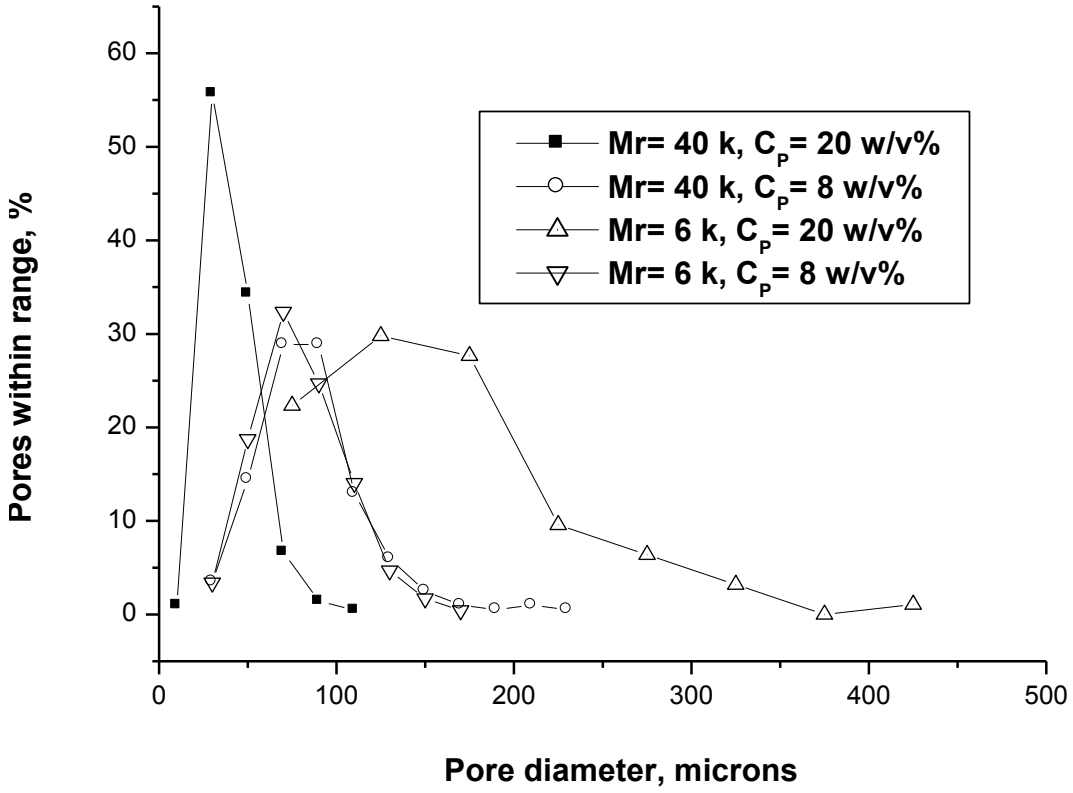


Fig. 5.15 Pore size distributions for solid HIPEs of dextran prepared using dextran with a molecular weight (Mr) of 40 k and 6 k, respectively, and a polymer concentration (C_p) of 20 w/v % and 8 w/v %, respectively.

To sum up **section 5.2**, microgels showed obviously better emulsifying ability at pH 6.8 for o/w HIPEs containing dextran than at other pH including 3.7, 4.7 and 5.5, and resulted in solid HIPEs of dextran with narrower pore size distribution after freeze-drying. Thermostating the o/w HIPEs above the theta temperature of dextran could be used to tune the pore interconnectivity and the microstructures of pore walls within the resultant solid HIPEs. A reduction in the concentration of dextran with a molecule weight of 40 k led to more interconnected pore structures and larger pore sizes. At a concentration of 8 w/v %, varying the molecular weight of dextran from 40 k to 6 k had no obvious effect on the pore structures of solid HIPEs.

5.3 Dextran-*co*-polyNIPAAm macroporous structures from microgels stabilised o/w HIPEs

Stimuli-responsive polymers can adapt to an environmental change via a sharp variation of their properties and have vast potential for biomedical[610] and many other emerging applications,[611] such as self-healing coatings, micro- and nanoacutation and sensors to name a few. Modification of dextran via the incorporation of polyNIPAAm has been used to make dextran thermoresponsive for drug delivery applications.[612,613] Here, we aim to use polyNIPAAm-modified dextran (dextran-*co*-polyNIPAAm, synthesised and characterised by Zhou[600]) instead of dextran as the building material for macroporous structures. This modification would be especially useful for application in the physiological environment, since the cloud point of dextran-*co*-polyNIPAAm (34 °C as measured by Zhou[600]) does allow the material to be solidified at 37 °C without using chemical crosslinking. Moreover, due to the use of poly(NIPAAm-*co*-AA) microgels as emulsifiers, their stimuli-responsiveness and drug-delivery capability would potentially render the resultant macroporous structures multi-responsive and multi-functional.

5.3.1 Morphologies and thermal properties of dextran-*co*-polyNIPAAm macroporous structures

When dextran was replaced by dextran-*co*-polyNIPAAm in the preparation of microgels stabilised o/w HIPEs under identical conditions (pH 6.8), the resultant Pickering HIPE was

also stable and viscous. To obtain macroporous structures, the HIPEs were either frozen directly in LN_2 (**Fig. 5.16**) or thermostatted at 38 °C for 30 min prior to the freezing and freeze-drying process (**Fig. 5.17**). Since 38 °C was above the cloud point of dextran-*co*-polyNIPAAm (34 °C[600]), it was expected that coarsening effects[606-608] may impact on the microstructures of pore walls due to phase separation of polyNIPAAm during thermostating and offer us possibility to control cell behaviour[50] in the case of application as tissue engineering scaffolds.

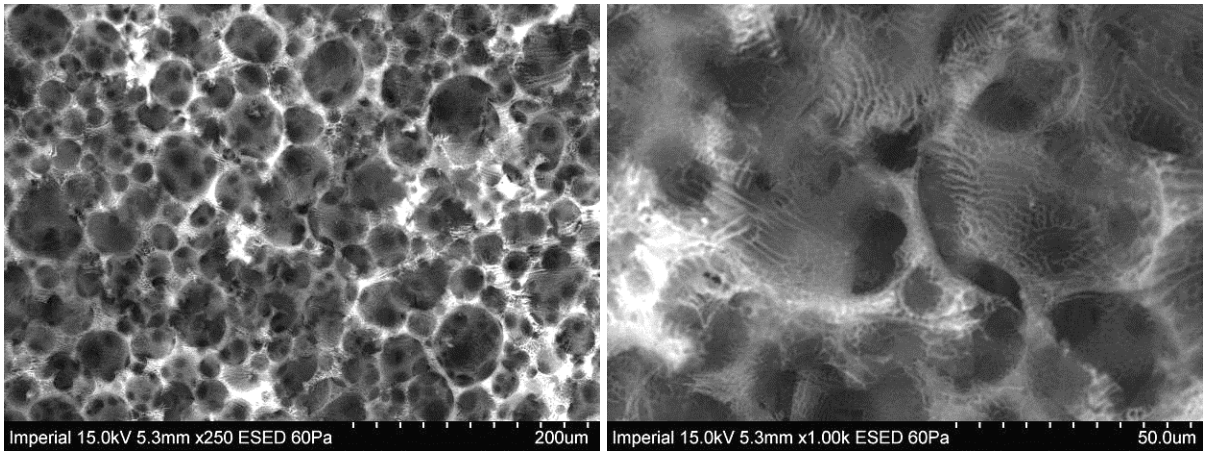


Fig. 5.16 Morphologies of dextran-*co*-polyNIPAAm macroporous structures prepared by directly freezing the HIPEs in LN_2 after emulsification and then freeze-drying.

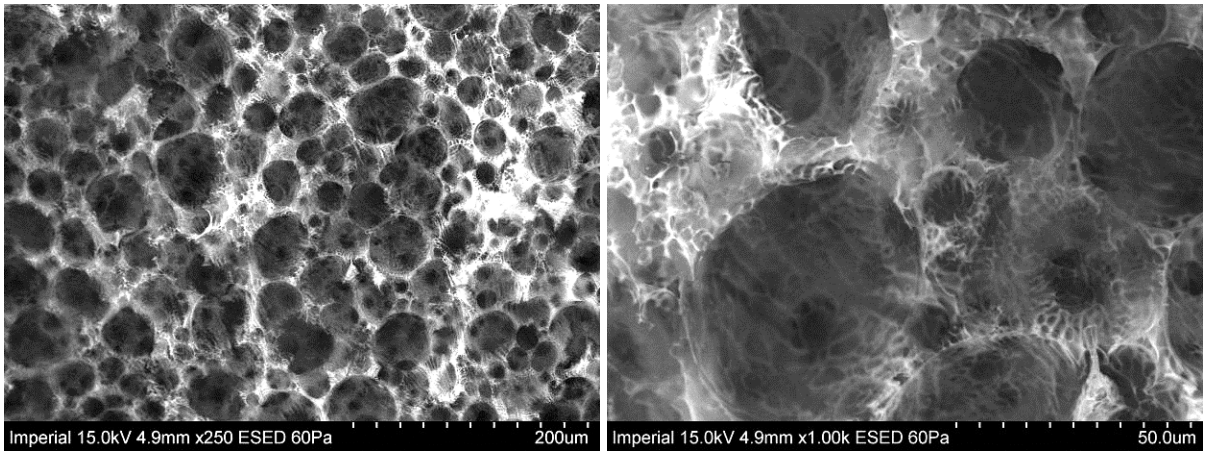


Fig. 5.17 Morphologies of dextran-*co*-polyNIPAAm macroporous structures prepared by thermostating the HIPEs at 38 °C for 30 min prior to the freezing and freeze-drying process.

The average pore size of dextran-*co*-polyNIPAAm macroporous structures (**Fig. 5.16**) was 44.6 ± 13.9 μm, similar to that of dextran solid HIPEs (41.5 ± 14.5 μm, **Fig. 5.4**), indicating that replacement of dextran by dextran-*co*-polyNIPAAm had little effect on the pore structures. Meanwhile, dextran-*co*-polyNIPAAm macroporous structures prepared using

a thermostating step (**Fig. 5.17**) had an average pore size of 38.7 ± 14.2 μm and exhibited a similar pore size distribution to its counterpart prepared without using the thermostating step (**Fig. 5.18**), suggesting that the thermostating process had no obvious effect on the pore structures. Meanwhile, the microstructures of pore walls in the above two dextran-*co*-polyNIPAAm macroporous structures did not show very obvious differences. This indicated that the thermostating conditions (38 °C for 30 min) might have not yet induced sufficiently high extent of phase separation in polyNIPAAm prior to the freezing step.

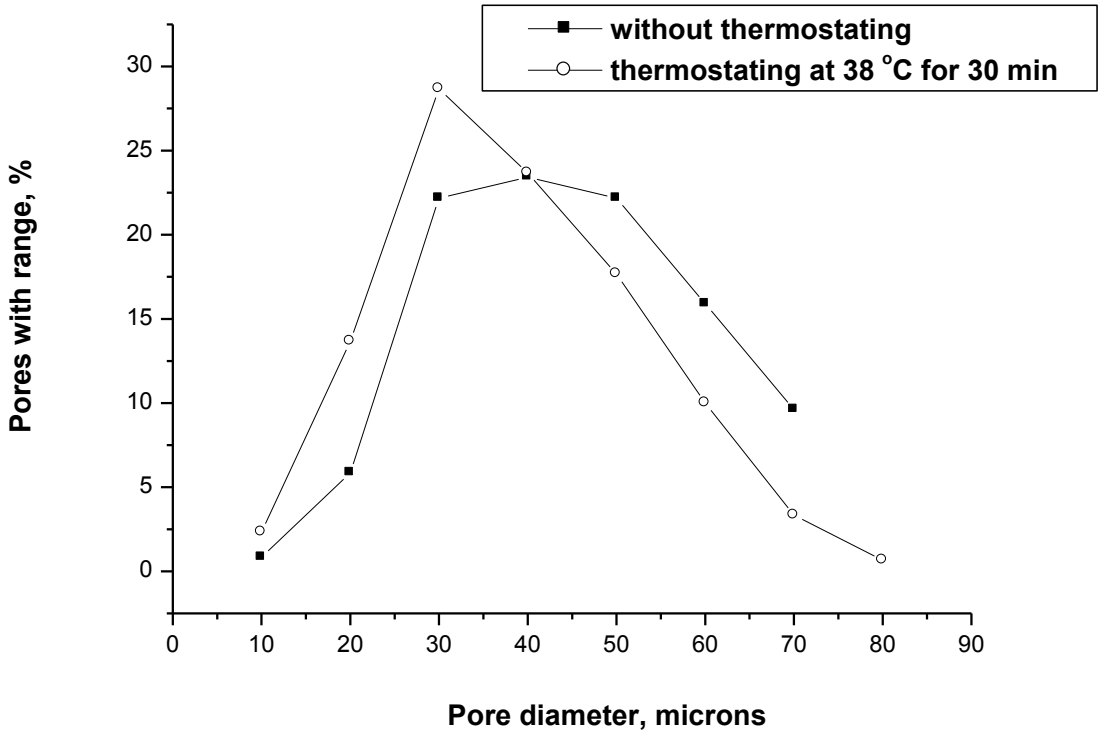


Fig. 5.18 Pore size distribution for dextran-*co*-polyNIPAAm macroporous structures prepared either by using a thermostating step (38 °C for 30 min) after emulsification but prior to the freezing and freeze-drying step or by freezing the HIPEs in LN_2 directly after emulsification and then freeze-drying.

Since the two dextran-*co*-polyNIPAAm macroporous structures maintained their structural integrity without using chemical crosslinking, the physical interactions among the polymer chains were expected to manifest and were investigated with DSC (**Fig. 5.19** and **Table 5.1**). As controls, dextran macroporous structures and microgel particles (**GP_pH6.8**) were also characterised using heating rates of 20 °C/min and 5 °C/min. As a result, a single glass transition temperature (T_g) of 221 °C was observed in the 2nd heating cycle of dextran macroporous structures. Zhang *et al.*[614] reported a similar T_g value (223°C) using a heating

rate of 20 °C/min and attributed this high value to strong hydrogen bonding among dextran molecules. This verified our early speculation that hydrogen bonding was responsible for the structural integrity of dextran solid HIPEs (**Section 5.2.1**). Meanwhile, the effect of microgels on the glass transition of the macroporous structures was not visible and therefore negligible, due to a relatively low content (2 wt %) in the matrix. For dextran-*co*-polyNIPAAm macroporous structures, two glass transitions were observed only when 20 °C/min was applied as the heating rate (**Fig. 5.19**). The steep transition at ~220 °C was similar to T_g of dextran solid HIPEs and therefore represented the glass transition of dextran segments. The other transition belonging to polyNIPAAm occurred in a range of 128~154 °C for dextran-*co*-polyNIPAAm macroporous structures and 133~146 °C for its counterpart prepared using the thermostating step, respectively. This phenomenon of two glass transitions indicated that dextran-*co*-polyNIPAAm phase separated and the resultant polyNIPAAm aggregates formed a second type of physical crosslinking as expected. Also, a narrower polyNIPAAm glass transition range for the latter sample suggested that the thermostating process used indeed resulted in a further phase separation of polyNIPAAm.

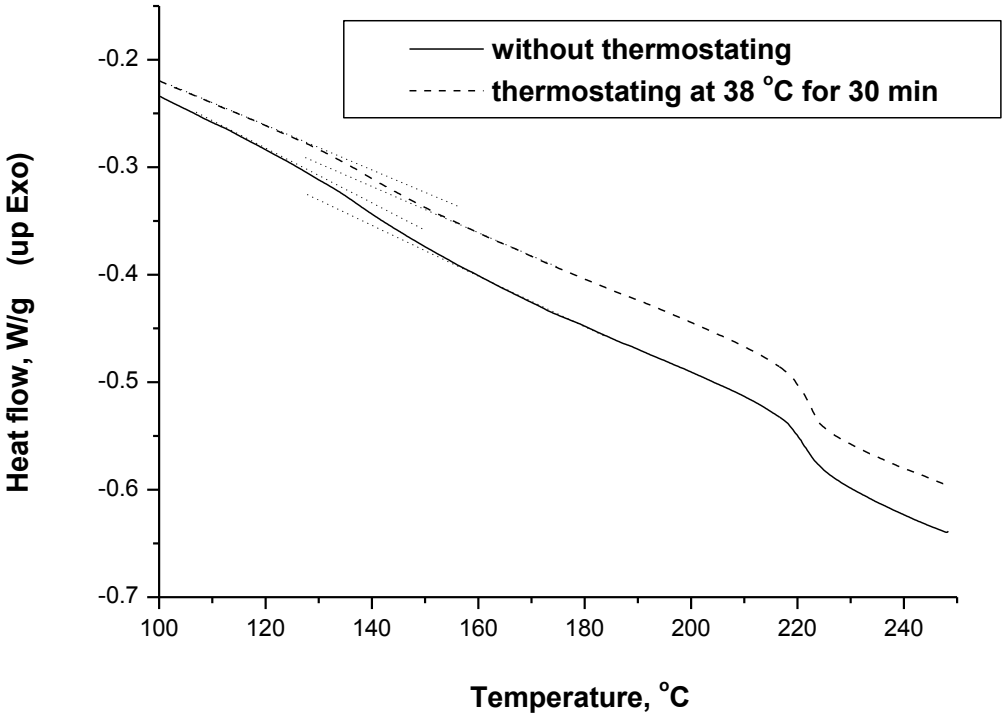


Fig. 5.19 Partial DSC curves for dextran-*co*-polyNIPAAm macroporous structures prepared either using or without using a thermostating step. The curves were obtained from the 2nd heating cycle at a heating rate of 20 °C/min and the rest of curves ranging from -50 °C to 100 °C were linear lines.

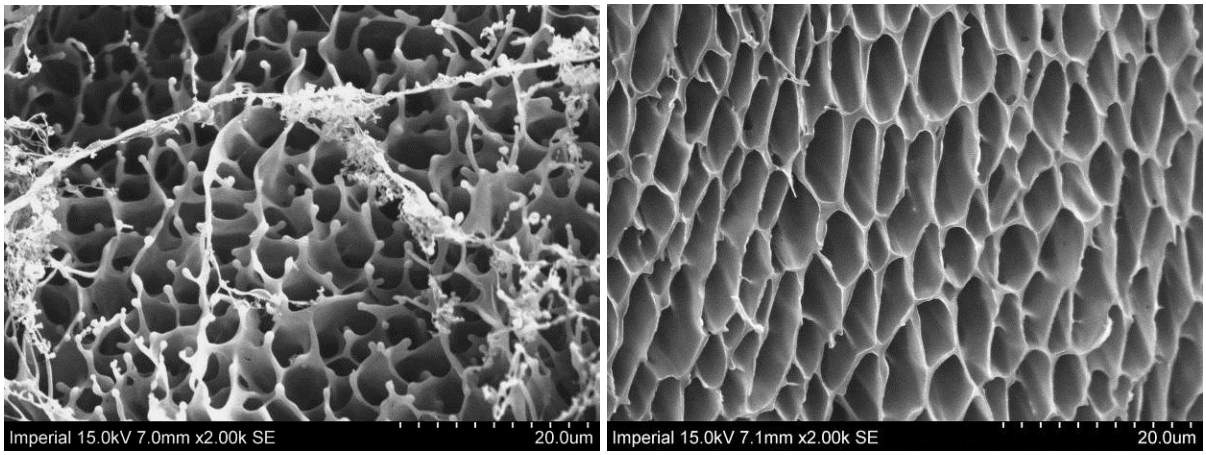
Table 5.1 A summary of glass transition temperatures (T_g) determined by DSC

	Dextran solid HIPEs		Dextran-*co*-polyNIPAAm	Dextran-*co*-polyNIPAAm (thermostating step)	**GP_pH6.8**	
	1	2			1	2
T_g, °C	206	221	138 and 221	139 and 223	152	157
Heating rate, °C/min	5	20	20	20	5	20

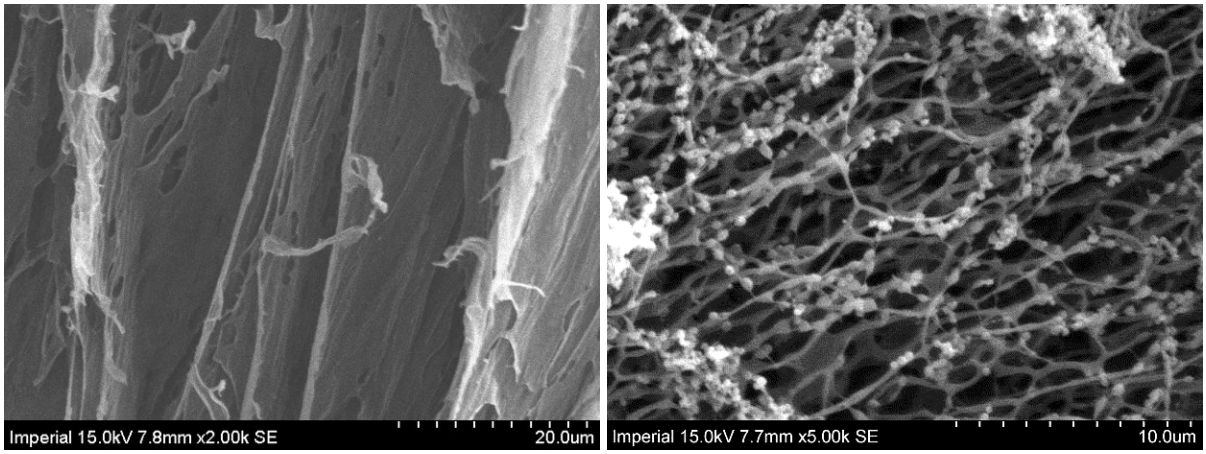
Therefore, dextran-*co*-polyNIPAAm was successfully used as the building materials of macroporous structures prepared from microgels stabilised o/w HIPEs. DSC revealed that phase separation of the copolymer provided a second physical crosslinking besides hydrogen bonding of dextran segments.

5.3.2 Morphologies of dextran-*co*-polyNIPAAm macroprous structures after durability tests in water

In order to evaluate the effects of aqueous environment on dextan-*co*-polyNIPAAm macroporous structures for implantation purpose, a preliminary durability test was carried out on the above two samples in 38 ± 2 °C water for 14 d. Although the scaffolds floated on top in water, the intermolecular hydrogen bonding of dextran segments was probably disrupted due to the good water-solubility of dextran. Thus, the structural integrity in water was mainly attributed to polyNIPAAm aggregates. After being frozen in LN_2 and freeze-dried, the tested samples exhibited various cellular morphologies (**Fig. 5.20** and **Fig. 5.21**).

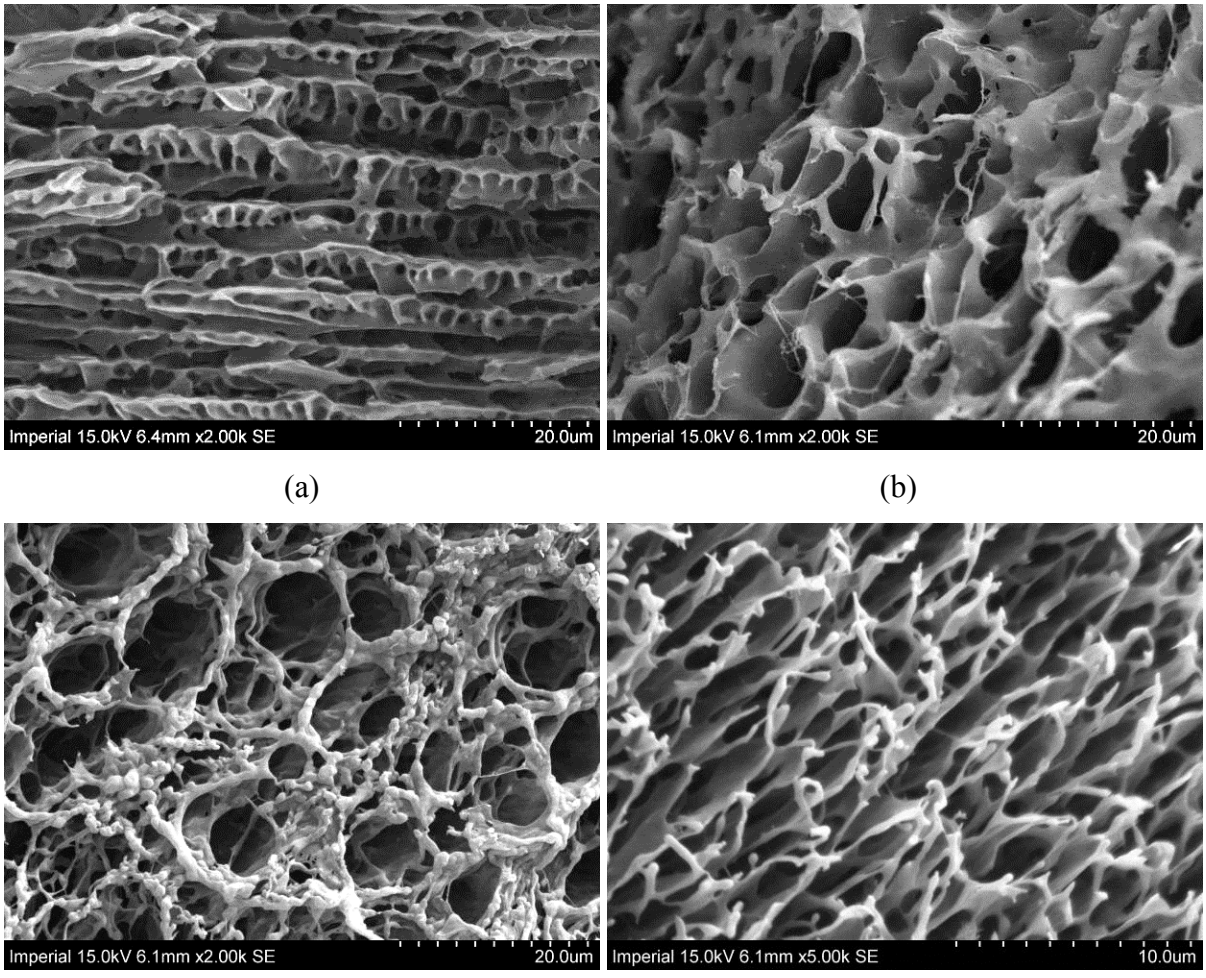


(a) (b)



(c) (d)

Fig. 5.20 Morphologies of dextran-*co*-polyNIPAAm macroporous structures frozen in LN_2 and freeze-dried after a 14 d durability test in water. The original emulsion-templated macroporous structures transformed into various new structures after freeze-drying.



(a) (b)

(c) (d)

Fig. 5.21 Morphologies of dextran-*co*-polyNIPAAm macroporous structures frozen in LN_2 and freeze-dried after a 14 d durability test in water. A thermostating step was used when preparing the original emulsion-templated macroporous structures prior to the test.

It was noticed that the emulsion-templated macroporous structures (**Fig. 5.16** and **Fig. 5.17**) disappeared and simply transformed into structures including pearl necklace-like [**Fig. 5.20** (d) and **Fig. 5.21** (c)], honeycomb-like [**Fig. 5.20** (b)], ladder-like [**Fig. 5.21** (a)], lamellae [**Fig. 5.20** (c)], etc. The sizes of pores were 2-10 μm in diameter, much smaller than those of emulsion-templated pores. Meanwhile, the polymer beads in the pearl necklace-like structures, formed due to a nucleation and growth mechanism[478,589,590] during freeze-drying, were a few hundred nanometers [**Fig. 5.20** (d)] or 1~2 μm [**Fig. 5.21** (c)] in diameter. The formation of various morphologies during phase separation was reported to be concentration dependent.[66,590,603,604,615] We believe this can also explain the various morphologies in our case, since dextran-*co*-polyNIPAAm floated in water during the test and the polymer concentration (C_p) was indeed spatially inhomogeneous prior to phase separation (freezing).

5.4 Summary

Poly(NIPAAm-*co*-AA) microgel particles stabilised o/w HIPEs were successfully used to fabricate macroporous dextran and dextran-*co*-polyNIPAAm. The pH of the aqueous phase was found crucial to the HIPE stability and pH 6.8 resulted in stable HIPEs without coalescence and pore structures with narrow pore size distribution after the freezing and freeze-drying process. Using dextran as the building material of macroporous structures, it was further found that thermostating HIPEs above the theta temperature of dextran prior to freezing did affect the pore interconnectivity of the resultant solid HIPEs as well as microstructures of the pore walls. Also, the pore interconnectivity was found to be increased upon reducing the dextran concentration from 20 w/v % to 8 w/v %. In the case of macroporous dextran-*co*-polyNIPAAm, phase-separated polyNIPAAm segments were found capable of keeping the material from dissolving in water at physiological temperatures. Combining the stimuli-responsiveness of microgel particles, macroporous dextran-*co*-polyNIPAAm could potentially be used as a multiply responsive scaffold.

Chapter 6 Conclusions and perspectives for future work

6.1 Conclusions

In the field of tissue engineering scaffolds, there is growing interest in the manufacture of complex multifunctional scaffolds designed to mimic the native extracellular matrix (ECM). By using emulsion templating to fabricate scaffolds, the work described in this thesis has gone some way towards this goal. We demonstrated the advantages of using poly(NIPAAm-*co*-AA) microgel particles as emulsifiers instead of the surfactants used for the preparation of conventional polyHIPEs.

By using dynamic light scattering, the sensitivity of poly(NIPAAm-*co*-AA) microgel particles to pH, temperature and KCl concentration was characterised. With this stimuli-responsive emulsifier, polyHIPEs with hydrophobic surfaces and polyHIPEs with hydrophilic surfaces have been both obtained by polymerisation of w/o HIPEs (DVB as the monomer) and o/w HIPEs (KAA as the monomer), respectively. Moreover, both polyHIPEs exhibited pore sizes of a few hundred micrometers, within the required range of pore size for bone tissue engineering scaffolds.

When using DVB as the oil phase, microgel suspensions of different pH were investigated in order to obtain w/o HIPEs. At pH 5, swollen-state microgel particles were so hydrophilic that only o/w emulsions were produced regardless of phase volume ratio or particle concentration. It was found that shrunken microgel particles at this pH were not suitable to stabilise emulsions. At pH 2.5 or pH 3, o/w emulsions were obtained below 32 °C while phase separation occurred above 32 °C due to particle aggregation. At pH 4, however, microgel particles in the shrunken state (>VPTT) resulted in the desired w/o emulsions (60 vol % internal phase) and HIPEs (80 vol % internal phase). Using photo-polymerisation at 40 °C, poly(DVB) Pickering-HIPEs with closed-pore morphology were then obtained. Investigation into the stabilisation mechanism suggested that the charges of microgel particles were crucial for the formation of stable particle layers at the water-oil interface.

For microgel particles stabilised o/w HIPEs with KAA dissolved in the aqueous phase, the HIPE stability against coalescence was found to be dependent on the KAA concentration and temperature while the stability against creaming was closely related to the stirring speed

used to produce the HIPEs since increasing the stirring speed reduced the size of emulsion droplets. To polymerise the o/w HIPEs, a crosslinker of high water solubility and reactivity, e.g. *N, N'*-methylenebisacrylamide (BIS), was preferred and photo initiation was found to be more convenient and efficient than initiation using the redox pair of APS/TMEDA. Although closed-pore morphologies were reported for most poly(Pickering HIPEs) in the literature, a systematic investigation into poly(KAA) Pickering-HIPEs here showed that open porous morphologies were attainable and that reducing the crosslinker content (BIS/KAA, mol/mol) strongly promoted the formation of pore throats. The critical BIS content was found to be 3.2 mol % for poly(KAA) Pickering-HIPEs prepared at a low stirring speed (400 rpm). For any BIS content lower than this, open pores became predominant. Other measures, such as increasing the stirring speed or the internal phase volume ratio and reducing the KAA concentration, would noticeably benefit the formation of pore throats only when the BIS content was sufficiently low (< 10 mol %). This vital role that BIS content played in pore-throat formation was also verified in poly(KMAA) Pickering-HIPEs. Via cryo-SEM, the driving force for pore throat formation was found to be non-solvent induced phase separation.

BET surface areas of poly(KAA) Pickering-HIPEs were below 2 m^2/g, although an increase was observed upon further removal of moisture. Skeleton densities of poly(KAA) Pickering-HIPEs measured by mercury intrusion porosimetry (MIP) were mostly below 1.0 $g.cm^{-3}$ and were even lower for those with closed-pore morphology. Alternatively, polymer blocks prepared by polymerising aqueous solutions with identical compositions to the aqueous phase of the corresponding o/w HIPEs and purifying in the same way as polyHIPEs were used in an indirect method. The measured densities of these polymer blocks, 1.19~1.35 $g.cm^{-3}$, were taken as the skeleton densities of poly(KAA) Pickering-HIPEs and were close to that of the reported PAA or poly(KAA). This indirect method also revealed that the porosity of the interior of poly(KAA) Pickering-HIPEs were as high as 97~98%.

By dispersing silica or Bioglass® into the aqueous phase of o/w HIPEs, poly(KAA) Pickering-HIPE composites were prepared without compromising the emulsion stability. The dispersion of silica within the composites was obviously improved when using a higher stirring speed (1000 rpm) during emulsification. A composite with 10 wt % nominal loading of silica exhibited a swelling ratio in SBF up to over 6000 wt %. In contrast to an unaffected polyHIPE morphology by silica, covered pore throats were sporadically observed within the poly(KAA)/Bioglass® Pickering-HIPE composites, probably due to dissolution of Bioglass® into the aqueous phase during emulsification.

Macroporous scaffolds loaded with active ingredients (A.I.) were also developed. This was achieved by using R6G dye- or paracetamol drug-loaded microgels as the emulsifiers of o/w HIPEs. It was found that the emulsifying ability of A.I. loaded microgels was closely related to the microgel-A.I. interaction. With an equivalent emulsifying ability to microgels, paracetamol-loaded microgel particles resulted in stable HIPEs at either low or high stirring speed and hence polyHIPEs of tunable morphologies.

Finally, microgels stabilised o/w HIPEs were successfully used to fabricate macroporous dextran and dextran-*co*-polyNIPAAm. The pH of the aqueous phase was found crucial to the HIPE stability and pH 6.8 resulted in stable HIPEs without coalescence and pore structures with narrow pore size distribution after the freezing and freeze-drying process. By thermostating HIPEs prior to freezing or by varying the dextran concentration, the pore structures of macroporous dextran were tunable. Macroporous dextran-*co*-polyNIPAAm could be potentially used as a multiply responsive scaffold. Besides the stimuli-responsiveness provided by microgel particles, polyNIPAAm segments of the copolymers enabled scaffold integrity in water due to phase separation at physiological temperature.

6.2 Perspectives for future work

Based on the investigation of poly(DVB) Pickering-HIPEs, there are two aspects in particular into which further research could be worthwhile. One possibility is to map out the charge density range of shrunken poly(NIPAAm-*co*-AA) microgel particles, at which stable microgel particle layers form at the interface and hence allow w/o HIPEs to be obtained. This study can start with pH 4, 1 mM KCl and 40 °C. Another area is to prepare open porous poly(Pickering HIPEs) by tuning the crosslinking density, the diluent and the solvents for extraction. DVB should be replaced by oil-soluble monomers that can turn into a rigid, biocompatible and biodegradable matrix for bone tissue engineering. A good example is the macromer of poly(propylene fumarate) (PPF), which has been investigated in conventional polyHIPEs.[68,218]

For microgel-stabilised o/w HIPE templates, further efforts are required in order to make use of the resultant polyHIPEs for bone cell growth: (i) to characterise and tune the mechanical properties of polyHIPEs in the wet state, i.e. macroporous hydrogels; (ii) to create biodegradable scaffolds; (iii) to carry out cell tests. Since poly(KAA) Pickering-HIPEs prepared using 80 vol % internal phase could have a porosity of up to 97%, reducing the

internal phase volume ratio would be a sensible measure to obtain higher mechanical strength. Meanwhile, copolymerising with another monomer is a feasible way to modify the hydrophobicity and mechanical properties of polyHIPEs. Alternatively, it is worth trying water-soluble monomers that may lead to rigid polyHIPEs. Poly(KAA) and poly(KMAA) are not biodegradable but using a biodegradable crosslinker, such as 2-hydroxyethyl methacrylate modified poly(L-glutamic acid),[616] would enable the scaffolds to biodegrade. Consideration of the osteoblast-polyHIPE scaffold interactions as investigated by Akay *et al.*[129,213] would be important during cell tests on macroporous hydrogels.

Fluorescence microscopy would be very useful to characterise dye-loaded microgel particles either in the aqueous solution[576] or at the water-oil interface.[381,617] The drug delivery functionality of poly(Pickering HIPEs) needs to be further quantified. Specifically, drug uptake/release measurements need to be made on both the microgel particles and the polymer matrix of polyHIPEs. Currently, the drug-microgel interactions are of a physical nature. However, the interactions could be extended to covalent ones, depending on the need of delivery. Moreover, bioactive molecules such as bone morphogenetic proteins (BMPs) and vascular endothelial growth factor (VEGF) are candidate molecules to deliver in any future study. In addition, since photo-initiation was used for both the w/o and the o/w templates, an attractive study could be to fabricate scaffolds in an injectable manner, especially for non-load-bearing bone sites.

Chapter 7 Experimental

7.1 Materials

Reagents and solvents were obtained from commercial sources and used as received, unless otherwise stated.

N-isopropylacrylamide (NIPAAm, 97%), acrylic acid (AA, ≥99.0%), *N, N'*-methylenebisacrylamide (BIS, ≥99.5%), ammonium persulphate (APS, >98%), Sodium dodecylbenzene sulfonate (NaDBS, technical grade), Amberlyst 15, sodium sulphide, divinylbenzene (DVB, 80%), styrene (>99%), α, α'-azoisobutyronitrile (AIBN, ≥98.0%), $CaCl_2.2H_2O$ (≥99%), di(ethyleneglycol) divinyl ether (DEGDVE, 99%), 1,5-hexadiene-3,4-diol (97%), Irgacure 2959 (98%), HCl in methanol solution (~1.25 M), N, N, N', N'-tetramethylethylenediamine (TMEDA, 99%), *p*-xylene (≥99%), dextran (Mr, 6,000), dextran (Mr, 40,000), Rhodamine 6G, dopamine. HCl, acetaminophen (or paracetamol) (≥99.0%), naproxen (98%), Tris (>99.9%), potassium phosphate monobasic ((≥99.0%), and potassium phosphate dibasic (K_2HPO_4) were purchased from Sigma-Aldrich Co. Ltd. (Gillingham, UK). K_2HPO_4 (>99%) from Fisher Scientific (Loughborough, UK) was also used.

Sodium dodecylbenzene sulfonate (NaDBS, 80% active constituent with sodium sulphate as the remainder), hydrochloric acid (35.4% or 37%, 1.18 g/cm^3), sulfuric acid (98%, 1.84 g/cm^3), nitric acid (69%, 1.42 g/cm^3), $NaH_2PO_4.H_2O$ (99.0%-102.0%), sodium hydroxide (≥99.0%), potassium hydroxide (86.0%), NaCl (99.5%), $NaHCO_3$ (99.9%), $MgCl_2.6H_2O$ (100.7%), $CaCl_2$ (95.3%), Na_2SO_4 (101%), and potassium chloride (≥99.5%) were all obtained from BDH Laboratory Supplies. Methacrylic acid (99.0%) was from Avocado Research Chemicals Ltd. (Lancashire, UK). Cerium (IV) ammonium nitrate (>99%) was purchased from Acros (Thermo Fisher Scientific Ltd., Loughborough, UK). Deuterium oxide (>99.92% D) was obtained from Apollo Scientific Ltd. (Stockport, UK).

Silica particles were kindly provided by Ortwin Rave Produkte and Dienstleistungen (Koblenz, Germany); Bioglass® (45S5, mean particle size < 5 μm) was a kind gift from Schott Glass (Mainz, Germany) and has a composition of 45% SiO_2, 24.5% Na_2O, 24.5% CaO, and 6% P_2O_5 (wt %), as the same as that of the first bioactive glass reported in 1971[546]. Hypermer 2296 was kindly supplied by UNIQEMA (Wirral, UK).

Distilled water was obtained from a Merit Water Still W4000 & W4000/Euro (Bibby Sterlin Ltd., Bargoed, UK). Amberlyst 15 was activated by using an aqueous HCl solution [5% (w/v)] at a volume ratio of 555 ml HCl solution/100 ml moist resin and was rinsed with distilled water in a column to neutral pH before use. DVB and styrene were purified through an aluminum oxide (active neutral, Merck, Germany) column to remove the inhibitors before use.

7.2 Synthesis and purification of poly(NIPAAm-*co*-AA) microgel particles

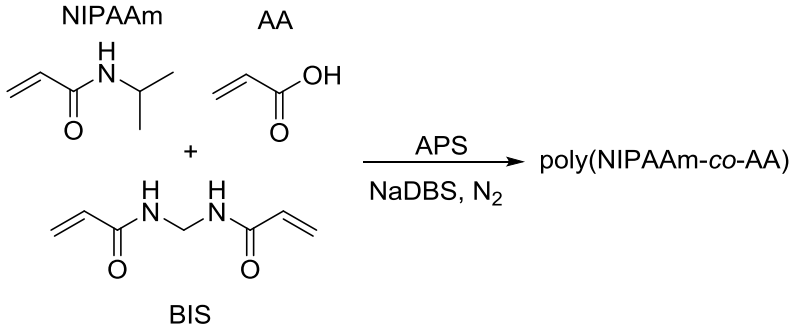


Fig. 7.1 Synthesis of poly(NIPAAm-*co*-AA) microgel particles

Poly(NIPAAm-*co*-AA) microgel particles (GP) were synthesised using a slightly modified protocol as described in the literature.[270,272] The free radical polymerisation was carried out in aqueous medium containing surfactant NaDBS (**Fig. 7.1**) and two feed ratios (molar) of NIPAAm, BIS and AA were used in this thesis, 94:1:5 (**GP1**) and 93:2:5 (**GP2**).

To synthesise **GP1** (batch 1 of GP), NIPAAm (6.38 g, 54.7 mmol) and BIS (0.093 g, 0.60 mmol) were mixed with 150 ml of an aqueous NaDBS solution (0.01 M) in a 250 ml three-necked round-bottom flask equipped with a condenser and a stirrer bar. AA (0.21 ml, 3.0 mmol) was then injected into the mixture. The monomer solution was made oxygen free by bubbling nitrogen at a speed of 2-3 bubbles per second through the reaction mixture for 30 min, and then above the solution surface for another 1 h. The polymerization was initiated by adding 0.5 ml of APS solution [7.5% (w/w)], which had been purged by bubbling N_2 in the same way as applied to the reaction mixture. The reaction lasted for 2 h at 60 °C with a stirring speed of 200 rpm, and then was terminated by introducing air into the flask. The gel particle suspension was purified by using dialysis (MWCO 12,000-14,000, Medicell International Ltd., UK) and an ionic exchange process and finally lyophilized for 2-3 days

using a Christ Alpha 1-2 LD Freeze drier. In synthesis of **GP2**, same procedures were followed except that NIPAAm (6.31 g, 54.1 mmol), BIS (0.185 g, 1.19 mmol) and AA (0.21 ml, 3.0 mmol) were used.

Six batches of **GP1** were prepared and employed in this thesis labeled as **GP1-1** to **GP1-6**. Particle size measurements were used to characterise microgel particles (**Section 7.3**).

The purification procedures of microgel particles were compared among **GP1-1**, **GP1-2**, **GP1-3** and **GP1-4**. Four factors involved in the procedure are coded as follows: (1) treatment of dialysis tubing, either simply washing with water (D) or following a three-step procedure[342] involving treatment with sodium sulfide and sulfuric acid (DT); (2) dialysis temperature, room temperature (20) or 60 °C (60); (3) dialysis type, either alkaline dialysis (OH) or acidic dialysis (H); (4) exchange resin, whether apply (EX) or not. For example, **GP1-1** was purified with procedure D20-OH-EX.

GP1-5, **GP1-6** and **GP2** were purified with simplified procedures. The dialysis tubing was only washed with running water and distilled water before use and dialysis was carried out at 60 °C against distilled water. Also, conductivity of the aqueous media was measured with a Hanna portable conductivity meter (HI 8733N, Fisher, UK). Dialysis was stopped once conductivity of the dialysis media showed no significant difference from that of distilled water at 60 °C (3-5 μS).

7.3 Analytical techniques and characterisation methods

NMR Spectroscopy ^{1}H NMR (400 MHz, D_2O) spectra were recorded on a Bruker DRX400 spectrometer at RT and processed with MestRe-C software (version 4.7.0.0.) using reference peak of HDO at 4.79 ppm.

Particle size measurement Hydrodynamic diameters (D_h) or particle sizes of the gel particles were measured in suspensions with predetermined concentrations of KCl (background electrolyte), particle concentrations and pH values based on dynamic light scattering (DLS). Gel particles were first weighed in a 50 ml plastic tube (Bibby Sterilin Ltd., UK). Then the required volume of KCl solution was calculated according to the target composition, measured from a stock solution with a 10 ml glass pipette (± 0.1 ml) and transferred to the tube, which was then sealed with screw cap and manually shaken at a frequency of 3-5 per second for about 1 min. The volume of gel suspension in one tube was normally controlled below 25 ml. Overnight or at least a few hours' rest was necessary before

the air bubbles produced in the tube gradually disappeared. The pH value was adjusted subsequently by using HCl solutions (pH 1 and pH 3) and KOH solutions (pH 12 and pH 13) and measured at RT with a Jenway Model 4330 Conductivity/ pH meter (Dunmow, UK) or an Euteck CyberScan PH11 pH/mV/C meter (Fisher, UK). Microgel suspensions prepared in other electrolyte solutions are specified elsewhere (**Section 7.4.6**). About 4 ml of the gel suspensions were pipetted or syringed into a disposable plastic cuvette, capped with a plastic lid and used for the particle size measurements, which were carried out using a Zeta PALS Zeta Potential Analyzer (Brookhaven Instruments Corporation, Worcestershire, UK) with a 35 mW diode laser at a scattering angle of 90° and using a Brookhaven Instruments Particle Sizing Software (9kpsdw32. exe ver. 3.81). The temperature of a tested gel suspension ranging from 10 °C to 70 °C was varied in situ via the instrument control. Each measurement result was obtained by using at least 5 runs and expressed in the form of mean ± standard error.

Optical microscopy Analysis was carried out on an optical microscope (BX51M microscope, Olympus UK LTD, Watford) equipped with an Olympus DP70 Digital Microscope Camera (12.5 mega pixels). For emulsion samples, a few emulsion drops were pipetted and placed on a cavity slide (76×26×1.35 mm, 1 cavity, ϕ 15-18mm, depth 0.6-0.8 mm, VWR, UK) and then sealed with a piece of cover glass before observation.

Photographs Four cameras were employed to take photographic images in this thesis: (1) a Nokia 6300 cell phone camera (2 mega pixels); (2) a Nokia N86 cell phone camera (8 mega pixels) (3) a Canon PowerShot A570 IS camera (7 mega pixels); (4) a Nikon D60 camera (10 mega pixels).

Scanning Electron Microscopy (SEM) Morphologies of polymerised products after purification and drying were characterised with three different instruments at RT in this thesis: (1) a JEOL JSM-5300 Scanning Electron Microscope (SEM) together with an Agar Auto Sputter Coater; (2) a JEOL JSM 5000 SEM together with an EMITECK K550 Sputter Coater; (3) a Hitachi S-3400N SEM performed either under variable pressure mode using an environmental secondary electron detector (ESED) for uncoated specimens or under normal SEM mode for specimens coated by an Agar Auto Sputter Coater. Porous structures were analyzed using Image-Pro® Plus (version 6.00.260, Media Cybernetics Inc.) where necessary.

Energy-dispersive X-ray spectroscopy (EDX) was carried out using a Hitachi S-3400N SEM fitted with an Oxford Instruments INCA 350 with X-act liquid nitrogen free detector and using software INCA suite version 4.11 (Oxford Instruments Analytical Limited, UK).

Cryo-SEM was carried out using a Hitachi S-3400N SEM equipped with an Alto 2100 Prep-Chamber (Gatan UK) as shown in **Fig. 7.2**. Detailed descriptions of the instrument and operations can be referred to the handbook.[504] A brief introduction of the process is given here (**Fig. 7.3**). In specimen mounting, a small sample piece was cut out of the bulk sample using a surgical scalpel (Swann-Moiton®, UK) and bound onto a copper stage with grove using glue named as Tissue-Tek® O.C.T™ compound (Sakuara Finetek Europe). The copper stage was subsequently connected to the transfer rod of vacuum transfer device (VTC) before slushing with LN_2. Sublimation of specimen after fracturing was to remove surface solvent and achieved by increasing the temperature of Gatan SEM Cold Stage Module in the SEM chamber. The vapors were condensed onto an Anti-contaminator, which was set at a temperature 10 °C lower than the cold stage. Keypad [**Fig. 7.2** (B)] was the control panel for cryo-preparation. SEM chamber was maintained at low temperature via cold N_2 gas supplied by (D) while the preparation chamber was cooled via LN_2 filled from (A)-4. Sublimation conditions used in the investigations of pore throat formation in poly(KAA) Pickering-HIPEs were varied (**Table 7.10**).



Fig. 7.2 Set-up for cyro-SEM: (A) Preparation chamber (1-Vacuum transfer device (VTD), 2-Pump assembly box, 3-Optical microscope, 4-Liquid N_2 filling port, 5-Sputter coater, 6-Fracture knife, 7-Ball valve assembly); (B) Keypad; (C) Slushing station; (D) Liquid N_2 bucket; (E) SEM chamber.

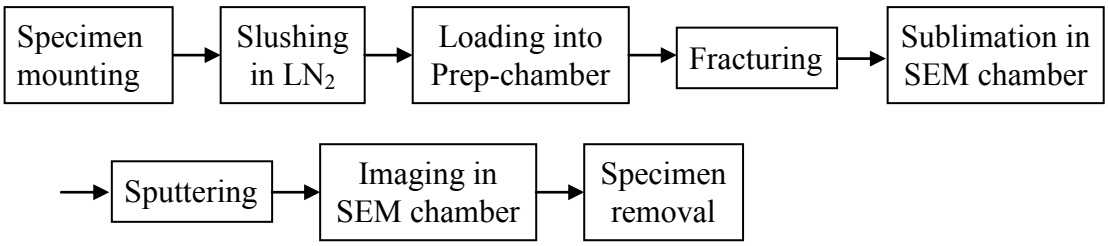


Fig. 7.3 Schematic process of a cryo-SEM experiment

Porosities of rigid polyHIPEs[139,142] Skeleton densities ($\rho_{skeleton}$) were measured with an AccuPyc1330 helium pycnometer (Micrometrics Ltd, Danstable, UK) using sample powders that can cover about half of the cell volume (12.0 ml). Envelope densities ($\rho_{envelope}$) were measured on a GeoPyc1360 Envelope Density Analyzer (Micrometrics Ltd, Danstable, UK) using Micromeritics DryFlo™ as the displacement medium. And porosity can be calculated according to Equation (7.1)

$$\text{Porosity} = (1 - \frac{\rho_{envelope}}{\rho_{skeleton}}) \times 100\% \quad \text{(7.1)}$$

Surface areas by gas adsorption[618] The nitrogen adsorption-desorption isotherms were obtained with a Micromeritics Tristar Surface Area and Porosity Analyzer at 77 K and using software Tristar 3000 v6.07. Prior to test, sample pieces of polyHIPEs were placed in a 3/8-inch bulb sample cell and degassed using a Micromeritics FlowPrep 060 Sample Degas System with helium flow at a rate of about 2 ml/min. Samples of poly(St/DVB) HIPEs (0.2018 g) was degassed at 100 °C for 12 h while poly(KAA) Pickering-HIPEs (20-100 mg) were degassed at 60 °C for various durations (**Table 7.11**). Surface areas were determined according to the Brunauer-Emmett-Teller (BET) method.[619,620]

Mercury Intrusion Porosimetry (MIP)[618] Porosity measurements of poly(KAA) Pickering-HIPEs were performed using a Micromeritics AutoPore IV 9500 mercury intrusion porosimeter at both low pressure (0-345 kPa) and high pressure (up to 228 MPa) and using software Autopore IV9500 v. 1.09. The penetrometer used has a capillary stem volume of 1.10 ml and a total volume of 3.99 ml. Calculations were based on the Washburn Equation[621] applying the physical properties of mercury: surface tension of 485.00 dyn/cm; density of 13.53 g/ml; contact angle of 130°. Sample pieces of size less than 0.5 mm in either dimension were cut out of the bulk piece in an inflatable glove chamber (Glove Bag™, Glas-Col®, Model X17-17, Indiana, US) filled with dry N_2 gas.

Liquid displacement Porosities of poly(KAA) Pickering-HIPEs were also assessed using liquid displacement[220,521-524] with hexane[220,524] or *p*-xylene[525] as the displacement liquid. A sample piece of known weight ($\mathbf{W_{dry}}$) was first immersed into the liquid and then removed when the volume of liquid became stable. 3 volumes, $\mathbf{V_1}$, $\mathbf{V_2}$ and $\mathbf{V_3}$ were recorded and used for the calculation of foam density, skeleton density and porosity with Equation (7.2), (7.3) and (7.4). $\mathbf{V_1}$ is the volume of liquid without sample; $\mathbf{V_2}$ is the stable volume recorded after sample is immersed into the liquid for long enough; $\mathbf{V_3}$ is the volume of remaining liquid recorded after the wet sample is taken out. Sample pieces of suitable size were cut out of the bulk materials in acetone and dried under vacuum before test.

$$\rho_{foam} = \frac{W_{dry}}{V_2 - V_3} \quad \text{(7.2)}$$

$$\rho_{skeleton} = \frac{W_{dry}}{V_2 - V_1} \quad \text{(7.3)}$$

$$\text{Porosity} = \frac{V_1 - V_3}{V_2 - V_3} \times 100\% \quad \text{(7.4)}$$

Thermal Analysis Thermal gravimetric analysis (TGA) was carried out using a Q500 Thermalgravimetric Analyzer and software TGA Q500 v6.7 Build 203 (TA Instruments). Sample pieces were placed in a platinum sample pan and tested in either air or N_2 atmosphere. Differential scanning calorimetry (DSC) was performed with a DSC Q2000 Differential Scanning Calorimeter and software DSC Q2000 v24.4 Build 116 (TA Instruments) using pan (Tzero Pan 901683.901) and pan lid (Tzero Hermetic Lid 901684.901). TGA and DSC data were analyzed using Universal V4.7A (TA Instruments).

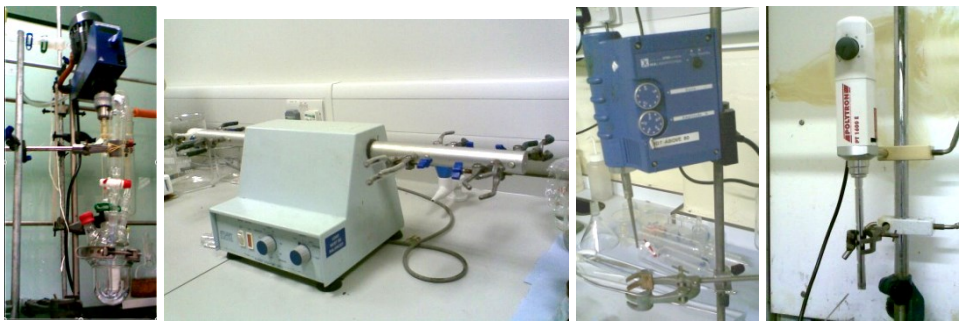
UV-vis spectroscopy All spectra were collected using a Perkin-Elmer Lamda 25 UV/Vis spectrophotometer over the range of 200-500 nm with 1 nm resolution at 20±2 °C. 1 cm path length quartz cuvettes were re-used during the tests by washing with distilled water and acetone in sequence and drying with N_2 flow. Background correction was performed using phosphate buffer (10 mM, pH 6.5) at both positions. Five tests were performed for each sample.

7.4 Preparation and characterisation of emulsions, HIPEs and polyHIPEs

7.4.1 Preparation of poly(styrene/DVB) HIPEs using surfactants as the emulsifier

HIPEs were prepared using an assembled mechanical stirrer [**Fig. 7.4** (a)], which consists of a mechanical overhead stirrer (IKA, RW 20 Digital), a reaction vessel (Soham Scientific, Fordham, UK), an anchor-shaped glass paddle (Soham Scientific, Fordham, UK), a stirrer bearing (Sigma-Aldrich, UK) and a dropping funnel. The oil phase (20 vol %) containing styrene (4 ml, 34.9 mmol), DVB (4 ml, 22.5 mmol), AIBN (0.105 g, 0.636 mmol) and Hypermer2296 (2 ml) was first added into the vessel. KCl aqueous solution (40 ml, 0.068 M) was then added dropwise into the oil mixture through a dropping funnel. Stirring speed was kept at 400 rpm during the addition at RT. And finally the mixture was stirred at 2000 rpm for another 5 min. HIPEs were obtained and transferred into a 50 ml plastic tube, sealed with a screw cap and placed into an oven at 70 °C for 1 d.

Afterwards, the polymerised products were removed from the tube and purified at RT by soaking in distilled water for 25 h and methanol for 39 h sequentially. Drying was carried out at 70 °C first in a convection oven for 6-7 h and then under vacuum until constant weight. The morphology of resultant polyHIPEs was characterised by SEM (1). Surface area was determined using a Micromeritics Tristar Surface Area and Porosity Analyzer. Densities and porosities were determined using an AccuPyc1330 helium pycnometer and a GeoPyc1360 Envelope Density Analyzer.



(a) (b) (c) (d)

Fig. 7.4 Apparatus used in emulsion preparation: (a) assembled mechanical stirrer; (b) flask shaker; (c) ultrasonic nozzle; (d) rotor-stator homogenizer.

7.4.2 Microgel particles stabilised emulsions using DVB as the oil phase

7.4.2.1 Emulsions prepared using microgel suspensions at pH 5

A POLYTRON PT 1600 E homogenizer with 1 cm head [**Fig. 7.4** (d)] was used for emulsification. Microgel suspension and DVB with determined volumes (**Table 7.1**) were put into a 50 ml plastic tube in sequence without mixing. For RT as the preparation temperature, homogenisation was carried out at 15, 000 rpm for 150 s with an interval of 1-2 min every 30 s. In the case where an elevated preparation temperature was used, the plastic tube containing microgel suspension and DVB was thermostatted to the temperature using an oil bath prior to homogenisation. For comparison, **No.1**~**No.5** were also prepared by manually shaking the plastic tube at a frequency of 3-5 per second for about 30 s at RT. Photos of the samples were taken with camera (1).

Table 7.1 Preparation of emulsions using DVB and microgel aqueous suspension of pH 5

No.	Preparation temperature	Microgel suspension			DVB volume /ml
		Composition	pH	Volume /ml	
1	RT	0.2 wt % in 1 mM KCl solution	5	2	8
2	RT	0.2 wt % in 1 mM KCl solution	5	4	6
3	RT	0.2 wt % in 1 mM KCl solution	5	5	5
4	RT	0.2 wt % in 1 mM KCl solution	5	6	4
5	RT	0.2 wt % in 1 mM KCl solution	5	8	2
6	RT	0.02 wt % in 1 mM KCl solution	5	6	4
7	RT	0.1 wt % in 1 mM KCl solution	5	6	4
8	RT	0.4 wt % in 1 mM KCl solution	5	6	4
9	40 °C	0.2 wt % in 1 mM KCl solution	5	8	2
10	50 °C	0.2 wt % in 1 mM KCl solution	5	8	2
11	65 °C	0.2 wt % in 1 mM KCl solution	5	8	2

For **No.1**~**No.8**, emulsion type and stability were recorded at t_1 = 20 min and t_2 = 20 h after preparation and optical microscopic analysis were carried out after the emulsion volumes became constant. Afterwards, AIBN (1.25 mol % relative to DVB) was mixed into **No.2**~**No.8** through homogenizing for 1 min at RT. Then the plastic tubes were sealed and

placed into an oven at 70 °C for 24-40 h. Polymerized products were removed from the plastic tubes, purified at RT with water and methanol and finally dried before characterized with SEM (1). The stability of emulsions prepared at 40 °C, 50 °C and 65 °C (No.9~No.11) was observed at RT after they were transferred into volumetric cylinders (10±0.1 ml).

7.4.2.2 Emulsions prepared using microgel suspensions at pH 2.5, 3 and 4

Using the established homogenising conditions (**Section 7.4.2.1**), different preparation temperatures were investigated for the emulsification of microgel suspensions of pH 3 and 40 vol % DVB (**Table 7.2**). AIBN (46.1 mg, 28.1 mmol) was dissolved into DVB (4 ml, 22.5 mmol) in a 50 ml plastic tube before 6 ml microgel suspension was added. The temperatures before and after homogenising and the sample states were recorded. Samples were then sealed and put into a 70 °C oven for 24 h. The polymerised products were purified and dried using the same procedures as described in **Section 7.4.2.1** and finally characterised with SEM (2).

Table 7.2 Emulsification of DVB and microgel suspension of pH 3 at different temperatures

No. *	$T_{preparation}$ /°C		Microgel suspension			DVB volume /ml
	Start	End	Composition	pH	Volume /ml	
1	18.5	22	0.4 wt % in 1 mM KCl solution	3	6	4
2	22	34	0.4 wt % in 1 mM KCl solution	3	6	4
3	34	34	0.4 wt % in 1 mM KCl solution	3	6	4

*Water baths of 18.5 °C and 34 °C were used in No.1 and No.3, respectively; no temperature control measure was used in No.2.

Particle sizes were measured using microgel suspensions (0.4 wt % and 0.6 wt) in 1 mM KCl solutions of pH 2.5, 3 and 4. Emulsions were prepared using DVB and microgel suspension of pH 2.5, 3 and 4 at different preparation temperatures ($T_{preparation}$). The obtained emulsions were transferred into graduated glass tubes (20 ml), sealed and placed in water baths with controlled temperatures (T_{ageing}) for stability observation (**Table 7.3**). Stability was recorded by observing the volume change of the emulsions over time. Optical microscopic samples were prepared using cavity slides at different time points during the ageing process.

Table 7.3 Stability study on microgel particles stabilised emulsions containing DVB

No.	Emulsion composition				Temperatures[#]		
	Microgel suspension*			DVB /ml	$T_{preparation}$ /°C	$T_{emulsions}$ /°C	T_{ageing} /°C
	Concentration	pH	Volume /ml				
1	0.4 wt %	3	6	4	16	22.5	24-26
2	0.4 wt %	3	6	4	15	21	31.5-32.0
3	0.4 wt %	3	6	4	15	21.5	37
4	0.4 wt %	2.5	6	4	15	21	25.0-25.5
5	0.4 wt %	2.5	6	4	16	24	31-32
6	0.4 wt %	4	6	4	50	-	50
7	0.4 wt %	4	6	4	37-38	-	50
8	0.4 wt %	4	6	4	15	21	50
9	0.4 wt %	4	6	4	16	22	25
10	0.8 wt %	4	6	4	15	21	25-25.5
11	0.8 wt %	4	6	4	15	24	50

*Microgel suspensions were all prepared in 1 mM KCl solution. [#]$T_{preparation}$: temperature of the water bath before homogenising; $T_{emulsions}$: temperature of the emulsions after homogenisation; T_{ageing}: temperature of the water bath used for stability (ageing) study.

7.4.2.3 Polymerisation of microgel particles stabilised water-in-DVB HIPEs

The preparation of microgel particles stabilised water-in-DVB HIPEs and poly(DVB) Pickering-HIPEs was carried out using 80 vol % DVB and microgel suspensions (0.4 wt % in 1 mM KCl solution) of pH 4. Initially, emulsification was carried out using a rotor-stator homoginizer at the speed of 15,000 rpm for 2.5 min. After microgel suspension (8 ml) and DVB (2 ml, 11.2 mmol) containing AIBN (23.1 mg, 0.141 mmol) were put into a plastic tube (50 ml) and thermostatted at 37 ºC water for 6 min, homogenising was applied using a procedure of (1.5 min on→ 2 min off→ 0.5 min on→ 2 min off→ 0.5 min on→ 2 min off). The sample was then sealed and placed in an oven at 70 ºC for polymerisation. The polymerised product was purified at RT by soaking into water and methanol for 1 d, respectively, and finally dried at 60 ºC.

Alternatively, HIPEs were prepared using assembled mechanical stirrer [**Fig. 7.2** (a)]. DVB (5 ml, 28.1 mmol) containing AIBN (57.6 mg, 0.351 mmol) was put into the reaction vessel and thermostatted using a 45 °C water bath. Microgel suspension (20 ml) was added

either through a dropping funnel in one route or through a modified column in condenser (**Fig. 7.5**) in another route. The difference between the two apparatuses was that temperature of the microgel suspension could be controlled in the latter case. When dropping funnel was used for addition of the microgel suspension into DVB (1 drop/ 3 s), stirring speed was kept at 400 rpm. The resultant emulsions were divided into two parts, which were polymerised either at 70 ºC for 24 h or at 50 ºC for 3 d. The polymerised products were purified at RT by soaking into water and methanol for 1 d, respectively, and finally dried at 60 ºC. When using the modified column in condenser for addition of microgel suspension, water (40 ºC) was circulated through the condenser to warm up the suspension inside the column. Microgel suspension (20 ml) was added (1 drop/ 3 s) into the reaction vessel (thermostatted at 40 ºC) while stirring was kept at 400 rpm. After the addition was finished, stirring was continued at 400 rpm for extra 30 min before increased to a higher speed, such as 600, 800 and 1000 rpm for 10 min. The obtained emulsions were quickly transferred into a glass vial (ext. diameter, 25 mm), capped and placed into a water bath (40 ºC) in front of a UV lamp (365 nm, 100W, UVP B-100 AP, Blak-Ray®, UK) with the centre distance of 15.5 cm. The UV exposure was stopped every 30 min to facilitate a 120º rotation of the glass vial. In total, UV light was used about 1.5 h. Samples were left in the bath (40 ºC) for 24 h in total. Polymerised samples were purified through Soxhlet extraction with water for 24 h and with methanol for another 24 h and finally dried at 60 ºC under vacuum. Morphologies of all the resultant polymers were characterized with SEM (2). Densities and porosities were determined using an AccuPyc1330 helium pycnometer and a GeoPyc1360 Envelope Density Analyzer.



Fig. 7.5 A modified column in condenser for the addition of microgel suspensions. The apparatus was connected to the neck of the vessel lid. Microgel suspension in the column was warmed up by circulated water in the condenser and added through the needle into the vessel containing DVB.

7.4.3 Poly(KAA) Pickering-HIPEs prepared from microgels stabilised o/w HIPEs

7.4.3.1 Selecting aqueous suspensions and organic solvents for HIPE preparation

Potassium acrylate (KAA) stock solution was prepared by neutralizing acrylic acid with KOH solution (3.0 M). The concentration of leading KAA solution was calculated using the following equation:

$$C_{KAA} = \frac{1000 d_{AA} V_{AA}}{M_{AA}(V_{AA} + V_{KOH})} \quad \text{……..……. (7.5)}$$

where d_{AA} is the density of AA, 1.051 $g.cm^{-3}$; M_{AA} is the molecular weight of AA, 72.06 $g.mol^{-1}$; V_{AA} and V_{KOH} are the volumes of AA and KOH in ml. KAA concentration of different batches is 2.56 ± 0.07 M.

This stock solution was mix with distilled water at different volume ratios to make up a series of 4 ml KAA solutions of different concentrations. Microgel suspensions (0.8 wt % in 1 mM KCl solution, 1 ml) were then mixed with the KAA solutions to make up the aqueous mixtures (5.0 ml) for HIPE preparation. Photos of microgel particles in these solutions were taken both at 25 ºC and at 32 ºC.

Above aqueous mixtures (5 ml) and selected oils (20 ml) were used for emulsion preparation (**Table 7.4**). The emulsification was carried out using assembled mechanical stirrer. In the cases where the one-speed stirring protocol was used, emulsion was stirred at 400 rpm for 30 min after addition of the oil was finished. For the two-speed stirring protocol, addition of the oil was carried out at the low speed; stirring was continued at this low speed for another 25~40 min after addition of oil; stirring at the high speed (1000 or 2000 rpm) was then uses for 5~10 min. The obtained emulsions were then transferred into a glass tube, sealed with a PE cap and left either at RT or at the selected temperature (e.g., 30 °C) for stability observation. Images of the samples were taken by camera (1). Particle size measurements were carried out using microgel suspensions (1.6 mg/ml and 3.2 mg/ml) in KAA solutions (0.82 M). Optical microscopic analysis was carried out on hexane-in-water HIPEs (**No.9** and **10** in **Table 7.4**) after the emulsion volumes became constant.

Table 7.4 Emulsification of microgel suspension in KAA solutions with various oils

No.	Microgel suspensions			Oil	Stirring protocol /rpm	Preparation temperature /°C
	[KAA] /M	[Microgel] /mg.ml^{-1}	Crosslinking degree of microgels /mol %			
1	1.33	1.6	1	Toluene	400	RT
2	1.12	1.6	1	Toluene	400	RT
3	1.02	1.6	1	Toluene	400	RT
4	0.92	1.6	1	Toluene	400	RT
5	0.82	1.6	1	Toluene	400	RT
6	0.82	1.6	1	Toluene	400→1000	RT
7	0.82	1.6	1	Toluene	400→2000	RT
8	0.82	3.2	1	Toluene	400→1000	RT
9	0.82	1.6	1	Hexane	426→1000	RT
10	0.82	1.6	1	Hexane	420→2000	RT
11	0.82	1.6	1	Hexane	430→1000	31~32
12	0.82	4.0	1	Hexane	420→1000	RT
13	0.82	1.6	2	Hexane	430→2000	RT
14	0.82	1.6	1	Cyclohexane	415	RT

7.4.3.2 Selecting crosslinker and initiator for polymerisation of HIPEs containing KAA

Three crosslinkers including di(ethyleneglycol) divinyl ether (DEGDVE), *N,N'*-isopropylacrylamide (BIS) and 1, 5-hexadiene-3, 4-diol as well as two initiating systems including APS/TMEDA and photo-initiator Irgacure2959 (I2959) were investigated. In the study, 5 ml aqueous solutions containing KAA (0.85 M), microgels (1.6 mg/ml), crosslinker and initiator were emulsified with 20 ml oil phase. The amount of crosslinker used was either 10 mol % or 20 mol % relative to KAA amount.

In the cases where APS and TMEDA were used for initiation, APS was mixed into the aqueous phase (2 mol %, relative to the total amount of double bonds) prior to emulsification. TMEDA was added during the stirring process, which was investigated together with the crosslinkers and stirring protocol (**Table 7.5**).

Table 7.5 Polymerisation of microgel-stabilised o/w HIPEs using redox initiation

No.	Oil phase	Crosslinker	Stirring protocol /rpm #	Adding TMEDA *	After adding TMEDA
1	Hexane	20 mol % DEGDVE	400→1000 (10 min)	0.05 ml, -3 min	(Emulsification at 32 °C) Phase separated after adding.
2	Toluene	20 mol % DEGDVE	400→1000 (5 min)	0.05 ml, -3 min	~12 ml oil out.
3	Toluene	20 mol % DEGDVE	400→1000 (2 min)	0.05 ml, -5 min	1.3 ml oil out; HIPEs can still flow after left at 30 °C for >15 h.
4	Toluene	10 mol % BIS	400	0.02 ml, -3 min	Stable HIPEs obtained; polymerised after left at 31 °C for 60 h (3.7 ml oil out).
5	Hexane	10 mol % BIS	400→1000 →400(3 min)	0.02 ml, -3 min	Stable HIPEs obtained; phase separated after left at 31 °C.
6	Toluene	10 mol % BIS	400→1000 (8 min)	0.02 ml, -3 min	Phase separated, ~13.3 ml oil out.
7	Toluene	10 mol % BIS	400→1000→ 245 (3 min)	0.02 ml, -3 min	0.55 ml oil out; HIPEs can flow after left at RT for 52 h; polymerised after left at 31 °C, 3.7 ml more oil out.
8	Toluene	10 mol % 1, 5-hexadiene-3, 4-diol	400	0.02 ml, -3 min	Stable HIPEs obtained; still can flow after 40 h at 31 °C.
9	Toluene	10 mol % 1, 5-hexadiene-3, 4-diol	400→1000→ 240 (3 min)	0.02 ml, -3 min	0.8 ml oil out; phase separated after left at 31 °C.

#Time in the bracket indicated duration of the stirring at that speed; * volume of TMEDA and the adding point calculated from the end of stirring.

In the cases where photo-initiator I2959 was used, I2959 and BIS were dissolved into the aqueous solution prior to emulsification with toluene using the one-speed stirring protocol (400 rpm). The obtained HIPEs were transferred into a glass tube (external diameter: 25 mm), sealed and put into a water bath in front of a UV lamp. The centre distance between UV lamp and glass tube was fixed at 13.5 cm. The glass tube containing HIPEs was either manually or continuously rotated during photo-polymerisation. For manual rotation, the glass tube was rotated 120° every 10-15 min and the UV exposure hence followed a procedure of (15 min on→15 min off→10 min on→15 min off→10 min on). For continuous rotation, the glass tube was rotated at a speed of 50~70 rpm in the water bath using an overhead stirrer during UV exposure (**Fig. 7.6**).

Polymerised samples were taken out of the glass tube by cracking the glass with a diamond knife and purified using Soxhlet extraction with HCl in MeOH solution (0.8 M) for 1 d and extraction with acetone for 1 d in sequence. Finally, samples were dried under vacuum. Morphologies of the obtained polyHIPEs were characterised using SEM (3). Particle size measurements were carried out using microgel suspensions (1.6 mg/ml) in KAA solutions (0.85 M) with and without BIS (10 mol %) and I2959 (2 mol %).



Fig. 7.6 Set-up for UV-polymerisation of o/w HIPEs. The glass tube containing HIPEs was rotated at a stirring speed of 50~70 rpm during UV exposure. A water bath was used to maintain the sample temperature around room temperature.

For photo-polymerisation using the continuous rotation protocol, the UV exposure time (t_{UV}) and the standing duration before purification (t_{stand}) were investigated (**Table 7.6**). For preparation of all the following polyHIPEs, argon was used to replace the air layer on top of the HIPEs in the glass tube prior to UV exposure and an UV exposure time of 1 h was used.

Table 7.6 Preparation of poly(KAA) Pickering-HIPEs using various t_{UV} and t_{stand}

No.		**1**	**2**	**3**	**4**
HIPE preparation	RT, °C	-	26	27	26.5
	$T_{water\ bath}$, °C	-	-	20	22.5
	Argon used	×	×	×	×
UV initiation	t_{UV}, min	30	60	60	30
	$T_{water\ bath}$, °C	25.5→26.6	25.9→28.0	21.8→25.9	21.8→23.4
t_{stand}		3 d	1 d	5 d	1 d
Soxhlet extraction	HCl in MeOH	0.8 M, 24 h	0.8 M, 24 h	0.8 M, 24 h	0.8 M, 24 h
	Acetone	24 h	24 h	24 h	24 h
Vacuum drying		50 °C	50 °C	50 °C	50 °C

The amount of I2959 necessary for photo-polymerisation of the o/w HIPEs was investigated by using 2.0, 1.5, 1.0 and 0.5 mol % I2959. Photos were taken after polymerisation. For preparation of all the following polyHIPEs, 2.0 mol % I2959 relative to total amount of double bonds was used unless otherwise stated.

7.4.3.3 Tuning the morphologies of poly(KAA) Pickering-HIPEs

Effects of the Soxhlet extraction and drying process on morphologies of poly(KAA) Pickering-HIPEs were investigated. The polyHIPEs were prepared using microgel suspension (1.6 mg/ml) in KAA solution (0.85 M) containing 10 mol % BIS and 2 mol % I2959 together with 80 vol % toluene. In contrast to the extraction and drying conditions stated in **Table 7.6**, various other conditions (**Table 7.7)** were used. Besides the route of two-step extraction and one-step drying sated in **Table 7.6**, three other routes were investigated (**Fig. 7.7**). In addition, a hydrogel sample was made by mixing polyHIPE piece (26.6 mg, **Table 7.6**) with distilled water (5.3103 g) in a round bottom flask and then frozen by LN_2 and freeze-dried.

Table 7.7 Various extraction and drying conditions for poly(KAA) Pickeirng-HIPEs

No.		**1**	**2**	**3**	**4***
Soxhlet extraction	HCl in MeOH	0.15 M, 40 h	0.15 M, 40 h	0.15 M, 40 h	0.15 M, 26 h
	Acetone	24 h	24 h	24 h	24 h
Drying		50 °C	70 °C	70 °C	60-70 °C

* A 1:1 (v/v) mixture of HCl in MeOH and distilled water was used instead of HCl in MeOH.

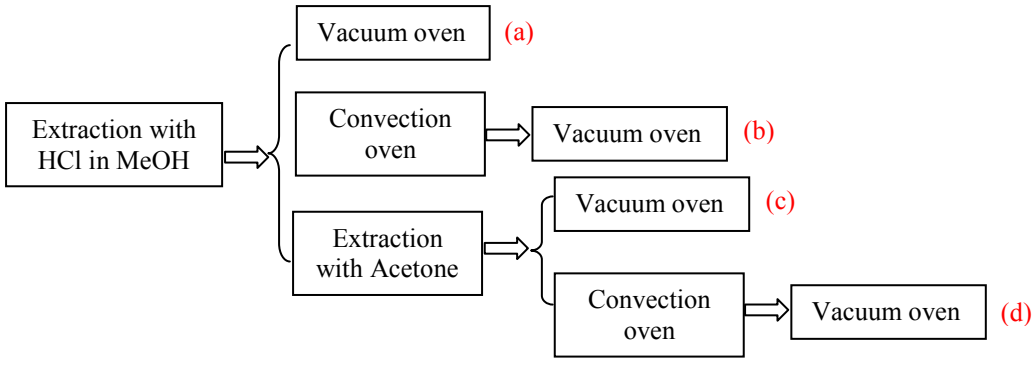


Fig. 7.7 Four purification-drying routes for poly(KAA) Pickering-HIPEs (a) One-step extraction and one-step drying; (b) one-step extraction and two-step drying; (c) two-step extraction and one-step drying; (d) two-step extraction and two-step drying.

For preparation of the following poly(KAA) Pickering-HIPEs, a purification-drying procedure (**Fig. 7.8**) was used unless otherwise specified. Polymerised HIPEs were taken out of the glass tube (Ext. diameter: 25 mm) by cracking the glass and then put into a thimble (Ext. diameter×Length, 28mm×80mm) for the subsequent Soxhlet extraction. In some cases, the polymerised HIPE sample was wrapped with a piece of toluene-wetted filter paper prior to putting into the thimble.

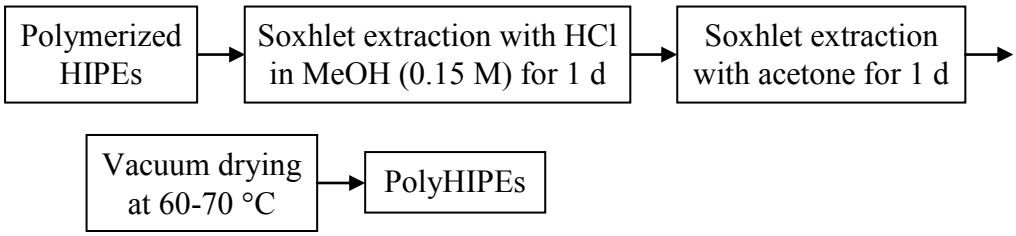


Fig. 7.8 An established procedure for purification and drying of poly(KAA) Pickering-HIPEs

To tune the morphology of poly(KAA) Pickering-HIPEs, a series of parameters involved in the preparation were varied (**Table 7.8**), including the internal phase volume ratio ($\phi_{int.}$), crosslinker content (relative to KAA amount), KAA amount, stirring speed and microgel concentration. For HIPEs prepared using 2.5 mol % BIS (**No.25** in **Table 7.8**), *p*-xylene was used instead of toluene as the internal phase in some cases. The resultant HIPEs were photo-polymerised and frozen in LN_2 and freeze-dried. When the one-speed stirring protocol was used for HIPE preparation, stirring was kept at 400 rpm during addition of toluene and for another 30 min after addition. For the two-speed stirring protocol, stirring was kept at 400 rpm during addition and for another 20 min after addition before finally increased to a higher speed for 10 min. Energy-dispersive X-ray spectroscopy (EDX) was used for polyHIPE elemental analysis during SEM observation.

To achieve a nominal $\phi_{int.}$ of 92.5%, several attempts were made using 2.5 ml aqueous solution and 31.5 ml toluene (**Table 7.9**). The aqueous solution contained 0.85 M KAA, 1.6 mg/ml microgels, 10 mol % BIS and 2 mol % I2959. The adding speed of toluene and the stirring protocol were varied. The volume of expelled toluene was measured for calculation of the actual $\phi_{int.}$.

Table 7.8 Poly(KAA) HIPEs prepared using various compositions and stirring protocols

No.	[KAA] /M	[Microgel] /mg.ml^{-1}	BIS content /mol %	$\phi_{int.}$ /vol %	Stirring protocol /rpm
1	0.85	1.6	10.0	80	One-speed (400)
2	0.85	1.6	10.0	85	One-speed (400)
3	0.85	1.6	10.0	90	One-speed (400)
4	0.85	1.6	7.5	80	One-speed (400)
5	0.85	1.6	5.0	80	One-speed (400)
6	0.85	1.6	4.0	80	One-speed (400)
7	0.85	1.6	3.8	80	One-speed (400)
8	0.85	1.6	3.6	80	One-speed (400)
9	0.85	1.6	3.4	80	One-speed (400)
10	0.85	1.6	3.2	80	One-speed (400)
11	0.85	1.6	2.5 (16.5 mg)	80	One-speed (400)
12	0.96	1.6	2.5 (18.5 mg)	80	One-speed (400)
13	0.75	1.6	5.0 (28.8 mg)	80	One-speed (400)
14	0.85	1.6	5.0 (32.9 mg)	85	One-speed (400)
15	0.96	1.6	2.5 (18.5 mg)	85	One-speed (400)
16	0.96	1.6	16.5 mg	80	One-speed (400)
17	1.07	1.6	16.5 mg	80	One-speed (400)
18	0.85	1.6	10.0	80	Two-speed (400→600)
19	0.85	1.6	10.0	80	Two-speed (400→700)
20	0.85	1.6	10.0	80	Two-speed (400→800)
21	0.85	1.6	10.0	80	Two-speed (400→1000)
22	0.85	1.6	5.0	80	Two-speed (400→1000)
23	0.85	1.6	4.0	80	Two-speed (400→1000)
24	0.85	1.6	3.2	80	Two-speed (400→1000)
25	0.85	1.6	2.5	80	Two-speed (400→1000)
26	0.85	16.0	2.5	80	Two-speed (400→1000)

Table 7.9 Preparation of o/w HIPEs for a nominal internal phase volume ratio of 92.5%

No.	Adding speed	Stirring at 400 rpm	1000 rpm	Actual $\phi_{int.}$
1	1 drop/3-4 s	4 h 30 min	N/A	90.6%
2	1 drop/ 3 s	2 h 15 min (adding) + 30 min	N/A	90.3%
3	1 drop/ 3 s	2 h 15 min (adding) + 30 min	N/A	88.6%
4	1 drop/ 1-2 s	1 h 15 min (adding) + 30 min	N/A	89.9%
5	1 drop/1-2 s	1 h (adding) + 1 h	10 min	Phase separated

Cryo-SEM investigations were carried out on polymerised HIPEs at three stages: (1) after photo-polymerization but before purification; (2) after Soxhlet extraction with MeOH; (3) after extraction with acetone but before vacuum drying. The samples used for this investigation were prepared following two of the compositions and stirring protocols (**No.22** and **No.25**) listed in **Table 7.8**, i.e., either 5.0 mol % or 2.5 mol % BIS content (relative to KAA) used. A series of sublimation conditions (**Table 7.10**) were used in the investigation.

Table 7.10 Conditions for cryo-SEM study on poly(KAA) Pickering-HIPEs

BIS content of the samples	Stage for investigation	Sublimation temperature /°C	Sublimation time
5.0 mol %	Stage (1)	-100	3 min 10 s
	Stage (2)	-110	3 min
		-86	3.5 min
	Stage (3)	-110	3 min
		-84 *	3 min
2.5 mol %	Stage (1)	-120	3 min
		-100	3 min 10 s
		-100	45 min
	Stage (2)	-110	3 min
		-86	3min
	Stage (3)	-84	3 min

* The sample used in this test was extracted with HCl in MeOH (0.15 M) for 1 d, followed with acetone for 3 d. All other Stage (3) samples were prepared through extraction with MeOH for 1 d, followed with acetone for 1 d. All Stage (2) samples were extracted with MeOH for 1 d.

7.4.3.4 Surface area measurements of poly(KAA) Pickering-HIPEs

Thermal gravimetric analysis (TGA) of poly(KAA) Pickering-HIPEs (**No.2** in **Table 7.8**, 7.797 mg) was carried out under a flow of N_2 gas, from 25 °C to 60 °C, at a heating rate of 10 °C/min. After maintained at 60 °C for 12 h, the sample was heated up to 150 °C at 10 °C/min and maintained for 1 h. The small pieces (< 5 mm in size) of polyHIPEs used for surface area measurements were prepared in two ways: (A) cut out of the bulk pieces in acetone and then dried under vacuum at ~70 °C; (B) torn with tweezers. Various degassing durations at 60 °C (**Table 7.11**) were used prior to the tests.

Table 7.11 Surface areas of poly(KAA) HIPEs measured using various degassing durations

Sample ID and cutting method #		Sample mass /g			Degassing duration /h			BET surface area /$m^2.g^{-1}$		
		1	2	3	1	2	3	1	2	3
No.1	A	0.0322	-	-	4	-	-	0.598	-	-
No.10	A	0.0344	-	-	4	-	-	0.100	-	-
No.11	A	0.0563	-	-	4	-	-	0.266	-	-
No.1	A	0.0430	0.0429	-	12	24	-	1.678	1.812	-
No.3	A	0.0723	0.0736	-	12	24	-	1.316	1.168	-
No.5	A*	0.0979	0.0966	-	4	12	-	0.002	0.022	-
No.6	B	0.0560	0.0457	-	4	12	-	0.368	0.452	-
No.12	A	0.0547	0.0498	-	4	12	-	0.282	0.250	-
No.13	B	0.0341	0.0387	0.0399	12	12	24	0.080	0.369	0.569
No.14	B	0.0233	0.0292	0.0273	12	12	24	0.002	0.273	0.644
No.15	B	0.0448	0.0497	0.0481	12	12	24	0.023	0.109	0.278
No.2	B	0.0349	0.0342	0.0341	23	12	24	0.409	0.981	1.330
No.4	A	0.0260	0.0266	0.0251	21	12	24	0.132	0.272	0.314
No.16	B	0.1043	0.1033	0.1035	20	12	24	0.017	0.082	0.083

Sample IDs are the same as the numbers in **Table 7.8**; *shrank to hard balls.

7.4.3.5 Porosity measurements of poly(KAA) Pickering-HIPEs

7.4.3.5.1 Porosity measurements using liquid displacement

Two set-ups were used for porosity measurements using liquid displacement. Firstly, each sample was immersed into a measuring cylinder (10 ml, ± 0.1 ml) containing hexane for

15~30 min. To prevent sample from floating, a metal block wrapped with a piece of thin cooper/steel wire (~10 cm) was put on top of the sample. The free end of the wire was curved as a hook that could fix to the top edge of the measuring cylinder. The volume of this metal block was included in V_1, V_2 and V_3 (refer to **Section 7.3** for what these volumes stand for). Porosities of three poly(KAA) Pickering-HIPEs were measured with this set-up (**Table 7.12**) and calculated using Equation (7.2)~(7.4).

Table 7.12 Porosity measurements using hexane as the displacement liquid

Sample #		W_{dry} /mg	V_1 /ml	V_2 * /ml	V_3 /ml	$W_{dry}/(V_2-V_3)$ /g.cm^{-3}	$W_{dry}/(V_2-V_1)$ /g.cm^{-3}	$(V_1-V_3)/(V_2-V_3)$ /%
No.1	1	16.5	6.45	7.00	6.25	0.0220	0.0300	26.7
	2	21.8	6.80	7.60	6.50	0.0198	0.0273	27.3
	3	12.6	6.20	6.68	5.90	0.0162	0.0263	38.5
No.2	1	11.26	6.20	6.40	6.09	0.0363	0.0563	35.5
	2	17.49	6.70	7.05	6.60	0.0400	0.0514	22.2
	3	10.15	7.30	7.48	7.10	0.0267	0.0564	52.6
	4	10.75	6.48	6.55	6.30	0.0430	0.1536	72.0
	5	15.78	7.00	7.17	6.90	0.0584	0.0928	37.0
No.6	1	22.2	6.40	6.90	6.19	0.0313	0.0444	29.6
	2	25.3	6.70	7.25	6.38	0.0291	0.0460	36.8
	3	19.2	7.38	7.70	7.18	0.0369	0.0600	38.5
	4	13.2	7.30	7.60	7.10	0.0264	0.0440	40.0
	5	24.0	7.00	7.49	6.68	0.0296	0.0490	39.5

Sample IDs are the same as the numbers in **Table 7.8**; * after an immersing duration of 15-30 min.

Secondly, evacuation-repressurization cycles[524] were used to drive air bubbles out of the polyHIPE sample through a self-designed device (**Fig. 7.9**). *p*-Xylene was used as the displacement liquid. "Evacuation" was the process to create a low pressure in the tube by exhausting air with a syringe and then quickly sealing the tube via a Young's tap. "Repressurization" was to open the tap when production of air bubbles became significantly slow. The glass tube was gently shaken to free those air bubbles attached to the sample surface. The cycle was repeated for a few times until no obvious production of air bubbles (40 min-2 h) visible. Porosities of five poly(KAA) Pickeirng-HIPEs were measured with this

set-up (**Table 7.13**) and calculated using Equation (7.2)~(7.4). Porosities of poly(St/DVB) HIPEs were also measured with this set-up in comparison with the data obtained before using an AccuPyc1330 helium pycnometer and a GeoPyc1360 Envelope Density Analyzer.

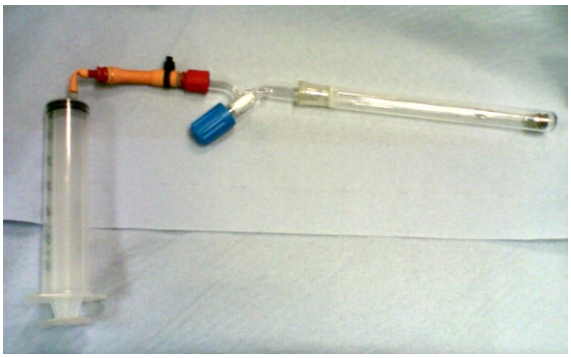


Fig. 7.9 Assembled device for density measurement using liquid displacement. The device was made up with a plastic syringe (50 ml), a two-way Young's tap, a graduated glass tube (20 ml, ± 0.1 ml), a wire-wrapped metal block, rubber tubings and connectors.

Table 7.13 Porosity measurements using *p*-xylene as the displacement liquid

Sample ID #		W_{dry} /mg	V_1 /ml	V_2 /ml	V_3 /ml	$W_{dry}/(V_2-V_3)$ /g.cm^{-3}	$W_{dry}/(V_2-V_1)$ /g.cm^{-3}	$(V_1-V_3)/(V_2-V_3)$ /%
No.1	1	21.54	17.55	17.78	16.86	0.023	0.094	75.0
	2	15.51	17.40	17.50	16.90	0.026	0.155	83.3
	3	22.80	19.20	19.50	18.50	0.023	0.076	70.0
No.2	1	28.70	17.59	17.65	16.80	0.034	0.478	92.9
	2	22.10	18.35	18.50	17.80	0.032	0.147	78.6
No.3	1	17.56	18.10	18.30	17.70	0.029	0.088	66.7
	2	11.88	17.55	17.80	17.30	0.024	0.048	50.0
	3	38.44	17.80	17.98	17.58	0.096	0.214	55.0
No.6	1	37.18	18.00	18.20	17.20	0.037	0.186	80.0
	2	25.70	16.81	16.95	16.20	0.034	0.184	81.3
	3	20.10	17.90	18.10	17.20	0.022	0.101	77.8
No.11	1	50.20	18.40	18.50	18.00	0.100	0.502	80.0
PS*	1	69.85	17.59	17.67	17.15	0.134	0.873	84.6
	2	83.45	16.80	16.90	16.20	0.119	0.835	85.7

Sample IDs are the same as the numbers in **Table 7.8**; * poly(St/DVB) HIPEs, 1 and 2 were measured using *p*-xylene and distilled water as the displacement liquid, respectively.

7.4.3.5.2 Porosities measurements using mercury intrusion porosimetry

Porosities of five poly(KAA) Pickering-HIPEs with BIS content of 10, 5, 4, 3.2 and 2.5 mol % were measured using mercury intrusion porosimetry (MIP) (**Table 7.14**).

Table 7.14 Porosity measurements of poly(KAA) Pickering-HIPEs using MIP

Sample #		Mass /g	Bulk density at 0.22 psia /g.cm^{-3}	Apparent density /g.cm^{-3}	Porosity /%
No.21	1	0.0295	0.029	0.408	92.9
	2	0.0493	0.038	0.293	87.0
	mean±std dev.	-	0.034±0.006	0.351±0.081	89.9±4.2
No.22	1	0.0787	0.086	0.629	86.3
No.23	1	0.0573	0.062	0.707	91.3
	2	0.0495	0.064	0.873	92.6
	mean±std dev.	-	0.063±0.002	0.790±0.118	92.0±1.0
No.24	1	0.0609	0.074	0.556	86.8
	2	0.0580	0.082	1.086	92.5
	3	0.0672	0.084	1.297	93.5
	mean±std dev.	-	0.080±0.005	0.980±0.382	90.9±3.6
No.25	1	0.0503	0.044	0.518	91.6
	2	0.0518	0.051	0.615	91.8
	3	0.0507	0.066	0.843	92.2
	mean±std dev.	-	0.053±0.011	0.659±0.167	91.8±0.3

Sample IDs are the same as the numbers in **Table 7.8**. The polyHIPEs were obtained by polymerising HIPEs that were prepared using 10, 5, 4, 3.2 and 2.5 mol % BIS contents and using the two-speed stirring protocol.

7.4.3.5.3 Porosity measurements using a designed indirect method

Two or three small cuboid-shaped pieces were cut out of the bulk polyHIPE sample using a surgical scalpel within an inflatable glove chamber filled with dry N_2. These small pieces of polyHIPEs were weighed, followed by dimension measurements (length × width × height) with a caliper in the glove chamber (**Table 7.15**). The foam densities of poly(KAA) Pickering-HIPEs were then calculated using the weights and volumes.

Table 7.15 Weights and dimensions of cuboid pieces of poly(KAA) Pickering-HIPEs

Sample #		Weight /g	Length /mm	Width /mm	Height /mm	Volumn /mm^3
No.21	1	0.01908	16.31±0.77	9.36±0.09	7.33±0.86	1118.78±141.77
	2	0.02761	17.46±0.74	11.01±0.09	6.63±0.41	1274.51±95.49
	3	0.01636	12.49±1.13	8.98±0.34	7.28±0.07	816.74±80.15
No.22	1	0.02905	13.53±0.54	8.93±0.63	6.78±0.24	819.97±72.61
	2	0.03225	15.77±1.41	7.28±1.09	6.64±0.56	763.28±148.02
No.23	1	0.01881	14.28±0.32	8.57±0.22	5.40±0.30	660.82±43.46
	2	0.02492	13.88±0.29	9.53±0.10	6.99±0.32	923.89±47.61
	3	0.01756	14.37±0.43	7.12±0.19	6.47±0.38	661.31±46.90
No.24	1	0.02179	12.72±0.31	7.37±0.37	5.84±0.45	548.00±51.74
	2	0.01558	12.78±0.31	9.25±0.62	5.52±0.87	652.42±113.13
	3	0.0235	13.54±0.29	8.24±0.83	5.69±0.37	634.75±77.31
No.25	1	0.02951	16.60±0.14	9.32±0.25	6.65±0.23	1028.53±45.57
	2	0.02145	13.54±0.48	9.65±0.55	6.28±0.40	821.24±76.13
	3	0.02443	16.88±0.39	9.71±0.37	6.19±0.50	1014.69±93.26

Sample IDs are the same as the numbers in **Table 7.8**. The polyHIPEs were obtained by polymerising HIPEs that were prepared using 10, 5, 4, 3.2 and 2.5 mol % BIS contents and using the two-speed stirring protocol.

The skeleton densities of poly(KAA) Pickering-HIPEs were measured using an indirect method. Polymer blocks (**PB1**~ **PB5**) were prepared by polymerising aqueous solutions with identical compositions to those of the aqueous phase of HIPEs (BIS content varied from 10, to 5, 4, 3.2 and 2.5 mol %). The obtained hydrogels after polymerisation were purified and dried in the same way as polymerised HIPEs. Before Soxhlet extraction, dimensions of the hydrogels (wet state) were measured. After drying, densities and volumes of the PBs (dry state) were measured with an Accupyc1330 helium pycnometer (**Table 7.16**). The obtained densities of PBs were taken as the skeleton densities of the corresponding polyHIPEs. Porosities of the polyHIPEs were then calculated using the obtained foam densities and skeleton densities according to Equation (7.1). Photos of PBs in the wet state and in the dry state were taken. The morphology of the surface of dried **PB1** and **PB5** were characterised with SEM (3).

Table 7.16 Dimensional measurements of polymer blocks in both wet and dry states

		PB1	**PB2**	**PB3**	**PB4**	**PB5**
BIS content		10.0 mol %	5.0 mol %	4.0 mol %	3.2 mol %	2.5 mol %
Wet	D /mm	24	18	23	23	23
	H /mm	16	11	23.5	24.5	22
	V /cm^3	7.238	2.799	9.764	10.179	9.141
Dry *	V /cm^3	0.438±0.001	0.448±0.001	0.952±0.001	0.778±0.001	0.835±0.001
	ρ /g. cm^{-3}	1.346±0.002	1.294±0.004	1.193±0.001	1.325±0.001	1.248±0.002

* One sample of each PB was measured for 10 times in the test. Values are mean ± standard deviation.

Dimensions of bulk poly(KAA) Pickering-HIPEs before Soxhlet extraction (wet) and after drying (dry) were measured (**Table 7.17**). Yields of the polyHIPEs were also calculated.

Table 7.17 Dimensions of poly(KAA) Pickering-HIPEs in the wet and dry states

Sample #	**No.21**	**No.22**	**No.23**	**No.24**	**No.25**
L_{wet} /mm	51.0	51.0	50.0	49.5	52.0
D_{dry}, /mm	21.1±0.1	19.9±0.9	19.3±0.2	17.7±1.0	19.3±1.6
L_{dry} /mm	54.4±1.4	48.1±0.7	44.5±1.0	41.9±1.2	42.7±0.4
Yield	89.0%	82.2%	85.2%	80.8%	79.3%

Sample IDs are the same as the numbers in **Table 7.8**. The polyHIPEs were obtained by polymerising HIPEs that were prepared using 10, 5, 4, 3.2 and 2.5 mol % BIS contents and using the two-speed stirring protocol. Values are mean ± standard deviation.

7.4.4 Preparation and characterisation of poly(KAA) Pickering-HIPE composites

In the preparation of poly(KAA)/silica Pickering-HIPE composites, BIS (3.2 mol % relative to KAA) and I2959 (2 mol %) were first dissolved into the KAA solution (4 ml, 0.82~0.85 M) in a glass tube. Microgel suspension (1.0 ml, 8 mg/ml in 1 mM KCl solution) and various amounts of silica (1, 5 10 and 15 wt %, relative the weight sum of BIS and KAA) were then mixed with the aqueous solution in the vessel prior to the addition of toluene (20 ml, 80 vol %). Emulsification was carried out using either the one-speed stirring protocol (400 rpm) or the two-speed stirring protocol (400→1000 rpm). As control (silica instead of microgels), emulsification was carried out at the stirring speed of 400 rpm using toluene (20 ml) and an aqueous suspension made up with silica particles (8 mg), KAA solution (4 ml, 4.27 mmol) and KCl solution (1 ml, 1 mM). For the polyHIPE composite prepared using 10

wt % silica and using the two-speed stirring protocol during emulsification, swelling tests were carried out in a saturated $CaCl_2$ solution, distilled water and a simulated body fluid (SBF) prepared following the Kokubo protocol.[622] For tests in SBF, a cylindrical piece of the polyHIPE composite was cut out of the bulk sample. Weights and dimensions (diameter × height) of the piece were measured prior to soaking into SBF, after soaking into 36 °C SBF for about 1 d and 5 d, respectively.

Poly(KAA)/Bioglass® Pickering-HIPE composites were prepared following the procedure for preparation of poly(KAA)/silica Pickering-HIPE composites. Various amounts of Bioglass® relative to the weight sum of KAA and BIS (2, 5, 10, 15 and 20 wt %) and the two-speed stirring protocol were used. Instead of using glass tubes, the HIPEs obtained were transferred into two plastic tubes (15 ml) for UV polymerization. During purification, the two samples taken out of the plastic tubes were wrapped with filter paper and put into two thimbles (Int. diameter×length: 19 mm×90 mm) for Soxhlet extraction. TGA was carried out on Bioglass® and the composites using a heating rate of 10 °C/min (**Table 7.18**).

Table 7.18 TGA of Bioglass® and poly(KAA)/Bioglass® Pickering-HIPE composites

Sample ID *	W_0 /mg	Gas	Protocol /[Temperature (isothermal duration)]
2 wt %_(a)	20.60	N_2	600 °C (1 min)
5 wt %_(a)	32.49	N_2	600 °C (1 min)
10 wt %_(a)	13.42	N_2	600 °C (1 min)
2 wt %_(b)	11.54	Air	600 °C (10 min)
2 wt %_(c)	8.24	Air	900 °C (10 min)
2 wt %_(d)	3.96	Air	900 °C (40 min)
2 wt %_(e)	2.20	Air	900 °C (60 min) → 1000 °C (5 min)
Bioglass®	9.42	Air	900 °C (60 min) → 1000 °C (5 min)
5 wt %_(b)	3.72	Air	900 °C (40 min)
10 wt %_(b)	1.40	Air	900 °C (40 min)
10 wt %_(c)	4.37	Air	900 °C (60 min) → 1000 °C (5 min)
15 wt %_(a)	7.21	Air	900 °C (40 min)
20 wt %_(a)	2.62	Air	900 °C (40 min)

* The ratios were the nominal ratios of Bioglass® to the weight sum of KAA and BIS.

7.4.5 Microgel particles stabilised o/w HIPEs containing potassium methacrylate

To obtain a potassium methacrylate (KMAA) stock solution, KOH solutions of four concentrations were prepared (0.5, 1.0, 1.5 and 3.0 M) and used to neutralize MAA. Lots of salts precipitated at RT when 3.0 M KOH was used whereas KMAA solutions were obtained for the other three. For HIPE preparation, the KMAA solution prepared from 1.5 M KOH was hence used, whose concentration was 1.30 M calculated according to Equation (7.5).

In the preparation of poly(KMAA) Pickering-HIPEs, an aqueous solution made up with KMAA solution (3.28 ml, 1.30 M, pH 7.05), distilled H_2O (0.72 ml), microgel (**GP1-6)** suspension (1.0 ml, 8 mg/ml in 1 mM KCl solution), various BIS contents and I2959 (2 mol %) was emulsified with toluene (20 ml, 80 vol %) using the two-speed stirring protocol. BIS contents used were 15.0, 5.0 and 3.2 mol % relative to amount of KMAA. Morphologies of the resultant polyHIPEs were characterised with SEM (3). Particle size measurements were carried out in the temperature range of 20~34 °C using microgel suspension (1.6 mg/ml) in KMAA solution (0.85 M).

7.4.6 Poly(KAA) HIPEs prepared using dye/drug loaded-microgels as the emulsifiers

The aqueous suspension selected for this study was made up with KAA stock solution (1.68 ml, pH 7.0, 4.27 mmol), distilled water (2.32 ml), BIS (21.07 mg, 3.2 mol % relative to KAA), I2959 (20.38 mg, 2 mol %) and microgel suspension (1.0 ml, 8 mg/ml). Introduction of dye/drug into the aqueous suspension was investigated using dye/drug aqueous solutions (2.32 ml) instead of distilled water (2.32 ml). For HIPE preparation, *p*-xylene (80 vol %) was used as the internal phase. Photo-polymerised HIPEs were frozen in LN_2 and freeze-dried using a HETO Power Dry LL1500 Freeze-drier (Thermo Scientific).

7.4.6.1 Poly(KAA) HIPEs prepared using dye-loaded microgels as the emulsifiers

Fluorescence emission spectra of rhodamine 6G (R6G) dye solutions with and without microgels were obtained using a Varian Cary Eclipse Spectrometer over a range of 540~750 nm. The excited wavelength was 528 nm. The R6G solution without microgels was prepared by mixing a dye solution (2.32 ml, 196 μg dye) with a KCl solution (1.0 ml, 1 mM) while the

dye solution with microgels was prepared by mixing the above solution (1.5 ml) with a microgel suspension (0.5 ml, 8 mg/ml in 1 mM KCl solution). The loading of R6G dye into microgels (**GP1-6**) and HIPE preparation were investigated (**Table 7.19**). Centrifugation was carried out using a Gallenhamp Angle Head Centrifuge at 5000 rpm for 1 h (RT, **No.1** and **No.3**) or using a Sigma 2-16K SciQuip centrifuge at 12 k rpm for 30 min and at 15 k rpm for 1 h (4 ºC, **No.6**). The mixture of microgel and dye was shaken overnight using a Stuart SSM4 Mini See-saw Rocker at 70 osc./min (**No.4**~**No.6**). Stable HIPEs obtained from **No.2** and **No.4** were photo-polymerised.

Table 7.19 Emulsification using dye-loaded microgel particles as the emulsifiers

No.	Solution background		Dye/microgel weight ratio	Aqueous mixture used for HIPE preparation	Stirring protocol #
	Dye	Microgel			
1	H_2O	1 mM KCl	0.196/8	Supernatant of (dye + microgels + KAA + BIS + I2959)	Two-speed
2	H_2O	1 mM KCl	0.196/8	Uncentrifuged mixture of (dye+ microgels+ KAA+ BIS+ I2959)	One-speed
3	H_2O	1 mM KCl	0.196/8	Supernatant of (dye + microgels + KAA + BIS + I2959)	One-speed
4	H_2O	1 mM KCl	0.39/8	Uncentrifuged mixture of (dye+ microgels+ KAA+ BIS+ I2959)	One-speed
5	H_2O	1 mM KCl	0.39/8	Uncentrifuged mixture of (dye+ microgels+ KAA+ BIS+ I2959)	Two-speed
6	Buffer	Buffer	0.39/8	KAA+ BIS+ I2959+ solution of the precipitate from centrifuged mixture of (dye+ microgels)	One-speed
7	Buffer	Buffer	0.39/8	Uncentrifuged mixture of (dye+ microgels+ KAA)	One-speed
8	-	Buffer	-	KAA+ microgels	One-speed

*Buffer refers to phosphate buffer (10 mM, pH 6.5); one-speed (400 rpm) and two-speed (400→1000 rpm).

For aqueous solutions/suspensions used in this study (**Table 7.20**), particle size measurements were carried out at 22 °C on un-centrifuged **S(1)**~**S(4)**, supernatants from centrifuged **S(2)**, **S(3)** and **S(5)** (5000 rpm for 1 h) and **S(6)**~**S(10)**. **S(9)** was the same solution as used in **No.6** of **Table 7.19**.

Table 7.20 Compositions of the aqueous solutions/suspensions used in dye loading study

No.	Solution/suspension composition	pH
S(1)	2.32 ml H_2O + 1 ml microgel suspension (8 mg/ml in 1 mM KCl solution)	-
S(2)	2.32 ml R6G solution (192 μg) + 1 ml KCl solution (1 mM)	5.54
S(3)	2.32 ml R6G solution (192 μg) + 1 ml microgel suspension (8 mg/ml in 1 mM KCl solution)	6.77
S(4)	**S(3)** + 1.68 ml KAA stock solution	6.68
S(5)	**S(4)** + BIS (21.07 mg) + I2959 (20.38 mg)	6.71
S(6)	Microgel suspension in buffer* (8 mg/ml)	5.28
S(7)	1 ml microgel suspension in buffer (8 mg/ml) + 2.32 ml dye buffer solution (0.39 mg dye)	6.53
S(8)	**S(7)** + 1.68 ml KAA	6.53
S(9)	Precipitate of centrifuged **S(7)** re-dissolved into 3.32 ml buffer + 1.68 ml KAA + BIS (21.07 mg) + I2959 (20.38 mg)	6.58
S(10)	Supernatant of centrifuged **S(7)**	6.40

* Buffer used in **S(6)**~**S(10)** was phosphate buffer (10 mM, pH 6.5).

7.4.6.2 Poly(KAA) HIPEs prepared using drug-loaded microgels as the emulsifiers

Aqueous solutions were prepared by mixing drugs (dopamine.HCl or paracetamol), microgel particles, KAA stock solutions (2.54 M, pH 7.0) in sequence into phosphate buffer solution (pH 6.5, 10 mM) following a ratio of 90 μmol drug: 3.32 ml buffer: 8 mg microgels: 1.68 ml KAA. Before and after adding KAA stock solution, the mixture was shaken using a shaker (Stuart SSM4 Mini See-saw Rocker, UK) at 70 osc./min overnight. The aqueous solutions were stored at 4 °C before use. Particle size measurements were carried out using the two solutions and a control solution without drug.

Prior to HIPE preparation, BIS (3.2 mol % relative to KAA) and I2959 (2 mol %) were dissolved into aqueous solutions containing paracetamol. Emulsification of the aqueous mixture and *p*-xylene (80 vol %) was carried out using either the one-speed (400 rpm) or the two speed stirring protocol (400→1000 rpm) at 20-22 °C. Microgel species with 1 mol % (**GP1-6**) and 2 mol % (**GP2**) crosslinking degree were both used in this study.

To test the loading and release of paracetamol, five aqueous solutions were used: (1) paracetamol in phosphate buffer (90 μmol per 3.32 ml); (2) **GP1-6** + paracetamol in

phosphate buffer (8 mg: 90 μmol: 3.32 ml); (3) **GP1-6** + paracetamol in phosphate buffer + KAA (8 mg: 90 μmol: 3.32 ml: 1.68 ml); (4) **GP2** + paracetamol in phosphate buffer (8 mg: 90 μmol: 3.32 ml); (5) **GP2** + paracetamol in phosphate buffer + KAA (8 mg: 90 μmol: 3.32 ml: 1.68 ml). UV-vis was performed using a mixture solution of solution (1) (7.5 μl) and phosphate buffer (3 ml, 10 mM, pH 6.5). Centrifugation was carried out using a Sigma 2-16K SciQuip centrifuge at 15 k rpm. Solution (2) was centrifuged for 30 min at 18 °C followed by 30 min at 4 °C while solution (4) was centrifuged for 30 min at 18 °C. UV-vis adsorption spectrum with an adsorption peak wavelength at 243 nm (**Fig. 7.10**) was collected by using a mixed solution of phosphate buffer (3 ml, 10 mM, pH 6.5) and the investigated solution (0.75 μl), including solution (1), solution (2), solution (4) and supernatants from centrifuged solution (2) and (4) (**Table 7.21**).

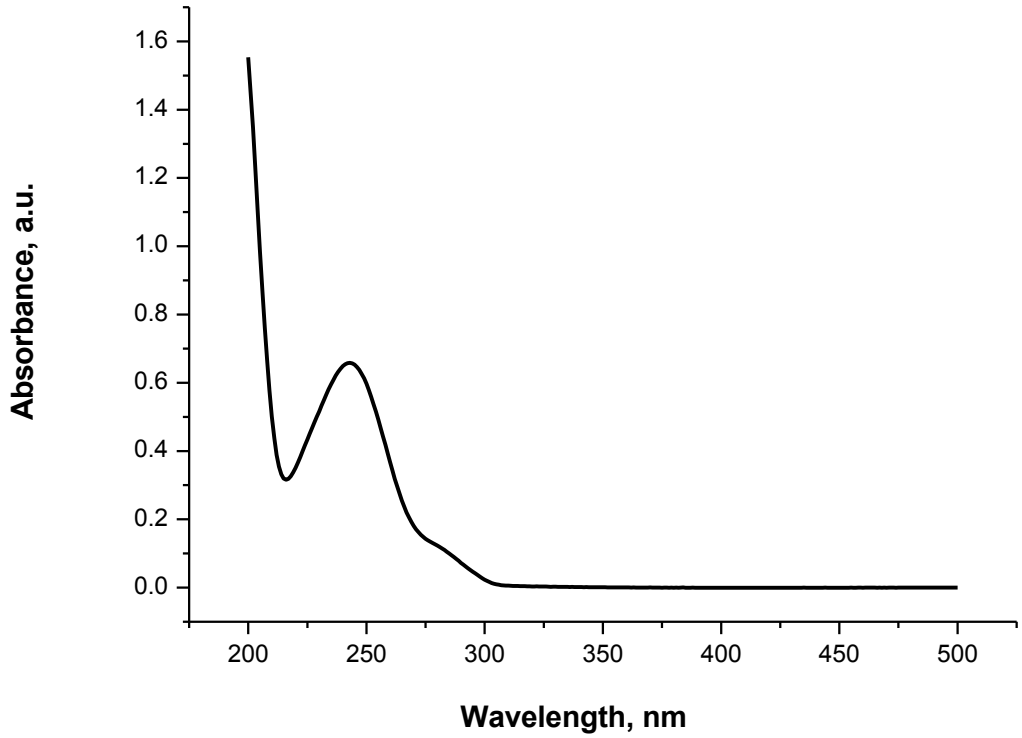


Fig. 7.10 Absorbance of paracetamol in phosphate buffer (peak wavelength at 243 nm)

Table 7.21 Absorbance of drug paracetamol and drug-loaded microgel particles at 243 nm

	Solution (1)	**Solution (2)**	**Supernatant of solution (2)**	**Solution (4)**	**Supernatant of solution (4)**
Average	0.64	0.65	0.65	0.68	0.69
Std deviation	0.01	0.02	0.03	0.03	0.03

7.4.7 Microgel particles stabilised o/w HIPEs containing dextran and its derivatives

(This part of work was in collaboration with Shengzhong Zhou)

7.4.7.1 Synthesis and characterisation of dextran-*co*-polyNIPAAm

(Done by Shengzhong Zhou)

Dextran-*co*-polyNIPAAm was prepared using ammonium cerium (IV) nitrate as a radical redox initiator, as described by Wang *et al.*[613] Dextran (5.00 g) was dissolved in distilled water (50 ml) in a three necked flask, which was placed in an oil bath at 27 °C and purged with nitrogen. The nitrogen atmosphere was maintained throughout the copolymerisation reaction. Cerium (IV) ammonium nitrate (0.01 mol, 5.50 g), nitric acid (69 %, 6.10 g) and NIPAAm (5.00 g) were added to the reaction system. After 4 h, the reaction was stopped by addition of sodium hydroxide solution (1 N). The reaction mixture was transferred to a dialysis tube (MWCO = 12,000 Da) and dialyzed against distilled water for 3 d (distilled water was changed twice a day). A white fluffy product was obtained after freeze drying. The yield is 44%, (this low yield is attributed to the removal of low molecular weight polymers during dialysis). The ratio of dextran glucose units to NIPAAm units in the copolymer was determined to be 1:0.67 by ^{1}H NMR spectra (400 MHz, D_2O). Aqueous gel permeation chromatography (GPC) was carried out at Smithers Rapra Technology Ltd. (UK), where pullulan polysaccharide was used for calibration. M_n = 13,600, PDI= 2.06.

The LCST of dextran-*co*-polyNIPAAm was also measured. A glass test tube containing an aqueous solution of dextran-*co*-polyNIPAAm (0.2 w/v %, 10 ml) was placed in a thermostatted water bath. The cloud point of the solution was observed by increasing temperature from 24 °C to 38 °C at 4 °C/h and then cooling down to room temperature. A sudden change of the solution from transparent to cloudy was observed at 34 °C both during increase of temperature and decrease of temperature. This temperature was used as the LCST of dextran-*co*-polyNIPAAm.

7.4.7.2 Preparation of microgel particles stabilised o/w HIPEs containing dextran and dextran-*co*-polyNIPAAm

HIPE preparation was carried out using the assembled mechanical stirrer [**Fig. 7.2** (a)]. A microgel suspension (2.5 ml, 0.4 wt % in 1 mM KCl solution) was measured with a syringe and injected into the reaction vessel while dextran or dextran-*co*-polyNIPAAm (0.5 g) was

weighed in a glass tube and then mixed with microgel suspension in the vessel. The aqueous mixture was stirred at 400 rpm for 10-20 min until all the materials were dissolved. *p*-Xylene (10 ml) was then added into the reaction vessel dropwise through a dropping funnel under stirring at 400 rpm. Stirring was continued for 10-15 min after addition of *p*-xylene was finished. The obtained emulsion sample was transferred into a round-bottom flask (50/100 ml), frozen in LN_2 and freeze-dried using a Christ Alpha 1-2 LD freeze-drier. In the cases where a thermostating step was used, the round-bottom flask containing HIPEs was thermostatted in a water bath prior to the freezing and freeze-drying steps. The variables investigated include pH of the microgel suspension, the thermostating temperature, dextran molecular weight and dextran concentration (**Table 7.22**). Particle size measurements were carried out using microgel suspensions (0.4 wt % in 1 mM KCl solution) in two series: (1) pH 3.7, 4.7, 5.5 and 6.8 at 22 °C; (2) pH 6.8 over a temperature range of 20-70 °C.

Table 7.22 Variables in preparation of macroporous dextran and dextran-*co*-polyNIPAAm

No.	Material	Concentration of material, w/v %	pH	Thermostating conditions
1	Dextran (40 k)	20	3.7	-
2	Dextran (40 k)	20	4.7	-
3	Dextran (40 k)	20	5.5	-
4	Dextran (40 k)	20	6.8	-
5	Dextran (40 k)	20	6.8	45 ºC for 1 h
6	Dextran (40 k)	20	6.8	50 ºC for 1 h
7	Dextran (40 k)	20	6.8	55 ºC for 1 h
8	Dextran (40 k)	20	6.8	60 ºC for 1 h
9	Dextran (40 k)	8	6.8	-
10	Dextran (6 k)	20	6.8	-
11	Dextran (6 k)	8	6.8	-
12	Dextran-*co*-polyNIPAAm	20	6.8	-
13	Dextran-*co*-polyNIPAAm	20	6.8	38 ºC for 0.5 h

7.4.7.3 Characterisation of macroprous dextran and dextran-*co*-polyNIPAAm

Morphologies of macroporous dextran and dextran-*co*-polyNIPAAm were characterised with SEM (3). Pore sizes were analysed using the SEM images (**Table 7.23**).

Table 7.23 Pore structure analysis of macroporous dextran and dextran-*co*-polyNIPAAm

No.*	**2**	**3**	**4**	**6**	**9**	**10**	**11**	**12**	**13**
Mean /μm	99.0	81.2	41.5	36.0	85.3	153.6	79.2	44.6	38.7
Std dev. /μm	55.3	35.9	14.5	14.2	32.1	71.2	25.9	13.9	14.2
Min. size /μm	23.2	25.4	19.0	11.2	29.0	51.6	23.4	12.6	8.4
Max. size /μm	276.0	200.6	120.0	84.6	236.0	415.6	178.8	74.0	84.2
Number of pores	201	209	210	237	201	94	235	239	300

* Samples numbers were the same as those in **Table 7.22**.

TGA was carried out under a flow of N_2 gas, from 30 °C to 600 °C, at a heating rate of 20 °C/min (**Fig. 7.12**). Tested samples include microgels (2.87 mg) obtained by freezing a suspension (0.4 wt % in 1 mM KCl solution, pH 6.8) in LN_2 and freeze-drying, abbreviated as **GP_pH6.8**, commercial dextran (27.12 mg, M_r 40 k), macroporous dextran (**No.4** in **Table 7.22**, 4.03 mg), macroporous dextran-*co*-polyNIPAAm (**No.12** in **Table 7.22**, 2.20 mg) and macroporous dextran-*co*-polyNIPAAm prepared using a thermostating step (**No.13** in **Table 7.22**, 3.74 mg).

GP_pH6.8, macroporous dextran (**No.4** in **Table 7.22**), macroporous dextran-*co*-polyNIPAAm (**No.12** in **Table 7.22**) and macroporous dextran-*co*-polyNIPAAm prepared using a thermostating step (**No.13** in **Table 7.22**) were then analysed using DSC. For all four samples, three cycles of heating and cooling were recorded between -50 °C and 250 °C after an initial quenching from RT to -50 °C. Tests were carried out using 5 °C/min and 20 °C/min as the ramp rate, respectively. For macroporous dextran (**No.4**), tests were also performed using other procedures (**Table 7.24**). All the steps and peaks observed in DSC tests of the samples were analysed (**Table 7.25**).

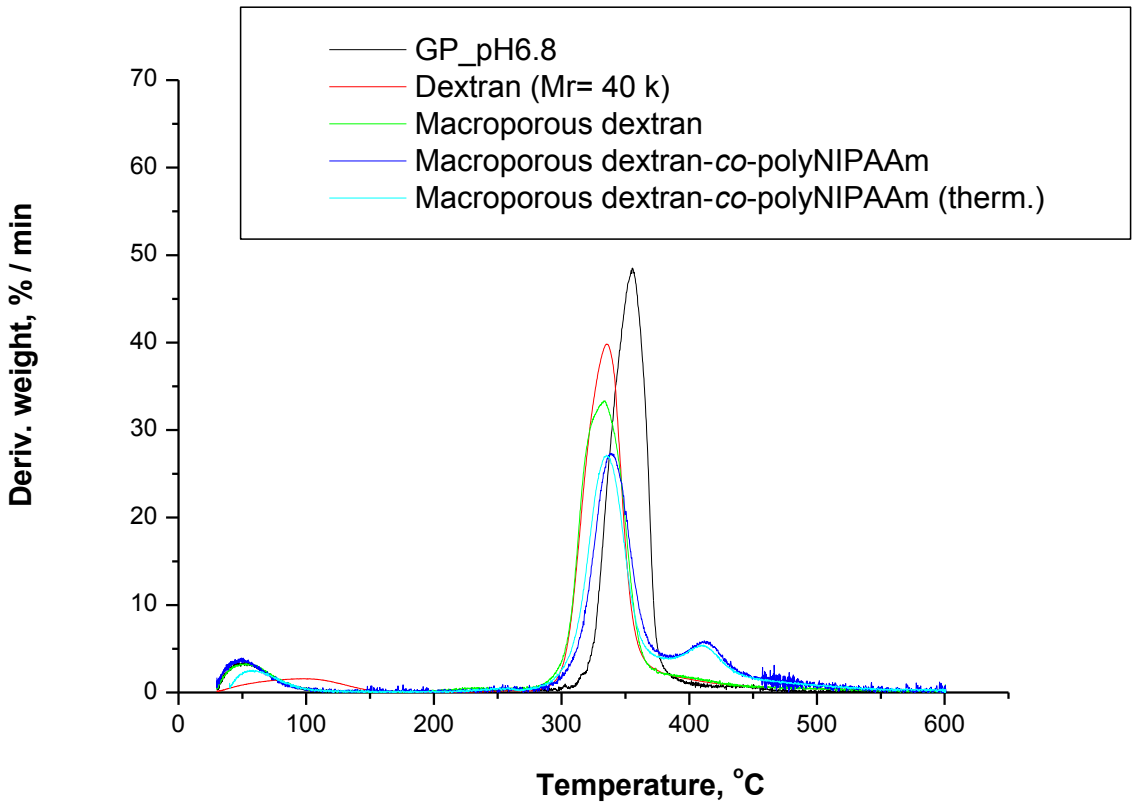


Fig. 7.11 TGA of macroporous dextran and dextran-*co*-polyNIPAAm and control samples

Table 7.24 Different test procedures used in DSC analysis of macroporous dextran

Sample ID*	Mass /mg	Ramp /°C. min^{-1}	Cycle 1 /°C	Cycle 2 /°C	Cycle 3 /°C	Cycle 4 /°C	Cycle 5 /°C	Cycle 6 /°C
No.4-1	1.43	5	[-50, 250]	[250, -50]	[-50, 250]			
No.4-2	1.36	20	[-50, 250]	[250, -50]	[-50, 250]			
No.4-3	1.83	20	[-50, 235]	[235, -50]	[-50, 235]			
No.4-4	1.75	20	[-50, 235]	[235, -50]	[-50, 250]			
No.4-5	2.14	20	[-50, 250]	[250, -50]	[-50, 250]			
No.4-6	1.74	20	[-50, 200]	[200, -50]	[-50, 250]	[250, -50]	[-50, 250]	[250, 30]

* Sample IDs are the same as the numbers used in **Table 7.22**.

Table 7.25 Summaries of steps and endothermic peaks observed in DSC

Sample ID *	Mass /mg	Ramp rate /°C. min^{-1}	Test cycle	Steps				Endothermic peaks		
				Onset /°C	Infection /°C	End /°C	ΔCp /J. g^{-1}.°C^{-1}	Onset /°C	Peak /°C	Area /J.g^{-1}
No.4-1	1.43	5	1st	97.2	103.3	108.3	0.971	128.5	129.4	0.604
								150.5	150.9	16.64
			2nd	-	-	-	-	244.6	244.0	57.13

			3rd	202.0	206.4	208.7	0.817	-	-	-
No.12-1	1.18	5	1st	-	-	-	-	149.5	150.1	4.620
No.13-1	1.04	5	1st	-	-	-	-	162.1	162.4	5.320
GP_pH6.8-1	1.44	5	1st	80.1	88.1	91.4	1.263	166.8	181.3	107.2
			3rd	145.1	152.2	153.8	0.992	-	-	-
No.4-2	1.36	20	1st	82.4	86.8	89.4	0.547	152.4	159.7	34.97
								241.8	242.7	40.96
			2nd	-	-	-	-	249.6	248.4	7.017
			3rd	217.1	220.7	222.6	0.563	-	-	-
No.12-2	1.43	20	1st	54.6	58.4	60.6	0.253	132.8	136.5	170.0
				72.6	76.0	78.5	0.438			
			3rd	128.1	137.6	154.0	0.264	-	-	-
				217.6	221.0	225.3	0.171			
No.13-2	1.70	20	1st	56.9	61.1	62.8	0.513	104.6	140.0	194.9
				73.3	76.4	79.7	0.494			
			3rd	132.5	138.7	145.7	0.118	-	-	-
				219.1	222.7	224.9	0.175			
GP_pH6.8-2	2.06	20	1st	-	-	-	-	57.3	64.4	4.574
								153.7	154.8	12.68
								237.1	238.4	54.10
			3rd	150.2	157.1	160.7	0.675	-	-	-
No.4-3	1.83	20	1st	43.9	57.8	62.6	0.235	160.5	161.4	60.46
				80.9	84.0	86.7	0.416			
			3rd	56.7	70.0	126.5	2.319	-	-	-
No.4-4	1.75	20	1st	48.2	56.2	58.7	0.453	154.3	154.6	59.28
				71.4	76.6	80.5	0.794			
				101.4	108.4	113.5	0.553			
				129.5	131.1	131.9	0.172			
			2nd	-	-	-	-	234.6	233.8	52.3
			3rd	215.9	220.4	221.9	0.570	-	-	-
No.4-5	2.14	20	1st	217.6	220.2	223.7	0.457	58.7	105.0	351.4
			3rd	218.2	223.0	225.5	0.773	-	-	-
No.4-6	1.74	20	1st	56.3	60.8	63.3	0.501	132.3	133.5	3.440
				76.3	80.7	83.8	0.654	152.3	152.8	23.38
				109.4	116.4	119.4	0.381			
			3rd	43.9	55.3	127.6	3.798	241.1	242.4	52.27
			5th	214.8	218.3	220.1	0.428	-	-	-

* Sample IDs are the same as the numbers used in **Table 7.22**.

Durability tests were carried out on macroporous dextran-*co*-polyNIPAAm that was prepared either without using (0.0139 g) or using a thermostating step (0.0132 g). The samples with determined weights were placed into two round-bottomed flasks containing H_2O and then maintained at 38 ± 2 °C for 14 d. Afterwards, both samples were frozen in LN_2 and freeze-dried. Morphologies of the dried materials were characterised with SEM (3).

References

(1) Klawitter, J. J.; Hulbert, S. F. *J. Biomed. Mater. Res.* **1971**, *5*, 161-229.
(2) Whang, K.; Healy, K. E.; Elenz, D. R.; Nam, E. K.; Tsai, D. C.; Thomas, C. H.; Nuber, G. W.; Glorieux, F. H.; Travers, R.; Sprague, S. M. *Tissue Eng.* **1999**, *5*, 35-51.
(3) Mooney, D.; Baldwin, D.; Suh, N.; Vacanti, L.; Langer, R. *Biomaterials* **1996**, *17*, 1417-1422.
(4) Langer, R.; Vacanti, J. P. *Science* **1993**, *260*, 920-926.
(5) Langer, R. *Pharm. Res.* **1997**, *14*, 840-841.
(6) Polak, J. M.; Mantalaris, S. *Pediatr. Res.* **2008**, *63*, 461-466.
(7) Griffith, L. G.; Naughton, G. *Science* **2002**, *295*, 1009-1014.
(8) Logeart-Avramoglou, D.; Anagnostou, F.; Bizios, R.; Petite, H. *J. Cell. Mol. Med.* **2005**, *9*, 72-84.
(9) Cullinane, D. M.; Einhorn, T. A. In *Principles of Bone Biology, second edition*; Bilezikian, J. P., Raisz, L. G., Rodan, G. A., Eds.; Academic Press, 2002; Vol. 1.
(10) Weiner, S.; Wagner, H. D. *Annu. Rev. Mater. Sci.* **1998**, *28*, 271-298.
(11) Marks, S. C.; Odgren, P. R. In *Principles of Bone Biology, second edition*; John P. Bilezikian, L. G. R., Gideon A. Rodan, Ed.; Academic Press: London, 2002; Vol. 1.
(12) Marks, S. C.; Popoff, S. N. *Am. J. Anat.* **1988**, *183*, 1-44.
(13) Parfitt, A. M. *J. Cell. Biochem.* **1994**, *55*, 273-286.
(14) Tuan, R. S.; Boland, G.; Tuli, R. *Arthritis Res. Ther.* **2003**, *5*, 32-45.
(15) Wagner, W.; Wein, F.; Seckinger, A.; Frankhauser, M.; Wirkner, U.; Krause, U.; Blake, J.; Schwager, C.; Eckstein, V.; Ansorge, W.; Ho, A. D. *Exp. Hematol.* **2005**, *33*, 1402-1416.
(16) Caplan, A. *J. Orthop. Res.* **1991**, *9*, 641-650.
(17) Pittenger, M. F.; Mackay, A. M.; Beck, S. C.; Jaiswal, R. K.; Douglas, R.; Mosca, J. D.; Moorman, M. A.; Simonetti, D. W.; Craig, S.; Marshak, D. R. *Science* **1999**, *284*, 143-147.
(18) Caplan, A. *J. Cell. Physiol.* **2007**, *213*, 341-347.
(19) Meyerrose, T.; Olson, S.; Pontow, S.; Kalomoiris, S.; Jung, Y.; Annett, G.; Bauer, G.; Nolta, J. A. *Adv. Drug Deliv. Rev.* **2010**, *62*, 1167-1174.
(20) Takahashi, K.; Yamanaka, S. *Cell* **2006**, *126*, 663-676.
(21) Yu, J.; Vodyanik, M. A.; Smuga-Otto, K.; Antosiewicz-Bourget, J.; Frane, J. L.; Tian, S.; Nie, J.; Jonsdottir, G. A.; Ruotti, V.; Stewart, R.; Slukvin, I. I.; Thomson, J. A. *Science* **2007**, *318*, 1917-1920.
(22) Takahashi, K.; Tanabe, K.; Ohnuki, M.; Narita, M.; Ichisaka, T.; Tomoda, K.; Yamanaka, S. *Cell* **2007**, *131*, 861-872.
(23) Duan, X.; Tu, Q.; Zhang, J.; Ye, J.; Sommer, C.; Mostoslavsky, G.; Kaplan, D.; Yang, P.; Chen, J. *J. Cell. Physiol.* **2011**, *226*, 150-157.
(24) Karaplis, A. C. In *Principles of Bone Biology, second edition*; John P. Bilezikian, L. G. R., Gideon A. Rodan, Ed.; Academic Press: London, 2002; Vol. 1.
(25) Hall, B. K.; Miyake, T. *Bioessays* **2000**, *22*, 138-147.
(26) Teitelbaum, S. L. *Science* **2000**, *289*, 1504-1508.
(27) Kenley, R. A.; Yim, K.; Abrams, J.; Ron, E.; Turek, T.; Marden, L. J.; Hollinger, J. O. *Pharm. Res.* **1993**, *10*, 1393-1401.
(28) Salgado, A. J.; Coutinho, O. P.; Reis, R. L. *Macromol. Biosci.* **2004**, *4*, 743-765.
(29) Damien, C. J.; Parsons, J. R. *J. Appl. Biomater.* **1991**, *2*, 187-208.

(30) Geetha, M.; Singh, A. K.; Asokamani, R.; Gogia, A. K. *Prog. Mater. Sci.* **2009**, *54*, 397-425.
(31) Khan, Y.; Yaszemski, M. J.; Mikos, A. G.; Laurencin, C. T. *J. Bone Joint Surg. Am.* **2008**, *90A*, 36-42.
(32) Marolt, D.; Knezevic, M.; Novakovic, G. *Stem Cell Res. Ther.* **2010**, *1*, 10.
(33) Gersbach, C. A.; Phillips, J. E.; Garcia, A. J. *Annu. Rev. Biomed. Eng.* **2007**, *9*, 87-119.
(34) Ulrich-Vinther, M. *Acta Orthop.* **2007**, *78*, 5-64.
(35) Phillips, J. E.; Gersbach, C. A.; Garcia, A. J. *Biomaterials* **2007**, *28*, 211-229.
(36) Bleiziffer, O.; Eriksson, E.; Yao, F.; Horch, R. E.; Kneser, U. *J. Cell. Mol. Med.* **2007**, *11*, 206-223.
(37) Hench, L. L.; Polak, J. M. *Science* **2002**, *295*, 1014-1017.
(38) Huebsch, N.; Mooney, D. J. *Nature* **2009**, *462*, 426-432.
(39) Xia, Z.; Triffitt, J. T. *Biomed. Mater.* **2006**, *1*, R1-R9.
(40) Williams, D. F. *Biomaterials* **2008**, *29*, 2941-2953.
(41) Stevens, M. M. *Mater. Today* **2008**, *11*, 18-25.
(42) Rezwan, K.; Chen, Q. Z.; Blaker, J. J.; Boccaccini, A. R. *Biomaterials* **2006**, *27*, 3413-3431.
(43) Place, E. S.; George, J. H.; Williams, C. K.; Stevens, M. M. *Chem. Soc. Rev.* **2009**, *38*, 1139-1151.
(44) Yunos, D. M.; Bretcanu, O.; Boccaccini, A. R. *J. Mater. Sci.* **2008**, *43*, 4433-4442.
(45) Sitharaman, B.; Shi, X. F.; Tran, L. A.; Spicer, P. P.; Rusakova, I.; Wilson, L. J.; Mikos, A. G. *J. Biomater. Sci. Polym. Ed.* **2007**, *18*, 655-671.
(46) Abarrategi, A.; Gutierrez, M. C.; Moreno-Vicente, C.; Hortiguela, M. J.; Ramos, V.; Lopez-Lacomba, J. L.; Ferrer, M. L.; del Monte, F. *Biomaterials* **2008**, *29*, 94-102.
(47) Karageorgiou, V.; Kaplan, D. *Biomaterials* **2005**, *26*, 5474-5491.
(48) Nguyen, L. H.; Annabi, N.; Nikkhah, M.; Bae, H.; Binan, L.; Park, S.; Kang, Y. Q.; Yang, Y. Z.; Khademhosseini, A. *Tissue Eng., B: Rev.* **2012**, *18*, 363-382.
(49) Graziano, A.; D'Aquino, R.; Angelis, M.; De Francesco, F.; Giordano, A.; Laino, G.; Piattelli, A.; Traini, T.; De Rosa, A.; Papaccio, G. *J. Cell. Physiol.* **2008**, *214*, 166-172.
(50) Alves, N. M.; Pashkuleva, I.; Reis, R. L.; Mano, J. F. *Small* **2010**, *6*, 2208-2220.
(51) Dado, D.; Levenberg, S. *Semi. Cell Dev. Biol.* **2009**, *20*, 656-664.
(52) Reilly, G. C.; Engler, A. J. *J. Biomech.* **2010**, *43*, 55-62.
(53) Kuboki, Y.; Takita, H.; Kobayashi, D.; Tsuruga, E.; Inoue, M.; Murata, M.; Nagai, N.; Dohi, Y.; Ohgushi, H. *J. Biomed. Mater. Res.* **1998**, *39*, 190-199.
(54) Ishaug, S. L.; Crane, G. M.; Miller, M. J.; Yasko, A. W.; Yaszemski, M. J.; Mikos, A. G. *J. Biomed. Mater. Res.* **1997**, *36*, 17-28.
(55) Roosa, S. M. M.; Kemppainen, J. M.; Moffitt, E. N.; Krebsbach, P. H.; Hollister, S. J. *J. Biomed. Mater. Res., A* **2010**, *92A*, 359-368.
(56) Arnett, T. *Proc. Nutr. Soc.* **2003**, *62*, 511-520.
(57) Mikos, A. G.; Thorsen, A. J.; Czerwonka, L. A.; Bao, Y.; Langer, R.; Winslow, D. N.; Vacanti, J. P. *Polymer* **1994**, *35*, 1068-1077.
(58) Lu, L. C.; Mikos, A. G. *MRS Bull.* **1996**, *21*, 28-32.
(59) Lu, L.; Peter, S. J.; Lyman, M. D.; Lai, H. L.; Leite, S. M.; Tamada, J. A.; Uyama, S.; Vacanti, J. P.; Langer, R.; Mikos, A. G. *Biomaterials* **2000**, *21*, 1837-1845.
(60) Shi, X. F.; Sitharaman, B.; Pham, Q. P.; Liang, F.; Wu, K.; Billups, W. E.; Wilson, L. J.; Mikos, A. G. *Biomaterials* **2007**, *28*, 4078-4090.
(61) Dehghani, F.; Annabi, N. *Curr. Opin. Biotechnol.* **2011**, *22*, 661-666.
(62) Yoshimoto, H. *Biomaterials* **2003**, *24*, 2077-2082.

(63) Tuzlakoglu, K.; Bolgen, N.; Salgado, A. J.; Gomes, M. E.; Piskin, E.; Reis, R. L. *J. Mater. Sci. Mater. Med.* **2005**, *16*, 1099-1104.
(64) Venugopal, J.; Low, S.; Choon, A. T.; Ramakrishna, S. *J. Biomed. Mater. Res., B: Appl. Biomater.* **2008**, *84B*, 34-48.
(65) Pham, Q. P.; Sharma, U.; Mikos, A. G. *Tissue Eng.* **2006**, *12*, 1197-1211.
(66) Lo, H.; Ponticiello, M. S.; Leong, K. W. *Tissue Eng.* **1995**, *1*, 15-28.
(67) Sachlos, E.; Reis, N.; Ainsley, C.; Derby, B.; Czernuszka, J. T. *Biomaterials* **2003**, *24*, 1487-1497.
(68) Christenson, E. M.; Soofi, W.; Holm, J. L.; Cameron, N. R.; Mikos, A. G. *Biomacromolecules* **2007**, *8*, 3806-3814.
(69) Park, T. H.; Shuler, M. L. *Biotechnol. Prog.* **2003**, *19*, 243-253.
(70) Rajagopalan, S. *Med. Image Anal.* **2006**, *10*, 693-712.
(71) Khademhosseini, A. *Proc. Natl. Acad. Sci. U.S.A.* **2006**, *103*, 2480-2487.
(72) Borenstein, J. T.; Weinberg, E. J.; Orrick, B. K.; Sundback, C.; Kaazempur-Mofrad, M. R.; Vacanti, J. P. *Tissue Eng.* **2007**, *13*, 1837-1844.
(73) Park, H.; Cannizzaro, C.; Vunjak-Novakovic, G.; Langer, R.; Vacanti, C. A.; Farokhzad, O. C. *Tissue Eng.* **2007**, *13*, 1867-1877.
(74) Yang, S. F.; Leong, K. F.; Du, Z. H.; Chua, C. K. *Tissue Eng.* **2001**, *7*, 679-689.
(75) Liu, C.; Xia, Z.; Czernuszka, J. T. *Chem. Eng. Res. Des.* **2007**, *85*, 1051-1064.
(76) Hollister, S. J. *Adv. Mater.* **2009**, *21*, 3330-3342.
(77) Biondi, M.; Ungaro, F.; Quaglia, F.; Netti, P. A. *Adv. Drug Deliv. Rev.* **2008**, *60*, 229-242.
(78) Patel, Z. S.; Young, S.; Tabata, Y.; Jansen, J. A.; Wong, M. E. K.; Mikos, A. G. *Bone* **2008**, *43*, 931-940.
(79) Kanczler, J.; Ginty, P.; White, L.; Clarke, N.; Howdle, S.; Shakesheff, K. *Biomaterials* **2010**, *31*, 1242-1250.
(80) Young, S.; Patel, Z. S.; Kretlow, J. D.; Murphy, M. B.; Mountziaris, P. M.; Baggett, L. S.; Ueda, H.; Tabata, Y.; Jansen, J. A.; Wong, M.; Mikos, A. G. *Tissue Eng., A* **2009**, *15*, 2347-2362.
(81) Kempen, D. H. R.; Lu, L. C.; Heijink, A.; Hefferan, T. E.; Creemers, L. B.; Maran, A.; Yaszemski, M. J.; Dhert, W. J. A. *Biomaterials* **2009**, *30*, 2816-2825.
(82) Hou, Q. P.; De Bank, P. A.; Shakesheff, K. M. *J. Mater. Chem.* **2004**, *14*, 1915-1923.
(83) Kretlow, J. D.; Young, S.; Klouda, L.; Wong, M.; Mikos, A. G. *Adv. Mater.* **2009**, *21*, 3368-3393.
(84) Bilodeau, K.; Mantovani, D. *Tissue Eng.* **2006**, *12*, 2367-2383.
(85) Ratcliffe, A.; Niklason, L. E. *Ann. N.Y. Acad. Sci.* **2002**, *961*, 210-215.
(86) Rauh, J.; Milan, F.; Guenther, K.-P.; Stiehler, M. *Tissue Eng., B: Rev.* **2011**, *17*, 263-280.
(87) Salter, E.; Goh, B.; Hung, B.; Hutton, D.; Ghone, N.; Grayson, W. L. *Tissue Eng., B: Rev.* **2012**, *18*, 62-75.
(88) Jagodzinski, M.; Krettek, C. *Injury* **2007**, *38*, S3-S10.
(89) Zhang, H.; Cooper, A. I. *Soft Matter* **2005**, *1*, 107-113.
(90) Imhof, A.; Pine, D. J. *Adv. Mater.* **1998**, *10*, 697-700.
(91) Kimmins, S. D.; Cameron, N. R. *Adv. Funct. Mater.* **2011**, *21*, 211-225.
(92) Whang, K.; Thomas, C. H.; Healy, K. E.; Nuber, G. *Polymer* **1995**, *36*, 837-842.
(93) Baker, S. C.; Rohman, G.; Southgate, J.; Cameron, N. R. *Biomaterials* **2009**, *30*, 1321-1328.
(94) Butler, R.; Davies, C. M.; Cooper, A. I. *Adv. Mater.* **2001**, *13*, 1459-1463.
(95) Cameron, N. R.; Sherrington, D. C. *J. Chem. Soc., Faraday Trans.* **1996**, *92*, 1543-1547.

(96) Cameron, N. R.; Sherrington, D. C. *Macromolecules* **1997**, *30*, 5860-5869.
(97) Vilchez, S.; Perez-Carrillo, L. A.; Miras, J.; Solans, C.; Esquena, J. *Langmuir* **2012**, *28*, 7614-7621.
(98) Shirshova, N.; Bismarck, A.; Steinke, J. H. G. *Macromol. Rapid Commun.* **2011**, *32*, 1899-1904.
(99) Shirshova, N.; Johansson, P.; Marczewski, M. J.; Kot, E.; Ensling, D.; Bismarck, A.; Steinke, J. H. G. *J. Mater. Chem. A* **2013**, *1*, 9612-9619.
(100) Li, J.; Zhang, J.; Zhao, Y.; Han, B.; Yang, G. *Chem. Commun.* **2012**, *48*, 994-996.
(101) Gokmen, M. T.; Van Camp, W.; Colver, P. J.; Bon, S. A. F.; Du Prez, F. E. *Macromolecules* **2009**, *42*, 9289-9294.
(102) Wu, R. T.; Menner, A.; Bismarck, A. *J. Polym. Sci., A: Polym. Chem.* **2010**, *48*, 1979-1989.
(103) Ikem, V. O.; Menner, A.; Horozov, T. S.; Bismarck, A. *Adv. Mater.* **2010**, *22*, 3588-3592.
(104) Wong, L. L. C.; Ikem, V. O.; Menner, A.; Bismarck, A. *Macromol. Rapid Commun.* **2011**, *32*, 1563-1568.
(105) Hua, Y.; Li, Y.; Zhang, S.; Chen, J.; Perchyonok, V. T. *Curr. Org. Chem.* **2012**, *16*, 2415-2422.
(106) Zou, S.; Yang, Y.; Liu, H.; Wang, C. *Colloids Surf., A: Physicochem. Eng. Asp.* **2013**, *436*, 1-9.
(107) Grosse, M. T.; Lamotte, M.; Birot, M.; Deleuze, H. *J. Polym. Sci., A: Polym. Chem.* **2008**, *46*, 21-32.
(108) David, D.; Silverstein, M. S. *J. Polym. Sci., A: Polym. Chem.* **2009**, *47*, 5806-5814.
(109) Lovelady, E.; Kimmins, S. D.; Wu, J. J.; Cameron, N. R. *Polym. Chem.* **2011**, *2*, 559-562.
(110) Sergent, B.; Birot, M.; Deleuze, H. *React. Funct. Polym.* **2012**, *72*, 962-966.
(111) Caldwell, S.; Johnson, D. W.; Didsbury, M. P.; Murray, B. A.; Wu, J. J.; Przyborski, S. A.; Cameron, N. R. *Soft Matter* **2012**, *8*, 10344-10351.
(112) Deleuze, H.; Faivre, R.; Herroguez, V. *Chem. Commun.* **2002**, 2822-2823.
(113) Benmachou, K.; Deleuze, H.; Heroguez, V. *React. Funct. Polym.* **2003**, *55*, 211-217.
(114) Kovacic, S.; Krajnc, P.; Slugovc, C. *Chem. Commun.* **2010**, *46*, 7504-7506.
(115) Kovacic, S.; Jerabek, K.; Krajnc, P.; Slugovc, C. *Polym. Chem.* **2012**, *3*, 325-328.
(116) Kovacic, S.; Matsko, N. B.; Jerabek, K.; Krajnc, P.; Slugovc, C. *J. Mater. Chem. A* **2013**, *1*, 487-490.
(117) Moine, L.; Deleuze, H.; Maillard, B. *Tetrahedron Lett.* **2003**, *44*, 7813-7816.
(118) Cummins, D.; Wyman, P.; Duxbury, C. J.; Thies, J.; Koning, C. E.; Heise, A. *Chem. Mater.* **2007**, *19*, 5285-5292.
(119) Cummins, D.; Duxbury, C. J.; Quaedflieg, P. J. L. M.; Magusin, P. C. M. M.; Koning, C. E.; Heise, A. *Soft Matter* **2009**, *5*, 804-811.
(120) Gurevitch, I.; Silverstein, M. S. *Macromolecules* **2011**, *44*, 3398-3409.
(121) Lamson, M.; Epshtein-Assor, Y.; Silverstein, M. S.; Matyjaszewski, K. *Polymer* **2013**, *54*, 4480-4485.
(122) Luo, Y.; Wang, A.-N.; Gao, X. *Soft Matter* **2012**, *8*, 1824-1830.
(123) Pulko, I.; Krajnc, P. *Macromol. Rapid Commun.* **2012**, *33*, 1731-1746.
(124) Boyere, C.; Favrelle, A.; Leonard, A. F.; Boury, F.; Jerome, C.; Debuigne, A. *J. Mater. Chem. A* **2013**, *1*, 8479-8487.
(125) Silverstein, M. S. *Prog. Polym. Sci.* **2014**, *39*, 199-234.
(126) Tebboth, M.; Menner, A.; Kogelbauer, A.; Bismarck, A. *Curr. Opin. Chem. Eng.* **2014**, *4*, 114-120.
(127) Menner, A.; Bismarck, A. *Macromol. Symp.* **2006**, *242*, 19-24.

(128) Williams, J. M.; Gray, A. J.; Wilkerson, M. H. *Langmuir* **1990**, *6*, 437-444.
(129) Akay, G.; Birch, M. A.; Bokhari, M. A. *Biomaterials* **2004**, *25*, 3991-4000.
(130) Carnachan, R. J.; Bokhari, M.; Przyborski, S. A.; Cameron, N. R. *Soft Matter* **2006**, *2*, 608-616.
(131) Zhang, S.; Chen, J.; Perchyonok, V. T. *Polymer* **2009**, *50*, 1723-1731.
(132) Hayman, M. W.; Smith, K. H.; Cameron, N. R.; Przyborski, S. A. *Biochem. Biophys. Res. Commun.* **2004**, *314*, 483-488.
(133) Hayman, M. W.; Smith, K. H.; Cameron, N. R.; Przyborski, S. A. *J. Biochem. Biophys. Methods* **2005**, *62*, 231-240.
(134) Tadros, T. F.; Vincent, B. In *Encyclopedia of Emulsion Technology, Volume 1, Basic Theory*; Becher, P., Ed.; Marcel Dekker, Inc.: New York, 1983; Vol. 1.
(135) Taylor, P. *Adv. Colloid Interface Sci.* **1998**, *75*, 107-163.
(136) Williams, J. M.; Wrobleski, D. A. *Langmuir* **1988**, *4*, 656-662.
(137) Cameron, N. R.; Sherrington, D. C.; Albiston, L.; Gregory, D. P. *Colloid Polym. Sci.* **1996**, *274*, 592-595.
(138) Barby, D.; Haq, Z. European Patent, EP 0060138, 1982.
(139) Menner, A.; Haibach, K.; Powell, R.; Bismarck, A. *Polymer* **2006**, *47*, 7628-7635.
(140) Youssef, C.; Backov, R.; Treguer, M.; Birot, M.; Deleuze, H. *J. Polym. Sci., A: Polym. Chem.* **2010**, *48*, 2942-2947.
(141) Normatov, J.; Silverstein, M. S. *Macromolecules* **2007**, *40*, 8329-8335.
(142) Haibach, K.; Menner, A.; Powell, R.; Bismarck, A. *Polymer* **2006**, *47*, 4513-4519.
(143) Menner, A.; Powell, R.; Bismarck, A. *Soft Matter* **2006**, *2*, 337-342.
(144) Lepine, O.; Birot, M.; Deleuze, H. *J. Polym. Sci., A: Polym. Chem.* **2007**, *45*, 4193-4203.
(145) Menner, A.; Salgueiro, M.; Shaffer, M. S. P.; Bismarck, A. *J. Polym. Sci., A: Polym. Chem.* **2008**, *46*, 5708-5714.
(146) Ramsden, W. *Proc. R. Soc.* **1903**, *72*, 156-164.
(147) Pickering, S. U. *J. Chem. Soc.* **1907**, 2001-2021.
(148) Binks, B. P. *Curr. Opin. Colloid Interface Sci.* **2002**, *7*, 21-41.
(149) Aveyard, R.; Binks, B. P.; Clint, J. H. *Adv. Colloid Interface Sci.* **2003**, *100*, 503-546.
(150) Binks, B. P.; Lumsdon, S. O. *Langmuir* **2000**, *16*, 8622-8631.
(151) Lopetinsky, R. J. G.; Masliyah, J. H.; Xu, Z. In *Colloidal Particles at Liquid Interfaces*; Binks, B. P., Horozov, T. S., Eds.; Cambridge University Press: Cambridge, 2006.
(152) Binks, B. P.; Lumsdon, S. O. *Langmuir* **2000**, *16*, 2539-2547.
(153) Velev, O. D.; Furusawa, K.; Nagayama, K. *Langmuir* **1996**, *12*, 2374-2384.
(154) Aveyard, R.; Clint, J. H.; Nees, D.; Paunov, V. N. *Langmuir* **2000**, *16*, 1969-1979.
(155) Binks, B. P.; Lumsdon, S. O. *Langmuir* **2001**, *17*, 4540-4547.
(156) Read, E. S.; Fujii, S.; Amalvy, J. I.; Randall, D. P.; Armes, S. P. *Langmuir* **2004**, *20*, 7422-7429.
(157) Amalvy, J. I.; Unali, G. F.; Li, Y.; Granger-Bevan, S.; Armes, S. P.; Binks, B. P.; Rodrigues, J. A.; Whitby, C. P. *Langmuir* **2004**, *20*, 4345-4354.
(158) Amalvy, J. I.; Armes, S. P.; Binks, B. P.; Rodrigues, J. A.; Unali, G. F. *Chem. Commun.* **2003**, 1826-1827.
(159) Golemanov, K.; Tcholakova, S.; Kralchevsky, P. A.; Ananthapadmanabhan, K. P.; Lips, A. *Langmuir* **2006**, *22*, 4968-4977.
(160) Morse, A. J.; Armes, S. P.; Thompson, K. L.; Dupin, D.; Fielding, L. A.; Mills, P.; Swart, R. *Langmuir* **2013**, *29*, 5466-5475.
(161) Dupin, D.; Armes, S. P.; Connan, C.; Reeve, P.; Baxter, S. M. *Langmuir* **2007**, *23*, 6903-6910.

(162) Fujii, S.; Aichi, A.; Muraoka, M.; Kishimoto, N.; Iwahori, K.; Nakamura, Y.; Yamashita, I. *J. Colloid Interface Sci.* **2009**, *338*, 222-228.
(163) van Rijn, P.; Mougin, N. C.; Franke, D.; Park, H.; Boker, A. *Chem. Commun.* **2011**, *47*, 8376-8378.
(164) van Rijn, P.; Park, H.; Ozlem Nazli, K.; Mougin, N. C.; Boker, A. *Langmuir* **2013**, *29*, 276-284.
(165) Li, Z.; Xiao, M.; Wang, J.; Ngai, T. *Macromol. Rapid Commun.* **2013**, *34*, 169-174.
(166) Tan, H.; Sun, G. Q.; Lin, W.; Mu, C. D.; Ngai, T. *ACS Appl. Mater. Interfaces* **2014**, *6*, 13977-13984.
(167) Liu, F.; Tang, C.-H. *J. Agric. Food Chem.* **2014**, *62*, 2644-2654.
(168) Liu, F.; Tang, C.-H. *J. Agric. Food Chem.* **2013**, *61*, 8888-8898.
(169) Ghosh, S.; Rousseau, D. *Curr. Opin. Colloid Interface Sci.* **2011**, *16*, 421-431.
(170) Rousseau, D. *Food Res. Int.* **2000**, *33*, 3-14.
(171) Andresen, M.; Stenius, P. *J. Dispersion Sci. Technol.* **2007**, *28*, 837-844.
(172) Wege, H. A.; Kim, S.; Paunov, V. N.; Zhong, Q.; Velev, O. D. *Langmuir* **2008**, *24*, 9245-9253.
(173) Blaker, J. J.; Lee, K.-Y.; Li, X.; Menner, A.; Bismarck, A. *Green Chem.* **2009**, *11*, 1321-1326.
(174) Kalashnikova, I.; Bizot, H.; Cathala, B.; Capron, I. *Langmuir* **2011**, *27*, 7471-7479.
(175) Kalashnikova, I.; Bizot, H.; Cathala, B.; Capron, I. *Biomacromolecules* **2012**, *13*, 267-275.
(176) Zoppe, J. O.; Venditti, R. A.; Rojas, O. J. *J. Colloid Interface Sci.* **2012**, *369*, 202-209.
(177) Venkataraman, P.; Tang, J.; Frenkel, E.; McPherson, G. L.; He, J.; Raghavan, S. R.; Kolesnichenko, V.; Bose, A.; John, V. T. *ACS App. Mater. Interfaces* **2013**, *5*, 3572-3580.
(178) Wei, Z.; Wang, C.; Zou, S.; Liu, H.; Tong, Z. *Polymer* **2012**, *53*, 1229-1235.
(179) Wei, Z.; Yang, Y.; Yang, R.; Wang, C. *Green Chem.* **2012**, *14*, 3230-3236.
(180) Yang, Y.; Wei, Z.; Wang, C.; Tong, Z. *Chem. Commun.* **2013**, *49*, 7144-7146.
(181) Qian, Y.; Zhang, Q.; Qiu, X.; Zhu, S. *Green Chem.* **2014**, *16*, 4963-4968.
(182) Timgren, A.; Rayner, M.; Sjoo, M.; Dejmek, P. *Proc. Food Sci.* **2011**, *1*, 95-103.
(183) Yusoff, A.; Murray, B. S. *Food Hydrocolloids* **2011**, *25*, 42-55.
(184) Li, C.; Li, Y.; Sun, P.; Yang, C. *Colloids Surf., A: Physicochem. Eng. Asp.* **2013**, *431*, 142-149.
(185) Tzoumaki, M. V.; Moschakis, T.; Kiosseoglou, V.; Biliaderis, C. G. *Food Hydrocolloids* **2011**, *25*, 1521-1529.
(186) Perrin, E.; Bizot, H.; Cathala, B.; Capron, I. *Biomacromolecules* **2014**, *15*, 3766-3771.
(187) Qi, F.; Wu, J.; Sun, G.; Nan, F.; Ngai, T.; Ma, G. *J. Mater. Chem. B* **2014**, *2*, 7605-7611.
(188) Whitby, C. P.; Lim, L. H.; Eskandar, N. G.; Simovic, S.; Prestidge, C. A. *J. Colloid Interface Sci.* **2012**, *375*, 142-147.
(189) Chevalier, Y.; Bolzinger, M.-A. *Colloids Surf., A: Physicochem. Eng. Asp.* **2013**, *439*, 23-34.
(190) Colver, P. J.; Bon, S. A. F. *Chem. Mater.* **2007**, *19*, 1537-1539.
(191) Menner, A.; Ikem, V.; Salgueiro, M.; Shaffer, M. S. P.; Bismarck, A. *Chem. Commun.* **2007**, 4274-4276.
(192) Menner, A.; Verdejo, R.; Shaffer, M.; Bismarck, A. *Langmuir* **2007**, *23*, 2398-2403.
(193) Ikem, V. O.; Menner, A.; Bismarck, A. *Angew. Chem. Int. Ed.* **2008**, *47*, 8277-8279.
(194) Gurevitch, I.; Silverstein, M. S. *J. polym. Sci., A: Polym. Chem.* **2010**, *48*, 1516-1525.
(195) Li, T.; Liu, H.; Zeng, L.; Yang, S.; Li, Z.; Zhang, J.; Zhou, X. *J. Mater. Chem.* **2011**, *21*, 12865-12872.

(196) Vilchez, A.; Rodriguez-Abreu, C.; Esquena, J.; Menner, A.; Bismarck, A. *Langmuir* **2011**, *27*, 13342-13352.
(197) Zhang, S. M.; Chen, J. D. *Chem. Commun.* **2009**, 2217-2219.
(198) Zhang, S. M.; Zhu, Y.; Hua, Y.; Jegat, C.; Chen, J. D.; Taha, M. *Polymer* **2011**, *52*, 4881-4890.
(199) Zhu, Y.; Zhang, S.; Chen, J.; Hu, C. *J. Polym. Sci., A: Polym. Chem.* **2010**, *48*, 4356-4360.
(200) Zhu, Y.; Zhang, S.; Hua, Y.; Chen, J.; Hu, C. *Polymer* **2010**, *51*, 3612-3617.
(201) Hermant, M. C.; Klumperman, B.; Koning, C. E. *Chem. Commun.* **2009**, 2738-2740.
(202) Ikem, V. O.; Menner, A.; Bismarck, A. *Langmuir* **2010**, *26*, 8836-8841.
(203) Cameron, N. R. *Polymer* **2005**, *46*, 1439-1449.
(204) Schoo, H. F. M.; Challa, G.; Rowatt, B.; Sherrington, D. C. *React. Polym.* **1992**, *16*, 125-136.
(205) Pierre, S. J.; Thies, J. C.; Dureault, A.; Cameron, N. R.; van Hest, J. C. M.; Carette, N.; Michon, T.; Weberskirch, R. *Adv. Mater.* **2006**, *18*, 1822-1826.
(206) Wakeman, R. J.; Bhumgara, Z. G.; Akay, G. *Chem. Eng. J.* **1998**, *70*, 133-141.
(207) Krajnc, P.; Leber, N.; Stefanec, D.; Kontrec, S.; Podgornik, A. *J. Chromatogr. A* **2005**, *1065*, 69-73.
(208) Pulko, I.; Smrekar, V.; Podgornik, A.; Krajnc, P. *J. Chromatogr. A* **2011**, *1218*, 2396-2401.
(209) Bokhari, M.; Carnachan, R. J.; Cameron, N. R.; Przyborski, S. A. *Biochem. Biophys. Res. Commun.* **2007**, *354*, 1095-1100.
(210) Bokhari, M.; Carnachan, R. J.; Cameron, N. R.; Przyborski, S. A. *J. Anat.* **2007**, *211*, 567-576.
(211) Barbetta, A.; Massimi, M.; Di Rosario, B.; Nardecchia, S.; De Colli, M.; Devirgiliis, L. C.; Dentini, M. *Biomacromolecules* **2008**, *9*, 2844-2856.
(212) Barbetta, A.; Massimi, M.; Devirgiliis, L. C.; Dentini, M. *Biomacromolecules* **2006**, *7*, 3059-3068.
(213) Bokhari, M. A.; Akay, G.; Zhang, S. G.; Birch, M. A. *Biomaterials* **2005**, *26*, 5198-5208.
(214) Busby, W.; Cameron, N. R.; Jahoda, C. A. B. *Biomacromolecules* **2001**, *2*, 154-164.
(215) Busby, W.; Cameron, N. R.; Jahoda, A. B. C. *Polym. Int.* **2002**, *51*, 871-881.
(216) Lumelsky, Y.; Zoldan, J.; Levenberg, S.; Silverstein, M. S. *Macromolecules* **2008**, *41*, 1469-1474.
(217) Lumelsky, Y.; Lalush Michael, I.; Levenberg, S.; Silverstein, M. *J. Polym. Sci., A: Polym. Chem.* **2009**, *47*, 7043-7053.
(218) Moglia, R. S.; Holm, J. L.; Sears, N. A.; Wilson, C. J.; Harrison, D. M.; Cosgriff-Hernandez, E. *Biomacromolecules* **2011**, *12*, 3621-3628.
(219) Barbetta, A.; Dentini, M.; De Vecchis, M. S.; Filippini, P.; Formisano, G.; Caiazza, S. *Adv. Funct. Mater.* **2005**, *15*, 118-124.
(220) Barbetta, A.; Dentini, M.; Zannoni, E. M.; De Stefano, M. E. *Langmuir* **2005**, *21*, 12333-12341.
(221) Barbetta, A.; Barigelli, E.; Dentini, M. *Biomacromolecules* **2009**, *10*, 2328-2337.
(222) Murray, M.; Snowden, M. *Adv. Colloid Interface Sci.* **1995**, *54*, 73-91.
(223) Saunders, B.; Vincent, B. *Adv. Colloid Interface Sci.* **1999**, *80*, 1-25.
(224) Funke, W.; Okay, O.; Joos-Müller, B. *Adv. Polym. Sci.* **1998**, *136*, 139-234.
(225) Pelton, R. *Adv. Colloid Interface Sci.* **2000**, *85*, 1-33.
(226) Gil, E. S.; Hudson, S. M. *Prog. Polym. Sci.* **2004**, *29*, 1173-1222.
(227) Motornov, M.; Roiter, Y.; Tokarev, I.; Minko, S. *Prog. Polym. Sci.* **2010**, *35*, 174-211.
(228) Das, M.; Zhang, H.; Kumacheva, E. *Annu. Rev. Mater. Res.* **2006**, *36*, 117-142.

(229) Lyon, L. A.; Meng, Z.; Singh, N.; Sorrell, C. D.; St. John, A. *Chem. Soc. Rev.* **2009**, *38*, 865-874.
(230) Fernandez-Barbero, A.; Suarez, I. J.; Sierra-MartÌn, B.; Fernandez-Nieves, A.; de las Nieves, F. J.; Marquez, M.; Rubio-Retama, J.; Lopez-Cabarcos, E. *Adv. Colloid Interface Sci.* **2009**, *147-148*, 88-108.
(231) Thorne, J. B.; Vine, G. J.; Snowden, M. J. *Colloid Polym. Sci.* **2011**, *289*, 625-646.
(232) Guan, Y.; Zhang, Y. *Soft matter* **2011**, *7*, 6375-6384.
(233) Ngai, T.; Behrens, S. H.; Auweter, H. *Chem. Commun.* **2005**, 331-333.
(234) Fujii, S.; Read, E. S.; Binks, B. P.; Armes, S. P. *Adv. Mater.* **2005**, *17*, 1014-1018.
(235) Ngai, T.; Auweter, H.; Behrens, S. H. *Macromolecules* **2006**, *39*, 8171-8177.
(236) Binks, B. P.; Murakami, R.; Armes, S. P.; Fujii, S. *Langmuir* **2006**, *22*, 2050-2057.
(237) Fujii, S.; Armes, S. P.; Binks, B. P.; Murakami, R. *Langmuir* **2006**, *22*, 6818-6825.
(238) Brugger, B.; Richtering, W. *Adv. Mater.* **2007**, *19*, 2973-2978.
(239) Zhang, Y.; Zhu, W.; Wang, B.; Ding, J. *J. Control. Release* **2005**, *105*, 260-268.
(240) Hamidi, M.; Azadi, A.; Rafiei, P. *Adv. Drug Deliv. Rev.* **2008**, *60*, 1638-1649.
(241) Kabanov, A.; Vinogradov, S. *Angew. Chem. Int. Ed.* **2009**, *48*, 5418-5429.
(242) Raemdonck, K.; Demeester, J.; De Smedt, S. *Soft matter* **2009**, *5*, 707-715.
(243) Oh, J.; Lee, D.; Park, J. *Prog. Polym. Sci.* **2009**, *34*, 1261-1282.
(244) Malmsten, M.; Bysell, H.; Hansson, P. *Curr. Opin. Colloid Interface Sci.* **2010**, *15*, 435-444.
(245) Zha, L.; Banik, B.; Alexis, F. *Soft Matter* **2011**, *7*, 5908-5916.
(246) Lee, K.; Silva, E. A.; Mooney, D. J. *J. R. Soc. Interface* **2011**, *8*, 153-170.
(247) Schmaljohann, D. *Adv. Drug Deliv. Rev.* **2006**, *58*, 1655-1670.
(248) Pelton, R. H.; Chibante, P. *Colloids Surf., A: Physicochem. Eng. Asp.* **1986**, *20*, 247-256.
(249) Pelton, R. H.; Pelton, H. M.; Morphesis, A.; Rowell, R. L. *Langmuir* **1989**, *5*, 816-818.
(250) Kawaguchi, H.; Fujimoto, K.; Mizuhara, Y. *Colloid Polym. Sci.* **1992**, *270*, 53-57.
(251) Saunders, B.; Vincent, B. *J. Chem. Soc., Faraday Trans.* **1996**, *92*, 3385-3389.
(252) Heskins, M.; Guillet, J. E. *J. Macromol. Sci., A: Pure Appl. Chem.* **1968**, *A2*, 1441-1455.
(253) Fujishige, S.; Kubota, K.; Ando, I. *J. Phys. Chem.* **1989**, *93*, 3311-3313.
(254) Schild, H. G.; Tirrell, D. A. *J. Phys. Chem.* **1990**, *94*, 4352-4356.
(255) Hirokawa, Y.; Tanaka, T. *J. Chem. Phys.* **1984**, *81*, 6379-6380.
(256) Kubota, K.; Fujishige, S.; Ando, I. *J. Phys. Chem.* **1990**, *94*, 5154-5158.
(257) Yamamoto, I.; Iwasaki, K.; Hirotsu, S. *J. Phys. Soc. Jpn.* **1989**, *58*, 210-215.
(258) Wu, C.; Zhou, S. *Macromolecules* **1995**, *28*, 5388-5390.
(259) Wu, C.; Zhou, S. *Macromolecules* **1995**, *28*, 8381-8387.
(260) Wang, X.; Qiu, X.; Wu, C. *Macromolecules* **1998**, *31*, 2972-2976.
(261) Wu, C.; Wang, X. *Phys. Rev. Lett.* **1998**, *80*, 4092-4094.
(262) Li, Y.; Tanaka, T. *Annu. Rev. Mater. Sci.* **1992**, *22*, 243-277.
(263) Otake, K.; Inomata, H.; Konno, M.; Saito, S. *Macromolecules* **1990**, *23*, 283-289.
(264) Wu, C.; Zhou, S. Q.; Au-yeung, S. C. F.; Jiang, S. H. *Angew. Makromol. Chem.* **1996**, *240*, 123-136.
(265) Tanaka, T.; Sato, E.; Hirokawa, Y.; Hirotsu, S.; Peetermans, J. *Phys. Rev. Lett.* **1985**, *55*, 2455-2458.
(266) Schild, H. G. *Prog. Polym. Sci.* **1992**, *17*, 163-249.
(267) Hirose, Y.; Amiya, T.; Hirokawa, Y.; Tanaka, T. *Macromolecules* **1987**, *20*, 1342-1344.

(268) Snowden, M. J.; Chowdhry, B. Z.; Vincent, B.; Morris, G. E. *J. Chem. Soc., Faraday Trans.* **1996**, *92*, 5013-5016.
(269) Kratz, K.; Hellweg, T.; Eimer, W. *Colloids Surf., A: Physicochem. Eng. Asp.* **2000**, *170*, 137-149.
(270) Ito, S.; Ogawa, K.; Suzuki, H.; Wang, B. L.; Yoshida, R.; Kokufuta, E. *Langmuir* **1999**, *15*, 4289-4294.
(271) Morris, G. E.; Vincent, B.; Snowden, M. J. *J. Colloid Interface Sci.* **1997**, *190*, 198-205.
(272) Ogawa, K.; Nakayama, A.; Kokufuta, E. *Langmuir* **2003**, *19*, 3178-3184.
(273) Chen, G.; Hoffman, A. S. *Nature* **1995**, *373*, 49-52.
(274) McPhee, W.; Tam, K.; Pelton, R. *J. Colloid Interface Sci.* **1993**, *156*, 24-30.
(275) Oh, K. S.; Oh, J. S.; Choi, H. S.; Bae, Y. C. *Macromolecules* **1998**, *31*, 7328-7335.
(276) Kratz, K.; Eimer, W. *Ber. Bunsen-Ges. Phys. Chem.* **1998**, *102*, 848-854.
(277) Eichenbaum, G. M.; Kiser, P. F.; Dobrynin, A. V.; Simon, S. A.; Needham, D. *Macromolecules* **1999**, *32*, 4867-4878.
(278) Senff, H.; Richtering, W. *Colloid Polym. Sci.* **2000**, *278*, 830-840.
(279) Varga, I.; Gilanyi, T.; Meszaros, R.; Filipcsei, G.; Zrinyi, M. *J. Phys. Chem. B* **2001**, *105*, 9071-9076.
(280) Wu, X.; Pelton, R. H.; Hamielec, A. E.; Woods, D. R.; McPhee, W. *Colloid Polym. Sci.* **1994**, *272*, 467-477.
(281) Berne, B.; Weeks, J.; Zhou, R. *Annu. Rev. Phys. Chem.* **2009**, *60*, 85-103.
(282) Ben-Naim, A. *Hydrophobic Interactions*; Plenum Press: New York, 1980.
(283) Shibayama, M.; Morimoto, M.; Nomura, S. *Macromolecules* **1994**, *27*, 5060-5066.
(284) Maeda, Y.; Kitano, H. *Spectrochim. Acta A* **1995**, *51*, 2433-2446.
(285) Israelachvili, J.; Wennerstrom, H. *Nature* **1996**, *379*, 219-225.
(286) Israelachvili, J. N. *Intermolecular and Surface Forces*; Second ed.; Academic Press, Harcout Brace & Company, Publishers: London, 1992.
(287) Israelachvili, J.; Pashley, R. *Nature* **1982**, *300*, 341-342.
(288) Shibayama, M.; Tanaka, T. *Adv. Polym. Sci.* **1993**, *109*, 1-62.
(289) Lum, K.; Chandler, D.; Weeks, J. *J. Phys. Chem. B* **1999**, *103*, 4570-4577.
(290) Meyer, E. E.; Rosenberg, K. J.; Israelachvili, J. *Proc. Natl. Acad. Sci. U.S.A.* **2006**, *103*, 15739-15746.
(291) Ilmain, F.; Tanaka, T.; Kokufuta, E. *Nature* **1991**, *349*, 400-401.
(292) Cho, J. K.; Meng, Z. Y.; Lyon, L. A.; Breedveld, V. *Soft Matter* **2009**, *5*, 3599-3602.
(293) Woodward, N. C.; Snowden, M. J.; Chowdhry, B. Z.; Jenkins, P.; Larson, I. *Langmuir* **2002**, *18*, 2089-2095.
(294) Agbugba, C. B.; Hendriksen, B. A.; Chowdhry, B. Z.; Snowden, M. J. *Colloids Surf., A: Physicochem. Eng. Asp.* **1998**, *137*, 155-164.
(295) Snowden, M. J.; Thomas, D.; Vincent, B. *Analyst* **1993**, *118*, 1367-1369.
(296) Verwey, E. J. W.; Overbeek, J. T. G. *Theory of the Stability of Lyophobic Colloids*; Elsevier Publishing Company, Inc.: New York, 1948.
(297) *CRC Handbook of Chemistry and Physics*; 90th ed.; Lide, D. R., Ed.; CRC Press: Boca Raton, FL, 2009, P8-43.
(298) Ahn, J.-S.; Choi, H.-K.; Cho, C.-S. *Biomaterials* **2001**, *22*, 923-928.
(299) Myung, D.; Koh, W. U.; Ko, J. M.; Hu, Y.; Carrasco, M.; Noolandi, J.; Ta, C. N.; Frank, C. W. *Polymer* **2007**, *48*, 5376-5387.
(300) Kawasaki, H.; Sasaki, S.; Maeda, H. *J. Phys. Chem. B* **1997**, *101*, 5089-5093.
(301) Suzuki, H.; Wang, B. L.; Yoshida, R.; Kokufuta, E. *Langmuir* **1999**, *15*, 4283-4288.
(302) Christensen, M. L.; Keiding, K. *Colloids Surf., A: Physicochem. Eng. Asp.* **2005**, *252*, 61-69.

(303) Hoare, T.; Pelton, R. *Langmuir* **2006**, *22*, 7342-7350.
(304) Shibayama, M.; Mizutani, S.-y.; Nomura, S. *Macromolecules* **1996**, *29*, 2019-2024.
(305) Arleth, L.; Xia, X. H.; Hjelm, R. P.; Wu, J. Z.; Hu, Z. B. *J. Polym. Sci., B: Polym. Phys.* **2005**, *43*, 849-860.
(306) Ricka, J.; Tanaka, T. *Macromolecules* **1984**, *17*, 2916-2921.
(307) Capriles-Gonzalez, D.; Sierra-Martin, B.; Fernandez-Nieves, A.; Fernandez-Barbero, A. *J. Phys. Chem. B* **2008**, *112*, 12195-12200.
(308) Barrat, J.; Joanny, J.; Pincus, P. *J. Phys. II* **1992**, *2*, 1531-1544.
(309) Flory, P. J. *Principles of Polymer Chemistry*; Cornell Press: Ithaca, NY, 1953.
(310) Kawasaki, H.; Sasaki, S.; Maeda, H. *J. Phys. Chem. B* **1997**, *101*, 4184-4187.
(311) Kratz, K.; Hellweg, T.; Eimer, W. *Ber. Bunsen-Ges. Phys. Chem.* **1998**, *102*, 1603-1608.
(312) Bokias, G.; Staikos, G.; Iliopoulos, I. *Polymer* **2000**, *41*, 7399-7405.
(313) Keerl, M.; Smirnovas, V.; Winter, R.; Richtering, W. *Angew. Chem. Int. Ed.* **2008**, *47*, 338-341.
(314) Bradley, M.; Ramos, J.; Vincent, B. *Langmuir* **2005**, *21*, 1209-1215.
(315) Zhang, Y.; Furyk, S.; Bergbreiter, D.; Cremer, P. *J. Am. Chem. Soc.* **2005**, *127*, 14505-14510.
(316) Lopez-Leon, T.; Fernandez-Nieves, A. *Phys. Rev. E* **2007**, *75*, 011801.
(317) Hou, Y.; Yu, C.; Liu, G.; Ngai, T.; Zhang, G. *J. Phys. Chem. B* **2010**, *114*, 3799-3803.
(318) Routh, A. F.; Vincent, B. *Langmuir* **2002**, *18*, 5366-5369.
(319) Daly, E.; Saunders, B. R. *Langmuir* **2000**, *16*, 5546-5552.
(320) Schoch, R. B.; Han, J.; Renaud, P. *Rev. Mod. Phys.* **2008**, *80*, 839-883.
(321) Arditty, S.; Whitby, C. P.; Binks, B. P.; Schmitt, V.; Leal-Calderon, F. *Eur. Phys. J. E* **2003**, *11*, 273-281.
(322) Binks, B. P.; Philip, J.; Rodrigues, J. A. *Langmuir* **2005**, *21*, 3296-3302.
(323) Frelichowska, J.; Bolzinger, M.-A.; Chevalier, Y. *J. Colloid Interface Sci.* **2010**, *351*, 348-356.
(324) Fernandez-Barbero, A.; Fernandez-Nieves, A.; Grillo, I.; Lopez-Cabarcos, E. *Phys. Rev. E* **2002**, *66*, 051803.
(325) Stieger, M.; Richtering, W.; Pedersen, J. S.; Lindner, P. *J. Chem. Phys.* **2004**, *120*, 6197-6206.
(326) Saunders, B. R.; Laajam, N.; Daly, E.; Teow, S.; Hu, X. H.; Stepto, R. *Adv. Colloid Interface Sci.* **2009**, *147-48*, 251-262.
(327) Hofl, S.; Zitzler, L.; Hellweg, T.; Herminghaus, S.; Mugele, F. *Polymer* **2007**, *48*, 245-254.
(328) Ogawa, K.; Sato, S.; Kokufuta, E. *Langmuir* **2005**, *21*, 4830-4836.
(329) Rasmusson, M.; Routh, A.; Vincent, B. *Langmuir* **2004**, *20*, 3536-3542.
(330) Kaszuba, M.; McKnight, D.; Connah, M. T.; McNeil-Watson, F. K.; Nobbmann, U. *J. Nanopart. Res.* **2008**, *10*, 823-829.
(331) Binks, B. P.; Clint, J. H. *Langmuir* **2002**, *18*, 1270-1273.
(332) Lele, A. K.; Hirve, M. M.; Badiger, M. V.; Mashelkar, R. A. *Macromolecules* **1997**, *30*, 157-159.
(333) Wu, C.; Zhou, S. Q. *J. Macromol. Sci., B: Phys.* **1997**, *B36*, 345-355.
(334) Wu, C. *Polymer* **1998**, *39*, 4609-4619.
(335) Gilanyi, T.; Varga, I.; Meszaros, R.; Filipcsei, G.; Zrinyi, M. *Phys. Chem. Chem. Phys.* **2000**, *2*, 1973-1977.
(336) Percot, A.; Zhu, X. X.; Lafleur, M. *J. Polym. Sci., B: Polym. Phys.* **2000**, *38*, 907-915.
(337) Maeda, Y.; Higuchi, T.; Ikeda, I. *Langmuir* **2000**, *16*, 7503-7509.
(338) Maeda, Y.; Yamamoto, H.; Ikeda, I. *Colloid Polym. Sci.* **2004**, *282*, 1268-1273.

(339) Kogure, H.; Nanami, S.; Masuda, Y.; Toyama, Y.; Kubota, K. *Colloid Polym. Sci.* **2005**, *283*, 1163-1171.
(340) Ono, Y.; Shikata, T. *J. Am. Chem. Soc.* **2006**, *128*, 10030-10031.
(341) Ahmed, Z.; Gooding, E.; Pimenov, K.; Wang, L.; Asher, S. *J. Phys. Chem. B* **2009**, *113*, 4248-4256.
(342) In http://www.visking.com/Visk_Tech_Clean.htm.
(343) In http://www.visking.com/Visk_TempTol.htm.
(344) van den Hul, H. J.; Vanderhoff, J. W. *J. Colloid Interface Sci.* **1968**, *28*, 336-337.
(345) Tam, K. C.; Ragaram, S.; Pelton, R. H. *Langmuir* **1994**, *10*, 418-422.
(346) Suzuki, H.; Kokufuta, E. *Colloids Surf., A: Physicochem. Eng. Asp.* **1999**, *147*, 233-240.
(347) Gilanyi, T.; Varga, I.; Meszaros, R.; Filipcsei, G.; Zrinyi, M. *Langmuir* **2001**, *17*, 4764-4769.
(348) Bradley, M.; Vincent, B.; Burnett, G. *Langmuir* **2007**, *23*, 9237-9241.
(349) Wilkinson, M. C.; Hearn, J.; Cope, P.; Chainey, M. *Br. Polym. J.* **1981**, *13*, 82-89.
(350) Hearn, J.; Wilkinson, M. C.; Goodall, A. R. *Adv. Colloid Interface Sci.* **1981**, *14*, 173-236.
(351) Wilkinson, M. C.; Hearn, J.; Steward, P. A. *Adv. Colloid Interface Sci.* **1999**, *81*, 77-165.
(352) Porter, M. R. *Handbook of surfactants*; second ed.; Blackie Academic & Professional: London, 1994.
(353) Schmidt, S.; Hellweg, T.; von Klitzing, R. *Langmuir* **2008**, *24*, 12595-12602.
(354) Williams, J. M. *Langmuir* **1988**, *4*, 44-49.
(355) Williams, J. M. *Langmuir* **1991**, *7*, 1370-1377.
(356) Hainey, P.; Huxham, I. M.; Rowatt, B.; Sherrington, D. C.; Tetley, L. *Macromolecules* **1991**, *24*, 117-121.
(357) Choi, J. S.; Chun, B. C.; Lee, S. J. *Macromol. Res.* **2003**, *11*, 104-109.
(358) Lepine, O.; Birot, M.; Deleuze, H. *Colloid Polym. Sci.* **2008**, *286*, 1273-1280.
(359) Manley, S. S.; Graeber, N.; Grof, Z.; Menner, A.; Hewitt, G. F.; Stepanek, F.; Bismarck, A. *Soft Matter* **2009**, *5*, 4780-4787.
(360) Cameron, N. R.; Sherrington, D. C. *Adv. Polym. Sci.* **1996**, *126*, 163-214.
(361) Cameron, N. R.; Barbetta, A. *J. Mater. Chem.* **2000**, *10*, 2466-2472.
(362) Barbetta, A.; Cameron, N. R. *Macromolecules* **2004**, *37*, 3188-3201.
(363) Barbetta, A.; Cameron, N. R. *Macromolecules* **2004**, *37*, 3202-3213.
(364) Brugger, B.; Rosen, B. A.; Richtering, W. *Langmuir* **2008**, *24*, 12202-12208.
(365) Brugger, B.; Richtering, W. *Langmuir* **2008**, *24*, 7769-7777.
(366) Binks, B. P.; Whitby, C. P. *Langmuir* **2004**, *20*, 1130-1137.
(367) Yan, N. X.; Gray, M. R.; Masliyah, J. H. *Colloids Surf., A: Physicochem. Eng. Asp.* **2001**, *193*, 97-107.
(368) Binks, B. P.; Lumsdon, S. O. *Phys. Chem. Chem. Phys.* **2000**, *2*, 2959-2967.
(369) Demond, A. H.; Lindner, A. S. *Environ. Sci. Technol.* **1993**, *27*, 2318-2331.
(370) Chen, H. H.; Ruckenstein, E. *J. Colloid Interface Sci.* **1990**, *138*, 473-479.
(371) Stiller, S.; Gers-Barlag, H.; Lergenmueller, M.; Pflucker, F.; Schulz, J.; Wittern, K. P.; Daniels, R. *Colloids Surf., A: Physicochem. Eng. Asp.* **2004**, *232*, 261-267.
(372) Tambe, D. E.; Sharma, M. M. *Adv. Colloid Interface Sci.* **1994**, *52*, 1-63.
(373) Binks, B. P.; Fletcher, P. D. I.; Holt, B. L.; Beaussoubre, P.; Wong, K. *Phys. Chem. Chem. Phys.* **2010**, *12*, 11954-11966.
(374) Gautier, F.; Destribats, M.; Perrier-Cornet, R.; Dechezelles, J. F.; Giermanska, J.; Heroguez, V.; Ravaine, S.; Leal-Calderon, F.; Schmitt, V. *Phys. Chem. Chem. Phys.* **2007**, *9*, 6455-6462.

(375) Wiley, R. M. *J. Colloid Sci.* **1954**, *9*, 427-437.
(376) Whitesides, T. H.; Ross, D. S. *J. Colloid Interface Sci.* **1995**, *169*, 48-59.
(377) Dixon, K. W. In *Polymer handbook*; 4th ed.; Brandrup, J., Immergut, E. H., Grulke, E. A., Eds.; John Wiley & Sons, Inc.: New York, 1999.
(378) Bresme, F.; Oettel, M. *J. Phys.: Condens. Matter* **2007**, *19*, 413101.
(379) Thieme, J.; Abend, S.; Lagaly, G. *Colloid Polym. Sci.* **1999**, *277*, 257-260.
(380) Horozov, T.; Binks, B.; Gottschalk-Gaudig, T. *Phys. Chem. Chem. Phys.* **2007**, *9*, 6398-6404.
(381) Destribats, M.; Lapeyre, V.; Wolfs, M.; Sellier, E.; Leal-Calderon, F.; Ravaine, V.; Schmitt, V. *Soft Matter* **2011**, *7*, 7689-7698.
(382) Binks, B. P.; Lumsdon, S. O. *Langmuir* **2000**, *16*, 3748-3756.
(383) Binks, B. P.; Murakami, R. *Nature Mater.* **2006**, *5*, 865-869.
(384) Binks, B. P.; Murakami, R.; Armes, S. P.; Fujii, S. *Angew. Chem. Int. Ed.* **2005**, *44*, 4795-4798.
(385) Brooks, B. W.; Richmond, H. N. *Chem. Eng. Sci.* **1994**, *49*, 1053-1064.
(386) Sun, G.; Li, Z.; Ngai, T. *Angew. Chem. Int. Ed.* **2010**, *49*, 2163-2166.
(387) Menon, V. B.; Wasan, D. T. In *Encyclopedia of Emulsion Technology, Volume 2, Applications*; Becher, P., Ed.; Marcel Dekker, Inc.: New York, 1985; Vol. 2.
(388) Kunieda, H.; Evans, D. F.; Solans, C.; Yoshida, M. *Colloids Surf.* **1990**, *47*, 35-43.
(389) Li, Z.; Geisel, K.; Richtering, W.; Ngai, T. *Soft Matter* **2013**, *9*, 9939-9946.
(390) Walstra, P. In *Encyclopedia of Emulsion Technology, Volume 1, Basic Theory*; Becher, P., Ed.; Marcel Dekker, Inc.: New York, 1983; Vol. 1.
(391) Pawar, A. B.; Caggioni, M.; Ergun, R.; Hartel, R. W.; Spicer, P. T. *Soft Matter* **2011**, *7*, 7710-7716.
(392) Schmidt, S.; Liu, T. T.; Rutten, S.; Phan, K. H.; Moller, M.; Richtering, W. *Langmuir* **2011**, *27*, 9801-9806.
(393) Destribats, M.; Lapeyre, V.; Sellier, E.; Leal-Calderon, F.; Schmitt, V.; Ravaine, V. *Langmuir* **2011**, *27*, 14096-14107.
(394) Monteux, C.; Marliere, C.; Paris, P.; Pantoustier, N.; Sanson, N.; Perrin, P. *Langmuir* **2010**, *26*, 13839-13846.
(395) Lucassen-Reynders, E. H.; Van Den Tempel, M. *J. Phys. Chem.* **1963**, *67*, 731-734.
(396) Yin, D.; Zhang, Q.; Yin, C.; Jia, Y.; Zhang, H. *Colloids Surf., A: Physicochem. Eng. Asp.* **2010**, *367*, 70-75.
(397) Nikolaides, M. G.; Bausch, A. R.; Hsu, M. F.; Dinsmore, A. D.; Brenner, M. P.; Weitz, D. A.; Gay, C. *Nature* **2002**, *420*, 299-301.
(398) Tarimala, S.; Ranabothu, S. R.; Vernetti, J. P.; Dai, L. L.; Ranabothu, S.; Vernetti, J.; Dai, L. *Langmuir* **2004**, *20*, 5171-5173.
(399) Tamada, Y.; Ikada, Y. *J. Biomed. Mater. Res.* **1994**, *28*, 783-789.
(400) Webb, K.; Hlady, V.; Tresco, P. A. *J. Biomed. Mater. Res.* **1998**, *41*, 422-430.
(401) Krajnc, P.; Stefanec, D.; Pulko, I. *Macromol. Rapid Commun.* **2005**, *26*, 1289-1293.
(402) Zhang, H.; Cooper, A. I. *Chem. Mater.* **2002**, *14*, 4017-4020.
(403) Kovacic, S.; Stefanec, D.; Krajnc, P. *Macromolecules* **2007**, *40*, 8056-8060.
(404) Kulygin, O.; Silverstein, M. S. *Soft Matter* **2007**, *3*, 1525-1529.
(405) Zhang, H.; Cooper, A. I. *Adv. Mater.* **2007**, *19*, 2439-2444.
(406) Grant, N. C.; Cooper, A. I.; Zhang, H. *ACS Appl. Mater. Interfaces* **2010**, *2*, 1400-1406.
(407) Li, Z.; Ming, T.; Wang, J.; Ngai, T. *Angew. Chem. Int. Ed.* **2009**, *48*, 8490-8493.
(408) Li, Z.; Ngai, T. *Colloid Polym. Sci.* **2011**, *289*, 489-496.
(409) Li, Z.; Wei, X.; Ngai, T. *Chem. Commun.* **2011**, *47*, 331-333.

(410) Chen, Y. M.; Shiraishi, N.; Satokawa, H.; Kakugo, A.; Narita, T.; Gong, J. P.; Osada, Y.; Yamamoto, K.; Ando, J. *Biomaterials* **2005**, *26*, 4588-4596.
(411) Park, B. J.; Pantina, J. P.; Furst, E. M.; Oettel, M.; Reynaert, S.; Vermant, J. *Langmuir* **2008**, *24*, 1686-1694.
(412) Babak, V. G. *Colloids Surf., A: Physicochem. Eng. Asp.* **1994**, *85*, 279-294.
(413) Arditty, S.; Schmitt, V.; Giermanska-Kahn, J.; Leal-Calderon, F. *J. Colloid Interface Sci.* **2004**, *275*, 659-664.
(414) Binks, B. P.; Lumsdon, S. O. *Phys. Chem. Chem. Phys.* **1999**, *1*, 3007-3016.
(415) Mishchuk, N. A.; Sanfeld, A.; Steinchen, A. *Adv. Colloid Interface Sci.* **2004**, *112*, 129-157.
(416) Ruckenstein, E.; Park, J. S. *Polymer* **1992**, *33*, 405-417.
(417) Ruckenstein, E. *Adv. Polym. Sci.* **1997**, *127*, 1-58.
(418) Kizling, J.; Kronberg, B. *Colloids Surf.* **1990**, *50*, 131-140.
(419) Kizling, J.; Kronberg, B. *Adv. Colloid Interface Sci.* **2001**, *89*, 395-399.
(420) Kizling, J.; Kronberg, B.; Eriksson, J. C. *Adv. Colloid Interface Sci.* **2006**, *123*, 295-302.
(421) Princen, H. M. *J. Colloid Interface Sci.* **1990**, *134*, 188-197.
(422) Girifalco, L. A.; Good, R. J. *J. Phys. Chem.* **1957**, *61*, 904-909.
(423) Arditty, S.; Schmitt, V.; Lequeux, F.; Leal-Calderon, F. *Eur. Phys. J. B* **2005**, *44*, 381-393.
(424) Chen, H. H.; Ruckenstein, E. *J. Colloid Interface Sci.* **1991**, *145*, 260-269.
(425) Howdle, S. M.; Watson, M. S.; Whitaker, M. J.; Popov, V. K.; Davies, M. C.; Mandel, F. S.; Wang, J. D.; Shakesheff, K. M. *Chem. Commun.* **2001**, 109-110.
(426) Lepock, J. R.; Frey, H. E.; Ritchie, K. P. *J. Cell Biol.* **1993**, *122*, 1267-1276.
(427) Bischof, J. C.; Padanilam, J.; Holmes, W. H.; Ezzell, R. M.; Lee, R. C.; Tompkins, R. G.; Yarmush, M. L.; Toner, M. *Biophys. J.* **1995**, *68*, 2608-2614.
(428) He, X. *Open Biomed. Eng. J.* **2011**, *5*, 47-73.
(429) Tokuyama, H.; Kanehara, A. *Langmuir* **2007**, *23*, 11246-11251.
(430) Fernandez-Trillo, F.; van Hest, J. C. M.; Thies, J. C.; Michon, T.; Weberskirch, R.; Cameron, N. R. *Adv. Mater.* **2009**, *21*, 55-59.
(431) Butler, R.; Hopkinson, I.; Cooper, A. I. *J. Am. Chem. Soc.* **2003**, *125*, 14473-14481.
(432) Tanny, G. B.; Kenigsberg, Y.; Shchori, E. European Patent, EP 0216622, 1987.
(433) Thunhorst, K. L.; Gehlsen, M. D.; Wright, R. E.; Nelson, E. W.; Koecher, S. D.; Gold, D. World Patent, WO 0121693, 2001.
(434) Clear, S. C.; Parthasarathy, R. V.; Sura, R. K.; Soo, P. P. US Patent, US 6890963, 2005.
(435) Burdick, J. A.; Anseth, K. S. *Biomaterials* **2002**, *23*, 4315-4323.
(436) Williams, C. G.; Kim, T. K.; Taboas, A.; Malik, A.; Manson, P.; Elisseeff, J. *Tissue Eng.* **2003**, *9*, 679-688.
(437) Bryant, S. J.; Bender, R. J.; Durand, K. L.; Anseth, K. S. *Biotechnol. Bioeng.* **2004**, *86*, 747-755.
(438) Williams, C. G.; Malik, A. N.; Kim, T. K.; Manson, P. N.; Elisseeff, J. H. *Biomaterials* **2005**, *26*, 1211-1218.
(439) Bryant, S. J.; Arthur, J. A.; Anseth, K. S. *Acta Biomater.* **2005**, *1*, 243-252.
(440) Burdick, J. A.; Chung, C.; Jia, X.; Randolph, M. A.; Langer, R. *Biomacromolecules* **2005**, *6*, 386-391.
(441) Hwang, N. S.; Varghese, S.; Theprungsirikul, P.; Canver, A.; Elisseeff, J. *Biomaterials* **2006**, *27*, 6015-6023.
(442) Nuttelman, C. R.; Benoit, D. S. W.; Tripodi, M. C.; Anseth, K. S. *Biomaterials* **2006**, *27*, 1377-1386.

(443) Fedorovich, N. E.; Oudshoorn, M. H.; van Geemen, D.; Hennink, W. E.; Alblas, J.; Dhert, W. J. A. *Biomaterials* **2009**, *30*, 344-353.
(444) Sabnis, A.; Rahimi, M.; Chapman, C.; Nguyen, K. T. *J. Biomed. Mater. Res. A* **2009**, *91A*, 52-59.
(445) Tokuyama, H.; Kato, Y. *Colloids Surf., B: Biointerfaces* **2008**, *67*, 92-98.
(446) Tokuyama, H.; Sumida, H.; Kanehara, A.; Nii, S. *Colloid Polym. Sci.* **2009**, *287*, 115-121.
(447) Kitagawa, N. World Patent, WO 9900187, 1999.
(448) Yan, Y.; Masliyah, J. H. *Colloids Surf., A: Physicochem. Eng. Asp.* **1993**, *75*, 123-132.
(449) Yan, N. X.; Masliyah, J. H. *Colloids Surf., A: Physicochem. Eng. Asp.* **1995**, *96*, 243-252.
(450) Lou, X.; Dalton, P. D.; Chirila, T. V. *J. Mater. Sci. Mater. Med.* **2000**, *11*, 319-325.
(451) Arriola, D. J.; Cutie, S. S.; Henton, D. E.; Powell, C.; Smith, P. B. *J. Appl. Polym. Sci.* **1997**, *63*, 439-451.
(452) Yin, Y.-L.; Prud'homme, R. K.; Stanley, F. In *Polyelectrolyte Gels: Properties, Preparation, and Applications*; Harland, R. S., Prud'homme, R. K., Eds.; American Chemical Society: Washington, DC, 1992; Vol. ACS Symposium Series 480.
(453) Lindemann, B.; Schroder, U. P.; Oppermann, W. *Macromolecules* **1997**, *30*, 4073-4077.
(454) Ruan, W.; Wang, X.; Lian, Y.; Huang, Y.; Niu, A. *J. Appl. Polym. Sci.* **2006**, *101*, 1181-1187.
(455) Zimmerman, R. L.; Jones, G. D.; Nummy, W. R. *Ind. Eng. Chem. Prod. Res. Dev.* **1963**, *2*, 296-303.
(456) Clayton, A. B.; Chirila, T. V.; Dalton, P. D. *Polym. Int.* **1997**, *42*, 45-56.
(457) Clayton, A. B.; Chirila, T. V.; Lou, X. *Polym. Int.* **1997**, *44*, 201-207.
(458) Decker, C. *Prog. Polym. Sci.* **1996**, *21*, 593-650.
(459) Oh, S. H.; Park, I. K.; Kim, J. M.; Lee, J. H. *Biomaterials* **2007**, *28*, 1664-1671.
(460) Otsuki, B.; Takemoto, M.; Fujibayashi, S.; Neo, M.; Kokubo, T.; Nakamura, T. *Biomaterials* **2006**, *27*, 5892-5900.
(461) Decker, C.; Jenkins, A. D. *Macromolecules* **1985**, *18*, 1241-1244.
(462) Andrzejewska, E. *Prog. Polym. Sci.* **2001**, *26*, 605-665.
(463) Bartl, V. H.; von Bonin, W. *Makromol. Chem.* **1962**, *57*, 74-95.
(464) Lissant, K. J.; Mayhan, K. G. *J. Colloid Interface Sci.* **1973**, *42*, 201-208.
(465) Litt, M. H.; Hsieh, B. R.; Krieger, I. M.; Chen, T. T.; Lu, H. L. *J. Colloid Interface Sci.* **1987**, *115*, 312-329.
(466) Jerabek, K.; Pulko, I.; Soukupova, K.; Stefanec, D.; Krajnc, P. *Macromolecules* **2008**, *41*, 3543-3546.
(467) Pakeyangkoon, P.; Magaraphan, R.; Malakul, P.; Nithitanakul, M. *Macromol. Symp.* **2008**, *264*, 149-156.
(468) Maurer, J. J.; Eustace, D. J.; Ratcliffe, C. T. *Macromolecules* **1987**, *20*, 196-202.
(469) Hughes, L. J.; Britt, G. E. *J. Appl. Polym Sci.* **1961**, *5*, 337-348.
(470) Nemec, J. W.; Bauer, W., Jr. In *Encyclopedia of Polymer Science and Engineering*; 2nd ed.; Mark, H. F., Bikales, N. M., Overberger, C. G., Menges, G., Eds.; John Wiley & Sons: New York, 1985; Vol. 1.
(471) Sherrington, D. C. In *Polymer-supported Reactions in Organic Chemistry*; Hodge, P., Sherrington, D. C., Eds.; John Wiley & Sons: Chichester, 1980.
(472) Ellis, T. S.; Karasz, F. E.; Ten Brinke, G. *J. Appl. Polym. Sci.* **1983**, *28*, 23-32.
(473) Wieczorek, P. P.; Kolarz, B. N.; Galina, H. *Angew. Makromol. Chem.* **1984**, *126*, 39-50.
(474) Okay, O.; Balkaş, T. I. *J. Appl. Polym. Sci.* **1986**, *31*, 1785-1795.

(475) Okay, O. *J. Appl. Polym. Sci.* **1986**, *32*, 5533-5542.
(476) Diego, R. B.; Ribelles, J. L. G.; Sánchez, M. S. *J. Appl. Polym. Sci.* **2007**, *104*, 1475-1481.
(477) Okay, O. *Prog. Polym. Sci.* **2000**, *25*, 711-779.
(478) van de Witte, P.; Dijkstra, P. J.; van den Berg, J. W. A.; Feijen, J. *J. Memb. Sci.* **1996**, *117*, 1-31.
(479) Liapis, A.; Pikal, M.; Bruttini, R. *Drying Technol.* **1996**, *14*, 1265-1300.
(480) Hilgen, H.; De Jong, G. J.; Sederel, W. L. *J. Appl. Polym. Sci.* **1975**, *19*, 2647-2654.
(481) Galina, H.; Kolarz, B. N. *J. Appl. Polym. Sci.* **1979**, *24*, 891-900.
(482) Poinescu, I. C.; Beldie, C.; Vlad, C. *J. Appl. Polym. Sci.* **1984**, *29*, 23-34.
(483) Sherrington, D. *Chem. Commun.* **1998**, 2275-2286.
(484) Refojo, M. F.; Yasuda, H. *J. Appl. Polym. Sci.* **1965**, *9*, 2425-2435.
(485) Šprincl, L.; Kopeček, J.; Lím, D. *J. Biomed. Mater. Res.* **1971**, *5*, 447-458.
(486) Chirila, T. V.; Chen, Y.-C.; Griffin, B. J.; Constable, I. J. *Polym. Int.* **1993**, *32*, 221-232.
(487) Monleon Pradas, M.; Gomez Ribelles, J. L.; Serrano Aroca, A.; Gallego Ferrer, G.; Suay Anton, J.; Pissis, P. *Polymer* **2001**, *42*, 4667-4674.
(488) Dziubla, T. D.; Torjman, M. C.; Joseph, J. I.; Murphy-Tatum, M.; Lowman, A. M. *Biomaterials* **2001**, *22*, 2893-2899.
(489) Elliott, J. E.; Macdonald, M.; Nie, J.; Bowman, C. N. *Polymer* **2004**, *45*, 1503-1510.
(490) Silverstein, M. S.; Tai, H. W.; Sergienko, A.; Lumelsky, Y. L.; Pavlovsky, S. *Polymer* **2005**, *46*, 6682-6694.
(491) Leber, N.; Fay, J. D. B.; Cameron, N. R.; Krajnc, P. *J. Polym. Sci., A: Polym. Chem.* **2007**, *45*, 4043-4053.
(492) Barbetta, A.; Dentini, M.; Leandri, L.; Ferraris, G.; Coletta, A.; Bernabei, M. *React. Funct. Polym.* **2009**, *69*, 724-736.
(493) Pakeyangkoon, P.; Magaraphan, R.; Malakul, P.; Nithitanakul, M. *J. Appl. Polym. Sci.* **2009**, *114*, 3041-3048.
(494) Dušek, K. *J. Polym. Sci., B: Polym. Lett.* **1965**, *3*, 209-212.
(495) Dušek, K. *J. Polym. Sci., C: Polym. Symp.* **1967**, *16*, 1289-1299.
(496) Millar, J. R.; Smith, D. G.; Marr, W. E.; Kressman, T. R. E. *J. Chem. Soc.* **1963**, 218-225.
(497) Serrano Aroca, A.; Campillo Fernandez, A. J.; Gomez Ribelles, J. L.; Monleon Pradas, M.; Gallego Ferrer, G.; Pissis, P. *Polymer* **2004**, *45*, 8949-8955.
(498) Okay, O.; Yilmaz, Y.; Kaya, D.; Keskinel, M.; Pekcan, Ö. *Polym. Bull.* **1999**, *43*, 425-431.
(499) Yasuda, H.; Gochin, M.; Stone, W. *J. Polym. Sci., A-1: Polym. Chem.* **1966**, *4*, 2913-2927.
(500) Po, R. *J. Macromol. Sci., C: Polym. Rev.* **1994**, *34*, 607-662.
(501) Abbasian, Z.; Moghbeli, M. R. *J. App. Polym. Sci.* **2010**, *116*, 986-994.
(502) Suzuki, M.; Hirasa, O.; Dušek, K. *Adv. Polym. Sci.* **1993**, *110*, 241-261.
(503) Yoshinobu, M.; Morita, M.; Higuchi, M.; Sakata, I. *J. Appl. Polym. Sci.* **1994**, *53*, 1203-1209.
(504) *Alto 2100 Operation Handbook*.
(505) Nishiyama, Y.; Satoh, M. *J. Polym. Sci., B: Polym. Phys.* **2000**, *38*, 2791-2800.
(506) Moussaid, A.; Candau, S. J.; Joosten, J. G. H. *Macromolecules* **1994**, *27*, 2102-2110.
(507) Chen, J. H.; Ruckenstein, E. *J. Appl. Polym. Sci.* **1992**, *45*, 377-386.
(508) Shibayama, M. *Macromol. Chem. Phys.* **1998**, *199*, 1-30.
(509) Zhang, X.; Wu, D.; Chu, C. *J. Polym. Sci., B: Polym. Phys.* **2003**, *41*, 582-593.
(510) Yazici, I.; Okay, O. *Polymer* **2005**, *46*, 2595-2602.

(511) Boyan, B. D.; Hummert, T. W.; Dean, D. D.; Schwartz, Z. *Biomaterials* **1996**, *17*, 137-146.
(512) Anselme, K. *Biomaterials* **2000**, *21*, 667-681.
(513) Hing, K. A. *Int. J. Appl. Ceram. Technol.* **2005**, *2*, 184-199.
(514) Zhang, L.; Webster, T. *Nano Today* **2009**, *4*, 66-80.
(515) Chen, V. J.; Ma, P. X. *Biomaterials* **2006**, *27*, 3708-3715.
(516) McNeill, I.; Alston, A. *Angew. Makromol. Chem.* **1998**, *262*, 157-172.
(517) Rao, K. M.; Anbananthan, N.; Rajulu, A. V. *Soft Matter* **2011**, *7*, 10780-10786.
(518) Hellman, N. N.; Melvin, E. H. *J. Am. Chem. Soc.* **1950**, *72*, 5186-5188.
(519) Sing, K. S. W.; Everett, D. H.; Haul, R. A. W.; Moscou, L.; Pierotti, R. A.; Rouquerol, J.; Siemieniewska, T. *Pure Appl. Chem.* **1985**, *57*, 603-619.
(520) Hiraoka, K.; Gotanda, M.; Yokoyama, T. *Polym. Bull.* **1980**, *2*, 631-636.
(521) Hsu, Y.-Y.; Gresser, J. D.; Trantolo, D. J.; Lyons, C. M.; Gangadharam, P. R. J.; Wise, D. L. *J. Biomed. Mater. Res.* **1997**, *35*, 107-116.
(522) Zhang, R.; Ma, P. X. *J. Biomed. Mater. Res.* **1999**, *44*, 446-455.
(523) Zhang, R.; Ma, P. X. *J. Biomed. Mater. Res.* **1999**, *45*, 285-293.
(524) Palocci, C.; Barbetta, A.; La Grotta, A.; Dentini, M. *Langmuir* **2007**, *23*, 8243-8251.
(525) Hiraoka, K.; Shin, H.; Yokoyama, T. *Polym. Bull.* **1982**, *8*, 303-309.
(526) Hiraoka, K.; Shirouzu, T.; Yokoyama, T. *Report of The Faculty of Eng., Nagasaki Univ.* **1983**, *13*, 67-72.
(527) Hiraoka, K.; Yokoyama, T. *J. Polym. Sci., B: Polym. Phys.* **1986**, *24*, 769-778.
(528) Audouin, F.; Birot, M.; Pasquinet, E.; Deleuze, H.; Besnard, O.; Poullain, D. *J. Appl. Polym. Sci.* **2008**, *108*, 2808-2813.
(529) Yao, C.; Qi, L.; Jia, H.; Xin, P.; Yang, G.; Chen, Y. *J. Mater. Chem.* **2009**, *19*, 767-772.
(530) Ho, S. T.; Hutmacher, D. W. *Biomaterials* **2006**, *27*, 1362-1376.
(531) Schadler, L. S. In *Nanocomposite Science and Technology*; Ajayan, P. M., Schadler, L. S., Braun, P. V., Eds.; WILEY-VCH Verlag GmbH & Co. KGaA: Weinheim, 2003.
(532) Jordan, J.; Jacob, K. I.; Tannenbaum, R.; Sharaf, M. A.; Jasiuk, I. *Mater. Sci. Eng. A* **2005**, *393*, 1-11.
(533) Tjong, S. C. *Mater. Sci. Eng. R* **2006**, *53*, 73-197.
(534) Hussain, F.; Hojjati, M.; Okamoto, M.; Gorga, R. E. *J. Compos. Mater.* **2006**, *40*, 1511-1575.
(535) Paul, D. R.; Robeson, L. M. *Polymer* **2008**, *49*, 3187-3204.
(536) Ma, P. X.; Zhang, R.; Xiao, G.; Franceschi, R. *J. Biomed. Mater. Res.* **2001**, *54*, 284-293.
(537) Wei, G.; Ma, P. X. *Biomaterials* **2004**, *25*, 4749-4757.
(538) Laschke, M. W.; Strohe, A.; Menger, M. D.; Alini, M.; Eglin, D. *Acta Biomater.* **2010**, *6*, 2020-2027.
(539) Heinemann, S.; Heinemann, C.; Jager, M.; Neunzehn, J.; Wiesmann, H. P.; Hanke, T. *ACS Appl. Mater. Interfaces* **2011**, *3*, 4323-4331.
(540) Boccaccini, A.; Erol, M.; Stark, W.; Mohn, D.; Hong, Z.; Mano, J. *Compos. Sci. Technol.* **2010**, *70*, 1764-1776.
(541) Wang, S.; Zhang, Z.; Liu, H.; Zhang, W.; Qian, Z.; Wang, B. *Colloid Polym. Sci.* **2010**, *288*, 1031-1039.
(542) Zou, H.; Wu, S.; Shen, J. *Chem. Rev.* **2008**, *108*, 3893-3957.
(543) Tasaki, I.; Byrne, P. M. *Biopolymers* **1992**, *32*, 1019-1023.
(544) Cho, J.; Tay, F.; Heng, J.; Ho, R.; Kazarian, S.; Hwang, Y. *Biomaterials* **2009**, *30*, 499-507.
(545) Hench, L. L. *J. Am. Ceram. Soc.* **1998**, *81*, 1705-1728.

(546) Hench, L. L.; Splinter, R. J.; Allen, W. C.; Greenlee, T. K. *J. Biomed. Mater. Res.* **1971**, *5*, 117-141.
(547) Hench, L. L. *J. Mater. Sci. Mater. Med.* **2006**, *17*, 967-978.
(548) Roether, J. A.; Boccaccini, A. R.; Hench, L. L.; Maquet, V.; Gautier, S.; Jerome, R. *Biomaterials* **2002**, *23*, 3871-3878.
(549) Gough, J.; Boccaccini, A.; Hench, L.; Maquet, V.; Jerome, R.; Roether, J. *J. Mater. Sci. Mater. Med.* **2002**, *13*, 1207-1214.
(550) Blaker, J. J.; Gough, J. E.; Maquet, V.; Notingher, I.; Boccaccini, A. R. *J. Biomed. Mater. Res. A* **2003**, *67A*, 1401-1411.
(551) Boccaccini, A. R.; Maquet, V. *Compos. Sci. Technol.* **2003**, *63*, 2417-2429.
(552) Maquet, V.; Boccaccini, A. R.; Pravata, L.; Notingher, I.; Jerome, R. *J. Biomed. Mater. Res. A* **2003**, *66A*, 335-346.
(553) Maquet, V.; Boccaccini, A. R.; Pravata, L.; Notingher, I.; Jerome, R. *Biomaterials* **2004**, *25*, 4185-4194.
(554) Olsen-Claire, J.; Blaker, J. J.; Roether, J. A.; Boccaccini, A. R.; Schmack, G.; Gliesche, K. *Mat.-wiss. u. Werkstofftech.* **2006**, *37*, 577-583.
(555) Xynos, I. D.; Edgar, A. J.; Buttery, L. D. K.; Hench, L. L.; Polak, J. M. *Biochem. Biophys. Res. Commun.* **2000**, *276*, 461-465.
(556) Day, R. M. *Tissue Eng.* **2005**, *11*, 768-777.
(557) Gorustovich, A. A.; Roether, J. A.; Boccaccini, A. R. *Tissue Eng., B: Rev.* **2010**, *16*, 199-207.
(558) Lu, H. H.; El-Amin, S. F.; Scott, K. D.; Laurencin, C. T. *J. Biomed. Mater. Res. A* **2003**, *64A*, 465-474.
(559) Boccaccini, A. R.; Blaker, J. J. *Expert Rev. Med. Devices* **2005**, *2*, 303-317.
(560) Gkioni, K.; Leeuwenburgh, S. C. G.; Douglas, T. E. L.; Mikos, A. G.; Jansen, J. A. *Tissue Eng., B: Rev.* **2010**, *16*, 577-585.
(561) Cerruti, M.; Greenspan, D.; Powers, K. *Biomaterials* **2005**, *26*, 1665-1674.
(562) McNeill, I. C.; Sadeghi, S. M. T. *Polym. Degrad. Stabil.* **1990**, *30*, 213-230.
(563) McNeill, I. C.; Sadeghi, S. M. T. *Polym. Degrad. Stabil.* **1990**, *29*, 233-246.
(564) Lehman, R. L.; Gentry, J. S.; Glumac, N. G. *Thermochim. Acta* **1998**, *316*, 1-9.
(565) Chatzistavrou, X.; Zorba, T.; Kontonasaki, E.; Chrissafis, K.; Koidis, P.; Paraskevopoulos, K. M. *Phys. Stat. Sol. A* **2004**, *201*, 944-951.
(566) Ilavsky, M.; Mikes, J.; Dusek, K. *Polym. Bull.* **1980**, *3*, 481-487.
(567) Garcia, D.; Escobar, J.; Bada, N.; Casquero, J.; Hernaez, E.; Katime, I. *Eur. Polym. J.* **2004**, *40*, 1637-1643.
(568) Lopez, V. C.; Hadgraft, J.; Snowden, M. J. *Int. J. Pharm.* **2005**, *292*, 137-147.
(569) Ramanan, R. M. K.; Chellamuthu, P.; Tang, L. P.; Nguyen, K. T. *Biotechnol. Prog.* **2006**, *22*, 118-125.
(570) Rzaev, Z. M. O.; Dincer, S.; Piskin, E. *Prog. Polym. Sci.* **2007**, *32*, 534-595.
(571) Chen, H. Y.; Gu, Y. Q.; Hu, Y. Z. *J. Mater. Sci. Mater. Med.* **2008**, *19*, 651-658.
(572) Lee, S.-H.; Shin, H. *Adv. Drug Deliv. Rev.* **2007**, *59*, 339-359.
(573) Chen, F. M.; Zhang, M.; Wu, Z. F. *Biomaterials* **2010**, *31*, 6279-6308.
(574) Lynch, I.; Dawson, K. A. *J. Phys. Chem. B* **2004**, *108*, 10893-10898.
(575) Lynch, I.; de Gregorio, P.; Dawson, K. A. *J. Phys. Chem. B* **2005**, *109*, 6257-6261.
(576) Das, M.; Mardyani, S.; Chan, W. C. W.; Kumacheva, E. *Adv. Mater.* **2006**, *18*, 80-83.
(577) Hoare, T.; Pelton, R. *Langmuir* **2008**, *24*, 1005-1012.
(578) Palit, S. R.; Ghosh, P. *J. Polym. Sci.* **1962**, *58*, 1225-1232.
(579) Sivakumaran, D.; Maitland, D.; Hoare, T. *Biomacromolecules* **2011**, *12*, 4112-4120.
(580) Strichartz, G. R.; Sanchez, V.; Arthur, R. G.; Chafetz, R.; Martiny, D. *Anesth. Analg.* **1990**, *71*, 158-170.

(581) Bernardo, M. V.; Blanco, M. D.; Olmo, R.; Teijon, J. M. *J. Appl. Polym. Sci.* **2002**, *86*, 327-334.
(582) Duvvuri, M.; Gong, Y.; Chatterji, D.; Krise, J. P. *J. Biol. Chem.* **2004**, *279*, 32367-32372.
(583) Gombotz, W. R.; Pankey, S. C.; Bouchard, L. S.; Ranchalis, J.; Puolakkainen, P. *J. Biomater. Sci. Polym. Ed.* **1993**, *5*, 49-63.
(584) Lo, H.; Kadiyala, S.; Guggino, S.; Leong, K. *J. Biomed. Mater. Res.* **1996**, *30*, 475-484.
(585) Coughlan, D. C.; Quilty, F. P.; Corrigan, O. I. *J. Control. Release* **2004**, *98*, 97-114.
(586) Huo, D. X.; Li, Y. N.; Qian, Q. W.; Kobayashi, T. *Colloids Surf., B: Biointerfaces* **2006**, *50*, 36-42.
(587) Chiklis, C. K.; Grasshoff, J. M. *J. Polym. Sci., A-2: Polym. Phys.* **1970**, *8*, 1617-1626.
(588) Aubert, J. H.; Clough, R. L. *Polymer* **1985**, *26*, 2047-2054.
(589) Tsai, F.-J.; Torkelson, J. M. *Macromolecules* **1990**, *23*, 775-784.
(590) Nam, Y. S.; Park, T. G. *Biomaterials* **1999**, *20*, 1783-1790.
(591) Mehvar, R. *J. Control. Release* **2000**, *69*, 1-25.
(592) Heinze, T.; Liebert, T.; Heublein, B.; Hornig, S. *Adv. Polym. Sci.* **2006**, *205*, 199-291.
(593) Van Tomme, S. R.; Hennink, W. E. *Expert Rev. Med. Devices* **2007**, *4*, 147-164.
(594) Cai, Q.; Yang, J.; Bei, J.; Wang, S. *Biomaterials* **2002**, *23*, 4483-4492.
(595) Levesque, S. G.; Lim, R. M.; Shoichet, M. S. *Biomaterials* **2005**, *26*, 7436-7446.
(596) Chen, F.-M.; Zhao, Y.-M.; Sun, H.-H.; Jin, T.; Wang, Q.-T.; Zhou, W.; Wu, Z.-F.; Jin, Y. *J. Control. Release* **2007**, *118*, 65-77.
(597) Ferreira, L. S.; Gerecht, S.; Fuller, J.; Shieh, H. F.; Vunjak-Novakovic, G.; Langer, R. *Biomaterials* **2007**, *28*, 2706-2717.
(598) Bölgen, N.; Yang, Y.; Korkusuz, P.; Guzel, E.; El Haj, A. J.; Piskin, E. *Tissue Eng., A* **2008**, *14*, 1743-1750.
(599) Sun, G.; Zhang, X.; Shen, Y.-I.; Sebastian, R.; Dickinson, L. E.; Fox-Talbot, K.; Reinblatt, M.; Steenbergen, C.; Harmon, J. W.; Gerecht, S. *Proc. Natl. Acad. Sci. U.S.A.* **2011**, *108*, 20976-20981.
(600) Zhou, S.; Bismarck, A.; Steinke, J. H. G. *Macromol. Rapid Commun.* **2012**, *33*, 1833-1839.
(601) Dong, X.; Wang, Y.; Huang, Y.; Liu, J.; Jing, X. *J. Mater. Chem.* **2011**, *21*, 16147-16152.
(602) Zhou, S.; Bismarck, A.; Steinke, J. H. G. *J. Mater. Chem.* **2012**, *22*, 18824-18829.
(603) Young, A. T. *J. Vac. Sci. Technol. A* **1986**, *4*, 1128-1133.
(604) Schugens, C.; Maquet, V.; Grandfils, C.; Jerome, R.; Teyssie, P. *Polymer* **1996**, *37*, 1027-1038.
(605) Güner, A. *J. Appl. Polym. Sci.* **1999**, *72*, 871-876.
(606) Song, S.-W.; Torkelson, J. M. *Macromolecules* **1994**, *27*, 6389-6397.
(607) Song, S.-W.; Torkelson, J. M. *J. Memb. Sci.* **1995**, *98*, 209-222.
(608) Aubert, J. H. *Macromolecules* **1990**, *23*, 1446-1452.
(609) Stenekes, R. J. H.; Talsma, H.; Hennink, W. E. *Biomaterials* **2001**, *22*, 1891-1898.
(610) Alarcon, C.; Pennadam, S.; Alexander, C. *Chem. Soc. Rev.* **2005**, *34*, 276-285.
(611) Stuart, M. A. C.; Huck, W. T. S.; Genzer, J.; Mueller, M.; Ober, C.; Stamm, M.; Sukhorukov, G. B.; Szleifer, I.; Tsukruk, V. V.; Urban, M.; Winnik, F.; Zauscher, S.; Luzinov, I.; Minko, S. *Nature Mater.* **2010**, *9*, 101-113.
(612) Huh, K. M.; Hashi, J.; Ooya, T.; Yui, N. *Macromol. Chem. Phys.* **2000**, *201*, 613-619.
(613) Wang, L. Q.; Tu, K. H.; Li, Y. P.; Zhang, J.; Jiang, L. M.; Zhang, Z. H. *React. Funct. Polym.* **2002**, *53*, 19-27.
(614) Zhang, Y. L.; Chu, C. C. *J. Mater. Sci. Mater. Med.* **2002**, *13*, 773-781.

(615) Ma, P. X.; Zhang, R. *J. Biomed. Mater. Res.* **2001**, *56*, 469-477.
(616) Gao, X.; He, C.; Xiao, C.; Zhuang, X.; Chen, X. *Mater. Lett.* **2012**, *77*, 74-77.
(617) Whitby, C. P.; Fischer, F. E.; Fornasiero, D.; Ralston, J. *J. Colloid Interface Sci.* **2011**, *361*, 170-177.
(618) Webb, P. A.; Orr, C. In *Analytical Methods in Fine Particle Technology*; Micromeritics Instrument Corporation: Norcross, GA USA, 1997.
(619) Brunauer, S.; Emmett, P. H.; Teller, E. *J. Am. Chem. Soc.* **1938**, *60*, 309-319.
(620) Brunauer, S.; Deming, L. S.; Deming, W. E.; Teller, E. *J. Am. Chem. Soc.* **1940**, *62*, 1723-1732.
(621) Washburn, E. W. *Phys. Rev.* **1921**, *17*, 273-283.
(622) Kokubo, T.; Takadama, H. *Biomaterials* **2006**, *27*, 2907-2915.